ANALYSIS OF STIFFENED

TALL BUILDING STRUCTURES

by

OTTO WING-HUNG LAU

B.Sc., C.Eng., M.I.Struct.E.

A.M.I.C.E.

A thesis presented for the degree of

Doctor of Philosophy

of the

University of Glasgow

in the

Department of Civil Engineering

1991

ProQuest LLC.
789 East Eisenhower Parkway
P.O. Box 1346
Ann Arbor, MI 48106 – 1346

Dedicated to my parents

and my wife

CONTENTS

		page
Acknowledgements		
Synopsis		
Chapter 1	INTRODUCTION	1
	1.1 Development of tall buildings	2
	1.2 Previous research	8
	1.3 Present research	14
Chapter 2	STATIC ANALYSIS OF OUTRIGGER-BRACED STRUCTURES	18
	2.1 Introduction	22
	2.2 Analysis	24
	2.2.1 One outrigger	25
	2.2.2 Two outriggers	29
	2.2.3 Three outriggers	32
	2.2.4 n outriggers	36
	2.3 Solutions for different load cases	41
	2.3.1 Uniformly distributed load	42
	2.3.2 Triangularly distributed load	44
	2.3.3 Point load at the top	46
	2.3.4 General polynomial loading	48
	2.3.5 Combined triangularly distributed load and a point load at the top	51
	2.4 Performance of outrigger-braced structures	54
	2.4.1 Drift reduction efficiency	54
	2.4.2 Moment reduction efficiency	59

2.5 Structural optimisation of top drift 63

2.5.1 Top drift minimisation 63

2.5.2 Core base moment minimisation 66

2.5.3 Core moment minimisation 67

2.6 Multiple linear regression 69

2.7 Uniformly spaced outriggers 72

2.8 Numerical results 73

Chapter 3 STATIC ANALYSIS OF MULTI-OUTRIGGER-BRACED STRUCTURES USING CONTINUUM TECHNIQUE 78

3.1 Introduction 81

3.2 Analysis 82

3.3 Numerical results 97

3.3.1 Design curves 97

3.2.2 Accuracy of results 98

Chapter 4 STATIC ANALYSIS OF SHEAR WALL AND OUTRIGGER-BRACED STRUCTURES USING TRANSFER MATRIX TECHNIQUE 101

4.1 Introduction 104

4.2 Structural behaviour of outrigger structures and stiffened linked shear walls 105

4.3 Analysis of coupled shear walls 110

4.4 Analysis of stiffened linked shear walls using transfer matrix technique 114

4.4.1 One stiffening beam 117

4.4.2 Two stiffening beams 119

4.4.3 Three stiffening beams 124

4.4.4 n stiffening beams 128

4.4.5 Boundary conditions 133

4.5 Corresponding case of outrigger-braced core 136

4.6 Numerical results 138

Chapter 5 DYNAMIC ANALYSIS OF OUTRIGGER-BRACED STRUCTURES USING TRANSFER MATRIX TECHNIQUE 141

5.1 Introduction 144

5.2 Analysis 145

5.2.1 One outrigger 145

5.2.2 Two outriggers 151

5.2.3 Three outriggers 156

5.2.4 n outriggers 159

5.2.5 Frequency equation 165

5.3 Corresponding case of linked shear walls 172

5.4 Application to coupled shear wall structures 173

5.5 Numerical examples 175

5.5.1 Example (5.1) 175

5.5.2 Example (5.2) 176

Chapter 6 STATIC ANALYSIS OF STIFFENED COUPLED SHEAR WALL STRUCTURES 178

6.1 Introduction 181

6.2 Analysis 184

6.2.1 Coupled shear walls with an intermediate stiffening beam 184

6.2.2 Coupled shear walls with two intermediate stiffening beams 207

	6.2.3 Two different types of connecting beams	220
	6.3 Significance of structural parameters	230
	6.4 Performance of coupled shear wall structures	233
	6.4.1 Reduction of the top drift	234
	6.4.2 Reduction of the base moment	235
	6.5 Numerical results	235
Chapter 7	DYNAMIC ANALYSIS OF COUPLED SHEAR WALLS USING CONTINUUM TECHNIQUE	243
	7.1 Introduction	245
	7.2 Analysis	246
	7.3 Numerical results	254
Chapter 8	CONCLUSIONS AND RECOMMENDATIONS FOR FUTURE WORK	256
	8.1 Conclusions	257
	8.2 Recommendations for future work	264
REFERENCES		268
Appendix I	Elements of transfer matrix U	275
Appendix II	Evaluation of parameter Kθ	277

ACKNOWLEDGEMENTS

The author wishes to express his gratitude and appreciation to Professor A. Coull, Regius Professor of Civil Engineering, University of Glasgow, for his supervision, guidance, encouragement and invaluable advice during the course of study and throughout the preparation of this thesis.

Grateful thanks are also due to:-
Professor H.B. Sutherland, former Cormack Professor of Civil Engineering, University of Glasgow, for his help and general advice on various occasions.

University of Glasgow and the Committee of Vice-Chancellors and Principals of the Universities of the United Kingdom for University Scholarship granted for the study of this piece of research work.

My colleagues, Dr. C.K. Wong, Dr. J. Tubman, Dr. J. Burns, Dr. S.K. Himmo and Mr. A. To for their company and useful discussions.

Among many who supported morally with the writing of this work, I particularly thank Dr. I.A. Smith for his immense encouragement during a critical period.

My parents for their moral and financial support throughout my education, without which this work would not have been possible.

Last but not least to Nyuk Ching, Joe and Florence for their love and support throughout the period of preparation of this work.

SYNOPSIS

This thesis presents static and dynamic analyses of stiffened tall building structures. The structures dealt with include stiffened linked and coupled shear walls and cores stiffened by outrigger bracings. The discrete matrix approach is used to investigate the effects due to different degrees of base flexibility on the optimum locations of outriggers to minimise top drift and core moment. Investigations are carried out into the static behaviour of outrigger structures subjected to different lateral load cases including uniformly distributed load, point load, triangularly distributed load, polynomial distributed load and a combination of point and triangularly distributed load. A study of equal spacings of the outriggers is made. A multiple regression technique is applied to established results to develop formulae for the optimum locations of outriggers.

An approximate solution for the static analysis based on the continuum method for multi-outrigger structures supported on both rigid and flexible foundation is presented. A comparison of the results is made with that based on drift minimisation and equally spaced outrigger using the discrete matrix approach.

The field transfer matrix technique is used to investigate the static and dynamic behaviour of linked shear walls with multi-stiffening beams. In the determination of the natural frequencies of vibration, the effects of bending, shear and rotatory inertias are included in the analysis. It is shown that there is an analogy between the behaviour of stiffened linked shear walls and outrigger-braced structures, and the same

governing equations apply in each case.

The continuum technique for the analysis of coupled shear walls is extended to cover the cases of up to two intermediate stiffening beams and two different types of connecting beams allowing the estimation of the effects of these beams on structural stiffening in and behaviour of coupled shear walls supported on both rigid and flexible foundations.

Finally, the 'continuum method' used earlier is employed to analyse the free bending of multi-outrigger-braced structures. The natural modes and frequencies of vibration are determined using the Galerkin technique. A comparison of results between the continuum method and that using the transfer matrix technique is made.

CHAPTER ONE

INTRODUCTION

1.1 DEVELOPMENT OF TALL BUILDINGS

As society developed, the need for sheltered spaces began to include the need for privacy and protection and thus evolved walled homes, walled cities and towers. In the beginning, however, sheltered spaces were for combined living and working purposes, or for the storage of goods and animals. These usable spaces were limited in height by materials and structural methods. The very tall structures were protective or symbolic in nature, and were infrequently used - for example, the pyramids of Egypt and medieval castle towers.

The modern skyscraper was a completely new invention with almost no antecedents prior to the middle of the 19th century. Until the use of structural steel became common and the art of modern city planning began its development, multi-storey housing in particular was not distinctly designed as a vertical mode of urban living. It was rather the result of simply crowding together into existing urban places forming a third dimension of high-density living.

The first skyscrapers were designed for commercial uses, and their appropriateness for this propose was acknowledged almost immediately. The development of high rise buildings follows closely to the growth of the city. Gradually they were a natural response to dense population concentration, scarcity of land and high land costs. Furthermore, the socioeconomic developments in industrialised nations have increasingly required the construction of tall apartment and office buildings. Today the incidence of

tall office buildings or of tall housing usually reflects the relative economic strength of government or of private business within a society. Apart from those forces, which generate the development of tall buildings, the technology exists to enable man to build as high as he wishes. As a result, a large number of tall buildings have been constructed to meet these social and economic demands.

Tallness is a relative matter. The tall building cannot be defined in specific terms related to height or number of floors. There is a number of variable factors in each society and therefore a measurable definition of the tall building cannot be universally applied. From a structural point of view, a tall building may be defined as one in which lateral forces play an important role in the structural design. On the other hand, low-rise buildings are generally designed to resist gravitational loads.

The rapid increase in the number of tall buildings, for both commercial and residential purposes, has illuminated the necessity for new philosophies and strategies for designing tall buildings. Particularly, it is necessary to provide methods of analysis capable of giving rapid and accurate assessments of their overall strength and stiffness.

As buildings increase in height, the major forces that determine the design of structure change from vertical loads to horizontal loads. Horizontal loads are caused either by wind or by seismic activity. It then becomes more important to ensure adequate

lateral stiffness to resist loads. This stiffness may be achieved in various ways with respect to different structural framing systems. The efficiency of a particular system is directly related to the quantity of materials used. Thus optimization of a structure for certain spatial requirements should yield the maximum stiffness with the least weight. This results in innovative structural systems applicable to certain height ranges.

Historically, bearing wall structures have been of thick, heavy masonry construction. Their high weight and inflexibility in plan layout made them rather inefficient for multi-storey application. However the development of new technologies in the use of engineering masonry and prefabricated concrete panels has made the bearing wall concept economical in the medium high-rise range.

As greater flexibility in layout and larger open spaces are needed for partitioning, a common solution is to gather vertical transportation and energy distribution systems (e.g. elevators, stairs, water supply, mechanical shafts) to form a core or cores, depending on the size and function of the building. These cores are utilised as shear cores to provide the necessary lateral stability for the building. The response of a core to lateral loading is dependent on its shape, the degree of homogeneity and rigidity, and the direction of the load. The cores can be made of steel, concrete, or a combination of both. The advantage of steel framed cores lies in the relatively rapid assembling of the prefabricated members. The lack of ductility inherent in concrete as a material is a disadvantage with respect to earthquake

loading.

The braced frame becomes inefficient above approximately 40 stories, since large amounts of material are needed to make the bracing sufficiently stiff and strong. The efficiency of the building structure may be improved by using horizontal outrigger belt trusses to tie the exterior frame to the core. The outriggers are fixed rigidly to the core and are simply connected to the exterior columns. The response of outrigger-braced core frame structures are studied in this thesis. The strength and stiffness of the system is further increased by adding additional belt trusses at intermediate levels within the building. At each braced level the system is restrained from bending. The bending moment at the base of the building is further reduced due to the greater transfer of lateral forces to axial forces and the building sway is further decreased.

The development of cross-wall structures for tall buildings has led to the extensive use of shear walls as efficient load-bearing elements. The structural systems, as shown in Fig.[1.1], will generally include regular parallel assemblies of cross-walls and one or more service cores which act as strong points in the building. Those shear walls are two- or three-dimensional vertical structural beam-like elements introduced into the design of tall buildings to provide lateral stability against horizontal loads. The layout of the shear wall buildings is always designed to carry a share of gravity loads as well as horizontal loads. This type of construction has been found to be efficient for buildings up to

about 30 storeys in height. A shear wall is usually perforated with openings in a regular manner as a result of the presence of corridors and windows. Shear walls with a series of regular vertical openings have come to be known as coupled shear walls. If the bending stiffness of the connecting members, or their wall connections, is low, they behave effectively as pin-ended links, the total lateral moment and shear force at any level will be shared between the walls in proportion to their flexural rigidities. The treatment for both types of shear wall is reported in this thesis.

For buildings over 30 storeys in height, the framed-tube form of construction has been found to be very efficient. The concept of the tubular system is a recent development in structural design. In its basic form, as shown in Fig.[1.2], the system consists of closely spaced exterior columns tied at each floor level by deep spandrel beams to form a rectangular tube perforated by holes for the windows. Alternatively it may be regarded as a system of four orthogonal rigidly jointed frame panels forming a closed rectangular system. Both steel and concrete have been used in the construction of such structures. From the point of view of construction economy, the framed tube compares favourably with the normal shear wall type of construction for medium rise buildings, but provides a distinctly economic advantage for taller buildings. Moreover, the closely spaced column system has the great advantage of also being the window wall system, thus replacing the vertical mullions for the support of the glass windows. This system was first used in 1963 for the 43-storey De Witt Chestnut Apartment

Building, in Chicago, U.S.A. Since then, the concept has been widely adopted by designers all over the world. The most significant one is the 110-storey twin towers for the World Trade Centre in New York, U.S.A. For still taller structures, especially where a large plan area is involved, the modular tube or bundled-tube system may be used. This system consists basically of a bundling of smaller size tubes which reduces the shear lag effect and thereby induces more effective participation of the interior columns in resisting the wind load. The Sears Towers, Chicago, the world's tallest building, with 109 storeys for a height of 442 metres above ground level was designed as a bundled-tube structure[1,2,3].

The structural systems given for certain heights should not be considered an absolute rule. In fact, the 102-storey Empire State Building is characterised by a rigid frame-shear wall interaction system, indicated as applying to buildings less than 40 storeys high. However, in the old days, the architectural design was so different from now. Additional stiffness was induced due to heavy masonry cladding and interior partitions which are seldom seen in present building designs. Low- to medium-rise buildings are normally designed for gravity loads, then checked for their ability to resist lateral loads. However high-rise buildings are much more susceptible to lateral force action. With respect to gravity loads, the weight of the structure increases almost linearly with the number of stories. However the amount of material needed for resistance of lateral forces increases at a drastically accelerating rate.

1.2 PREVIOUS RESEARCH

A substantial amount of work reported in this thesis is on the analysis of shear wall structures. From a structural point of view, shear wall structures stand between a solid vertical cantilevered beam and a normal single bay multistorey frame with rigid joints. They may be analysed by four distinct methods, namely (1) finite element analysis (2) the wide column frame analogy (3) simple cantilever walls (4) the continuum method.

Method 1 (finite element analysis) can be accurate and provides a powerful analytical tool but is highly complex. Generally the accuracy of the solution depends on the type and size of element used. The finite element method is not recommended for the analysis of coupled shear walls because of its time and cost limitations. A powerful digital computer is usually a prerequisite for this method. For the purpose of practical design in the office, it is not as readily used as other methods. However, the finite element method of analysis is particularly useful for the detailed analysis of localised stresses and displacements in complex structures or for comparison with results obtained by other methods of analysis.

Method 2 (the wide column frame analogy) is basically an extension of the stiffness method of analysis of normal frames to take account of the finite width of the columns (i.e. the walls of the structure) which are very deep in comparison with the beams. The

structural idealisation of a coupled shear wall is shown in Fig.[1.3]. The method is relatively versatile in that variations in wall thickness, storey height, and opening sizes may be taken into account. Standard computer programs are now available. In cases of buildings of less than six storeys where the assumptions made in the continuum theory are difficult to justify, the wide column analogy is appropriate.

Method 3 (simple cantilever walls) is simple but is only applicable where the walls are in fact independent solid walls (i.e. linked shear walls). It will generally give an underestimate of the stiffness of a building if applied to cases where composite action between walls could occur.

Method 4 (the continuum method) is attractive because as a result of the assumption of a continuous shear connecting medium, a single governing equation expressed as a second order differential equation can be set up. Although it is applicable to uniform systems only, the simplicity of the technique enables the production of simple design curves and tables, giving moments, shears and deflections in the system. The method allows a rapid and accurate solution to be worked out for a particular structural system under standard load cases.

The first conference on the behaviour of tall buildings was held in Southampton University[4] in 1966. Since then a number of regional conferences and symposia have been held all over the world, notably that at Lehigh University[5] in the United States

in 1972 and at Chicago in 1986. The Council on Tall Buildings and Urban Habitat series of Monographs[6] are a few of the many publications on the design and planning of tall buildings. These describe the main work to bring together knowledge about tall buildings themselves, which need not be repeated here.

The analysis of coupled shear wall structures has attracted many investigators. Shear walls of uniform cross-section for the full height of the building subjected to wind loading was treated using the continuum technique by Chitty and Wan[7], Beck[8], Rosman[9,10] and Magnus[11] extended the analysis to take into account the rotation of the cross-sections of the relatively wide walls, the axial forces in the walls and the effects of different boundary conditions. Coull[12,13] extended the basic analysis to cover different load cases, the cases of variable wall thickness[14], variable cross sections[15] and flexible foundations[16]. Based on the continuum method of analysis, Tso and Chan[17] extended the study to coupled shear walls resting on a flexible foundation and subjected to lateral loadings. A large range of foundation stiffnesses was studied. The influence of a stiff top beam on the structural response of coupled shear walls supported on flexible foundations was studied by Coull[18]. It was found that the undesirable effects of foundation movements may be reduced by providing one or more stiff connecting beams between the walls. Based on the continuous connection technique, Choo and Coull[19,20] extended the study to cover the case of a stiff base beam and found it to be more effective in reducing the effects of foundation flexibility. The analysis, based on the continuous

connection technique, is extended in this thesis to investigate the stiffening of coupled shear walls on rigid or flexible foundations. The cases of shear walls with one or more stiffening beams and two different types of connecting beams are included.

Initially most of the work was concerned with the case of plane walls undergoing bending, but in the last two decades, work has been carried out on core structures as a major component in resisting bending and torsional loading. Using an energy method, Jenkins and Harrison[21] analysed core structures by assuming torsional displacements and rotations in the form of polynomials and applying the minimum potential energy theorem to determine the rotations. Stafford Smith and Taranath[22] considered the warping displacements as a seventh degree of freedom of the section, and the effect of bracings was taken into account by adding their warping stiffness to the warping stiffness of the open section. In similar investigations by Heidebrecht and Stafford Smith[23] a braced open section was solved. Based on the same theory, Khan and Stafford Smith[24] converted a braced open section to an equivalent closed section by introducing a continuous connection to allow the shear flow to circulate around the profile of the core. Using the engineering theory of bending, Michael[25] considered a simple doubly-symmetric core to be composed of two equal separate channels and obtained a second order differential equation relating the bending moment in the walls and the applied torque. Similarly, Tso and Biswas[26] analysed the same core by formulating the problem in terms of the direct equilibrium of forces and considering the rotation as the unknown variable in the

governing equation. By considering the core to consist of vertical plates rigidly connected together along their edges and by using the continuous connection method and the folded plate approach, Coull[27] derived a third order equation for structures on fixed or flexible foundations. Coull and Tawfik[28,29] extended the technique to obtain closed-form solutions for a wide range of cross-sectional platforms, including asymmetric, multi-cell and multi-bay structures. The same form of governing third order differential equation may be used to describe the torsional behaviour of the majority of practical situations.

Stiffening of a core structure by using outrigger-bracings as shown diagramatically in Fig.[1.4] was first studied by Taranath[30]. He investigated single outrigger structures and showed that the optimum location of an outrigger was close to the mid-height of the building. McNabb and Muvdi[31] verified Taranath's result for a single outrigger structure and showed that the optimum locations for two outriggers were 0.312 and 0.685 of the total height from the top. Stafford Smith and Nwake[32] produced generalized results for the optimum locations in multi-outrigger structures. They showed that if the outriggers are located at equidistant height intervals, but excluding one at the top of the structures, a close to optimum reduction in drift is achieved. In each of the above investigations, the assumption of flexurally rigid outriggers was adopted and only a uniformly distributed lateral load was examined to simplify the solution of the problem. It was noted, however, that the flexibility of the outriggers would have an influence on the total drift and on the

core moment. This flexibility would also affect the optimum location of the outriggers for the maximum reduction in drift. Stafford Smith and Salim[33,34] investigated further the multi-outrigger structure with flexible outriggers. They developed equations and formulae to allow the optimum locations of the outriggers and magnitude of drift and reduction in core moment to be estimated. All the works on the optimisation of the outrigger-braced structures were concerned with the reduction of the top drift of buildings as the prime factor. Reduction in the base moment was considered as a secondary factor in the analysis. Boggs and Gasparini[35] presented generalized results for the case of a single outrigger at a particular height, considering a flexible outrigger, non-prismatic elements and a triangularly distributed lateral load.

Most of the works on the subject mentioned so far were mainly concerned with the design parameters governing drift reduction under lateral loading. However, with a trend towards taller, lighter and more wind sensitive structures, it is of importance to be able to access the dynamic properties of the building in order to evaluate dynamic loading. The topic has been previously studied by Rutenburg[36]. The response spectrum technique was used in the analysis. The case of a single outrigger, assuming no flexibility in the outrigger arm, was considered. Coull and Moudarres[37,38] used the field transfer matrix technique to investigate the static and dynamic behaviour of single outrigger-braced and stiffened linked shear wall structures. The effect of bending, shear and rotatory inertia are included in the analysis. The first natural

frequency of the structure was found. The technique was found to be relatively simple and efficient.

1.3 PRESENT RESEARCH

This thesis is concerned with the analyses of the stiffening of high-rise buildings essentially comprising outrigger-braced structures, coupled shear wall and linked shear wall structures, under the action of lateral loads. Particular attention is paid to the structural behaviour and optimisation of the structure.

In Chapter 2, based on the discrete matrix approach, an analysis is presented to cover the important lateral load design cases, namely (i) uniformly distributed load, (ii) an equivalent quasi-static earthquake loading, in which the total specified base shear is represented by a combination of a triangularly distributed inertia loading and a concentrated load at the top, the latter being included to represent the dynamic influence of the higher modes which may be excited and (iii) any form of wind force distribution which may be represented by a polynomial of the form $p(1-(x/H)^z)$, in which z is any integer and (x/H) is the height ratio. Using the discrete matrix approach, the optimisation of outrigger-braced structures to minimise both top drift and core moment is presented. Any elastic rotational flexibility at the base is included in the analysis. A multiple linear regression is applied in the analysis to enable designers to obtain the optimum locations of the outriggers to minimise either the lateral drift or the core moment, for a range of relative stiffnesses of the

core, outriggers and columns.

In Chapter 3, an approximate analysis of multi-braced-structures based on the continuum approach, in which the set of outriggers is smeared over the height to give an equivalent uniform bracing system, is presented.

In Chapter 4, the field transfer matrix technique is used to investigate the static behaviour of stiffened linked shear walls. It has been shown that there is an analogy between the behaviour of outrigger-braced structures and linked shear walls which are stiffened by a series of stiff connecting beams. The analysis and results are shown to apply equally well to both forms of structure. Furthermore, the developed theory was also demonstrated for applying to the analysis of a coupled shear wall structure.

In Chapter 5, an investigation of the dynamic behaviour of outrigger structures and linked shear walls structures using the field transfer matrix technique is presented. The field transfer matrix technique is used to handle the discontinuities at the outrigger or the stiffening beams positions. The effect of bending, shear and rotatory inertias are included in the analysis. In addition, the possibility of any elastic rotational flexibility at the core base is included. Its influence on the natural frequencies is demonstrated in the numerical studies. A series of numerical studies are made, and the first three natural frequencies are determined for one, two and three outriggers. The relative influences of the flexural rigidities of the core and

outriggers, and the axial rigidities of the columns are examined. The determination of the first natural frequency is more important for wind actions, but the higher modes become of importance when considering seismic behaviour. The behaviour of outrigger braced core and stiffened linked shear walls is analogous, and so the analysis, equations and results apply equally well to both forms of stiffened structure. Only the important governing parameters need to be redefined in a manner appropriate to the particular structure being considered.

Chapter 6 describes the elastic analysis of stiffened coupled shear wall structures. When the connecting beams of the coupled shear walls are weak, the two walls will behave more like two independent cantilevered walls. When the connecting beams are stiff, the two walls will tend to act as a monolithic cantilever and thus increase the structural efficiency. It was shown that the structural response of a coupled shear wall with weak coupling beams may be improved by introducing a stiffer beam at some position along the height on the building. Here, the continuous connection technique is extended to cover the stiffened coupled shear wall structures with up to two stiffening beams and two layers of connecting beams with different stiffnesses.

In Chapter 7, the continuous connection method is employed to analyse the free bending of multi-outrigger-braced structures. The natural modes and frequencies of vibration are determined from the Galerkin technique.

In Chapter 8, the conclusions drawn from the above studies and suggestions for future works are included.

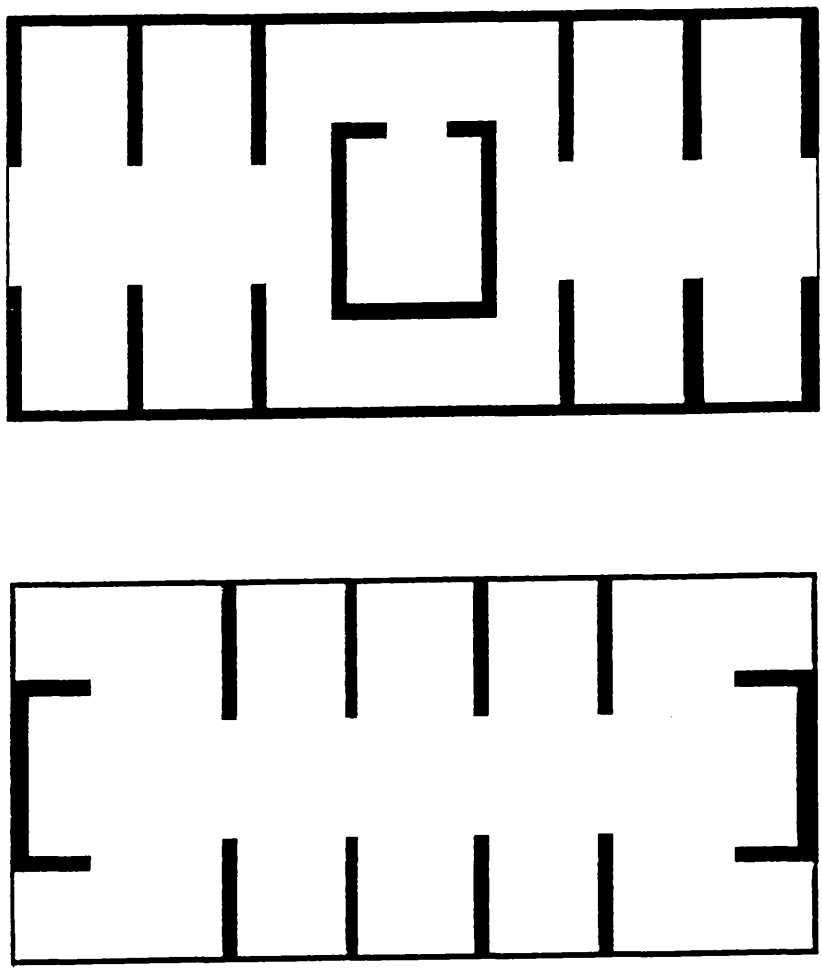

FIG. [1.1] PLAN-FORMS OF REGULAR SYMMETRIC CROSS-WALL STRUCTURES

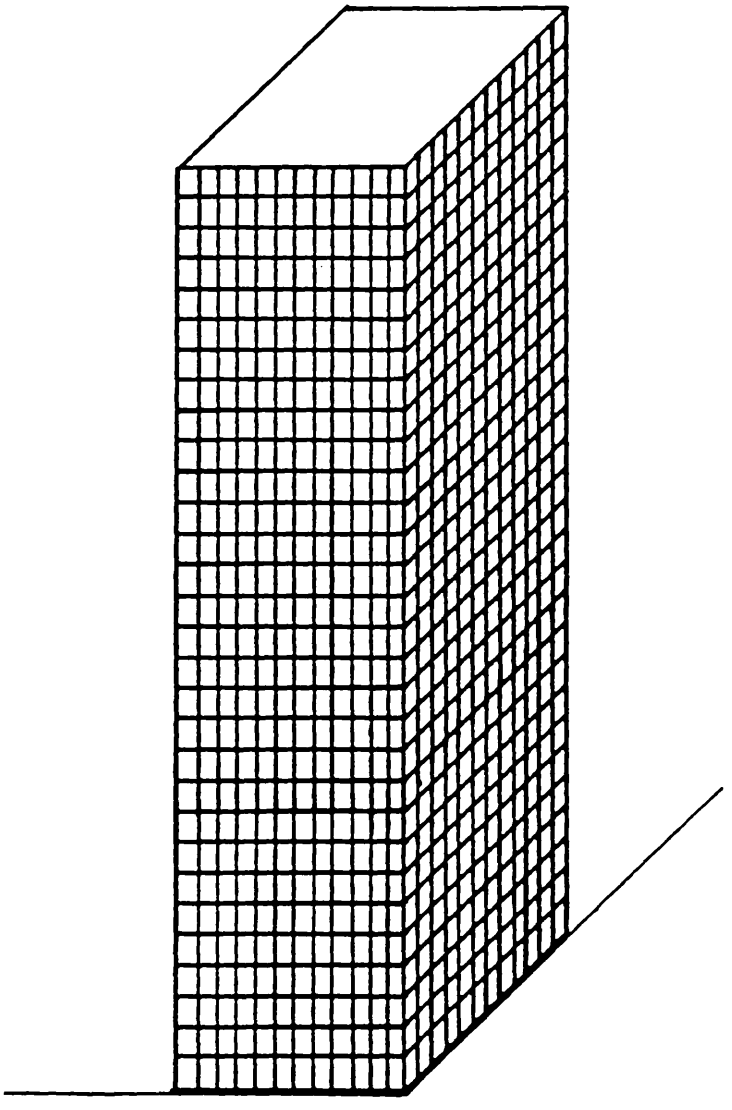

FIG. [1.2] REPRESENTATION OF A FRAMED-TUBE STRUCTURE

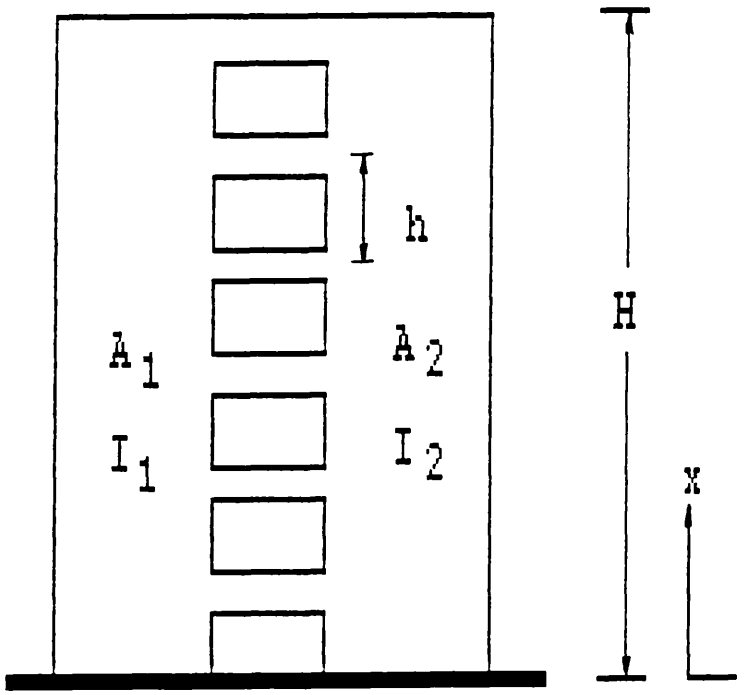

Coupled shear walls

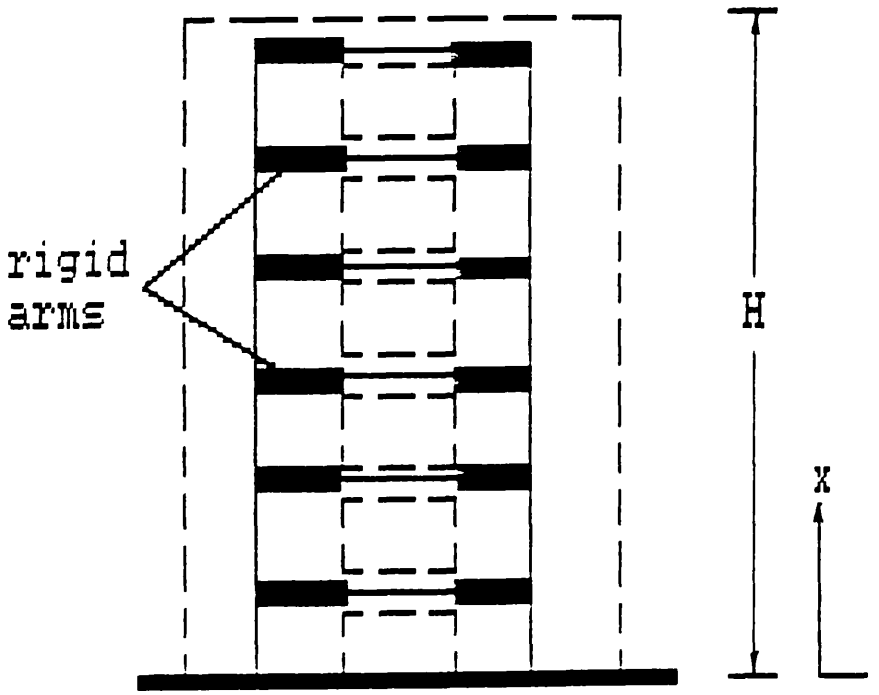

Equivalent frame

FIG. [1.3] COUPLED SHEAR WALLS AND EQUIVALENT FRAME FOR ANALYSIS BY THE FRAME ANALOGY METHOD

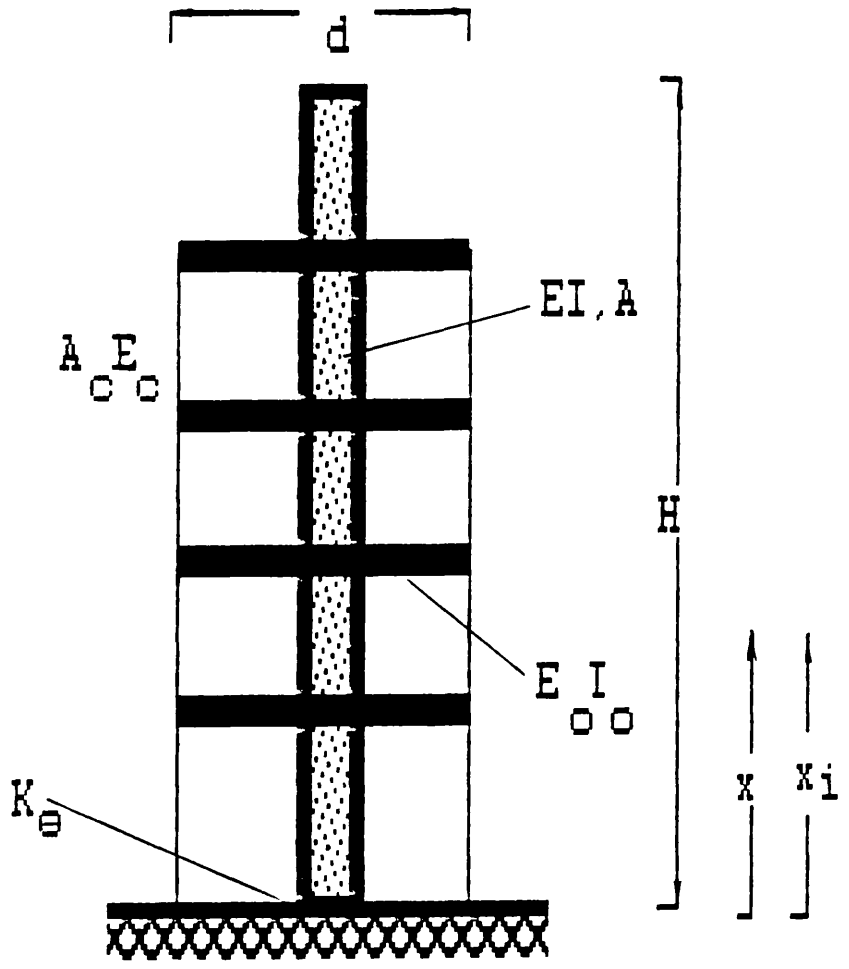

SECTION A-A

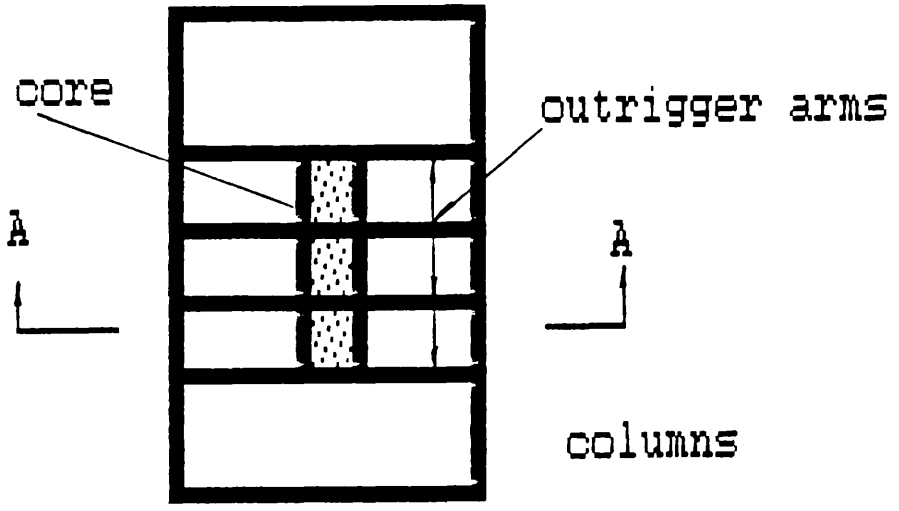

Fig.[1.4] TYPICAL PLAN

CHAPTER TWO

STATIC ANALYSIS OF OUTRIGGER-BRACED STRUCTURES

NOTATION of Chapter 2

$\mathbb{A}$, $\mathbb{B}$, $\mathbb{C}$	matrices containing structural parameters
A_c	sectional area of column
d	distance between columns
E	elastic modulus of core
E_c	elastic modulus of column
E_o	elastic modulus of outrigger
$F_1..F_i..F_n$	tip shear of outriggers 1..i.. and n
H	height of structure
I	moment of inertia of core
I_o	effective moment of inertia of outrigger
I_r	actual moment of inertia of outrigger
k	structural parameter
M_a	applied moment due to external loads
M_{aB}	applied moment at the base of the structure
M_B	core moment at the base of the structure
M_c	reduction in core moment for an infinitely rigid outrigger structure with a rigid base
M_{cf}	reduction in core moment for an infinitely rigid outrigger structure with a flexible base
M_{Bir}	core moment at the base of an outrigger structure with an infinite number of infinitely rigid outriggers and a rigid base
M_{Bif}	core moment at the base of an outrigger structure with an infinite number of infinitely rigid outriggers and a flexible base
$M_1..M_i..M_n$	restraining moments due to outriggers 1..i..n
M_x	core moment at level x measured from the top

P	point load at the top of the structure
p	maximum load intensity of a general polynomial load
r_m	moment reduction efficiency
r_y	drift reduction efficiency
S, S_1	structural parameters
w	horizontal load per unit height
w_t	maximum load intensity of a upper triangular distributed load
$x_1..x_i..x_n$	distance of outriggers 1..i..n from top of structure
y_c	reduction in top drift for an infinitely rigid outrigger structure with a rigid base
y_{cf}	reduction in top drift for an infinitely rigid outrigger structure with a flexible base
y_{Tir}	top drift of an outrigger structure with an infinite number of infinitely rigid outriggers and a rigid base
y_{Tif}	top drift of an outrigger structure with an infinite number of infinitely rigid outriggers and a flexible base
y_{FFT}	top drift of the free bending of the core with a flexible foundation
y_{FT}	top drift of the free bending of the core with a rigid base
y_T	top drift of the structure
α, β	structural parameters
$\xi_1..\xi_i..\xi_n$	non-dimensional height (x_i/H)
$\vartheta_1..\vartheta_i..\vartheta_n$	rotation of core at outriggers 1..i..and n

K_ϑ	rotational stiffness
ω	non-dimensional characteristic parameter
$\mathbb{M}$	matrix for restraining moments

Other subsidiary symbols are defined locally in the text.

2.1 INTRODUCTION

An outrigger-braced tall building structure, as shown in Fig.[2.1], consists of a stiff interior core, comprising either a braced steel frame or a system of shear walls, connected to exterior columns by a flexurally stiff cantilever beam or truss. When the structure is subjected to lateral forces, the outriggers and columns resist the rotation of the core and thus reduce the lateral deflections and base moment which would have occurred in a free-standing core. Outrigger bracing is one of the most effective and economic systems for controlling drift in tall buildings, and, as the outriggers are generally incorporated within the plant levels in the building, they interfere only minimally with the usable space. This form of bracing has been used for many very tall buildings in both steel and reinforced concrete. The magnitude of the reductions in drift and core moments depends on the relative flexural rigidities, the outriggers and the columns acting axially about the centroid of the core, as well as on the locations of the outriggers within the height of the core. An idealised representation of a single outrigger-braced structure and its typical floor plan are shown in Fig.[2.2].

The analysis is based on the pioneering work of Stafford Smith[32,33] who investigated the influence of single or multi-outriggers on the behaviour of structures subjected to uniformly distributed lateral loading. Both of the papers have studied the influence of the flexibility and the locations of the outriggers on the reduction in drift which was the main criterion considered, under uniform distributed loading only. In this Chapter, the analysis is extended to include any elastic rotational flexibility at the base of the core and to cover five important lateral load cases, (i) a uniformly distributed load w;

(ii) a triangularly distributed lateral load, whose intensity varies linearly from zero at the base to a value w_t at the top; (iii) a concentrated top load P at the top; (iv) a general lateral loading whose intensity at any level is defined by the polynomial $p[\ 1-(x/H)\ ]^z$ and (v) a combined triangularly distributed and a point load at the top based on the recommendation of the Canadian Code of Practice[42]. The work on optimum locations of outriggers for the above load cases includes not only the main criterion of top drift, but includes also the core moment on the structure.

A study is made to determine the location of the outriggers to give a maximum reduction of the top drift. However, it is noted that outriggers located for optimum drift reduction do not give a maximum core base moment reduction. The core base moment progressively reduces as the outriggers are placed lower on the structure. This becomes more important when the core at the foundation level is not rigid. In this chapter, a study is made to determine also the location of the outriggers to give a maximum reduction of the core moment. A numerical example is presented and the balance of the two requirements is discussed at the end of this Chapter. Discussion is also made on the importance of the balance of the two aspects on the design of the structure.

A multiple linear regression analysis is used to determine the optimum locations of the outriggers to minimise either the lateral drift or the core moments, for a range of relative stiffnesses of core, outriggers and columns. Although it is possible to obtain for a particular structure the optimum outrigger locations using a flexibility analysis, it is mathematically complicated and if

repeated analyses are necessary in the process of adjusting the design of the structure, it is extremely time-consuming. Therefore the multiple linear regression is applied to the results of flexibility analysis to develop general formulae for estimating the optimum levels of outriggers to minimise the drift in an idealised, uniform outrigger-braced structures. A set of design curves which illustrate the influence of the flexibility of the outrigger/s on the optimum location either to lateral drift or to the core moment are given for the different load cases. Finally, the results of a study on the comparison of structural response between the optimum outrigger system and the equally spaced outrigger system subject to different lateral loadings are presented.

2.2 ANALYSIS

The development of the analysis is based on the following simplified assumptions:-

1. The structure behaves linear elastically.
2. The outriggers are pinned to the columns and axial forces only are induced in the columns.
3. The outriggers are rigidly attached to the core.
4. The sectional properties of the core, columns and outrigger do not change throughout the height of the structure.

The analysis is based on the discrete matrix approach to establish equations for the compatibility and equilibrium of the core and outriggers at the outrigger levels. Their solution gives the

restraining moment applied to the core by each outrigger, and hence gives the moment diagram for the core.

2.2.1 ONE OUTRIGGER

Where the core rests on an elastic foundation or a rotational stiffness exists due to the formation of the basement or substructure, the rotational deformation ϑ_B at the base will be included. The required boundary condition is obtained by using the base compatibility equation. The rotational deformation is proportional to the core moment.

$$\vartheta_B = K_\vartheta M_B$$

where K_ϑ is the rotational flexibility at the base of the structure or of the substructure

$$M_B = M_{aB} - M_1$$

in which

M_B is the core moment at base

M_{aB} is the applied core moment at base

M_1 is the restraining moment of the outrigger

The restraining moment of the outrigger is defined as the product of the outrigger tip shear and the distance between columns. The tip shear is equal to the difference between the axial forces in the columns above and below the outrigger concerned. In the one-outrigger case,

$$M_1 = F_1 d$$

where F_1 is the outrigger tip shear and d is the distance between columns.

The analysis is expressed initially in terms of any lateral applied loading, and specific cases are established subsequently. The core rotation at the level where the outrigger is placed can be shown by using the moment-area method to be,

$$\vartheta = \frac{1}{EI} \int_{x_1}^{H} (M_a - M_1)dx + K_\vartheta M_B \qquad (2.1)$$

where

M_a is the external moment at level x

x_1 is the distance of the outrigger measured from the top of the structure

E is the elastic modulus of the core

I is the moment of inertia of the core

H is the height of the core structure

The corresponding expression for the rotation of the outrigger will now be developed to establish compatibility with the core. The rotation of the inboard end of an outrigger where it attaches to the core consists of two components, one due to differential axial deformation of the columns and the other due to the outrigger bending under the action at its ends of the column forces. The component of rotation due to axial deformations of the

columns is given by

$$\vartheta_a = \frac{2M_1(H-x_1)}{d^2E_cA_c} \qquad (2.2)$$

while that due to the bending of the outrigger is given by

$$\vartheta_b = \frac{M_1 d}{12E_oI_o} \qquad (2.3)$$

Equations (2.1), (2.2) and (2.3) can be used to express the compatibility of the core and outrigger rotations at the level of the outrigger, thus

$$\vartheta_a + \vartheta_b = \vartheta$$

or

$$\frac{2M_1(H-x_1)}{d^2E_cA_c} + \frac{M_1 d}{12E_oI_o} = \frac{1}{EI}\int_{x_1}^{H}(M_a-M_1)dx + K_\vartheta M_B \qquad (2.4)$$

where

E_c is the elastic modulus of the column

A_c is the area of the column

E_o is the elastic modulus of the outrigger

I_o is the moment of inertia of outrigger

Since the width of the central core is not generally negligible, rotations of the core cross-section under bending will impose displacements of magnitude $a\frac{dy}{dx}$ at the inner ends of the outriggers

where a is half of the central core width. This is shown in Fig.[2.3]. The inner segment of the outrigger, of length a, may then be regarded as infinitely stiff. This effect may be included in the analysis by replacing the true flexural rigidity $E_o I_r$ by an equivalent value $E_o I_o$ of magnitude.

$$E_o I_o = \frac{E_o I_r}{(1-2a/d)^3} \qquad (2.5)$$

Equation (2.4) can be rewritten as,

$$M_1 [\ S_1 + S(H-x_1)\ ] = \frac{1}{EI} \int_{x_1}^{H} M_a dx + K_\vartheta M_B \qquad (2.6)$$

in which S and S_1 are the parameters

$$S = \frac{1}{EI} + \frac{2}{d^2 E_c A_c} \qquad (2.6a)$$

and

$$S_1 = \frac{d}{12 E_o I_o} \qquad (2.6b)$$

The expression for the restraining moment is then

$$M_1 = \frac{1}{S_1 + S(H-x_1) + K_\vartheta} \left[\frac{1}{EI} \int_{x_1}^{H} M_a dx + K_\vartheta M_{aB} \right] \qquad (2.7)$$

The restraining moment M_1 can be subtracted from the "free" bending moment diagram to give the resulting bending moment distribution in the core. The forces in the columns below the

outrigger becomes $+M_1/d$ for the tension side and $-M_1/d$ for the compression side. The maximum moments in the outriggers will then be the product of the tip shear and the free length of the outrigger.

The moment-area method is a simple means of determining the top drift of the outrigger structure. The top drift of the core is obtained as

$$y_T = \frac{1}{EI}\left[\int_0^{x_1} M_a x dx + \int_{x_1}^{H} (M_a - M_1) x dx\right] + \vartheta_B H \qquad (2.8)$$

2.2.2 TWO OUTRIGGERS

The core rotations at levels 1 and 2 in Fig.[2.4] can be shown by the moment-area method to be respectively

$$\vartheta_1 = \frac{1}{EI}\int_{x_1}^{x_2}(M_a - M_1)\, dx + \frac{1}{EI}\int_{x_2}^{H}(M_a - M_1 - M_2)\, dx + K_\vartheta M_B \qquad (2.9a)$$

$$\vartheta_2 = \frac{1}{EI}\int_{x_2}^{H}(M_a - M_1 - M_2) dx + K_\vartheta M_B \qquad (2.9b)$$

In the above equations, M_1 and M_2 are the restraining moments from the two outriggers given by

$$M_1 = F_1 d$$

$$M_2 = F_2 d$$

where F_1 is the shear force at the tip of the first outrigger and F_2 is the shear force at the tip of the second outrigger.

The components of rotation at 1 and 2 due to axial deformations of the columns are given by

$$\vartheta_{a1} = \frac{2M_1(H-x_1)}{d^2E_cA_c} + \frac{2M_2(H-x_2)}{d^2E_cA_c} \qquad (2.10a)$$

$$\vartheta_{a2} = \frac{2(M_1+M_2)(H-x_2)}{d^2E_cA_c} \qquad (2.10b)$$

while those due to the bending of the outrigger are given by

$$\vartheta_{b1} = \frac{M_1 d}{12E_oI_o} \qquad (2.11a)$$

$$\vartheta_{b2} = \frac{M_2 d}{12E_oI_o} \qquad (2.11b)$$

Equations (2.9a), (2.10a) and (2.11a) can be used to express the compatibility of the core and outrigger rotations at the level of the upper outrigger, thus

$$\vartheta_{a1} + \vartheta_{b1} = \vartheta_1$$

or

$$\frac{2M_1(H-x_1)}{d^2E_cA_c} + \frac{2M_2(H-x_2)}{d^2E_cA_c} + \frac{M_1d}{12E_oI_o} =$$

$$\frac{1}{EI}\left[\int_{x_1}^{x_2}(M_a-M_1)dx + \int_{x_2}^{H}(M_a-M_1-M_2)dx\right] + K_\vartheta M_B \qquad (2.12a)$$

Equations (2.9b), (2.10b) and (2.11b) can be used to express the compatibility of the core and outrigger rotations at the lower outrigger.

$$\vartheta_{a2} + \vartheta_{b2} = \vartheta_2$$

$$\frac{2(M_1+M_2)(H-x_2)}{d^2E_cA_c} + \frac{M_2d}{12E_oI_o} =$$

$$\frac{1}{EI}\int_{x_2}^{H}(M_a-M_1-M_2)dx + K_\vartheta M_b \qquad (2.12b)$$

Equations (2.12a) and (2.12b) may be rewritten as

$$M_1[S_1+S(H-x_1)]+M_2S(H-x_2) = \frac{1}{EI}\int_{x_1}^{H} M_a + K_\vartheta M_B \qquad (2.13a)$$

$$M_1S(H-x_2)+M_2[S_1+S(H-x_2)] = \frac{1}{EI}\int_{x_2}^{H} M_a + K_\vartheta M_B \qquad (2.13b)$$

where x_1 and x_2 are the distances of the outriggers measured from the top of the structure, and

$$M_B = M_{aB} - M_1 - M_2$$

Equations (2.13a) and (2.13b) can be written in matrix form as follows

$$\begin{bmatrix} M_1 \\ M_2 \end{bmatrix} = \begin{bmatrix} S_1+S(H-x_1)+K_\vartheta & S(H-x_2)+K_\vartheta \\ S(H-x_2)+K_\vartheta & S_1+S(H-x_2)+K_\vartheta \end{bmatrix}^{-1} \cdot \begin{bmatrix} \frac{1}{EI}\int_{x_1}^{H} M_a dx+K_\vartheta M_{aB} \\ \frac{1}{EI}\int_{x_2}^{H} M_a dx+K_\vartheta M_{aB} \end{bmatrix} \tag{2.14}$$

Using the moment-area method, the top drift becomes

$$y_T = \frac{1}{EI}\left[\int_0^{x_1} M_a x dx + \int_{x_1}^{x_2}(M_a-M_1)x dx + \int_{x_2}^{H}(M_a-M_1-M_2)x dx\right] + \vartheta_B H \tag{2.15}$$

where

$$\vartheta_B = K_\vartheta(M_{aB}-M_1-M_2)$$

2.2.3 THREE OUTRIGGERS

Similar procedures can be used for structures with three or more outriggers, as shown in Fig.[2.5], to form compatibility equations corresponding to the core and outriggers at each level of the outrigger as

$$\vartheta_1 = \frac{1}{EI}\int_{x_1}^{x_2}(M_a - M_1)dx + \frac{1}{EI}\int_{x_2}^{x_3}(M_a - M_1 - M_2)dx + \frac{1}{EI}\int_{x_2}^{H}(M_a - M_1 - M_2 - M_3)dx + K_\vartheta M_B \quad (2.16a)$$

$$\vartheta_2 = \frac{1}{EI}\int_{x_2}^{x_3}(M_a - M_1 - M_2)dx + \frac{1}{EI}\int_{x_3}^{H}(M_a - M_1 - M_2 - M_3)dx + K_\vartheta M_B \quad (2.16b)$$

$$\vartheta_3 = \frac{1}{EI}\int_{x_3}^{H}(M_a - M_1 - M_2 - M_3)dx + K_\vartheta M_B \quad (2.16c)$$

where

x_1, x_2 and x_3 are the distances of the outrigger measured from the top of the structure.

$M_B = M_{aB} - M_1 - M_2 - M_3$

M_1, M_2 and M_3 are the restraining moments from the three outriggers given by

$$M_1 = F_1 d$$

$$M_2 = F_2 d$$

$$M_3 = F_3 d$$

F_1, F_2 and F_3 are the tip shears of the outriggers concerned.

The components of rotation due to axial deformations of the columns are given by

$$\vartheta_{a1} = \frac{2M_1(H-x_1)}{d^2 E_c A_c} + \frac{2M_2(H-x_2)}{d^2 E_c A_c} + \frac{2M_3(H-x_3)}{d^2 E_c A_c} \quad (2.17a)$$

$$\vartheta_{a2} = \frac{2(M_1+M_2)(H-x_2)}{d^2E_cA_c} + \frac{2M_3(H-x_3)}{d^2E_cA_c} \qquad (2.17b)$$

$$\vartheta_{a3} = \frac{2(M_1+M_2+M_3)(H-x_3)}{d^2E_cA_c} \qquad (2.17c)$$

while those due to the bending of the outrigger are given by

$$\vartheta_{b1} = \frac{M_1 d}{12E_oI_o} \qquad (2.18a)$$

$$\vartheta_{b2} = \frac{M_2 d}{12E_oI_o} \qquad (2.18b)$$

$$\vartheta_{b3} = \frac{M_3 d}{12E_oI_o} \qquad (2.18c)$$

Equations (2.16), (2.17) and (2.18) can be used to express the compatibility of the core and outrigger rotations at each level of outrigger, as

$$\vartheta_{a1} + \vartheta_{b1} = \vartheta_1$$

$$\vartheta_{a2} + \vartheta_{b2} = \vartheta_2$$

$$\vartheta_{a3} + \vartheta_{b3} = \vartheta_3$$

Hence,

$$M_1[S_1+S(H-x_1)] + M_2S(H-x_2) + M_3S(H-x_3) = \frac{1}{EI}\int_{x_1}^{H} M_a + K_\vartheta M_B \qquad (2.19a)$$

$$M_1 S(H-x_2) + M_2[S_1+S(H-x_2)] + M_3 S(H-x_3) = \frac{1}{EI}\int_{x_2}^{H} M_a + K_\vartheta M_B \qquad (2.19b)$$

$$M_1 S(H-x_3) + M_2 S(H-x_3) + M_3(S_1+S(H-x_3)] = \frac{1}{EI}\int_{x_3}^{H} M_a + K_\vartheta M_B \qquad (2.19c)$$

Equation (2.19) can be written in matrix form as follows,

$$\begin{bmatrix} M_1 \\ M_2 \\ M_3 \end{bmatrix} = \begin{bmatrix} S_1+S(H-x_1)+K_\vartheta & S(H-x_2)+K_\vartheta & S(H-x_3)+K_\vartheta \\ S(H-x_2)+K_\vartheta & S_1+S(H-x_2)+K_\vartheta & S(H-x_3)+K_\vartheta \\ S(H-x_3)+K_\vartheta & S(H-x_3)+K_\vartheta & S_1+S(H-x_3)+K_\vartheta \end{bmatrix}^{-1} \cdot \begin{bmatrix} \frac{1}{EI}\int_{x_1}^{H} M_a dx + K_\vartheta M_{aB} \\ \frac{1}{EI}\int_{x_2}^{H} M_a dx + K_\vartheta M_{aB} \\ \frac{1}{EI}\int_{x_3}^{H} M_a dx + K_\vartheta M_{aB} \end{bmatrix} \qquad (2.20)$$

The top drift is,

$$y_T = \frac{1}{EI}\left[\int_0^{x_1} M_a x dx + \int_{x_1}^{x_2} M_a x dx + \int_{x_1}^{x_2} (M_a - M_1) x dx + \int_{x_2}^{x_3} (M_a - M_1 - M_2) x dx + \frac{1}{EI}\int_{x_3}^{H} (M_a - M_1 - M_2 - M_3) x dx \right] + \vartheta_B H \qquad (2.21)$$

where

$$\vartheta_B = K_\vartheta (M_{FB} - M_1 - M_2 - M_3)$$

2.2.4 n OUTRIGGERS

The solution of multi-outrigger structures with four or more outriggers leads to the complexity of formulating a large number of compatibility equations for the core and outriggers to give moment and drift. The recognition of patterns allows generalised equations to be written. These are expressed best in matrix form for simultaneous computer solution.

$$\mathbb{M} = \mathbb{P}^{-1}.\mathbb{L} \qquad (2.22)$$

where $\mathbb{M}$ is a column matrix containing the restraining moments M_1, M_2 ..M_i .. and $M_n$due to outriggers 1, 2 .. i .. and n.

$$\mathbb{M} = \begin{bmatrix} M_1 \\ M_2 \\ \vdots \\ M_i \\ \vdots \\ M_n \end{bmatrix}$$

$\mathbb{L}$ is a column matrix containing the load terms due to the applied moment at levels x_1, x_2, .. x_i .. and x_n.

$$\mathbb{L} = \begin{bmatrix} \frac{1}{EI}\int_{x_1}^{H} M_a dx + K_\vartheta M_{aB} \\ \frac{1}{EI}\int_{x_2}^{H} M_a dx + K_\vartheta M_{aB} \\ \vdots \\ \frac{1}{EI}\int_{x_i}^{H} M_a dx + K_\vartheta M_{aB} \\ \vdots \\ \frac{1}{EI}\int_{x_n}^{H} M_a dx + K_\vartheta M_{aB} \end{bmatrix}$$

and $\mathbb{P}$ is a square matrix containing the structural properties of the structure given by,

$$\mathbb{P} = \begin{bmatrix} S_1+S(H-x_1)+K_\vartheta & S(H-x_2)+K_\vartheta & \cdots & S(H-x_i)+K_\vartheta & \cdots & S(H-x_n)+K_\vartheta \\ S(H-x_2)+K_\vartheta & S_1+S(H-x_2)+K_\vartheta & \cdots & S(H-x_i)+K_\vartheta & \cdots & S(H-x_n)+K_\vartheta \\ \vdots & \vdots & & \vdots & & \vdots \\ S(H-x_i)+K_\vartheta & S(H-x_i)+K_\vartheta & \cdots & S(H-x_i)+K_\vartheta & \cdots & S(H-x_i)+K_\vartheta \\ \vdots & \vdots & & \vdots & & \vdots \\ S(H-x_n)+K_\vartheta & S(H-x_n)+K_\vartheta & \cdots & S_1+S(H-x_n)+K_\vartheta & \cdots & S_1+S(H-x_n)+K_\vartheta \end{bmatrix}$$

Equation (2.22) can be expressed further in terms of non-dimensional variables, as

$$\mathbb{M} = \frac{1}{SH}\, \mathbb{P}^{*-1}.\mathbb{L} \qquad (2.23a)$$

where $\mathbb{P}^*$ is a matrix given by,

$$
\mathbb{P}^{*} = \begin{bmatrix}
\omega+(1-\varepsilon_1) + R/k & (1-\varepsilon_2) + R/k & \ldots(1-\varepsilon_i) + R/k & \ldots(1-\varepsilon_n) + R/k \\
(1-\varepsilon_2) + R/k & \omega+(1-\varepsilon_2) + R/k & \ldots(1-\varepsilon_i) + R/k & \ldots(1-\varepsilon_n) + R/k \\
\vdots & \vdots & \vdots & \vdots \\
(1-\varepsilon_i) + R/k & (1-\varepsilon_i) + R/k & \ldots\omega+(1-\varepsilon_i) + R/k & \ldots(1-\varepsilon_n) + R/k \\
\vdots & \vdots & \vdots & \vdots \\
(1-\varepsilon_n) + R/k & (1-\varepsilon_n) + R/k & \ldots(1-\varepsilon_n) + R/k & \ldots\omega+(1-\varepsilon_n) + R/k
\end{bmatrix}
\tag{2.23b}
$$

where

$$k = \frac{1}{EIS} \tag{2.24a}$$

$$R = \frac{K_{\vartheta} EI}{H} \tag{2.24b}$$

$$\omega = \frac{S_1}{SH} \tag{2.24c}$$

and ε_i is a non-dimensional height term given by

$$\varepsilon_i = x_i/H$$

The term k is related to the core-to-column relative stiffness ratio, α, given by

$$\alpha = \frac{2EI}{d^2 E_c A_c} \tag{2.25}$$

where EI is the flexural rigidity of the core and $A_c E_c$ is the axial rigidity of the columns. By substituting equation (2.6a) into (2.24a), k can be rewritten as,

$$k = \frac{E_c A_c d^2/2}{EI+E_c A_c d^2/2} = \frac{1}{1+\alpha} \qquad (2.26)$$

For a high column stiffness α=0.1, k is equal to 0.9. For a low column stiffness α=10, k is equal to 0.09. For an outrigger structure, k generally lies in the region between 0.1 and 1.0.

The term R is to measure the rotational stiffness at the base of the structure. The practical range of R lies in the region between zero and one. For a case of an outrigger structure at an infinitely rigid base, R is equal to zero. However, a certain degree of rotational flexibility always exists at the base of the structure. The designer should take that into account for the determination of the optimum locations of the outriggers. The stiffer the base of the structure is, R will tend to zero.

For a stiff foundation, for example, with structural properties as follows,

K_θ=2E-11(Rad/Nm)

E=24.5E+9(N/m^2)

I=50m^4

H=100m

R lies in the region of 0.2. For a weak foundation, for example

with K_θ=10E-11(Rad/Nm), R lies in the region of 1.2.

The evaluation of parameter K_θ is discussed in Appendix 2.
The stiffer the soil is, the term R reduces to zero. For a rigid base, the term R therefore vanishes.

The term ω is a measure of the relative bending flexibility of the outriggers. By substituting S and S_1 from equations (2.6a) and (2.6b) to (2.24c) and rearranging, ω can be expressed in term of k (related to the core-column inertia ratio) and the core-outrigger inertia ratio β. They are defined as,

$$\omega = \frac{k\beta}{12} \qquad (2.27)$$

and

$$\beta = \frac{EI\ d}{E_o I_o H} \qquad (2.28)$$

From equation (2.27), the term ω generally lies between 0 and 1 which represent the flexibility of the outrigger being infinitely rigid and relatively flexible respectively.

After the restraining moments are obtained from equation (2.22), the forces throughout the structure may be determined.

Using the moment-area method, the top drift of the structure becomes,

$$y_T = \frac{1}{EI}\left[\int_0^{x_1} M_a x dx + \int_{x_1}^{x_2} (M_a - M_1) x dx + .. + \int_{x_i}^{x_{i+1}} (M_a - M_1 .. M_{i+1}) x dx + .. + \int_{x_n}^{H} (M_a - M_1 .. M_n) x dx\right] + \vartheta_B H \tag{2.28}$$

On integrating, equation (2.28) is simplified as,

$$y_T = y_{FT} - \frac{1}{2EI} \sum_{i=1}^{n} M_i (H^2 - x_i^2) + \vartheta_B H \tag{2.29}$$

where y_{FT} is the drift of a free cantilever core with a rigid foundation due to the applied load and is expressed as,

$$y_{FT} = \frac{1}{EI} \int_0^H M_a x dx \tag{2.29a}$$

and

$$\vartheta_B H = K_\vartheta (M_{aB} - \sum_{i=1}^{n} M_i) H \tag{2.29b}$$

The second term of the equation (2.29) represents the reduction due to the restraining moments from the outriggers.

2.3 SOLUTIONS FOR DIFFERENT LOAD CASES

In this section, solutions are presented for three fundamental load cases, (i) a uniformly distributed load w, (ii) a concentrated top load P and (iii) a triangularly distributed lateral load, whose intensity varies linearly from zero at the base to a value w_t at the top. In addition, two more different

loading combinations are considered. They are (i) a general lateral loading whose intensity at any level is defined by the polynomial $p[\ 1-(x/H)\ ]^z$ and (ii) a combination of a point load and a triangularly distributed load.

2.3.1 UNIFORMLY DISTRIBUTED LOAD

The moment at any distance x from the top is given by $wx^2/2$ where w is the load per unit height. Following the analysis presented above for one, two, three and n outriggers, the expressions for the restraining moment and top drift can be obtained by substituting $wx^2/2$ for M_a in the earlier equations. The corresponding equations for multi-outrigger structures with three or more outriggers in non-dimensional form can be obtained from equation (2.23) as follows,

$$\mathbb{M} = \frac{kwH^2}{6}\, \mathbb{P}^{*-1}.\mathbb{L}_1^{*} \qquad (2.30)$$

where

$$\mathbb{L}_1^{*} = \begin{bmatrix} 1-\xi_1^{\,3}+3R \\ 1-\xi_2^{\,3}+3R \\ \vdots \\ 1-\xi_i^{\,3}+3R \\ \vdots \\ 1-\xi_n^{\,3}+3R \end{bmatrix}$$

Substituting equation (2.30) into (2.29), the top drift of the structure becomes,

$$\frac{y_T}{\frac{wH^4}{8EI}} = 1 - 4\sum_{i=1}^{n} M_i^*(1-\xi_i^2) + 8R\left(\frac{1}{2} - \sum_{i=1}^{n} M_i^*\right) \qquad (2.31)$$

where M_i^* is the non-dimensional moment term and for this load case is given by $M_i/(wH^2)$

For simplicity, assumming the structure has a infinitively stiff system of foundation and the base. The term R vanishes. The corresponding equations (2.30) and (2.31) become,

$$\mathbb{M} = \frac{kwH^2}{6}\,\mathbb{P}_1^{*-1}.\mathbb{L}_2^* \qquad (2.32)$$

where

$$\mathbb{P}_1^* = \begin{bmatrix} \omega+(1-\varepsilon_1) & (1-\varepsilon_2) & ..(1-\varepsilon_i) & ..(1-\varepsilon_n) \\ (1-\varepsilon_2) & \omega+(1-\varepsilon_2) & ..(1-\varepsilon_i) & ..(1-\varepsilon_n) \\ \vdots & \vdots & \vdots & \vdots \\ (1-\varepsilon_i) & (1-\varepsilon_i) & ..\omega+(1-\varepsilon_i) & ..(1-\varepsilon_n) \\ \vdots & \vdots & \vdots & \vdots \\ (1-\varepsilon_n) & (1-\varepsilon_n) & ..(1-\varepsilon_n) & ..\omega+(1-\varepsilon_n) \end{bmatrix}$$

and

$$\mathbb{L}_2^* = \begin{bmatrix} 1-\xi_1^3 \\ 1-\xi_2^3 \\ \vdots \\ 1-\xi_i^3 \\ \vdots \\ 1-\xi_n^3 \end{bmatrix}$$

The drift of the structure becomes,

$$\frac{y_T}{\frac{wH^4}{8EI}} = 1 - 4 \sum_{i=1}^{n} M_i^* (1-\xi_i^2) \qquad (2.33)$$

2.3.2 TRIANGULARLY DISTRIBUTED LOAD

The moment at any distance x from the top of the structure is given by,

$$\frac{w_t x^2}{2} - \frac{w_t x^3}{6H}$$

where w_t is intensity of loading of the upper triangular distributed load. The applied moment at the base of the structure is therefore

$$M_{aB} = \frac{w_t H^2}{3}$$

Equation (2.23) becomes,

$$\mathbb{M} = \frac{kw_t H^2}{24} \mathbb{P}^{*-1} . \mathbb{L}_3^* \qquad (2.34)$$

where

$$\mathbb{L}_3^* = \begin{bmatrix} 3-4\xi_1^3+\xi_1^4+8R \\ 3-4\xi_1^3+\xi_1^4+8R \\ \vdots \\ 3-4\xi_i^3+\xi_i^4+8R \\ \vdots \\ 3-4\xi_n^3+\xi_n^4+8R \end{bmatrix}$$

Substituting equation (2.34) into (2.29), the top drift of the structure becomes,

$$\frac{y_T}{\frac{11w_t H^4}{120EI}} = 1 - \frac{60}{11} \sum_{i=1}^{n} M_i^* (1-\xi^2) + \frac{120}{11} R \left(\frac{1}{3} - \sum_{i=1}^{n} M_i^*\right) \qquad (2.35)$$

where M_i^* is the non-dimensional moment term and for this load case is given by $M_i/(w_t H^2)$

For the rigid foundation case, the corresponding equations (2.34) and (2.35) become,

$$\mathbb{M} = \frac{kwH^2}{24} \mathbb{P}^{*-1} . \mathbb{L}_4^* \qquad (2.36)$$

where

$$\mathbb{L}_4^* = \begin{bmatrix} 3-4\xi_1^3+\xi_1^4 \\ 3-4\xi_1^3+\xi_1^4 \\ \vdots \\ 3-4\xi_i^3+\xi_i^4 \\ \vdots \\ 3-4\xi_n^3+\xi_n^4 \end{bmatrix}$$

The top drift of the structure becomes,

$$\frac{y_T}{\frac{11w_tH^4}{120EI}} = 1 - \frac{60}{11}\sum_{i=1}^{n} M_i^*(1-\xi^2) \qquad (2.37)$$

2.3.3 POINT LOAD AT TOP

The moment at any distance x from the top is given by Px where P is the concentrated point load at the top of the structure.

The corresponding restraining moments in equation (2.23) become,

$$\mathbb{M} = \frac{kPH^2}{2}\,\mathbb{P}^{*-1}.\mathbb{L}_5^* \qquad (2.38)$$

where

$$\mathbb{L}_5^* = \begin{bmatrix} 1-\xi_1^2+2R \\ 1-\xi_1^2+2R \\ \vdots \\ 1-\xi_i^2+2R \\ \vdots \\ 1-\xi_n^2+2R \end{bmatrix}$$

Substituting equation (2.38) into (2.29), the top drift of the structure becomes,

$$\frac{y_T}{\frac{PH^3}{3EI}} = 1 - \frac{3}{2}\sum_{i=1}^{n} M_i^*(1-\xi^2) + 3R\ (1 - \sum_{i=1}^{n} M_i^*) \qquad (2.39)$$

where M_i^* is the non-dimensional moment term and for this load case is given by $M_i/(PH)$

For the rigid foundation case, the corresponding equations (2.38) and (2.39) become,

$$\mathbb{M} = \frac{kPH^2}{2}\,\mathbb{P}^{*-1}.\mathbb{L}_6^* \qquad (2.40)$$

The top drift of the structure becomes,

$$\frac{y_T}{\frac{PH^3}{3EI}} = 1 - \frac{3}{2}\sum_{i=1}^{n} M_i^*(1-\xi^2) \qquad (2.41)$$

2.3.4 GENERAL POLYNOMIAL LOADING

The uniformly distributed load and the triangularly distributed load at any height can be expressed by the following polynomial expression.

$$p_x = p\ [\ 1-(x/H)^z\ ]$$

where P_x is the load intensity of loading at the distance x from the top of the structure and p is the intensity of loading at the top.

Therefore when z=1, it reverts to a triangularly distributed lateral load whose intensity varies linearly from zero at the base to a value p at the top. For z becoming very large, it defines a uniformly distributed loading. This is shown in Fig.[2.6]. Integrating the product of the load expression and the lever arm distance from the top as below,

$$M_a = \int_0^x \int_0^x p[\ 1-(x/H)^z]dxdx$$

The moment at any distance x from the top of the structure is therefore represented by,

$$M_a = \frac{px^2}{2} - \frac{px^{z+2}}{H^z}\left(\frac{1}{(z+1)} - \frac{1}{(z+2)}\right)$$

and the applied moment at the base is given by

$$M_{aB} = K_2 pH^2$$

where

$$K_2 = \frac{1}{2} - \frac{1}{(z+1)(z+2)}$$

Equation (2.23) becomes,

$$\mathbb{M} = kpH^2 \mathbb{P}^{*-1} . \mathbb{L}_7^* \qquad (2.42)$$

where

$$\mathbb{L}_7^* = \begin{bmatrix} \frac{1}{6}(1-\xi_1^3) - \frac{1}{K_1}(1-\xi_1^{z+3}) + K_2 R \\ \frac{1}{6}(1-\xi_2^3) - \frac{1}{K_1}(1-\xi_2^{z+3}) + K_2 R \\ \vdots \\ \frac{1}{6}(1-\xi_i^3) - \frac{1}{K_1}(1-\xi_i^{z+3}) + K_2 R \\ \vdots \\ \frac{1}{6}(1-\xi_n^3) - \frac{1}{K_1}(1-\xi_n^{z+3}) + K_2 R \end{bmatrix}$$

and

$$K_1 = (z+1)(z+2)(z+3)$$

From equation (2.29), the corresponding expression for top drift becomes,

$$\frac{y_T}{K_3 \frac{pH^4}{EI}} = 1 - \frac{1}{2K_3} \sum_{i=1}^{n} M_i^* (1-\xi^2) + \frac{1}{K_3} R \left(K_2 - \sum_{i=1}^{n} M_i^*\right) \qquad (2.43)$$

where M_i^* is the non-dimensional moment term and for this load case is given by $M_i/(pH^2)$

and

$$K_3 = \frac{1}{8} - \frac{1}{(z+4)(z+2)(z+1)}$$

For the rigid foundation case, the corresponding equations (2.42) and (2.43) become,

$$\mathbb{M} = kpH^2 \mathbb{P}^{*-1} . \mathbb{L}_8^* \qquad (2.44)$$

where

$$\mathbb{L}_8^* = \begin{bmatrix} \frac{1}{6}(1-\xi_1^3) - \frac{1}{K_1}(1-\xi_1^{z+3}) \\ \frac{1}{6}(1-\xi_2^3) - \frac{1}{K_1}(1-\xi_2^{z+3}) \\ \vdots \\ \frac{1}{6}(1-\xi_i^3) - \frac{1}{K_1}(1-\xi_i^{z+3}) \\ \vdots \\ \frac{1}{6}(1-\xi_n^3) - \frac{1}{K_1}(1-\xi_n^{z+3}) \end{bmatrix}$$

From equation (2.29), the corresponding expression for top drift becomes,

$$\frac{y_T}{K_3 \frac{pH^4}{EI}} = 1 - \frac{1}{2K_3} \sum_{i=1}^{n} M_i^*(1-\xi^2) \qquad (2.45)$$

2.3.5 COMBINED TRIANGULARLY DISTRIBUTED LOAD AND A POINT LOAD AT THE TOP

One of the modern Codes of Practice, the Canadian Building Code of Practice, suggests that earthquake loading can be assumed to be composed of two components, a triangularly distributed load F_t and a point load F_P acting at the top. The two force components depend on the dimensions of the building structure itself.

The total lateral seismic force V at the base of the structure is therefore equal to the sum of F_t and F_P or,

$$V = w_t H/2 + P$$

The Code states that the total lateral seismic base force V must be distributed as follows,

a). A portion F_P shall be assumed to be concentrated at the top of the structure and equal to $0.004V(h_n/D_s)^2$, except that F_P need not exceed 0.15V and may be considered as zero for $(h_n/D_s) \leq 3$, where h_n is the height above the base of the structure and D_s is the dimension of the lateral force resisting system in a direction parallel to the applied forces.

b). The remainder, $V-F_P$, shall be distributed along the height of the building including the top level in accordance with the following formula,

$$F_x = (V-F_P)w_x h_x \,/\, \left(\sum_{i=1}^{n} w_i h_i\right) \qquad (2.46)$$

where

F_x is the lateral force applied to level x

h_i and h_x are the height above the base of the structure to "i" and "x" respectively

w_x and w_i are the load intensity at levels "x" and "i"

The F_t and F_P can be related to the total shear force, V, at the base of the structure as,

$$F_P = rV$$

and $F_t = (1-r)V$

where r is the ratio of F_P to the total lateral force, V, at the base.

Summing the moment due to F_P and F_t, the exteral moment M_a at any distance x from the top is represented by,

$$M_a = V\left(\frac{(1-r)x^2}{H} - \frac{(1-r)x^3}{3H^2} + rx\right) \qquad (2.47)$$

and

$$M_{aB} = (2+r)VH/3$$

Equation (2.23) becomes,

$$\mathbb{M} = k\mathbb{V}\mathbb{H}\mathbb{P}^{*-1}.\mathbb{L}_9^{*} \qquad (2.48)$$

where

$\mathbb{L}_9^{*}$ is a 1xn matrix with elements $L_1^{*}..L_i^{*}..L_n^{*}$ and

$$L_i = \frac{(1-r)(1-\xi_i^{3})}{3} - \frac{(1-r)(1-\xi_i^{4})}{12} + \frac{r(1-\xi_i^{2})}{2} + (2+r)R$$

From equation (2.29), the corresponding expression for top drift becomes,

$$\frac{y_T}{K_4 \frac{VH^3}{EI}} = 1 - \frac{1}{2K_4} \sum_{i=1}^{n} M_i^{*}(1-\xi^2) + \frac{1}{K_4} R[\frac{(2+r)}{3} - \sum_{i=1}^{n} M_i^{*}] \qquad (2.49)$$

where M_i^{*} is the non-dimensional moment term and for this load case is given by $M_i/(VH)$

$$K_4 = \frac{(11+9r)}{60}$$

For the rigid foundation case, the corresponding equations (2.48) and (2.49) become,

$$\mathbb{M} = k\mathbb{V}\mathbb{H}\mathbb{P}^{*-1}.\mathbb{L}_{10}^{*} \qquad (2.50)$$

where

$\mathbb{L}_{10}^{*}$ is a 1xn matrix with elements $L_1^{*}..L_i^{*}..L_n^{*}$ and

$$L_i = \frac{(1-r)(1-\xi_i^3)}{3} - \frac{(1-r)(1-\xi_i^4)}{12} + \frac{r(1-\xi_i^2)}{2}$$

and

$$\frac{y_T}{K_4 \frac{VH^3}{EI}} = 1 - \frac{1}{2K_4} \sum_{i=1}^{n} M_i^{*}(1-\xi^2) \qquad (2.51)$$

2.4 PERFORMANCE OF OUTRIGGER-BRACED STRUCTURES

The performance of outrigger structures will depend on the variation in the size and structural arrangements of the core, outriggers, and columns. These variations include the core-to-column and core-to-outrigger inertia ratios and the number and levels of the outriggers. The performance of the outrigger structures can be measured with respect to both their reduction in core moment and drift.

2.4.1 DRIFT REDUCTION EFFICIENCY

The performance of the outrigger system may be measured by a drift reduction factor r_y, defined as the ratio of the reduction in the drift to the maximum possible reduction that would occur if the core and columns behaved as a single composite unit for the rigid base case. That is, taken to the limit, rigid outriggers placed at an infinite number of levels would cause the columns to behave fully compositely with the core, acting about a common

neutral axis. The expression for the maximum possible reduction y_c for the outrigger system with a rigid base is given by,

$$y_c = y_{FT} - y_{Tir} \tag{2.52}$$

or y_c can be rewritten as

$$y_c = \kappa y_{FT} \tag{2.53}$$

where y_{FT} is the top drift of the free bending of the core with a rigid base given in equation (2.29a)

y_{Tir} is the top drift of an infinitely rigid outrigger structure on a rigid base.

For the case of an outrigger system with a flexible base, the maximum possible reduction y_{cf} is given by,

$$y_{cf} = y_{FFT} - y_{Tif} \tag{2.54}$$

where y_{FFT} is the top drift of the free bending of the core with a flexible base and is given by

$$y_{FFT} = y_{FT} + K_\theta M_B H \tag{2.55}$$

y_{Tif} is the top drift of an infinitely rigid outrigger structure with a flexible base.

The corresponding values of y_{FFT} and y_{Tif} can be obtained by either using a multi-outrigger structure with more than 50 rigid outriggers and with a rigid base or using the continuum technique to achieve a closed-form solution. The application of the continuum method for multi-outrigger-braced structures and the devivation of the corresponding limiting values for y_{Tir} and y_{Tif} are reported in Chapter 3.

For the case of a flexible base, the drift reduction efficiency is expressed by

$$r_y = \frac{y_{FFT} - y_T}{y_{cf}} \times 100\ \% \qquad (2.56)$$

For the case of a rigid base, the drift reduction efficiency becomes

$$r_y = \frac{y_{FT} - y_T}{y_c} \times 100\ \% \qquad (2.57)$$

UNIFORMLY DISTRIBUTED LOADING

From equation (2.55), y_{FFT} becomes

$$y_{FFT} = \frac{wH^4}{8EI}(1+4R) \qquad (2.58)$$

Substituting y_T from equation (2.31) and y_{FFT} from equation (2.58) into equation (2.56), the general expression for r_y becomes,

$$r_y = \frac{4R + 4\sum_{i=1}^{n} M_i^*(1-\xi^2) - 8R(\frac{1}{2} - \sum_{i=1}^{n} M_i^*)}{y_{cf}/y_{FT}} \times 100\,\% \qquad (2.59)$$

POINT LOAD AT TOP

From equation (2.55), y_{FFT} becomes

$$y_{FFT} = \frac{PH^3}{3EI}(1+3R) \qquad (2.60)$$

Substituting y_T from equation (2.35) and y_{FFT} from equation (2.60) into equation (2.56), the general expression for r_y becomes,

$$r_y = \frac{3R + \frac{3}{2}\sum_{i=1}^{n} M_i^*(1-\xi^2) - 3R(1 - \sum_{i=1}^{n} M_i^*)}{y_{cf}/y_{FT}} \times 100\,\% \qquad (2.61)$$

TRIANGULARLY DISTRIBUTED LOAD

From equation (2.55), y_{FFT} becomes

$$y_{FFT} = \frac{11w_tH^4}{120EI}(1+\frac{40}{11}R) \qquad (2.62)$$

Substituting y_T from equation (2.39) and y_{FFT} from equation (2.62) into equation (2.56), the general expression for r_y becomes,

$$r_y = \frac{\frac{40}{11}R + \frac{60}{11}\sum_{i=1}^{n} M_i^*(1-\xi^2) - \frac{120}{11}R(\frac{1}{3} - \sum_{i=1}^{n} M_i^*)}{y_{cf}/y_{FT}} \times 100\%$$

(2.63)

GENERAL POLYNOMIAL LOAD

From equation (2.55), y_{FFT} becomes

$$y_{FFT} = \frac{K_3 pH^4}{EI}(1 + \frac{K_2}{K_3}R) \qquad (2.64)$$

Substituting y_T from equation (2.43) and y_{FFT} from equation (2.64) into equation (2.56), the general expression for r_y becomes,

$$r_y = \frac{\frac{K_2}{K_3}R + \frac{1}{2K_3}\sum_{i=1}^{n} M_i^*(1-\xi^2) - \frac{1}{K_3}R(K_2 - \sum_{i=1}^{n} M_i^*)}{y_{cf}/y_{FT}} \times 100\%$$

(2.65)

COMBINATION OF TRIANGULARLY DISTRIBUTED LOAD AND POINT LOAD

From equation (2.55), y_{FFT} becomes

$$y_{FFT} = \frac{K_4 VH^3}{EI}[\ 1 + \frac{(2+r)}{3K_4}\ ] \qquad (2.66)$$

Substituting y_T from equation (2.49) and y_{FFT} from equation (2.66) into equation (2.56), the general expression for r_y becomes,

$$r_y = \frac{\frac{(2+r)}{3K_4} + \frac{1}{2K_4}\sum_{i=1}^{n} M_i^*(1-\xi^2) - \frac{1}{K_4}R[\frac{(2+r)}{3} - \sum_{i=1}^{n} M_i^*]}{y_{cf}/y_{FT}} \times 100\% \qquad (2.67)$$

2.4.2 MOMENT REDUCTION EFFICIENCY FOR MINIMUM CORE MOMENT

The performance of the outrigger system may be measured by a moment reduction factor r_m, defined as the ratio of the reduction in the core moment to the maximum possible reduction M_c that would occur if the core and columns behaved as a single composite unit for the rigid base case.

The expression for the maximum possible reduction M_c for the outrigger system with a rigid base is given by,

$$M_c = M_{aB} - M_{Bir} \qquad (2.68)$$

or it can be rewritten by

$$M_c = kM_{aB} \qquad (2.69)$$

where M_{aB} is the base moment of the free bending of the core with a rigid base.

M_{Bir} is the base moment of an infinitely rigid outrigger structure with a rigid base.

For the case of an outrigger system with a flexible base, the maximum possible reduction y_{cf} is given by,

$$M_{cf} = M_{aB} - M_{Bif} \tag{2.70}$$

where M_{Bif} is the base moment of an infinitely rigid outrigger structure with a flexible base.

Again the derviation of the corresponding limiting values for M_{Bir} and M_{Bif} are reported in Chapter 3.

For the case of a rigid base, the moment reduction efficiency for minimum core moment is given by,

$$r_m = \left(\frac{M_{aB} - M_x}{M_c} \right) .100\% \tag{2.71}$$

where M_x is the core moment at any level x measured from the top of the structure and

$$M_x = M_{ax} - \sum_{i=1}^{n} M_i \tag{2.72a}$$

and M_{ax} is the applied moment at any level x measured from the top of the structure.

If the minimisation of core moment at the base is concerned, the expression of M_x becomes

$$M_B = M_{aB} - \sum_{i=1}^{n} M_i \qquad (2.72b)$$

For the case of a flexible base, the drift reduction efficiency is expressed by

$$r_m = \left(\frac{M_{aB} - M_x}{M_{cf}} \right) .100\ \% \qquad (2.73)$$

The moment reduction efficiency can be obtained easily by substituting the appropriate equations for M_i and M_{aB} into either equation (2.71) or (2.73).

UNIFORMLY DISTRIBUTED LOAD

For the particular case where minimisation of the core moment at the base is concerned, r_m can be obtained by substituting M from equation (2.30) into (2.73). The expression for r_m becomes,

$$r_m = \frac{1}{3} \mathbb{P}^{*-1} . \mathbb{L}_1^{*} .100\ \% \qquad (2.74)$$

TRIANGULARLY DISTRIBUTED LOAD

Similarly, r_m can be obtained by substituting M from equation (2.34) into (2.73). The expression for r_m becomes,

$$r_m = \frac{1}{8} \mathbb{P}^{*-1} \mathbb{L}_3^* . 100\ \% \qquad (2.75)$$

POINT LOAD AT TOP

Similarly, r_m can be obtained by substituting M from equation (2.38) into (2.73). The expression for r_m becomes,

$$r_m = \frac{1}{2} \mathbb{P}^{*-1} . \mathbb{L}_5^* . 100\ \% \qquad (2.76)$$

GENERAL POLYNOMIAL LOADING

For the particular case where minimisation of core moment at the base is concerned, r_m can be obtained by substituting M from equation (2.42) into (2.73). The expression for r_m becomes,

$$r_m = \frac{1}{K_2} \mathbb{P}^{*-1} \mathbb{L}_7^* . 100\ \% \qquad (2.77)$$

COMBINATION OF TRIANGULARLY DISTRIBUTED LOAD AND POINT LOAD

Similarly, r_m can be obtained by substituting M from equation (2.48) into (2.73). The expression for r_m becomes,

$$r_m = \frac{3}{(2+r)} \mathbb{P}^{*-1} \mathbb{L}_9^* . 100\ \% \qquad (2.78)$$

2.5 STRUCTURAL OPTIMISATION OF TOP DRIFT

In this study, the reduction based on both the top drift and the core moment are considered for optimisation. Very often, the core moment is considered as secondary to the reduction in drift. However, a relatively weak foundation or basement substructure may affect greatly the structural performance of the structure. In some circumstances, the core moment at the base of the structure is as important as the top drift. Therefore it is useful to consider the optimisation of structural performance of the outrigger-braced structure based on the reduction of core moment at the base.

2.5.1 TOP DRIFT MINIMISATION

Minimisation of the top drift can be obtained by differentiation of equation (2.29) with respect to x_i (i=1,2,..n). For the rigid foundation case, this leads to a set of equations and can be expressed in matrix form as,

$$\mathbb{A}.\mathbb{B} - 2\mathbb{C} = 0 \qquad (2.79)$$

where

$$\mathbb{A} = \begin{bmatrix} M_{11} & M_{21} & M_{31} & \cdots & M_{i1} & \cdots & M_{n1} \\ M_{12} & M_{22} & M_{32} & \cdots & M_{i2} & \cdots & M_{n2} \\ \vdots & \vdots & \vdots & & \vdots & & \\ M_{ij} & M_{2j} & M_{3j} & \cdots & M_{ij} & \cdots & M_{nj} \\ \vdots & \vdots & \vdots & & \vdots & & \\ M_{in} & M_{2n} & M_{3n} & \cdots & M_{in} & \cdots & M_{nn} \end{bmatrix}$$

$$\mathbb{B} = \begin{bmatrix} H^2-x_1^2 \\ H^2-x_2^2 \\ \vdots \\ H^2-x_i^2 \\ \vdots \\ H^2-x_n^2 \end{bmatrix}$$

$$\mathbb{C} = \begin{bmatrix} x_1M_1 \\ x_2M_2 \\ \vdots \\ x_iM_i \\ \vdots \\ x_nM_n \end{bmatrix}$$

and $M_{ij} = \frac{dM_i}{dx_j} (i,j = 1,2,..,N)$

For the flexible foundation case, the solution becomes

$$\mathbf{A}.\mathbf{B} - 2\mathbf{C} + 2RH^2\mathbf{A} = 0 \qquad (2.80)$$

Theoretically by substituting expressions for the restraining moments from equation (2.23) and their corresponding derivatives, equations (2.77) and (2.78) can be solved to obtain the optimum locations of the outriggers. This method is feasible for one or two outriggers. As the number of outriggers increases, the solution of the expressions concerned becomes very complicated and a numerical solution is necessary. The optimisation techniques which are available for minimising an expression with a number of constraints generally require derivatives or gradients of the functions involved and tend to be manually tedious. The successful development of computer technology and the high performance of the micro-processors, such as 486s and Work-stations, now enable very complicated calculations to be performed in seconds. The speed of searching for the optimum solution from a group of contraints is no longer the problem. For the solution, a simple sequential searching technique was used to determine the optimum locations of the outriggers. A computer program based on 'divide and conquer' strategy was used. The range of values of the outrigger locations was divided up into subranges using a coarse grid. The bound of the optimum value of the drift as computed from equation (2.29) and its corresponding outrigger locations are obtained. The outrigger locations obtained from this search are then used as the subrange for another iteration. The solution is refined until the required accuracy is achieved.

2.5.2 CORE BASE MOMENT MINIMISATION

The "optimum outrigger levels" in the previous section were calculated for the maximum reduction in drift at the top of the structure. When the moment at the base is to be minimised to suit the design of the foundation or basement sub-structure the drift is no longer the most critical consideration. Reduction in the core base moment depends on the amount of restrained moment taken by the outriggers. A reduction in the core base moment is generally achieved by locating the outrigger lower than its "optimum" level for drift. For a rigid outrigger case, a hypothetical maximum reduction in core base moment can be achieved with an outrigger placed nearer to the base of the structure. The general expression for the core base moment is

$$M_B = M_{aB} - \sum_{i=1}^{n} M_i \qquad (2.81)$$

Minimisation of the core base moment can be obtained by diferentiation of equation (2.79) with respect to x_i. This leads to a set of simultaneous equations and can be expressed in matrix form as,

$$\mathbf{A} = 0 \qquad (2.82)$$

The same technique as in Section (2.5.1) is used.

2.5.3 CORE MOMENT MINIMISATION

Sometimes it is required to minimise the core moment for financial and architectural planning reasons. For the infinitely rigid outrigger case, it can be proved easily from equation (2.23) that for a single outrigger structure with an infinitely rigid outrigger arm the restraining moment induced in the outrigger arm increases the nearer the outrigger is placed to the base of the structure. Therefore the optimum location for minimum core moment is always found to be where M_x is equal to M_B. However, when the flexibility is introduced into the foundation and the outrigger arm, the optimum location can be found some distance up the height of the structure.

For a single outrigger structure subjected to a uniformly distributed load, there are three (1x2+1) representative points on the bending moment curve of the core. They are,

$$M_{core} = \left[\frac{wx^2}{2} \right]_{x=x_1^-}$$

$$M_{core} = \left[\frac{wx^2}{2} - M_1 \right]_{x=x_1^+}$$

where x_1^- and x_1^+ represent point just above and below the outrigger and

$$M_{core} = M_B = \left[M_{aB} - M_1 \right]_{x=H} \qquad (2.83)$$

where M_{core} is the core moment of the outrigger structure.

For an n-outrigger structure, there are (nx2+1) representative points on the bending moment curve of the core. They are given by,

$$M_{core} = \left[\frac{wx^2}{2} \right]_{x = x_1^-}$$

$$M_{core} = \left[\frac{wx^2}{2} - M_1 \right]_{x = x_1^+ \text{ and } x = x_2^-}$$

$$M_{core} = \left[\frac{wx^2}{2} - M_1 - M_2 \right]_{x = x_2^+ \text{ and } x = x_3^-}$$

.

.

$$M_{core} = \left[\frac{wx^2}{2} - M_1 - M_2 \,..\, - M_i \right]_{x = x_i^+ \text{ and } x_{i+1}^-}$$

.

.

$$M_{core} = M_B = \left[M_{aB} - M_1 - M_2 \,..\, - M_i \,..\, - M_n \right]_{x=H}$$

(2.84)

Minimisation of the core moment can be obtained by differentiation of M_{core} with respect to x_i (i=1,2,..n). For the rigid foundation case, this will lead to a set of equations as before. By substituting expressions for the restraining moments from equation (2.23) and their corresponding derivatives, the equations can be solved to obtain the optimum locations of the outriggers for minimum core moment. This method is tedious and complicated in the implementation of a computer solution. As the number of outriggers increases, the solution of the expressions concerned becomes very

complicated and a numerical solution is necessary. Therefore, a similar optimisation technique as in section [2.5.1] was used. The solution is refined through a number of iterations until the required accuracy is achieved.

2.6 MULTIPLE LINEAR REGRESSION

The analysis presented in the earlier sections is mathematically complicated and, if repeated analyses are necessary in the process of adjusting the design of the structure, it is extremely time-consuming. Therefore, a wide range of analytical results obtained in the earlier sections using the compatibility analyses is used to develop a mathematical model which can provide a reasonably accurate estimate of the optimum outrigger levels in terms of a single characteristic parameter ω.

Multiple linear regression is applied to the results of the earlier sections to develop general formulae for estimating the optimum levels of outriggers to minimise both top drift and core moment at the base of the structure. The purpose of a multiple regression analysis is to investigate the relationships between variables and to develop a mathematical model of one variable in terms of the other. The method of least squares is used to evaluate the unknown coefficients b_i in a linear mathematical model of the form,

$$x_{i(optimum)} = b_o + \sum_{i=1}^{n} b_i Y_i \qquad (2.85)$$

where Y_1, Y_2, .. Y_n are the variables and b_o, b_1 .. b_n are unknown coefficients to be estimated from the available data. The type of model shown in equation (2.85) appears to be restrictive. However, many other models may be reduced to this form by redefining or transforming the variables. For example,

$$x_i = b_o + b_1\omega + b_2\omega^2$$

The model above after redefining $Y_1=\omega$ and $Y_2=\omega^2$ will become

$$x_i = b_o + b_1Y_1 + b_2Y_2$$

Therefore, although the models that may be investigated using multiple linear analysis are linear, the variables themselves need not be. The models may include powers of variables, exponentials, logarithms, etc. The disadvantages of this analysis are that difficulties may be encountered when determining functional relationships in complex situations, and the models that can be found are seldom accurate over the entire range of variables. Most computer installations provide access to one of the forms of multiple linear regression analysis as part of a statistical analysis package. A MINITAB program was used in the analysis.

The optimum outrigger location in a single-outrigger structure was investigated first, using the mathematical model in equation (2.85). In the simplest form, the curve of the optimum location of the outrigger could be represented by only a minimum number of terms, that is, a set of straight lines,

$$x_1 = b_o + b_1 Y_1$$

It is found to be more efficient and convenient to use the single parameter ω in the computation and the regression analysis procedure, than to use the relative stiffnesses of the core to columns, α, and the core to outrigger, β.

The model in equation (2.85), after transforming the variables Y_i into ω^i becomes,

$$x_{i(optimum)} = b_o + \sum_{i=1}^{n} b_i \omega^i \qquad (2.86)$$

The table below demonstrates the stepwise regression results of the optimum location of outrigger for a single outrigger case under the triangularly distributed load. The stepwise procedure was used to allow the program to introduce variables one at a time into the model so that the greatest improvement was achieved at each step.

b_o	b_1	b_2	b_3	b_4	b_5	$R_{adjusted}$
0.417	-0.433	0.224	0	0	0	0.988
0.427	-0.583	0.617	0.262	0	0	0.997
0.425	-0.543	0.440	0	-0.124	0	0.998
0.420	-0.442	0	0.670	-0.454	0.004	0.999

$R_{adjusted}$ is an adjusted multiple correlation coefficient and is a measure of how well regression equation fits the data. The closer R is to unity, the better the approximation.

Having derived the mathematical models for the optimum locations, the approximate outrigger positions may be obtained by substituting the characteristic parameter ω into the equation below,

$$x_i = b_o+b_1\omega+b_2\omega^2+b_3\omega^3+b_4\omega^4+b_5\omega^5 \qquad (2.87)$$

The reduction in drift and the restraining moments may then be determined by substituting the approximate values of x_i into the appropriate equations (2.23) to (2.29).

2.7 UNIFORMLY SPACED OUTRIGGERS

So far only the optimum location of the outriggers for maximum reduction in top drift or core base moment have been considered. It is usually convenient, as well as necessary from strength considerations, to make the outrigger at least a full storey depth. Their bulk, and obstructive configuration, often makes it appropriate for them to share the plant room levels.

In order to allow the integration of the outriggers within the normal floor intervals, as well as for architectural and plant considerations, it may be more convenient to locate the outriggers at equally spaced positions rather than at the optimum locations. Aesthetic architectural considerations, as well as structural

factors, will all have to be taken into account in deciding the final number and location of the outriggers. From the structural engineer's point of view, it would be useful if the relative performance of systems with different numbers of outriggers at different locations and with different spacings of outriggers were known. Then the structural and cost penalties incurred by departures from the structural optimum could be determined.

In this section, the moment and drift reduction efficiencies for uniformly spaced outrigger structures subjected to the fundamental load cases of uniformly distributed load, triangularly load and a concentrated point load at the top are presented. Different arrangements of placing the outrigger/s, as shown in Fig.[2.7], are presented. Their corresponding efficiencies are compared with that of the optimum locations for the top drift minimisation.

2.8 NUMERICAL RESULTS

The numerical investigations carried out on the elastic behaviour of outrigger-braced structures are presented mainly in graphical forms. For the areas of study such as those on base flexibility and more complicated lateral loadings, in which more governing parameters are involved, the results are presented in a tabular form.

In order to assess the order of relative importance of the parameters ω, k and R on the structural behaviour of outrigger-braced structures subjected to different loading conditions, an extensive parametric study was conducted, mainly

for the case of a rigid base. First of all, design curves based on the approach of the minimisation of top drift showing the variation of the optimum location of the outriggers with ω for the case of a rigid base subjected to the three fundamental load cases, uniformly distributed load, triangularly distributed load and a concentrated point load at the top, are given in Figs.[2.8] to [2.19]. For the case of a rigid base, the optimum locations of the outriggers remain the same throughout the range of values of k. The curves show that as the outriggers become more flexible, the other properties remaining constant, the optimum levels will tend to be nearer to the top of the structure. The curves showing their corresponding moment and drift efficiency are given in Figs.[2.20] to [2.25]. It can be seen that as the number of outriggers increases, other factors being constant, both moment and drift efficiencies increase. However, the increments of increase in efficiency reduce for each additional outrigger. It was also indicated that increasing outrigger flexibility reduces both the moment and drift efficiency of the structure, but with a smaller reduction for the more flexible outrigger systems.

Based on the approach of the minimisation of base moment, the curves showing the variation of optimum location of outriggers with ω and their corresponding moment and drift efficiency are given in Fig.[2.26] to [2.43]. The curves show that as the outriggers become more rigid, the other properties remaining constant, the optimum levels will tend to be nearer to the base of the structure. It suggests that a rigid outrigger located near to the base is always desirable to control the base moment and maintain the rigidity at the base of the structure. The lower the

outrigger the greater the resisting moment it always provides. However, the benefit of placing it very low on the structure to give a high resisting moment is offset by the fact that it would not be as effective in reducing drift as reducing the base moment. It can be seen from the curves showing moment and drift efficiencies that a price of poor drift efficiency has to be paid for locating outriggers near to the base of the structure. Therefore depending on which is the primary consideration for the structure, a balance of both the top drift and the base core moment must be made as reductions in core moments can be only achieved by placing the outriggers lower in the structure than drift consideration would suggest.

The minimum design core moment may not necessary occur at the base. Fig.[2.44] and [2.45] show the profile of the core moment above the outrigger and at the base for the case of a single outrigger system with a rigid base. It clearly indicates that the minimum design core moment may not occur at where the core moment just above the outrigger is equal to the base moment at the base of the structure. Depending on the flexibility of the outrigger and the parameter k, the optimum location of the outriggers varies within the height of the structure.

If the flexibility at the base of the structure due to a weak basement substructure or a weak soil foundation is taken into consideration, the optimum locations of the outriggers based on the minimisation of the top drift or the core moment will involve extra parameters such as R and 1/EIS. Figs.[2.46] to [2.48] show the variation of optimum location of outriggers based on the drift

minimisation approach with ω for different base flexibilities. A selection of curves showing the variation of location of outriggers with their top deflections under a uniformly distributed load are presented in Fig.[2.49]. Tables [2.1] to [2.3] show a summary of the study of outrigger structures with different base flexibilities based on the optimisation of top drift approach for the three fundamental load cases. The results show that an infinitely rigid outrigger is very efficient in controlling both the drift and core moment of the structure. As the outriggers become slightly flexible the efficiency diminishes very quickly.

For the case of a single outrigger and a flexible base, the core base moment appears to be very sensitive to the location of the outrigger for very rigid outriggers. Fig.[2.50] and Fig.[2.51] show the profile of the core moment above the outrigger and at the base for the case of a single outrigger system with a flexible base. Fig.[2.52] and [2.53] show the variation of the optimum location of the outrigger with ω based on the core moment approach for different base flexibilities. Tables [2.4] to [2.6] show a summary of the study of outrigger structures with different base flexibilities based on the optimisation of the core moment.

Tables [2.7] to [2.9] show a summary of the study of outrigger structures with different base flexibilities for different values of z in the general polynomial load case. It is interesting to note the variation of the optimum location of outriggers, base moment, top drift, moment and drift reduction factors with z.

Tables [2.10] to [2.12] show a summary of the study of outrigger structures with different base flexibilities for different values of r in the case of the combined triangularly distributed load and a point load at the top. The variation of the optimum location of outriggers does not appear to be sensitive to r.

A summary of the study of the mathematical models for the optimum outriggers location based on both top drift and base moment optimisation using the multiple linear regression technique is presented. The coefficients b_i in equation (2.86), using 5 terms in the series, for three standard load cases, are shown in Tables [2.13] to [2.18]. Coefficients are given for one to four outrigger levels. They enable a designer to work on a set of generalised formulae to determine the optimum outrigger locations.

Finally, comparison of efficiencies for different spacing arrangements as shown in Fig.[2.7] are presented in Figs.[2.54] to [2.77] for up to four outriggers. It is evident that for a system with the same number of uniformly spaced outriggers, those with an outrigger at the top are relatively inefficient in minimising the top drift. Similarly, those with an outrigger close to the base are relatively efficient in reducing the core base moment of the structure.

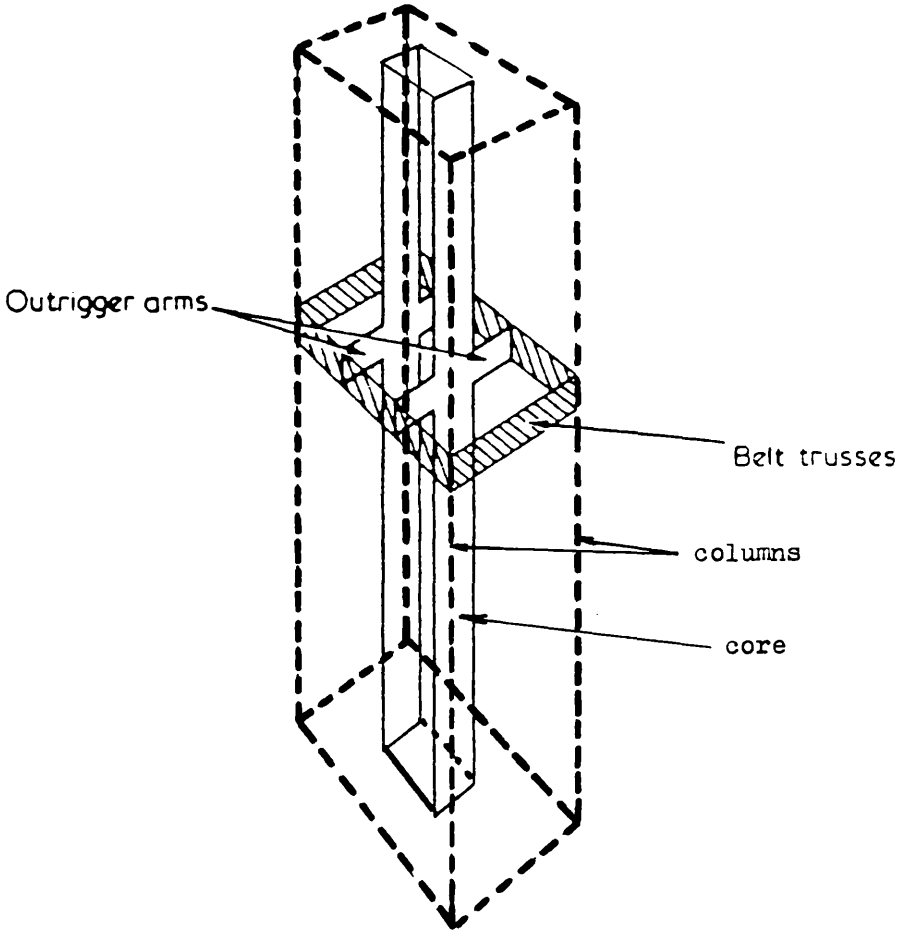

FIG. [2.1] REPRESENTATION OF AN OUTRIGGER-BRACED TALL BUILDING STRUCTURE

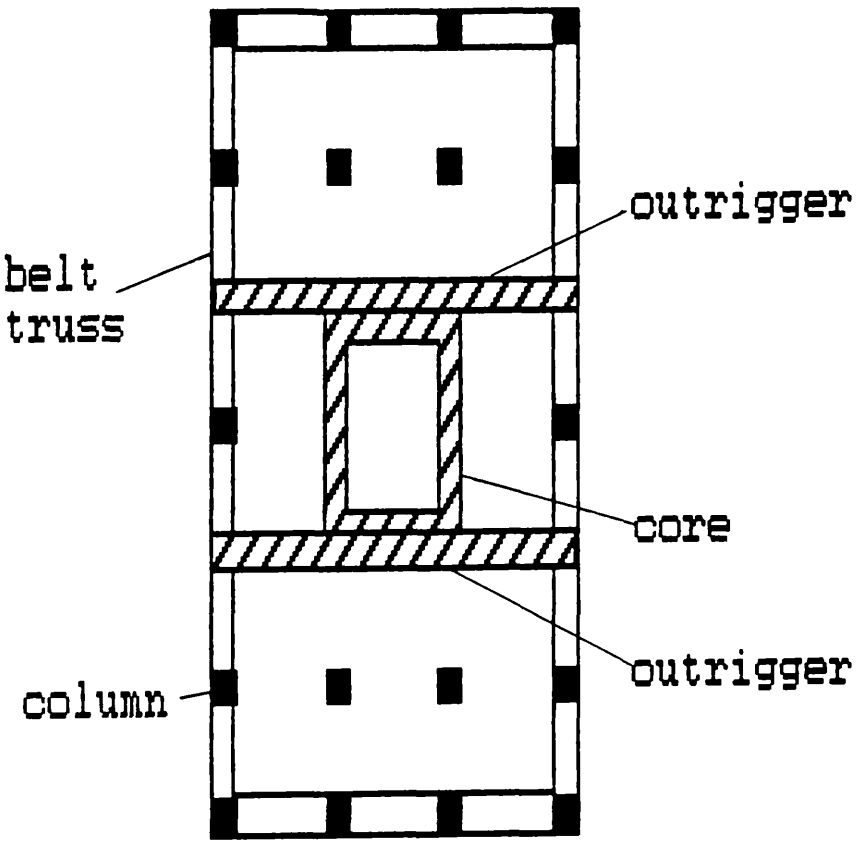

Floor plan of anoutrigger-braced structure

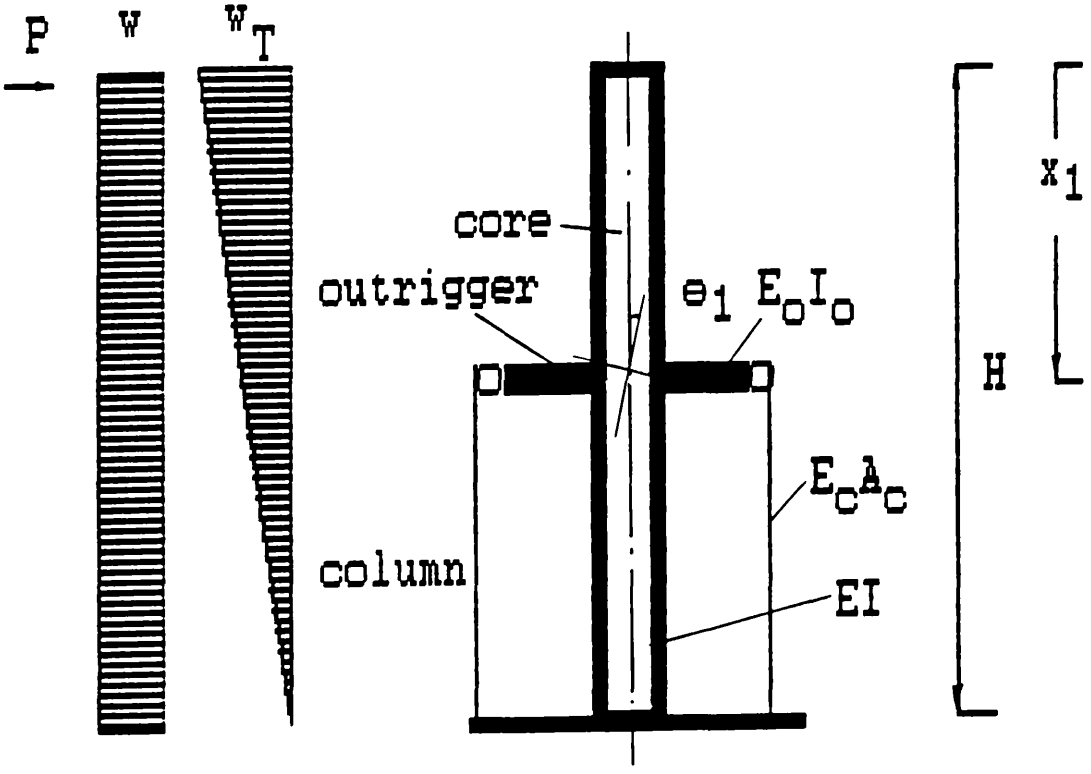

FIG.[2.2] A TYPICAL FLOOR PLAN OF ANOUTRIGGER STRUCTURE AND AN IDEALISED REPRESENTATION OF A SINGLE OUTRIGGER STRUCTURE

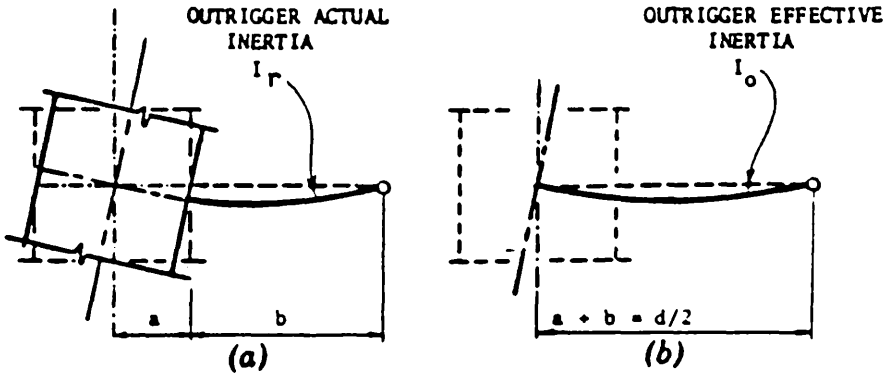

(a) Wide-column action of wall and outrigger
(b) Action of equivalent full-span outrigger

FIG. [2.3] FLEXURAL RIGIDITY OF A WIDE-COLUMN BEAM AND EQUIVALENT FULL-SPAN BEAM

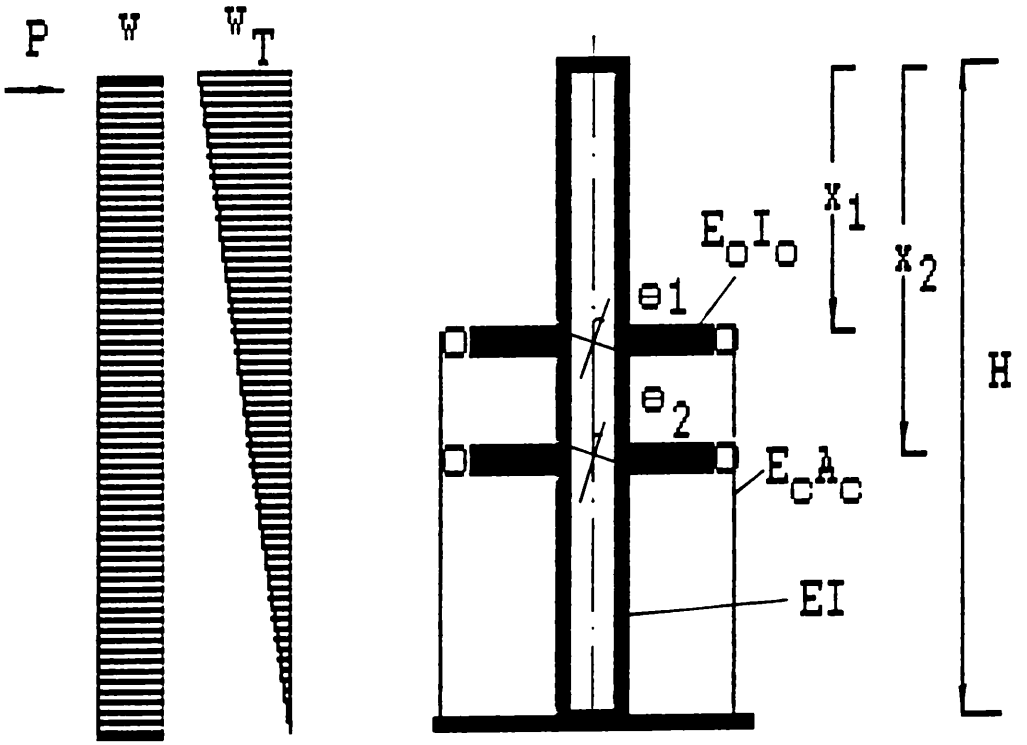

FIG.[2.4] TWO OUTRIGGER CASE

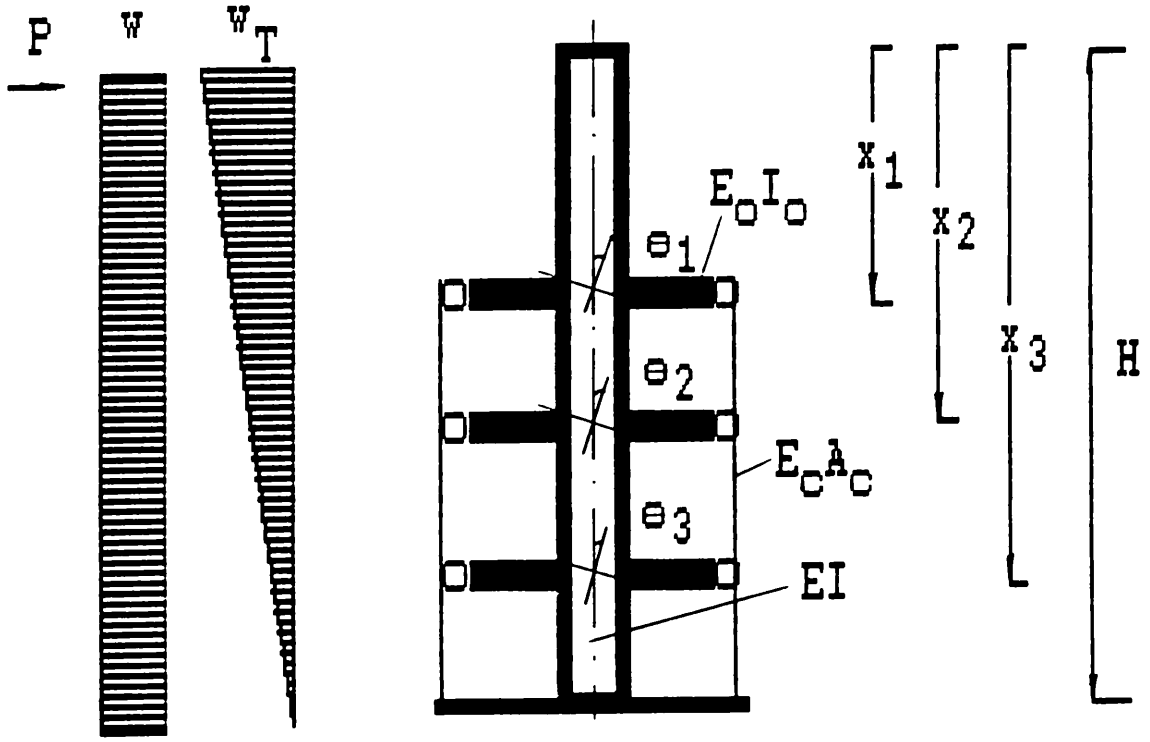

FIG.[2.5] THREE OUTRIGGER CASE

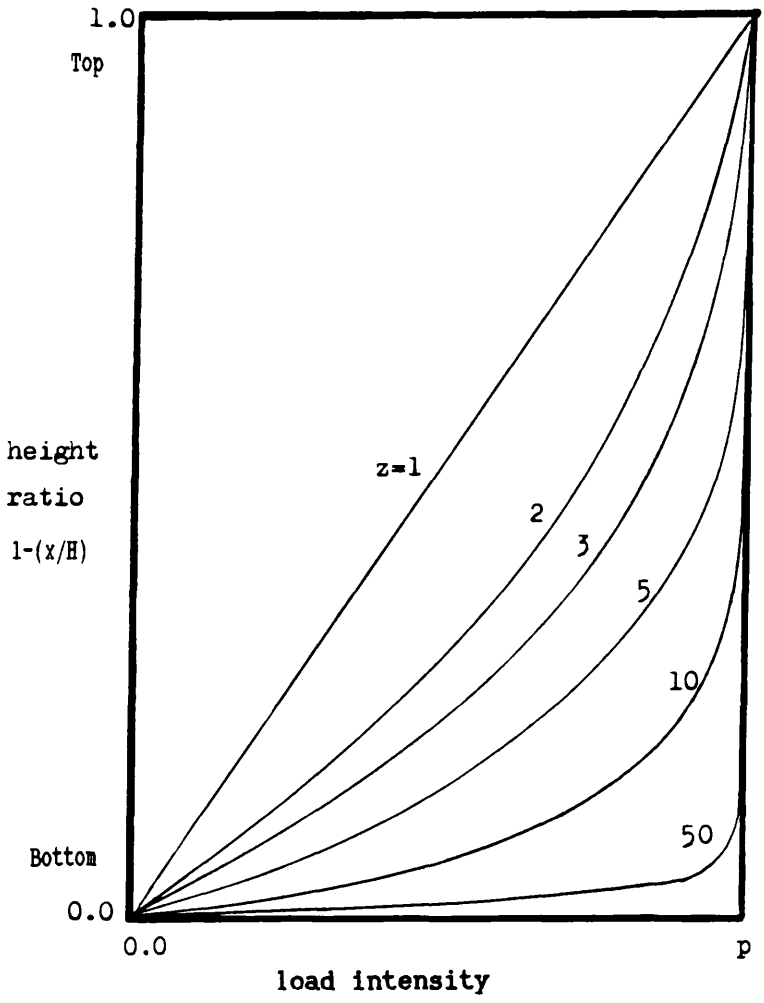

FIG.[2.6] VARIATION OF p_x WITH HEIGHT FOR DIFFERENT VALUES OF z

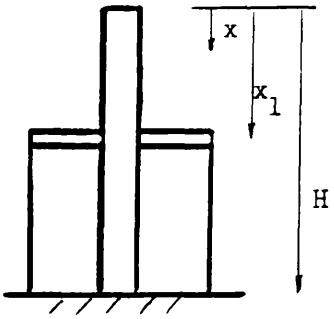

Type I	Type II
x_1= 0.0	x_1= 0.5H

Single Outrigger

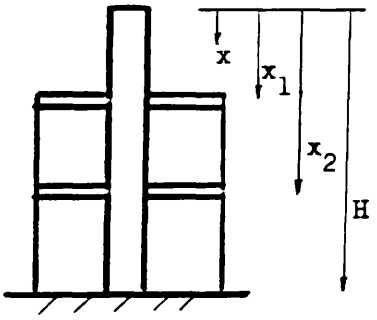

Type I	Type II	Type III
x_1= .33H	x_1= .25H	x_1=0.0
x_2= .67H	x_2= .75H	x_2= .5H

Two Outriggers

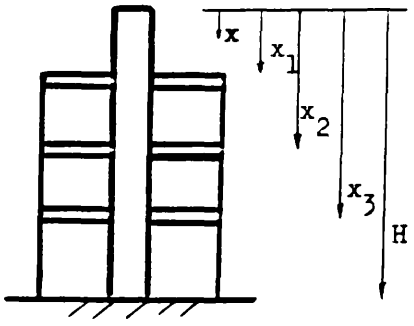

Type I	Type II	Type III
x_1= .25H	x_1= .167H	x_1=0.0
x_2= .50H	x_2= .50H	x_2= .33H
x_3= .75H	x_3= .833H	x_3= .67H

Three Outriggers

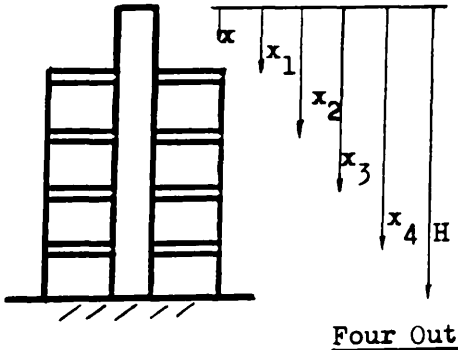

Type I	Type II	Type III
x_1= .20H	x_1= .125H	x_1=0.0
x_2= .40H	x_2= .375H	x_2= .25H
x_3= .60H	x_3= .625H	x_3= .50H
x_4= .80H	x_4= .875H	x_4= .75H

Four Outriggers

FIG. [2.7] DIFFERENT ARRANGEMENTS OF OUTRIGGERS

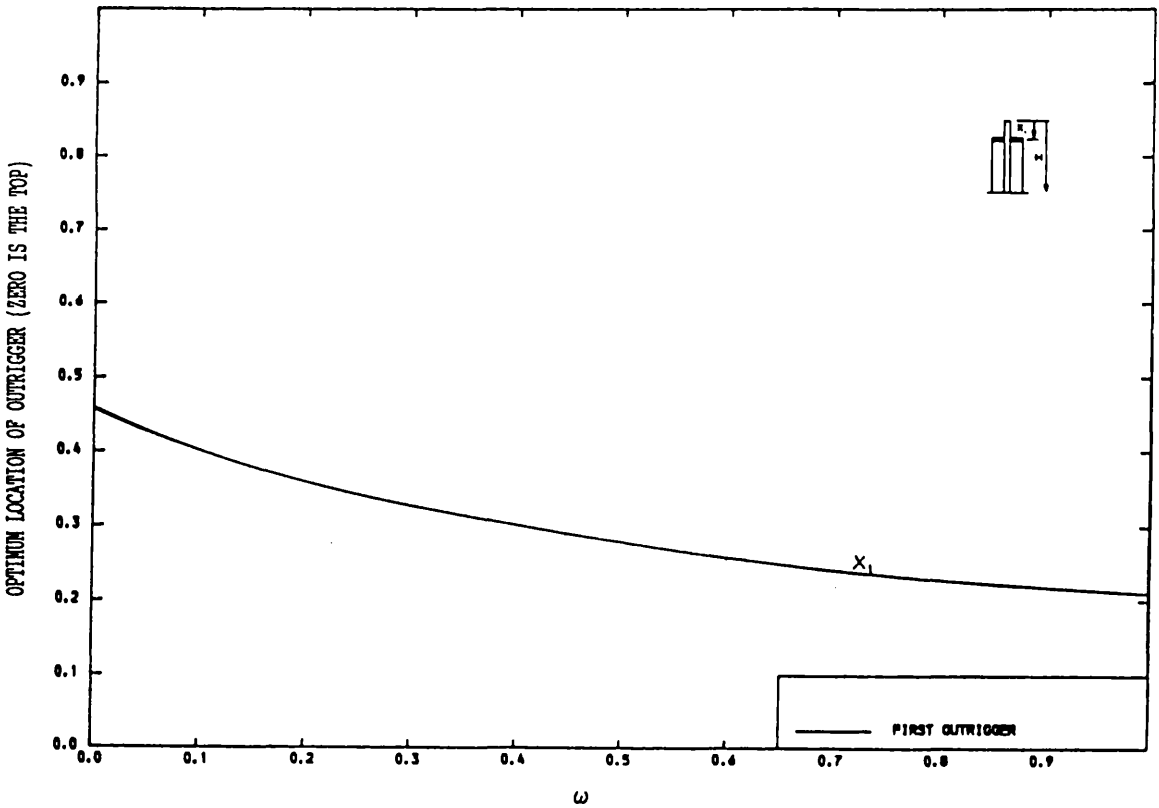

FIG.[2.8] VARIATION OF OPTIMUM LOCATION OF OUTRIGGER WITH ω
(R=0, CASE OF ONE OUTRIGGER, U.D.L.)
(MINIMISATION OF TOP DRIFT)

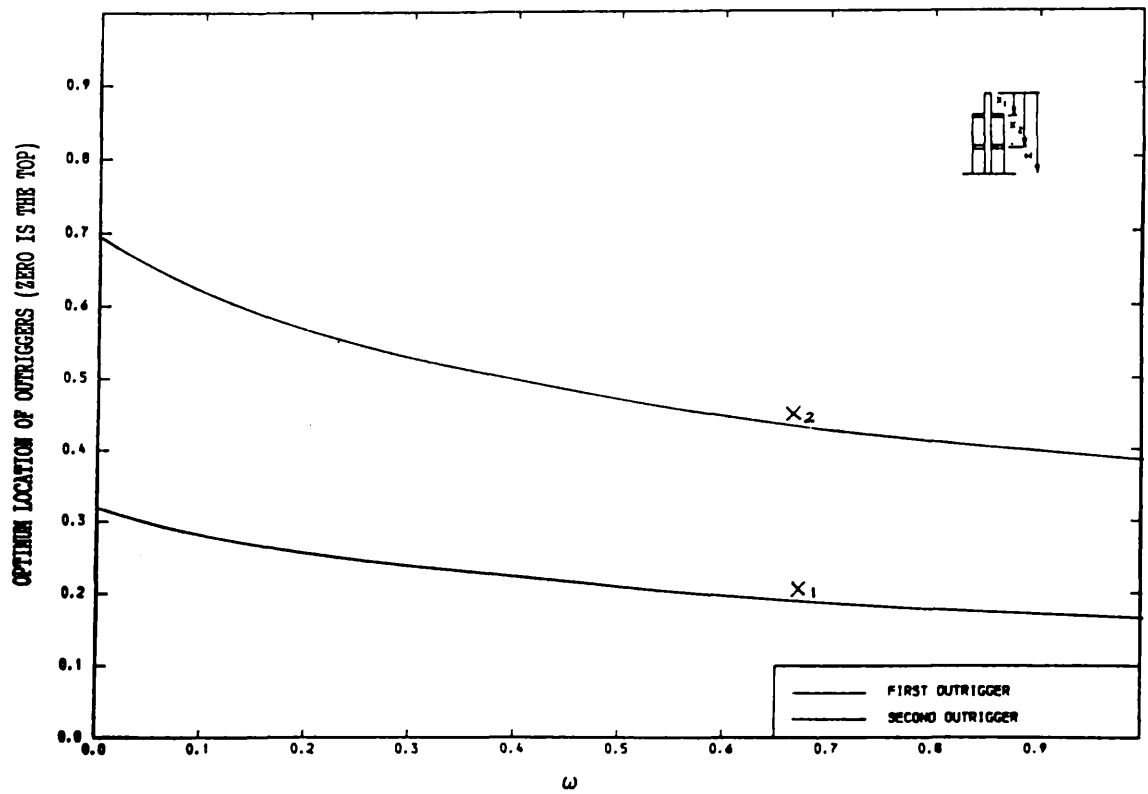

FIG.[2.9] VARIATION OF OPTIMUM LOCATIONS OF OUTRIGGERS WITH ω
(R=0, CASE OF TWO OUTRIGGERS, U.D.L.)
(MINIMISATION OF TOP DRIFT)

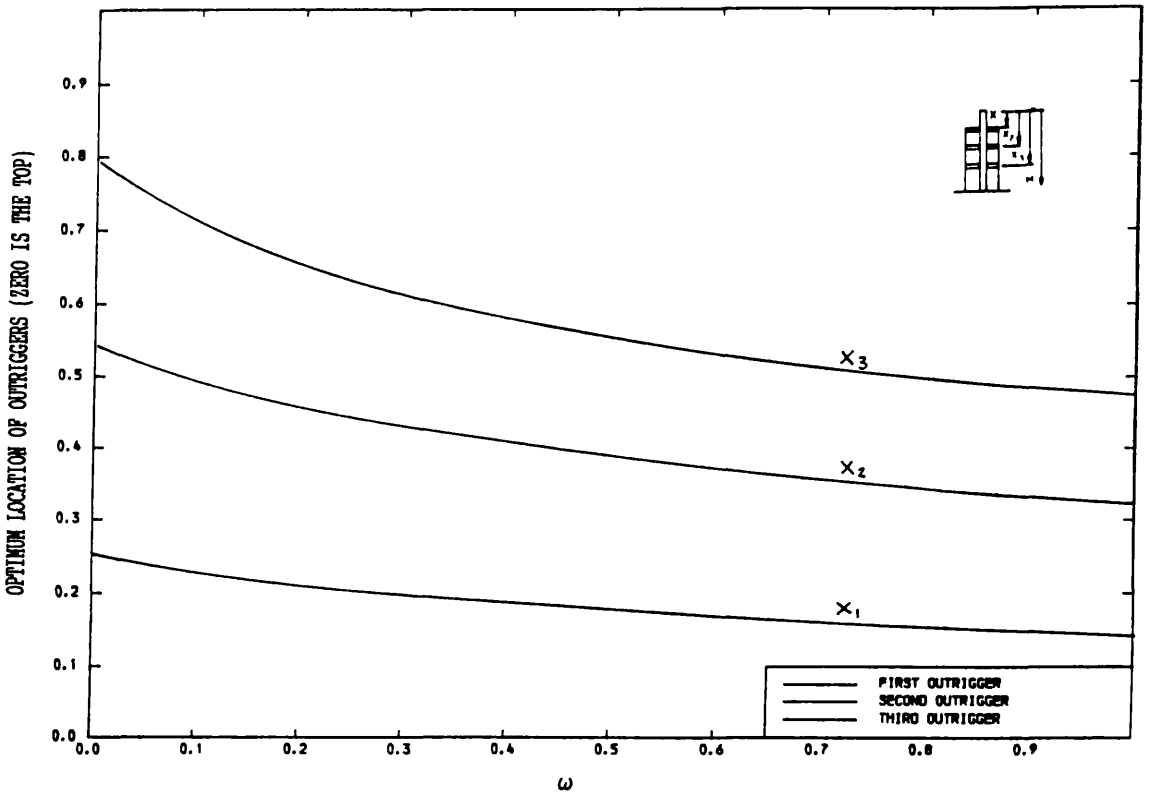

FIG. [2.10] VARIATION OF OPTIMUM LOCATIONS OF OUTRIGGERS WITH ω
(R=0, CASE OF THREE OUTRIGGERS, U.D.L.)
(MINIMISATION OF TOP DRIFT)

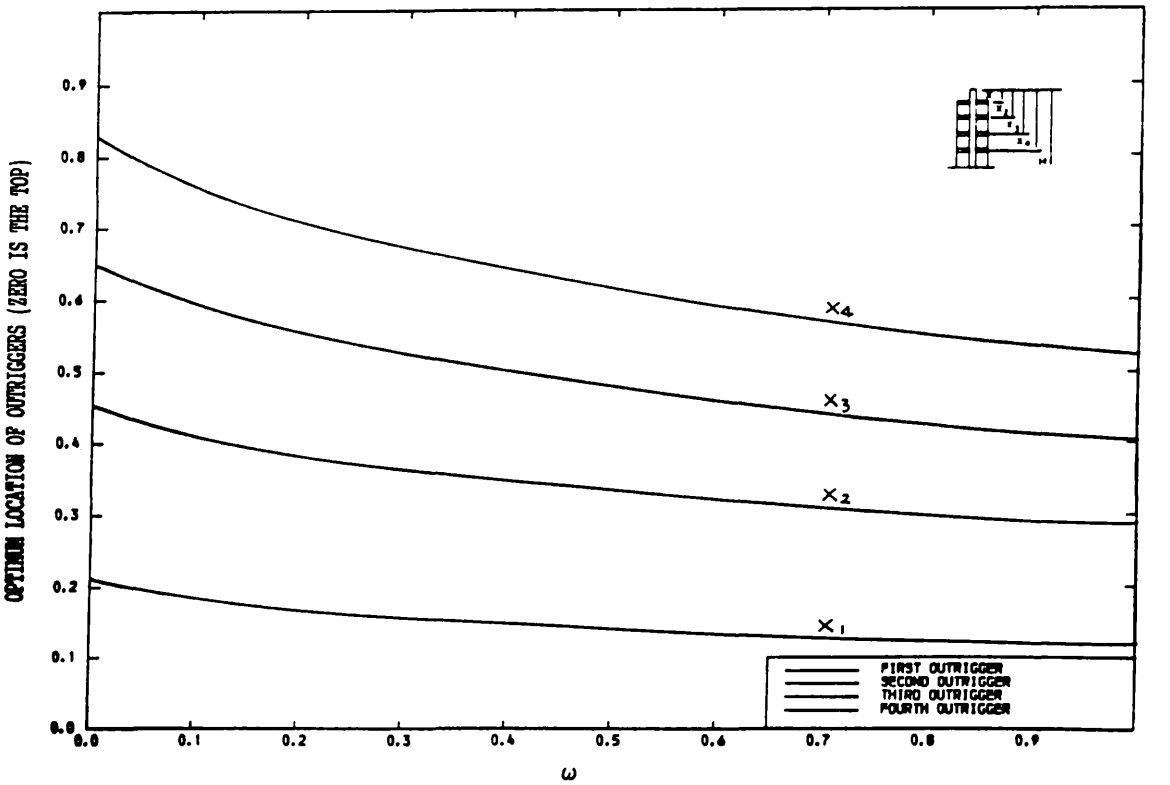

FIG. [2.11] VARIATION OF OPTIMUM LOCATIONS OF OUTRIGGERS WITH ω
(R=0, CASE OF FOUR OUTRIGGERS, U.D.L.)
(MINIMISATION OF TOP DRIFT)

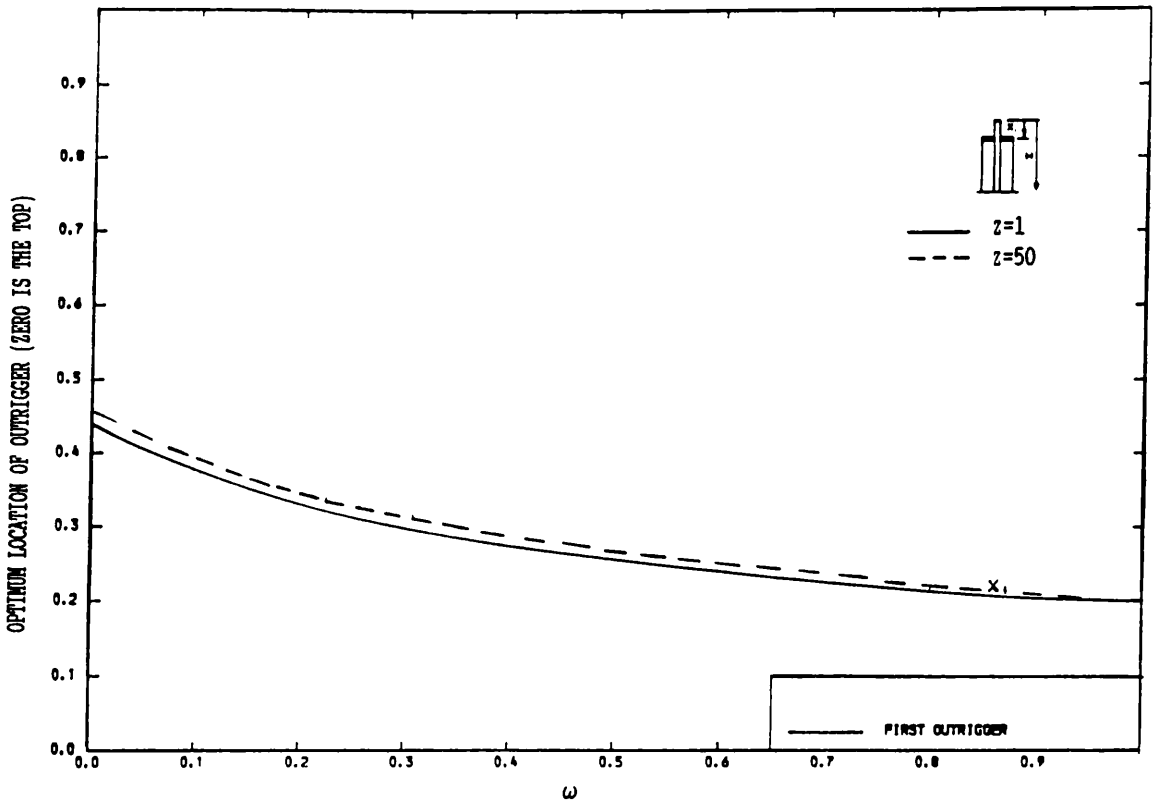

FIG.[2.12] VARIATION OF OPTIMUM LOCATION OF OUTRIGGER WITH ω
(R=0, CASE OF ONE OUTRIGGER)
(TRIANGULARLY DISTRIBUTED LOAD)
(MINIMISATION OF TOP DRIFT)

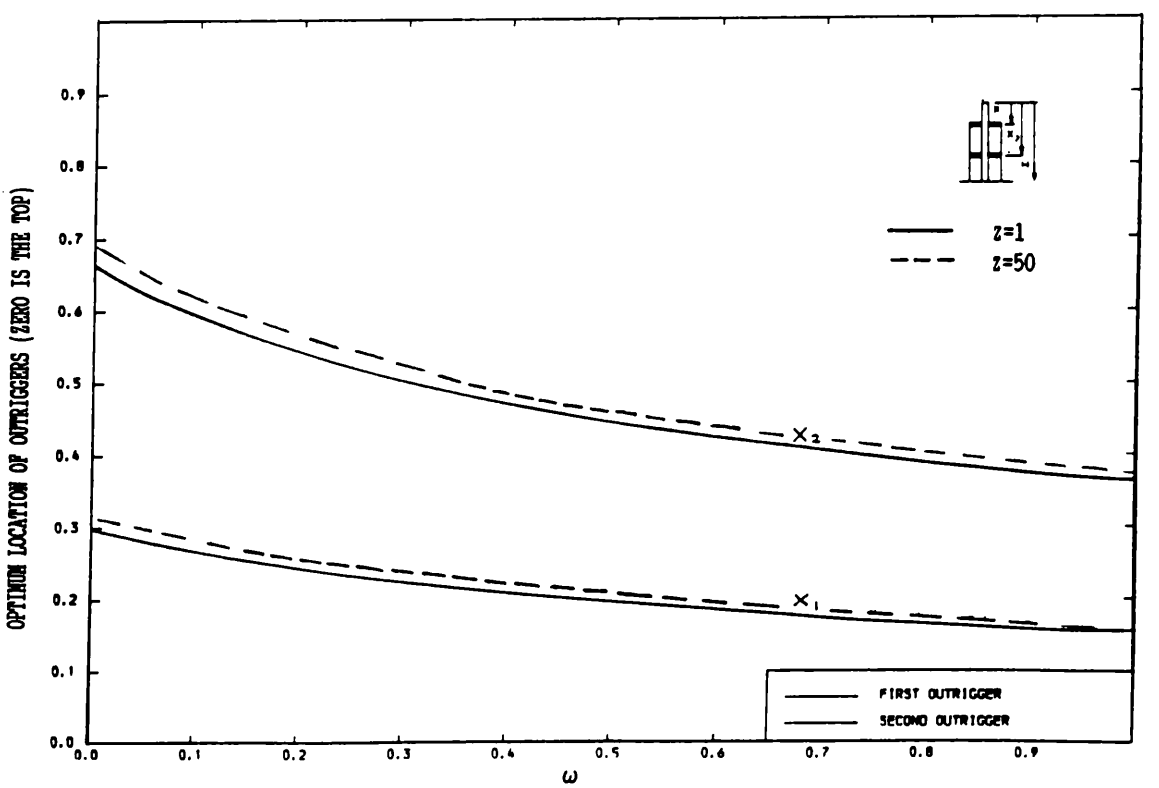

FIG.[2.13] VARIATION OF OPTIMUM LOCATIONS OF OUTRIGGERS WITH ω
(R=0, CASE OF TWO OUTRIGGERS)
(TRIANGULARLY DISTRIBUTED LOAD)
(MINIMISATION OF TOP DRIFT)

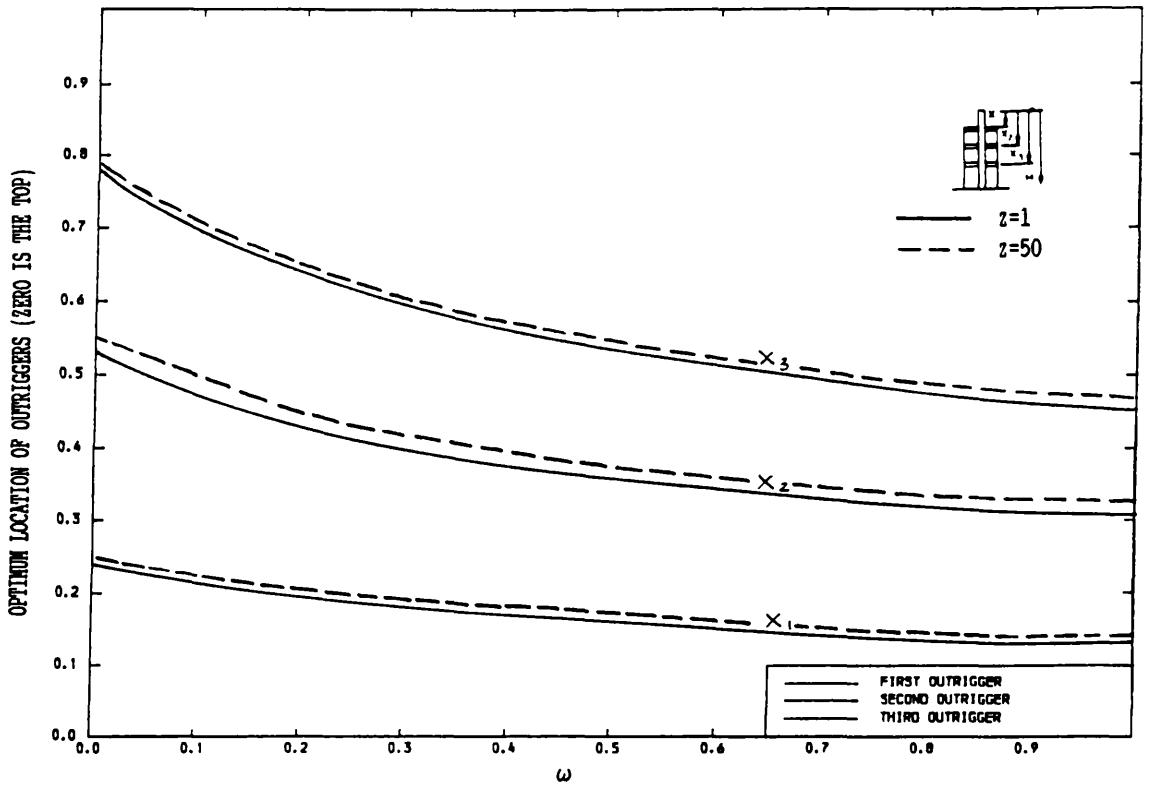

FIG.[2.14] VARIATION OF OPTIMUM LOCATIONS OF OUTRIGGERS WITH ω
(R=0, CASE OF THREE OUTRIGGERS)
(TRIANGULARLY DISTRIBUTED LOAD)
(MINIMISATION OF TOP DRIFT)

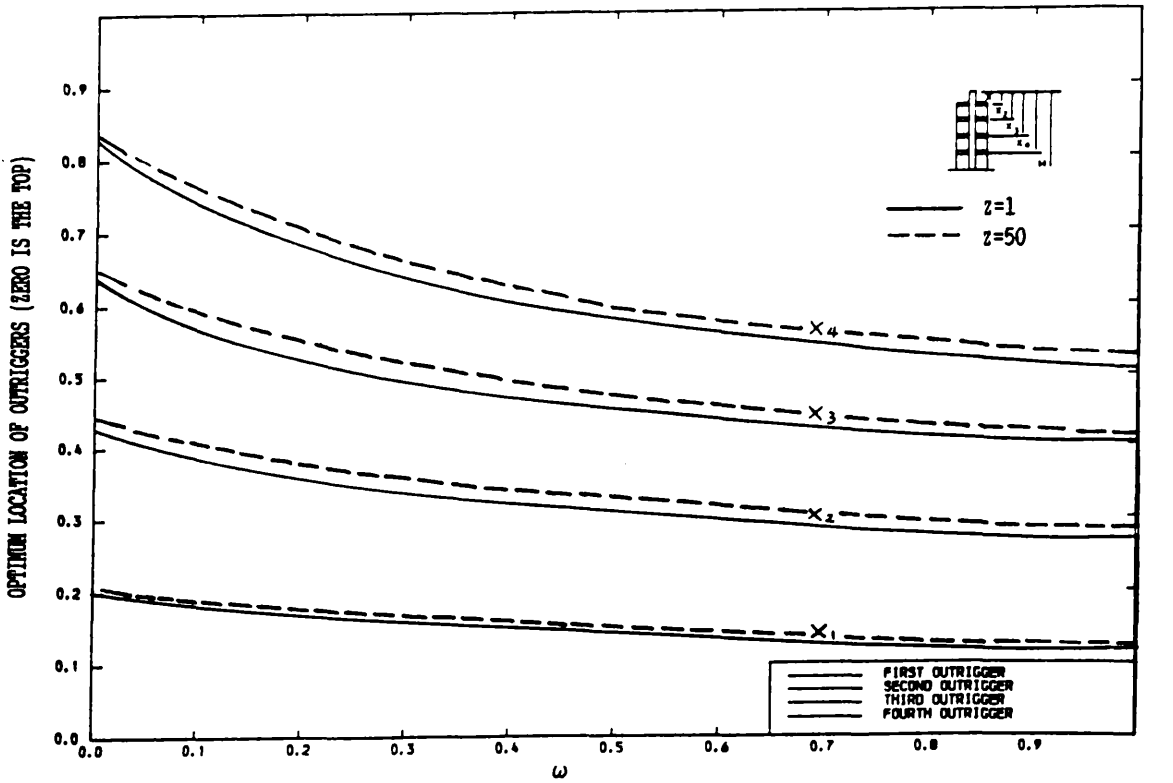

FIG.[2.15] VARIATION OF OPTIMUM LOCATIONS OF OUTRIGGERS WITH ω
(R=0, CASE OF FOUR OUTRIGGERS)
(TRIANGULARLY DISTRIBUTED LOAD)
(MINIMISATION OF TOP DRIFT)

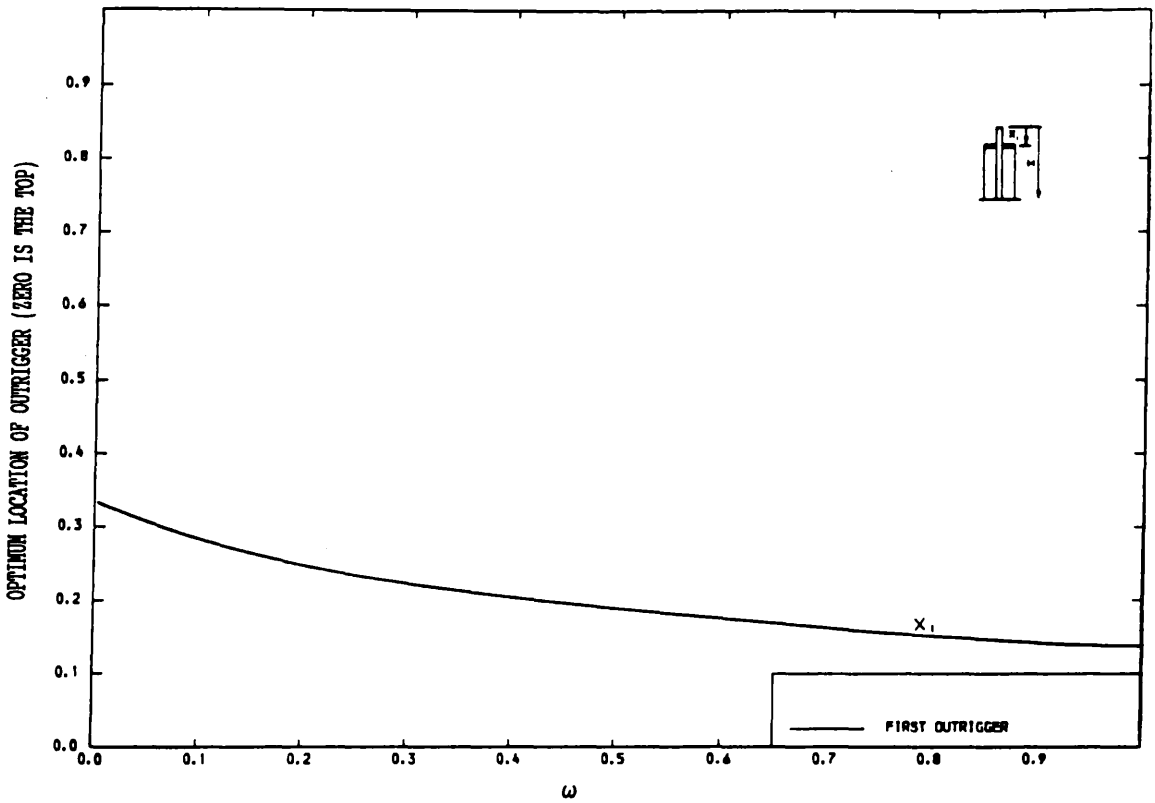

FIG.[2.16] VARIATION OF OPTIMUM LOCATION OF OUTRIGGER WITH ω
(R=0, CASE OF ONE OUTRIGGER, POINT LOAD AT THE TOP)
(MINIMISATION OF TOP DRIFT)

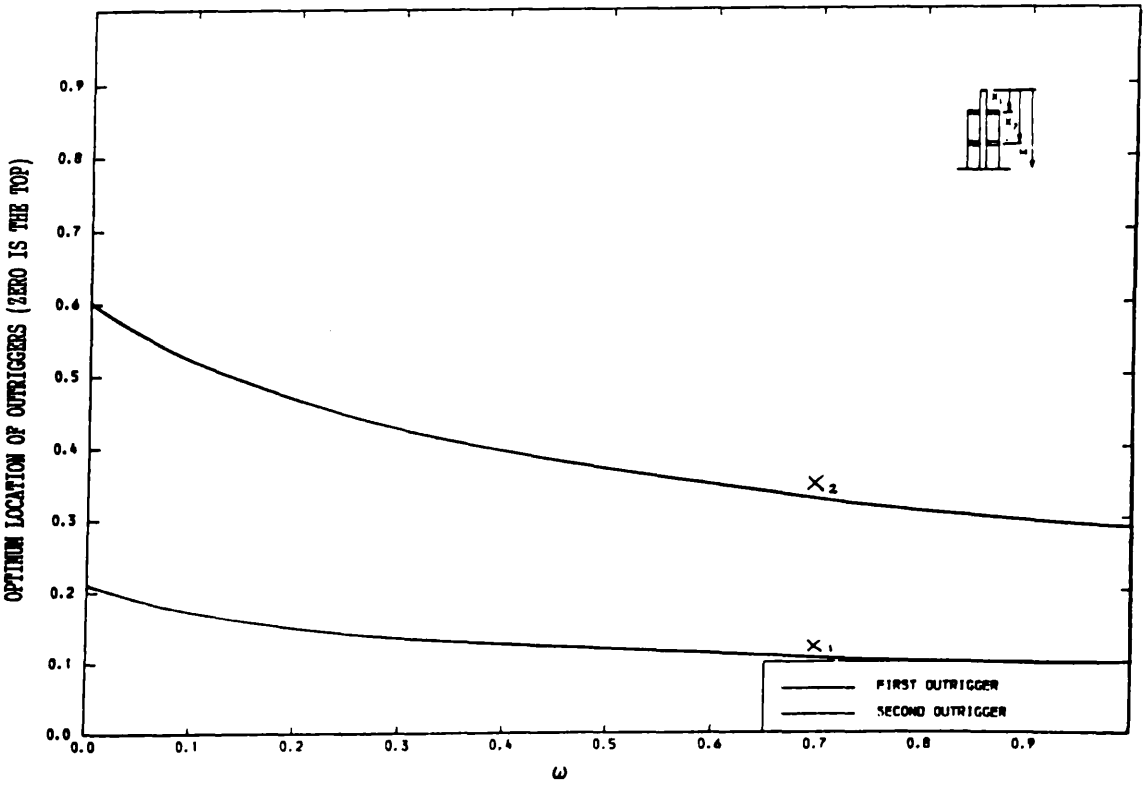

FIG.[2.17] VARIATION OF OPTIMUM LOCATIONS OF OUTRIGGERS WITH ω
(R=0, CASE OF TWO OUTRIGGERS, POINT LOAD AT THE TOP)
(MINIMISATION OF TOP DRIFT)

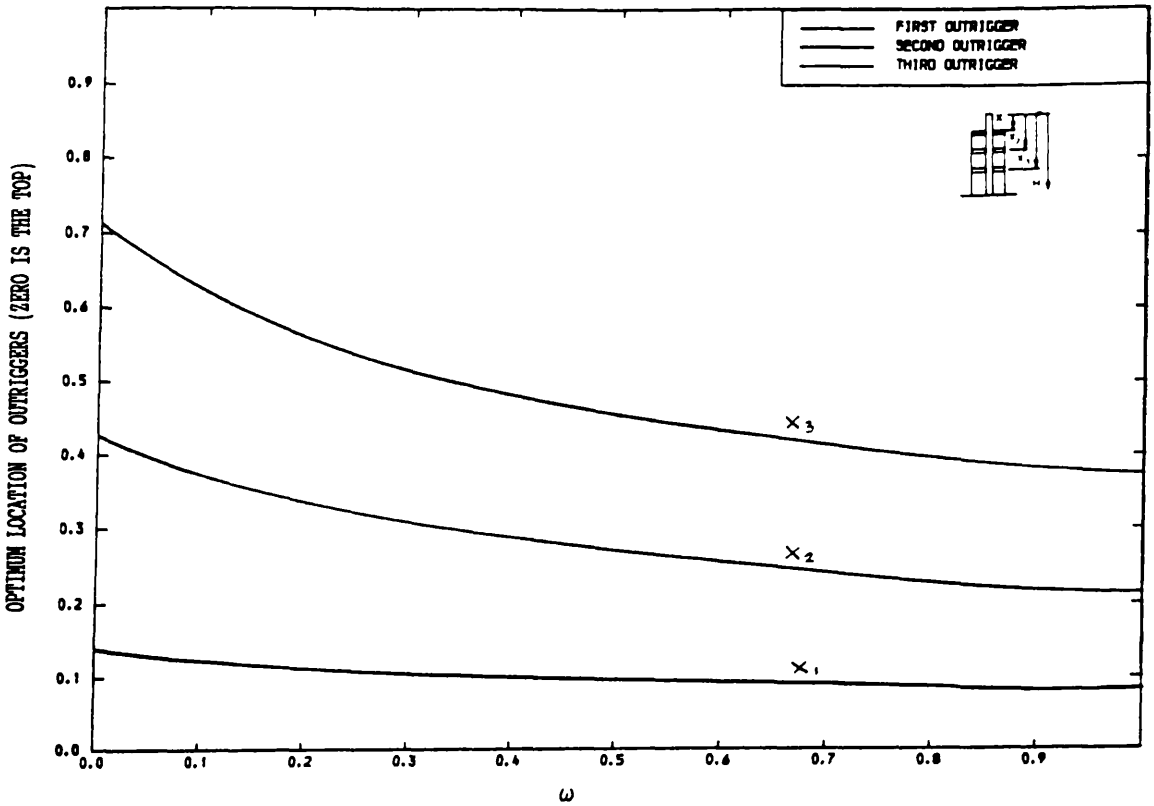

FIG.[2.18] VARIATION OF OPTIMUM LOCATIONS OF OUTRIGGERS WITH ω
(R=0, CASE OF THREE OUTRIGGERS, POINT LOAD AT THE TOP)
(MINIMISATION OF TOP DRIFT)

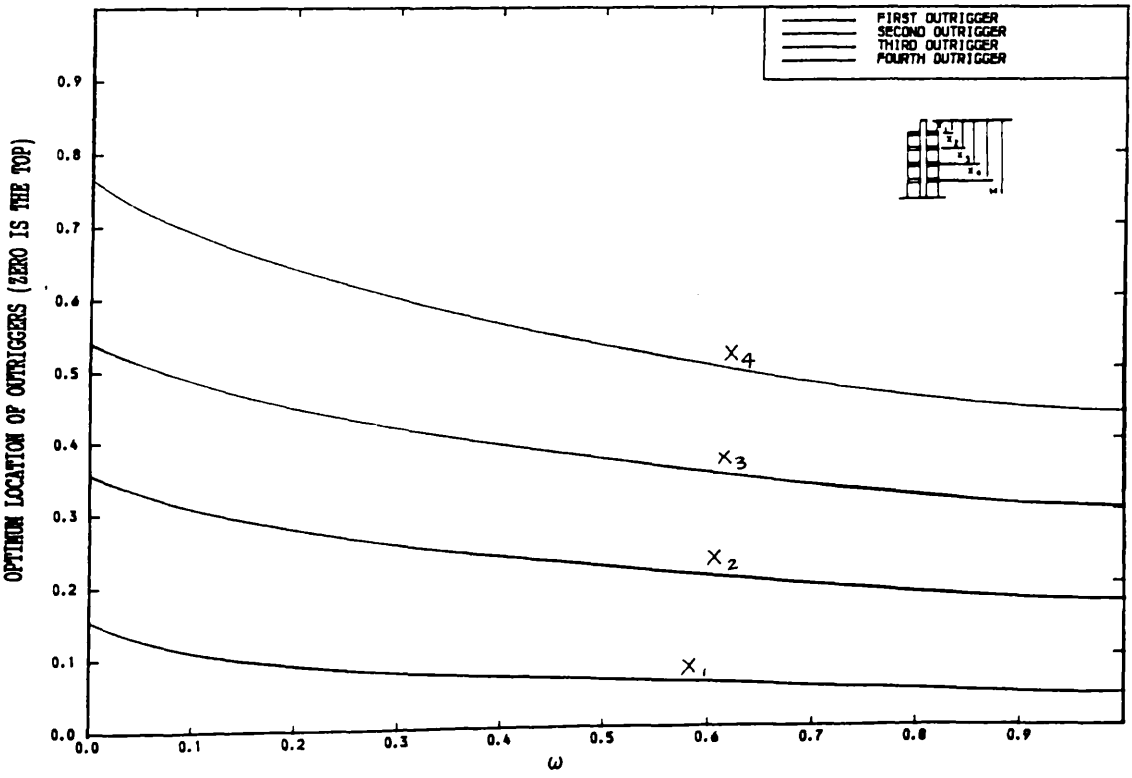

FIG.[2.19] VARIATION OF OPTIMUM LOCATIONS OF OUTRIGGERS WITH ω
(R=0, CASE OF FOUR OUTRIGGERS, POINT LOAD AT THE TOP)
(MINIMISATION OF TOP DRIFT)

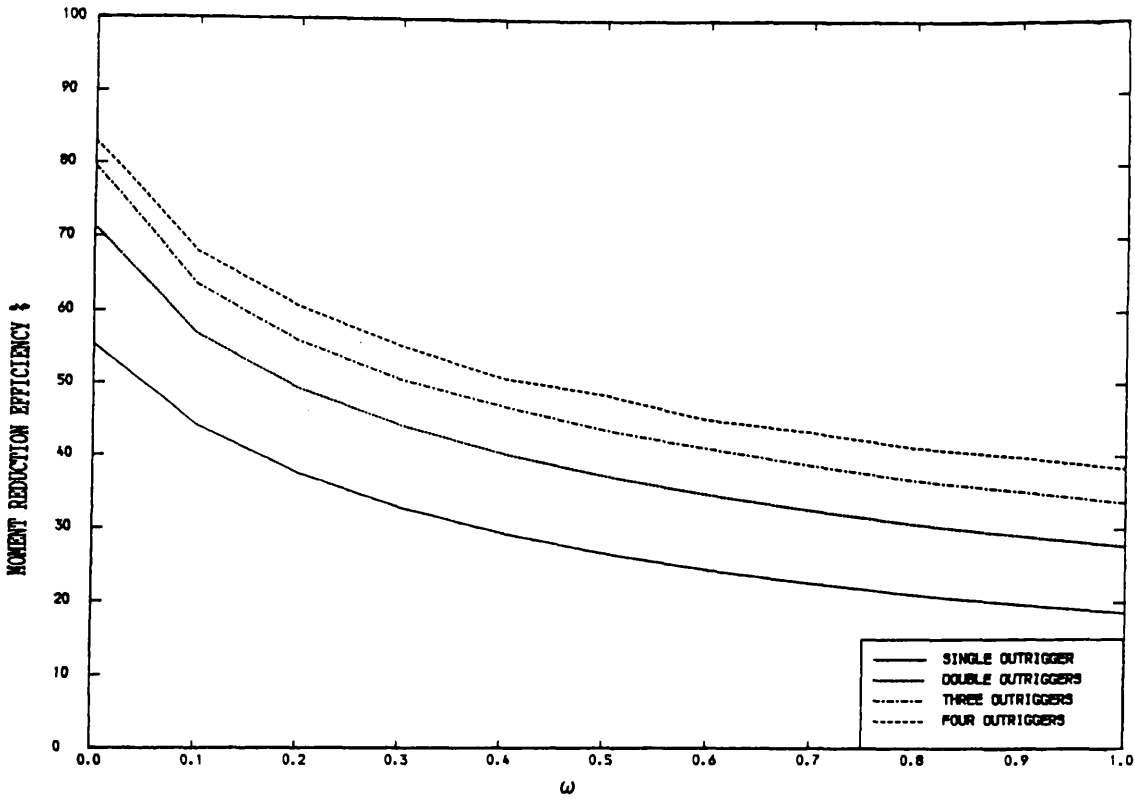

FIG. [2.20] COMPARISON OF MOMENT REDUCTION EFFICIENCY
(R=0, U.D.L.)
(MINIMISATION OF TOP DRIFT)

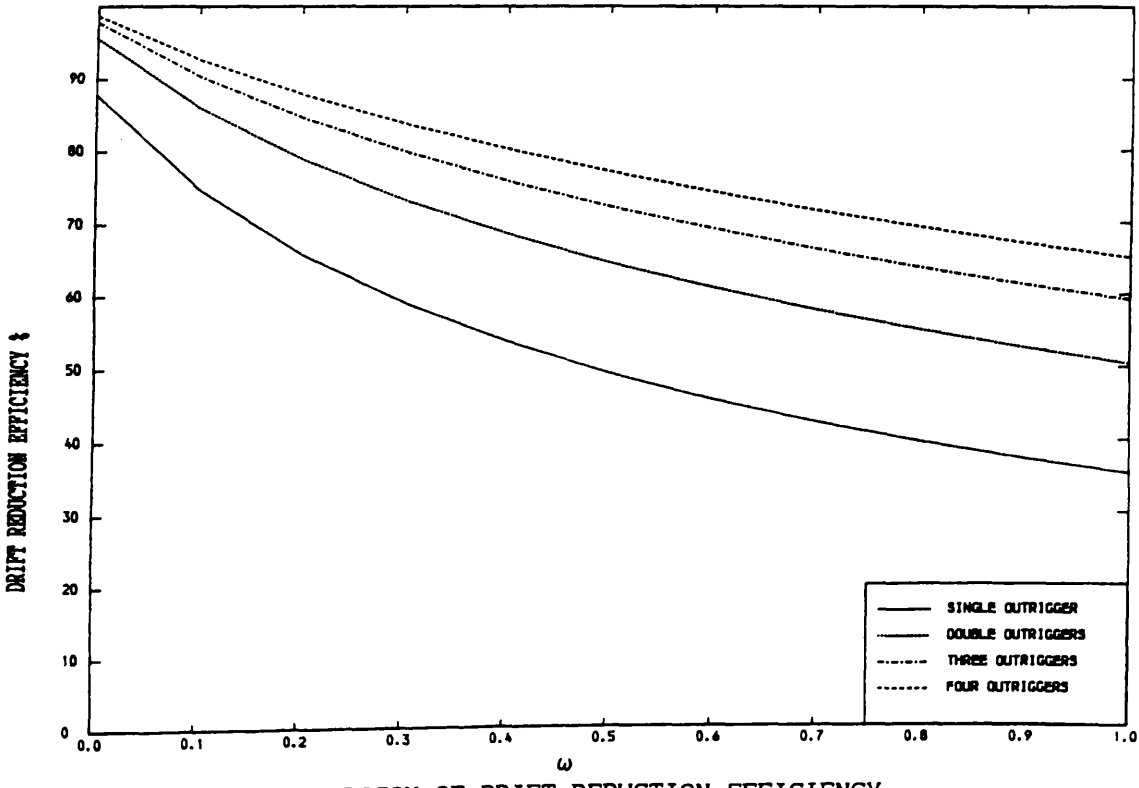

FIG. [2.21] COMPARISON OF DRIFT REDUCTION EFFICIENCY
(R=0, U.D.L.)
(MINIMISATION OF TOP DRIFT)

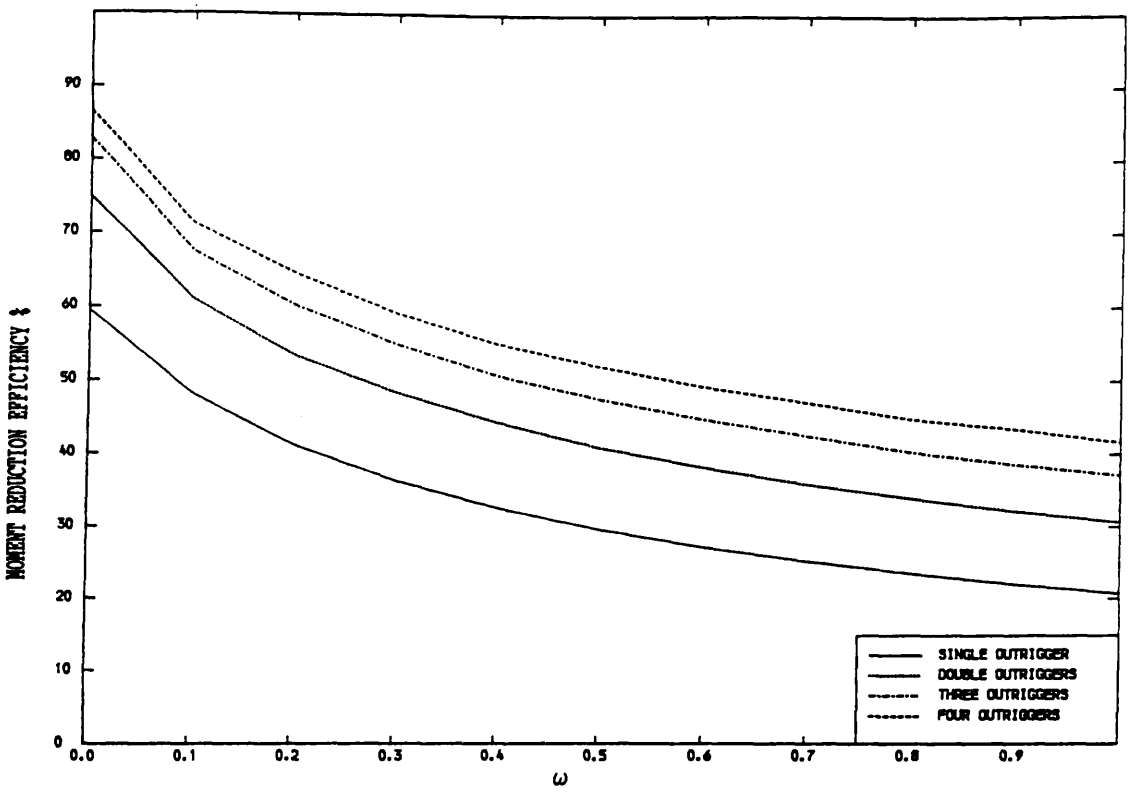

FIG.[2.22] COMPARISON OF MOMENT REDUCTION EFFICIENCY
(R=0, TRIANGULARLY DISTRIBUTED LOAD)
(MINIMISATION OF TOP DRIFT)

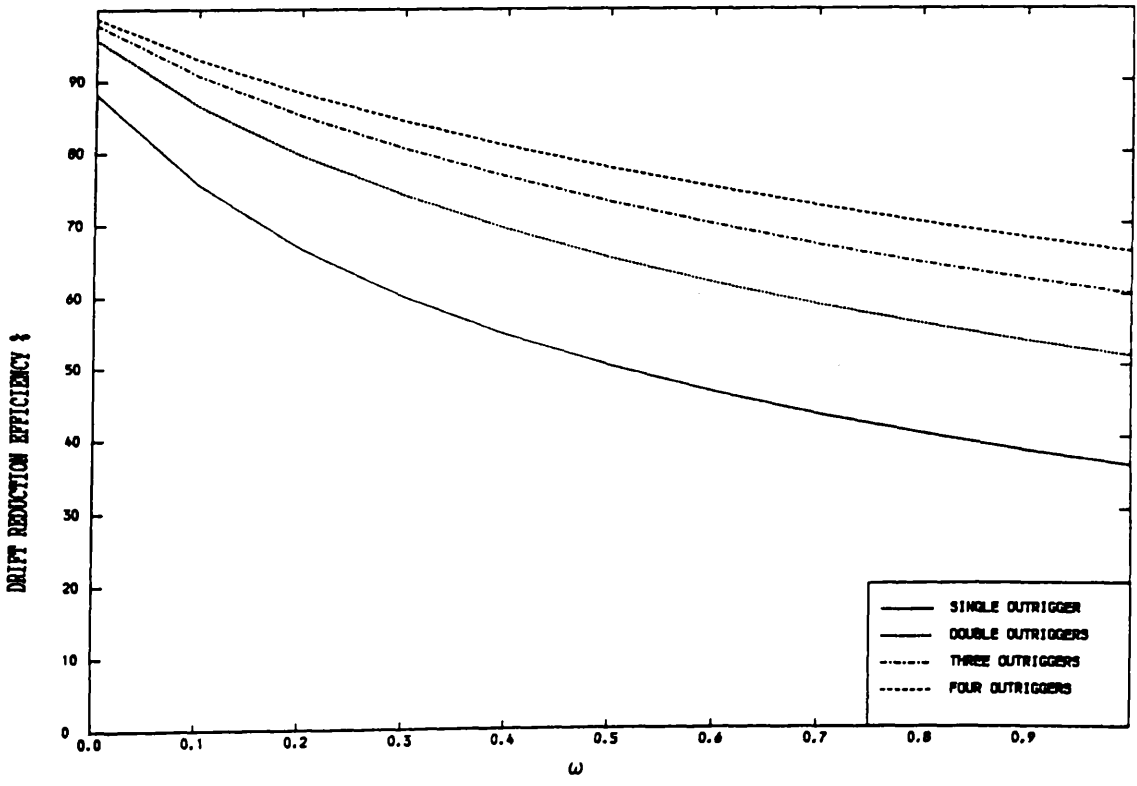

FIG.[2.23] COMPARISON OF DRIFT REDUCTION EFFICIENCY
(R=0, TRIANGULARLY DISTRIBUTED LOAD)
(MINIMISATION OF TOP DRIFT)

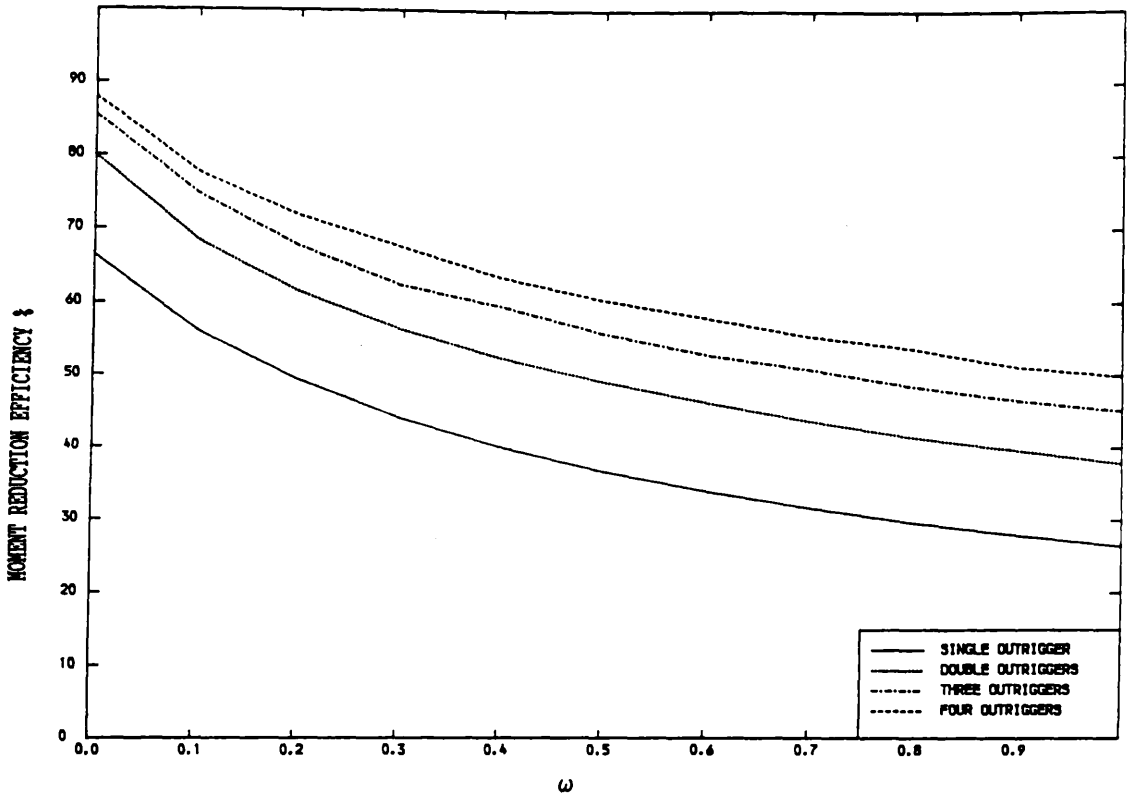

FIG. [2.24] COMPARISON OF MOMENT REDUCTION EFFICIENCY
(R=0, POINT LOAD AT THE TOP)
(MINIMISATION OF TOP DRIFT)

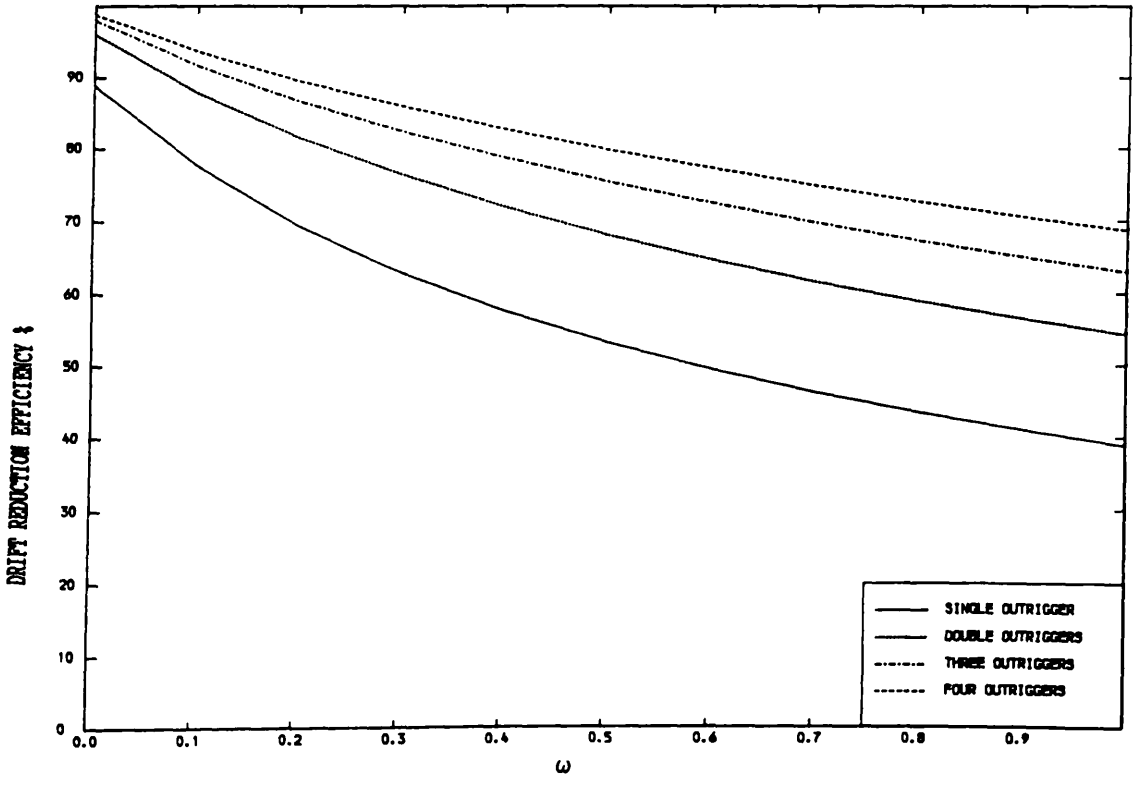

FIG. [2.25] COMPARISON OF DRIFT REDUCTION EFFICIENCY
(R=0, POINT LOAD AT THE TOP)
(MINIMISATION OF TOP DRIFT)

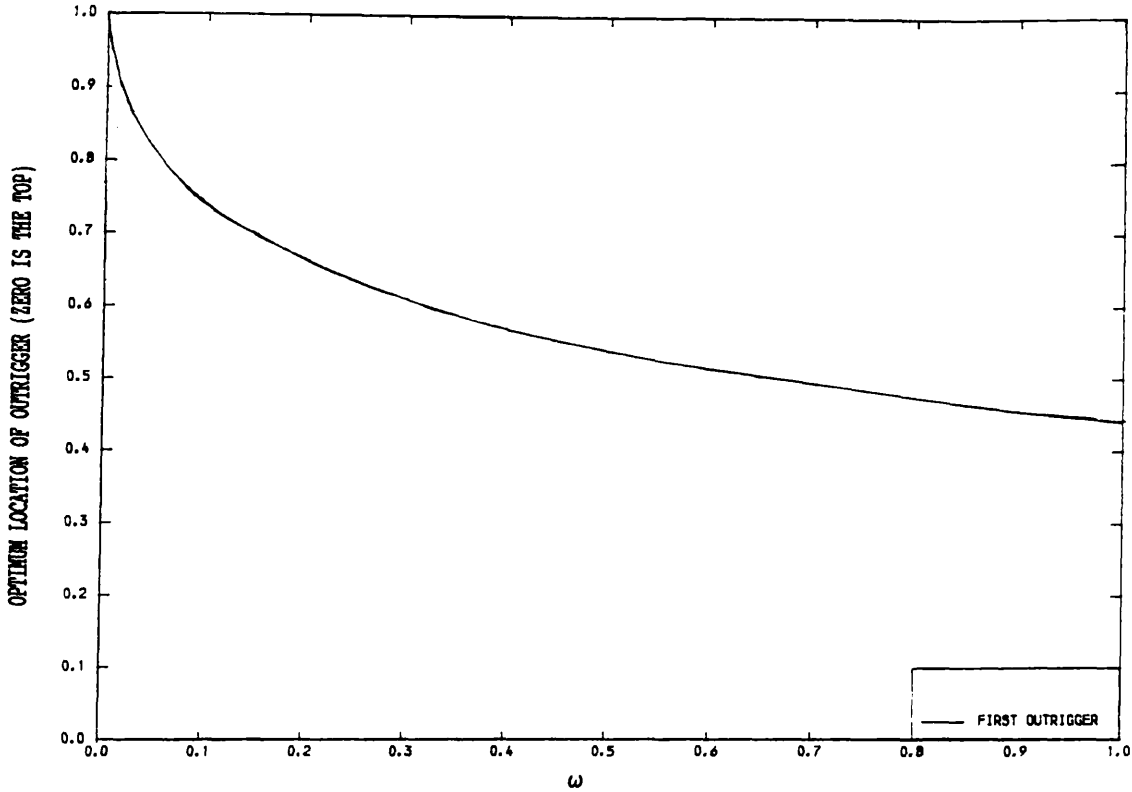

FIG. [2.26] VARIATION OF OPTIMUM LOCATION OF OUTRIGGER WITH ω
(R=0, CASE OF ONE OUTRIGGER, U.D.L.)
(MINIMISATION OF CORE MOMENT AT THE BASE)

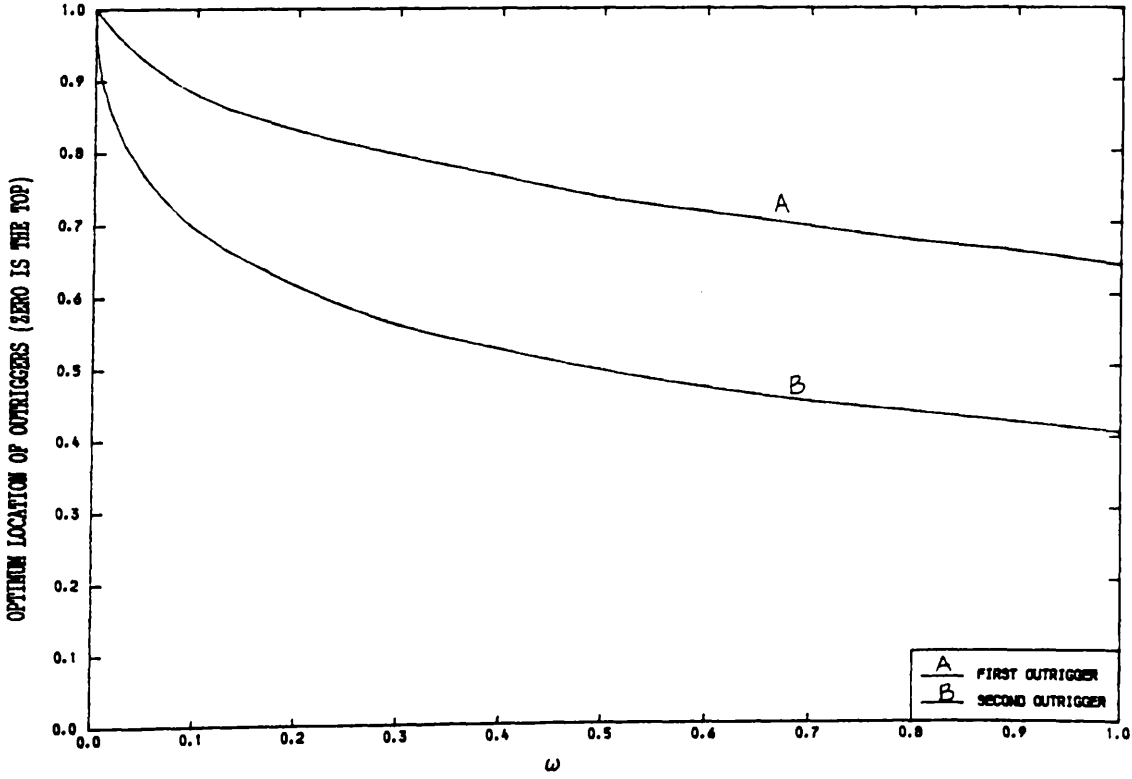

FIG. [2.27] VARIATION OF OPTIMUM LOCATIONS OF OUTRIGGERS WITH ω
(R=0, CASE OF TWO OUTRIGGERS, U.D.L.)
(MINIMISATION OF CORE MOMENT AT THE BASE)

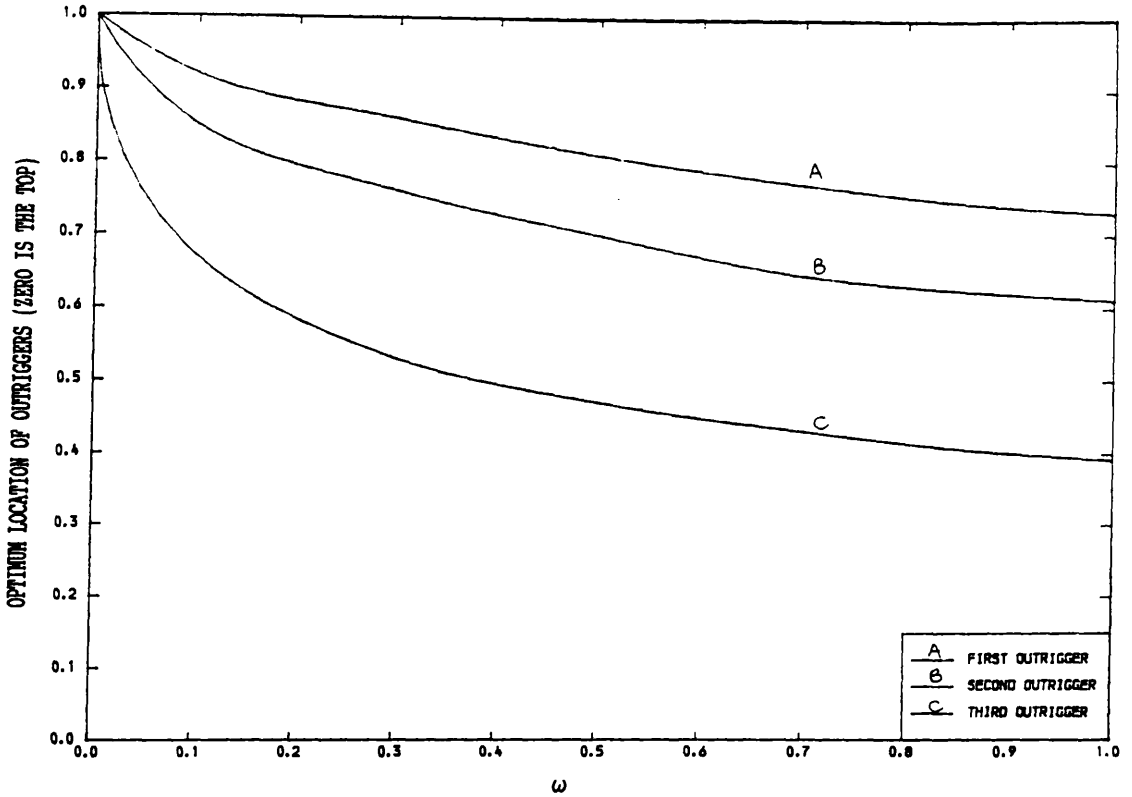

FIG.[2.28] VARIATION OF OPTIMUM LOCATIONS OF OUTRIGGERS WITH ω
(R=0, CASE OF THREE OUTRIGGERS, U.D.L.)
(MINIMISATION OF CORE MOMENT AT THE BASE)

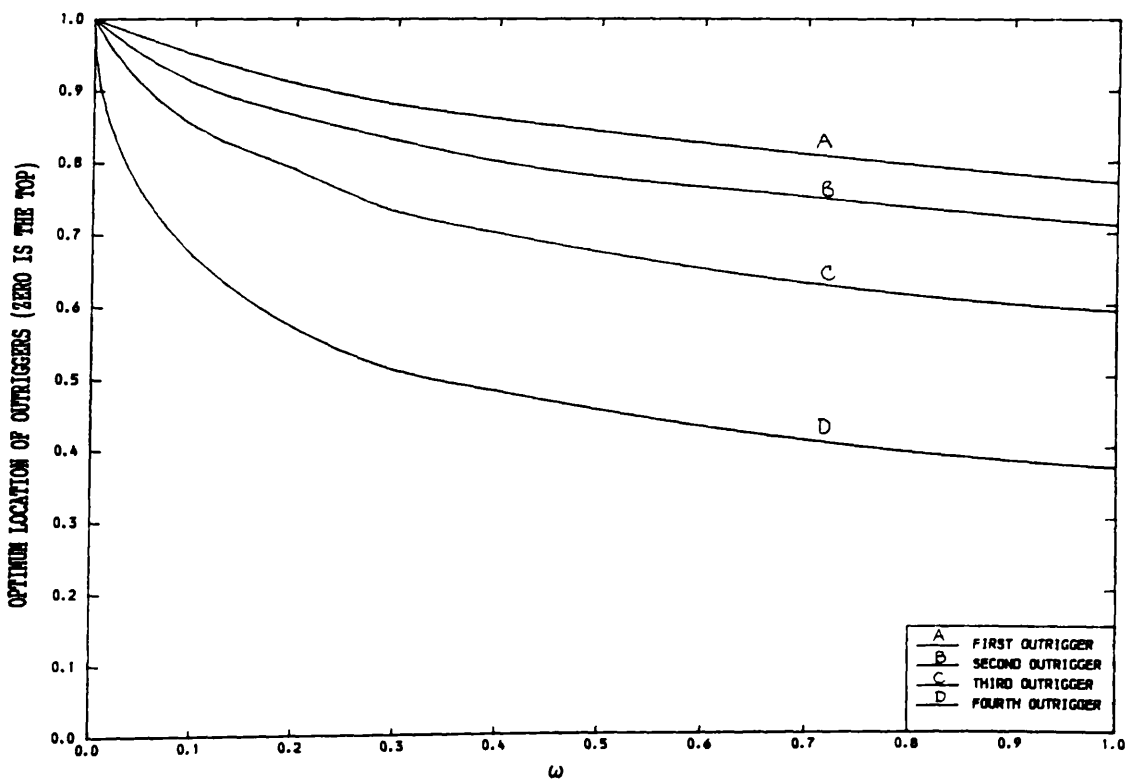

FIG.[2.29] VARIATION OF OPTIMUM LOCATIONS OF OUTRIGGERS WITH ω
(R=0, CASE OF FOUR OUTRIGGERS, U.D.L.)
(MINIMISATION OF CORE MOMENT AT THE BASE)

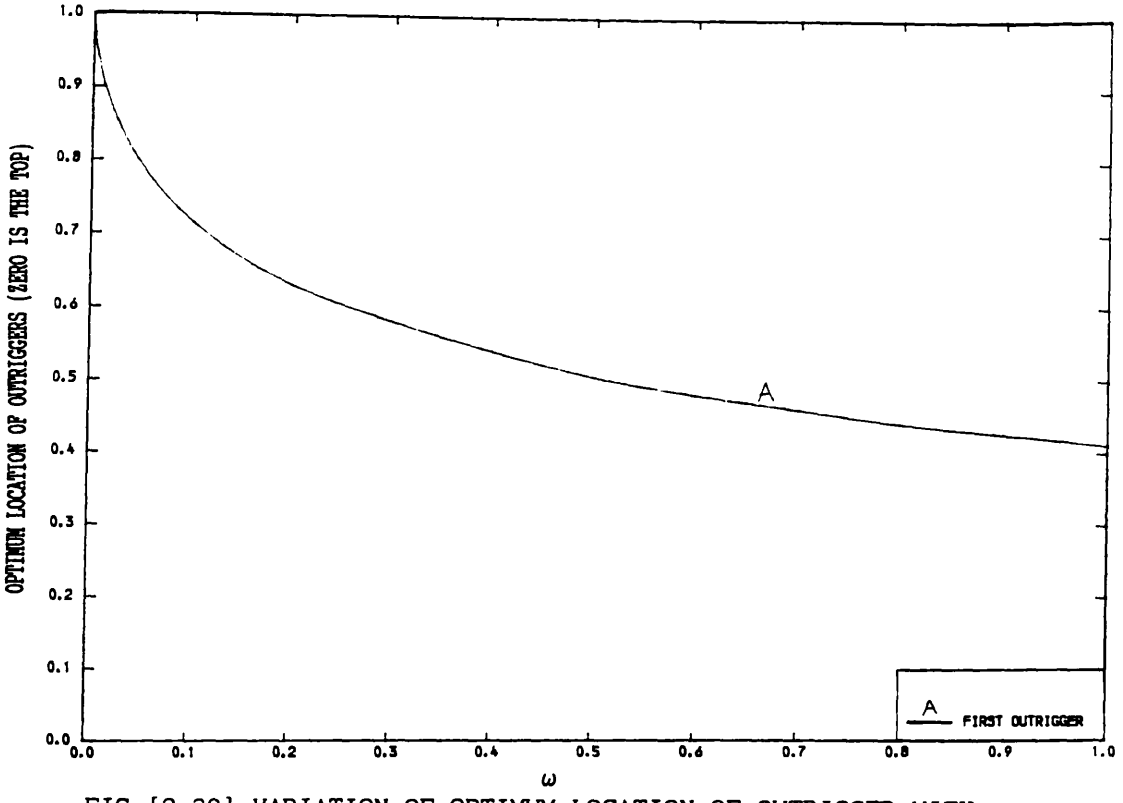

FIG.[2.30] VARIATION OF OPTIMUM LOCATION OF OUTRIGGER WITH ω
(R=0, CASE OF ONE OUTRIGGER)
(TRIANGULARLY DISTRIBUTED LOAD)
(MINIMISATION OF CORE MOMENT AT THE BASE)

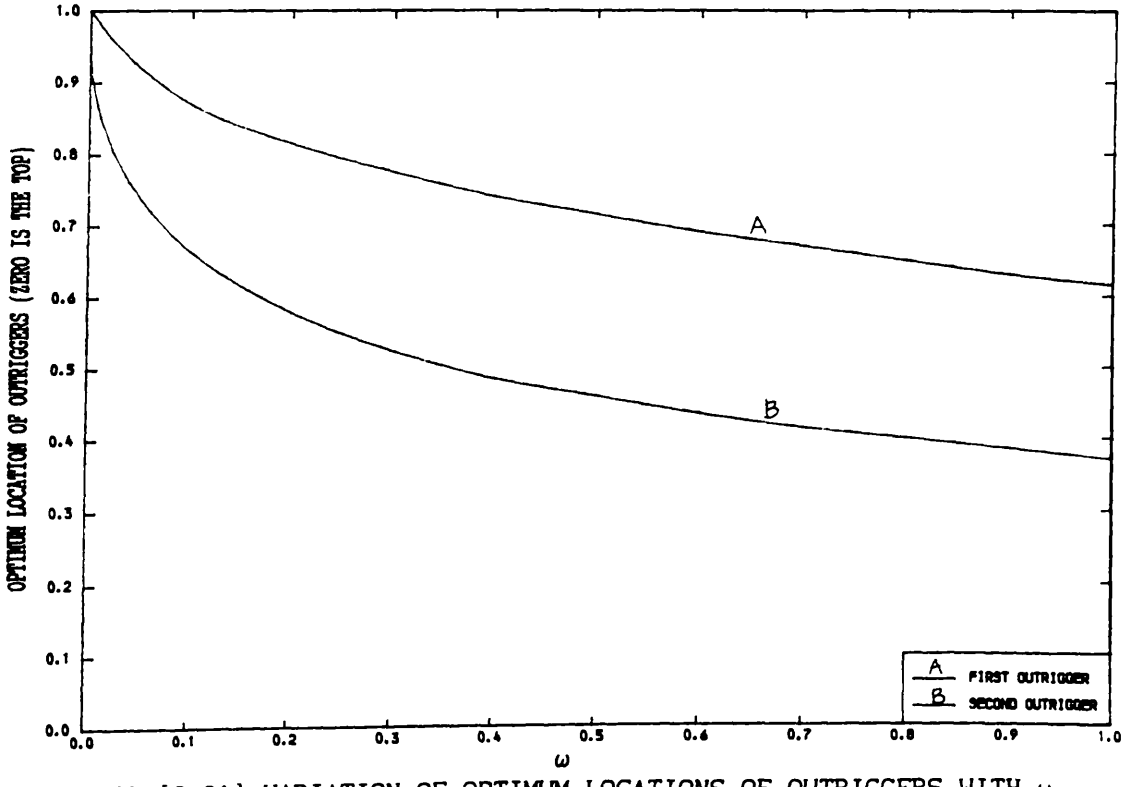

FIG.[2.31] VARIATION OF OPTIMUM LOCATIONS OF OUTRIGGERS WITH ω
(R=0, CASE OF TWO OUTRIGGERS)
(TRIANGULARLY DISTRIBUTED LOAD)
(MINIMISATION OF CORE MOMENT AT THE BASE)

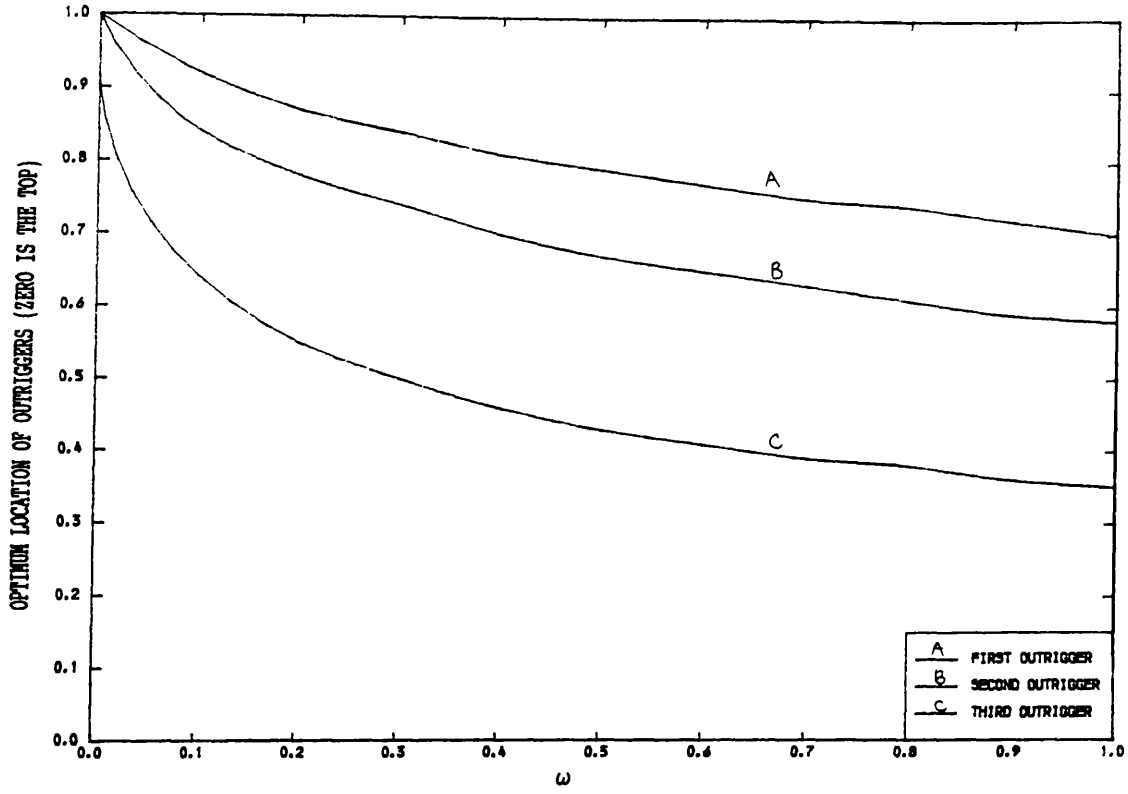

FIG. [2.32] VARIATION OF OPTIMUM LOCATIONS OF OUTRIGGERS WITH ω
(R=0, CASE OF THREE OUTRIGGERS)
(TRIANGULARLY DISTRIBUTED LOAD)
(MINIMISATION OF CORE MOMENT AT THE BASE)

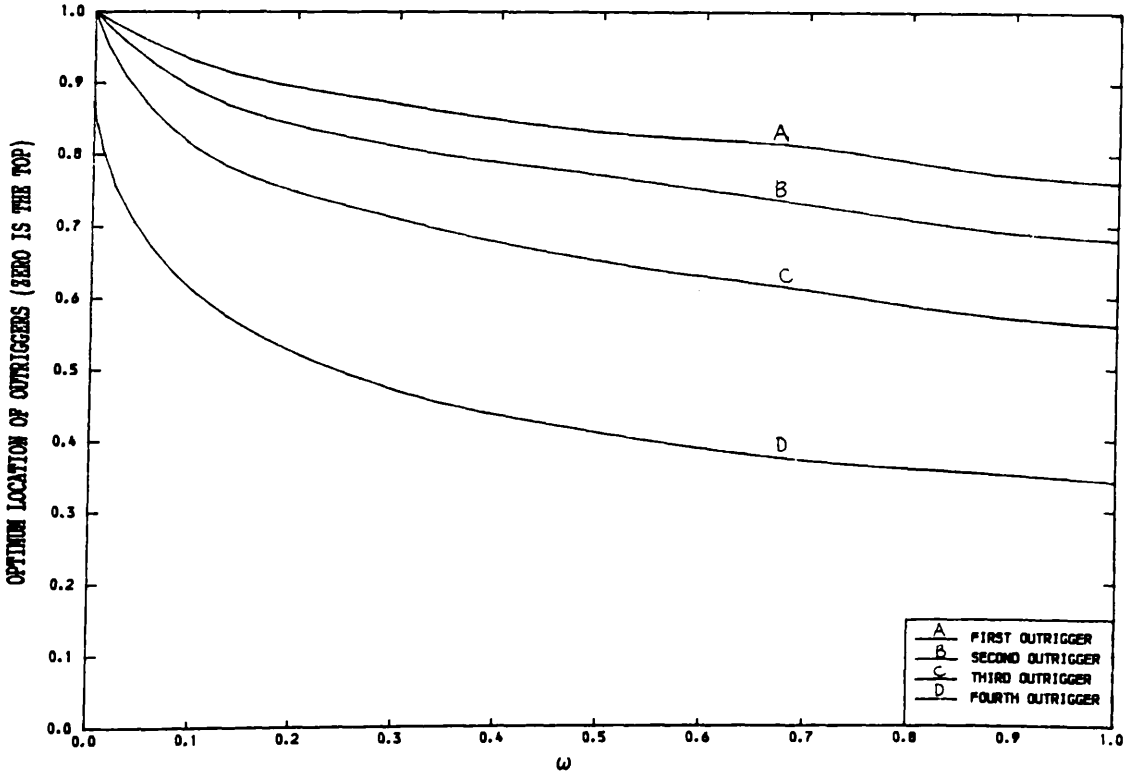

FIG. [2.33] VARIATION OF OPTIMUM LOCATIONS OF OUTRIGGERS WITH ω
(R=0, CASE OF FOUR OUTRIGGERS)
(TRIANGULARLY DISTRIBUTED LOAD)
(MINIMISATION OF CORE MOMENT AT THE BASE)

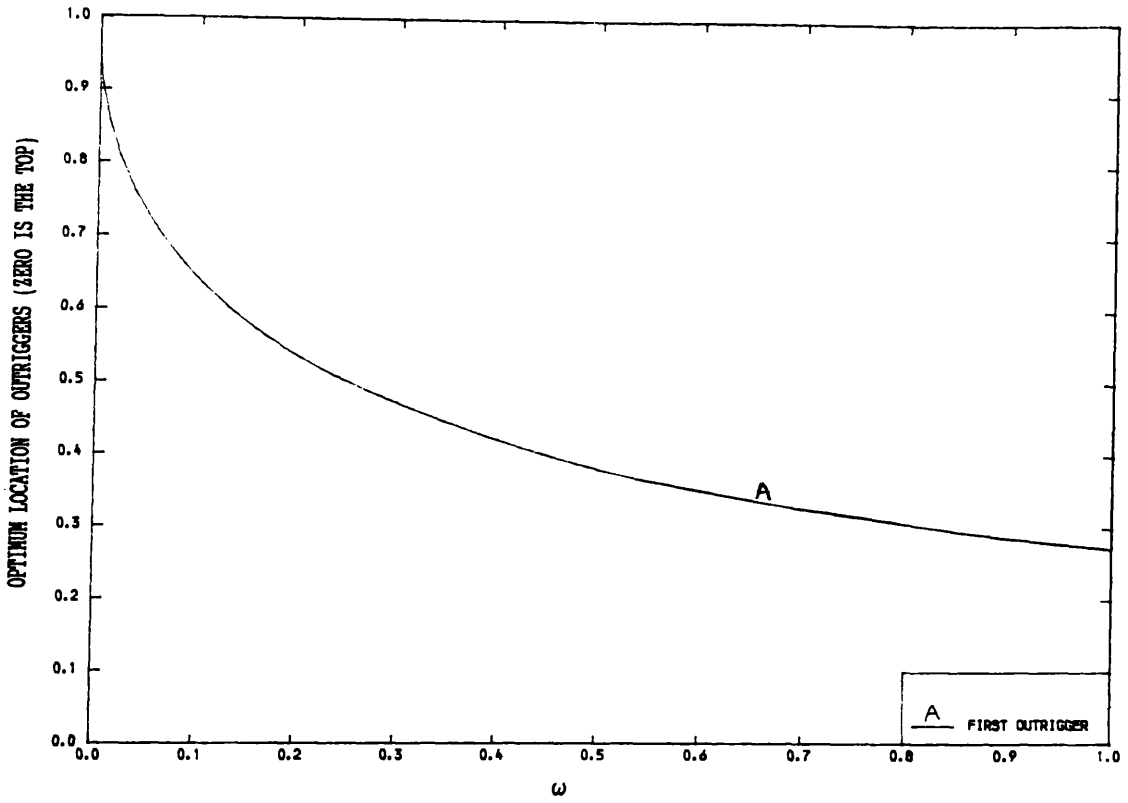

FIG. [2.34] VARIATION OF OPTIMUM LOCATION OF OUTRIGGER WITH ω
(R=0, CASE OF ONE OUTRIGGER, POINT LOAD AT THE TOP)
(MINIMISATION OF CORE MOMENT AT THE BASE)

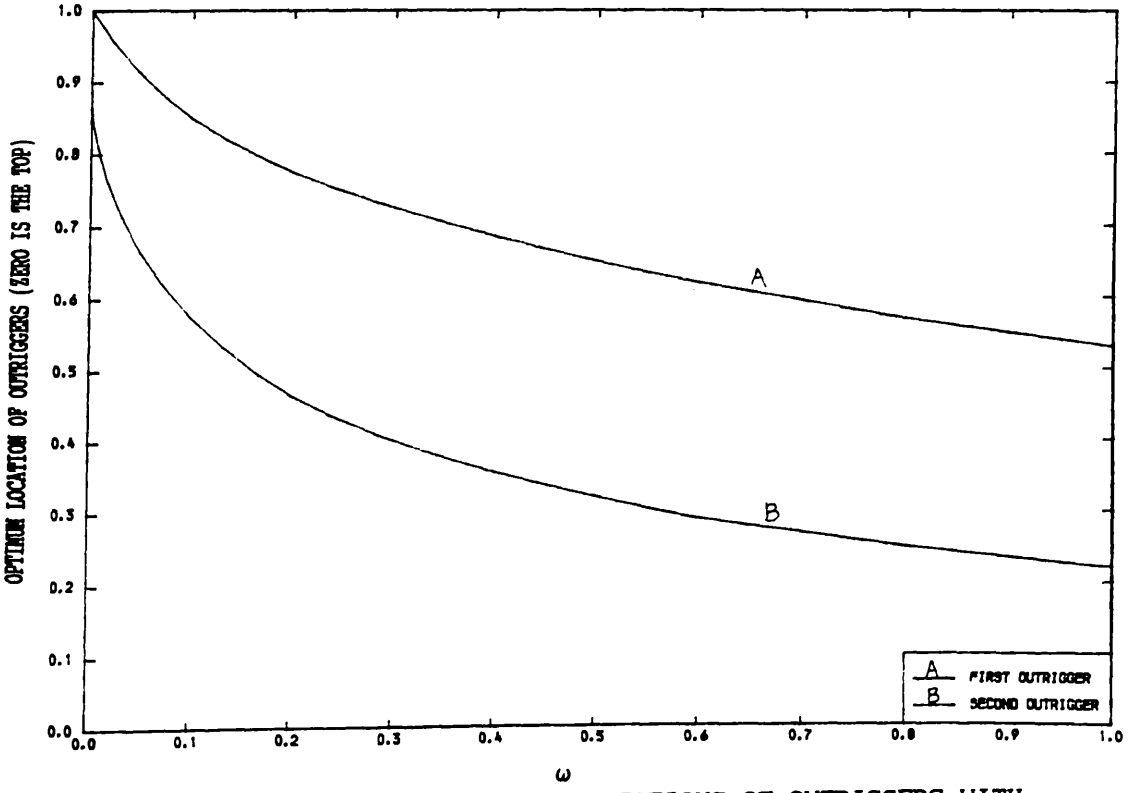

FIG. [2.35] VARIATION OF OPTIMUM LOCATIONS OF OUTRIGGERS WITH ω
(R=0, CASE OF TWO OUTRIGGERS, POINT LOAD AT THE TOP)
(MINIMISATION OF CORE MOMENT AT THE BASE)

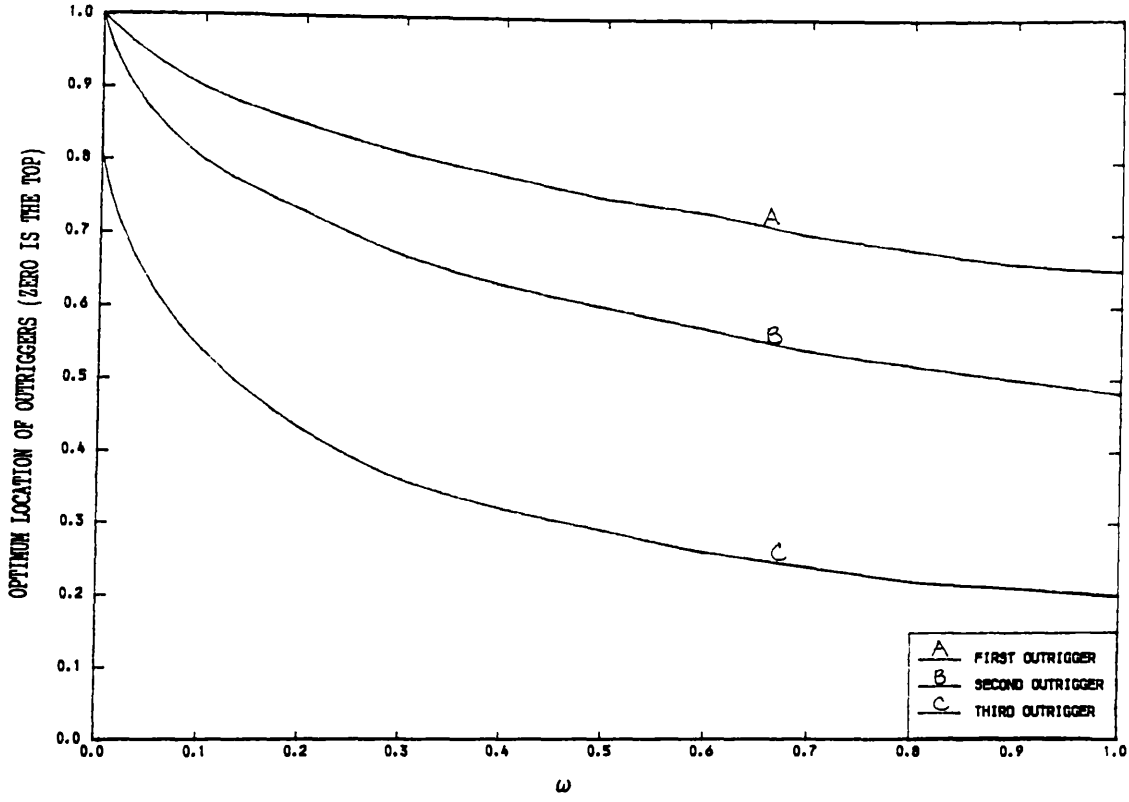

FIG.[2.36] VARIATION OF OPTIMUM LOCATIONS OF OUTRIGGERS WITH ω
(R=0, CASE OF THREE OUTRIGGERS, POINT LOAD AT THE TOP)
(MINIMISATION OF CORE MOMENT AT THE BASE)

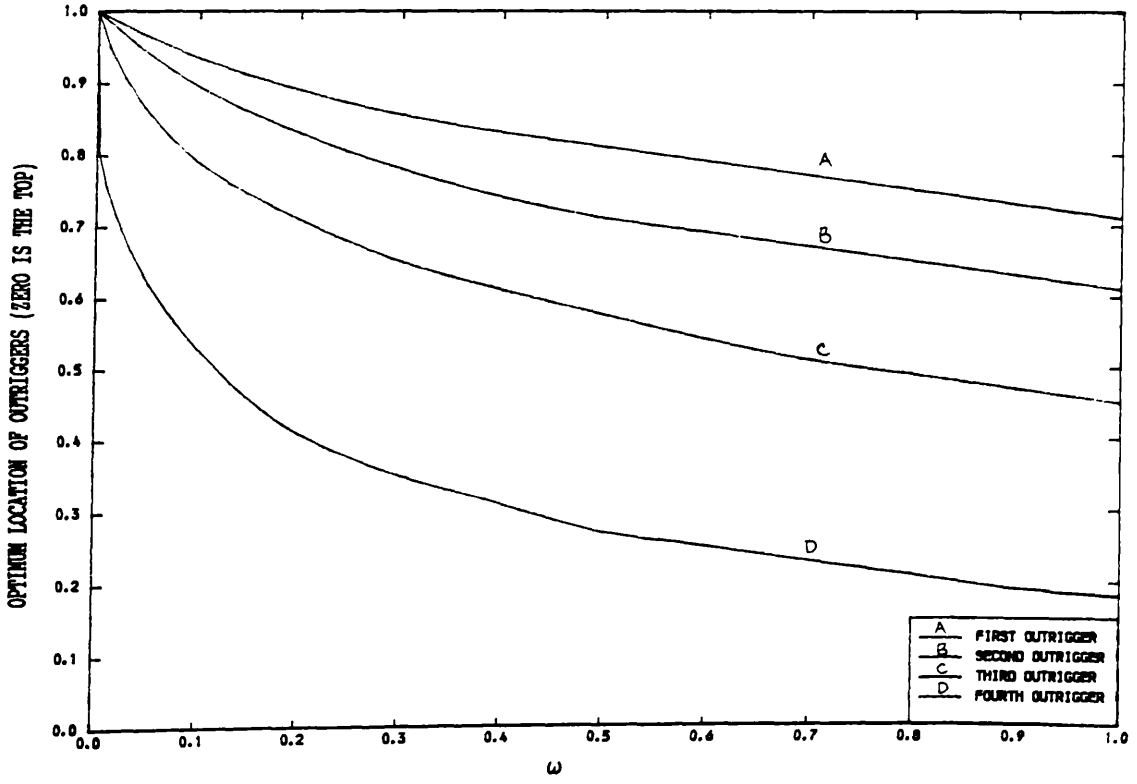

FIG.[2.37] VARIATION OF OPTIMUM LOCATIONS OF OUTRIGGERS WITH ω
(R=0, CASE OF FOUR OUTRIGGERS, POINT LOAD AT THE TOP)
(MINIMISATION OF CORE MOMENT AT THE BASE)

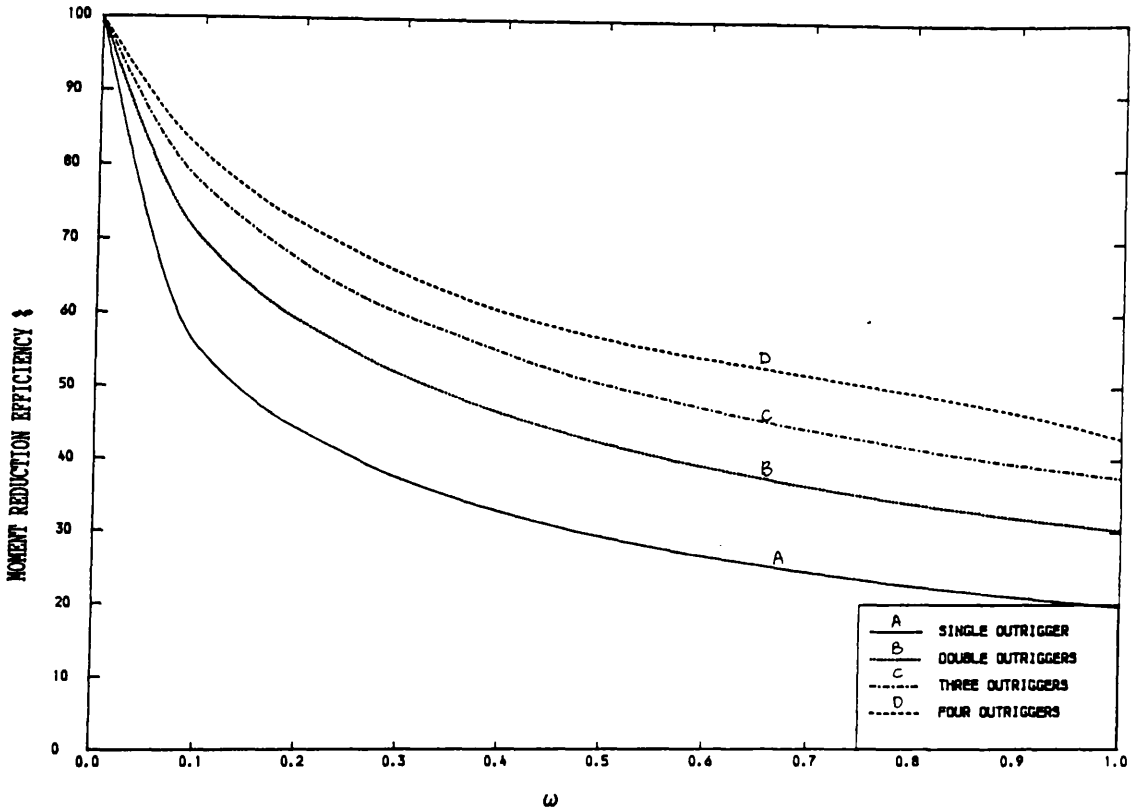

FIG. [2.38] VARIATION OF MOMENT REDUCTION EFFICIENCY WITH ω
(R=0, U.D.L.)
(MINIMISATION OF CORE MOMENT AT THE BASE)

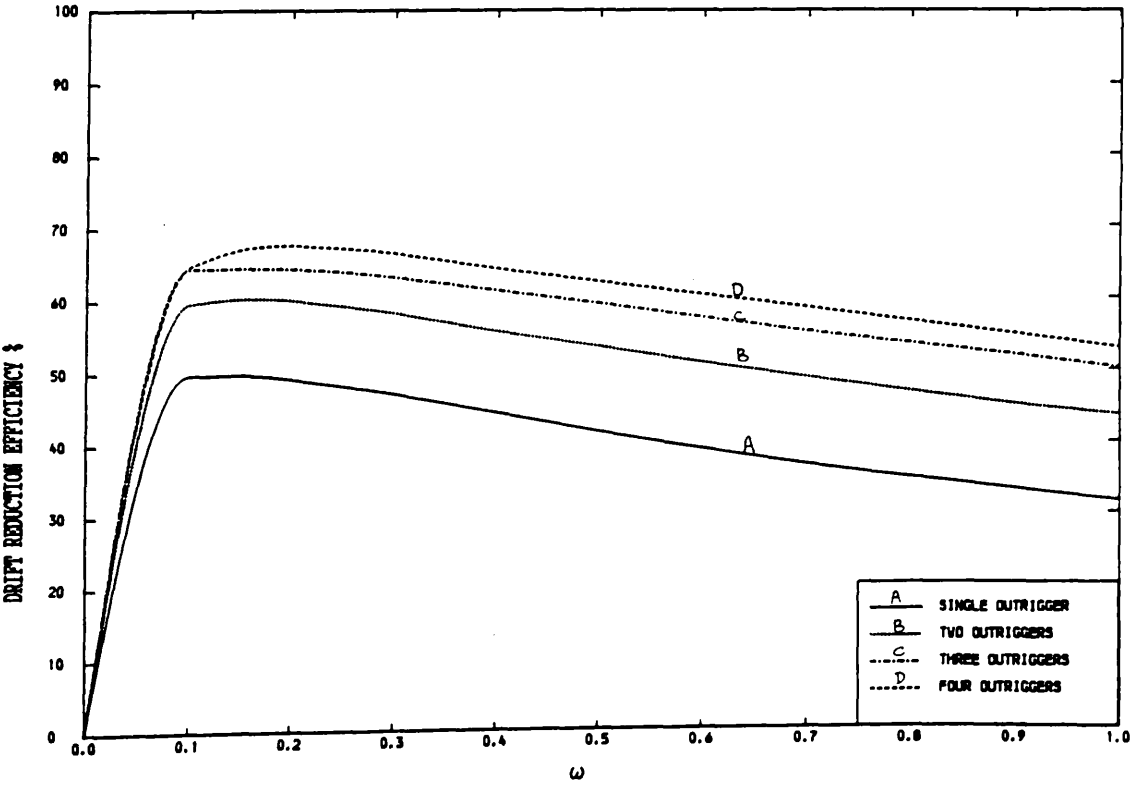

FIG. [2.39] VARIATION OF DRIFT REDUCTION EFFICIENCY WITH ω
(R=0, U.D.L.)
(MINIMISATION OF CORE MOMENT AT THE BASE)

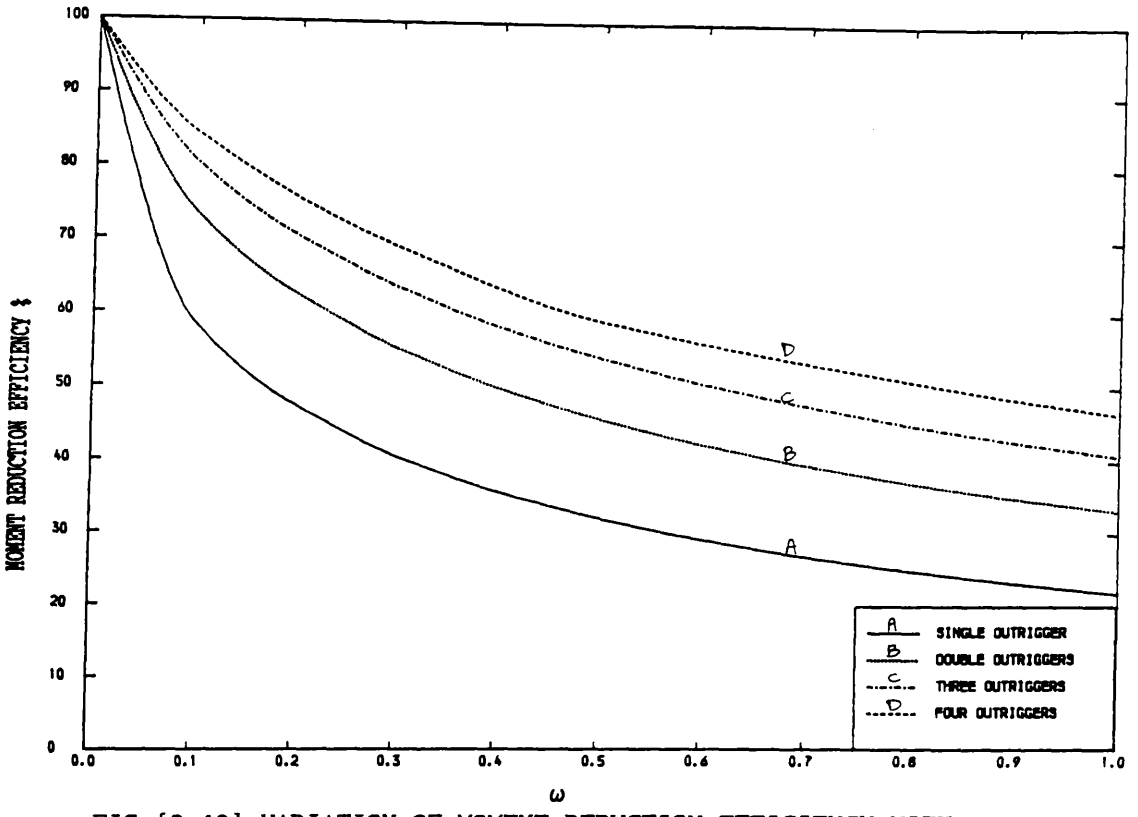

FIG.[2.40] VARIATION OF MOMENT REDUCTION EFFICIENCY WITH ω
(R=0, TRIANGULARLY DISTRIBUTED LOAD)
(MINIMISATION OF CORE MOMENT AT THE BASE)

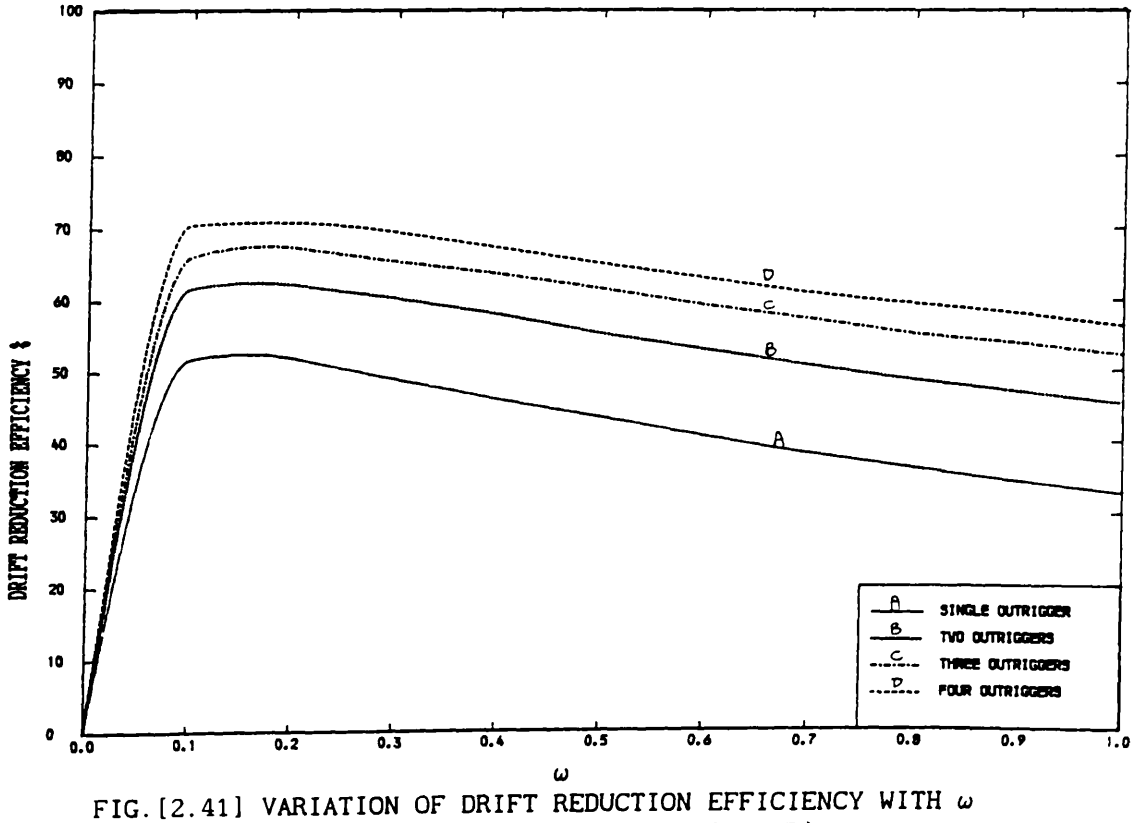

FIG.[2.41] VARIATION OF DRIFT REDUCTION EFFICIENCY WITH ω
(R=0, TRIANGULARLY DISTRIBUTED LOAD)
(MINIMISATION OF CORE MOMENT AT THE BASE)

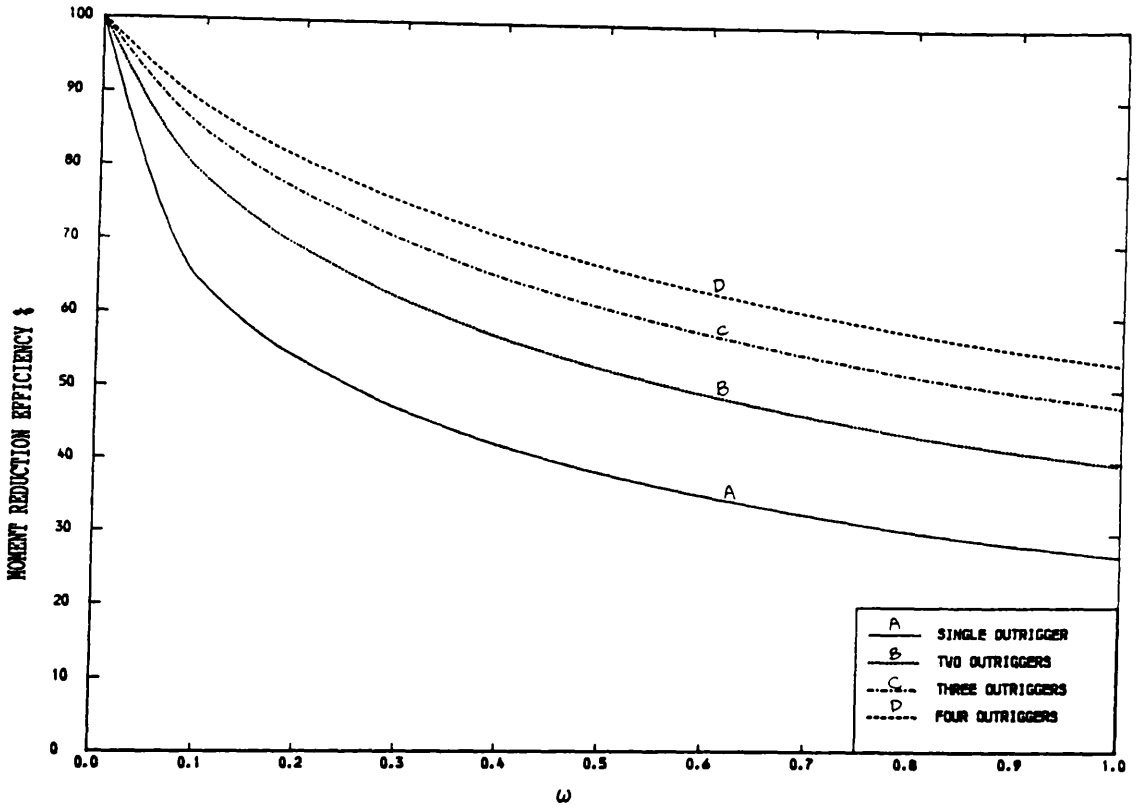

FIG. [2.42] VARIATION OF MOMENT REDUCTION EFFICIENCY WITH ω
(R=0, POINT LOAD AT THE TOP)
(MINIMISATION OF CORE MOMENT AT THE BASE)

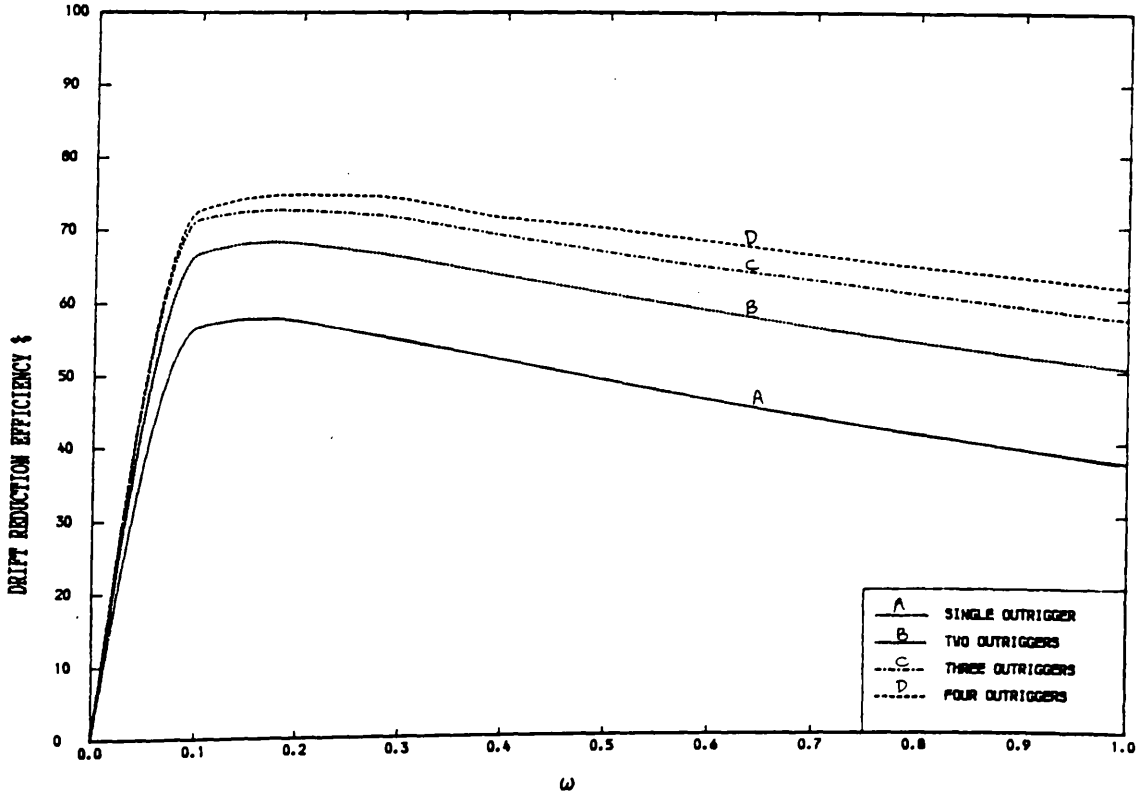

FIG. [2.43] VARIATION OF DRIFT REDUCTION EFFICIENCY WITH ω
(R=0, POINT LOAD AT THE TOP)
(MINIMISATION OF CORE MOMENT AT THE BASE)

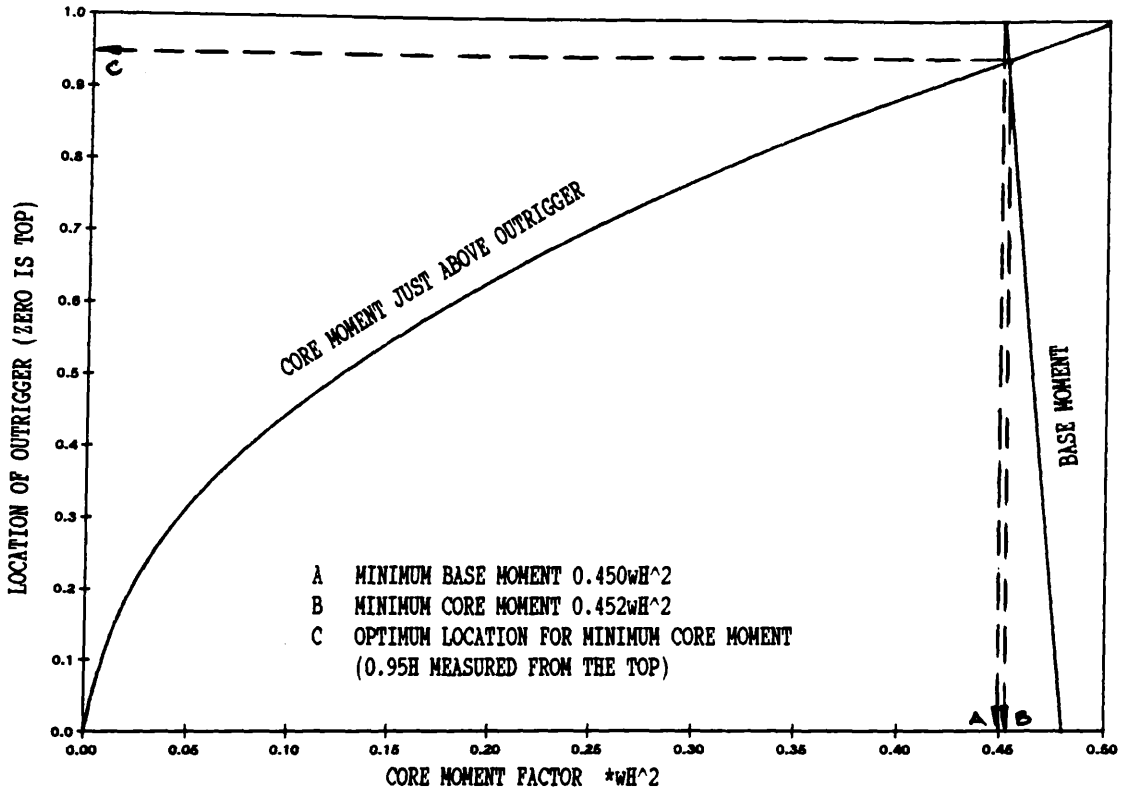

FIG.[2.44] VARIATION OF OUTRIGGER LOCATION WITH CORE MOMENT
(CASE OF ONE OUTRIGGER, U.D.L.)
(ω=0, 1/EIS=0.1, R=0)

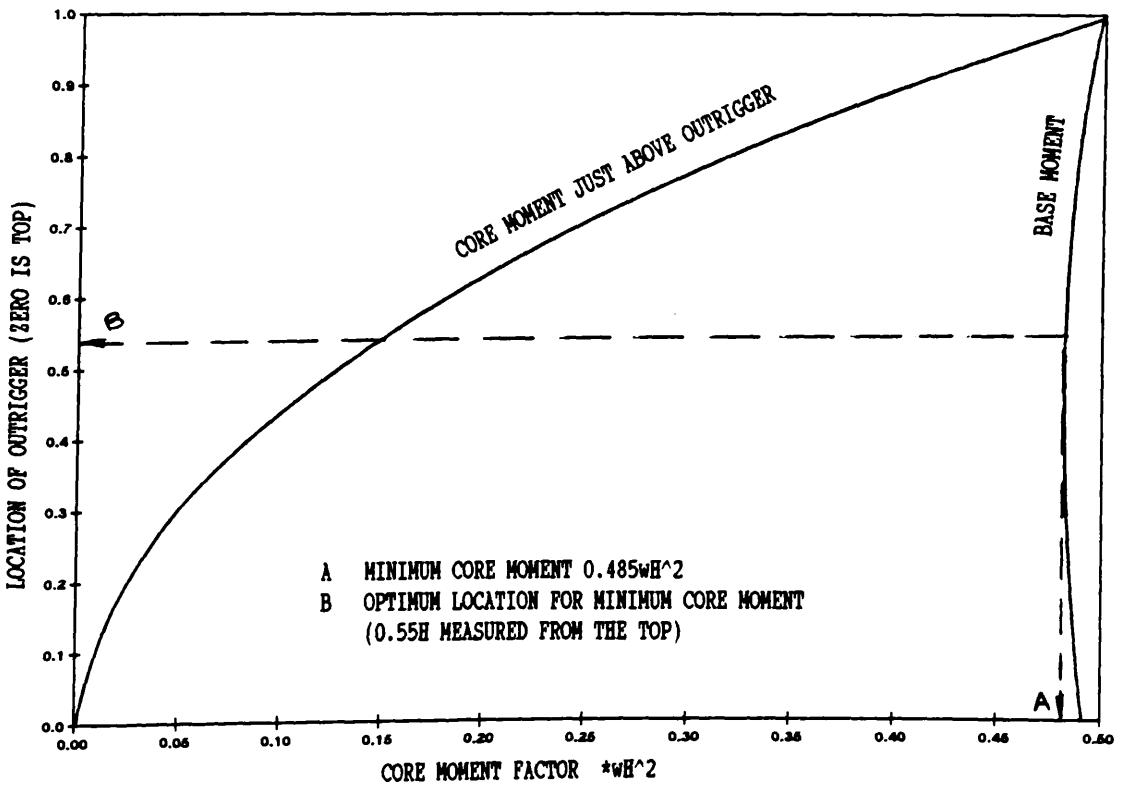

FIG.[2.45] VARIATION OF OUTRIGGER LOCATION WITH CORE MOMENT
(CASE OF ONE OUTRIGGER, U.D.L.)
(ω=0.5, 1/EIS=0.1, R=0)

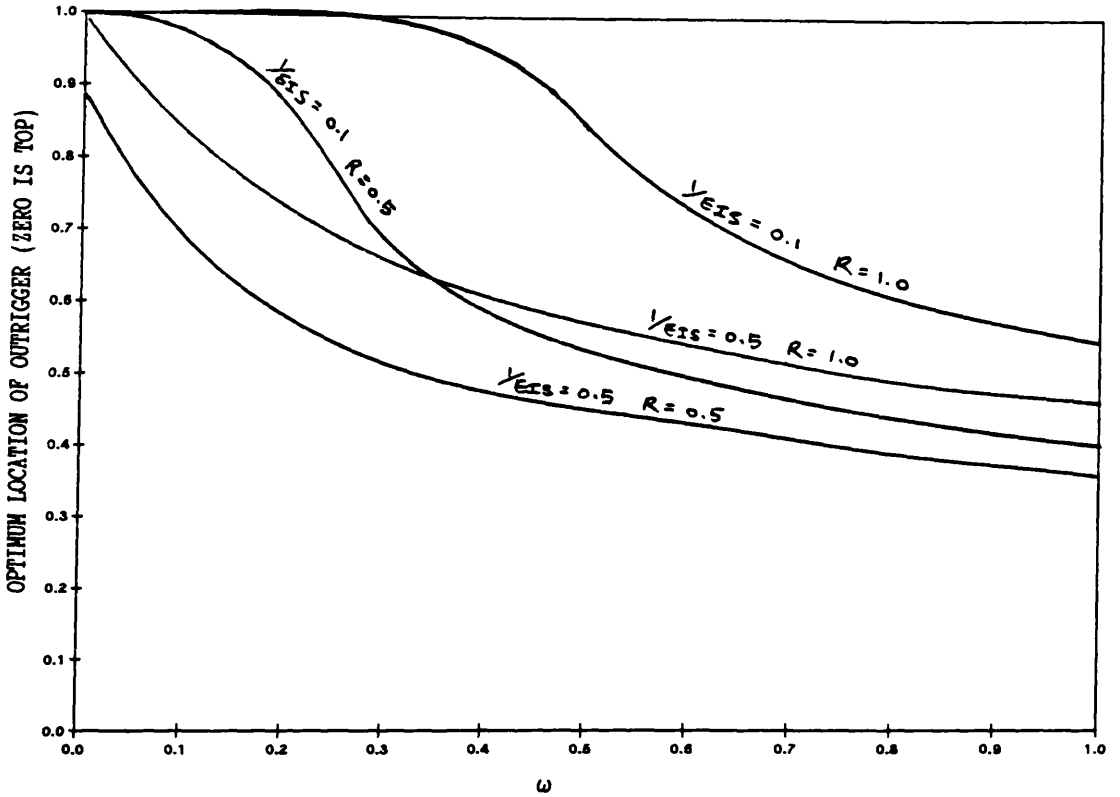

FIG. [2.46] VARIATION OF OPTIMUM LOCATION OF OUTRIGGER WITH ω
(CASE OF ONE OUTRIGGER, U.D.L.)
(MINIMISATION OF TOP DRIFT)

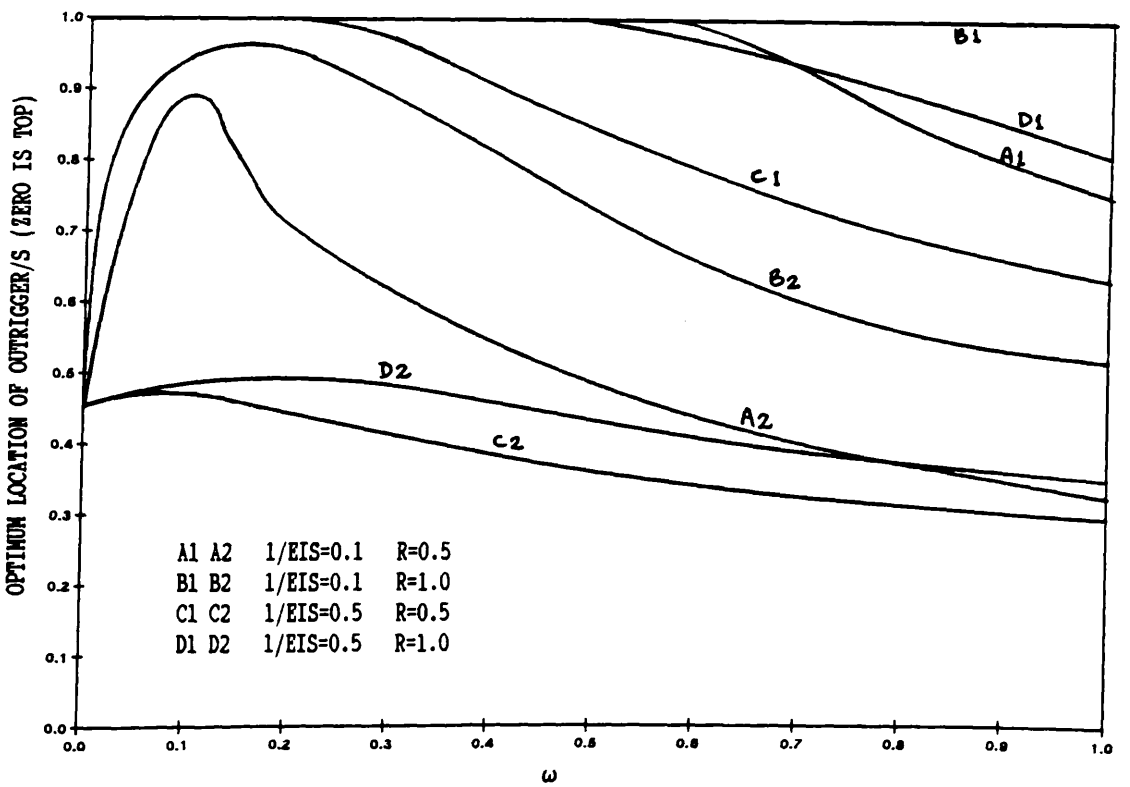

FIG. [2.47] VARIATION OF OPTIMUM LOCATIONS OF OUTRIGGERS WITH ω
(CASE OF TWO OUTRIGGERS, U.D.L.)
(MINIMISATION OF TOP DRIFT)

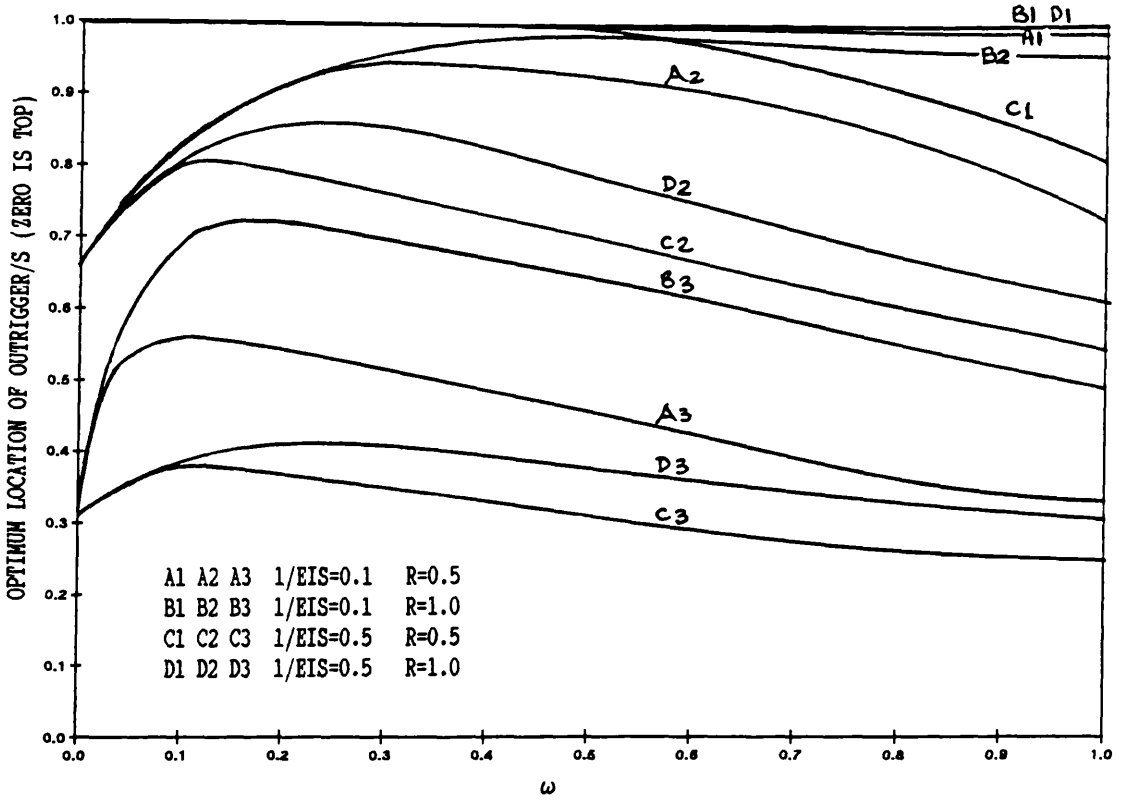

FIG.[2.48] VARIATION OF OPTIMUM LOCATIONS OF OUTRIGGERS WITH ω
(CASE OF THREE OUTRIGGERS, U.D.L.)
(MINIMISATION OF TOP DRIFT)

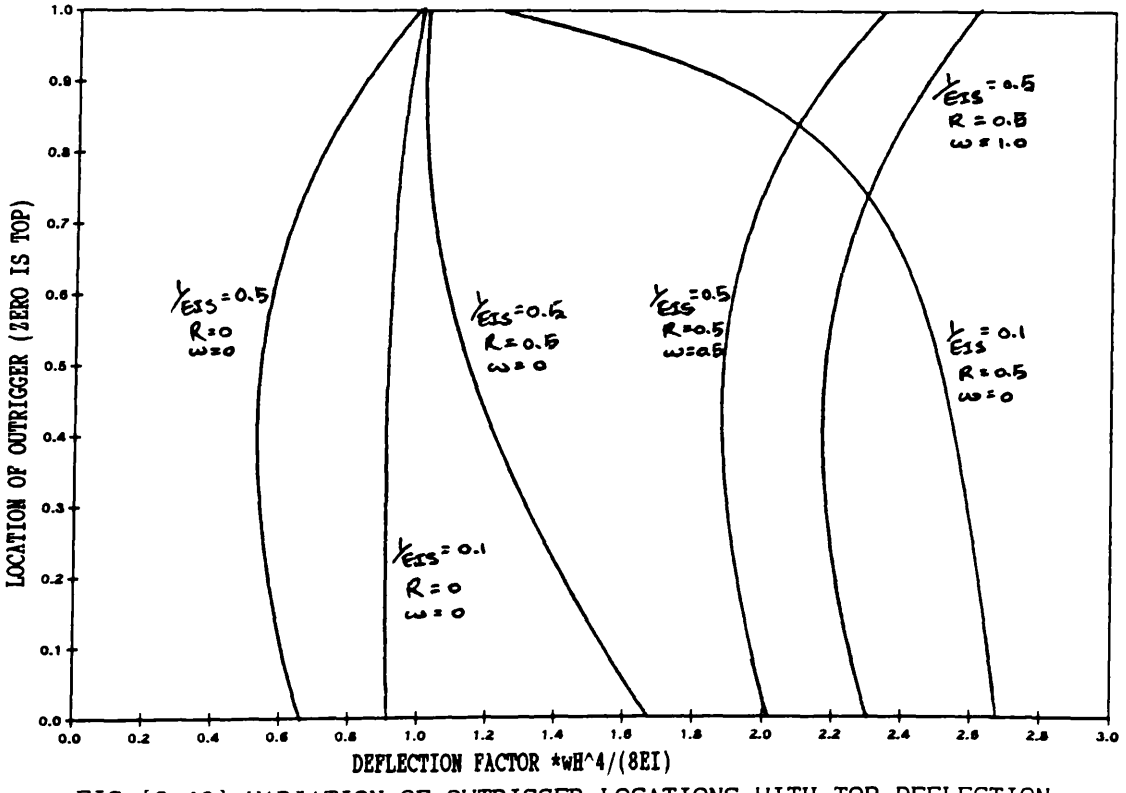

FIG.[2.49] VARIATION OF OUTRIGGER LOCATIONS WITH TOP DEFLECTION
(CASE OF ONE OUTRIGGERS, U.D.L.)

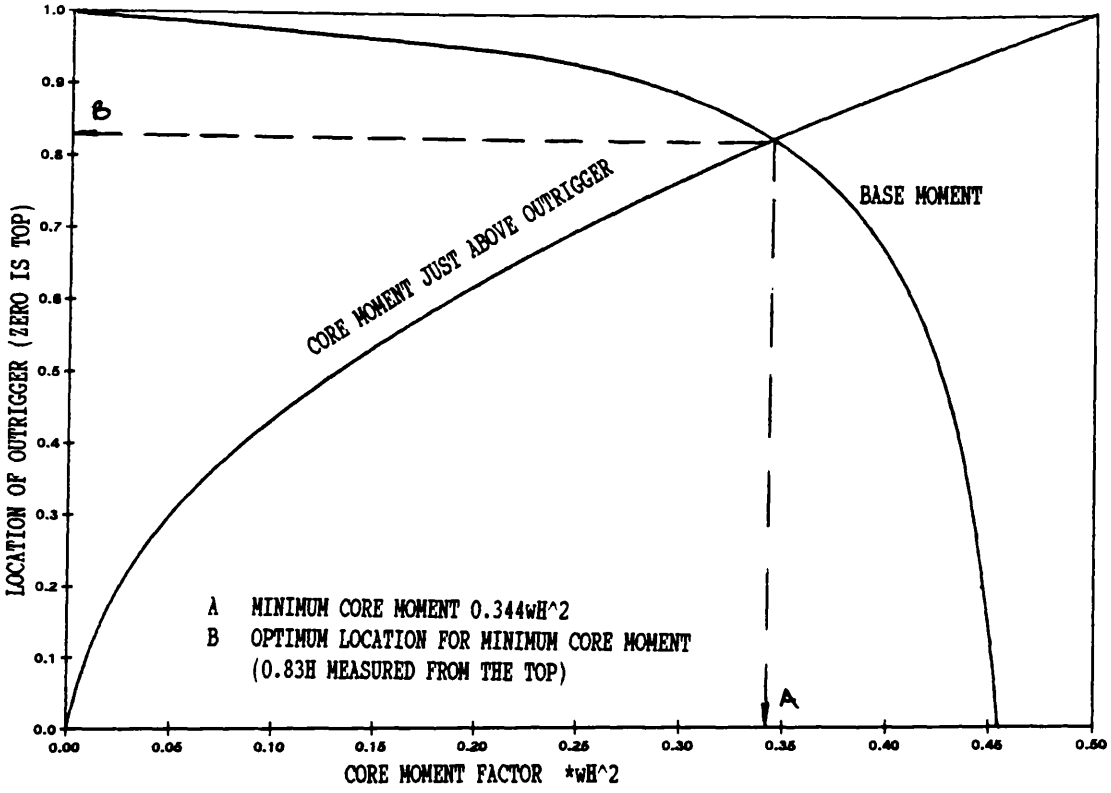

FIG.[2.50] VARIATION OF OUTRIGGER LOCATION WITH CORE MOMENT
(CASE OF ONE OUTRIGGER, U.D.L.)
(ω=0, 1/EIS=0.1, R=0.5)

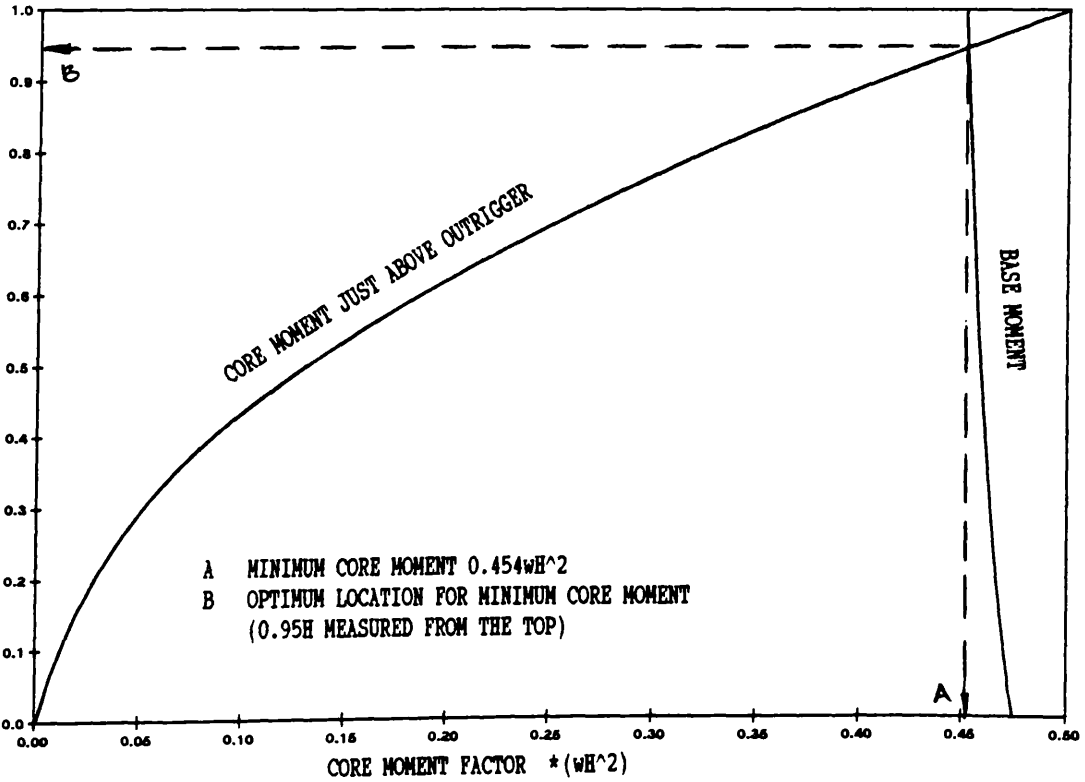

FIG.[2.51] VARIATION OF OUTRIGGER LOCATION WITH CORE MOMENT
(CASE OF ONE OUTRIGGER, U.D.L.)
(ω=0.5, 1/EIS=0.1, R=0.5)

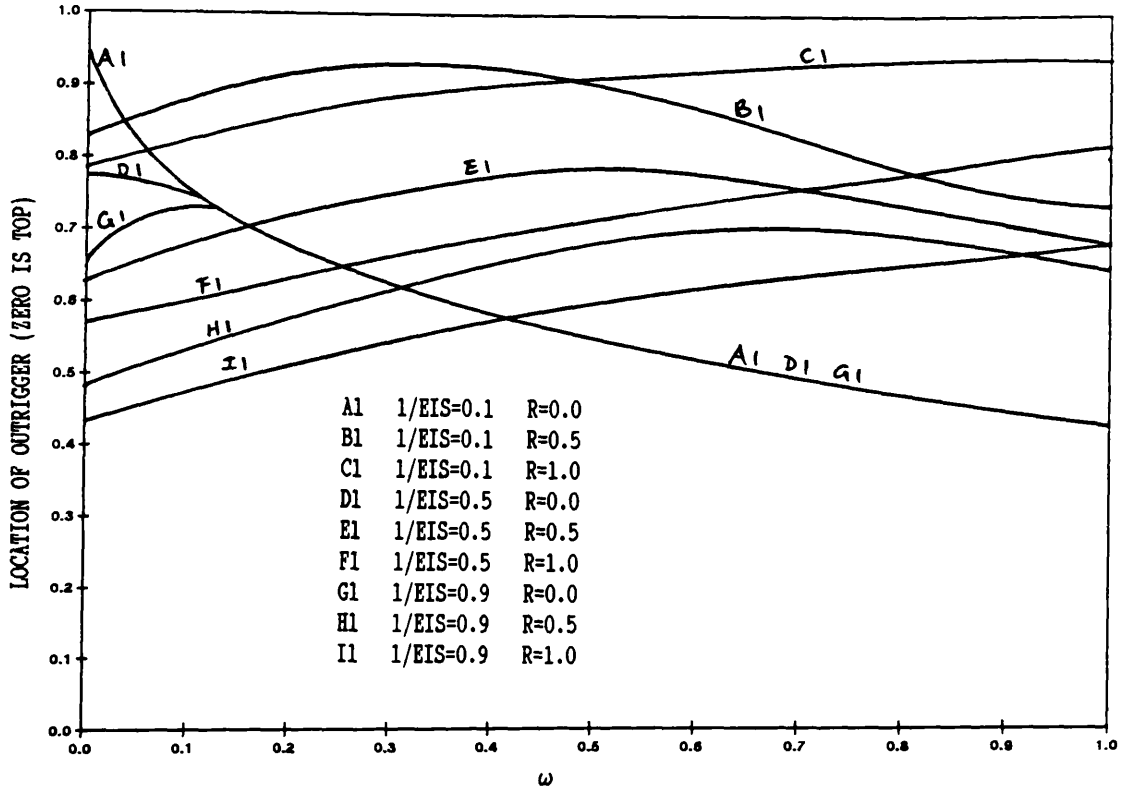

FIG. [2.52] VARIATION OF OPTIMUM LOCATION OF OUTRIGGER WITH ω
(CASE OF ONE OUTRIGGERS, U.D.L.)
(MINIMISATION OF CORE MOMENT AT THE BASE)

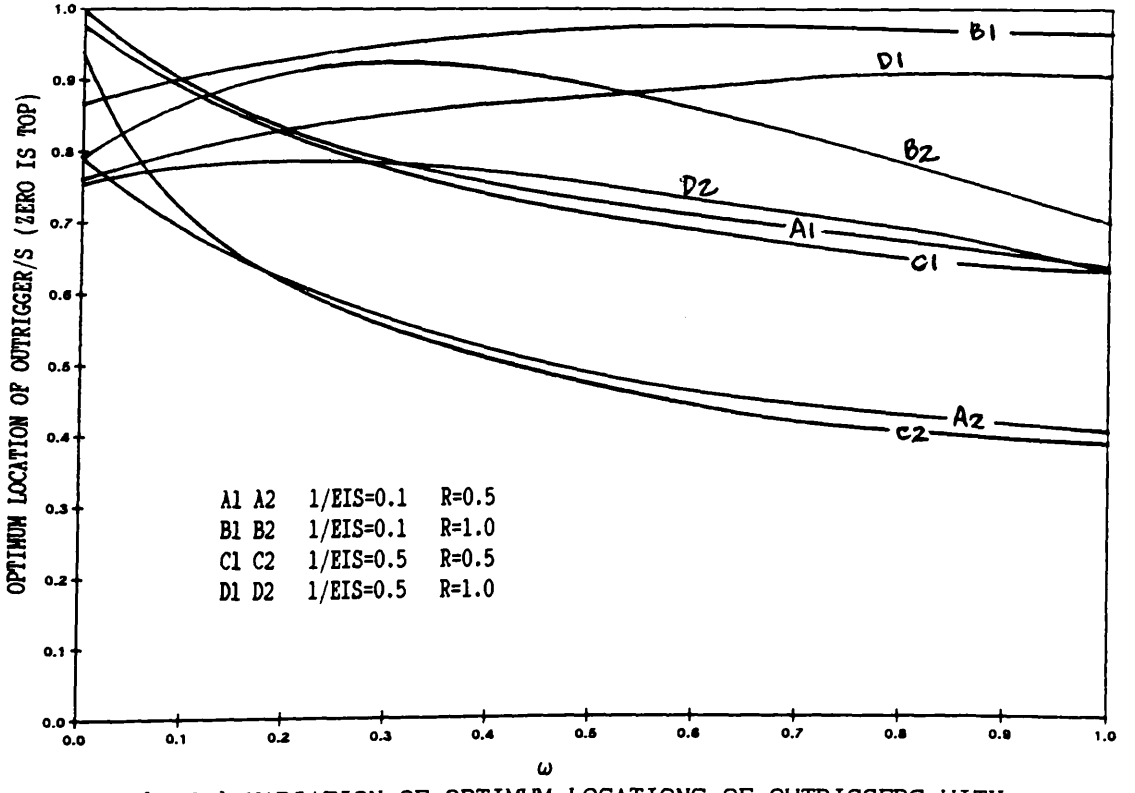

FIG. [2.53] VARIATION OF OPTIMUM LOCATIONS OF OUTRIGGERS WITH ω
(CASE OF TWO OUTRIGGERS, U.D.L.)
(MINIMISATION OF CORE MOMENT AT THE BASE)

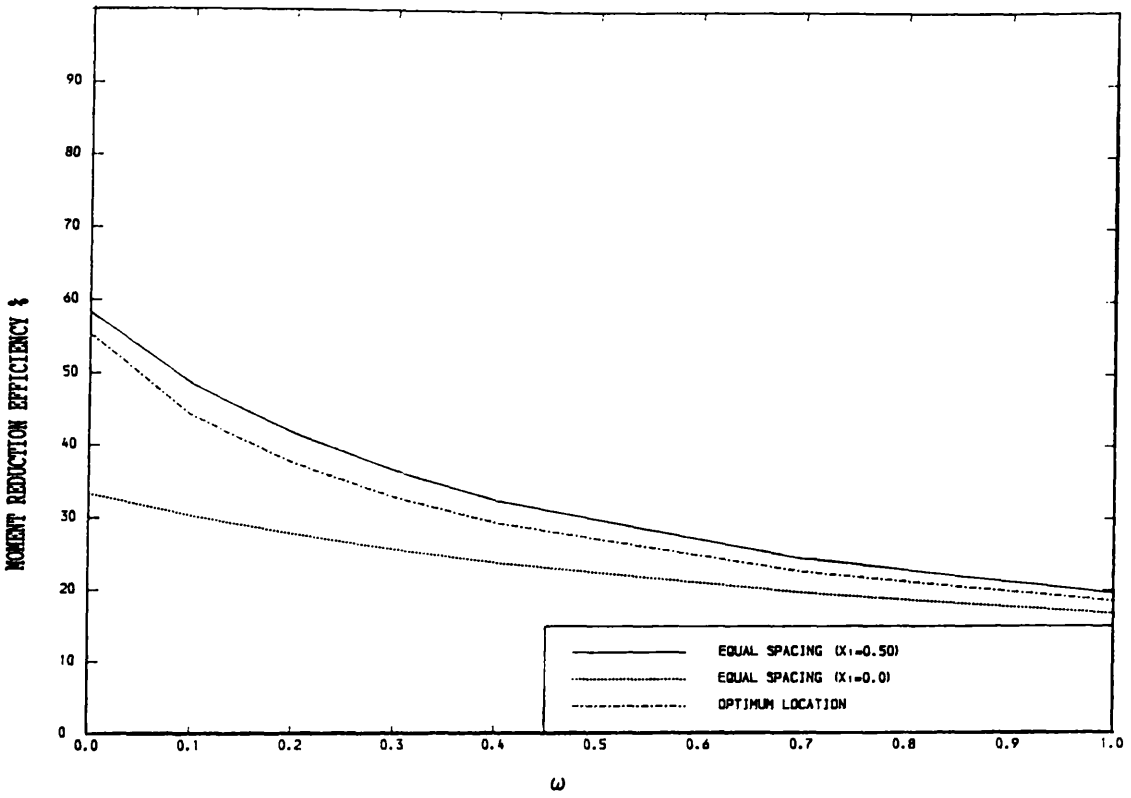

FIG. [2.54] VARIATION OF MOMENT REDUCTION EFFICIENCY WITH ω
(R=0, CASE OF ONE OUTRIGGER, U.D.L.)

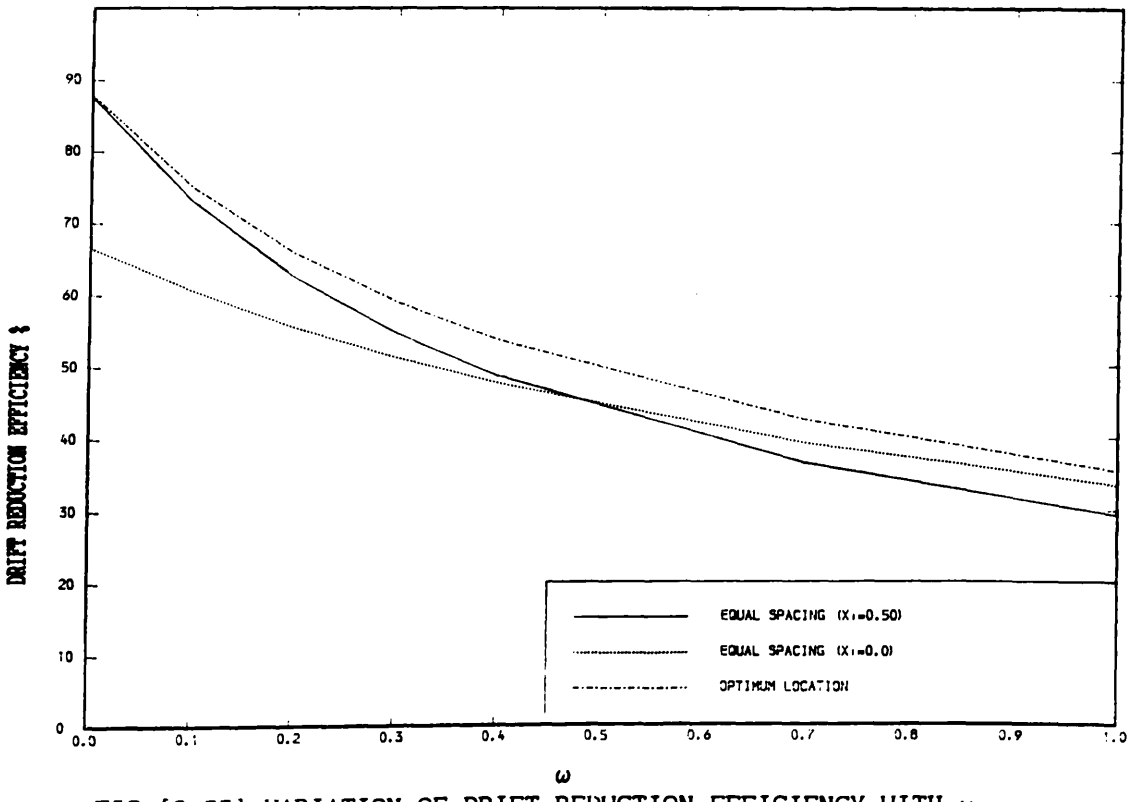

FIG. [2.55] VARIATION OF DRIFT REDUCTION EFFICIENCY WITH ω
(R=0, CASE OF ONE OUTRIGGER, U.D.L.)

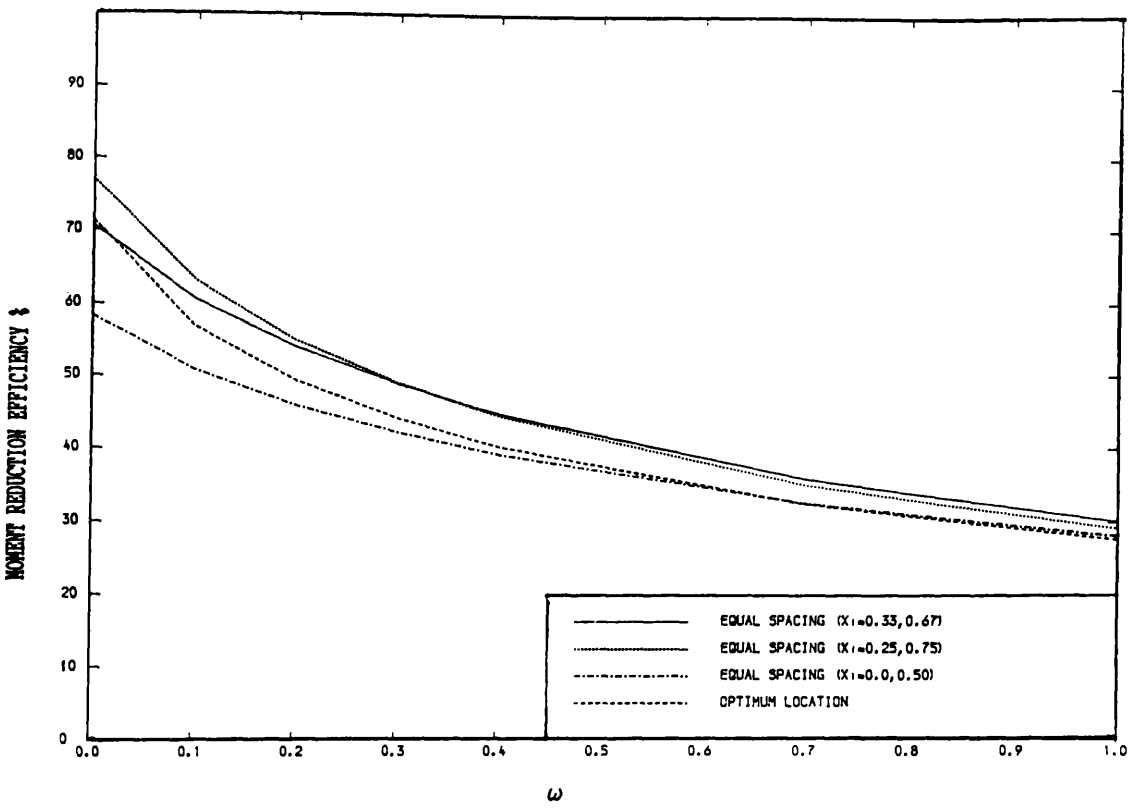

FIG.[2.56] VARIATION OF MOMENT REDUCTION EFFICIENCY WITH ω
(R=0, CASE OF TWO OUTRIGGERS, U.D.L.)

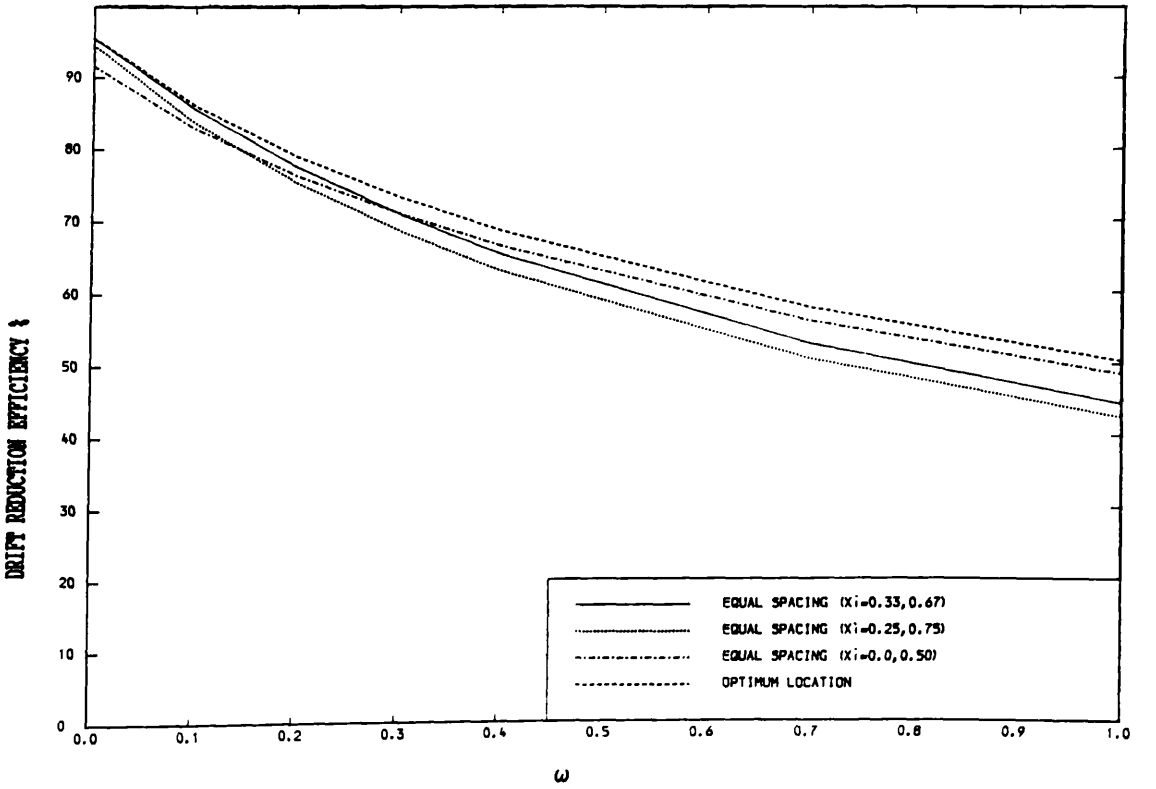

FIG.[2.57] VARIATION OF DRIFT REDUCTION EFFICIENCY WITH ω
(R=0, CASE OF TWO OUTRIGGERS, U.D.L.)

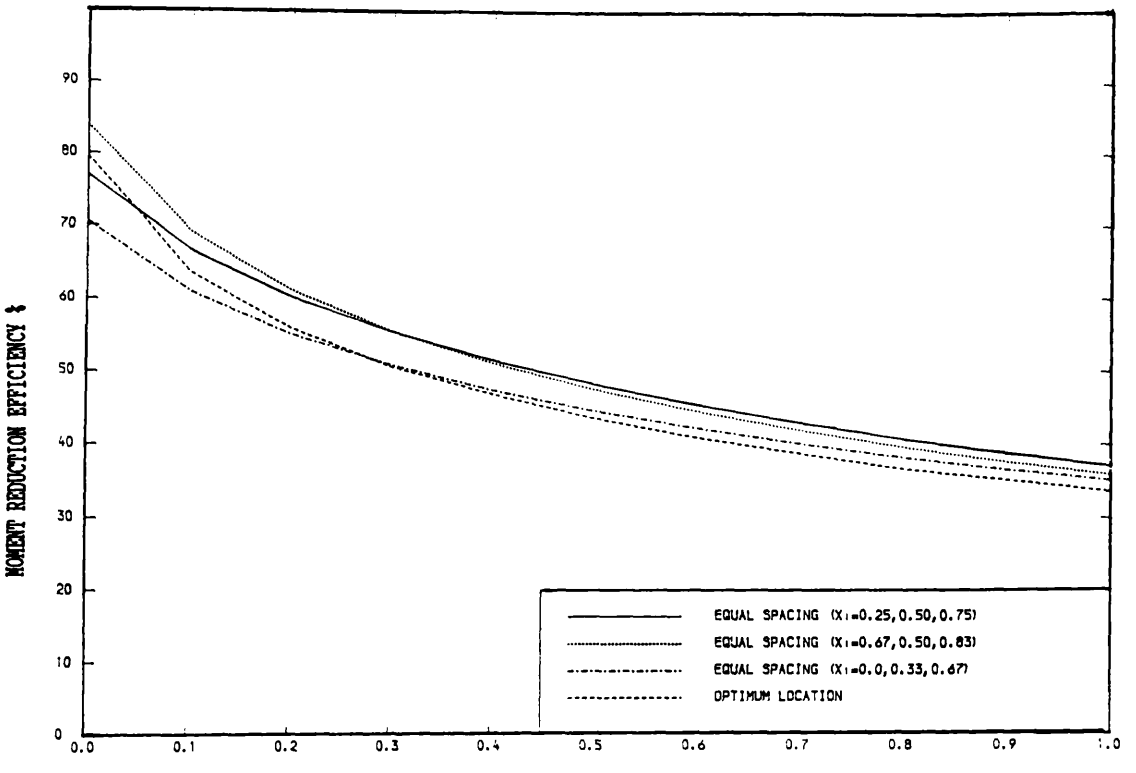

FIG.[2.58] VARIATION OF MOMENT REDUCTION EFFICIENCY WITH ω
(R=0, CASE OF THREE OUTRIGGERS, U.D.L.)

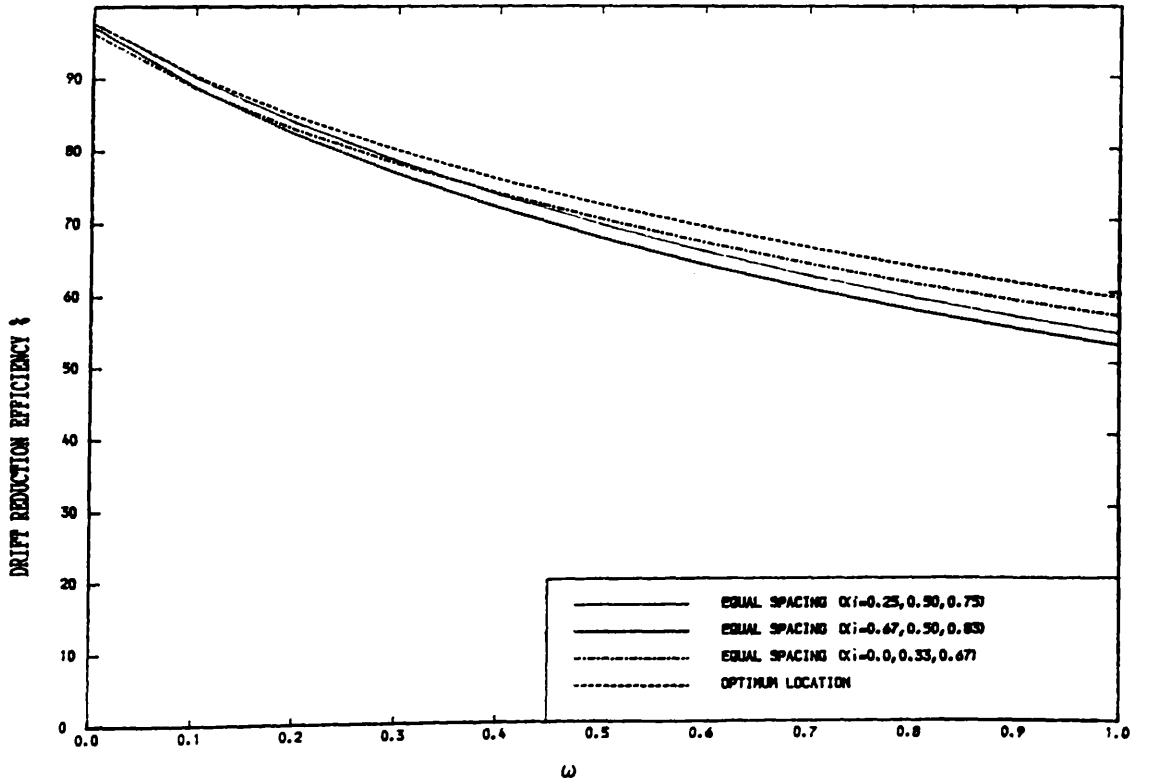

FIG.[2.59] VARIATION OF DRIFT REDUCTION EFFICIENCY WITH ω
(R=0, CASE OF THREE OUTRIGGERS, U.D.L.)

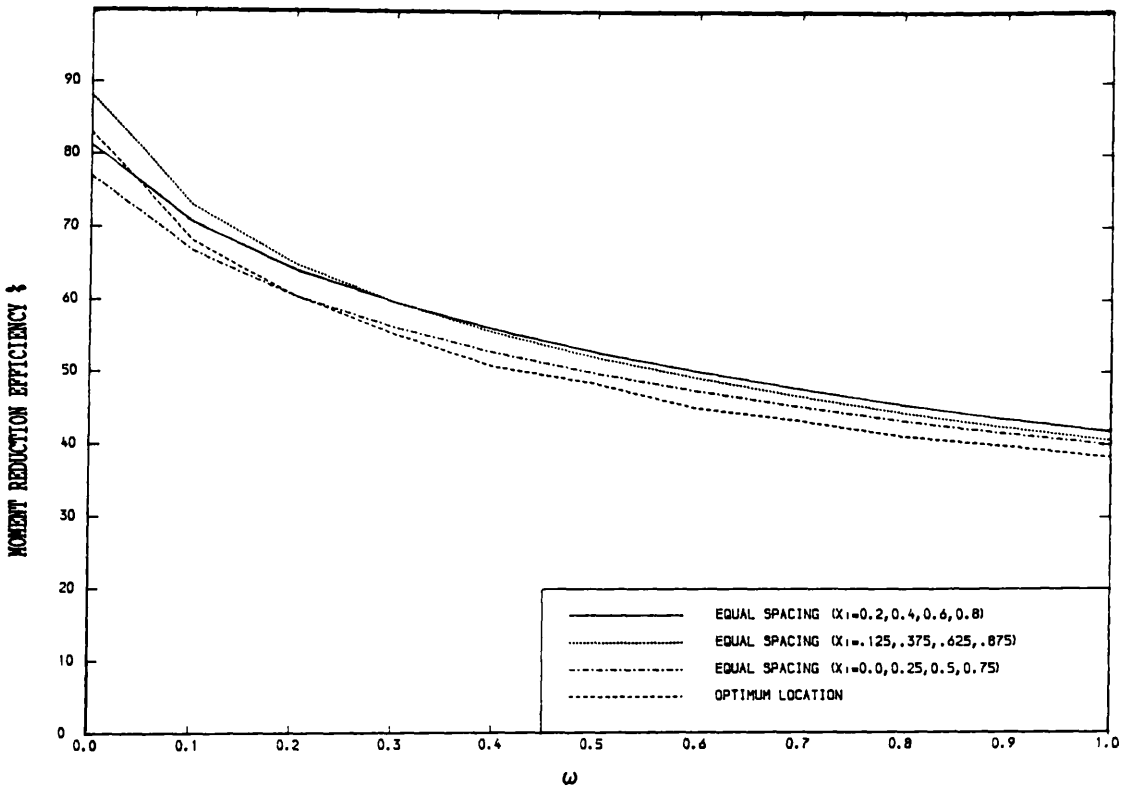

FIG.[2.60] VARIATION OF MOMENT REDUCTION EFFICIENCY WITH ω
(R=0, CASE OF FOUR OUTRIGGERS, U.D.L.)

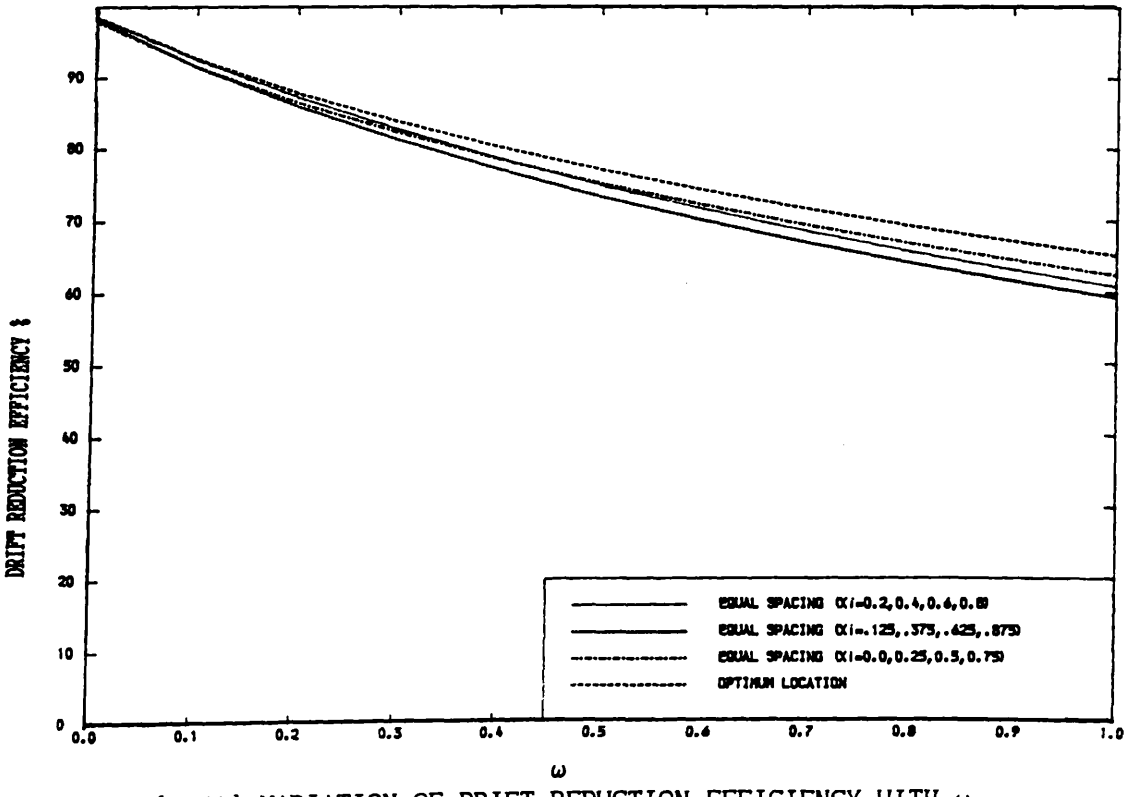

FIG.[2.61] VARIATION OF DRIFT REDUCTION EFFICIENCY WITH ω
(R=0, CASE OF FOUR OUTRIGGERS, U.D.L.)

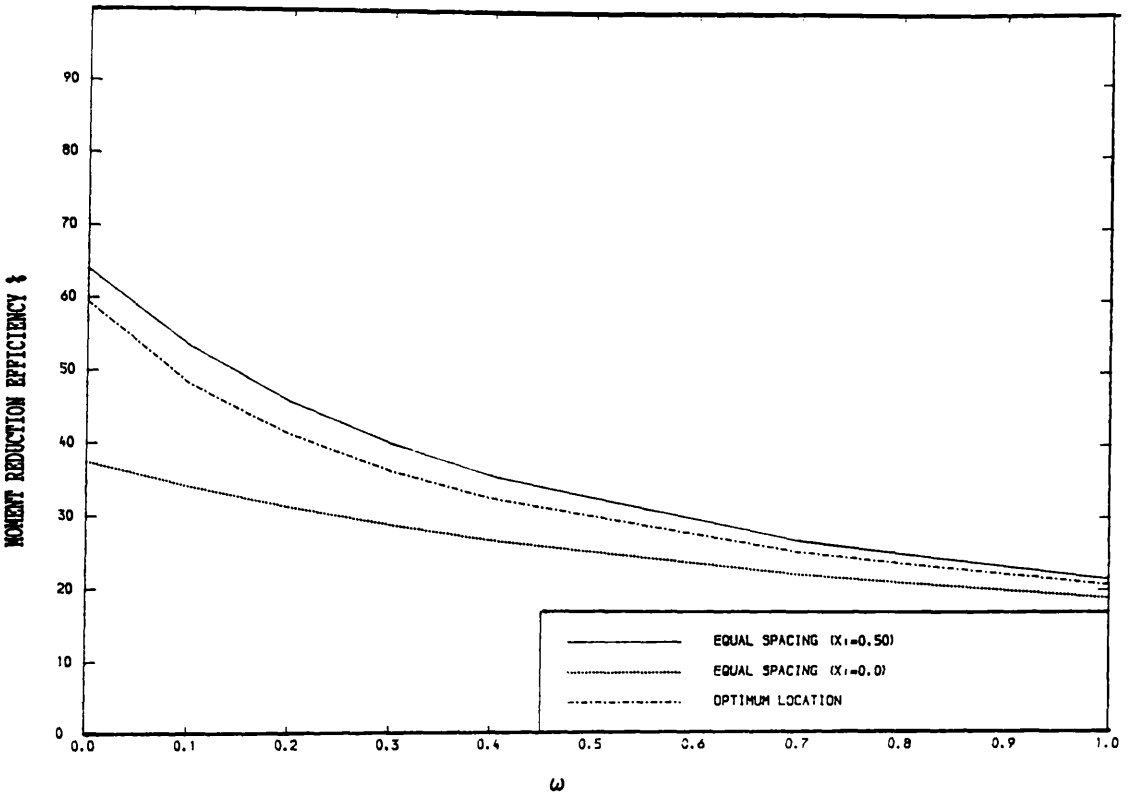

FIG. [2.62] VARIATION OF MOMENT REDUCTION EFFICIENCY WITH ω
(R=0, CASE OF ONE OUTRIGGER)
(POINT LOAD AT THE TOP)

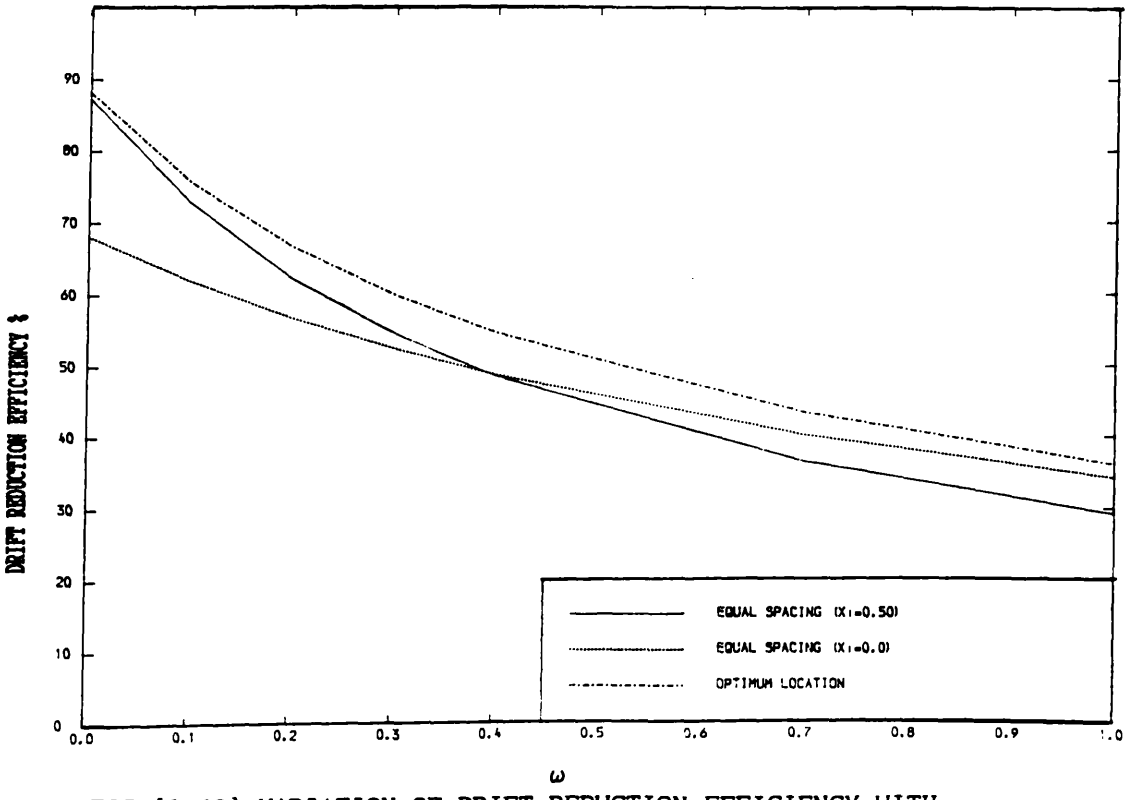

FIG. [2.63] VARIATION OF DRIFT REDUCTION EFFICIENCY WITH ω
(R=0, CASE OF ONE OUTRIGGER)
(POINT LOAD AT THE TOP)

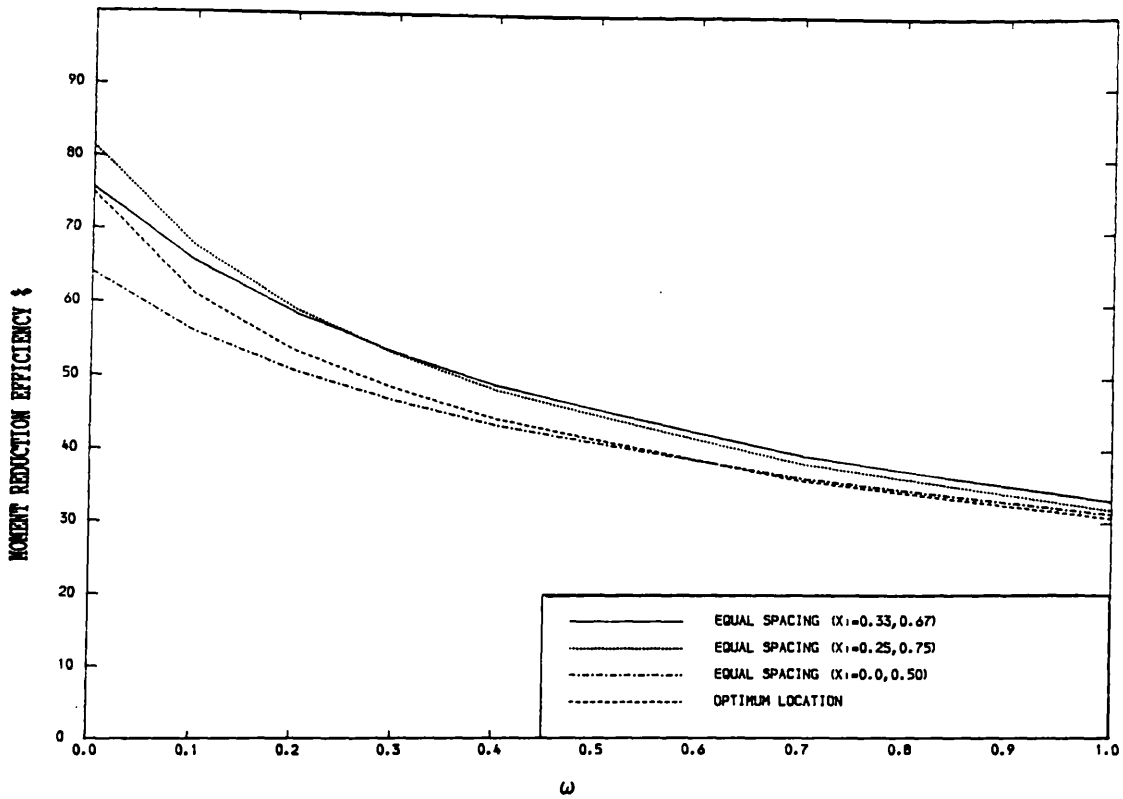

FIG.[2.64] VARIATION OF MOMENT REDUCTION EFFICIENCY WITH ω
(R=0, CASE OF TWO OUTRIGGERS)
(TRIANGULARLY DISTRIBUTED LOAD)

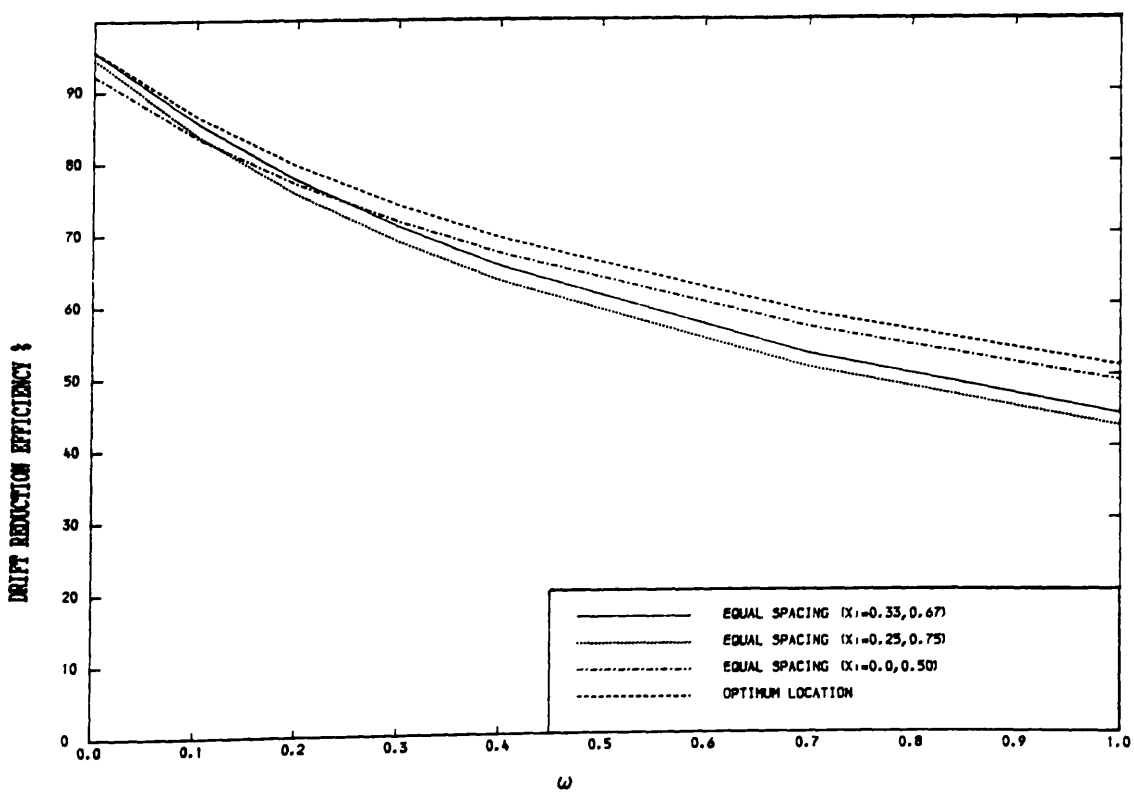

FIG.[2.65] VARIATION OF DRIFT REDUCTION EFFICIENCY WITH ω
(R=0, CASE OF TWO OUTRIGGERS)
(TRIANGULARLY DISTRIBUTED LOAD)

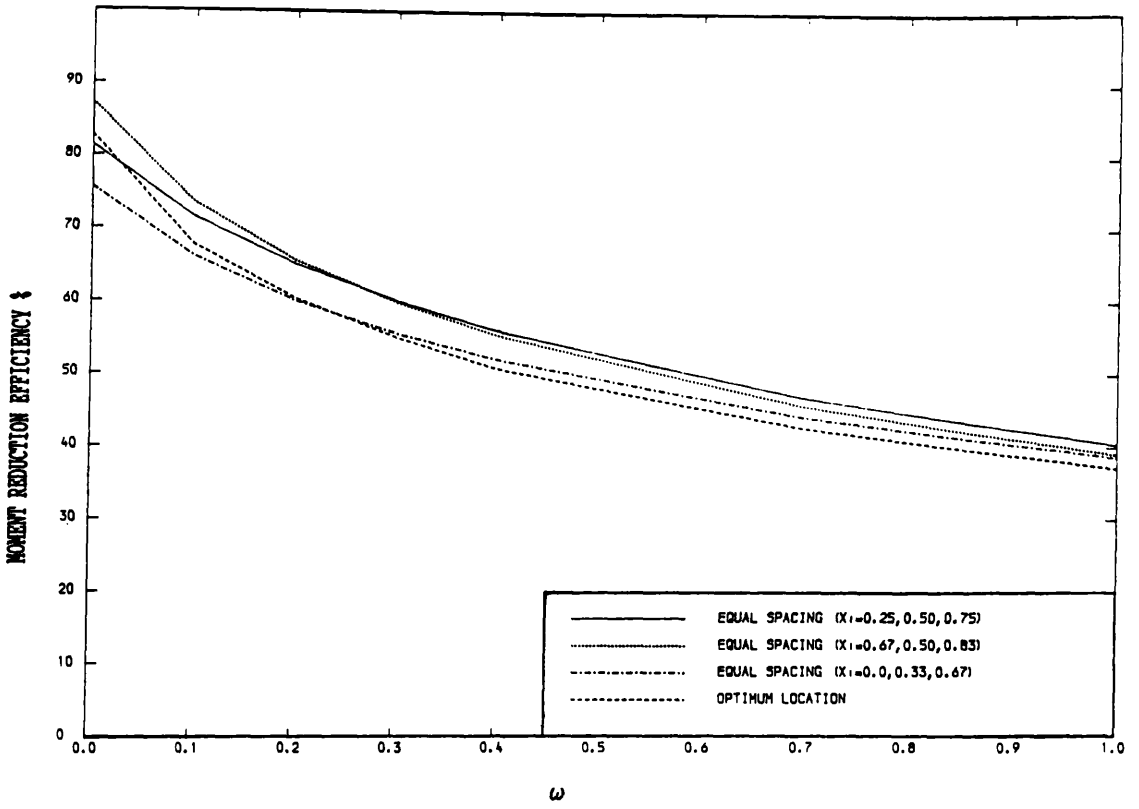

FIG. [2.66] VARIATION OF MOMENT REDUCTION EFFICIENCY WITH ω
(R=0, CASE OF THREE OUTRIGGERS)
(TRIANGULARLY DISTRIBUTED LOAD)

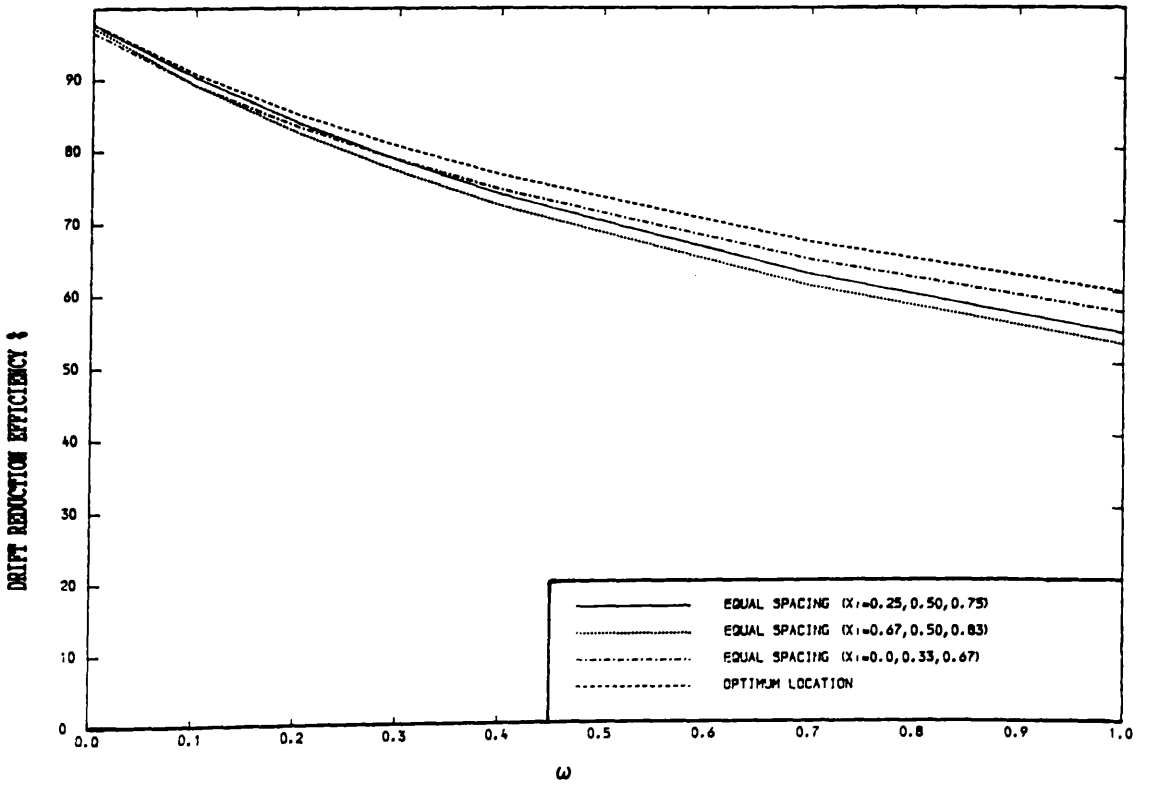

FIG. [2.67] VARIATION OF DRIFT REDUCTION EFFICIENCY WITH ω
(R=0, CASE OF THREE OUTRIGGERS)
(TRIANGULARLY DISTRIBUTED LOAD)

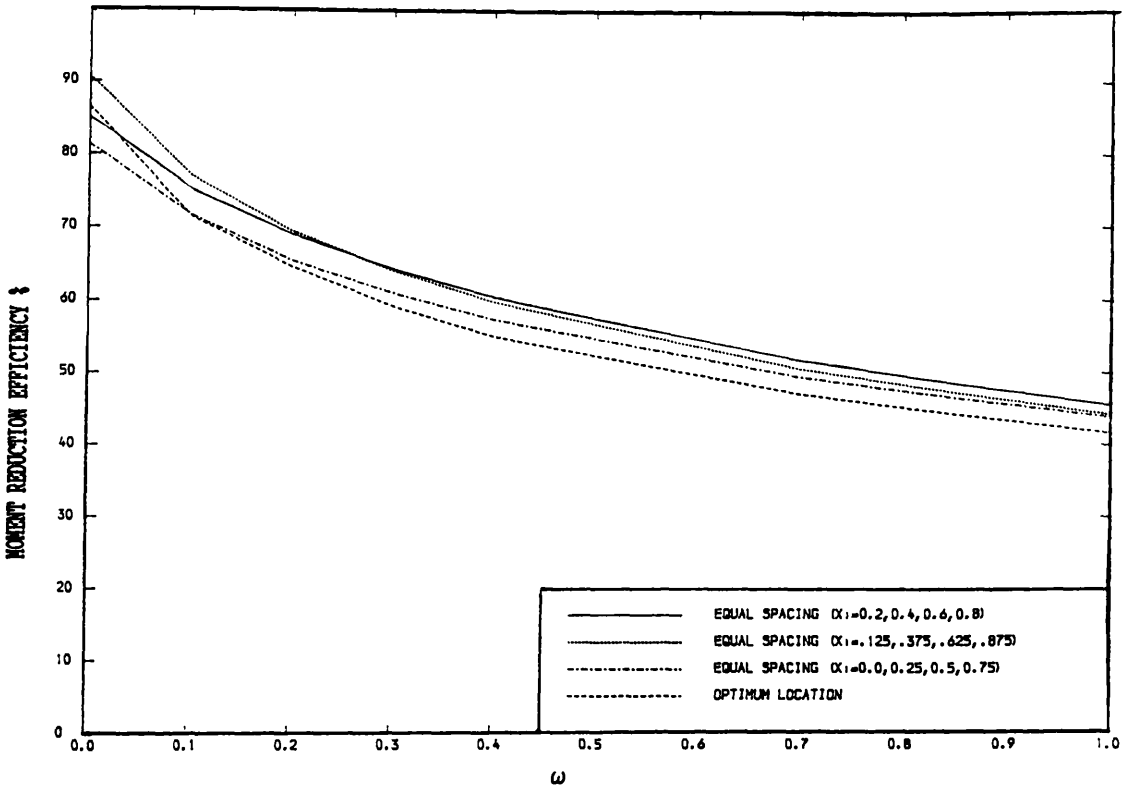

FIG. [2.68] VARIATION OF MOMENT REDUCTION EFFICIENCY WITH ω
(R=0, CASE OF FOUR OUTRIGGERS)
(TRIANGULARLY DISTRIBUTED LOAD)

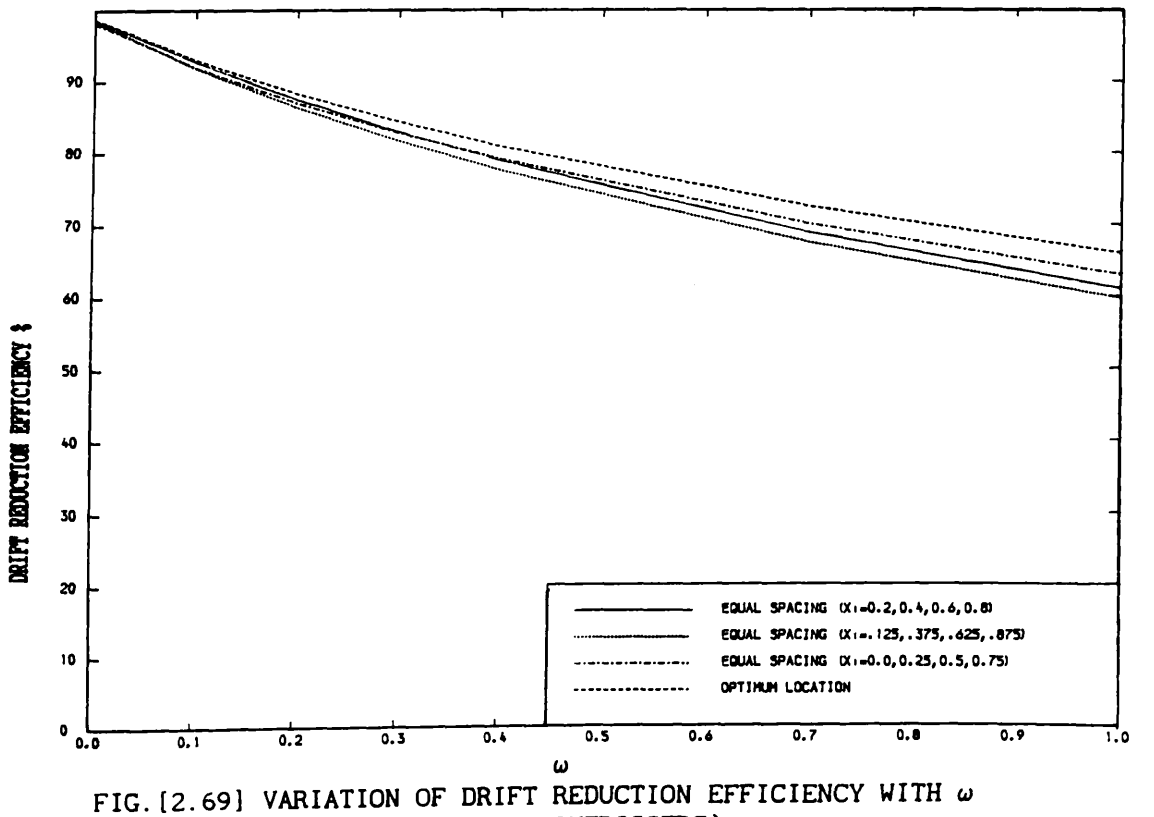

FIG. [2.69] VARIATION OF DRIFT REDUCTION EFFICIENCY WITH ω
(R=0, CASE OF FOUR OUTRIGGERS)
(TRIANGULARLY DISTRIBUTED LOAD)

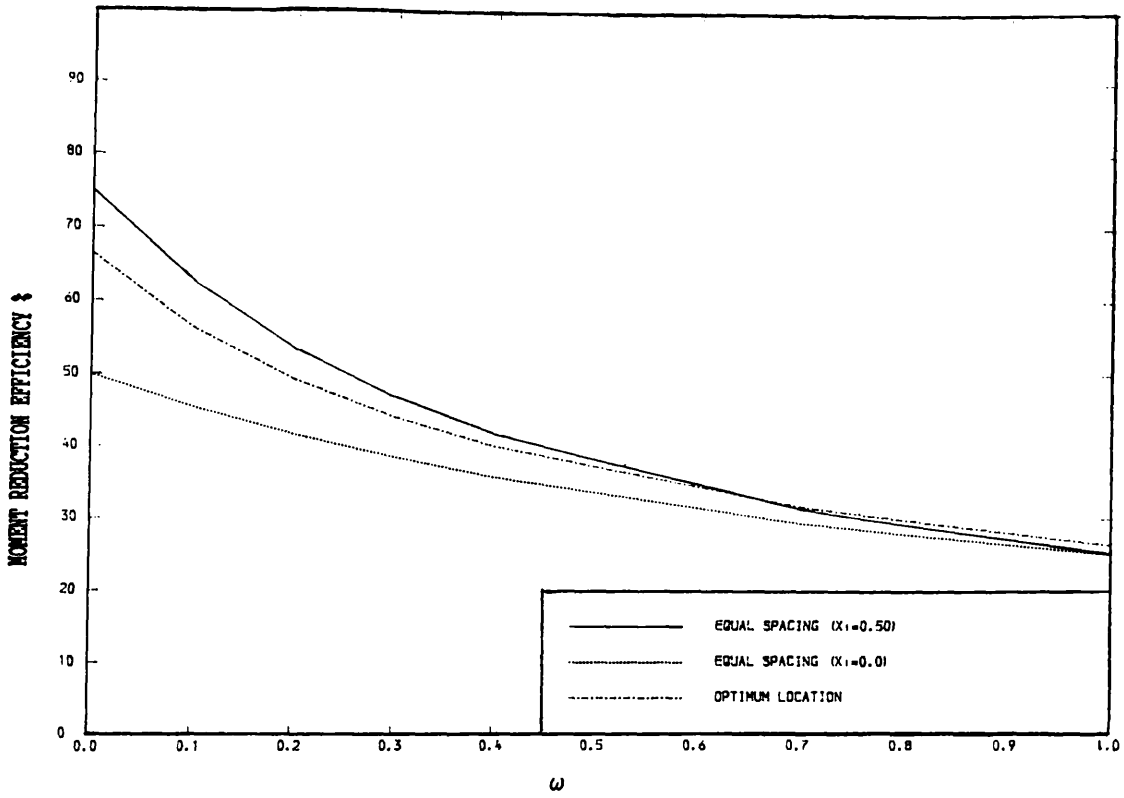

FIG. [2.70] VARIATION OF MOMENT REDUCTION EFFICIENCY WITH ω
(R=0, CASE OF ONE OUTRIGGER)
(POINT LOAD AT THE TOP)

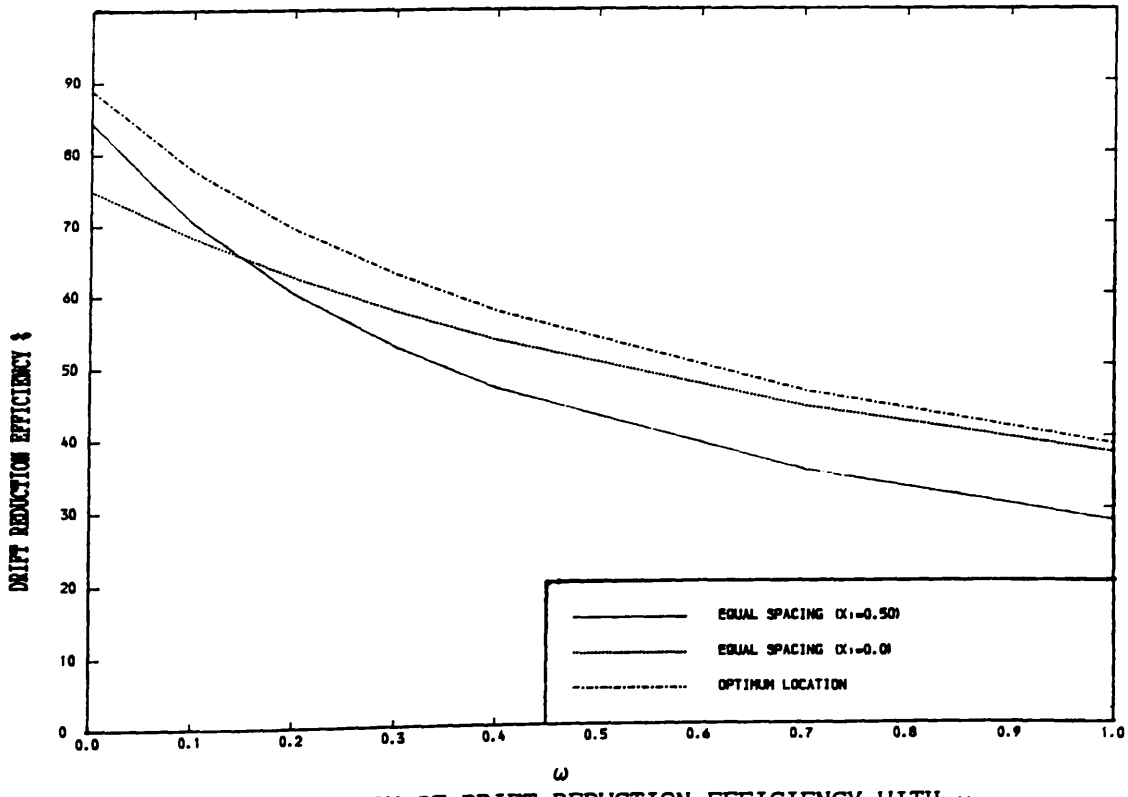

FIG. [2.71] VARIATION OF DRIFT REDUCTION EFFICIENCY WITH ω
(R=0, CASE OF ONE OUTRIGGER)
(POINT LOAD AT THE TOP)

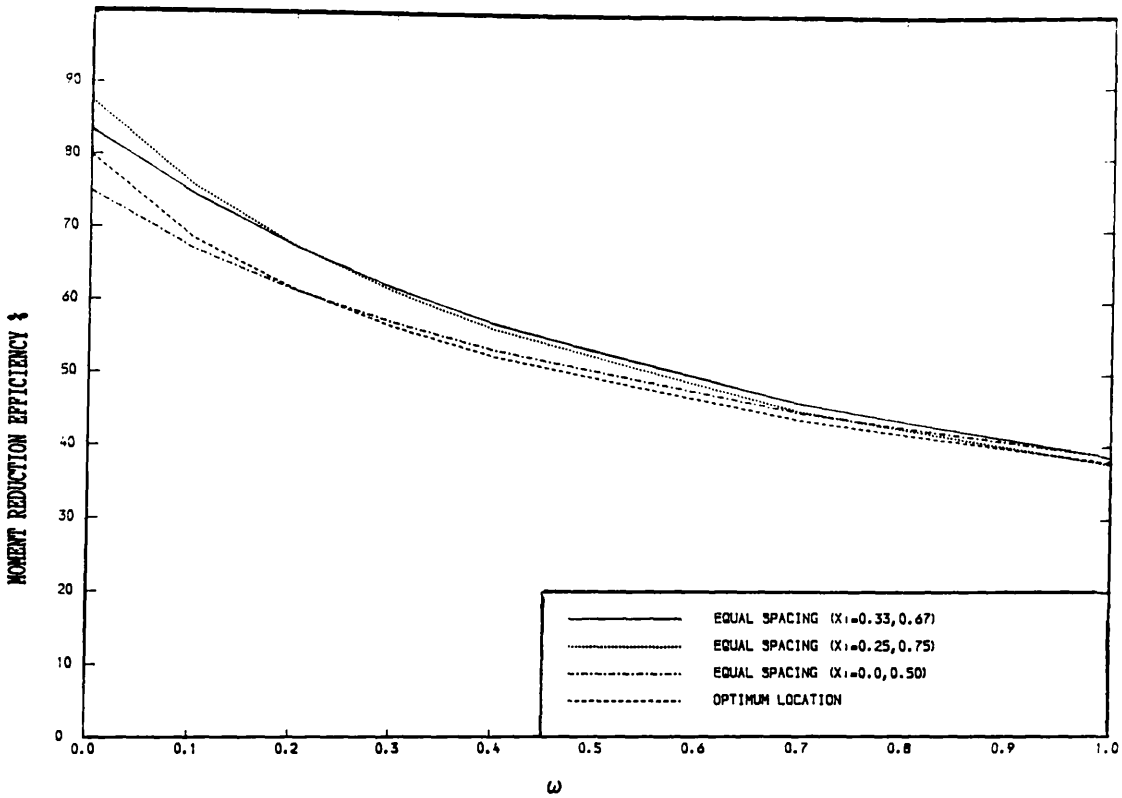

FIG. [2.72] VARIATION OF MOMENT REDUCTION EFFICIENCY WITH ω
(R=0, CASE OF TWO OUTRIGGERS)
(POINT LOAD AT THE TOP)

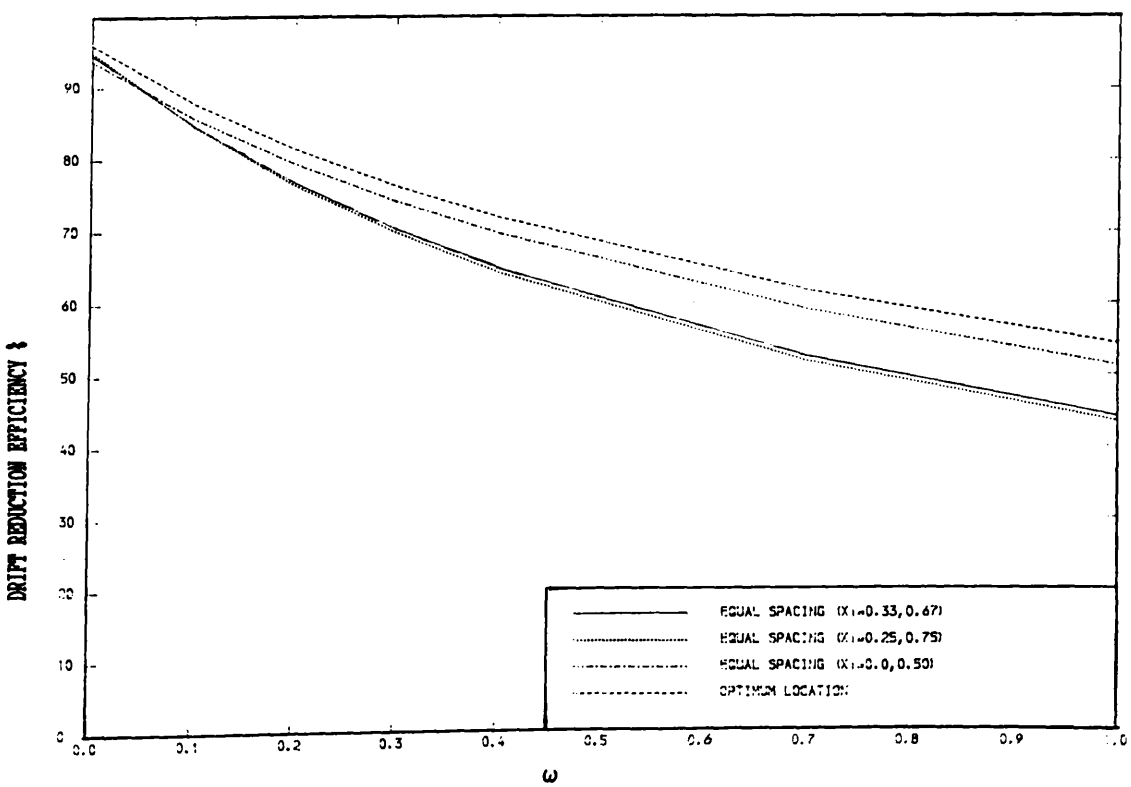

FIG. [2.73] VARIATION OF DRIFT REDUCTION EFFICIENCY WITH ω
(R=0, CASE OF TWO OUTRIGGERS)
(POINT LOAD AT THE TOP)

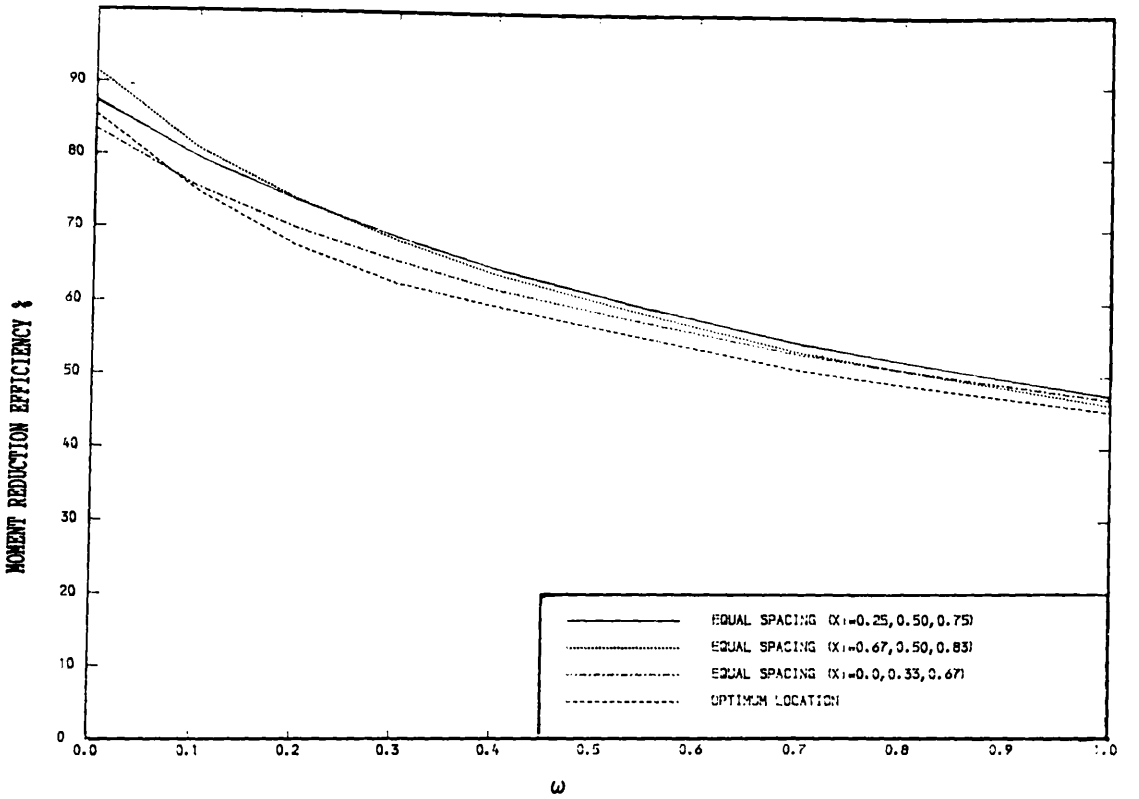

FIG.[2.74] VARIATION OF MOMENT REDUCTION EFFICIENCY WITH ω
(R=0, CASE OF THREE OUTRIGGERS)
(POINT LOAD AT THE TOP)

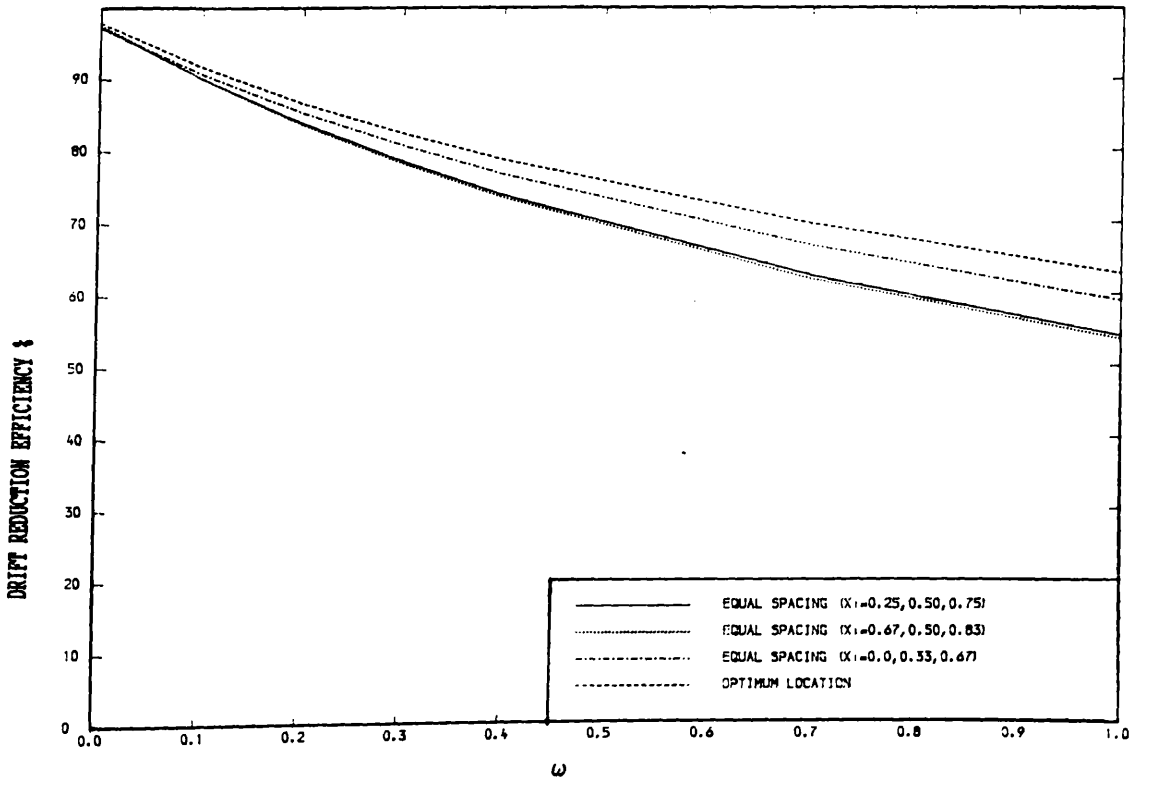

FIG.[2.75] VARIATION OF DRIFT REDUCTION EFFICIENCY WITH ω
(R=0, CASE OF THREE OUTRIGGERS)
(POINT LOAD AT THE TOP)

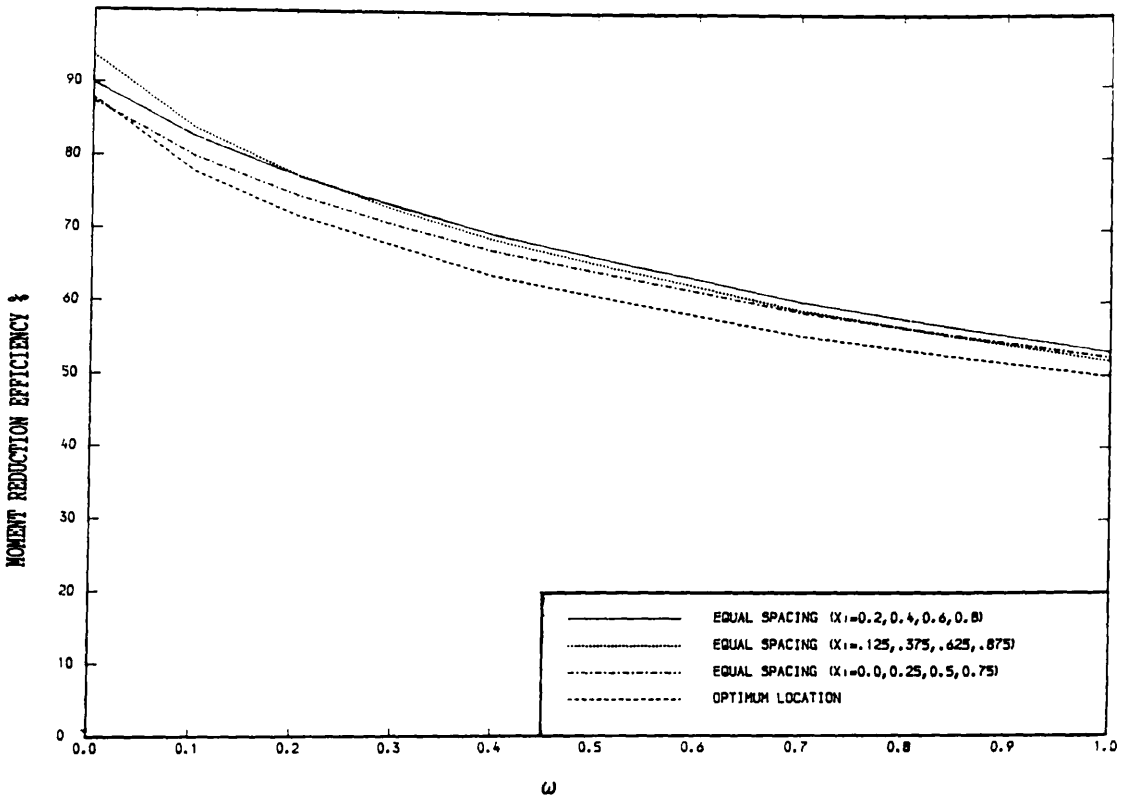

FIG. [2.76] VARIATION OF MOMENT REDUCTION EFFICIENCY WITH ω
(R=0, CASE OF FOUR OUTRIGGERS)
(POINT LOAD AT THE TOP)

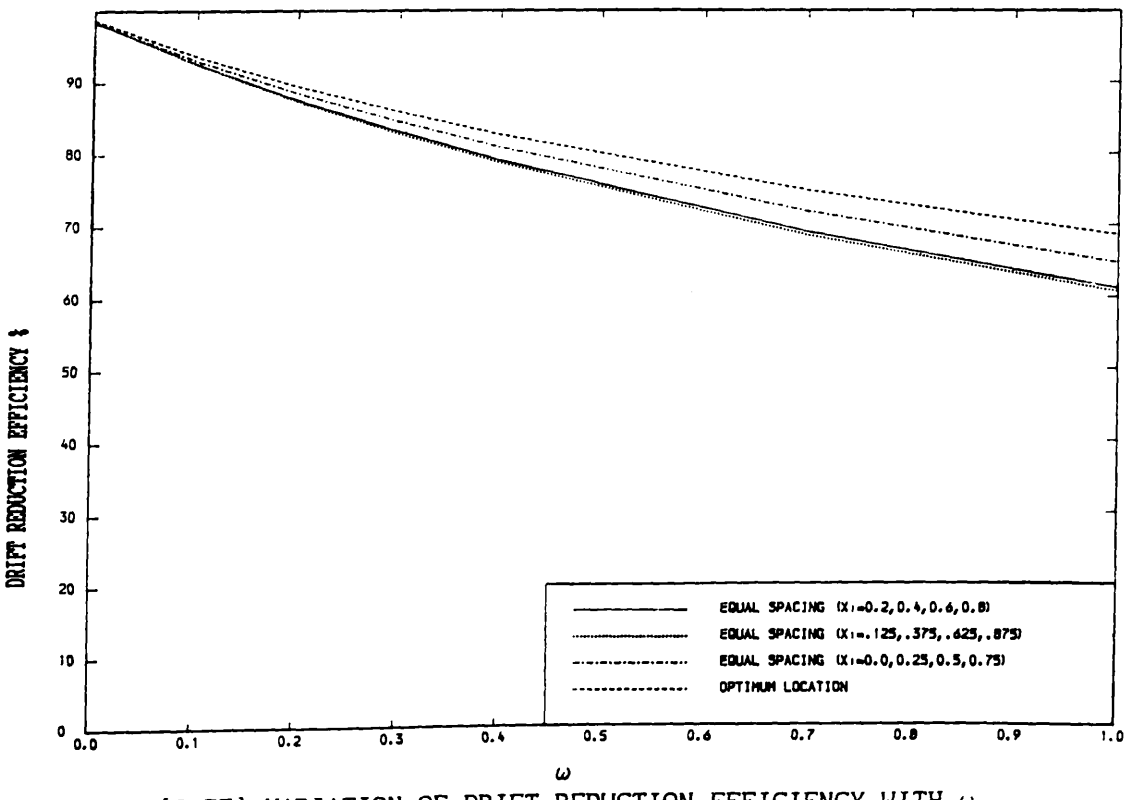

FIG. [2.77] VARIATION OF DRIFT REDUCTION EFFICIENCY WITH ω
(R=0, CASE OF FOUR OUTRIGGERS)
(POINT LOAD AT THE TOP)

Table [2.1] Summary of study of outrigger structures with different base flexibility terms R based on optimisation of top drift approach (U.D.L.)

Number of outrigger/s	R	1/EIS	ω	Optimum location/s x_1 x_2 x_i/H measured from top	Base moment $*M_{aB}$	Top drift $*y_{FT}$	r_m %	r_y %
1	0.0	0.1	0.0	0.46	0.944	0.912	55.72	87.85
			0.4	0.29	0.970	0.946	29.29	53.67
			0.8	0.23	0.980	0.960	20.97	39.73
		0.5	0.0	0.46	0.722	0.561	55.72	87.86
			0.4	0.29	0.854	0.732	29.30	53.67
			0.8	0.23	0.896	0.801	20.97	39.73
	0.5	0.1	0.0	0.99	0.150	1.267	99.99	96.17
			0.4	0.59	0.912	2.706	10.55	16.32
			0.8	0.43	0.944	2.794	6.71	11.43
		0.5	0.0	0.87	0.192	0.992	82.62	81.07
			0.4	0.49	0.658	1.795	34.97	48.65
			0.8	0.39	0.754	2.094	25.15	36.58
2	0.0	0.1	0.0	0.31 0.69	0.928	0.904	72.20	95.57
			0.4	0.21 0.49	0.960	0.931	40.36	68.51
			0.8	0.17 0.41	0.970	0.945	30.67	55.06
		0.5	0.0	0.31 0.69	0.638	0.522	72.20	95.57
			0.4	0.21 0.49	0.798	0.657	40.36	68.51
			0.8	0.17 0.41	0.848	0.725	30.67	55.06
	0.5	0.1	0.0	0.45 0.99	0.150	1.182	99.99	99.99
			0.4	0.55 0.99	0.820	2.524	20.95	26.42
			0.8	0.39 0.85	0.898	2.685	11.87	17.48
		0.5	0.0	0.45 0.99	0.140	0.578	87.93	97.78
			0.4	0.39 0.85	0.244	1.427	77.30	63.50
			0.8	0.31 0.69	0.632	1.745	37.63	50.67

Table [2.2] Summary of study of outrigger structures with different base flexibility terms R based on optimisation of top drift approach (Triangularly distributed load)

Number of outrigger/s	R	1/EIS	ω	Optimum location/s x_1 x_2 x_i/H measured from top	Base moment $*M_{aB}$	Top drift $*y_{FT}$	r_m %	r_y %
1	0.0	0.1	0.0	0.43	0.939	0.912	59.63	88.28
			0.4	0.28	0.957	0.945	32.60	54.58
			0.8	0.22	0.975	0.959	23.44	40.51
		0.5	0.0	0.43	0.702	0.559	59.63	88.28
			0.4	0.28	0.837	0.727	32.60	54.58
			0.8	0.22	0.882	0.797	23.44	40.51
	0.5	0.1	0.0	0.99	0.150	1.218	99.99	97.15
			0.4	0.54	0.909	2.403	10.89	25.19
			0.8	0.39	0.942	2.479	6.94	20.59
		0.5	0.0	0.75	0.294	0.933	72.19	82.06
			0.4	0.45	0.651	1.581	36.48	53.85
			0.8	0.35	0.747	1.844	25.87	42.40
2	0.0	0.1	0.0	0.29 0.67	0.924	0.904	75.78	95.73
			0.4	0.21 0.47	0.954	0.931	44.31	69.32
			0.8	0.17 0.39	0.966	0.944	33.95	55.93
		0.5	0.0	0.29 0.67	0.621	0.521	75.78	95.73
			0.4	0.21 0.47	0.780	0.653	44.31	69.32
			0.8	0.17 0.39	0.831	0.720	33.95	55.93
	0.5	0.1	0.0	0.43 0.99	0.147	1.133	99.99	99.99
			0.4	0.49 0.99	0.822	2.252	21.32	34.37
			0.8	0.35 0.79	0.900	2.386	11.97	26.22
		0.5	0.0	0.43 0.99	0.140	0.570	87.93	97.86
			0.4	0.35 0.79	0.495	1.271	51.64	67.34
			0.8	0.27 0.63	0.627	1.540	38.13	55.64

Table [2.3] Summary of study of outrigger structures with different base flexibility terms R based on optimisation of top drift approach (Point load at the top)

Number of outrigger/s	R	1/EIS	ω	Optimum location/s x_1 x_2 x_i/H measured from top		Base moment $*M_{aB}$	Top drift $*y_{FT}$	r_m %	r_y %
1	0.0	0.1	0.0	0.33		0.933	0.911	66.50	88.88
			0.4	0.20		0.960	0.942	40.00	57.60
			0.8	0.15		0.970	0.957	29.62	43.43
		0.5	0.0	0.33		0.670	0.556	66.50	88.89
			0.4	0.20		0.800	0.712	40.00	57.60
			0.8	0.15		0.852	0.783	29.62	43.43
	0.5	0.1	0.0	0.99		0.150	1.200	99.99	94.48
			0.4	0.45		0.910	2.258	10.78	17.59
			0.8	0.31		0.938	2.323	7.43	12.86
		0.5	0.0	0.67		0.331	0.944	33.84	78.47
			0.4	0.36		0.638	1.483	37.01	51.29
			0.8	0.27		0.729	1.718	27.71	39.44
2	0.0	0.1	0.0	0.19	0.59	0.920	0.904	79.50	95.99
			0.4	0.13	0.39	0.948	0.928	52.32	71.84
			0.8	0.11	0.31	0.958	0.941	41.48	58.86
		0.5	0.0	0.19	0.59	0.602	0.520	79.50	95.99
			0.4	0.13	0.39	0.738	0.641	52.32	71.84
			0.8	0.11	0.31	0.792	0.706	41.48	58.86
	0.5	0.1	0.0	0.33	0.99	0.150	1.114	99.99	99.99
			0.4	0.41	0.99	0.818	2.121	21.79	27.54
			0.8	0.25	0.77	0.897	2.241	12.34	18.82
		0.5	0.0	0.33	0.99	0.120	0.568	89.99	97.42
			0.4	0.25	0.77	0.483	1.205	52.86	65.31
			0.8	0.19	0.59	0.610	1.443	39.88	53.33

Table [2.4] Summary of study of outrigger structures with different base flexibility terms R based on optimisation of top drift approach (Combined triangularly distributed and a point load, r=0.05)

Number of outrigger/s	R	1/EIS	ω	Optimum location/s x_1 x_2 x_i/H measured from top	Base moment $*M_{aB}$	Top drift $*y_{FT}$	r_m %	r_y %
1	0.0	0.1	0.0	0.42	0.940	0.912	59.82	88.21
			0.4	0.27	0.967	0.945	33.01	54.79
			0.8	0.21	0.976	0.959	23.80	40.74
		0.5	0.0	0.42	0.701	0.559	59.82	88.21
			0.4	0.27	0.835	0.726	33.01	54.79
			0.8	0.21	0.881	0.796	23.80	40.74
	0.5	0.1	0.0	0.99	0.150	1.238	99.99	94.32
			0.4	0.54	0.911	2.518	10.65	19.35
			0.8	0.40	0.941	2.597	3.81	12.45
		0.5	0.0	0.79	0.263	0.975	75.36	83.26
			0.4	0.45	0.650	1.665	35.79	51.61
			0.8	0.36	0.746	1.939	25.97	39.07
2	0.0	0.1	0.0	0.27 0.65	0.971	0.904	74.89	95.69
			0.4	0.19 0.45	0.979	0.931	44.37	69.48
			0.8	0.17 0.39	0.983	0.944	34.54	56.13
		0.5	0.0	0.27 0.65	0.854	0.522	74.89	95.69
			0.4	0.19 0.45	0.897	0.653	44.37	69.48
			0.8	0.17 0.39	0.917	0.719	34.55	56.13
	0.5	0.1	0.0	0.41 0.99	0.150	1.153	99.99	99.99
			0.4	0.51 0.99	0.819	2.355	21.67	28.06
			0.8	0.35 0.83	0.897	2.499	12.33	19.35
		0.5	0.0	0.41 0.99	0.140	0.574	87.93	99.99
			0.4	0.35 0.83	0.485	1.335	52.66	66.74
			0.8	0.27 0.65	0.625	1.620	38.34	53.67

Table [2.5] Summary of study of outrigger structures with different base flexibility terms R based on optimisation of top drift approach (Combined triangularly distributed and a point load, r=0.10)

Number of outrigger/s	R	1/EIS	ω	Optimum location/s x_1 x_2 x_i/H measured from top	Base moment $*M_{aB}$	Top drift $*y_{FT}$	r_m %	r_y %
1	0.0	0.1	0.0	0.41	0.940	0.912	60.06	88.17
			0.4	0.26	0.967	0.945	33.42	54.99
			0.8	0.20	0.976	0.959	24.17	40.95
		0.5	0.0	0.41	0.700	0.559	60.06	88.17
			0.4	0.26	0.833	0.725	33.42	54.99
			0.8	0.20	0.897	0.795	24.17	40.95
	0.5	0.1	0.0	0.99	0.150	1.242	99.99	93.66
			0.4	0.55	0.911	2.543	10.66	11.88
			0.8	0.40	0.941	2.623	7.07	8.03
		0.5	0.0	0.78	0.271	0.973	74.54	87.35
			0.4	0.45	0.648	1.650	35.99	54.80
			0.8	0.35	0.745	1.919	26.07	41.88
2	0.0	0.1	0.0	0.27 0.65	0.925	0.904	75.46	95.68
			0.4	0.19 0.45	0.955	0.930	45.08	69.66
			0.8	0.15 0.37	0.965	0.944	34.78	56.35
		0.5	0.0	0.27 0.65	0.623	0.522	75.46	95.68
			0.4	0.19 0.45	0.954	0.930	45.76	69.81
			0.8	0.15 0.37	0.826	0.718	34.78	56.35
	0.5	0.1	0.0	0.41 0.99	0.150	1.240	99.99	99.99
			0.4	0.49 0.99	0.819	2.335	21.68	31.38
			0.8	0.35 0.83	0.897	2.476	12.35	21.66
		0.5	0.0	0.41 0.99	0.130	0.574	88.96	97.40
			0.4	0.35 0.83	0.484	1.324	61.70	70.48
			0.8	0.27 0.65	0.623	1.605	38.55	56.97

Table [2.6] Summary of study of outrigger structures with different base flexibility terms R based on optimisation of top drift approach (Combined triangularly distributed and a point load, r=0.15)

Number of outrigger/s	R	1/EIS	ω	Optimum location/s x_1 x_2 x_i/H measured from top	Base moment $*M_{aB}$	Top drift $*y_{FT}$	r_m %	r_y %
1	0.0	0.1	0.0	0.41	0.939	0.912	60.87	88.15
			0.4	0.26	0.966	0.945	34.00	55.19
			0.8	0.20	0.975	0.959	24.62	41.15
		0.5	0.0	0.41	0.696	0.559	60.87	88.15
			0.4	0.26	0.830	0.724	34.00	55.19
			0.8	0.20	0.877	0.794	24.62	41.15
	0.5	0.1	0.0	0.99	0.160	1.232	99.99	88.26
			0.4	0.53	0.911	2.474	10.66	8.13
			0.8	0.38	0.941	2.550	7.07	3.22
		0.5	0.0	0.77	0.278	0.972	73.82	82.09
			0.4	0.44	0.648	1.635	35.99	48.66
			0.8	0.34	0.744	1.902	26.18	35.20
2	0.0	0.1	0.0	0.27 0.65	0.924	0.904	76.01	95.67
			0.4	0.19 0.45	0.924	0.904	45.76	69.81
			0.8	0.15 0.37	0.965	0.943	35.36	56.55
		0.5	0.0	0.27 0.65	0.620	0.522	76.01	95.67
			0.4	0.19 0.45	0.771	0.651	45.76	69.81
			0.8	0.15 0.37	0.823	0.717	35.36	56.55
	0.5	0.1	0.0	0.41 0.99	0.150	1.147	99.99	93.74
			0.4	0.49 0.99	0.819	2.315	21.68	18.39
			0.8	0.33 0.81	0.898	2.455	12.22	9.35
		0.5	0.0	0.41 0.99	0.140	0.574	87.94	99.99
			0.4	0.33 0.81	0.489	1.314	52.25	66.63
			0.8	0.27 0.65	0.622	1.591	38.65	50.88

Table [2.7] Summary of study of outrigger structures with different base flexibility terms R based on optimisation of top drift approach (Polynomial loading, z=2)

Number of outrigger/s	R	1/EIS	ω	Optimum location/s x_1 x_2 x_i/H measured from top	Base moment $*M_{aB}$	Top drift $*y_{FT}$	r_m %	r_y %
1	0.0	0.1	0.0	0.44	0.942	0.912	58.32	88.18
			0.4	0.29	0.968	0.946	31.56	54.20
			0.8	0.22	0.977	0.960	22.52	40.18
		0.5	0.0	0.44	0.708	0.559	58.32	88.18
			0.4	0.29	0.842	0.729	31.56	54.20
			0.8	0.22	0.887	0.799	22.52	40.18
	0.5	0.1	0.0	0.99	0.150	1.250	99.99	97.01
			0.4	0.56	0.911	2.594	10.66	16.78
			0.8	0.42	0.942	2.676	6.95	11.88
		0.5	0.0	0.82	0.239	0.981	77.81	71.34
			0.4	0.47	0.653	1.717	35.48	43.62
			0.8	0.37	0.750	2.002	25.56	32.88
2	0.0	0.1	0.0	0.31 0.67	0.926	0.904	74.27	95.69
			0.4	0.21 0.47	0.957	0.931	42.79	69.01
			0.8	0.17 0.39	0.967	0.944	32.70	55.57
		0.5	0.0	0.31 0.67	0.629	0.522	74.27	95.69
			0.4	0.21 0.47	0.786	0.655	42.79	69.01
			0.8	0.17 0.39	0.837	0.722	32.70	55.57
	0.5	0.1	0.0	0.43 0.99	0.150	1.165	99.99	99.99
			0.4	0.53 0.99	0.819	2.423	21.68	26.98
			0.8	0.37 0.83	0.898	2.574	12.21	17.97
		0.5	0.0	0.43 0.99	0.140	0.575	87.93	86.63
			0.4	0.37 0.67	0.489	1.372	52.25	56.61
			0.8	0.29 0.67	0.627	1.670	38.14	45.39

Table [2.8] Summary of study of outrigger structures with different base flexibility terms R based on optimisation of top drift approach (Polynomial loading, z=5)

Number of outrigger/s	R	1/EIS	ω	Optimum location/s x_1 x_2 x_i/H measured from top	Base moment $*M_{aB}$	Top drift $*y_{FT}$	r_m %	r_y %
1	0.0	0.1	0.0	0.45	0.943	0.912	56.70	88.00
			0.4	0.29	0.970	0.946	30.20	53.82
			0.8	0.23	0.978	0.960	21.62	39.85
		0.5	0.0	0.45	0.716	0.560	56.70	88.00
			0.4	0.29	0.849	0.731	30.20	53.82
			0.8	0.23	0.892	0.801	21.62	39.85
	0.5	0.1	0.0	0.99	0.150	1.259	99.99	96.62
			0.4	0.58	0.911	2.657	10.66	16.55
			0.8	0.43	0.943	2.743	6.83	11.63
		0.5	0.0	0.84	0.222	0.987	79.55	80.75
			0.4	0.49	0.654	1.761	35.38	48.85
			0.8	0.38	0.753	2.055	25.26	36.73
2	0.0	0.1	0.0	0.31 0.69	0.926	0.904	73.90	95.62
			0.4	0.21 0.49	0.958	0.931	41.56	68.67
			0.8	0.17 0.41	0.968	0.945	31.60	55.21
		0.5	0.0	0.31 0.69	0.630	0.522	73.90	95.62
			0.4	0.21 0.49	0.792	0.657	41.56	68.67
			0.8	0.17 0.41	0.842	0.724	31.60	55.21
	0.5	0.1	0.0	0.45 0.99	0.150	1.175	99.99	99.99
			0.4	0.53 0.99	0.820	2.481	21.56	26.63
			0.8	0.39 0.85	0.898	2.637	12.22	17.70
		0.5	0.0	0.45 0.99	0.145	0.577	87.42	97.65
			0.4	0.39 0.85	0.486	1.403	52.56	63.02
			0.8	0.31 0.67	0.631	1.712	37.73	50.87

Table [2.9] Summary of study of outrigger structures with different base flexibility terms R based on optimisation of top drift approach (Polynomial loading, z=10)

Number of outrigger/s	R	1/EIS	ω	Optimum location/s x_1 x_2 x_i/H measured from top	Base moment $*M_{aB}$	Top drift $*y_{FT}$	r_m %	r_y %
1	0.0	0.1	0.0	0.45	0.944	0.912	55.72	87.90
			0.4	0.29	0.970	0.946	29.64	53.71
			0.8	0.23	0.979	0.960	21.22	39.76
		0.5	0.0	0.45	0.721	0.560	55.72	87.90
			0.4	0.29	0.852	0.731	29.64	53.71
			0.8	0.23	0.894	0.801	21.22	39.76
	0.5	0.1	0.0	0.99	0.150	1.264	99.99	96.40
			0.4	0.58	0.911	2.687	10.66	16.37
			0.8	0.43	0.943	2.773	6.83	11.53
		0.5	0.0	0.86	0.202	0.989	81.60	72.12
			0.4	0.49	0.656	1.782	35.17	43.36
			0.8	0.39	0.754	2.078	0.295	32.63
2	0.0	0.1	0.0	0.31 0.69	0.927	0.904	72.94	95.59
			0.4	0.21 0.49	0.959	0.931	40.83	68.56
			0.8	0.17 0.41	0.969	0.945	31.03	55.10
		0.5	0.0	0.31 0.69	0.635	0.522	72.94	95.59
			0.4	0.21 0.49	0.796	0.657	40.83	68.56
			0.8	0.17 0.41	0.845	0.724	31.03	55.10
	0.5	0.1	0.0	0.45 0.99	0.150	1.179	99.99	99.99
			0.4	0.55 0.99	0.820	2.507	21.56	26.49
			0.8	0.39 0.85	0.898	2.666	12.22	11.31
		0.5	0.0	0.45 0.99	0.145	0.577	87.42	87.06
			0.4	0.39 0.85	0.488	1.417	52.35	56.60
			0.8	0.31 0.69	0.630	1.732	37.83	45.18

Table [2.10] Summary of study of outrigger structures with different base flexibility terms R based on optimisation of core moment approach (U.D.L.)

Number of outrigger/s	R	1/EIS	ω	Optimum location/s x_1 x_2 x_i/H measured from top		Min. moment $*M_{aB}$	Top drift $*y_{FT}$	r_m %	r_y %
1	0.0	0.1	0.0	0.95		0.904	0.981	95.08	18.54
			0.4	0.57		0.968	0.956	32.72	44.18
			0.8	0.47		0.978	0.965	22.46	34.99
		0.5	0.0	0.77		0.606	0.679	78.76	64.13
			0.4	0.57		0.836	0.779	32.72	44.18
			0.8	0.47		0.888	0.825	22.46	34.99
	0.5	0.1	0.0	0.83		0.708	2.234	33.99	42.51
			0.4	0.93		0.866	2.753	15.60	13.71
			0.8	0.79		0.936	2.826	7.45	9.66
		0.5	0.0	0.63		0.396	1.061	61.76	78.28
			0.4	0.77		0.612	1.911	39.67	43.96
			0.8	0.73		0.734	2.218	27.20	31.57
2	0.0	0.1	0.0	0.79	0.99	0.900	0.939	99.00	60.58
			0.4	0.52	0.76	0.954	0.944	46.34	55.97
			0.8	0.43	0.67	0.966	0.953	33.90	47.26
		0.5	0.0	0.97	0.99	0.504	0.943	99.00	11.47
			0.4	0.52	0.76	0.768	0.720	46.34	55.97
			0.8	0.43	0.67	0.830	0.764	33.90	47.26
	0.5	0.1	0.0	0.80	0.86	0.672	2.162	38.18	46.50
			0.4	0.93	0.95	0.818	2.593	21.19	22.59
			0.8	0.77	0.97	0.886	2.718	13.27	15.65
		0.5	0.0	0.97	0.99	0.298	0.989	71.78	81.19
			0.4	0.52	0.76	0.468	1.556	54.40	58.30
			0.8	0.43	0.67	0.592	1.867	41.72	45.74

Table [2.11] Summary of study of outrigger structures with different base flexibility terms R based on optimisation of core moment approach (Triangularly distributed load)

Number of outrigger/s	R	1/EIS	ω	Optimum location/s x_1 x_2 x_i/H measured from top	Min. moment $*M_{aB}$	Top drift $*y_{FT}$	r_m %	r_y %
1	0.0	0.1	0.0	0.93	0.604	0.977	94.85	23.28
			0.4	0.53	0.642	0.953	35.72	46.65
			0.8	0.43	0.650	0.963	24.81	36.73
		0.5	0.0	0.73	0.400	0.660	80.07	67.94
			0.4	0.53	0.548	0.767	35.72	46.65
			0.8	0.43	0.584	0.816	24.81	36.73
	0.5	0.1	0.0	0.81	0.482	2.033	62.04	47.66
			0.4	0.91	0.594	2.452	48.62	22.22
			0.8	0.75	0.624	2.509	45.03	18.76
		0.5	0.0	0.57	0.276	0.973	74.03	80.32
			0.4	0.73	0.408	1.687	60.53	49.24
			0.8	0.69	0.486	1.955	52.57	37.57
2	0.0	0.1	0.0	0.81 0.99	0.600	0.951	99.26	49.24
			0.4	0.49 0.75	0.634	0.947	49.86	52.53
			0.8	0.39 0.65	0.642	0.955	36.97	44.89
		0.5	0.0	0.97 0.99	0.336	0.952	99.26	9.63
			0.4	0.49 0.75	0.500	0.737	49.86	52.53
			0.8	0.39 0.65	0.544	0.776	36.97	44.89
	0.5	0.1	0.0	0.83 0.85	0.456	1.988	65.45	50.39
			0.4	0.91 0.93	0.548	2.326	54.13	29.87
			0.8	0.71 0.95	0.590	2.420	49.10	24.17
		0.5	0.0	0.71 0.73	0.208	0.969	80.98	80.50
			0.4	0.69 0.83	0.314	1.414	70.14	61.12
			0.8	0.61 0.87	0.392	1.674	62.17	49.80

Table [2.12] Summary of study of outrigger structures with different base flexibility terms R based on optimisation of core moment approach (Point load at the top)

Number of outrigger/s	R	1/EIS	ω	Optimum location/s x_1 x_2 x_i/H measured from top	Min. moment $*M_{aB}$	Top drift $*y_{FT}$	r_m %	r_y %
1	0.0	0.1	0.0	0.90	0.905	0.973	95.00	27.08
			0.4	0.42	0.958	0.948	42.02	51.91
			0.8	0.30	0.970	0.959	30.33	41.41
		0.5	0.0	0.60	0.600	0.616	80.00	76.80
			0.4	0.42	0.790	0.740	42.02	51.91
			0.8	0.30	0.848	0.793	30.33	41.41
	0.5	0.1	0.0	0.76	0.755	1.977	29.34	38.00
			0.4	0.89	0.892	2.305	12.93	14.17
			0.8	0.66	0.934	2.346	7.90	11.19
		0.5	0.0	0.44	0.442	0.989	57.05	76.20
			0.4	0.66	0.671	1.729	33.64	38.88
			0.8	0.57	0.717	1.789	28.94	35.86
2	0.0	0.1	0.0	0.81 0.99	0.901	0.953	99.50	46.71
			0.4	0.35 0.69	0.943	0.936	56.87	63.51
			0.8	0.25 0.57	0.956	0.946	43.74	54.16
		0.5	0.0	0.97 0.99	0.503	0.956	99.50	8.73
			0.4	0.35 0.69	0.716	0.682	56.87	63.51
			0.8	0.25 0.57	0.781	0.729	43.74	54.16
	0.5	0.1	0.0	0.79 0.81	0.720	1.932	33.53	41.28
			0.4	0.87 0.91	0.828	2.188	20.60	22.67
			0.8	0.61 0.93	0.886	2.261	13.65	17.37
		0.5	0.0	0.65 0.67	0.331	0.931	68.40	79.12
			0.4	0.55 0.75	0.479	1.270	53.27	62.03
			0.8	0.45 0.81	0.582	1.501	42.74	50.38

Table [2.13] Summary of the approximate optimum outrigger locations by regression (U.D.L., Top drift optimisation)

No. of outriggers	Optimum location	Coefficients						R adjusted
		b_o	b_1	b_2	b_3	b_4	b_5	
1	x_1	0.491	-0.491	0	0.749	-0.503	0.005	0.999
2	x_1	0.308	-0.291	0	0.422	-0.278	0.003	0.999
	x_2	0.666	-0.577	0	0.909	-0.636	0.008	0.999
3	x_1	0.243	-0.197	0	0.263	-0.178	0.003	0.998
	x_2	0.521	-0.392	0	0.594	-0.410	0.004	0.999
	x_3	0.760	-0.611	0	1.080	-0.793	0.009	0.999
4	x_1	0.208	-0.173	0	0.193	-0.120	0.001	0.999
	x_2	0.443	-0.278	0	0.349	-0.237	0.003	0.999
	x_3	0.626	-0.444	0	0.763	-0.532	0.005	0.996
	x_4	0.816	-0.584	0	0.966	-0.677	0.006	0.999

Table [2.14] Summary of the approximate optimum outrigger locations by regression (Triangularly Distributed Load, Top drift optimisation)

No. of outriggers	Optimum location	Coefficients						R adjusted
		b_o	b_1	b_2	b_3	b_4	b_5	
1	x_1	0.420	-0.442	0	0.670	-0.454	0.004	0.999
2	x_1	0.291	-0.259	0	0.427	-0.315	0.004	0.998
	x_2	0.648	-0.529	0	0.641	-0.397	0.005	0.999
3	x_1	0.239	-0.199	0	0.237	-0.137	0.001	0.992
	x_2	0.520	-0.417	0	0.472	-0.270	0.003	0.996
	x_3	0.758	-0.603	0	0.833	-0.547	0.005	0.999
4	x_1	0.197	-0.138	0	0.105	-0.050	0.001	0.994
	x_2	0.421	-0.301	0	0.399	-0.244	0.004	0.997
	x_3	0.624	-0.414	0	0.422	-0.244	0.007	0.997
	x_4	0.814	-0.655	0	1.020	-0.683	0.007	0.999

Table [2.15] Summary of the approximate optimum outrigger locations by regression (Point load at top, Top drift optimisation)

No. of outriggers	Optimum location	Coefficients						R adjusted
		b_o	b_1	b_2	b_3	b_4	b_5	
1	x_1	0.324	-0.384	0	0.583	-0.397	0.002	0.999
2	x_1	0.203	-0.237	0	0.427	-0.302	0.003	0.999
	x_2	0.587	-0.579	0	0.805	-0.541	0.005	0.999
3	x_1	0.136	-0.130	0	0.254	-0.182	0.002	0.994
	x_2	0.417	-0.421	0	0.651	-0.437	0.006	0.997
	x_3	0.706	-0.687	0	1.010	-0.661	0.006	0.998
4	x_1	0.136	-0.236	0	0.462	-0.316	0.002	0.992
	x_2	0.339	-0.324	0	0.449	-0.291	0.004	0.999
	x_3	0.535	-0.461	0	0.711	-0.485	0.007	0.998
	x_4	0.751	-0.591	0	0.783	-0.516	0.008	0.999

Table [2.16] Summary of the approximate optimum outrigger locations by regression (U.D.L., Base moment optimisation)

No. of outriggers	Optimum location	Coefficients						R adjusted
		b_o	b_1	b_2	b_3	b_4	b_5	
1	x_1	0.954	-1.710	1.840	0	-0.665	0	0.955
2	x_1	0.943	-1.940	2.170	0	-0.788	0	0.937
	x_2	0.982	-0.871	0.979	0	-0.274	0	0.985
3	x_1	0.948	-2.190	2.560	0	-0.948	0	0.911
	x_2	0.978	-1.030	0.954	0	-0.299	0	0.964
	x_3	0.990	-0.578	0.445	0	-0.131	0	0.984
4	x_1	0.944	-2.060	2.540	0	-1.070	0	0.900
	x_2	0.977	-0.984	1.080	0	-0.491	0	0.956
	x_3	0.987	-0.627	0.685	0	-0.339	0	0.974
	x_4	0.996	-0.429	0.461	0	-0.259	0	0.995

Table [2.17] Summary of the approximate optimum outrigger locations by regression (Triangularly distributed load, Base moment optimisation)

No. of outriggers	Optimum location	Coefficients						R adjusted
		b_o	b_1	b_2	b_3	b_4	b_5	
1	x_1	0.948	-1.850	2.010	0	-0.721	0	0.948
2	x_1	0.937	-2.110	2.400	0	-0.885	0	0.931
	x_2	0.981	-0.956	0.882	0	-0.299	0	0.985
3	x_1	0.931	-2.240	2.590	0	-0.956	0	0.922
	x_2	0.975	-1.120	1.080	0	-0.365	0	0.977
	x_3	0.992	-0.696	0.613	0	-0.213	0	0.995
4	x_1	0.935	-2.490	2.990	0	-1.110	0	0.900
	x_2	0.972	-1.310	1.370	0	-0.493	0	0.951
	x_3	0.986	-0.815	0.785	0	-0.283	0	0.973
	x_4	0.993	-0.573	0.536	0	-0.201	0	0.986

Table [2.18] Summary of the approximate optimum outrigger locations by regression (Point load at top, Base moment optimisation)

No. of outriggers	Optimum location	Coefficients						R adjusted
		b_o	b_1	b_2	b_3	b_4	b_5	
1	x_1	0.935	-2.340	2.570	0	-0.917	0	0.947
2	x_1	0.919	-2.670	3.060	0	-1.120	0	0.926
	x_2	0.980	-1.170	1.060	0	-0.347	0	0.988
3	x_1	0.910	-2.830	3.300	0	-1.210	0	0.914
	x_2	0.969	-1.400	1.380	0	-0.474	0	0.976
	x_3	0.986	-0.762	0.600	0	-0.181	0	0.990
4	x_1	0.907	-2.910	3.430	0	-1.280	0	0.912
	x_2	0.967	-1.480	1.450	0	-0.490	0	0.976
	x_3	0.992	-0.957	0.842	0	-0.271	0	0.997
	x_4	0.995	-0.601	0.484	0	-0.172	0	0.997

CHAPTER THREE

STATIC ANALYSIS OF MULTI-OUTRIGGER-BRACED STRUCTURES USING THE CONTINUUM TECHNIQUE

NOTATION for Chapter 3

A_c	sectional area of column
d	distance between columns
E	elastic modulus of core
E_c	elastic modulus of columns
E_o	elastic modulus of outrigger
H	height of structure
I	moment of inertia of core
I_o	effective moment of inertia of outrigger
I_r	actual moment of inertia of outrigger
M	moment in the core
M_a	applied moment due to external loads
M_{aB}	applied moment at the base of the structure
M_B	core moment at the base of the structure
M_{Bir}	core moment at the base of an outrigger structure with an infinite number of infinitely rigid outriggers and a rigid base
M_{Bif}	core moment at the base of an outrigger structure with an infinite number of infinitely rigid outriggers and a flexible base
P	point load at the top of the structure
q	shear force per unit height in the 'continuous medium'
S, S_1	structural parameters
T	axial force in columns
T_B	axial force in columns at the base of the structure
w	horizontal load per unit height

w_t	maximum load intensity of a upper triangular distributed load
y_T	top drift of the structure
y_{Tir}	top drift of an outrigger structure with an infinite number of infinitely rigid outriggers and a rigid base
y_{Tif}	top drift of an outrigger structure with an infinite number of infinitely rigid outriggers and a flexible base
α, β	structural parameters
ω	non-dimensional characteristic parameter

Other subsidiary symbols are defined locally in the text.

3.1 INTRODUCTION

The continuum technique has been used widely in the last few decades especially for the analysis of the coupled shear walls. The technique is relatively simple and makes the basic assumptions that the discrete system of connections, formed by lintel beams or floor slabs, may be replaced by an equivalent continuous medium and that the walls deflect equally throughout the height. The method is amenable to hand calculation for regular or partially regular systems. By assuming a fixed vertical line of contraflexure in the connecting system, conditions of compatibility and equilibrium yield a governing linear differential equation of the second order, enabling a general closed mathematical solution to be obtained for specific applied load functions. The simplicity of the technique enables the production of simple design curves and tables, which allow a rapid and accurate solution to be worked out for a particular structural system under standard load cases. The method is suitable for design office use.

The technique has been used in the past[14],[15,[16] to analyse structures of uniform cross-section, variable wall thickness, variable cross-section and flexible foundations. So far, the technique has been applied to describe the structural behaviour of coupled shear wall structures. Since there is an analogy in the structural behaviour between coupled shear wall and outrigger-braced structures, the same governing equations will apply with a new set of governing parameters α and β, used in the earlier analysis, redefined for an outrigger-braced structures. In this Chapter, an approximate analysis of a multi-outrigger-braced structure, based on the continuum approach used previously on coupled shear wall structures, is presented. In this method, the set of outriggers is smeared over the height to give an equivalent uniform bracing system. The equations of equilibrium and compatibility yield a second-order governing differential

equation, which, when solved, leads to closed-form solutions which are independent of the number of outriggers. The closed-form solutions are used to produce generalised design curves. The analysis appears to give reasonably accurate results for even a small number of outrigger, and accurate results for a large number of outriggers.

3.2 ANALYSIS

In the multi-outrigger-braced structure of Fig.(3.1a), the 'n' outriggers are rigidly connected to the central core and pin-connected to the external columns to ensure that the latter carry only axial forces. The discrete set of outriggers, each of flexural rigidity $E_o I_o$, is assumed smeared over the height to produce an equivalent uniform bracing medium of flexural rigidity $E_o I_o n/H$ per unit height as shown in Fig.(3.1b).

Consideration of the equilibrium of a small element of column and outrigger medium shows that

$$T = \int_x^H q \, dx \qquad (3.1)$$

In equation (3.1), T is the axial force in a column at any height x measured from the base of the structure, and q is the shear force per unit height in the bracing medium. From equation (3.1), q can be written as,

$$q = - \frac{dT}{dx} \qquad (3.2)$$

The equation of vertical deflection compatibility at the junction between external columns and outriggers, is

$$\frac{d}{2}\frac{dy}{dx} - \frac{q(d/2)^3 H}{3E_o I_o n} - \frac{1}{E_c A_c}\int_0^x T\,dx = 0 \qquad (3.3)$$

where

d is the distance between columns

$E_c A_c$ is the axial rigidity of the columns

In equation (3.3), the three terms represent the relative vertical displacements due respectively to bending of the core, bending of the outriggers, and axial deformations of the columns.

The moment-curvature relationship for the core is

$$EI\frac{d^2y}{dx^2} = M = M_a - Td \qquad (3.4a)$$

where

M is the moment in the core

M_a is the applied moment

EI is the flexural rigidity of the core

The axial force, T, in a column at any height x is therefore given by,

$$T = \frac{M_a - M}{d} \qquad (3.4b)$$

The load systems shown in Fig.[3.1] are considered in this Chapter. This is the sum of three loadings, namely a uniformly distributed load, a point load at the top and a triangularly distributed load. The static applied moment Ma is given by

$$M_a = P(H-x) + \frac{w(H-x)^2}{2} + \left[\frac{w_t(H-x)^2}{2} - \frac{w_t(H-x)^3}{6H} \right] \qquad (3.5)$$

The static moment at the base M_{aB} is given by

$$M_{aB} = PH + \frac{wH^2}{2} + \frac{w_t H^2}{3}$$

On differentiating equation (3.3), and substituting in equation (3.4), the governing differential equation in terms of the column axial force T becomes,

$$\frac{d^2T}{dx^2} - \alpha^2 T = -\beta^2 M_a \qquad (3.6)$$

where

$$\alpha^2 = \frac{Sn}{S_1 H} \qquad (3.7)$$

$$\beta^2 = \frac{1}{EIS_1} \left(\frac{n}{dH}\right) \qquad (3.8)$$

with

$$S = \frac{1}{EI} + \frac{2}{d^2 E_c A_c} \tag{3.9}$$

$$S_1 = \frac{d}{12 E_o I_o} \tag{3.10}$$

Thus from equations (3.7) and (3.8),

$$\frac{\beta^2}{\alpha^2} = \frac{1}{EISd} \tag{3.11}$$

The parameters S and S_1 are defined in the same manner as in equations (2.6a) and (2.6b) in Chapter 2. The parameter S is a function of the flexural rigidities of the core and the column areas acting about the centroidal axis of the core, and S_1 depends on the flexural rigidity of the outriggers.

The complete solution to the governing ordinary differential equation (3.6) is given by the sum of the complementary function and the particular integral. The complementary function is,

$$T_c = B \cosh\alpha x + C \sinh\alpha x \tag{3.12}$$

and the particular integral is,

$$T_p = \beta^2/\alpha^2 \{1 - D^2/\alpha^2 + D^4/\alpha^2 - ..\} M_a \tag{3.13}$$

in which D is the operator d/dx, and B and C are integration constants which must be determined from the appropriate boundary conditions.

From equations (3.12) and (3.13), the complete solution becomes,

$$T = B \cosh\alpha x + C \sinh\alpha x + \beta^2/\alpha^2 \{ M_a + w/\alpha^2 + w_t/\alpha^2 - w_t(H-x)/(\alpha^2 H) \} \quad (3.14)$$

Substituting equation (3.11) into (3.2), the shear flow q is given by,

$$q = -\alpha (B \sinh\alpha x + C \cosh\alpha x) - \beta^2/\alpha^2 \{ dM_a/dx + w_t/(\alpha^2 H) \} \quad (3.15)$$

where

$$\frac{dM_a}{dx} = - P - w(H-x) - \left[w_t(H-x) - \frac{w_t(H-x)^2}{2H} \right]$$

The integration constants B and C are found by considering the upper and lower boundary conditions of the structure.

At the top of the structure, there is no axial force. Thus at x=H, the axial force at the top of structure T_T becomes,

$$T_T = 0 \quad (3.16)$$

Substituting equation (3.14) into (3.16) and simplifying gives,

$$B = -C \tanh\alpha H - \frac{\beta^2 (w+w_t)}{\alpha^4 \cosh\alpha H} \qquad (3.17)$$

Consider the general case where a certain degree of rotational flexibility exists at the base of the structure. At the base of the structure, the rotation is proportional to the base moment M_B as,

$$\frac{dy}{dx} = K_\vartheta M_B \qquad (3.18a)$$

where K_ϑ is the rotational stiffness at the base of the structure or of the substructure

Therefore substituting equation (3.18a) into (3.3), the boundary condition at the base becomes,

$$q_B = \frac{nK_\vartheta}{S_1 dH} (M_{aB} - T_B\, d) \qquad (3.18b)$$

where q_B is the shear force per unit height in the connecting medium at the base of the structure and T_B is the axial force in the columns at the base of structure.

For the case where the base of the outrigger structure is considered to be fully rigid. The lower boundary condition as obtained from the basic compatibility equation (3.3) as,

$$q_B = 0 \qquad (3.19)$$

Therefore for a general case where the rotational flexibility at the base of the structure is included, substituting T and q from equations (3.14) and (3.15) into equation (3.18), the constant C becomes,

$$C = \frac{(\alpha H)^2 R}{EISH}\left[\frac{-M_{aB}}{d} - \frac{\beta^2(w+w_t)}{\alpha^4 \cosh\alpha H} + \frac{\beta^2}{\alpha^2}\left(M_{aB} + \frac{w}{\alpha^2}\right)\right].I_1$$

$$- \frac{\beta^2}{\alpha^2}\left[\frac{dM_{aB}}{dx} - \frac{w_t}{\alpha^2 H}\right].I_1 \qquad (3.20)$$

where

$$I_1 = \frac{1}{\frac{(\alpha H)^2 R}{EISH}\tanh\alpha H + \alpha}$$

For the case of a rigid base, C reduces to

$$C = \frac{\beta^2}{\alpha^3}\left(wH + \frac{w_t H}{2} - \frac{w_t}{\alpha^2 H} + P\right) \qquad (3.21)$$

Therefore the constant B can be obtained by substituting the above expression for C into equation (3.17).

Once the constants B and C are obtained, the distribution of axial forces T in the columns and the shear flow q are given by equations (3.14) and (3.15).

Although they are constant between outriggers in the discrete structure, the column forces vary continuously throughout the height in the continuum model. Therefore, when relating the results to the prototype structure, the average value of column force for the level concerned should be used.

The shear V_i in any particular outrigger at level x_i is equal to the difference between the column forces at the mid-storey height position above and below the outrigger concerned. That is,

$$V_i = T(i-h/2) - T(i+h/2) \tag{3.22}$$

where h is the storey height.

Substituting equation (3.14) into (3.4), and integrating twice, the lateral deflection of the structure can be found as,

$$y = \frac{L(x)}{EI} - \frac{1}{EI} 1 \left\{ \frac{B}{\alpha^2} \cosh\alpha x + \frac{C}{\alpha^2} \sinh\alpha x + \frac{\beta^2}{\alpha^2} \left[L(x) + \frac{wx^2}{2\alpha} + \frac{w_t H x^3}{6(\alpha H)^2} \right] \right\} + D\,x + E \tag{3.23}$$

where

$$L(x) = \frac{P(H-x)^3}{6} + \frac{w(H-x)^4}{24} + \left[\frac{w_t(H-x)^4}{24} - \frac{w_t(H-x)^5}{120H} \right]$$

The constants D and E can be obtained by considering the boundary conditions at the base of the structure.

$$y_{(x=0)} = 0$$

$$\frac{dy}{dx} = \vartheta_{(x=0)} = K_{\vartheta} M_B$$

The constants D and E are given by,

$$D = \frac{1}{EI}\left[\frac{PH^2}{2} + \frac{wH^3}{6} + \frac{w_t H^3}{8} + \frac{C\,1}{\alpha} - \frac{\beta^2}{\alpha^2}\,1\left(\frac{wH^3}{6} + \frac{w_t H^3}{8} + \frac{PH^2}{2}\right)\right] + \vartheta_{(x=0)}$$

$$E = \frac{1}{EI}\left[\frac{E\,1}{\alpha^2} + \frac{\beta^2}{\alpha^2}\,1\left(\frac{wH^4}{24} + \frac{w_t H^4}{30} + \frac{PH^3}{6}\right) - \left(\frac{wH^4}{24} + \frac{w_t H^4}{30} + \frac{PH^3}{6}\right)\right]$$

where $\vartheta_{(x=0)}$ is obtained by considering equations (3.4a) and (3.18a) and is given by

$$\vartheta_{(x=0)} = \frac{RH}{EI}\left[M_{aB} + dC\tanh\alpha H + \frac{\beta^2(w+w_t)}{\alpha^4 \cosh\alpha H} - \frac{\beta^2}{\alpha^2}\left(M_{aB} + \frac{w}{\alpha^2}\right)\right]$$

One of the most important design criteria is the drift, or top deflection y_T, which is obtained by substituting x=H into equation (3.23) leading to the complete general expression for the top drift as,

$$y_T = -\frac{1}{EI} 1 \left\{ \frac{B}{\alpha^2} \cosh\alpha H + \frac{C}{\alpha^2} \sinh\alpha H + \frac{\beta^2}{\alpha^2} \left[\frac{wH^2}{2\alpha} + \frac{w_t H^4}{6(\alpha H)^2} \right] \right\} + DH + E \qquad (3.24)$$

where the constants B, C, D and E were presented earlier. The expression of the top drift in the above equation includes the effect due to the rotational flexibility of the base of the structure. It can be expressed in terms of non-dimensional parameters αH, 1/EIS and R.

For the special case where the base is considered to be infinitely rigid, R is equal to zero. The equation (3.24) reduces to a much more managableleable form.

For a uniformly distributed load,

$$\frac{y_T}{\frac{wH^4}{8EI}} = 1 - \frac{1}{EIS} \left[\frac{8}{(\alpha H)^4} \left(\frac{1}{\cosh\alpha H} - 1 \right) + \frac{8}{(\alpha H)^3} \tanh\alpha H - \frac{4}{(\alpha H)^2} + 1 \right] \qquad (3.25)$$

For a point load at the top of the structure,

$$\frac{y_T}{\frac{PH^3}{3EI}} = 1 - \frac{1}{EIS}\left[\frac{3}{(\alpha H)^3}\tanh\alpha H - \frac{3}{(\alpha H)^2} + 1\right] \qquad (3.26)$$

For a triangularly distributed load,

$$\frac{y_T}{\frac{11w_tH^4}{120EI}} = 1 - \frac{120}{11EIS}\left[\frac{-1}{(\alpha H)^5}\tanh\alpha H + \frac{1}{(\alpha H)^4\cosh\alpha H}\right.$$

$$\left. + \frac{\tanh\alpha H}{2(\alpha H)^3} - \frac{1}{3(\alpha H)^2} + \frac{11}{120}\right] \qquad (3.27)$$

The other important criterion is the maximum moment. The general expression for core moment M at any level can be obtained by substituting T into equation (3.4a) and becomes,

$$M = M_a - d\left\{B\cosh\alpha x + C\sinh\alpha x + \right.$$

$$\left.\beta^2/\alpha^2\ [\ M_a + w/\alpha^2 + w_t/\alpha^2 - w_t(H-x)/(\alpha^2 H)\ ]\right\} \qquad (3.28)$$

Minimisation of the core base moment can be obtained by differentiating equation (3.28) with respect to x. It leads to the equation as,

$$\frac{dM}{dx} = 0 = \frac{dM_a}{dx} - d\left\{\frac{B}{\alpha}\sinh\alpha H + \frac{C}{\alpha}\cosh\alpha H + \frac{\beta^2}{\alpha^2}\left[\frac{dM_a}{dx} + \frac{w_t}{\alpha^2}\right]\right\} \qquad (3.29)$$

Either solving the equation (3.29) or by means of some searching techniques as described in Chapter 2, the level at which the maximum core moment occurs can be obtained.

The stiffening effect of the outriggers is shown by expressing the core moment at the base, M_B, as a ratio of the static base moment M_{aB} which would occur in the core alone. The expression for the core moment and the base moment in the core for the rigid foundation case are presented below.

For a uniformly distributed load,

$$M = \frac{w(H-x)^2}{2} - \frac{w}{EIS}\left[\frac{-H}{\alpha}\tanh\alpha H.\cosh\alpha x - \frac{1}{\alpha^2}\frac{\cosh\alpha x}{\cosh\alpha H} + \frac{H}{\alpha}\sinh\alpha x + \frac{(H-x)^2}{2} + \frac{1}{\alpha^2}\right] \qquad (3.30)$$

and the expression for the core moment at the base is given by,

$$\frac{M_B}{\frac{wH^2}{2}} = 1 - \frac{1}{EIS}\left[\frac{-2}{\alpha H}\tanh\alpha H - \frac{2}{(\alpha H)^2\cosh\alpha H}\right.$$

$$\left. + \frac{2}{(\alpha H)^2} + 1\right] \qquad (3.31)$$

For a point load at the top of the structure,

$$M = P(H-x) - \frac{W}{EIS}\left[\frac{-1}{\alpha}\tanh\alpha H\cosh\alpha x\right.$$

$$\left. + \frac{1}{\alpha}\sinh\alpha x + (H-x)\right] \qquad (3.32)$$

and the expression for the core moment at the base M_B is given by,

$$\frac{M_B}{PH} = 1 - \frac{1}{EIS}\left[\frac{-1}{\alpha H}\tanh(\alpha H) + 1\right] \qquad (3.33)$$

For a triangularly distributed load,

$$M = w_t \left\{ \left[\frac{(H-x)^2}{2} - \frac{(H-x)^3}{6H} \right] \right.$$

$$- \frac{1}{EIS} \left[\frac{1}{\alpha} \left(\frac{-H}{2} + \frac{1}{\alpha^2 H} \right) \tanh\alpha H \cosh\alpha x \right.$$

$$- \frac{\cosh\alpha x}{\alpha^2 \cosh\alpha H} + \frac{1}{\alpha} \left(\frac{H}{2} - \frac{1}{\alpha^2 H} \right) \sinh\alpha x$$

$$\left. \left. + \frac{(H-x)^2}{2} - \frac{(H-x)^3}{6H} + \frac{1}{\alpha^2} - \frac{(H-x)}{\alpha^2 H} \right] \right\} \qquad (3.34)$$

and the expression for the core moment at the base is given by,

$$\frac{M_B}{\frac{w_t H^2}{3}} = 1 - \frac{1}{EIS} \left[\frac{3}{(\alpha H)^3} \tanh\alpha H - \frac{3}{(\alpha H)^2} \frac{1}{\cosh(\alpha H)} \right.$$

$$\left. - \frac{3}{(\alpha H)} \left(\frac{1}{2} \tanh\alpha H \right) + 1 \right] \qquad (3.35)$$

The second terms in equations (3.25), (3.26), (3.27), (3.31), (3.33) and (3.35) give respectively the relative reductions in the drift and base moment which result from the outrigger bracing. They thus form a measure of the efficiency of the bracing.

The axial force in the columns at the base T_B can be obtained easily by substituting M_B from equations (3.27), (3.29) and (3.31) into equation (3.4b) as,

$$T_B = \frac{M_{aB} - M_B}{d} \tag{3.36}$$

For a uniformly distributed load,

$$T_B = \frac{wH^2}{EISd}\left[\frac{-1}{\alpha H}\tanh\alpha H - \frac{1}{(\alpha H)^2\cosh\alpha H} + \frac{1}{(\alpha H)^2} + \frac{1}{2}\right] \tag{3.37}$$

For a point load at the top of the structure,

$$T_B = \frac{PH}{EISd}\left[\frac{-1}{\alpha H}\tanh(\alpha H) + 1\right] \tag{3.38}$$

For a triangularly distributed load,

$$T_B = \frac{w_t H^2}{EISd}\left[\frac{1}{(\alpha H)^3}\tanh\alpha H - \frac{1}{(\alpha H)^2}\frac{1}{\cosh(\alpha H)} - \frac{1}{(\alpha H)}\left(\frac{1}{2}\tanh\alpha H\right) + \frac{1}{3}\right] \tag{3.39}$$

The variation of the relative deflection and core moment, over the practical range of the two controlling structural parameters αH and $1/EIS$, are shown in Figs.[3.11] to [3.16], respectively. The curves illustrate the significant increase in lateral stiffness

$$T_B = \frac{M_{aB} - M_B}{d} \qquad (3.36)$$

For a uniformly distributed load,

$$T_B = \frac{wH^2}{EISd}\left[\frac{-1}{\alpha H}\tanh\alpha H - \frac{1}{(\alpha H)^2\cosh\alpha H} + \frac{1}{(\alpha H)^2} + \frac{1}{2}\right] \qquad (3.37)$$

For a point load at the top of the structure,

$$T_B = \frac{PH}{EISd}\left[\frac{-1}{\alpha H}\tanh(\alpha H) + 1\right] \qquad (3.38)$$

For a triangularly distributed load,

$$T_B = \frac{w_t H^2}{EISd}\left[\frac{1}{(\alpha H)^3}\tanh\alpha H - \frac{1}{(\alpha H)^2}\frac{1}{\cosh(\alpha H)} - \frac{1}{(\alpha H)}\left(\frac{1}{2}\tanh\alpha H\right) + \frac{1}{3}\right] \qquad (3.39)$$

The variation of the relative deflection and core moment, over the practical range of the two controlling structural parameters αH and $1/EIS$, are shown in Figs.[3.11] to [3.16], respectively. The curves illustrate the significant increase in lateral stiffness

and the reduction in core moment, which can be achieved with outrigger bracing.

3.3 NUMERICAL RESULTS

The numerical investigations using the continuum technique are presented in two sections. Firstly, a series of design curves which allow for rapid solution are presented in Figs.[3.2] to [3.25]. Secondly, a series of numerical calculations based on the flexibility approach of Chapter 2 and the continuum technique are presented and compared in Tables [3.1] to [3.6].

3.3.1 DESIGN CURVES

Within the assumptions made, Figs.[3.2] to [3.19] define the behaviour of all multi-outrigger-braced structures for the three load cases considered. The increase in stiffness and reduction in core moment can be determined directly for any bracing configuration, from a knowledge of the three parameters R, αH and 1/EIS which are all in nondimensional form. The design curves presented can be used for assessing the lateral drift and the core base moment for any structural parameters. The curves allow a direct assessment of the effectiveness of any number of outriggers.

A series of design curves showing the variation of top drift and base moment with the parameters 1/EIS and R for the limiting case of outriggers with infinite αH are presented in Figs.[3.20] to [3.25]. From the curves, a set of limiting values of y_{Tir}, y_{Tif},

M_{Bir} and M_{Bif} can be obtained to be used in defining both the drift and moment efficiencies of the outrigger-braced system in Chapter 2. Figs.[3.26] to [3.31] show variation of the bending moment profile with different base flexibilities for the three load cases. Representative values of αH of 2 and 6 are presented showing the changes in the maximum core moment. As the outrigger arms become stiffer, the effect of base flexibilities will tend to shift the position of maximum core moment higher up from the base.

However, the results rely on the validity of the continuum representation of the outriggers along the height. It is therefore of importance to examine the accuracy of this basic assumption.

3.3.2 ACCURACY OF RESULTS

A series of numerical examples was also used to investigate the accuracy of the method of analysis for structures involving a relatively small number of outriggers. The results were compared with the data obtained from an accurate flexibility analysis for both the optimum locations of the outriggers to minimise the drift, optimum locations of the outriggers to minimise the core moment at the base and equal spacings of outriggers. A range of values for the significant parameters was used to vary the relative stiffness of the core, outriggers and columns over the range of practical configurations and of different base flexibilities.

In order to allow a direct comparison with the results presented in Chapter 2, the more general relative stiffness parameter ω is

used in the numerical examples presented in this Chapter. For simplicity, the parameter ω can be written in terms of n, αH, S and S_1 as,

$$\omega = \frac{n}{(\alpha H)^2} = \frac{S_1}{SH} = \frac{d}{12H}\left[\frac{EI}{E_o I_o}\right]\left[1 + \frac{2EI}{E_c A_c d^2}\right]^{-1} \qquad (3.40)$$

The number of outriggers investigated ranged from one to three, the latter being normally regarded as about the maximum number which would normally be used in practice.

The comparisons between relative drifts are shown in Tables (3.1) to (3.6), in which "Optimum spacings (drift)", "Uniform spacings Type (i), (ii) and (iii)" and "Continuum" refer to the values when the outriggers are located at their optimum levels for top drift, uniformly spaced and in the continuum configuration. Three different forms of uniform spacing were examined, as follows: Type (i), the outriggers were spaced at intervals of H/n+1, with no outrigger at the top; Type (ii), the spacings were H/n, apart from the top and bottom, where the spacings were H/2n; and Type (iii), the spacings were H/n, with one outrigger always positioned at the top.

Tables [3.1] to [3.6] indicates that the continuum approach gives reasonably accurate values for the lateral drift and core moment at the base for even a very small number of outriggers. The results become more accurate as the number of outriggers and the stiffness at the base increases. Results of similar accuracy were

obtained for the core base moments. By establishing the maximum possible reductions in lateral deflection and core base moment for a very large number of outriggers, the relative efficiency of a limited number may be assessed.

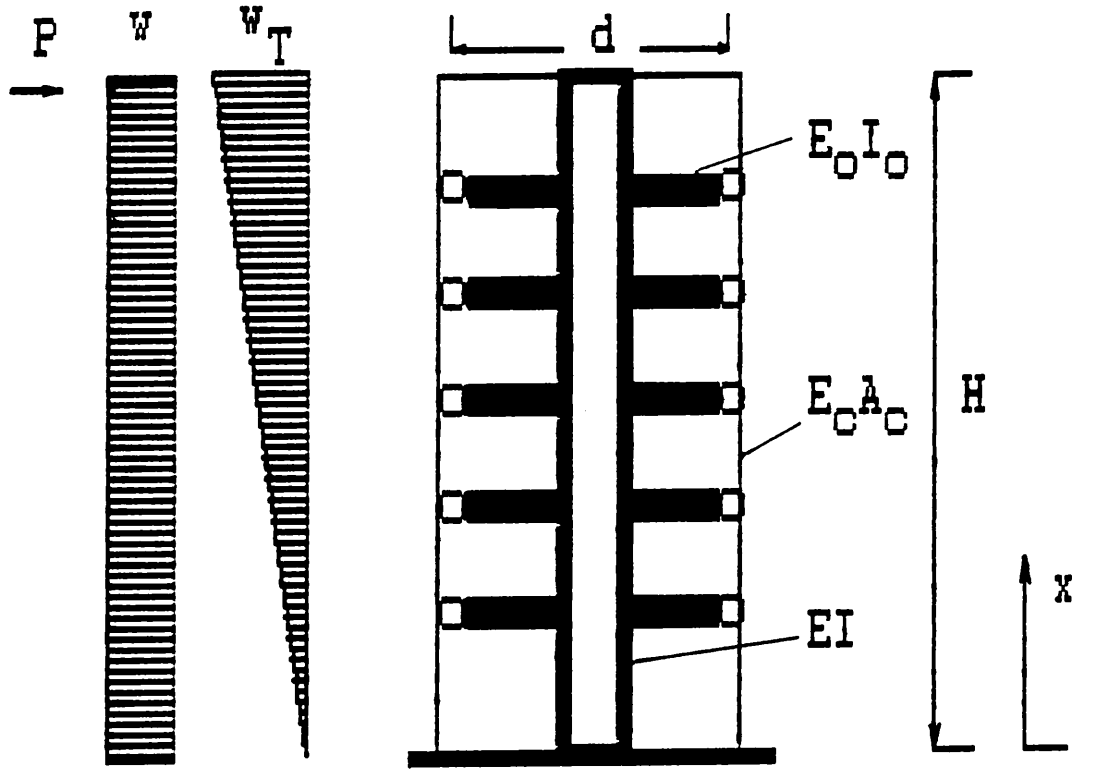

Multi-outrigger-braced structure

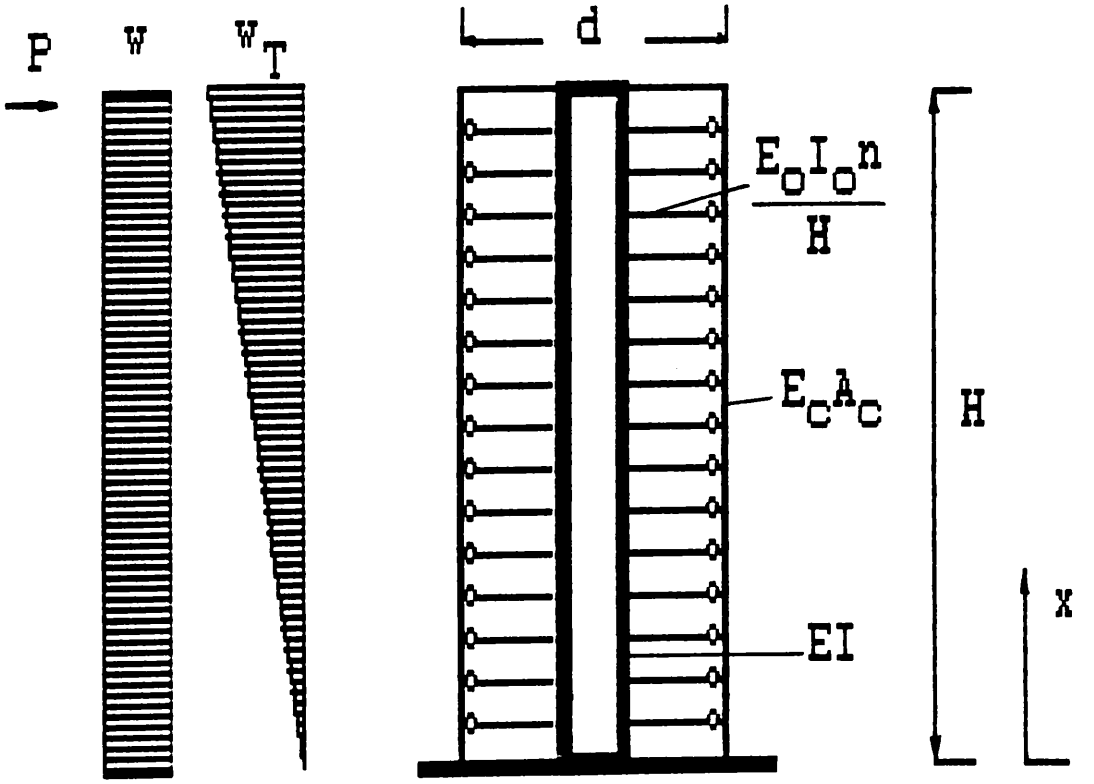

FIG. [3.1] MULTI-OUTRIGGER-BRACED STRUCTURE AND ITS EQUIVALENT SUBSTITUTE SYSTEM

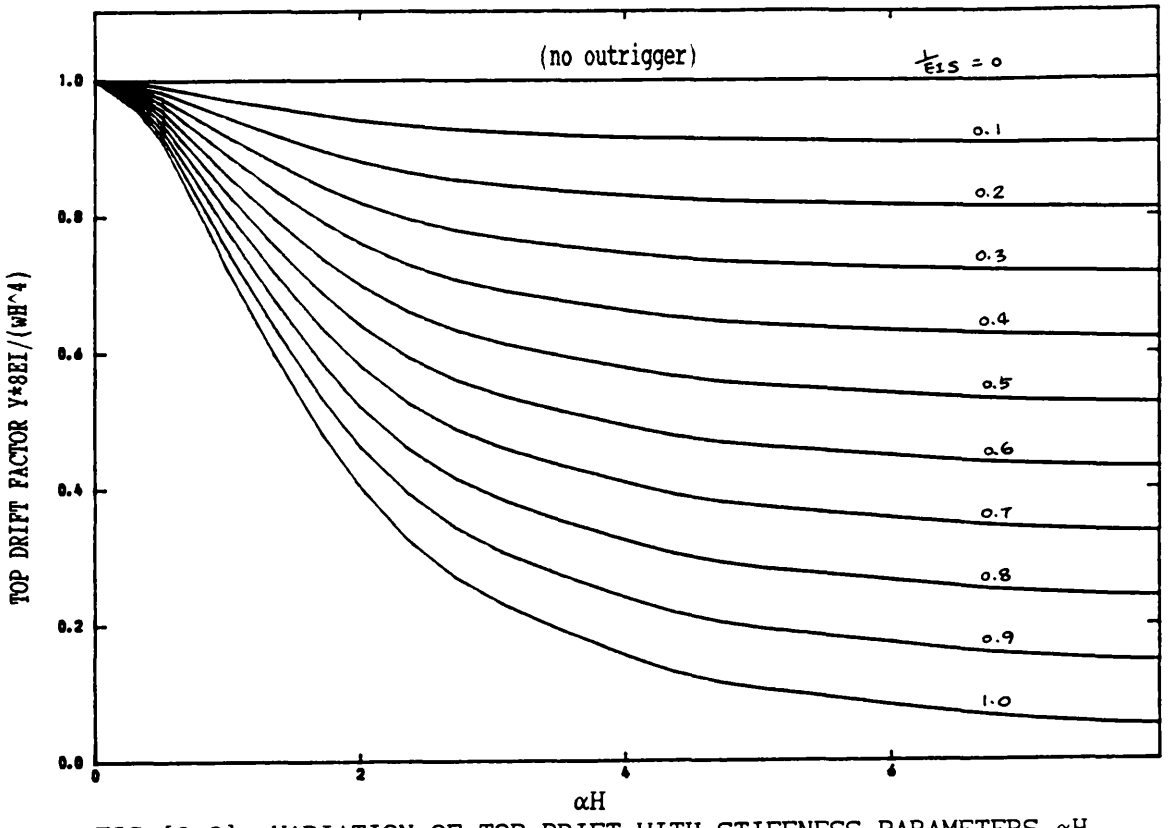

FIG. [3.2] VARIATION OF TOP DRIFT WITH STIFFNESS PARAMETERS αH AND 1/EIS
(U.D.L., R=0)

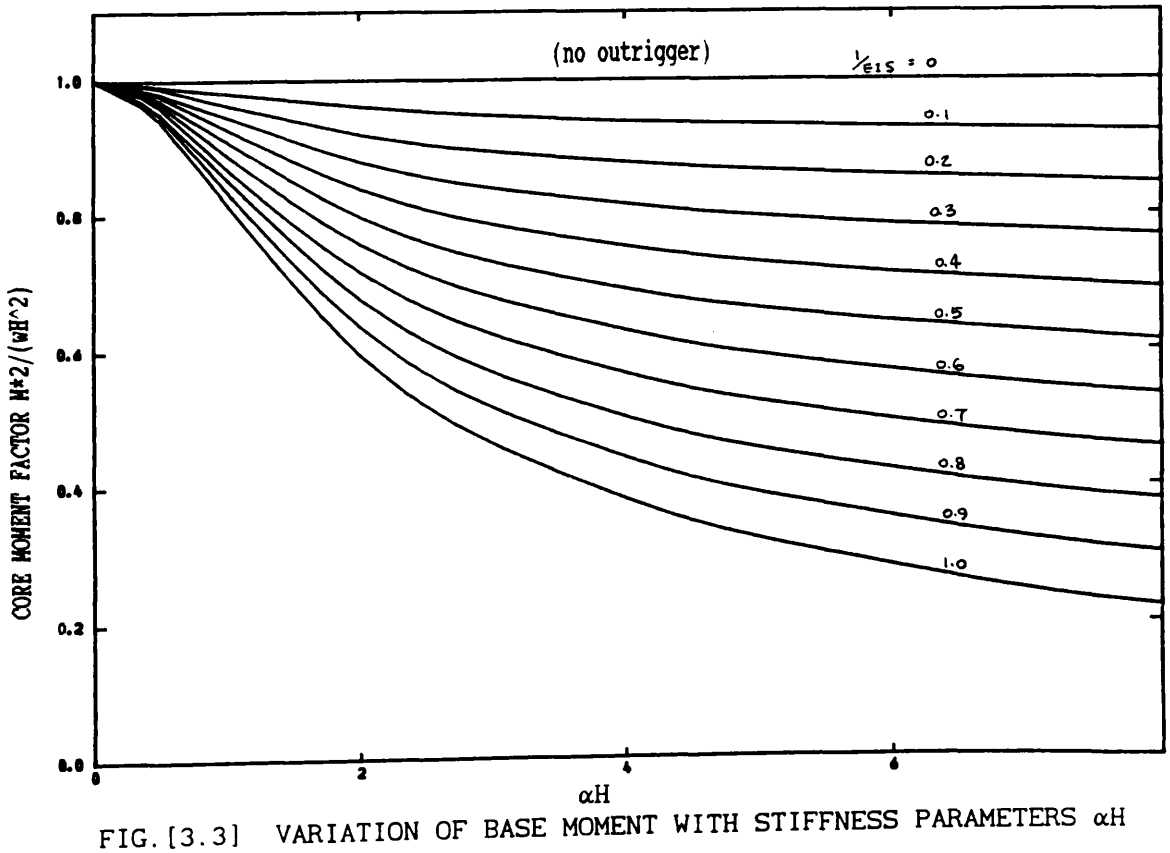

FIG. [3.3] VARIATION OF BASE MOMENT WITH STIFFNESS PARAMETERS αH AND 1/EIS
(U.D.L., R=0)

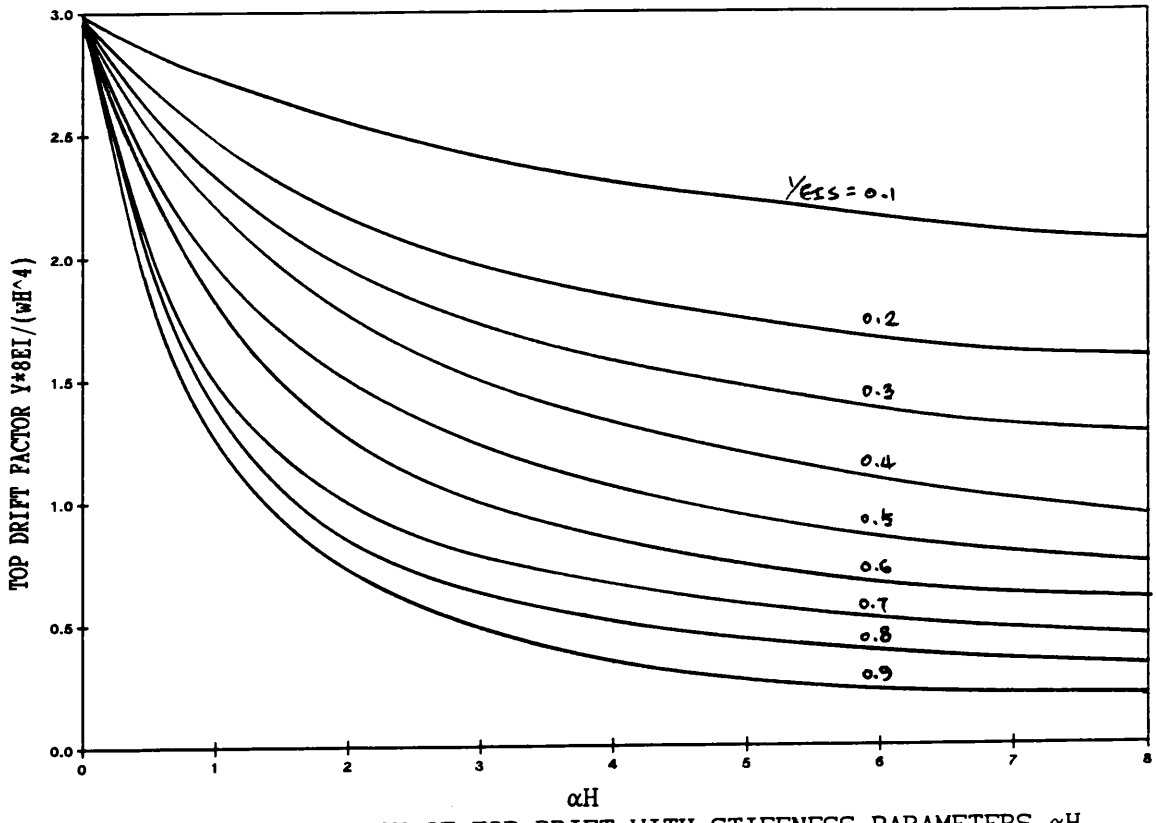

FIG. [3.4] VARIATION OF TOP DRIFT WITH STIFFNESS PARAMETERS αH AND 1/EIS
(U.D.L., R=0.5)

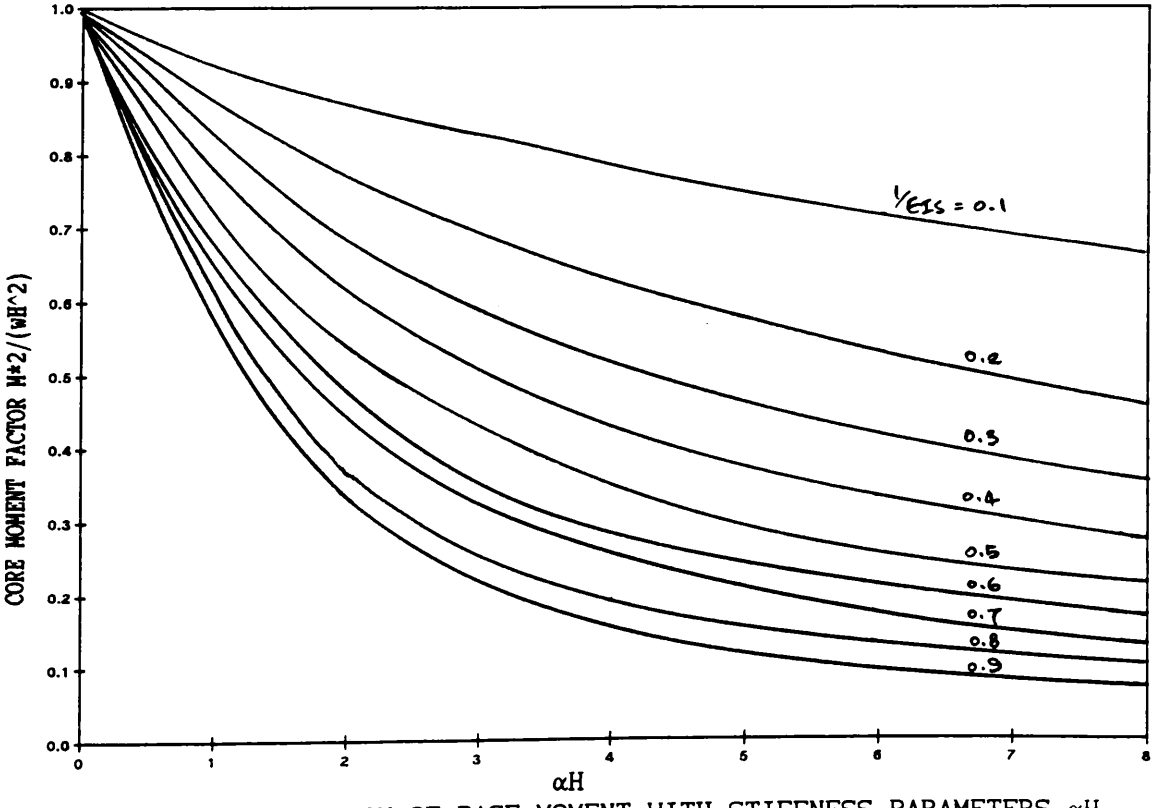

FIG. [3.5] VARIATION OF BASE MOMENT WITH STIFFNESS PARAMETERS αH AND 1/EIS
(U.D.L., R=0.5)

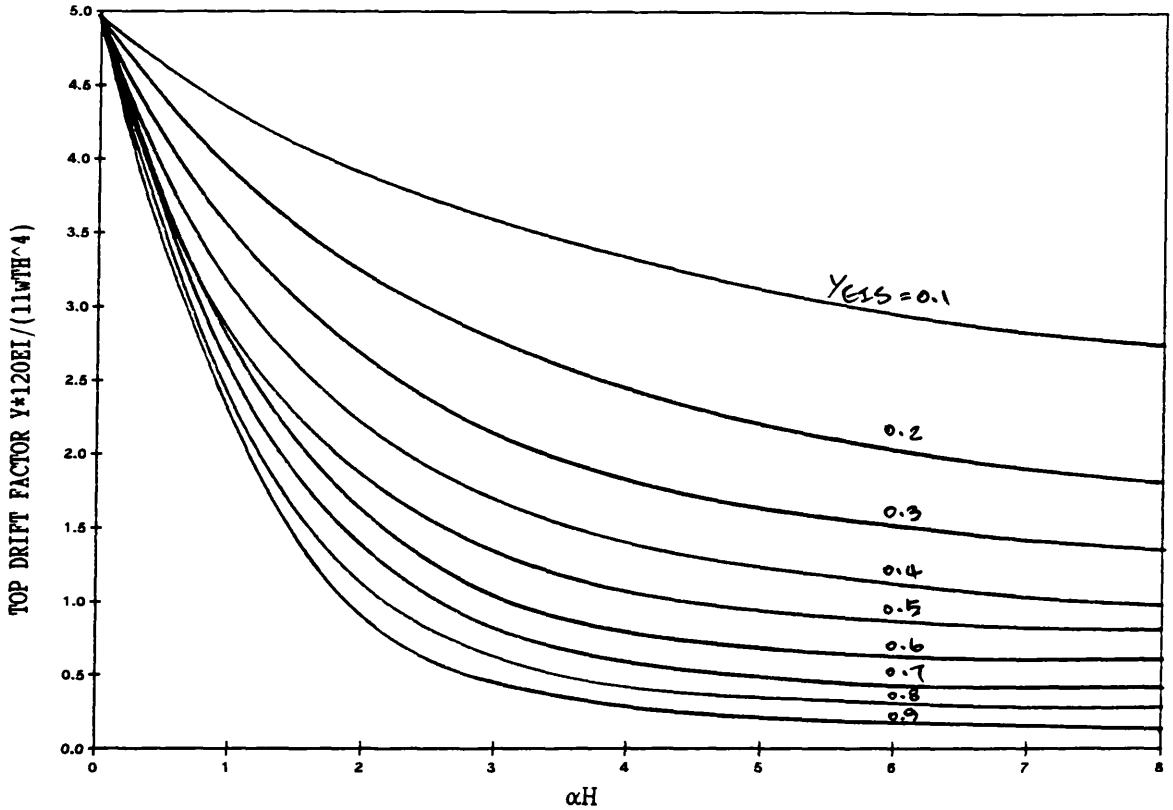

FIG. [3.6] VARIATION OF TOP DRIFT WITH STIFFNESS PARAMETERS αH AND 1/EIS
(U.D.L., R=1.0)

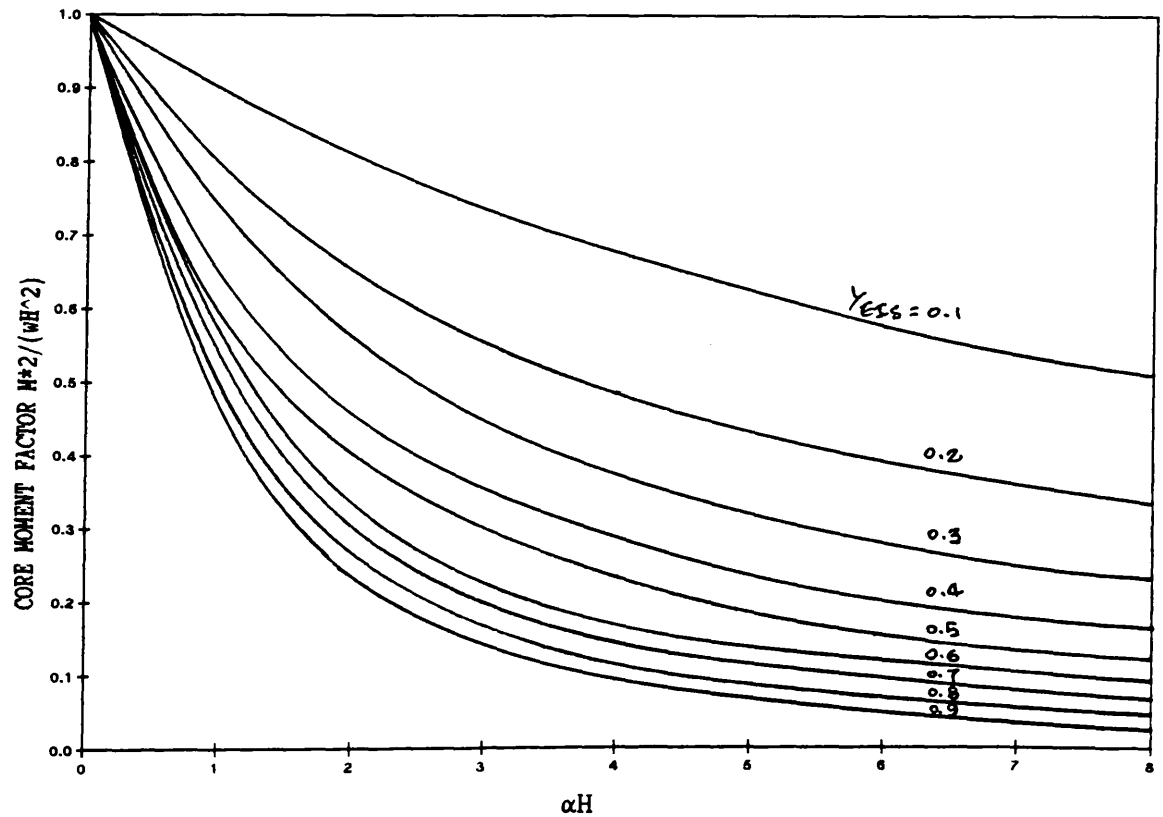

FIG. [3.7] VARIATION OF BASE MOMENT WITH STIFFNESS PARAMETERS αH AND 1/EIS
(U.D.L., R=1.0)

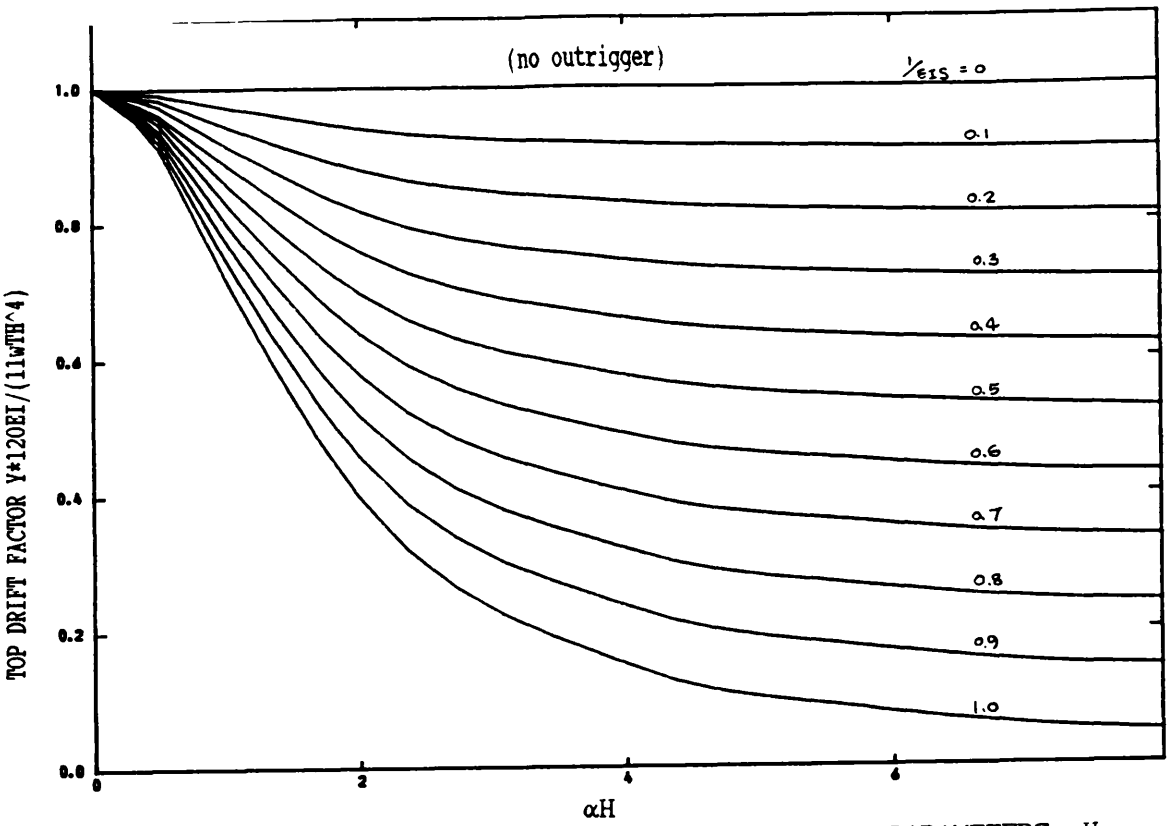

FIG. [3.8] VARIATION OF TOP DRIFT WITH STIFFNESS PARAMETERS αH AND 1/EIS
(TRIANGULARLY DISTRIBUTED LOAD, R=0)

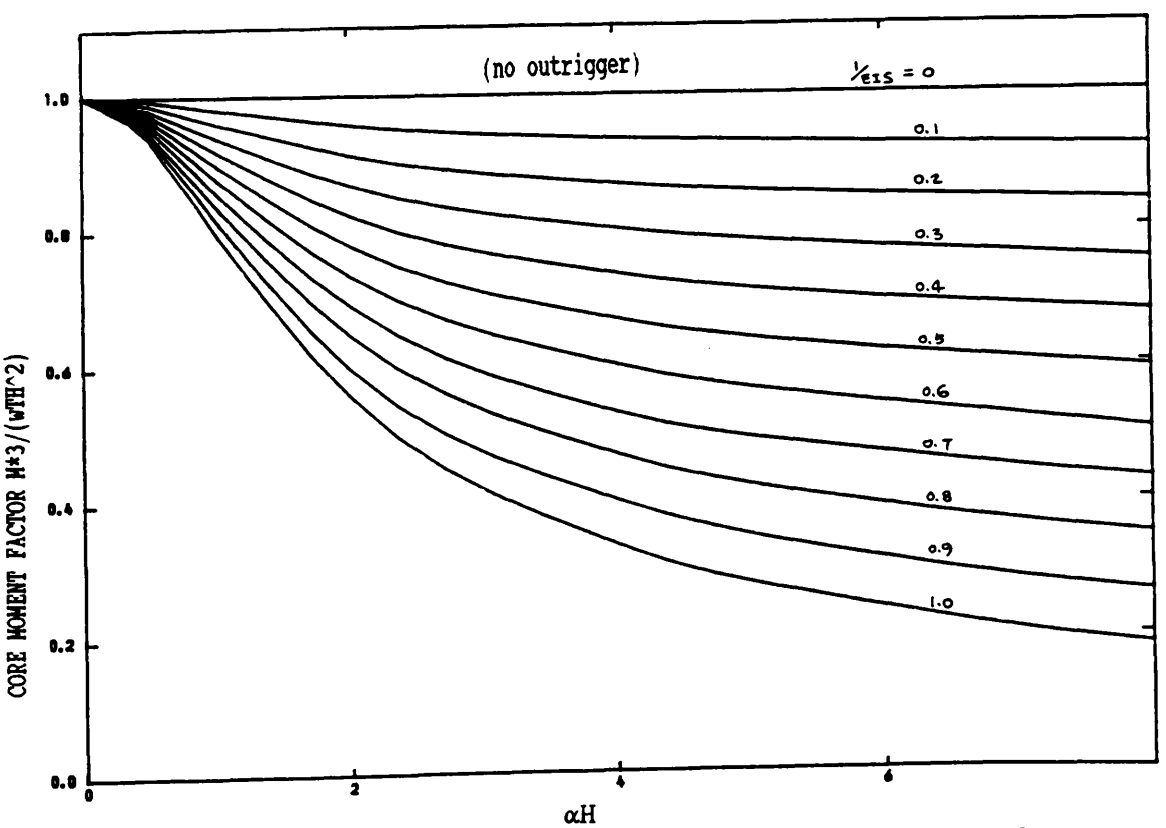

FIG. [3.9] VARIATION OF BASE MOMENT WITH STIFFNESS PARAMETERS αH AND 1/EIS
(TRIANGULARLY DISTRIBUTED LOAD, R=0)

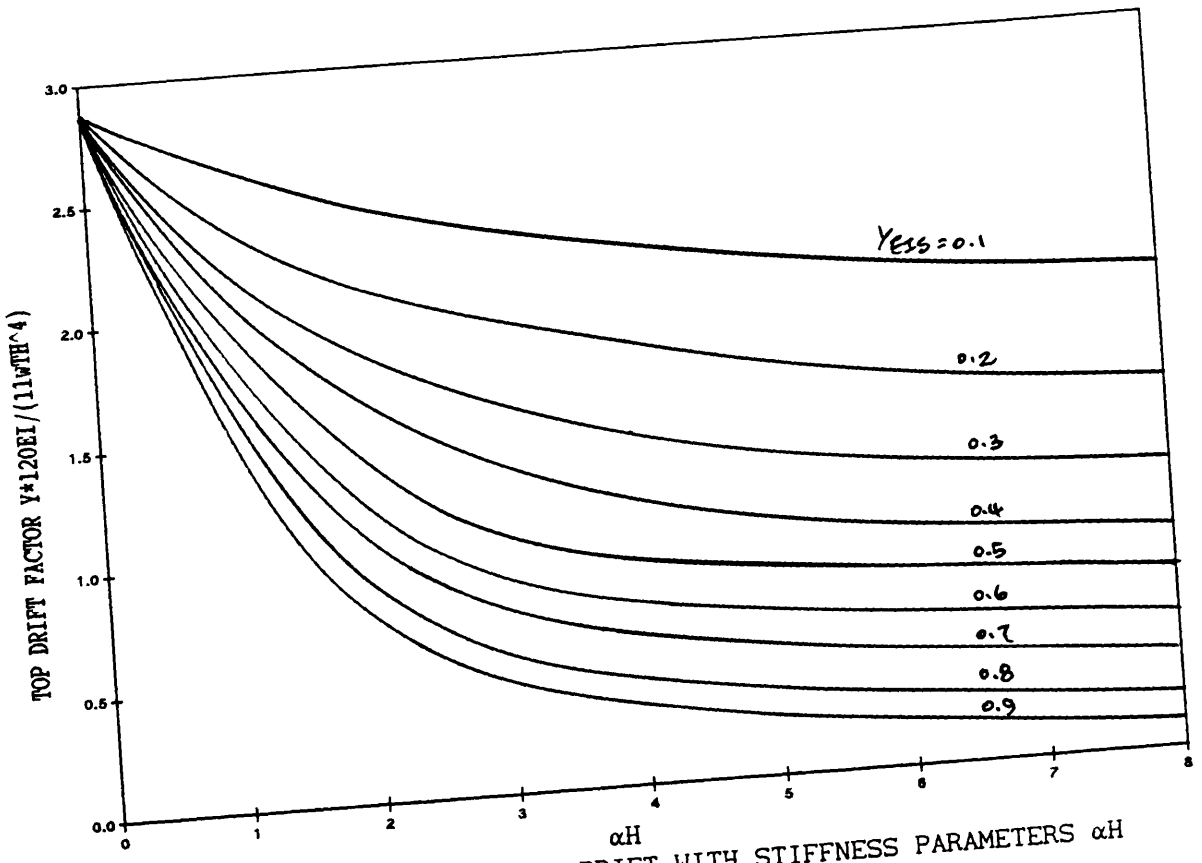

FIG.[3.10] VARIATION OF TOP DRIFT WITH STIFFNESS PARAMETERS αH AND 1/EIS
(TRIANGULARLY DISTRIBUTED LOAD, R=0.5)

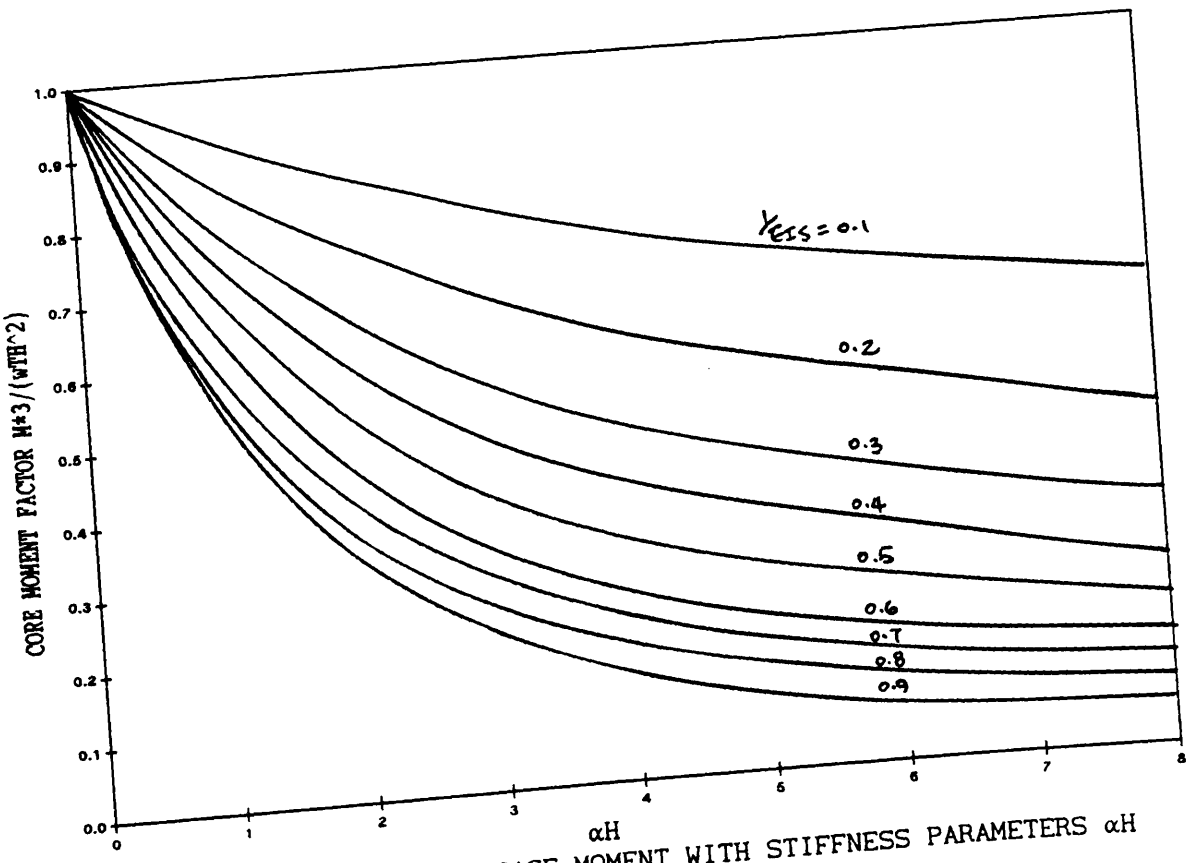

FIG.[3.11] VARIATION OF BASE MOMENT WITH STIFFNESS PARAMETERS αH AND 1/EIS
(TRIANGULARLY DISTRIBUTED LOAD, R=0.5)

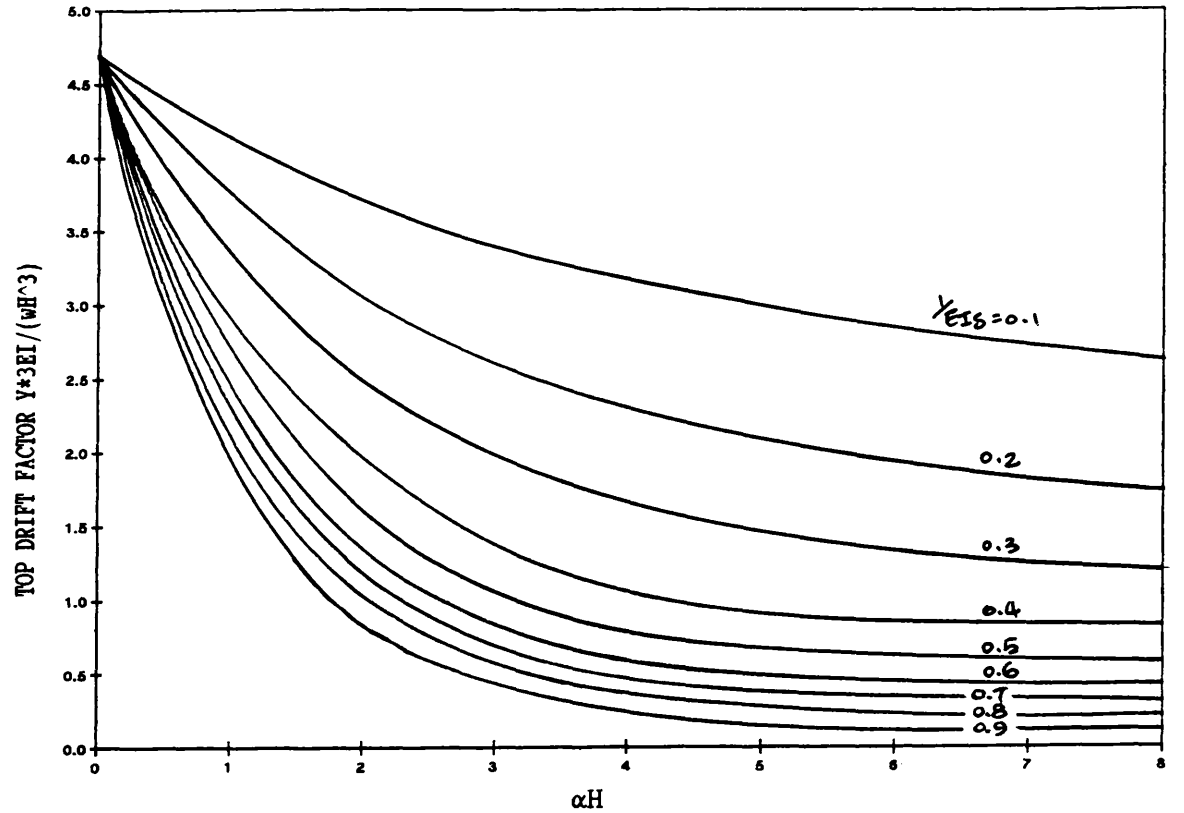

FIG.[3.12] VARIATION OF TOP DRIFT WITH STIFFNESS PARAMETERS αH AND 1/EIS
(TRIANGULARLY DISTRIBUTED LOAD, R=1.0)

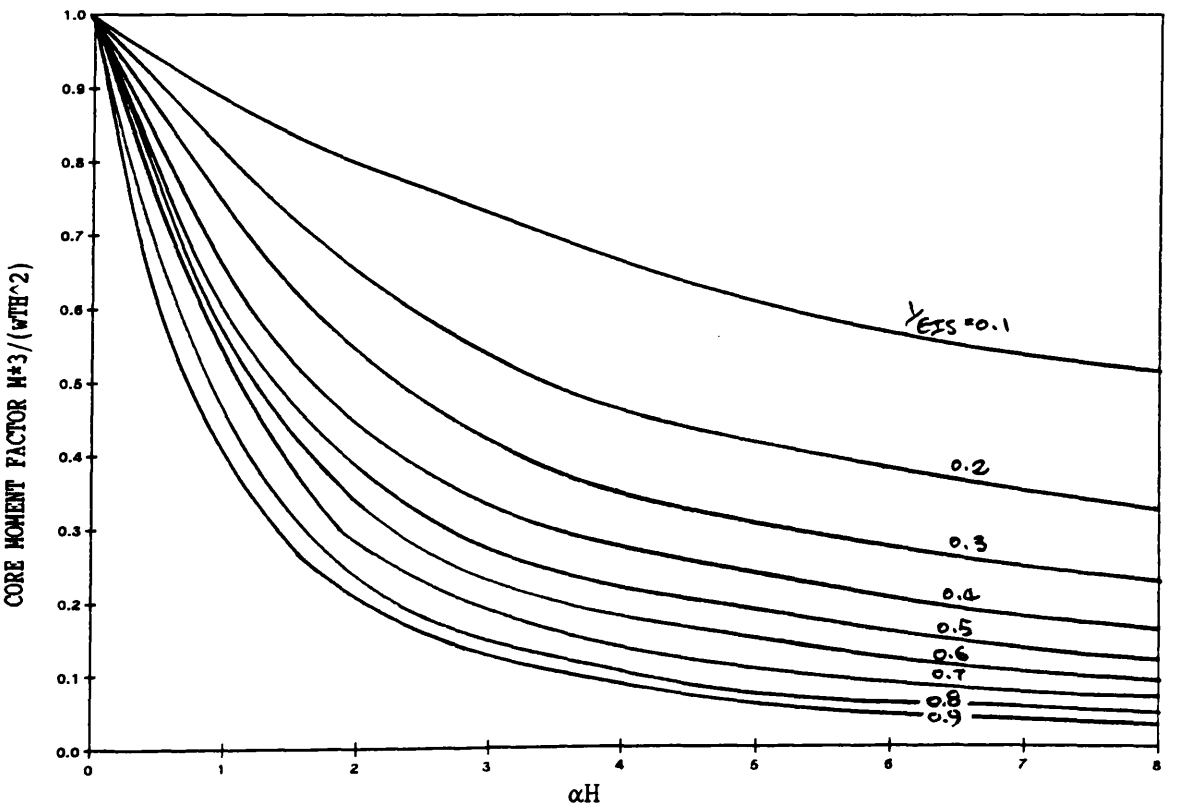

FIG.[3.13] VARIATION OF BASE MOMENT WITH STIFFNESS PARAMETERS αH AND 1/EIS
(TRIANGULARLY DISTRIBUTED LOAD, R=1.0)

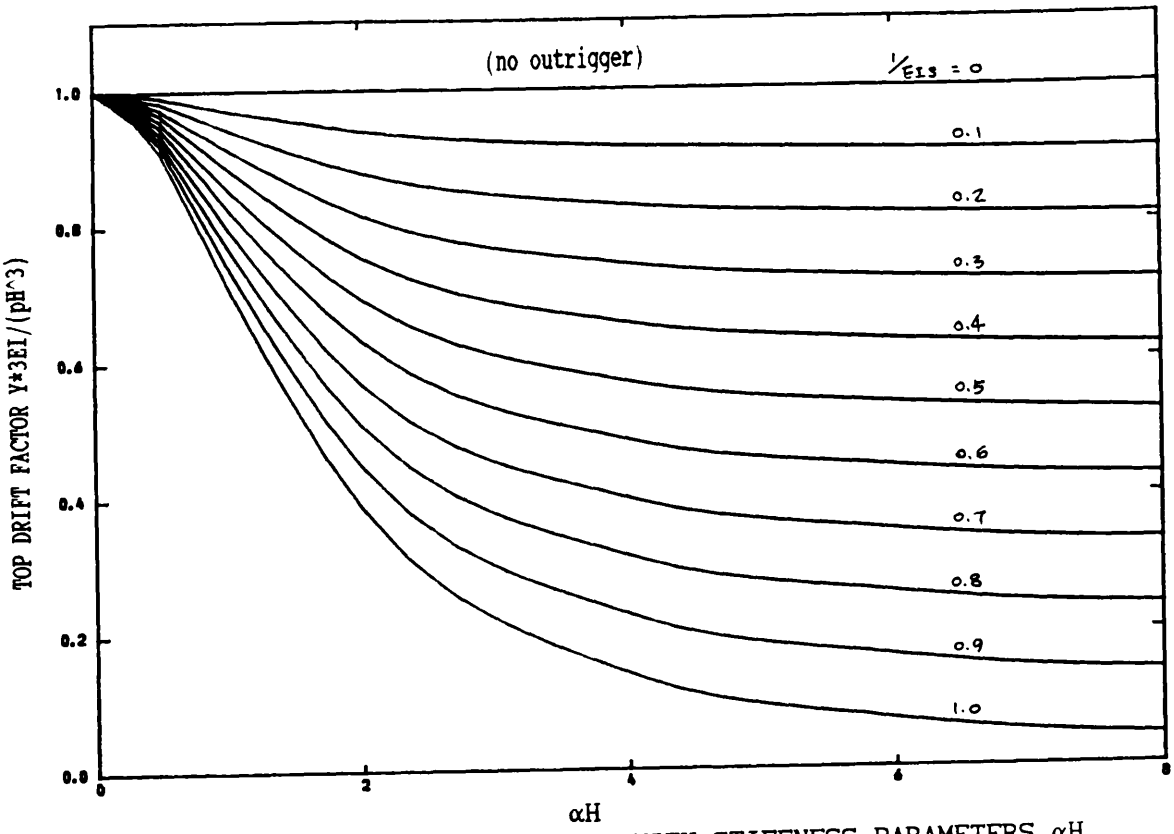

FIG. [3.14] VARIATION OF TOP DRIFT WITH STIFFNESS PARAMETERS αH AND 1/EIS
(POINT LOAD AT THE TOP, R=0)

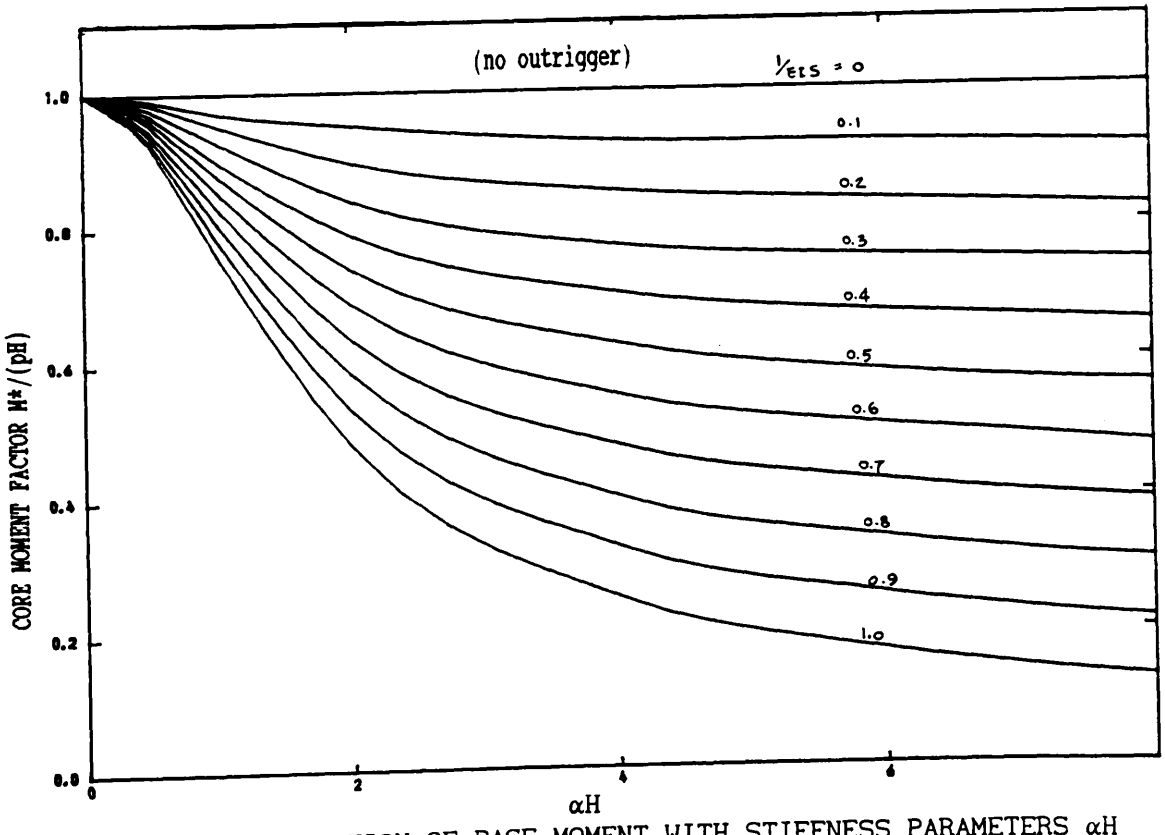

FIG. [3.15] VARIATION OF BASE MOMENT WITH STIFFNESS PARAMETERS αH AND 1/EIS
(POINT LOAD AT THE TOP, R=0)

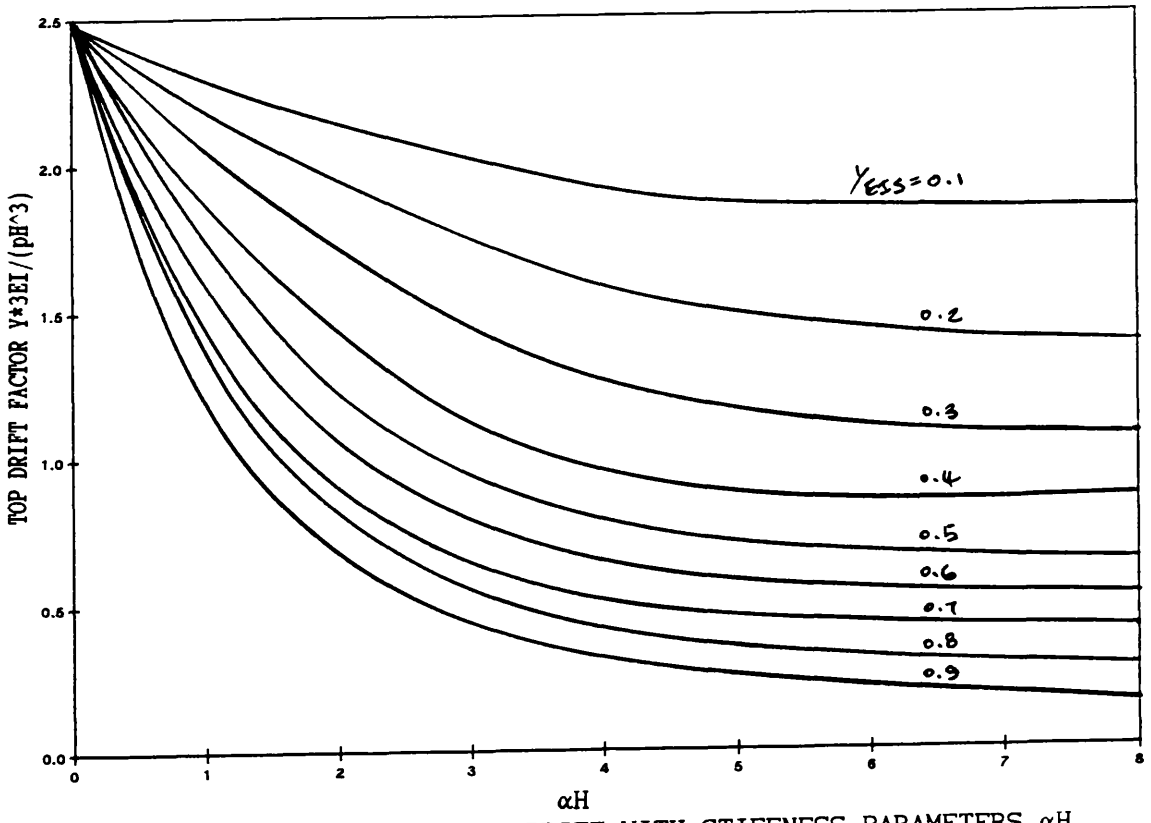

FIG.[3.16] VARIATION OF TOP DRIFT WITH STIFFNESS PARAMETERS αH AND 1/EIS
(POINT LOAD AT THE TOP, R=0.5)

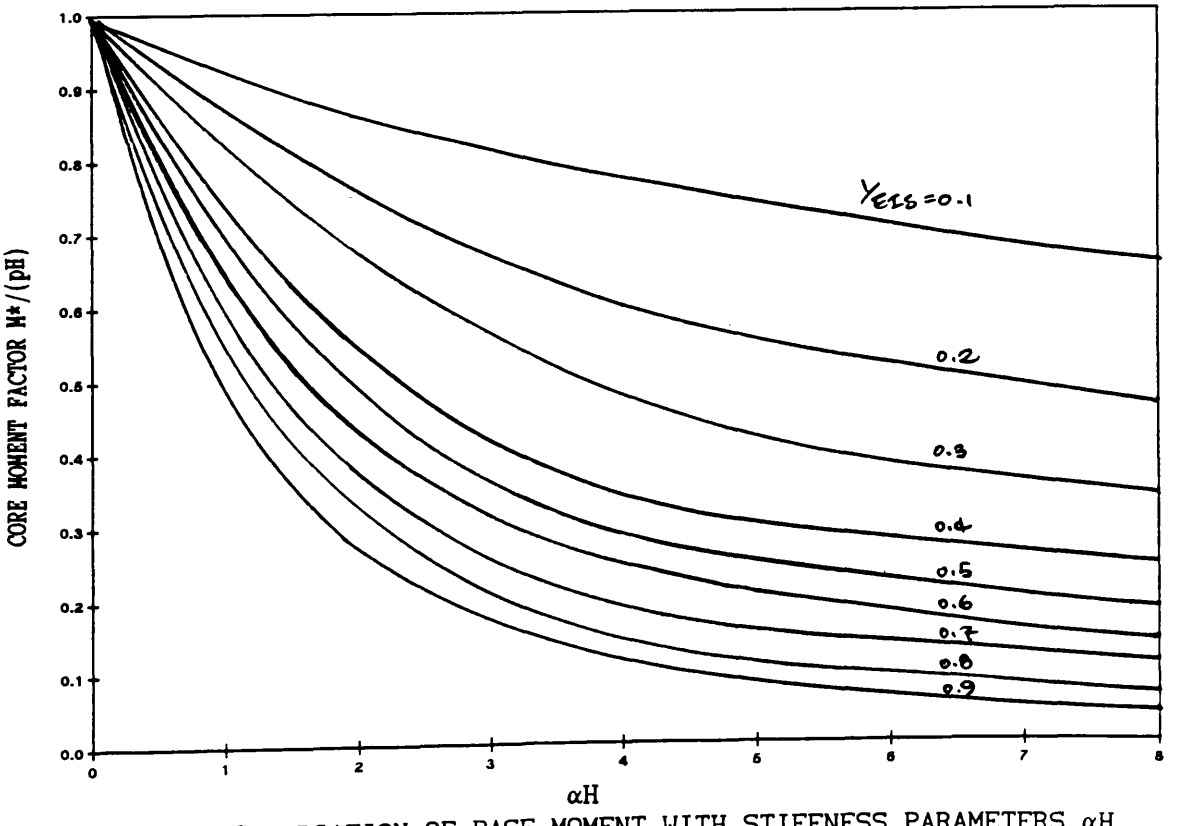

FIG.[3.17] VARIATION OF BASE MOMENT WITH STIFFNESS PARAMETERS αH AND 1/EIS
(POINT LOAD AT THE TOP, R=0.5)

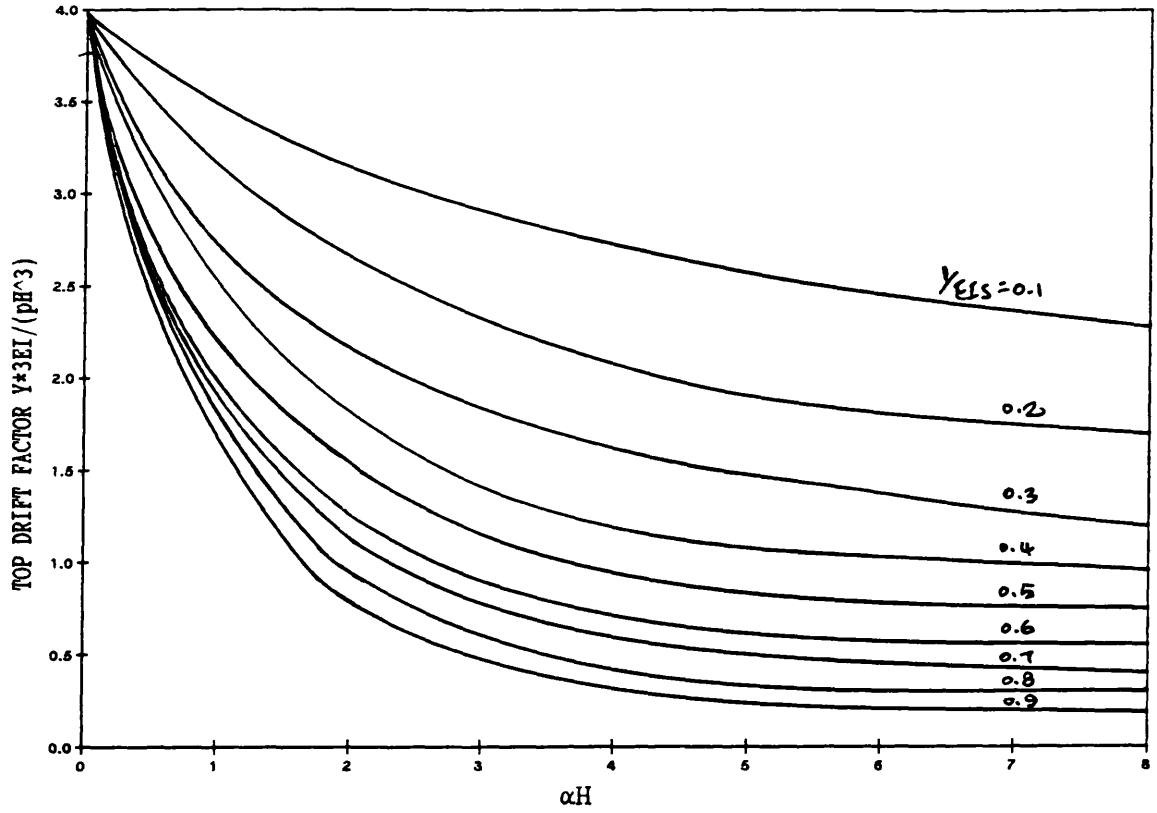

FIG.[3.18] VARIATION OF TOP DRIFT WITH STIFFNESS PARAMETERS αH AND 1/EIS
(POINT LOAD AT THE TOP, R=1.0)

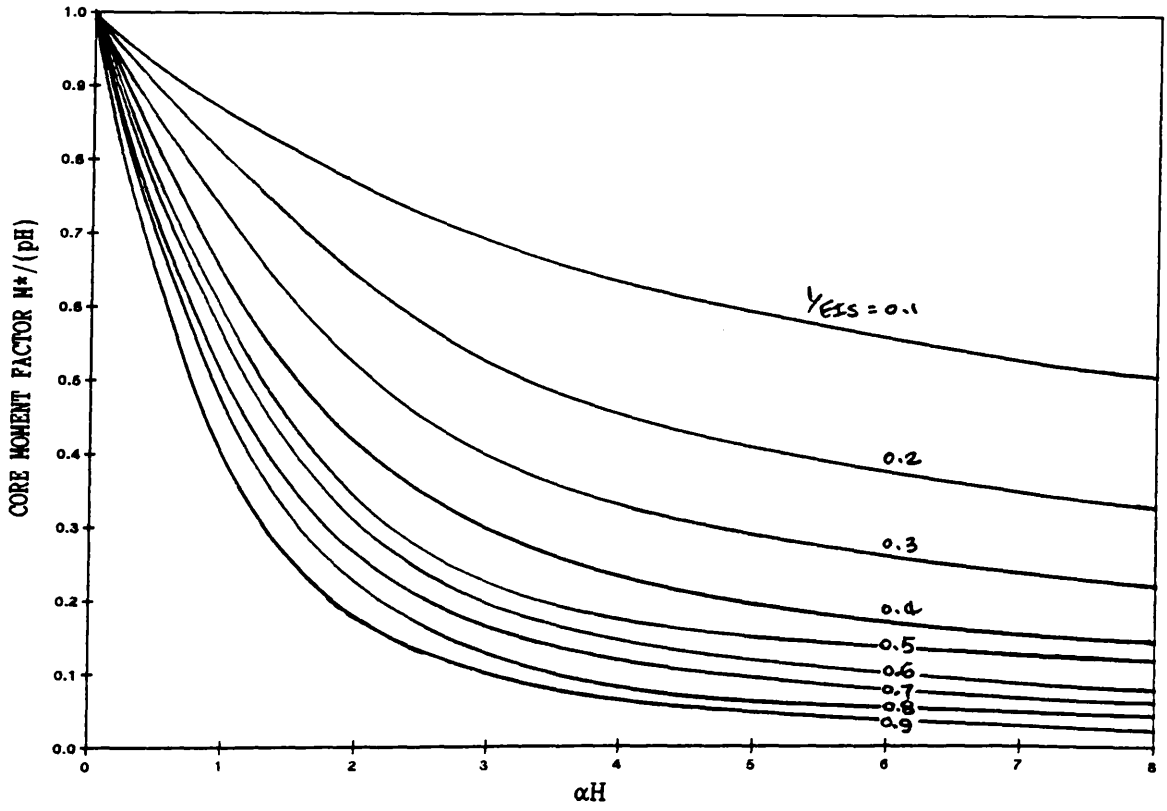

FIG.[3.19] VARIATION OF BASE MOMENT WITH STIFFNESS PARAMETERS αH AND 1/EIS
(POINT LOAD AT THE TOP, R=1.0)

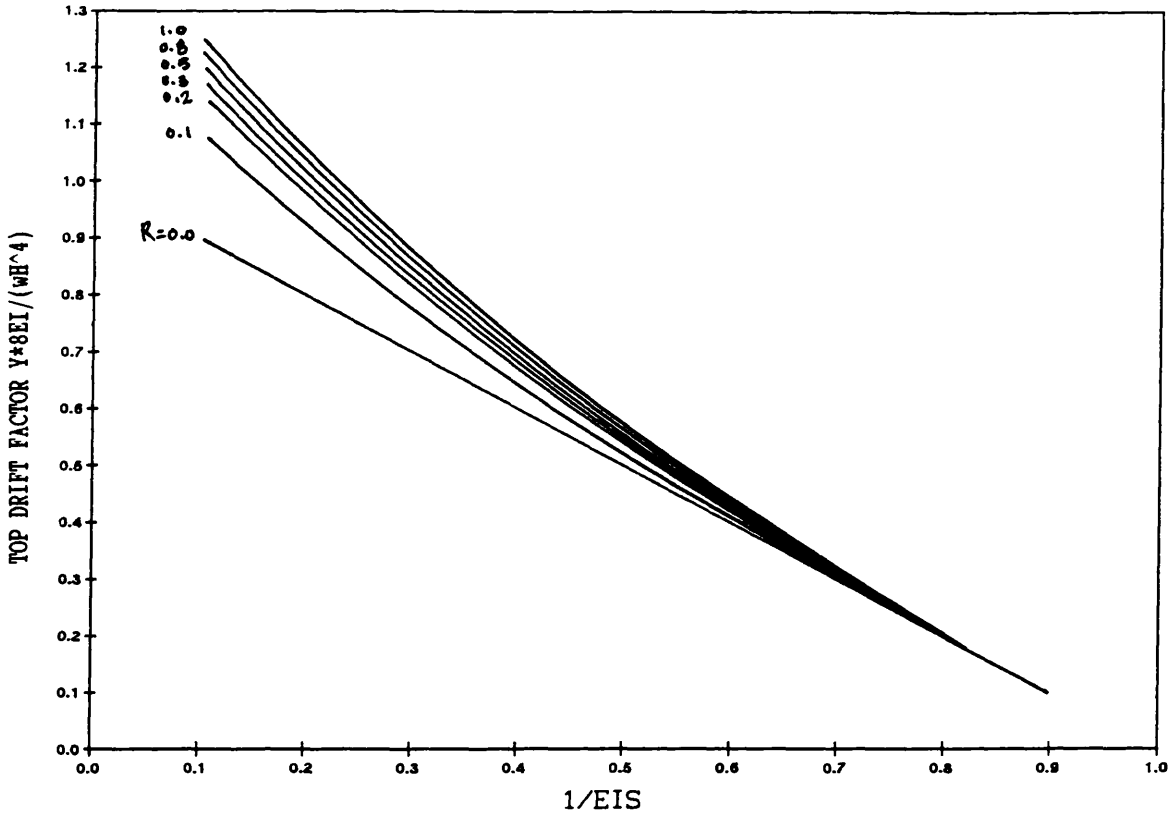

FIG. [3.20] VARIATION OF TOP DRIFT WITH PARAMETERS 1/EIS AND R (U.D.L., LIMITING CASE)

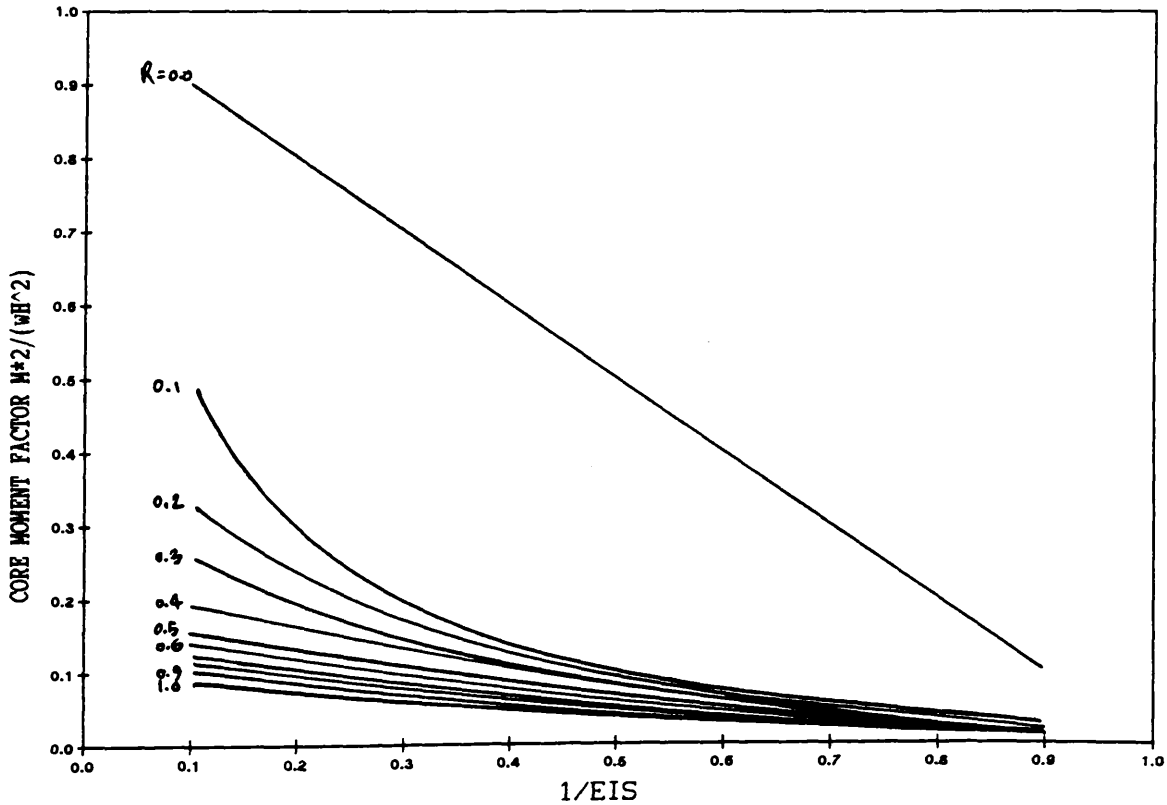

FIG. [3.21] VARIATION OF BASE MOMENT WITH PARAMETERS 1/EIS AND R (U.D.L., LIMITING CASE)

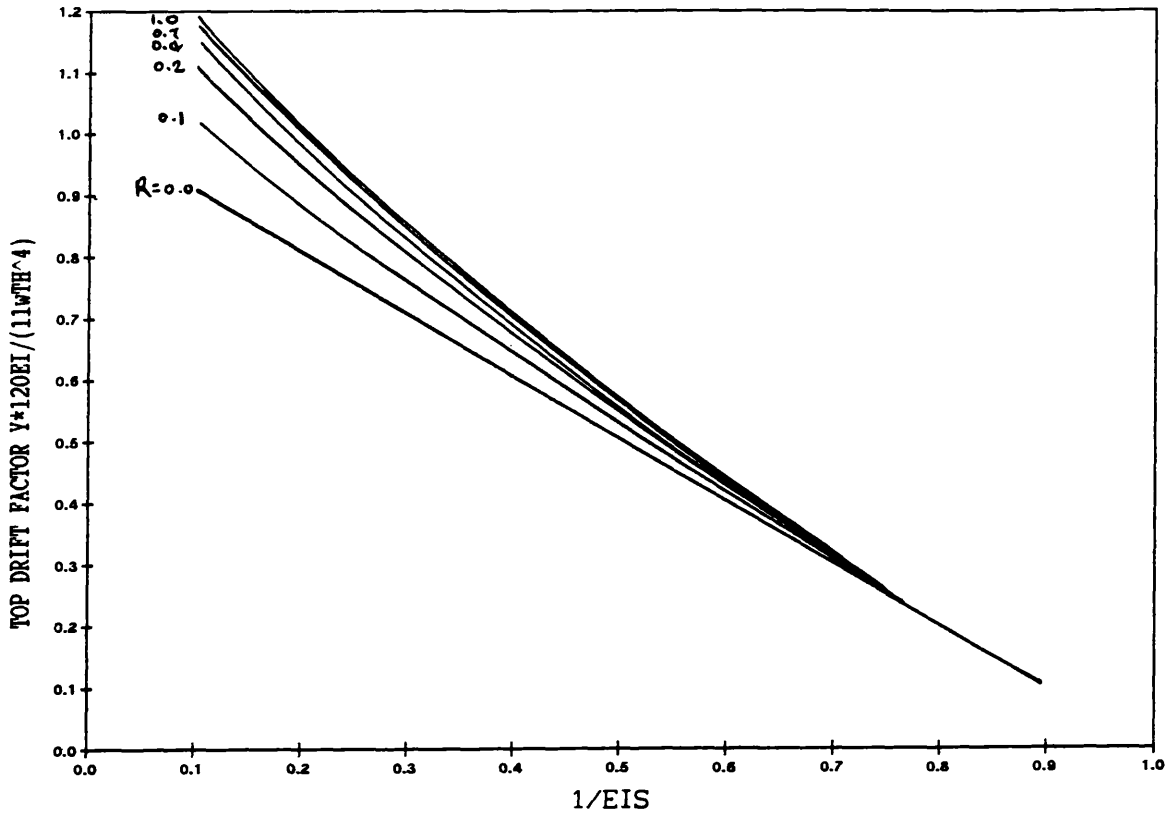

FIG.[3.22] VARIATION OF TOP DRIFT WITH PARAMETERS 1/EIS AND R
(TRIANGULARLY DISTRIBUTED LOAD, LIMITING CASE)

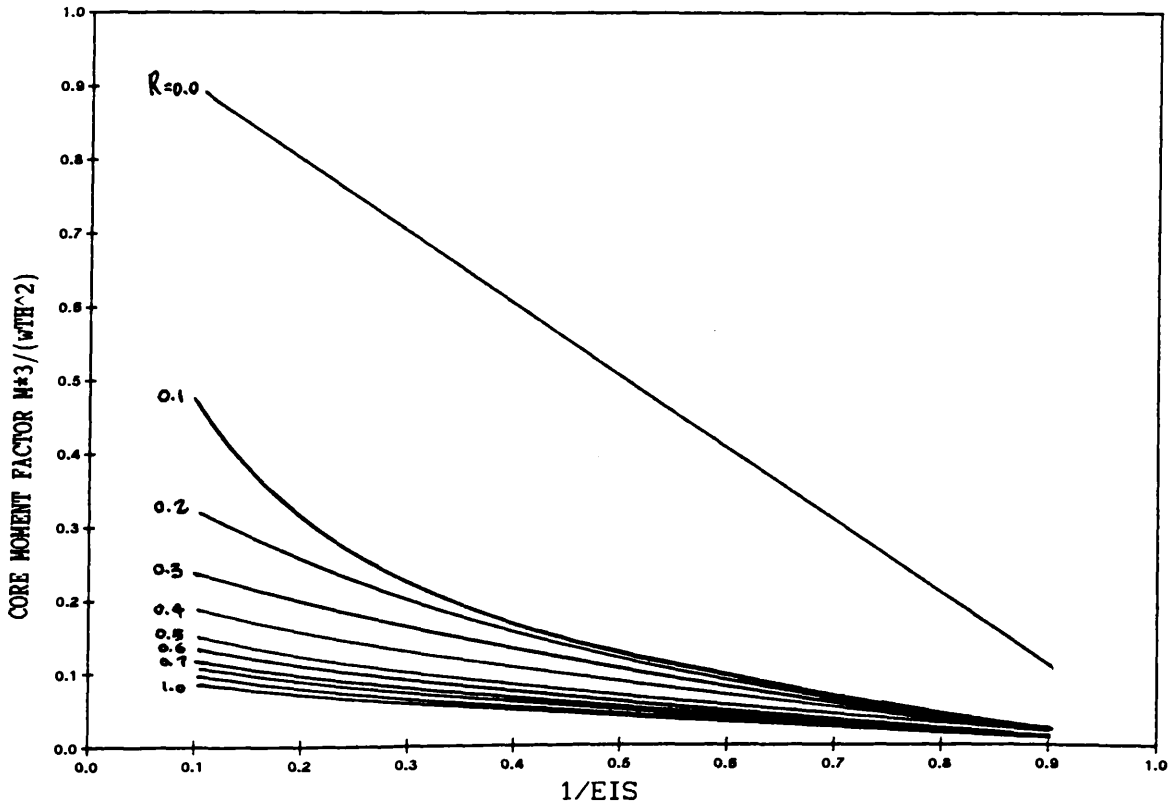

FIG.[3.23] VARIATION OF BASE MOMENT WITH PARAMETERS 1/EIS AND R
(TRIANGULARLY DISTRIBUTED LOAD, LIMITING CASE)

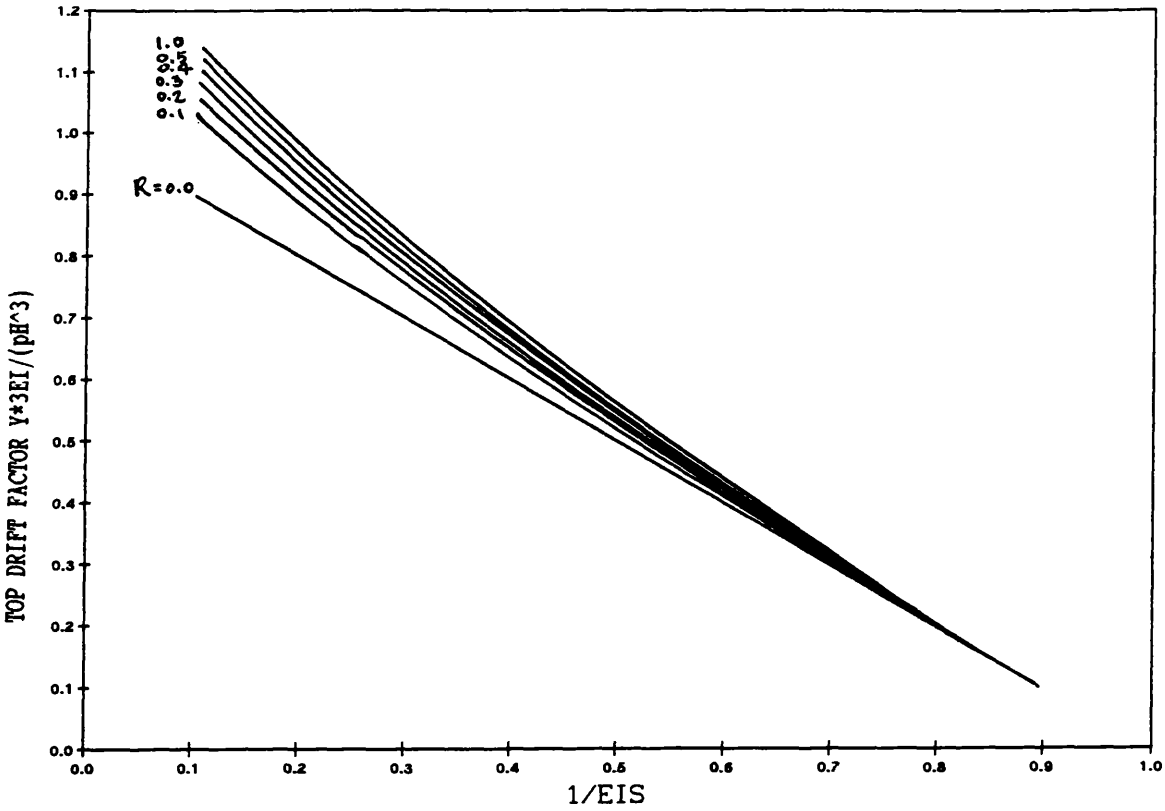

FIG.[3.24] VARIATION OF TOP DRIFT WITH PARAMETERS 1/EIS AND R
(POINT LOAD AT THE TOP, LIMITING CASE)

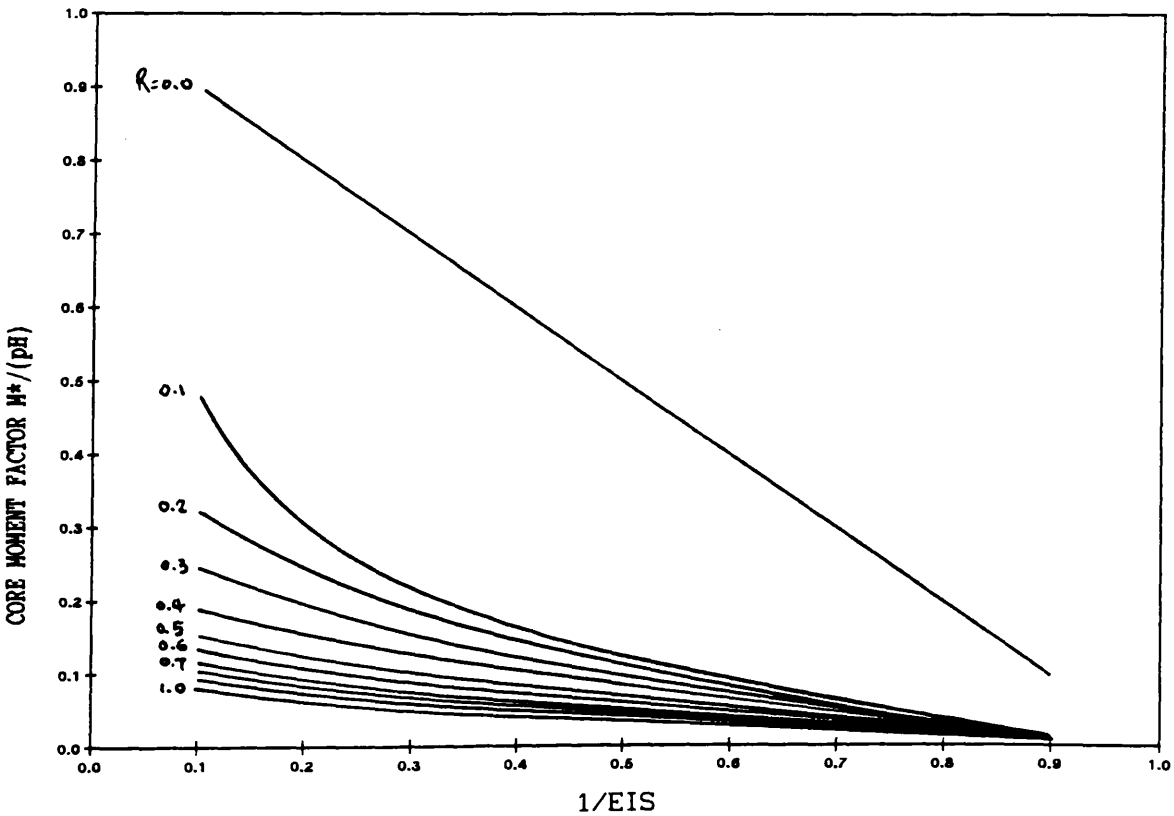

FIG.[3.25] VARIATION OF BASE MOMENT WITH PARAMETERS 1/EIS AND R
(POINT LOAD AT THE TOP, LIMITING CASE)

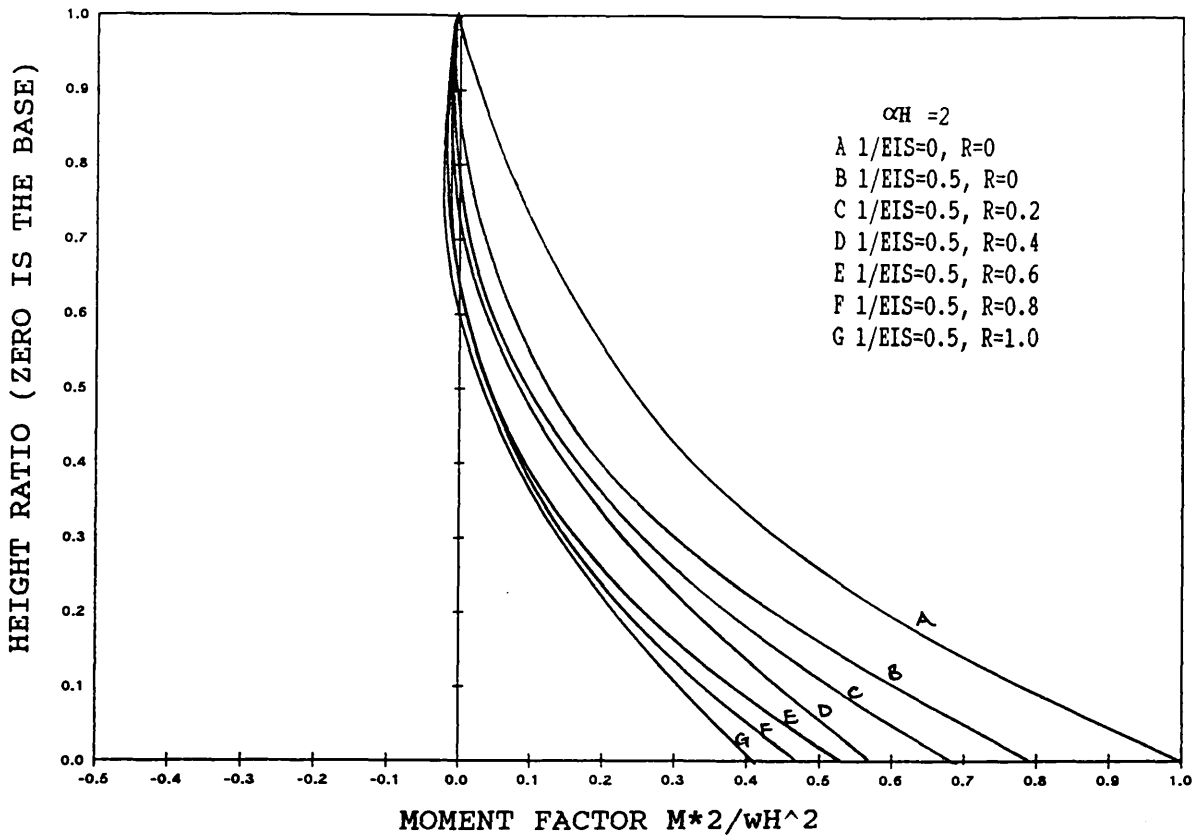

FIG.[3.26] VARIATION OF BENDING MOMENT WITH HEIGHT FOR DIFFERENT BASE FLEXIBILITIES FACTOR R (U.D.L.)

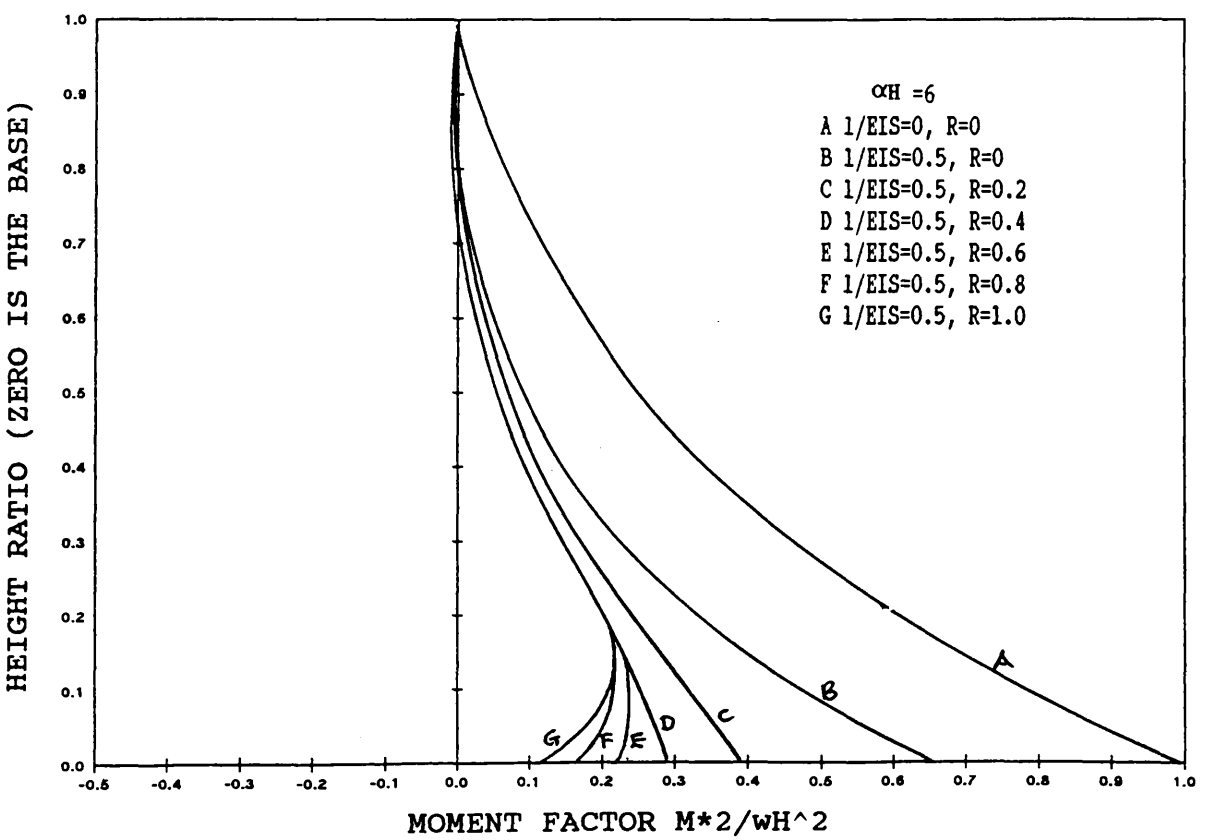

FIG.[3.27] VARIATION OF BENDING MOMENT WITH HEIGHT FOR DIFFERENT BASE FLEXIBILITIES FACTOR R (U.D.L.)

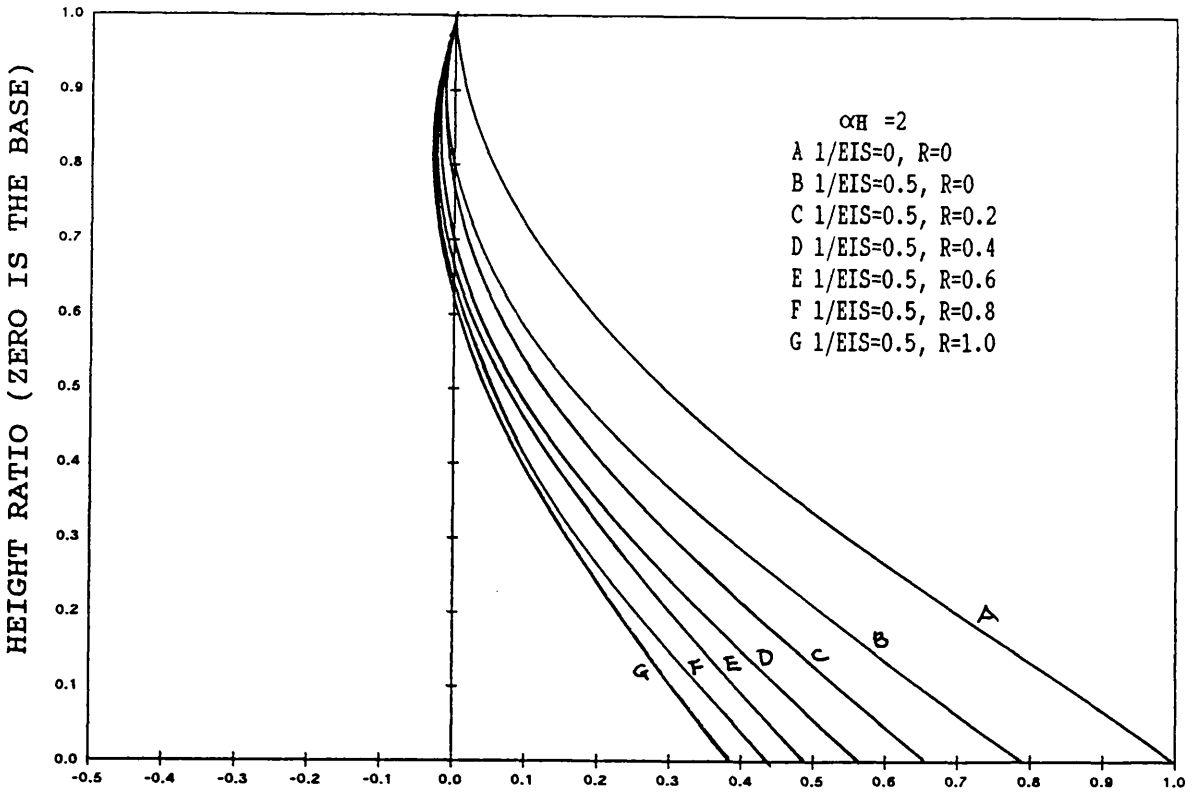

FIG.[3.28] VARIATION OF BENDING MOMENT WITH HEIGHT FOR DIFFERENT BASE FLEXIBILITIES FACTOR R (TRIANGULARLY DISTRIBUTED LOAD)

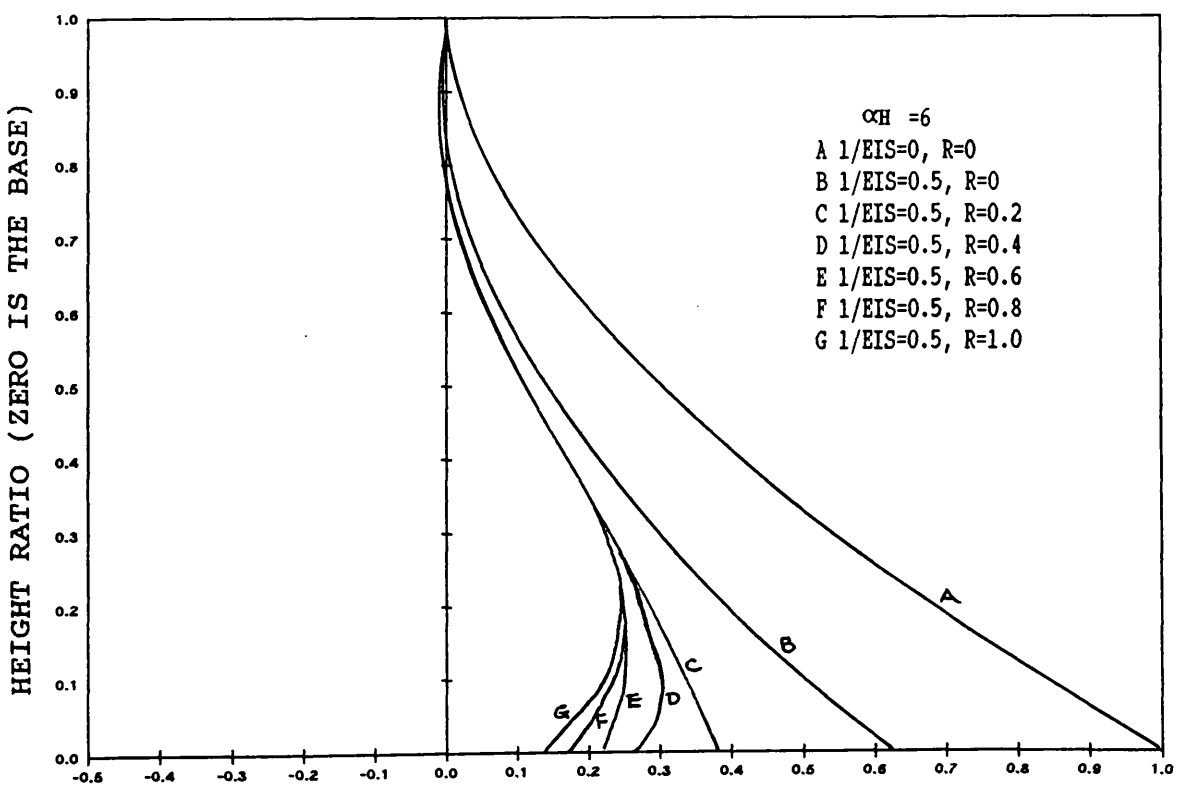

FIG.[3.29] VARIATION OF BENDING MOMENT WITH HEIGHT FOR DIFFERENT BASE FLEXIBILITIES FACTOR R (TRIANGULARLY DISTRIBUTED LOAD)

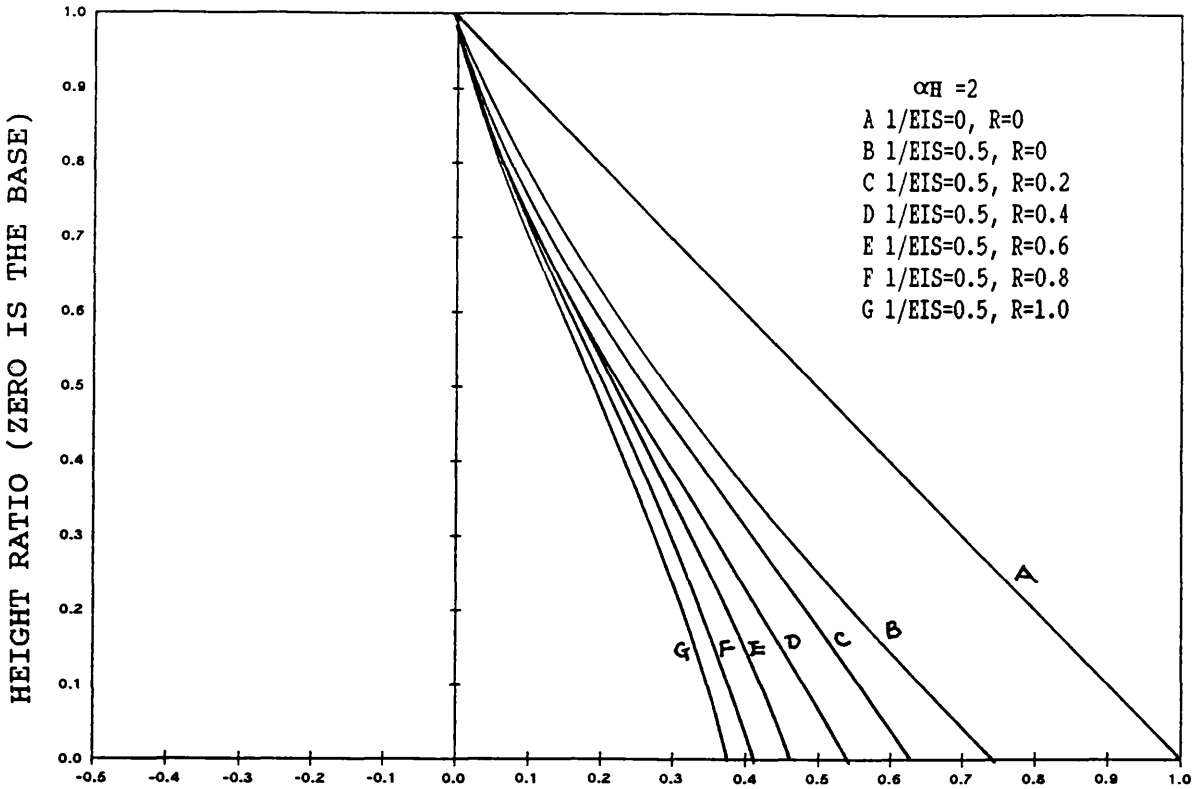

FIG.[3.30] VARIATION OF BENDING MOMENT WITH HEIGHT FOR DIFFERENT BASE FLEXIBILITIES FACTOR R (POINT LOAD AT THE TOP)

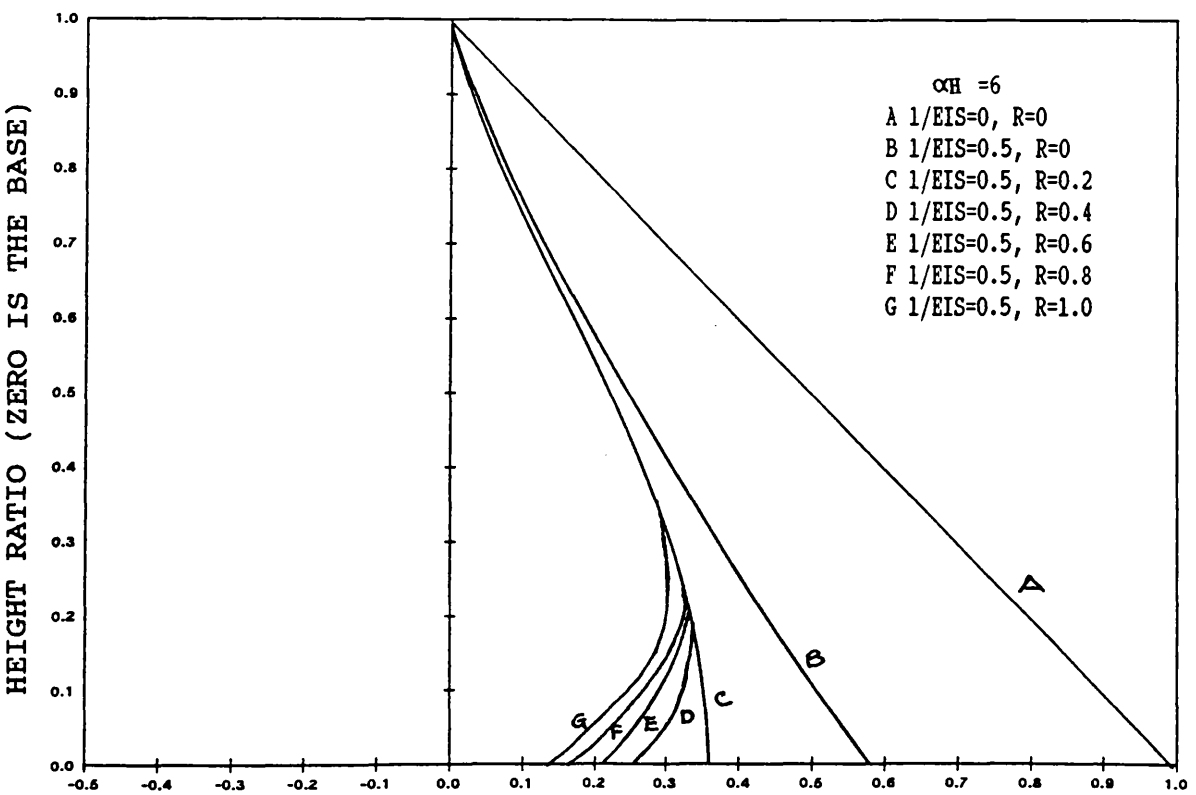

FIG.[3.31] VARIATION OF BENDING MOMENT WITH HEIGHT FOR DIFFERENT BASE FLEXIBILITIES FACTOR R (POINT LOAD AT THE TOP)

Table [3.1] Comparison of relative top drift factors (y_T/y_{FT}) for U.D.L.

R	n	ω (αH)	1/EIS	Optimum spacing (Drift)	Uniform spacings Type (i)	Type (ii)	Type (iii)	Continuum
0.0	1	0.1	0.1	0.925	0.940	0.927		0.922
		(3.162)	0.5	0.626	0.700	0.635		0.610
		0.5	0.1	0.951	0.956	0.956		0.957
		(1.414)	0.5	0.754	0.781	0.778		0.785
	2	0.1	0.1	0.914	0.915	0.916	0.917	0.913
		(4.472)	0.5	0.570	0.572	0.582	0.586	0.565
		0.5	0.1	0.936	0.940	0.941	0.938	0.940
		(2.000)	0.5	0.678	0.700	0.709	0.688	0.700
	3	0.1	0.1	0.909	0.910	0.911	0.911	0.909
		(5.477)	0.5	0.545	0.550	0.556	0.557	0.546
		0.5	0.1	0.928	0.930	0.932	0.930	0.931
		(2.449)	0.5	0.640	0.653	0.662	0.650	0.657
	50	0.1	0.1					0.900
		(22.361)	0.5					0.503
		0.5	0.1					0.903
		(10.000)	0.5					0.516
0.5	1	0.1	0.1	2.350	2.710	2.574		2.443
		(3.162)	0.5	1.328	1.765	1.370		1.413
		0.5	0.1	2.736	2.785	2.736		2.717
		(1.414)	0.5	1.890	2.048	1.892		1.847
	2	0.1	0.1	2.060	2.465	2.424	2.549	2.323
		(4.472)	0.5	0.907	1.116	1.069	1.281	0.955
		0.5	0.1	2.583	2.625	2.617	2.664	2.600
		(2.000)	0.5	1.526	1.539	1.535	1.630	1.500
	3	0.1	0.1	1.938	2.400	2.335	2.459	2.250
		(5.477)	0.5	0.795	1.004	0.943	1.095	0.871
		0.5	0.1	2.464	2.559	2.544	2.593	2.530
		(2.449)	0.5	1.315	1.363	1.349	1.430	1.326
	50	0.1	0.1					1.677
		(22.361)	0.5					0.590
		0.5	0.1					2.017
		(10.000)	0.5					0.702
1.0	1	0.1	0.1	3.057	4.333	3.985		3.599
		(3.162)	0.5	1.570	2.500	1.771		1.349
		0.5	0.1	4.314	4.500	4.354		4.281
		(1.414)	0.5	2.621	3.000	2.632		2.500
	2	0.1	0.1	2.476	3.712	3.585	3.943	3.297
		(4.472)	0.5	0.951	1.316	1.265	1.656	1.075
		0.5	0.1	3.826	4.083	4.047	4.206	3.992
		(2.000)	0.5	1.890	2.013	1.979	2.219	1.907
	3	0.1	0.1	2.352	3.540	3.348	3.704	3.116
		(5.477)	0.5	0.827	1.183	1.072	1.338	0.958
		0.5	0.1	3.505	3.922	3.862	4.023	3.818
		(2.449)	0.5	1.536	1.722	1.674	1.861	1.628
	50	0.1	0.1					1.916
		(22.361)	0.5					0.597
		0.5	0.1					2.574
		(10.000)	0.5					0.733

Table [3.2] Comparison of relative top drift factors (y_T/y_{FT}) for triangularly distributed load

R	n	ω (αH)	1/EIS	Optimum spacing (Drift)	Uniform spacings Type (i)	Type (ii)	Type (iii)	Continuum
0.0	1	0.1	0.1	0.924	0.938	0.927		0.922
			0.5	0.622	0.690	0.636		0.608
		0.5	0.1	0.950	0.955	0.956		0.957
			0.5	0.750	0.773	0.782		0.783
	2	0.1	0.1	0.913	0.914	0.916	0.916	0.912
			0.5	0.567	0.572	0.581	0.582	0.563
		0.5	0.1	0.935	0.940	0.941	0.937	0.940
			0.5	0.674	0.698	0.707	0.684	0.700
	3	0.1	0.1	0.909	0.910	0.911	0.911	0.909
			0.5	0.547	0.548	0.554	0.554	0.545
		0.5	0.1	0.925	0.930	0.932	0.929	0.931
			0.5	0.635	0.652	0.660	0.646	0.655
	50	0.1	0.1					0.900
			0.5					0.500
		0.5	0.1					0.903
			0.5					0.516
0.5	1	0.1	0.1	2.122	2.400	2.283		2.298
		(3.162)	0.5	1.187	1.536	1.203		1.078
		0.5	0.1	2.428	2.468	2.428		2.552
		(1.414)	0.5	1.664	1.794	1.671		1.734
	2	0.1	0.1	1.874	2.188	2.155	2.258	2.188
		(4.472)	0.5	0.841	0.983	0.950	1.114	0.906
		0.5	0.1	2.301	2.330	2.324	2.361	2.443
		(2.000)	0.5	1.354	1.357	1.357	1.425	1.409
	3	0.1	0.1	1.761	2.135	2.082	2.184	2.122
		(5.477)	0.5	0.744	0.891	0.847	0.962	0.830
		0.5	0.1	2.203	2.274	2.262	2.301	2.378
		(2.449)	0.5	1.181	1.204	1.196	1.255	1.247
	50	0.1	0.1					1.605
		(22.361)	0.5					0.580
		0.5	0.1					1.912
		(10.000)	0.5					0.679
1.0	1	0.1	0.1	2.710	3.740	3.444		3.344
		(3.162)	0.5	1.407	2.116	1.511		1.260
		0.5	0.1	3.745	3.887	3.766		3.970
		(1.414)	0.5	2.261	2.559	2.263		2.318
	2	0.1	0.1	2.223	3.213	3.109	3.404	3.069
		(4.472)	0.5	0.875	1.168	1.097	1.400	1.012
		0.5	0.1	3.335	3.532	3.504	3.633	3.704
		(2.000)	0.5	1.660	1.729	1.706	1.888	1.770
	3	0.1	0.1	2.105	3.073	2.916	3.208	2.906
		(5.477)	0.5	0.769	1.027	0.944	1.146	0.906
		0.5	0.1	3.067	3.397	3.349	3.481	3.544
		(2.449)	0.5	1.361	1.484	1.449	1.590	1.515
	50	0.1	0.1					1.822
		(22.361)	0.5					0.587
		0.5	0.1					2.416
		(10.000)	0.5					0.707

Table [3.3] Comparison of relative top drift factors (y_T/y_{FT}) for point load at the top

R	n	ω (αH)	1/EIS	Optimum spacing (Drift)	Uniform spacings Type (i)	Type (ii)	Type (iii)	Continuum
	1	0.1	0.1	0.922	0.932	0.930		0.921
			0.5	0.612	0.659	0.649		0.603
		0.5	0.1	0.947	0.950	0.958		0.956
			0.5	0.734	0.750	0.789		0.779
	2	0.1	0.1	0.912	0.915	0.915	0.914	0.912
			0.5	0.561	0.576	0.577	0.572	0.558
		0.5	0.1	0.932	0.940	0.941	0.934	0.939
			0.5	0.660	0.700	0.703	0.672	0.694
	3	0.1	0.1	0.908	0.910	0.910	0.909	0.908
			0.5	0.542	0.550	0.551	0.547	0.541
		0.5	0.1	0.925	0.931	0.931	0.927	0.930
			0.5	0.624	0.653	0.655	0.635	0.649
	50	0.1	0.1					0.901
			0.5					0.503
		0.5	0.1					0.903
			0.5					0.514
0.5	1	0.1	0.1	2.012	2.147			2.045
		(3.162)	0.5	1.148	1.149			0.966
		0.5	0.1	2.279	2.281			2.264
		(1.414)	0.5	1.556	1.581			1.535
	2	0.1	0.1	1.788	2.061	2.030	2.117	1.955
		(4.472)	0.5	0.815	0.943	0.908	1.036	0.823
		0.5	0.1	2.164	2.189	2.183	2.211	2.169
		(2.000)	0.5	1.279	1.286	1.279	1.321	1.250
	3	0.1	0.1	1.680	2.012	1.964	2.052	1.901
		(5.477)	0.5	0.727	0.550	0.550	0.908	0.762
		0.5	0.1	2.075	2.136	2.124	2.157	2.113
		(2.449)	0.5	1.120	0.652	0.655	1.169	1.109
	50	0.1	0.1					1.480
		(22.361)	0.5					0.565
		0.5	0.1					1.731
		(10.000)	0.5					0.643
1.0	1	0.1	0.1	2.243	3.190			2.900
		(3.162)	0.5	1.375	1.422			1.106
		0.5	0.1	3.475	3.484			3.426
		(1.414)	0.5	2.107	2.109			2.000
	2	0.1	0.1	2.107	2.982	2.890	3.145	2.675
		(4.472)	0.5	0.848	1.108	1.042	1.286	0.905
		0.5	0.1	3.102	3.270	3.243	3.352	3.200
		(2.000)	0.5	1.556	1.616	1.590	1.727	1.533
	3	0.1	0.1	1.994	2.855	2.715	2.972	2.543
		(5.477)	0.5	0.752	0.979	0.903	1.071	0.821
		0.5	0.1	2.857	3.145	3.100	3.214	3.066
		(2.449)	0.5	1.286	1.388	1.353	1.463	1.318
	50	0.1	0.1					1.659
		(22.361)	0.5					0.570
		0.5	0.1					2.145
		(10.000)	0.5					0.665

Table [3.4] Comparison of relative base moment factors (M_B/M_{aB}) for U.D.L.

R	n	ω (αH)	1/EIS	Optimum spacing (Drift)	Uniform spacings Type (i)	Type (ii)	Type (iii)	Continuum
0.0	1	0.1	0.1	0.973	0.970	0.951		0.945
			0.5	0.867	0.849	0.757		0.724
		0.5	0.1	0.956	0.978	0.971		0.972
			0.5	0.779	0.889	0.854		0.858
	2	0.1	0.1	0.943	0.939	0.937	0.949	0.935
			0.5	0.716	0.697	0.684	0.746	0.675
		0.5	0.1	0.963	0.959	0.959	0.963	0.960
			0.5	0.814	0.793	0.796	0.817	0.798
	3	0.1	0.1	0.936	0.933	0.931	0.939	0.930
			0.5	0.682	0.667	0.654	0.695	0.650
		0.5	0.1	0.956	0.952	0.953	0.955	0.953
			0.5	0.782	0.759	0.763	0.777	0.746
	50	0.1	0.1					0.909
			0.5					0.543
		0.5	0.1					0.918
			0.5					0.590
0.5	1	0.1	0.1	0.681	0.928	0.878		0.816
		(3.162)	0.5	0.461	0.691	0.534		0.405
		0.5	0.1	0.923	0.946	0.925		0.914
		(1.414)	0.5	0.690	0.762	0.683		0.653
	2	0.1	0.1	0.547	0.838	0.815	0.875	0.764
		(4.472)	0.5	0.205	0.434	0.392	0.523	0.319
		0.5	0.1	0.845	0.890	0.883	0.909	0.875
		(2.000)	0.5	0.542	0.571	0.557	0.628	0.539
	3	0.1	0.1	0.546	0.809	0.774	0.837	0.730
		(5.477)	0.5	0.173	0.378	0.325	0.432	0.274
		0.5	0.1	0.790	0.867	0.857	0.883	0.850
		(2.449)	0.5	0.423	0.510	0.490	0.552	0.477
	50	0.1	0.1					0.429
		(22.361)	0.5					0.082
		0.5	0.1					0.612
		(10.000)	0.5					0.169
1.0	1	0.1	0.1	0.519	0.889	0.815		0.718
		(3.162)	0.5	0.268	0.583	0.413		0.281
		0.5	0.1	0.854	0.917	0.883		0.863
		(1.414)	0.5	0.553	0.667	0.569		0.527
	2	0.1	0.1	0.381	0.756	0.722	0.811	0.646
		(4.472)	0.5	0.118	0.315	0.275	0.402	0.209
		0.5	0.1	0.737	0.830	0.819	0.860	0.805
		(2.000)	0.5	0.348	0.446	0.429	0.510	0.407
	3	0.1	0.1	0.381	0.715	0.663	0.755	0.601
		(5.477)	0.5	0.097	0.263	0.216	0.314	0.174
		0.5	0.1	0.663	0.796	0.779	0.821	0.768
		(2.449)	0.5	0.278	0.384	0.361	0.428	0.346
	50	0.1	0.1					0.281
		(22.361)	0.5					0.045
		0.5	0.1					0.459
		(10.000)	0.5					0.098

Table [3.5] Comparison of relative base moment factors (M_B/M_{aB}) for triangularly distributed load

R	n	ω (αH)	1/EIS	Optimum spacing (Drift)	Uniform spacings Type (i)	Type (ii)	Type (iii)	Continuum
0.0	1	0.1	0.1	0.952	0.966	0.947		0.940
			0.5	0.759	0.830	0.733		0.702
		0.5	0.1	0.970	0.975	0.968		0.969
			0.5	0.852	0.875	0.840		0.844
	2	0.1	0.1	0.939	0.932	0.944		0.931
			0.5	0.674	0.662	0.720		0.653
		0.5	0.1	0.959	0.955	0.956	0.959	0.956
			0.5	0.796	0.775	0.779	0.797	0.780
	3	0.1	0.1	0.932	0.929	0.927	0.934	0.926
			0.5	0.663	0.643	0.633	0.670	0.628
		0.5	0.1	0.953	0.948	0.949	0.951	0.949
			0.5	0.763	0.738	0.743	0.756	0.744
	50	0.1	0.1					0.907
			0.5					0.533
		0.5	0.1					0.915
			0.5					0.574
0.5	1	0.1	0.1	0.681	0.924	0.874		0.812
		(3.162)	0.5	0.474	0.676	0.517		0.393
		0.5	0.1	0.922	0.943	0.922		0.912
		(1.414)	0.5	0.683	0.750	0.672		0.643
	2	0.1	0.1	0.603	0.833	0.811	0.870	0.761
		(4.472)	0.5	0.200	0.417	0.379	0.504	0.308
		0.5	0.1	0.844	0.886	0.880	0.905	0.872
		(2.000)	0.5	0.539	0.557	0.545	0.613	0.527
	3	0.1	0.1	0.546	0.805	0.771	0.833	0.727
		(5.477)	0.5	0.176	0.364	0.315	0.416	0.265
		0.5	0.1	0.789	0.863	0.854	0.879	0.847
		(2.449)	0.5	0.430	0.496	0.477	0.537	0.464
	50	0.1	0.1					0.428
		(22.361)	0.5					0.081
		0.5	0.1					0.610
		(10.000)	0.5					0.164
1.0	1	0.1	0.1	0.519	0.885	0.811		0.715
		(3.162)	0.5	0.296	0.570	0.400		0.272
		0.5	0.1	0.859	0.914	0.880		0.861
		(1.414)	0.5	0.554	0.656	0.560		0.519
	2	0.1	0.1	0.380	0.751	0.718	0.806	0.643
		(4.472)	0.5	0.116	0.303	0.265	0.388	0.202
		0.5	0.1	0.739	0.826	0.816	0.856	0.802
		(2.000)	0.5	0.355	0.435	0.419	0.498	0.397
	3	0.1	0.1	0.384	0.711	0.660	0.751	0.598
		(5.477)	0.5	0.100	0.254	0.209	0.302	0.168
		0.5	0.1	0.664	0.793	0.776	0.818	0.764
		(2.449)	0.5	0.277	0.373	0.351	0.416	0.337
	50	0.1	0.1					0.280
		(22.361)	0.5					0.044
		0.5	0.1					0.457
		(10.000)	0.5					0.096

Table [3.6] Comparison of relative base moment factors (M_B/M_{aB}) for point load at the top

R	n	ω (αH)	1/EIS	Optimum spacing (Drift)	Uniform spacings Type (i)	Type (ii)	Type (iii)	Continuum
0.0	1	0.1	0.1	0.944	0.955	0.938		0.932
			0.5	0.719	0.773	0.688		0.658
		0.5	0.1	0.963	0.967	0.963		0.963
			0.5	0.817	0.833	0.813		0.814
	2	0.1	0.1	0.932	0.925	0.924	0.933	0.922
			0.5	0.658	0.627	0.621	0.665	0.612
		0.5	0.1	0.951	0.947	0.948	0.950	0.948
			0.5	0.755	0.737	0.741	0.750	0.741
	3	0.1	0.1	0.925	0.920	0.919	0.925	0.918
			0.5	0.626	0.602	0.596	0.623	0.591
		0.5	0.1	0.944	0.939	0.940	0.942	0.940
			0.5	0.721	0.696	0.704	0.708	0.701
	50	0.1	0.1					0.904
			0.5					0.522
		0.5	0.1					0.910
			0.5					0.550
0.5	1	0.1	0.1	0.681	0.913	0.865		0.805
		(3.162)	0.5	0.479	0.630	0.485		0.368
		0.5	0.1	0.920	0.935	0.917		0.906
		(1.414)	0.5	0.667	0.714	0.650		0.620
	2	0.1	0.1	0.607	0.825	0.804	0.860	0.754
		(4.472)	0.5	0.194	0.390	0.356	0.466	0.289
		0.5	0.1	0.842	0.879	0.873	0.896	0.865
		(2.000)	0.5	0.527	0.530	0.519	0.577	0.500
	3	0.1	0.1	0.544	0.798	0.765	0.824	0.721
		(5.477)	0.5	0.173	0.341	0.296	0.387	0.250
		0.5	0.1	0.786	0.856	0.846	0.871	0.839
		(2.449)	0.5	0.405	0.468	0.450	0.503	0.437
	50	0.1	0.1					0.427
		(22.361)	0.5					0.079
		0.5	0.1					0.607
		(10.000)	0.5					0.157
1.0	1	0.1	0.1	0.519	0.875	0.804		0.708
		(3.162)	0.5	0.303	0.531	0.375		0.255
		0.5	0.1	0.861	0.906	0.875		0.855
		(1.414)	0.5	0.549	0.625	0.542		0.500
	2	0.1	0.1	0.381	0.744	0.712	0.797	0.637
		(4.472)	0.5	0.112	0.283	0.249	0.359	0.189
		0.5	0.1	0.741	0.820	0.809	0.848	0.795
		(2.000)	0.5	0.336	0.414	0.399	0.469	0.377
	3	0.1	0.1	0.384	0.705	0.655	0.744	0.593
		(5.477)	0.5	0.097	0.238	0.197	0.281	0.158
		0.5	0.1	0.663	0.786	0.769	0.810	0.757
		(2.449)	0.5	0.272	0.352	0.332	0.390	0.318
	50	0.1	0.1					0.279
		(22.361)	0.5					0.043
		0.5	0.1					0.455
		(10.000)	0.5					0.092

CHAPTER FOUR

STATIC ANALYSIS OF SHEAR WALL AND OUTRIGGER-BRACED STRUCTURES USING TRANSFER MATRIX TECHNIQUE

NOTATION of Chapter 4

A_1, A_2	cross-sectional areas of walls 1 and 2
A_c	sectional area of column
d	distance between columns
E	elastic moduli of walls
E_c	elastic modulus of column
E_o	elastic modulus of outrigger
E_s	elastic modulus of stiffening beam
$F_1..F_i..F_n$	tip shear of outriggers 1..i.. and n
H	height of structure
I_1, I_2	second moments of area of walls 1 and 2
I_o	effective moment of inertia of outrigger
l	distance between centroidal axis of walls
M_a	applied moment due to external loads
M_{aB}	applied moment at the base of the structure
$M_1..M_i..M_n$	restraining moments due to stiffening beams 1..i..n
P	point load at the top of the structure
S, S_1, S_2, ω	structural parameters
s, s_1, s_2, w	structural parameters
w	horizontal load per unit height
w_t	maximum load intensity of a upper triangular distributed load
V	shear force
$x_1..x_i..x_n$	distances of outriggers 1..i..n from top of structure
y_T	top drift of the structure
$\mathbb{U}_i, \mathbb{A}_i, \mathbb{B}_i, \mathbb{C}_i$	field transfer matrices

K_{ϑ}	rotational stiffness
δ, δ_a, δ_b	displacements at the point of contraflexure
ϑ_B	slope of the walls at the base of the structure
$\psi_1..\psi_i..\psi_n$	slopes of the walls or core
$\mathbb{M}_2..\mathbb{M}_i..\mathbb{M}_n$	matrix for restraining moments
$\mathbb{T}_2..\mathbb{T}_i..\mathbb{T}_n$	field transfer matrices
$\mathbb{Z}_{n+1}..\mathbb{Z}_i..\mathbb{Z}_n$	state vector of actions
$\Psi_1..\Psi_i..\Psi_n$	matrices of the slope terms

Other subsidiary symbols are defined locally in the text.

4.1 INTRODUCTION

Load bearing shear walls interconnected by floor slabs are extensively used in tall building structures. If the connections of the floor slabs are weak or the floor slabs are designed as simply supported systems to resist vertical forces only, the shear walls behave effectively as linked shear walls, as shown in Fig.[4.1].

The lack of moment resisting connections of the slabs to the walls ensures that the slabs only serve to transmit wind forces from the facade to the system of shear walls. The wind moments must then be resisted entirely by the bending moments in the walls, so that high tensile stresses may be induced in the extreme fibres.

Difficulties can arise in design, particularly with panel construction, if the self-weight of the building does not produce sufficient compressive stresses to overcome these tensile stresses. The high bending stresses can be substantially reduced if a portion of the applied moments can be resisted by axial forces in the walls. However, it may not be economical to introduce moment-resistant connections between walls and slabs in order to induce the desired axial tensile and compressive forces into the walls.

A simple alternative solution is to incorporate a stiffening beam or truss at some level in the building, which will induce the axial forces desired to resist the wind moments more effectively.

There is an analogy between the structural actions of laterally loaded stiffened linked shear walls and that of outrigger-braced structures. The structural configuration of the latter is described in detail in Chapter 2.

When the structure is subjected to lateral loads, the outriggers and columns resist the rotation of the core by inducing tensile and compressive stresses in the columns. In an analogous fashion to the actions in linked shear walls, a correspondingly large resisting moment is induced by the relatively low axial forces because of the lever arm action. The overall action reduces both the lateral deflection and the base moment which would have resulted in a free-standing core.

The analysis is based on the earlier work of Moudarres and Coull[38] who applied the transfer matrix technique to the analysis of stiffened linked shear walls with single stiffening beams and single outrigger structures under a uniformly distributed lateral load. The object of this Chapter is to extend the earlier work and apply the same transfer matrix technique to the analysis of stiffened linked shear walls with multi-stiffening beams, and multi-outrigger-braced structures under the other standard load cases of a triangularly distributed load and a point load at the top.

4.2 STRUCTURAL BEHAVIOUR OF OUTRIGGER STRUCTURES AND STIFFENED LINKED SHEAR WALLS

Consider a system of two linked shear walls, which are braced by a stiffening beam, rigidly connected at each wall at the level, as shown in Fig.[4.2a]. The walls are assumed to be linked by rigid pin-ended members which simulate the action of the floor slabs with weak end connections. The walls are assumed to deflect equally throughout the height. If a 'cut' is made along the points of contraflexure of the stiffening beam as shown in Fig.[4.2b], the relative vertical deflection of the cut ends of the stiffening

beam must be zero. The displacement of the cut ends of the stiffening beam consists of two components, one due to the stiffening beam bending under the action at its ends of the shear force F_1 and the other due to the differential axial deformations of the shear walls.

The vertical displacement δ due to the slope of the walls can be shown by the moment-area method to be,

$$\delta = l \left[\frac{1}{EI} \int_{H-x_1}^{H} (M_a - M_1)dx + \vartheta_B \right] \qquad (4.1a)$$

where

ϑ_B is the slope of the walls at the base of the structure

M_1 is the restraining moment caused by the stiffening beam

M_a is the applied bending moment at any levels due to the external loads P, w and w_t, given by,

$$M_a = P(H-x) + \frac{w(H-x)^2}{2} + \left[\frac{w_t(H-x)^2}{2} - \frac{w_t(H-x)^3}{6H} \right] \qquad (4.1b)$$

l is the distance between centroidal axes of walls

ϑ_B is the rotation of the walls at the base

H is height of the structure

EI is flexural rigidity of the walls

$$I = I_1 + I_2$$

and

I_1 and I_2 is the second moment of area of wall 1 and wall 2 respectively

$$\vartheta_B = K_\vartheta (M_{aB} - M_1) \tag{4.1c}$$

where

M_{aB} is the static applied moment at the base of the structure

K_ϑ is a rotational stiffness at the base of the structure and the restraining moment due to the stiffening beam is given by,

$$M_1 = F_1 l \tag{4.2}$$

The vertical displacement due to bending of the stiffening beam is given by,

$$\delta_b = \frac{F_1 b^3}{12 E_s I_s} \tag{4.3}$$

where

$E_s I_s$ is the flexural rigidity of the stiffening beam

b is the clear opening between walls

While that due to the axial deformation of the walls is,

$$\delta_a = \frac{F_1 x_1}{E} \left(\frac{1}{A_1} + \frac{1}{A_2} \right) \tag{4.4}$$

where A_1 and A_2 are the cross-sectional areas of walls 1 and 2.

Equations (4.1), (4.2) and (4.4) can be used to express the compatibility of the displacement at the point of contraflexure of the stiffening beam, thus

$$\delta = \delta_a + \delta_b$$

$$1 \left[\frac{1}{EI} \int_{H-x_1}^{H} (M_a - M_1)dx + \vartheta_B \right] =$$

$$\frac{F_1 b^3}{12E_s I_s} + \frac{F_1 x_1}{E} \left(\frac{1}{A_1} + \frac{1}{A_2} \right) \qquad (4.5)$$

Equation (4.5) can be rewritten as,

$$M_1 [s_1 + s x_1 + K_\vartheta] = \frac{1}{EI} \int_{H-x_1}^{H} M_a dx + K_\vartheta M_{aB} \qquad (4.6a)$$

where

$$s = \frac{1}{EI} + \frac{1}{EI^2} \left(\frac{1}{A_1} + \frac{1}{A_2} \right) \qquad (4.6b)$$

$$s_1 = \frac{b^3}{12E_s I_s l^2} \qquad (4.6c)$$

The expression for the restraining moment becomes,

$$M_1 = \frac{1}{s_1+sx_1+K_\vartheta}\left[\frac{1}{EI}\int_{H-x_1}^{H} M_a dx + K_\vartheta M_{aB}\right] \tag{4.7}$$

Equation (4.7) is expressed in a identical form to equation (2.7), with the parameters s_1 and s defined for the shear walls structure.

Following the procedure described above, corresponding equations of restraining moments for linked shear walls with two stiffening beams can be obtained as follows,

$$\begin{bmatrix} M_1 \\ M_2 \end{bmatrix} = \begin{bmatrix} s_1+s(H-x_1)+K_\vartheta & s(H-x_2)+K_\vartheta \\ s(H-x_2)+K_\vartheta & s_1+s(H-x_2)+K_\vartheta \end{bmatrix}^{-1} \begin{bmatrix} \frac{1}{EI}\int_{x_1}^{H} M_a dx+K_\vartheta M_{aB} \\ \frac{1}{EI}\int_{x_2}^{H} M_a dx+K_\vartheta M_{aB} \end{bmatrix} \tag{4.8}$$

where M_1 and M_2 are the restraining moments caused by the stiffening beams at level x_1 and x_2 respectively and M_{aB} is the static moment at the base of the structure.

Equation (4.8) is in an identical form to equation (2.14) in Chapter 2. The equations for the restraining moments M_1, $M_2..M_i..M_n$ can be shown to be identical to equations (2.7), (2.14), (2.20) and (2.22). Hence, the results of the parametric study in Chapter 2 can be applied directly to the linked shear walls structure with their corresponding parameters S, S_1 and ω defined respectively by, s, s_1 and w for the shear walls,

where

$$w = \frac{s_1}{sH} \tag{4.9}$$

4.3 ANALYSIS OF COUPLED SHEAR WALLS

There is an analogy between the structural actions of laterally loaded stiffened linked walls and outrigger-braced structures for very tall structures, as demonstrated in the section (4.2). As the number of stiffening beams in the linked shear walls increases, the structural behaviour will change being that of two independent cantilever walls with high bending moments and low axial forces towards that of a monolithic cantilever with relatively lower bending moments and higher axial forces for the same external load. That is, the structure begins to behave like coupled shear walls. Following the same argument, there is also an analogy between coupled shear walls and multi-outrigger-braced structures. It follows that, after redefinition of the parameters S and S_1, the discrete matrix analysis developed in Chapter 2 can be applied to analyse coupled shear walls. The analysis of the multi-outrigger-braced structure is discussed in detail in Chapter 3. The shear walls and the outrigger-braced type of structure are shown in Fig.[4.3]. The restraining moment M_i of the connecting beams between the shear walls can be expressed as in equation (2.22) and is given by,

$$\mathbb{M} = \mathbb{P}^{-1}\mathbb{L} \tag{4.10}$$

where $\mathbb{M}$ is a matrix containing the restraining moments M_1, M_2 .. M_i .. and M_n due to connecting beams 1, 2 .. i .. and n.

$$\mathbb{M} = \begin{bmatrix} M_1 \\ M_2 \\ \vdots \\ M_i \\ \vdots \\ M_n \end{bmatrix}$$

$\mathbb{L}$ is a matrix containing the load terms due to the applied moment at levels x_1, x_2, .. x_i .. and x_n.

$$\mathbb{L} = \begin{bmatrix} \frac{1}{EI}\int_{x_1}^{H} M_a dx + K_\vartheta M_{aB} \\ \frac{1}{EI}\int_{x_2}^{H} M_a dx + K_\vartheta M_{aB} \\ \vdots \\ \frac{1}{EI}\int_{x_i}^{H} M_a dx + K_\vartheta M_{aB} \\ \vdots \\ \frac{1}{EI}\int_{x_n}^{H} M_a dx + K_\vartheta M_{aB} \end{bmatrix}$$

and $\mathbb{P}$ is a matrix containing the structural properties of the structure given by,

$$\mathbb{P} = \begin{bmatrix} s_1+s(H-x_1)+K_\vartheta & s(H-x_2)+K_\vartheta & \cdots & s(H-x_i)+K_\vartheta & \cdots & s(H-x_n)+K_\vartheta \\ s(H-x_2)+K_\vartheta & s_1+s(H-x_2)+K_\vartheta & \cdots & s(H-x_i)+K_\vartheta & \cdots & s(H-x_n)+K_\vartheta \\ \vdots & \vdots & & \vdots & & \vdots \\ s(H-x_i)+K_\vartheta & s(H-x_i)+K_\vartheta & \cdots & s(H-x_i)+K_\vartheta & \cdots & s(H-x_i)+K_\vartheta \\ \vdots & \vdots & & \vdots & & \vdots \\ s(H-x_n)+K_\vartheta & s(H-x_n)+K_\vartheta & \cdots & s_1+s(H-x_n)+K_\vartheta & \cdots & s_1+s(H-x_n)+K_\vartheta \end{bmatrix}$$

The restraining moment, M_i, of the connecting beams can be obtained by solving the above equation (4.10) directly. Once the restraining moments are obtained, the axial force in the walls at level x_i becomes,

$$T_i = \frac{\sum_{i=i}^{n} M_i}{l} \qquad (4.11)$$

where T_i is the axial force between level x_{i-1} and x_i.

The shear force F_i in any connecting beam becomes,

$$F_i = M_i/l \qquad (4.12)$$

The moment curvature relationships of the walls are,

$$EI\frac{d^2y}{dx^2} = M_a - T_i l$$

$$= M_a - \sum_{i=i}^{n} M_i \qquad (4.13)$$

Using the moment-area method, the top drift of the structure becomes,

$$y_T = \frac{1}{EI}\left[\int_0^{x_1} M_a x dx + \int_{x_1}^{x_2}(M_a - M_1)x dx + \right.$$
$$\left. .. \int_{x_i}^{x_{i+1}}(M_a - M_1 .. M_{i+1})x dx + \int_x^H (M_a - M_1 .. M_n)x dx \right]$$
$$+ \vartheta_B H \qquad (4.14a)$$

On integrating, equation (4.13) is simplified as,

$$y_T = y_{FT} - \frac{1}{2EI}\sum_{i=1}^{n} M_i(H^2 - x_i^2) + \vartheta_B H \qquad (4.14b)$$

where y_{FT} is the drift of a free cantilever wall with a rigid foundation due to the applied load and is expressed as in equation (2.29).

The last term of equation (4.14b) represents the lateral deflection due to rotation at the base of the structure and is given by,

$$\vartheta_B H = K_\vartheta (M_{aB} - \sum_{i=1}^{n} M_i)H \qquad (4.14c)$$

The second term of the equation (4.14c) represents the reduction due to the restraining moments from the connecting beam.

4.4 STATIC ANALYSIS OF STIFFENED LINKED SHEAR WALLS USING THE TRANSFER MATRIX TECHNIQUE

Considering a linked shear wall structure subjected to a uniformly distributed lateral load of intensity w, the fundamental governing differential equation is,

$$\frac{d^4y}{dx^4} - \frac{w}{EI} = 0 \qquad (4.15)$$

where y is the deflection at level x. Since both walls deflect equally at all levels, the curvatures are also equal, and the two walls may be lumped together in the analysis. Equation (4.15) may readily be integrated to give the deflection and associated structural actions for a given set of boundary conditions. The relationships between the state vectors of actions at two points "i" and "i-1", a distance l apart, may then be expressed in matrix form,

$$\begin{bmatrix} -y \\ \psi \\ M \\ V \\ 1 \end{bmatrix}_i = \begin{bmatrix} 1 & l & 12rl & 4rl^2 & -wrl^3 \\ 0 & 1 & 24r & 12rl & -4wrl^2 \\ 0 & 0 & 1 & l & \frac{-wl^2}{2} \\ 0 & 0 & 0 & 1 & -wl \\ 0 & 0 & 0 & 0 & 1 \end{bmatrix} \cdot \begin{bmatrix} -y \\ \psi \\ M \\ V \\ 1 \end{bmatrix}_{i-1} \qquad (4.16)$$

where ψ, M and V are, respectively, the rotation of the cross section, the bending moment, and the shear force. The sign conventions employed for the quantities are shown in Fig.[4.4], and

$$r = \frac{l}{24EI} \tag{4.17}$$

If the structure is subjected to a triangularly distributed lateral load, whose intensity varies linearly from zero at the base to a value w_t at a height H, the fundamental governing differential equation is,

$$\frac{d^4y}{dx^4} - \frac{w_t x}{EIH} = 0 \tag{4.18}$$

The relationships between the state vectors of actions at two points "i" and "i-1", a distance l apart, may be expressed in matrix form

$$\begin{bmatrix} -y \\ \psi \\ M \\ V \\ 1 \end{bmatrix}_i = \begin{bmatrix} 1 & l & 12rl & 4rl^2 & -\frac{w_t}{H}(\frac{l^4 r}{5} + x_{i-1} l^3 r) \\ 0 & 1 & 24r & 12rl & -\frac{w_t}{H}(l^3 r + 4x_{i-1} l^2 r) \\ 0 & 0 & 1 & l & -\frac{w_t}{H}(\frac{l^3}{6} + x_{i-1}\frac{l^2}{2}) \\ 0 & 0 & 0 & 1 & -\frac{w_t}{H}(\frac{l^2}{2} + x_{i-1} l) \\ 0 & 0 & 0 & 0 & 1 \end{bmatrix} \cdot \begin{bmatrix} -y \\ \psi \\ M \\ V \\ 1 \end{bmatrix}_{i-1} \tag{4.19}$$

where x_{i-1} is the distances measured from the base to station point "i-1". Again, the extended 5x5 matrices are used in order to include the distributed loading. Since the triangularly distributed lateral load varies along the height of the structure, the x_{i-1} is used to determine the loading condition at the starting station point "i-1". Unlike the U.D.L. case, the transfer matrices at each station point are formulated with different load terms and *l*.

If the structure is subjected to a point load P at the top of the structure, the fundamental governing equation is,

$$\frac{d^3y}{dx^3} + \frac{P}{EI} = 0 \qquad (4.20)$$

For the case of point load applied at the top, the load term becomes zero for a formulation based on a distributed load. The transfer matrices can further be reduced to 4x4 matrices by discarding the last row and column. The load term will only come into effect in the top boundary condition. However, in order to generalise a method for all load cases, 5x5 matrices are used throughout.

The relationships between the state vectors of actions at two points "i" and "i-1", a distance *l* apart, may be expressed in matrix form

$$\begin{bmatrix} -y \\ \psi \\ M \\ V \\ 1 \end{bmatrix}_i = \begin{bmatrix} 1 & l & 12rl & 4rl & 0 \\ 0 & 1 & 24r & 12rl & 0 \\ 0 & 0 & 1 & l & 0 \\ 0 & 0 & 0 & 1 & 0 \\ 0 & 0 & 0 & 0 & 1 \end{bmatrix} \cdot \begin{bmatrix} -y \\ \psi \\ M \\ V \\ 1 \end{bmatrix}_{i-1} \qquad (4.21)$$

The general symbolic form of the extended state vector at any particular point "i" on the structure will be denoted for convenience by,

$$\mathbb{Z}_i^k = \{ -y \quad \psi \quad M \quad V \quad 1 \}_i^k \qquad (4.22)$$

in which k will be assigned a superscript "+" or "-" to indicate that the position of the section considered is immediately above or below the point "i", respectively. The additional term in the extended column vector for the actions is required to include directly the applied load term. Equations (4.16), (4.19) and (4.21) may be expressed succinctly as,

$$\mathbb{Z}_i = \mathbb{U}\, \mathbb{Z}_{i-1} \qquad (4.23)$$

in which $\mathbb{Z}_i$ is the state vector at position "i" and $\mathbb{U}$ is the extended field transfer matrix whose elements u_{ij} are defined in equations (4.16), (4.19) and (4.21). The field transfer matrix enables the state vector of actions at any point "i" to be expressed in terms of the corresponding actions at any other point "i-1".

4.4.1 ONE STIFFENING BEAM

Consider linked shear walls with one stiffening beam positioned at height x_1, as shown in Fig.[4.5]. The state vectors of actions at point "1" on the structure may be expressed in terms of the state vectors at the other significant positions "0" and "2" by the relationship,

$$\mathbb{Z}_1^{-} = \mathbb{A}_1 . \mathbb{Z}_0 \qquad (4.24)$$

$$\mathbb{Z}_2 = \mathbb{A}_2 . \mathbb{Z}_1^{+} \qquad (4.25)$$

where $\mathbb{A}_1$ and $\mathbb{A}_2$ are transfer matrices of a form similar to $\mathbb{U}$, with elements $a1_{ij}$ and $a2_{ij}$ corresponding to those given for u_{ij} in equations (4.16), (4.19) and (4.21). The relationship between the state vectors $\mathbb{Z}_1^{-}$ and $\mathbb{Z}_1^{+}$ is,

$$\mathbb{Z}_1^{+} - \mathbb{Z}_1^{-} + \{\, 0 \quad 0 \quad M_1 \quad 0 \quad 0 \,\} = 0 \qquad (4.26)$$

At levels x_1, by establishing the condition of compatibility for vertical displacement at the point of contraflexure of the stiffening beam, the restraining moment M_1 due to the stiffening beam can be expressed in terms of the slope and is given by,

$$M_1 = t1.\psi_1 \tag{4.27a}$$

where ψ_1 is a scalar denoting the slope at the station point "1" and

$$t1 = - \frac{1}{s_1 + s_2 x_1} \tag{4.27b}$$

with

$$s_2 = \frac{1}{EI^2} \left(\frac{1}{A_1} + \frac{1}{A_2} \right) \tag{4.27c}$$

Substituting equation (4.27a) into (4.26), the relationship between the state vectors $\mathbb{Z}_1$ and $\mathbb{Z}_2$ is,

$$\mathbb{Z}_1^{+} = \mathbb{Z}_1^{-} + \mathbb{K}_1.\Psi_1 \tag{4.28a}$$

where

Ψ_1 is a vector given by $\mathbb{G}.\mathbb{Z}_1^{-}$ (4.28b)

and $\mathbb{K}_1$ and $\mathbb{G}$ are matrices of orders 5x1 and 1x5 respectively,

$$\mathbb{K}_1 = \begin{bmatrix} 0 \\ 0 \\ t1 \\ 0 \\ 0 \end{bmatrix} \qquad (4.28c)$$

$$\mathbb{G} = [\ 0 \quad 1 \quad 0 \quad 0 \quad 0\ ] \qquad (4.28d)$$

On substituting equations (4.24) and (4.28a) into equation (4.25), $\mathbb{Z}_2$ may be expressed as,

$$\mathbb{Z}_2 = \mathbb{R}_1 . \mathbb{Z}_0 \qquad (4.29)$$

where $\mathbb{R}_1$ is a transfer matrix of order 5x5 linking the state vector of actions at point "0" to the state vector at point "2" and is given by,

$$\mathbb{R}_1 = \mathbb{A}_2 . \mathbb{A}_1 + \mathbb{A}_2 . \mathbb{K}_1 . \mathbb{G} . \mathbb{A}_1 \qquad (4.30)$$

4.4.2 TWO STIFFENING BEAMS

Consider linked shear walls with two stiffening beams positioned at heights x_1 and x_2, as shown in Fig.[4.6]. The state vectors of actions at point "1" on the structure may be expressed in terms of the state vectors at the other significant positions "0" and "2" by the relationship,

$$\mathbb{Z}_1^{-} = \mathbb{B}_1 . \mathbb{Z}_0 \qquad (4.31)$$

$$\mathbb{Z}_2^- = \mathbb{B}_2 . \mathbb{Z}_1^+ \tag{4.32}$$

and the state vector at point "3" at the top of the structure may be expressed as

$$\mathbb{Z}_3 = \mathbb{B}_3 . \mathbb{Z}_2^+ \tag{4.33}$$

Matrices $\mathbb{B}_1$, $\mathbb{B}_2$ and $\mathbb{B}_3$ are transfer matrices of a form similar to $\mathbb{U}$ defined in equations (4.16), (4.19) and (4.21).

By establishing the condition of compatibility for vertical displacement at the point of contraflexure of the stiffening beams, the restraining moments M_1 and M_2 due to the stiffening beams can be expressed in terms of the slopes, given by,

$$\mathbb{M}_2 = \mathbb{T}_2 . \Psi_2 \tag{4.34a}$$

where

$$\mathbb{M}_2 = \begin{bmatrix} M_2 \\ M_1 \end{bmatrix} \tag{4.34b}$$

$$\mathbb{T}_2 = \begin{bmatrix} s_1 + s_2 x_2 & s_2 x_1 \\ s x_1 & s_1 + s_2 x_1 \end{bmatrix}^{-1} \tag{4.34c}$$

and

$$\Psi_2 = \begin{bmatrix} \psi_2 \\ \psi_1 \end{bmatrix} \tag{4.34d}$$

ψ_1, ψ_2 are the scalar denoting the slopes at the station points "1" and "2".

From equation (4.34a), M_1 and M_2 can be expressed as,

$$M_1 = \mathbb{K}_2 . \Psi_2 \tag{4.35a}$$

$$M_2 = \mathbb{K}_3 . \Psi_2 \tag{4.35b}$$

where $\mathbb{K}_2$ and $\mathbb{K}_3$ are matrices of the order 5x2,

$$\mathbb{K}_2 = \begin{bmatrix} 0 & 0 \\ 0 & 0 \\ t2_{21} & t2_{22} \\ 0 & 0 \\ 0 & 0 \end{bmatrix}$$

$$\mathbb{K}_3 = \begin{bmatrix} 0 & 0 \\ 0 & 0 \\ t2_{11} & t2_{12} \\ 0 & 0 \\ 0 & 0 \end{bmatrix}$$

in which $t2_{11}$, $t2_{12}$, $t2_{21}$ and $t2_{22}$ are the elements of matrix $\mathbb{T}_2$.

The relationship between the state vectors $\mathbb{Z}_1^+$ and $\mathbb{Z}_1^-$ at point "1" on the structure is,

$$\mathbb{Z}_1^+ = \mathbb{Z}_1^- + \mathbb{K}_2.\Psi_2 \qquad (4.36)$$

Substituting equation (4.31) into (4.36), $\mathbb{Z}_1^+$ becomes,

$$\mathbb{Z}_1^+ = \mathbb{B}_1.\mathbb{Z}_0 + \mathbb{K}_2.\Psi_2 \qquad (4.37)$$

Hence substituting equation (4.37) into (4.32), $\mathbb{Z}_2^-$ at point "2" on the structure is,

$$\mathbb{Z}_2^- = \mathbb{B}_2.\mathbb{B}_1.\mathbb{Z}_0 + \mathbb{B}_2.\mathbb{K}_2.\Psi_2 \qquad (4.38)$$

and the relationship between the state vectors $\mathbb{Z}_2^+$ and $\mathbb{Z}_2^-$ at point "2" on the structure is,

$$\mathbb{Z}_2^+ = \mathbb{Z}_2^- + \mathbb{K}_3.\Psi_2 \qquad (4.39)$$

After substituting equation (4.38) into (4.39), it becomes,

$$\mathbb{Z}_2^+ = \mathbb{B}_2.\mathbb{B}_1.\mathbb{Z}_0 + [\ \mathbb{B}_2.\mathbb{K}_2 + \mathbb{K}_3\ ].\Psi_2 \qquad (4.40)$$

From equation (4.31), ψ_1 can be expressed as

$$\psi_1 = \mathbb{G}.\mathbb{B}_1.\mathbb{Z}_0 \qquad (4.41)$$

From equation (4.38), ψ_2 can be expressed as

$$\psi_2 = \mathbb{G}.\mathbb{B}_2.\mathbb{B}_1.\mathbb{Z}_0 + \mathbb{G}.\mathbb{B}_2.\mathbb{K}_2.\Psi_2 \qquad (4.42)$$

Equations (4.41) and (4.42) can be expressed in matrix form as,

$$\begin{bmatrix} \psi_1 \\ \psi_2 \end{bmatrix} = \begin{bmatrix} \mathbb{G}.\mathbb{B}_1.\mathbb{Z}_0 \\ \mathbb{G}.\mathbb{B}_2.\mathbb{B}_1.\mathbb{Z}_0 + \mathbb{G}.\mathbb{B}_2.\mathbb{K}_2.\Psi_2 \end{bmatrix} \qquad (4.43a)$$

Equation (4.43) can be expressed further in terms of the state vector $\mathbb{Z}_0$ and Ψ_2 as,

$$\mathbb{I}.\Psi_2 = \begin{bmatrix} \mathbb{G}.\mathbb{B}_1 \\ \mathbb{G}.\mathbb{B}_2.\mathbb{B}_1 \end{bmatrix}.\mathbb{Z}_0 + \begin{bmatrix} 0 & 0 \\ \mathbb{G}.\mathbb{B}_2.\mathbb{K}_2 & \end{bmatrix}.\Psi_2 \qquad (4.43b)$$

where $\mathbb{I}$ is a 2x2 unit matrix.

Equation (4.43b) can be simplified to,

$$\psi_2 = \mathbb{J}_1^{-1}.\mathbb{J}_2.\mathbb{Z}_0 \qquad (4.43c)$$

where $\mathbb{J}_1$ and $\mathbb{J}_2$ are the matrices of the order 2x2 and 2x5 respectively and are given by,

$$\mathbb{J}_1 = \mathbb{I} - \begin{bmatrix} 0 & 0 \\ \mathbb{G}.\mathbb{B}_2.\mathbb{K}_2 & \end{bmatrix}$$

$$\mathbb{J}_2 = \begin{bmatrix} \mathbb{G}.\mathbb{B}_1 \\ \mathbb{G}.\mathbb{B}_2.\mathbb{B}_1 \end{bmatrix}$$

Substituting equations (4.43c), (4.38) and (4.39) into (4.33), the transfer matrix linking the point "0" at the base to the state vector of actions at point "3" at the top of structure is obtained as,

$$\mathbb{Z}_3 = \mathbb{R}_2.\mathbb{Z}_0 \qquad (4.44)$$

where

$$\mathbb{R}_2 = \mathbb{B}_3.\{\ \mathbb{B}_2.\mathbb{B}_1 + [\ \mathbb{B}_2.\mathbb{K}_2 + \mathbb{K}_3\ ].\mathbb{J}_1^{-1}.\mathbb{J}_2\ \}$$

4.4.3 THREE STIFFENING BEAMS

Consider linked shear walls with three stiffening beams positioned at heights x_1, x_2 and x_3, as shown in Fig.[4.7]. By establishing the condition of compatibility for vertical displacement at the point of contraflexure of the stiffening beams, the restraining moments M_1, M_2 and M_3 due to the stiffening beams can be expressed in terms of the slopes,

$$\mathbb{M}_3 = \mathbb{T}_3.\Psi_3 \qquad (4.45a)$$

where

$$\mathbb{M}_3 = \begin{bmatrix} M_3 \\ M_2 \\ M_1 \end{bmatrix} \qquad (4.45b)$$

$$\mathbb{T}_3 = \begin{bmatrix} s_1 + s_2x_3 & s_2x_2 & s_2x_1 \\ sx_2 & s_1 + s_2x_2 & s_2x_1 \\ sx_1 & sx_1 & s_1 + s_2x_1 \end{bmatrix}^{-1} \qquad (4.45c)$$

and

$$\Psi_3 = \begin{bmatrix} \psi_3 \\ \psi_2 \\ \psi_1 \end{bmatrix} \qquad (4.45d)$$

ψ_1, ψ_2 and ψ_3 are the scalar denoting the slopes at the stations points "1", "2" and "3".

Therefore M_1 , M_2 and M_3 can be expressed in terms of Ψ_3 as,

$$M_1 = \mathbb{K}_5 . \Psi_3 \qquad (4.46)$$

$$M_2 = \mathbb{K}_6 . \Psi_3 \qquad (4.47)$$

$$M_3 = \mathbb{K}_7 . \Psi_3 \qquad (4.48)$$

where $\mathbb{K}_5$, $\mathbb{K}_6$ and $\mathbb{K}_7$ are matrices of the order 5x3,

$$\mathbb{K}_5 = \begin{bmatrix} 0 & 0 & 0 \\ 0 & 0 & 0 \\ t3_{31} & t3_{32} & t3_{33} \\ 0 & 0 & 0 \\ 0 & 0 & 0 \end{bmatrix}$$

$$\mathbb{K}_6 = \begin{bmatrix} 0 & 0 & 0 \\ 0 & 0 & 0 \\ t3_{21} & t3_{22} & t3_{23} \\ 0 & 0 & 0 \\ 0 & 0 & 0 \end{bmatrix}$$

$$\mathbb{K}_7 = \begin{bmatrix} 0 & 0 & 0 \\ 0 & 0 & 0 \\ t3_{11} & t3_{12} & t3_{13} \\ 0 & 0 & 0 \\ 0 & 0 & 0 \end{bmatrix}$$

in which $t3_{ij}$ are the elements of matrix $\mathbb{T}_3$.

Following the same procedure as in the previous sections (4.4.1) and (4.4.2), the state vectors of actions at point "1", "2", "3" and "4" on the structure may be expressed in terms of the state vectors at the position "0" by the relationship,

$$\mathbb{Z}_1^- = \mathbb{C}_1 . \mathbb{Z}_0 \tag{4.49}$$

$$\mathbb{Z}_1^+ = \mathbb{C}_1 . \mathbb{Z}_0 + \mathbb{K}_4 . \Psi_3 \tag{4.50}$$

$$\mathbb{Z}_2^- = \mathbb{C}_2 . \mathbb{C}_1 . \mathbb{Z}_0 + \mathbb{C}_2 . \mathbb{K}_4 . \Psi_3 \tag{4.51}$$

$$\mathbb{Z}_2^+ = \mathbb{C}_2 . \mathbb{C}_1 . \mathbb{Z}_0 + [\mathbb{C}_2 . \mathbb{K}_4 + \mathbb{K}_5] . \Psi_3 \tag{4.52}$$

$$\mathbb{Z}_3^{-} = \mathbb{C}_3.\mathbb{C}_2.\mathbb{C}_1.\mathbb{Z}_0 + \mathbb{C}_3.[\mathbb{C}_2.\mathbb{K}_4 + \mathbb{K}_5].\Psi_3 \qquad (4.53)$$

$$\mathbb{Z}_3^{+} = \mathbb{C}_3.\mathbb{C}_2.\mathbb{C}_1.\mathbb{Z}_0 + \{\mathbb{C}_3.[\mathbb{C}_2.\mathbb{K}_4 + \mathbb{K}_5] + \mathbb{K}_6\}.\Psi_3 \qquad (4.54)$$

$$\mathbb{Z}_4 = \mathbb{C}_4.\mathbb{C}_3.\mathbb{C}_2.\mathbb{C}_1.\mathbb{Z}_0 + \{\mathbb{C}_4.\mathbb{C}_3.[\mathbb{C}_2.\mathbb{K}_4 + \mathbb{K}_5] + \mathbb{C}_4.\mathbb{K}_6\}.\Psi_3 \qquad (4.55)$$

where $\mathbb{C}_1$, $\mathbb{C}_2$, $\mathbb{C}_3$ and $\mathbb{C}_4$ are transfer matrices with corresponding elements $c1_{ij}$, $c2_{ij}$, $c3_{ij}$ and $c4_{ij}$ similar to u_{ij} of $\mathbb{U}$, given in equations (4.16), (4.19) and (4.21). The relationship between the state vectors $\mathbb{Z}_1^{-}$ and $\mathbb{Z}_1^{+}$ is,

From equations (4.49), (4.51) and (4.53), ψ_1, ψ_2 and ψ_3 can be extracted and written in a single matrix as,

$$\begin{bmatrix} \psi_1 \\ \psi_2 \\ \psi_3 \end{bmatrix} = \begin{bmatrix} \mathbb{G}.\mathbb{C}_1.\mathbb{Z}_0 \\ \mathbb{G}.\mathbb{C}_2.\mathbb{C}_1.\mathbb{Z}_0 + \mathbb{G}.\mathbb{C}_2.\mathbb{K}_4.\Psi_3 \\ \mathbb{G}.\mathbb{C}_3.\mathbb{C}_2.\mathbb{C}_1.\mathbb{Z}_0 + \mathbb{G}.\mathbb{C}_3.[\mathbb{C}_2.\mathbb{K}_4+\mathbb{K}_5].\Psi_3 \end{bmatrix} \qquad (4.56)$$

Equation (4.56) can be simplified further in terms of the state vector $\mathbb{Z}_0$ as,

$$\Psi_3 = \mathbb{J}_3^{-1}.\mathbb{J}_4.\mathbb{Z}_0 \qquad (4.57)$$

where $\mathbb{J}_3$ and $\mathbb{J}_4$ are matrices the order 3x3 and 3x5 respectively and are given by,

$$J_3 = I - \begin{bmatrix} 0 & 0 & 0 \\ G.C_2.K_4 & & \\ G.C_3.[C_2.K_4.+K_5] & & \end{bmatrix}$$

$$J_4 = \begin{bmatrix} G.C_1 \\ G.C_2.C_1 \\ G.C_3.C_2.C_1 \end{bmatrix}$$

and I is a 3x3 unit matrix.

Substituting equation (4.57) into (4.55), the transfer matrix linking the point "0" at the base to the top of structure is obtained as,

$$Z_4 = R_3.Z_0 \qquad (4.58)$$

where

$$R_3 = C_4.C_3.C_2.C_1.Z_0+\{C_4.C_3.[C_2.K_4+K_5]+C_4.K_6\}.J_3^{-1}.J_4$$

4.4.4 n STIFFENING BEAMS CASE

Consider linked shear walls with n stiffening beams positioned at heights x_1, x_2 .. x_i .. and x_n, as shown in Fig.[4.8]. By establishing the condition of compatibility for vertical displacement at the point of contraflexure of the stiffening beams, the general expression for the restraining moments M_1, M_2, .. M_i .. and M_n due to the stiffening beams is given by,

$$\mathbb{M} = \mathbb{T}_n . \Psi_n \qquad (4.59)$$

where

$$\mathbb{M} = \begin{bmatrix} M_n \\ \vdots \\ M_i \\ \vdots \\ M_2 \\ \\ M_1 \end{bmatrix}$$

$$\mathbb{T}_n = \begin{bmatrix} s_1+s_2x_n & s_2x_{n-1} & \cdot & \cdot & s_2x_2 & s_2x_1 \\ \vdots & \vdots & \vdots & \vdots & \vdots & \vdots \\ s_2x_i & s_1+s_2x_i & \cdot & \cdot & \cdot & s_2x_1 \\ \vdots & \vdots & \vdots & \vdots & \vdots & \vdots \\ s_2x_2 & s_2x_2 & \cdot & \cdot & s_1+s_2x_2 & s_2x_1 \\ \\ s_2x_1 & s_2x_1 & \cdot & \cdot & s_2x_1 & s_1+s_2x_1 \end{bmatrix}^{-1}$$

$$\Psi_n = \begin{bmatrix} \psi_n \\ \vdots \\ \psi_i \\ \vdots \\ \psi_2 \\ \\ \psi_1 \end{bmatrix}$$

Therefore the restraining moments M_1, M_2, .. M_i .. and M_n, due to the stiffening beams, can be expressed as

$$M_1 = \mathbb{K}1.\Psi_n \tag{4.60a}$$

$$M_2 = \mathbb{K}2.\Psi_n \tag{4.60b}$$

$$M_i = \mathbb{K}i.\Psi_n \tag{4.60c}$$

$$M_n = \mathbb{K}n.\Psi_n \tag{4.60d}$$

where $\mathbb{K}1$, $\mathbb{K}2$, .. $\mathbb{K}i$ .. $\mathbb{K}n$ are the matrices of the order 5xn,

$$\mathbb{K}1 = \begin{bmatrix} 0 & .. & 0 & .. & 0 \\ 0 & .. & 0 & .. & 0 \\ tn_{n1} & .. & tn_{ni} & .. & tn_{nn} \\ 0 & .. & 0 & .. & 0 \\ 0 & .. & 0 & .. & 0 \end{bmatrix}$$

$$\mathbb{K}2 = \begin{bmatrix} 0 & .. & 0 & .. & 0 \\ 0 & .. & 0 & .. & 0 \\ tn_{n-1\ 1} & .. & tn_{n-1\ i} & .. & tn_{n-1\ n} \\ 0 & .. & 0 & .. & 0 \\ 0 & .. & 0 & .. & 0 \end{bmatrix}$$

$$\mathbb{K}i = \begin{bmatrix} 0 & .. & 0 & .. & 0 \\ 0 & .. & 0 & .. & 0 \\ tn_{n-i+1\ 1} & .. & tn_{n-i+1\ i} & .. & tn_{n-i+1\ n} \\ 0 & .. & 0 & .. & 0 \\ 0 & .. & 0 & .. & 0 \end{bmatrix}$$

$$\mathbb{K}n = \begin{bmatrix} 0 & .. & 0 & .. & 0 \\ 0 & .. & 0 & .. & 0 \\ tn_{11} & .. & tn_{1i} & .. & tn_{1n} \\ 0 & .. & 0 & .. & 0 \\ 0 & .. & 0 & .. & 0 \end{bmatrix}$$

in which tn_{ij} are the elements of matrix $\mathbb{T}_n$.

By extension of the earlier analysis, the state vector at a point at the top of the structure may be expressed in a generalised form as,

$$\mathbb{Z}_{n+1} = \mathbb{U}_n.\mathbb{U}_{n-1}..\mathbb{U}_0.\mathbb{Z}_0 + [\ \mathbb{U}_n.\mathbb{U}_{n-1}..\mathbb{U}_1.\mathbb{K}1 + \mathbb{U}_n.\mathbb{U}_{n-1}..\mathbb{U}_2.\mathbb{K}2 + ..+ \mathbb{U}_n.\mathbb{U}_{n-1}..\mathbb{U}_i.\mathbb{K}i + .. + \mathbb{U}_n.\mathbb{K}n\ ].\Psi_n \qquad (4.61)$$

where

$\mathbb{Z}_n$ is the state vector at the top of the structure

$\mathbb{Z}_0$ is the state vector at the bottom of the structure

$\mathbb{U}_n$, $\mathbb{U}_{n-1}$, $\mathbb{U}_{n-2}$ .. $\mathbb{U}_i$ .. $\mathbb{U}_0$ are the transfer matrices

$\mathbb{K}1$, $\mathbb{K}2$, .. $\mathbb{K}i$ .. $\mathbb{K}n$ are the matrices formed from the elements of the matrix $\mathbb{T}_n$

Following the same procedure as in the previous sections, the general expression for ψ_1, ψ_2, ψ_3 .. ψ_i .. and ψ_n can be expressed as

$$\Psi_n = \mathbb{J}1^{-1}.\mathbb{J}2.\mathbb{Z}_0 \qquad (4.62)$$

where $\mathbb{J}1$ and $\mathbb{J}2$ are matrices of the order nxn and nx5 respectively and are given by,

$$\mathbb{J}1 = \mathbb{I} - \begin{bmatrix} 0 \; . \; . \; . \; . \; . \; . \; . \; . \; . \; . \; . \; . \; . \; . \; . \; . \; . \; . \; 0 \\ \mathbb{G}.\mathbb{U}_1.\mathbb{K}1 \\ \mathbb{G}.\mathbb{U}_2.\mathbb{U}_1.\mathbb{K}1 + \mathbb{G}.\mathbb{U}_2.\mathbb{K}2 \\ \vdots \\ \mathbb{G}.\mathbb{U}_n.\mathbb{U}_{n-1} \ldots \mathbb{U}_1.\mathbb{K}1 + \mathbb{G}.\mathbb{U}_n.\mathbb{U}_{n-1} \ldots \mathbb{U}_2.\mathbb{K}2 \\ + \ldots + \mathbb{G}.\mathbb{U}_n.\mathbb{K}n \end{bmatrix}$$

$$\mathbb{J}2 = \begin{bmatrix} \mathbb{G}.\mathbb{U}_0 \\ \mathbb{G}.\mathbb{U}_1.\mathbb{U}_0 \\ \mathbb{G}.\mathbb{U}_2.\mathbb{U}_1.\mathbb{U}_0 \\ \vdots \\ \mathbb{G}.\mathbb{U}_n.\mathbb{U}_{n-1} \ldots \mathbb{U}_i \ldots \mathbb{U}_0 \end{bmatrix}$$

where $\mathbb{I}$ is a nxn unit matrix.

Substituting equation (4.62) into (4.61), the transfer matrix linking the point "0" at the base to the top of structure is obtained as,

$$\mathbb{Z}_{n+1} = \mathbb{R}_n.\mathbb{Z}_0 \tag{4.63}$$

where $\mathbb{R}_n$ is the transfer matrix of the order 5x5 as

$$\mathbb{R}_n = \mathbb{U}_n.\mathbb{U}_{n-1}..\mathbb{U}_0 + [\, \mathbb{U}_n.\mathbb{U}_{n-1}..\mathbb{U}_1.\mathbb{K}1 + \mathbb{U}_n.\mathbb{U}_{n-1}..\mathbb{U}_2.\mathbb{K}2 + .. + \mathbb{U}_n.\mathbb{U}_{n-1}..\mathbb{U}_i.\mathbb{K}i + .. + \mathbb{U}_n.\mathbb{K}n \,].\mathbb{J}1^{-1}.\mathbb{J}2$$

4.4.5 BOUNDARY CONDITIONS

If the structure is rigidly built in at the base and free at the top, the boundary conditions for the uniformly distributed lateral load and triangularly distributed lateral load cases are,

$$y_B = \psi_B = 0 \tag{4.64a}$$

$$M_T = V_T = 0 \tag{4.64b}$$

where the subscript "B" and "T" denote bottom and top position of the structure respectively.

If the structure is rigidly built in at the base and free at the top subjected to the point load P applied at the top, the boundary conditions becomes,

$$y_B = \psi_B = 0 \tag{4.65a}$$

$$V_T = P \tag{4.65b}$$

$$M_T = 0 \tag{4.65c}$$

Substitution of the boundary conditions, equations (4.64) or (4.65), into equation (4.63) gives two equations to enable the bending moment M_B and shear force V_B to be determined in terms of the applied load.

For the uniformly distributed lateral load and triangularly distributed lateral load cases, Equation (4.63) becomes,

$$\begin{bmatrix} 0 \\ 0 \\ 1 \end{bmatrix} = \mathbb{P}. \begin{bmatrix} M_B \\ V_B \\ 1 \end{bmatrix} \tag{4.66a}$$

where

$$\mathbb{P} = \begin{bmatrix} rn_{33} & rn_{34} & rn_{35} \\ rn_{43} & rn_{44} & rn_{45} \\ rn_{53} & rn_{54} & rn_{55} \end{bmatrix} \tag{4.66b}$$

and rn_{ij} are specific elements of the transfer matrix $\mathbb{R}_n$ in equation (4.63).

For the case of point load P applied at the top, Equation (4.63) becomes,

$$\begin{bmatrix} 0 \\ P \\ 1 \end{bmatrix} = \mathbb{P}. \begin{bmatrix} M_B \\ V_B \\ 1 \end{bmatrix} \tag{4.66c}$$

Therefore M_B and V_B can be obtained from equation (4.66a) or (4.66c). For the uniformly distributed lateral load and triangularly distributed lateral load cases, M_B and V_B become,

$$M_B = p_{13} \tag{4.67a}$$

$$V_B = p_{23} \tag{4.67b}$$

where p_{13} and p_{23} are specific elements of the matrix $\mathbb{P}^{-1}$.

For the case of point load P applied at the top,

$$M_B = p_{12} P + p_{13} \tag{4.68a}$$

$$V_B = p_{22} P + p_{23} \tag{4.68b}$$

Having evaluated M_B and V_B, the lateral deflection at the top of the structure, y_T and ψ_T can be determined directly from equation (4.63).

For the uniformly distributed lateral load and triangularly distributed lateral load cases, y_T and ψ_T become,

$$y_T = rn_{13} p_{13} + rn_{14} p_{23} + rn_{15} \tag{4.69a}$$

$$\psi_T = rn_{23} p_{13} + rn_{24} p_{23} + rn_{25} \tag{4.69b}$$

For the case of point load P applied at the top,

$$y_T = rn_{13}(p_{12}P+p_{13}) + rn_{14}(p_{22}P+p_{23}) + rn_{15} \tag{4.70a}$$

$$\psi_T = rn_{23}(p_{12}P+p_{13}) + rn_{24}(p_{22}P+p_{23}) + rn_{25} \tag{4.70b}$$

If the structure is built at the flexible foundation and free at the top, the boundary conditions at the base become,

$$y_B = 0 \tag{4.71}$$

$$\psi_B = K_\vartheta M_B \tag{4.72}$$

The boundary conditions at the top for the uniformly distributed lateral load, triangularly distributed lateral and point load applied at the top cases are given as before in

equations (4.64b), (4.65b) and (4.65c).

Substituting the boundary conditions in equations (4.71) and (4.72) into equation (4.63), M_B and V_B can be determined in terms of the applied load. For the uniformly distributed lateral load and triangularly distributed lateral load cases, equation (4.63) becomes,

$$\begin{bmatrix} 0 \\ 0 \\ 1 \end{bmatrix} = \mathbb{Q}. \begin{bmatrix} M_B \\ V_B \\ 1 \end{bmatrix} \qquad (4.73a)$$

where $\mathbb{Q}$ is a matrix of the order 3x3,

$$\mathbb{Q} = \begin{bmatrix} rn_{32}.K_\vartheta + rn_{33} & rn_{34} & rn_{35} \\ rn_{42}.K_\vartheta + rn_{43} & rn_{44} & rn_{45} \\ rn_{52}.K_\vartheta + rn_{53} & rn_{54} & rn_{55} \end{bmatrix} \qquad (4.73b)$$

For the case of point load P applied at the top, Equation (4.63) becomes,

$$\begin{bmatrix} 0 \\ P \\ 1 \end{bmatrix} = \mathbb{Q}. \begin{bmatrix} M_B \\ V_B \\ 1 \end{bmatrix} \qquad (4.73c)$$

Therefore M_B and V_B can be obtained from equation (4.73a) or (4.73c). For the uniformly distributed lateral load and triangularly distributed lateral load cases, M_B and V_B become,

$$M_B = q_{13} \qquad (4.74a)$$

$$V_B = q_{23} \tag{4.74b}$$

where q_{13} and q_{23} are specific elements of the matrix $\mathbb{Q}^{-1}$.

For the case of point load P applied at the top,

$$M_B = q_{12}\, P + q_{13} \tag{4.75a}$$

$$V_B = q_{22}\, P + q_{23} \tag{4.75b}$$

Having evaluated M_B and V_B, the lateral deflection at the top of the structure, y_T and ψ_T can be determined directly from equation (4.63).

For the uniformly distributed lateral load and triangularly distributed lateral load cases, y_T and ψ_T become,

$$y_T = rn_{13}\, q_{13} + rn_{14}\, q_{23} + rn_{15} \tag{4.76a}$$

$$\psi_T = rn_{23}\, q_{13} + rn_{24}\, q_{23} + rn_{25} \tag{4.76b}$$

For the case of point load P applied at the top,

$$y_T = rn_{13}(q_{12}P+q_{13}) + rn_{14}(q_{22}P+q_{23}) + rn_{15} \tag{4.77a}$$

$$\psi_T = rn_{23}(q_{12}P+q_{13}) + rn_{24}(q_{22}P+q_{23}) + rn_{25} \tag{4.77b}$$

4.5 CORRESPONDING CASE OF OUTRIGGER-BRACED CORE

As demonstrated in Section 4.2 in this Chapter that there is an analogy between the outrigger and the linked shear walls. The developed theory in Section 4.4 for the linked shear walls can be used directly for the analysis of an outrigger-braced core.

In that case, the bending of the core wall under the action of lateral forces corresponds to the bending of the two walls, and the axial deformations in the columns correspond directly to the axial deformations in the two walls. The resisting moment produced by the stiffening beam in inducing the axial forces in the walls corresponds to the resisting moment produced by the outrigger. Consequently, the theory for static analysis of the outrigger structures by transfer matrix technique may be developed in an identical manner. The only differences in the analysis are the structural parameters S_1 and S_2 for the outrigger-braced core instead of s_1 and s_2 for linked shear walls.

For linked shear walls, the structural parameters s_1 and s_2 apply to the analysis as given in equations (4.6b) and (4.6c). For the outrigger-braced structure, the structural parameters S_1 and S_2 from equations (2.6a) and (2.6b) should be used. By setting up the state vectors of actions at station points, as shown in Fig.[4.9a] to [4.10b], and establishing the condition of rotational compatibility for the core and outriggers at outrigger levels, similar set of expressions for the outrigger-braced structures can be obtained accordingly. The general expression of the restraining moment M_1, M_2 .. M_i .. and M_n due to the outriggers at levels x_1,

$x_2 \; .. \; x_i \; .. \; x_n$ can be expressed in a same form as equation (4.59), where $\mathbb{T}_n$ is the transfer matrix of the order nxn containing the structural parameter S_1 and S_2, given by

$$\mathbb{T}_n = \begin{bmatrix} S_1+S_2x_n & S_2x_{n-1} & . \; . & S_2x_2 & s_2x_1 \\ \vdots & \vdots & \vdots \; \vdots & \vdots & \vdots \\ S_2x_i & S_1+S_2x_i & . \; . & . & S_2x_1 \\ \vdots & \vdots & \vdots \; \vdots & \vdots & \vdots \\ S_2x_2 & S_2x_2 & . \; . & S_1+S_2x_2 & S_2x_1 \\ S_2x_1 & S_2x_1 & . \; . & S_2x_1 & S_1+S_2x_1 \end{bmatrix}^{-1}$$

where

$$S_1 = \frac{d}{12E_oI_o} \qquad (4.78a)$$

and

$$S_2 = \frac{2}{d^2E_cA_c} \qquad (4.78b)$$

where

E_c is the elastic modulus of the column material

A_c is the area of the column

E_o is the elastic modulus of the outrigger material

I_o is the moment of inertia of outrigger

d is the distance between columns

Ψ_n is a matrix of the order nx1, with elements ψ_1, ψ_2 .. ψ_i .. ψ_n denoting the slopes of the core of at station points "1", "2" .. "i" .. "n".

The equations derived for the case of stiffened linked shear walls may thus be used directly for the static analysis of outrigger-braced cores, provided the structural parameter s_1 and s_2 are changed to S_1 and S_2 as shown in equations (4.78a) and (4.78b). Parameter studies made to investigate design trends may thus be used to examine the behaviour of the two seemingly different forms of structure.

4.6 NUMERICAL RESULTS

Three numerical examples were considered to illustrate the application of the transfer matrix technique to the analysis of shear wall structures. Calculations were performed on a representative 20-storey structure with the plan form shown in Fig.[4.13], subjected to a uniformly distributed loading of 10kN/m over the entire height H of 60m. The storey height was taken to be 3.0m.

In example [4.1], it is assumed that the structure has two linked shear walls and is stiffened either by one, two or three stiffening beams. Two type of stiffening beams were studied, Type A and Type B, with cross-sectional dimensions 300mmx400mm and 300mmx800mm. A wide range of stiffening beam positions was investigated. The use of uniform spacings and the optimum levels of the stiffening beams were included in the study. The results

for this example are shown in Table [4.1]. Since no additional assumptions were added to the analysis, the results were expected to be the same as those of the discrete matrix analysis.

The structural parameters in the example for the discrete matrix analysis are,

	Case of Type A lintel beams	Case of Type B lintel beams
w	1.4652	0.1831
1/(EIs)	0.8242	0.8242

The optimum locations corresponding to the above structural parameters can be obtained from Figs.[2.8], [2.9] and [2.10]. The optimumn locations of the stiffening beams are found to be in good agreement with those in Table [4.1].

In example [4.2], it is assumed that the structure is a coupled shear system supported on a rigid foundation. The deflection, base moment and shear force in the lintel beams are presented in Tables [4.2] and [4.3]. Results are given for the continuum solution, for comparative purposes. For the 20-storey structure, the results for the transfer matrix technique and the continuum solution are found to be in close agreement.

In example [4.3], it is assumed that the structure is a coupled shear wall system with openings 6m high at the top and the bottom. The elevation of the structure is shown in Fig.[4.14]. The

openings are intended to allow areas such as a canteen or assembly hall to be constructed within the structure. It is neccessary and of interest to find out the effect of those openings on the structural behaviour of the coupled shear system. Calculations using the transfer matrix technique were performed to determine the top deflection, base moment and shear force in the lintel beams for the cases of both top and bottom openings, top opening only and bottom opening only. The results are presented in Tables [4.4] to [4.6]. The increases in top drift and base moment in the structure due to the openings are given below,

Cases	Increase in top drift % Lintel beams		Increase in base moment % Lintel beams	
	Type A	Type B	Type A	Type B
Top and Bottom openings	1.8	0.3	1.9	6.4
Top opening only	1.6	0.1	0.2	0.0
Bottom opening only	0.1	0.2	1.7	6.4

The effect on the shear force distribution in the lintel beams was generally found to be localised near to the openings. As expected, the opening at the top will have a comparatively greater effect on top drift while the opening at the bottom will have a stronger effect on the base moment in the walls.

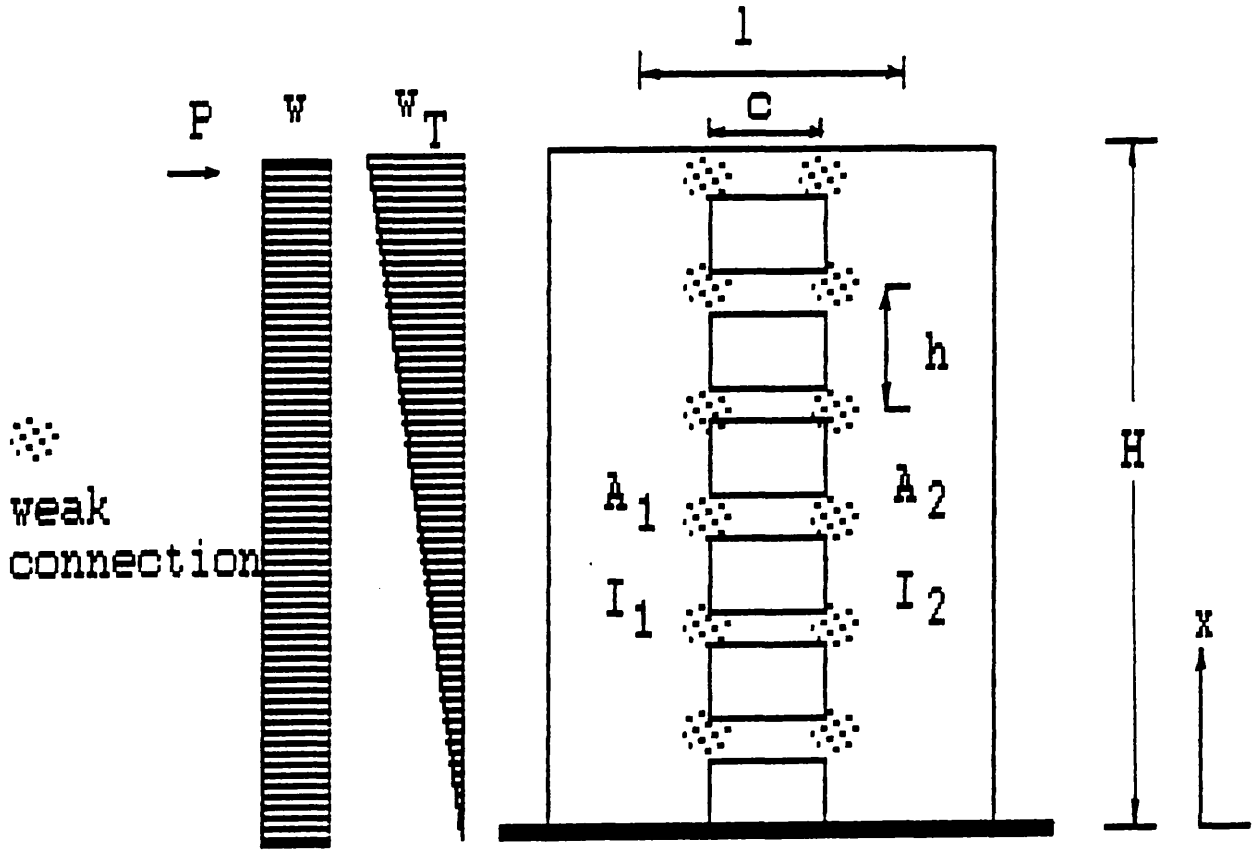

Linked shear walls and external loads

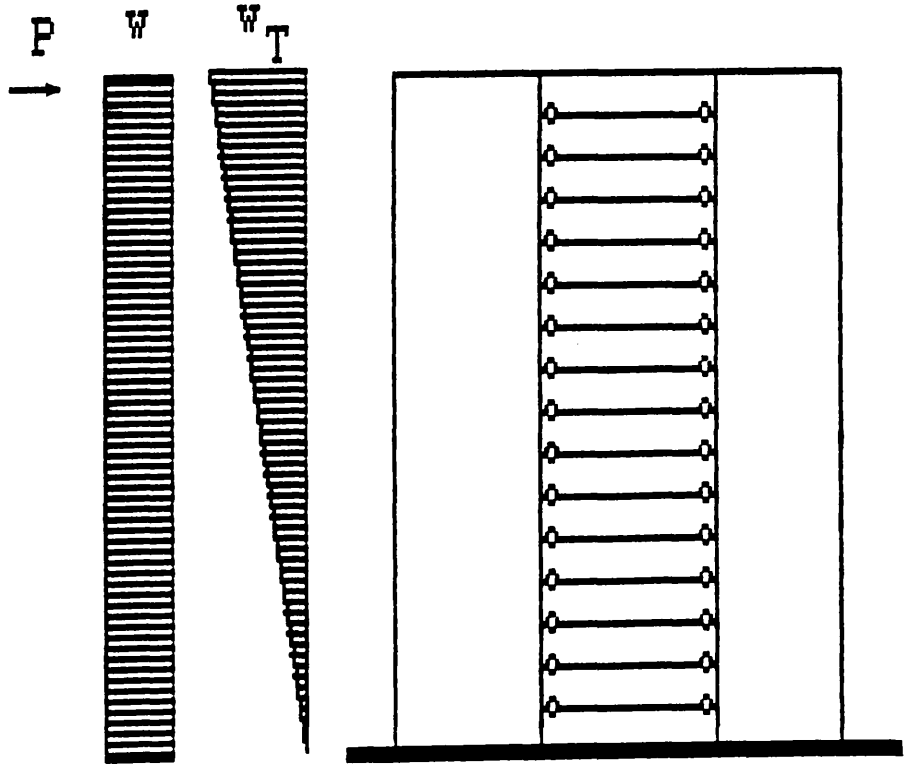

Equivalent substitute system

FIG.[4.1] A LINKED SHEAR WALL STRUCTURE AND THE EQUIVALENT SYSTEM

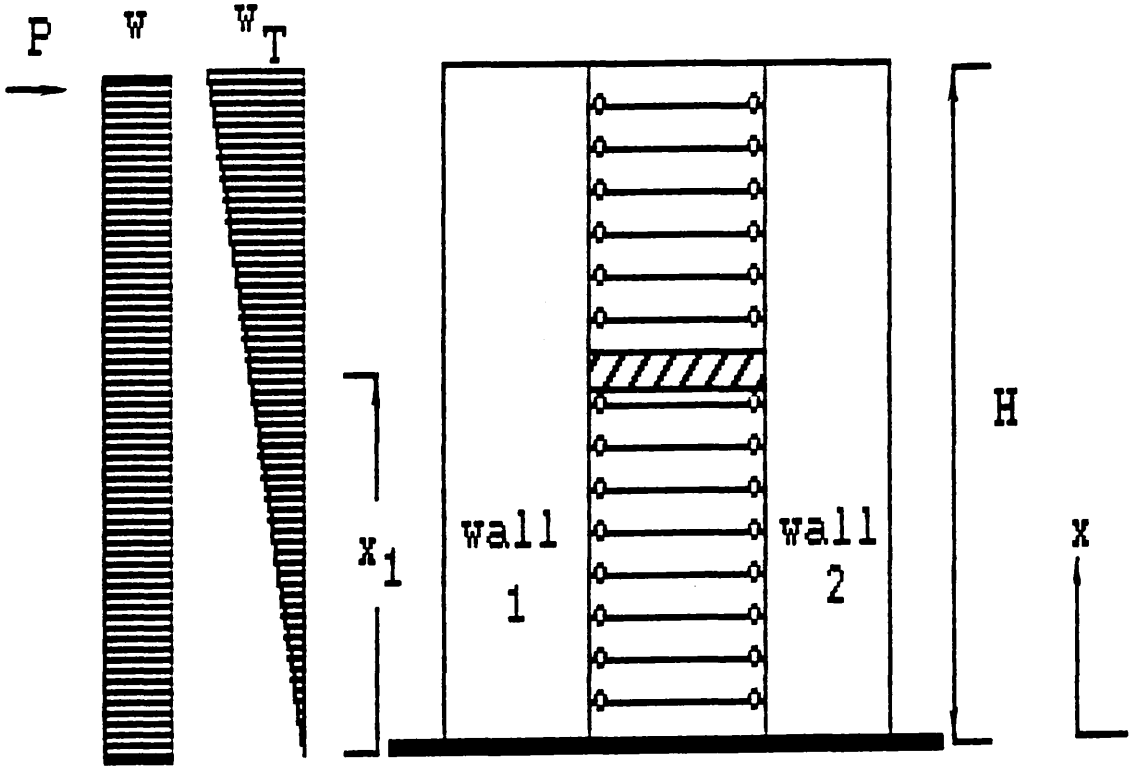

FIG. [4.2a] A linked shear walls with an intermediate stiffening beam

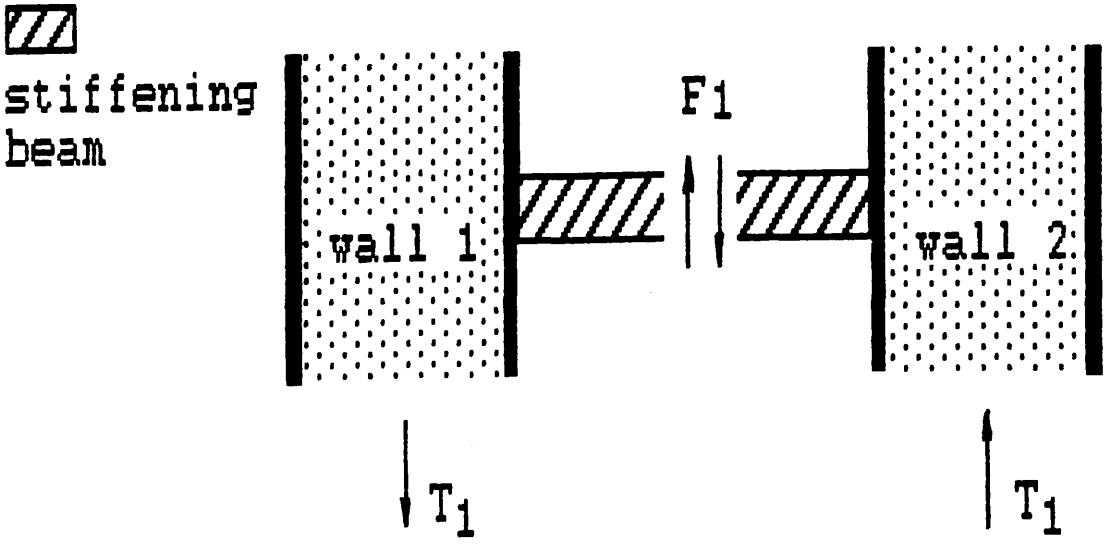

FIG. [4.2b] Action of vertical forces

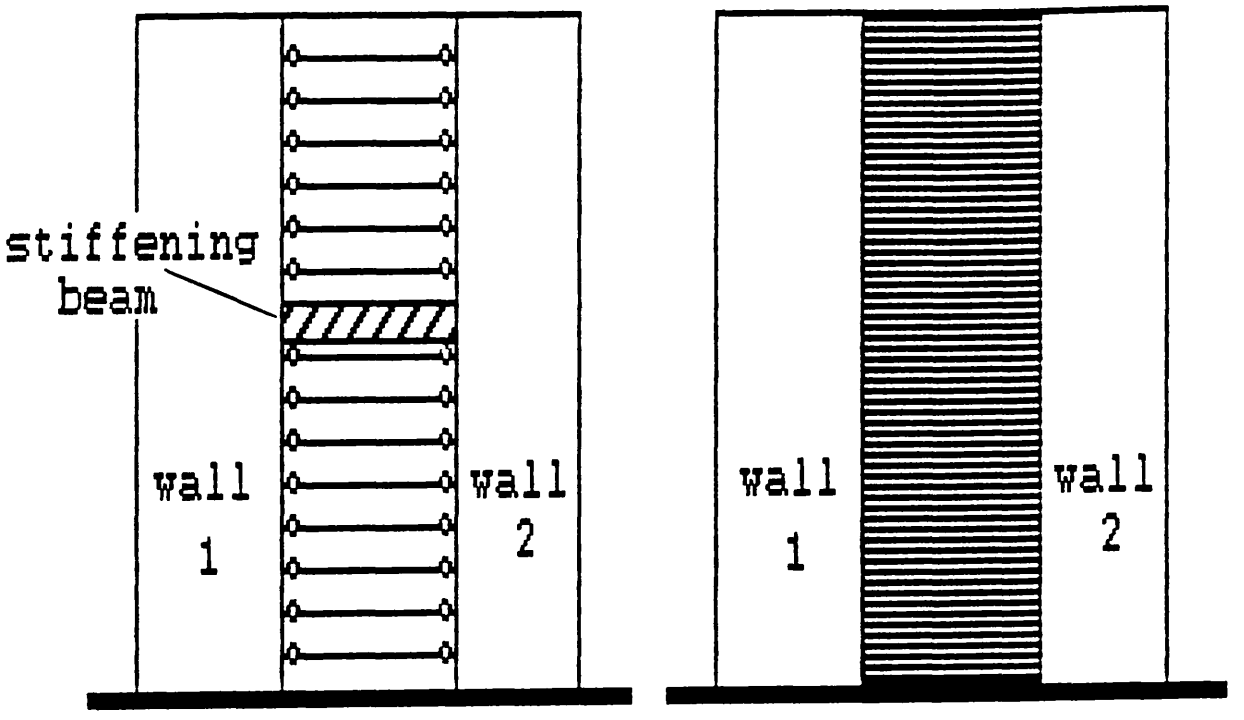

A linked and a coupled shear walls

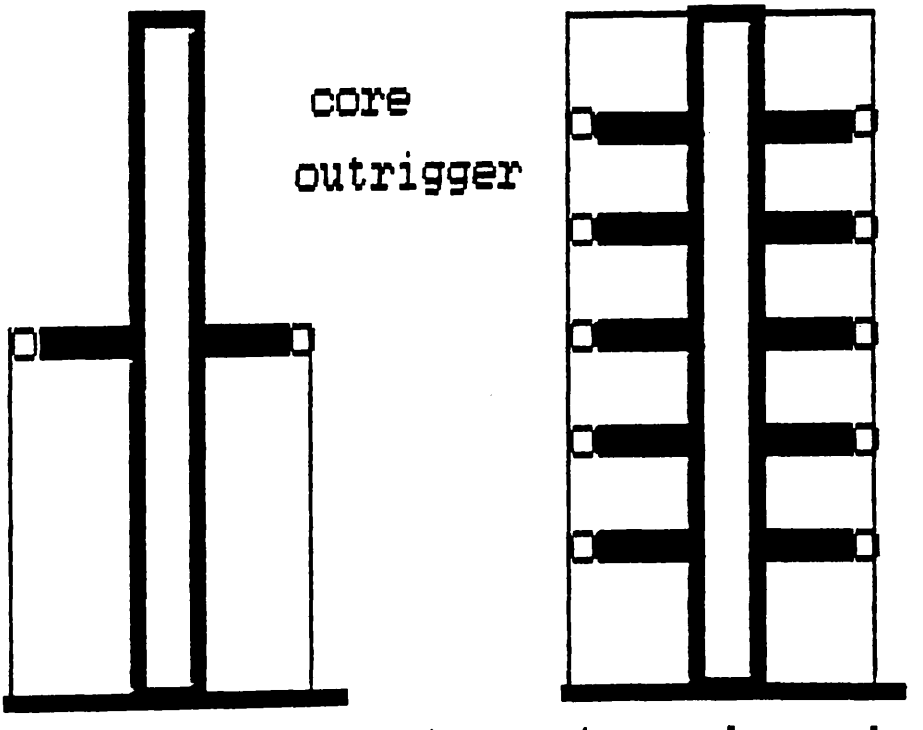

A single and a multi-outrigger-braced structure

FIG.[4.3] Analogy between the shear walls structures and the outrigger-braced structures

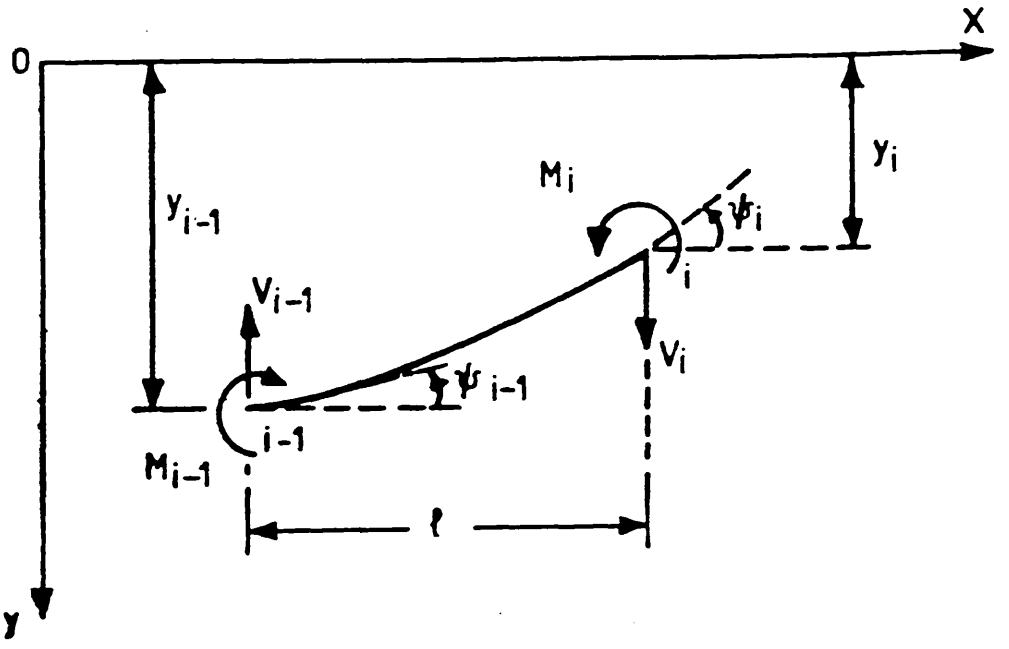

FIG. [4.4] SIGN CONVENTION FOR STRUCTURAL ACTIONS

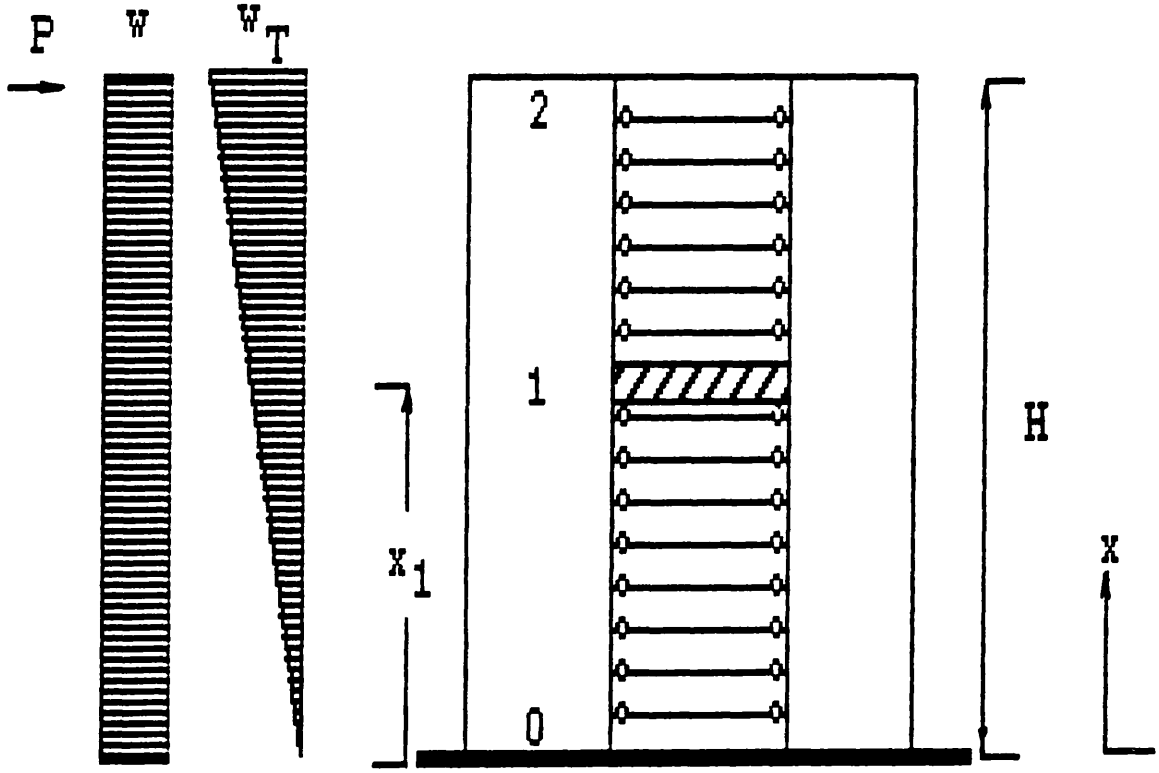

FIG. [4.5] A LINKED SHEAR WALL STRUCTURE WITH AN INTERMEDIATE STIFFENING BEAM

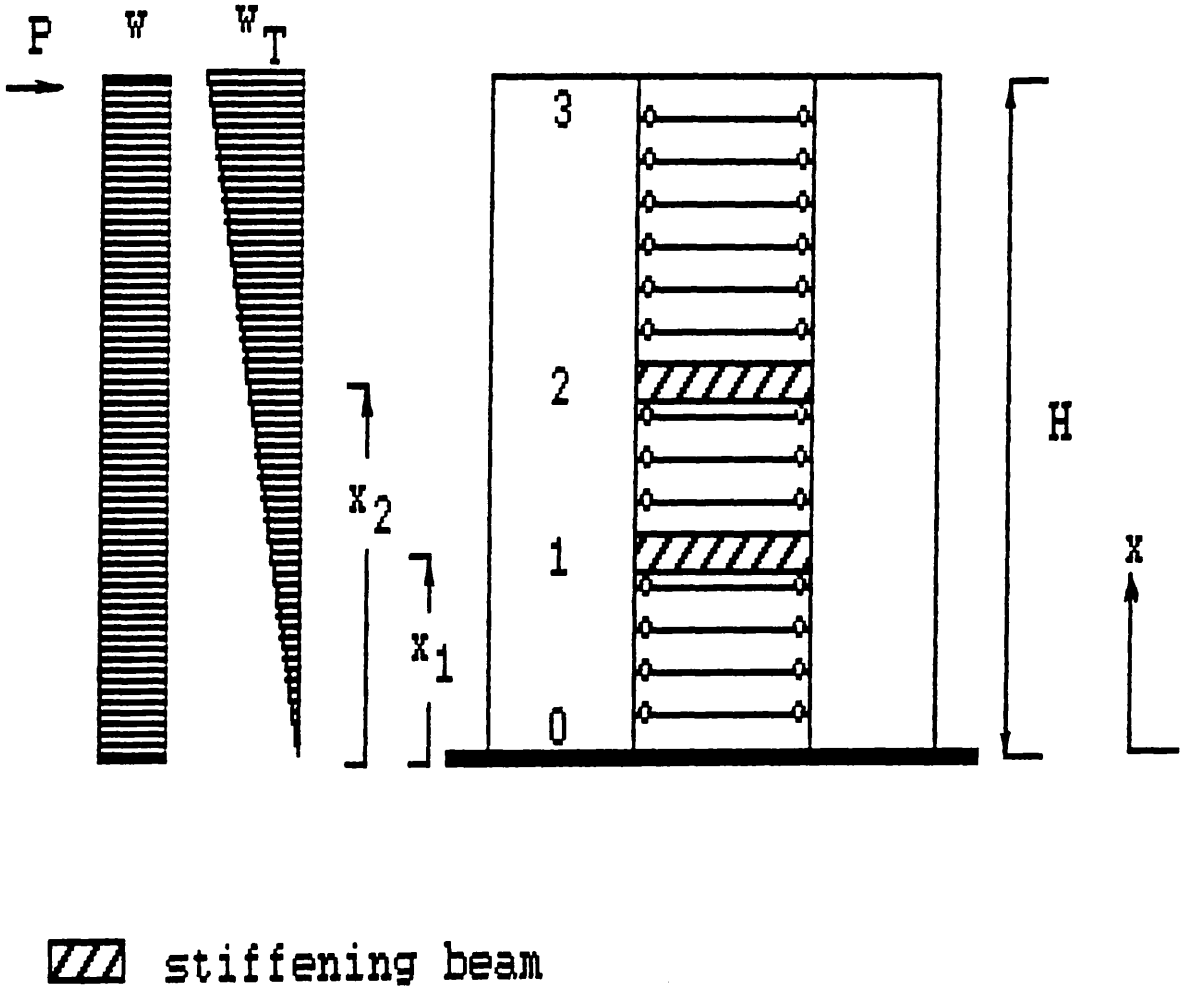

FIG. [4.6] A LINKED SHEAR WALL STRUCTURE WITH TWO INTERMEDIATE STIFFENING BEAMS

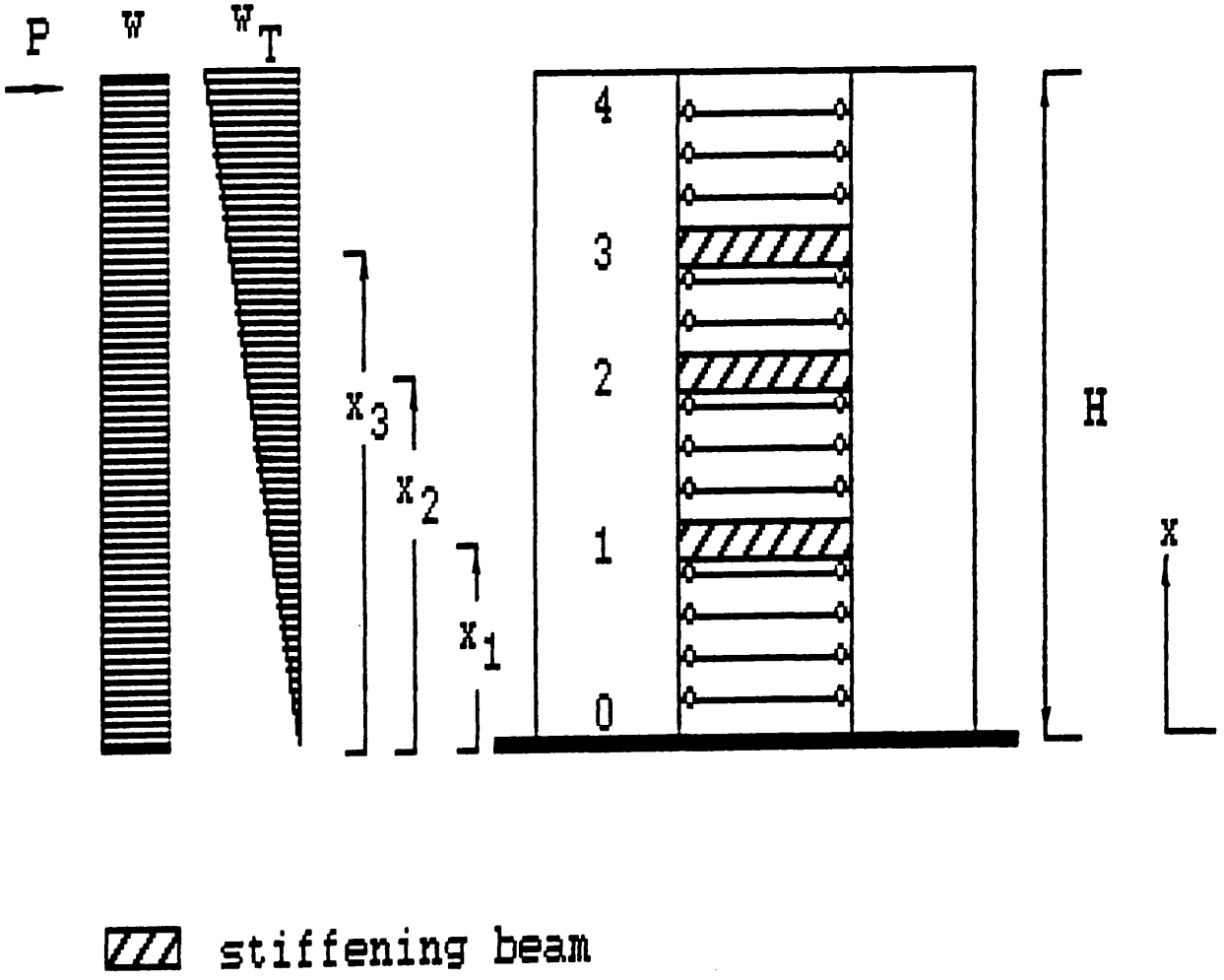

FIG.[4.7] A LINKED SHEAR WALL STRUCTURE WITH THREE INTERMEDIATE STIFFENING BEAMS

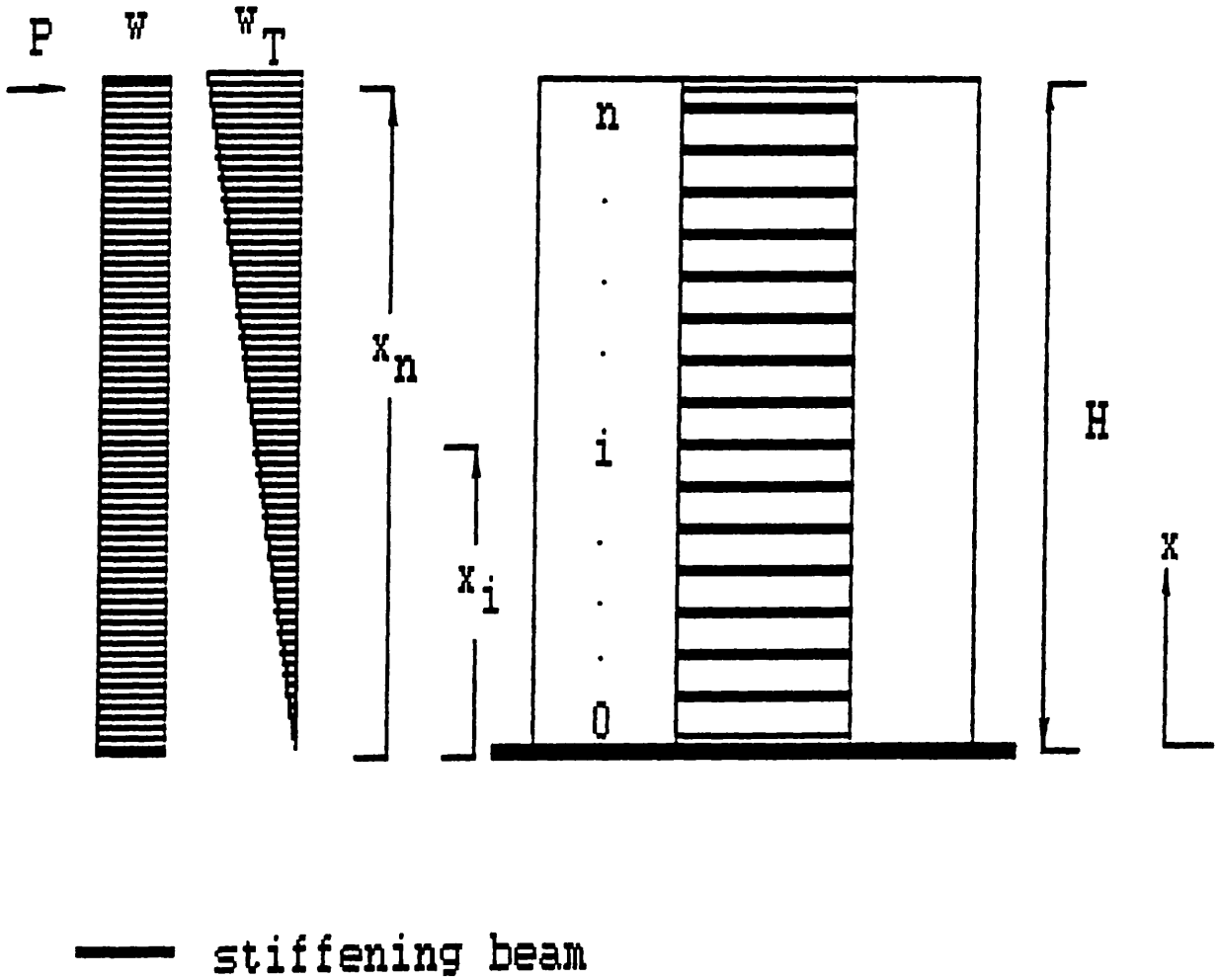

FIG.[4.8] A LINKED SHEAR WALL STRUCTURE WITH n INTERMEDIATE STIFFENING BEAMS

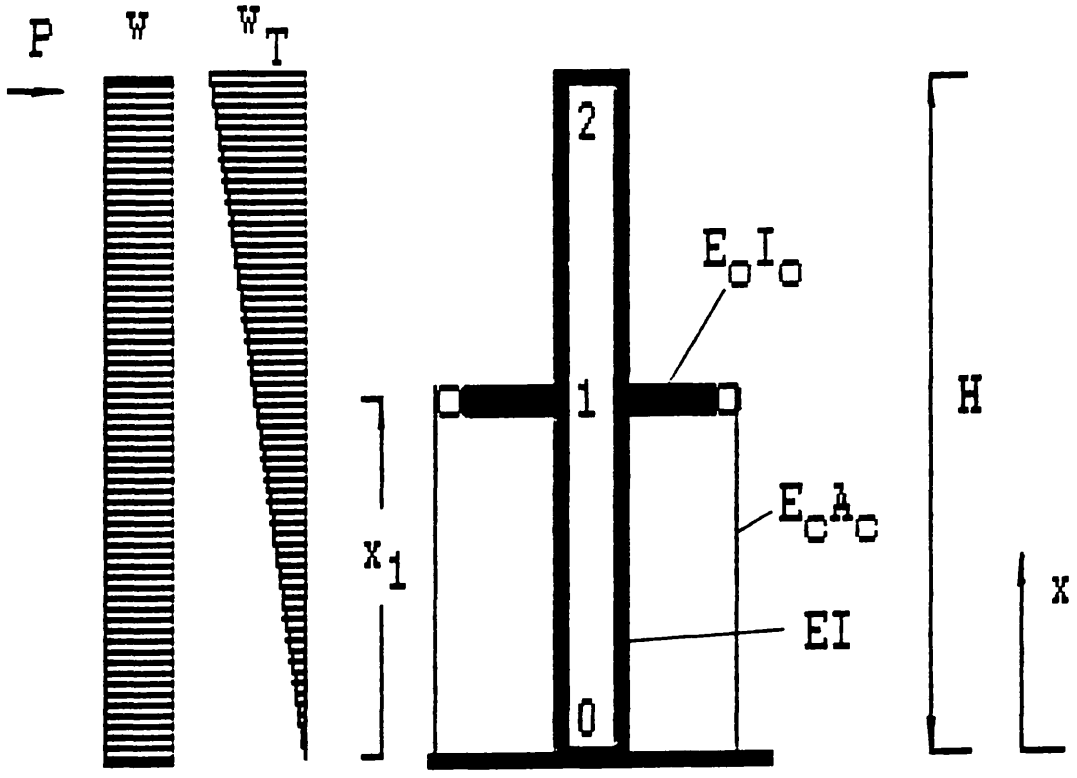

FIG.[4.9] ONE OUTRIGGER CASE

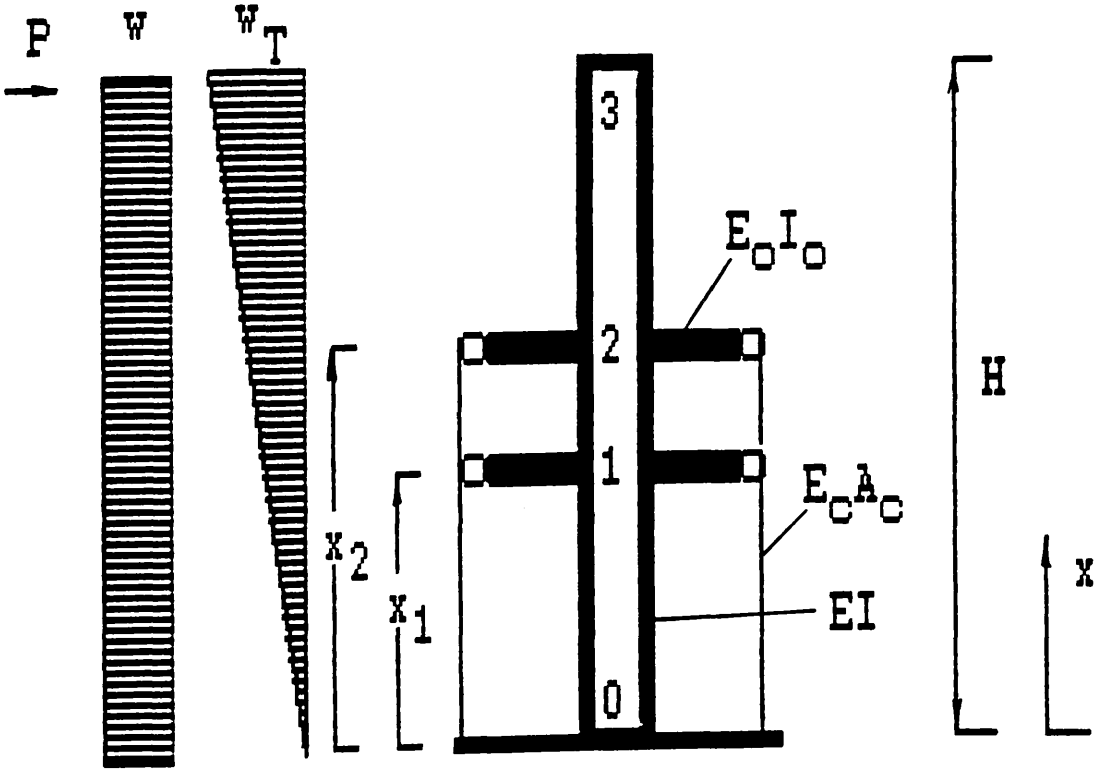

FIG.[4.10] TWO OUTRIGGER CASE

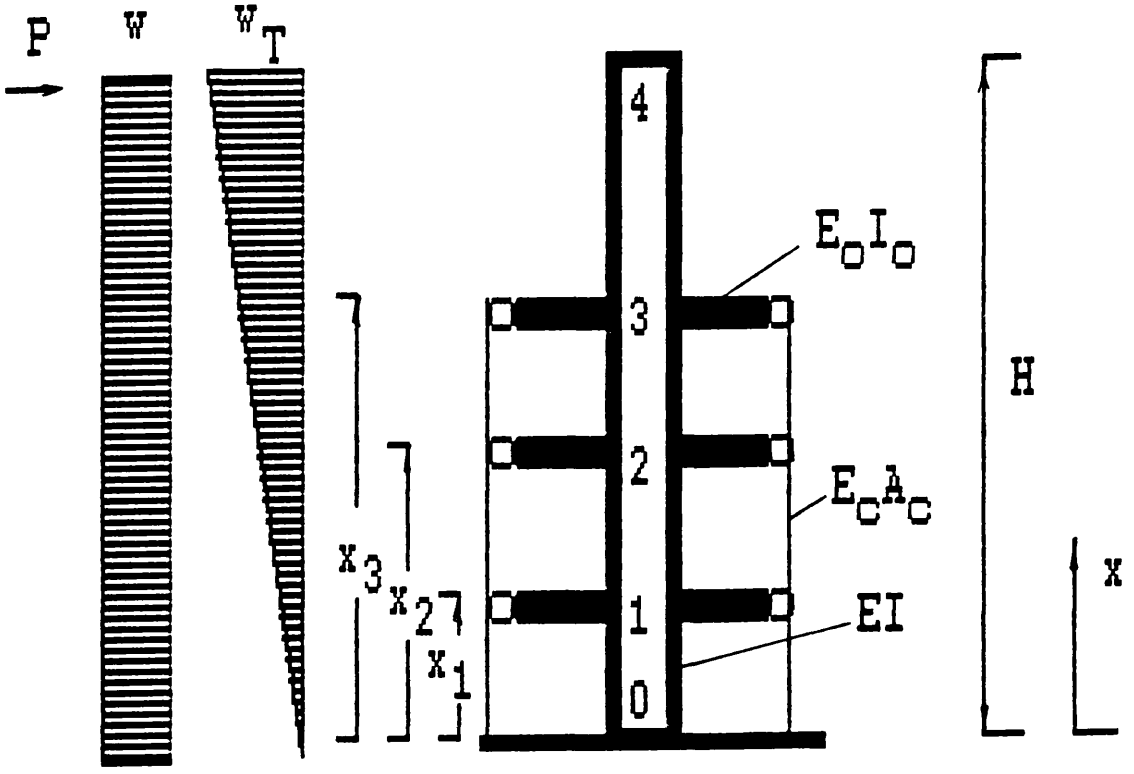

FIG.[4.11] THREE OUTRIGGER CASE

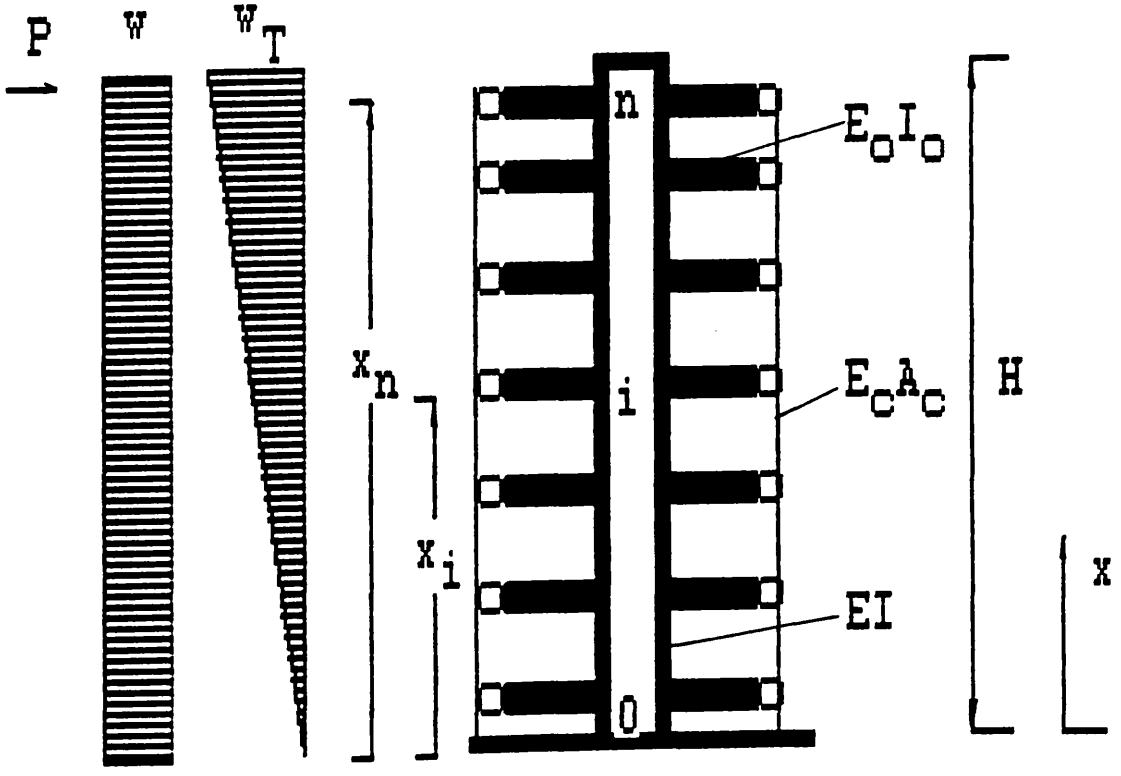

FIG.[4.12] n OUTRIGGER CASE

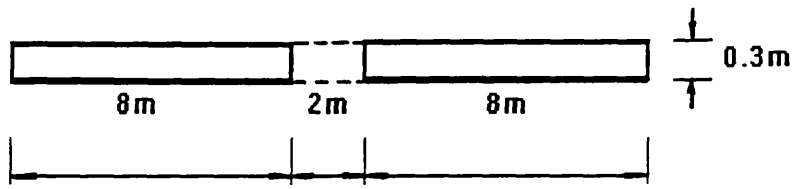

FIG. [4.13] EXAMPLE STRUCTURE, PLAN DIMENSIONS

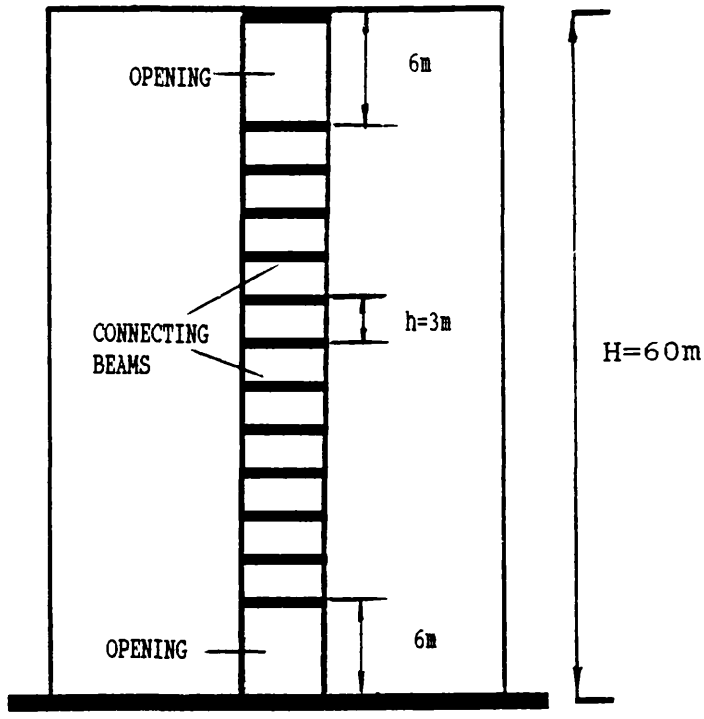

FIG.[4.14] EXAMPLE STRUCTURE, ELEVATION

Table [4.1] Results for example [4.1] using transfer matrix technique

Number of outriggers	x_1	x_2	x_3	Lintel beams			
	measured from the base (H)			Type A (300mmx400mm)		Type B (300mmx800mm)	
				M_B/M_{aB}	y_T/y_{FT}	M_B/M_{aB}	y_T/y_{FT}
1	0.0			1.000	1.000	1.000	1.000
	0.1			0.952	0.982	0.737	0.900
	0.2			0.918	0.941	0.650	0.748
	0.3			0.895	0.893	0.626	0.619
	0.4			0.882	0.849	0.631	0.527
	0.5			0.875	0.813	0.648	0.472
	(B*)0.6			0.873	0.787	0.672	0.448
	0.7			0.874	0.771	0.697	0.449
	0.8			0.878	0.765	0.722	0.468
	(A*)0.9			0.882	0.766	0.747	0.498
	1.0			0.887	0.773	0.768	0.535
2	0.33	0.66		0.799	0.702	0.547	0.351
	0.25	0.75		0.807	0.716	0.537	0.369
	0.50	1.00		0.807	0.664	0.616	0.363
	(A*)0.62	0.85		0.808	0.649		
	(B*)0.42	0.75				0.578	0.341
3	0.25	0.50	0.75	0.746	0.625	0.495	0.300
	0.17	0.50	0.83	0.755	0.637	0.486	0.314
	0.33	0.66	1.00	0.755	0.599	0.539	0.310
	(A*)0.52	0.68	0.86	0.759	0.576		
	(B*)0.32	0.52	0.79			0.518	0.296

A* Optimum locations of stiffening beams for Type A case
B* Optimum locations of stiffening beams for Type B case

Table [4.2] Comparison of results for example [4.2]
(Type A lintel beams 300mmx400mm)

Level x measured from the base (m)	Transfer matrix technique Shear force in lintel beams (kN)	M_B (kNm)	y_T (mm)	Continuum q.h (kN)	M_B (kNm)	y_T (mm)
60	28.80		13.43	*16.40		13.52
57	32.40			33.23		
54	32.40			34.72		
51	36.00			36.79		
48	39.60			39.31		
45	39.60			42.28		
42	43.20			45.25		
39	46.80			48.36		
36	50.40			51.33		
33	54.00			54.15		
30	57.00			56.38		
27	57.00			56.38		
24	57.00			58.90		
21	57.00			58.75		
18	57.00			57.27		
15	54.00			54.30		
12	50.40			49.25		
9	43.20			42.00		
6	32.40			31.75		
3	18.00			17.95		
0	0.00	9135.2		0.00	9126.0	

* q.h/2 for the top beam

Table [4.3] Comparison of results for example [4.2]
(Type B lintel beams 300mmx800mm)

Level x measured from the base (m)	Transfer matrix technique Shear force in lintel beams (kN)	M_B (kNm)	y_T (mm)	Continuum q.h (kN)	M_B (kNm)	y_T (mm)
60	10.80		8.49	*7.12		8.47
57	14.40			15.87		
54	18.00			19.89		
51	25.20			25.22		
48	32.40			31.45		
45	39.60			38.13		
42	43.20			45.10		
39	50.40			52.07		
36	57.60			59.34		
33	64.80			66.46		
30	72.00			73.44		
27	79.20			80.26		
24	86.00			86.79		
21	93.60			92.57		
18	97.20			97.47		
15	100.80			100.44		
12	100.80			100.29		
9	93.60			95.10		
6	79.20			81.30		
3	54.00			52.96		
0	0.00	5814.72		0.00	5724.00	

* q.h/2 for the top beam

Table [4.4] Forces and deformations for example [4.3]
(With top and bottom openings)

	Lintel beams type A			Lintel beams type B		
Level x measured from the base (m)	Shear force in lintel beams (kN)	M_B (kNm)	y_T (mm)	Shear force in lintel beams (kN)	M_B (kNm)	y_T (mm)
60	36.00		13.67	18.00		8.52
57						
54	36.00			21.60		
51	39.60			25.20		
48	39.60			32.40		
45	43.20			39.60		
42	46.80			46.80		
39	50.40			54.00		
36	54.00			61.20		
33	54.00			64.80		
30	57.60			72.00		
27	57.60			79.20		
24	57.60			86.40		
21	57.60			93.60		
18	57.60			97.20		
15	54.00			100.80		
12	50.40			100.80		
9	43.20			97.20		
6	32.40			86.40		
3						
0	0.00	9305.82		0.00	6188.40	

Table [4.5] Forces and deformations for example [4.3]
(With top opening only)

	Lintel beams type A			Lintel beams type B		
Level x measured from the base (m)	Shear force in lintel beams (kN)	M_B (kNm)	y_T (mm)	Shear force in lintel beams (kN)	M_B (kNm)	y_T (mm)
60	36.00		13.65	18.00		8.50
57						
54	36.00			21.60		
51	39.60			25.20		
48	39.60			32.40		
45	43.20			39.60		
42	46.80			46.80		
39	50.40			54.00		
36	54.00			61.20		
33	54.00			64.80		
30	57.60			72.00		
27	57.60			79.20		
24	57.60			86.40		
21	57.60			93.60		
18	57.60			97.20		
15	54.00			100.80		
12	50.40			100.80		
9	43.20			93.60		
6	32.40			79.20		
3	18.00			54.00		
0	0.00	9152.28		0.00	5814.72	

Table [4.6] Forces and deformations for example [4.3]
(With bottom opening only)

	Lintel beams type A			Lintel beams type B		
Level x measured from the base (m)	Shear force in lintel beams (kN)	M_B (kNm)	y_T (mm)	Shear force in lintel beams (kN)	M_B (kNm)	y_T (mm)
60	28.80		13.45	10.80		8.51
57	32.40			14.40		
54	32.40			18.00		
51	36.00			25.20		
48	39.60			32.40		
45	39.60			39.60		
42	43.20			43.20		
39	46.80			50.40		
36	50.40			57.60		
33	54.00			64.80		
30	57.60			72.00		
27	57.60			79.20		
24	57.60			86.40		
21	57.60			93.60		
18	57.60			97.20		
15	54.00			100.80		
12	50.40			100.80		
9	43.20			97.20		
6	32.40			86.40		
3						
0	0.00	9288.18		0.00	6188.40	

CHAPTER FIVE

DYNAMIC ANALYSIS OF OUTRIGGER-BRACED STRUCTURES

NOTATION of Chapter 5

$\mathbb{A}_i, \mathbb{B}_i, \mathbb{C}_i$	field transfer matrices
A	cross-sectional area of core
A_c	sectional area of column
d	distance between columns
E	elastic moduli of walls
E_c	elastic modulus of column
E_o	elastic modulus of outrigger
E_s	elastic modulus of stiffening beam
GA	shearing rigidity of core
H	height of structure
i	radius of gyration of core cross-section
I	second moment of area of core
I_1, I_2	second moments of area of walls 1 and 2
I_o	effective moment of inertia of outrigger
l	distance between centroidal axis of walls
m	mass per unit length of core
$M_1..M_i..M_n$	restraining moments due to outriggers 1..i..n
$\mathbb{R}$	field transfer matrix
S, S_1	structural parameters
s, s_1	structural parameters
$\mathbb{T}$	field transfer matrix
y	horizontal deflection of outrigger
y_T	top drift of the structure
$\mathbb{U}_i$	field transfer matrices
$\mathbb{Z}$	state vector of actions
K_ϑ	rotational stiffness
δ, δ_a, δ_b	displacements at the point of contraflexure

σ, τ, β	parameters
$\psi_1..\psi_i..\psi_n$	slopes of the walls or core
$\mathbb{M}_2..\mathbb{M}_i..\mathbb{M}_n$	matrix for retraining moments
$\mathbb{T}_2..\mathbb{T}_i..\mathbb{T}_n$	field transfer matrices
$\mathbb{Z}_{n+1}..\mathbb{Z}_i..\mathbb{Z}_n$	state vector of actions
$\Psi_1..\Psi_i..\Psi_n$	matrices of the slope terms

Other subsidiary symbols are defined locally in the text.

5.1 INTRODUCTION

The preceding Chapters on outrigger-braced structures have been concerned with static behaviour. As buildings become taller and lighter, they become more wind-sensitive and more vulnerable to seismic effects. For these and other reasons, it has become important to assess the effect of outriggers on the dynamic properties of the structures containing them.

There are essentially two kinds of lateral vibrations that a structure can undergo. These are free vibration and forced vibration. In free vibration a structure undergoes oscillatory motion while free of any external forces, whereas in forced vibration the structure responds to a system of time-varying external forces. An understanding of the free vibration of any structure is a prerequisite to the understanding of its response in forced vibration. Furthermore, it is found that in the majority of design problems, the solution of more complicated problem of forced vibration response is simplified by obtaining a solution for the free vibration problem. The free vibration of a real structure can occur in an infinite number of modal shapes, referred to as modes, and each modal shape has a discrete frequency associated with it. The first or fundamental mode is the mode associated with the lowest frequency. The second mode is that associated with the second lowest frequency, and so on. The second, third and the higher modes of vibration can often be neglected by the engineer. This is primarily because the number of nodal points increases directly with the higher mode number and much more energy is required to excite the higher modes to

appreciable amplitudes.

The field transfer matrix technique which is suitable for the analysis of elongated structures, can be used to determine the natural frequencies of outrigger-braced structures. The method has the advantage of requiring only a small size of matrix of maximum order 4x4. The dynamic analysis of such structures, which are essentially uniform but contain one or more structural discontinuities, may be handled conveniently by the transfer matrix technique.

The present analysis is based on the work of Moudarres and Coull[37], who used the transfer matrix technique to study the free vibrations of a single outrigger structure. In this Chapter, the same fundamental transfer matrix analysis used in the previous investigation is extended to study the free vibration of multi-outrigger-braced structures.

5.2 ANALYSIS

5.2.1 ONE OUTRIGGER

Consider the uniform core wall as shown in Fig.[5.1a], which is braced by an outrigger rigidly connected to the core at a height x_1. The uniform peripheral columns are positioned symmetrically about the centroidal axis of the core. The columns are assumed to be pin-ended so that they carry only axial forces. The core is assumed to act effectively as a vertical cantilever beam.

The governing differential equation for the free vibrations of a uniform elastic beam, including the effects of shear deformation and rotary inertia, is given by,

$$\frac{d^4y}{dx^4} + m\omega^2\left(\frac{i^2}{EI} + \frac{1}{GA}\right)\frac{d^2y}{dx^2} - \frac{m\omega^2}{EI}\left(1 - \frac{mi^2\omega^2}{GA}\right)y = 0 \qquad (5.1)$$

where

y is the bending deflection

m is the mass per unit length

EI is the flexural rigidity

GA is the shearing rigidity

i is the radius of gyration about the centroidal axis

ω is the circular natural frequency

Equation (5.1) can be expressed more succinctly in the form

$$\frac{d^4y}{dx^4} + \left(\frac{\sigma+\tau}{l^2}\right)\frac{d^2y}{dx^2} - \left(\frac{\beta^4-\sigma\tau}{l^4}\right)y = 0 \qquad (5.2)$$

where

$$\sigma = \frac{ml^2\omega^2}{GA} \qquad (5.3a)$$

$$\tau = \frac{mi^2l^2\omega^2}{EI} \qquad (5.3b)$$

$$\beta^4 = \frac{m l^4 \omega^2}{EI} \qquad (5.3c)$$

in which l is the length of beam considered.

Equation (5.2) is an ordinary differential equation with constant coefficients and may readily be solved to give the deflection and associated structural actions for a given set of boundary conditions. The solution may be expressed in terms of the relationship between the actions at the ends of a segment of length l. The relationship between the state vector of actions at points i and (i-1), a distance l apart, may then be expressed in matrix form as,

$$\begin{bmatrix} -y \\ \psi \\ M \\ V \end{bmatrix}_i = \begin{bmatrix} u_{11} & u_{12} & u_{13} & u_{14} \\ u_{21} & u_{22} & u_{23} & u_{24} \\ u_{31} & u_{32} & u_{33} & u_{34} \\ u_{41} & u_{42} & u_{43} & u_{44} \end{bmatrix} \cdot \begin{bmatrix} -y \\ \psi \\ M \\ V \end{bmatrix}_{i-1} \qquad (5.4)$$

in which ψ, M and V are the rotation of the cross-section, the bending moment and the shear force respectively. The sign conventions for these quantities are shown in Fig.[3.4]. The elements u_{ij} are functions of σ, τ and β, and are reproduced from Reference [39] in Appendix I.

For tall slender structures the effects of shearing deformations and rotatory inertia will generally be small, and may be neglected by omitting the terms in σ and τ respectively in the expressions

for u_{ij} in equation (5.4). In that case, the matrix $\mathbb{U}$ becomes symmetrical with respect to the cross diagonal.

The general symbolic form of the state vector at any particular point i on the structure will be denoted for convenience by

$$\mathbb{Z}_i^k = \{ -y \quad \psi \quad M \quad V \}_i^k \tag{5.5}$$

where k will be assigned one of the superscripts 'L', 'R', '+' or '-' to indicate that the position of the section considered is immediately to the left or right of point i for a horizontal member or above or below the point i for a vertical member respectively.

Equation (5.4) may be expressed more succinctly in the form

$$\mathbb{Z}_i = \mathbb{U}.\mathbb{Z}_{i-1} \tag{5.6}$$

in which $\mathbb{Z}_i$ is the state vector at any position i and U is the field transfer matrix. The field transfer matrix enables the state vector of any point i to be expressed in terms of the state vector at any other position i-1.

The state vector at a point just below "1" on the structure as shown in Fig.[5.1], may be expressed in terms of the state vectors at the other significant points "0" and "2" by the relationship

$$\mathbb{Z}_1^- = \mathbb{A}_1.\mathbb{Z}_0 \tag{5.7}$$

The state vector at the point "2" at the top of the core may be expressed as

$$\mathbb{Z}_2 = \mathbb{A}_2 . \mathbb{Z}_1^{+} \tag{5.8}$$

where $\mathbb{A}_1$ and $\mathbb{A}_2$ are transfer matrices of the order 4x4 of a form similar to $\mathbb{U}$ with corresponding elements $a1_{ij}$ and $a2_{ij}$ to those given in Appendix I.

Because of structural symmetry, only lateral deflections of the core occur, and the actions on the both outrigger arms will be antisymmetric. Only the behaviour of one representative arm need then be considered.

The vertical displacement x_d at the outer end of the outrigger arm is

$$x_d = \frac{F_1 x_1}{E_c A_c} \tag{5.9}$$

where F_1 is the axial force in the column equal to shear force at the outer end of the outrigger and $E_c A_c$ is the axial rigidity of the column.

The compatibility conditions at joint 1 are,

$$\psi_1^{L} = -\psi_1^{R} = -\psi_1^{+} = \psi_1 \tag{5.10}$$

$$x_1^{L} = \psi_1 (b/2) \tag{5.11}$$

$$y_1^- = y_1^+ = y_1 \tag{5.12}$$

where b is the width of the core.

By establishing the compatibility for the rotations at the inboard ends of the outrigger where it attaches to the core, the restraining moment M_1 due to the outrigger at level x_1 can be expressed in terms of the slope as,

$$M_1 = t1.\psi_1 \tag{5.13}$$

where ψ_1 is a scalar denoting the slope at the station point "1" and

$$t1 = -\frac{1}{S_1 + S_2 x_1} \tag{5.14}$$

where S_1 and S_2 are defined in equations (4.78a) and (4.78b) in Chapter 4.

The relationship between the state vectors $\mathbb{Z}_1^+$ and $\mathbb{Z}_1^+$ at point "1" on the core is

$$\mathbb{Z}_1^+ = \mathbb{Z}_1^- + \mathbb{K}_1.\Psi_1 \tag{5.15}$$

where $\mathbb{K}_1$ is a matrix of the order 4x1.

$$\mathbb{K}_1 = \begin{bmatrix} 0 \\ 0 \\ t_1 \\ 0 \end{bmatrix}$$

and $\Psi_1 = \mathbb{G}.\mathbb{Z}_1$ where $\mathbb{G}$ is a matrix of the order 1x4 given by,

$$\mathbb{G} = [\ 0 \quad 1 \quad 0 \quad 0\ ]$$

Substituting equations (5.6) and (5.15) into (5.7), $\mathbb{Z}_2$ may be expressed as

$$\mathbb{Z}_2 = \mathbb{R}_1.\mathbb{Z}_0 \qquad (5.16)$$

where $\mathbb{R}_1$ is a 4x4 matrix and is given by,

$$\mathbb{R}_1 = \mathbb{B}_1.\mathbb{A}_1 + \mathbb{B}_1.\mathbb{K}_1.\mathbb{G}.\mathbb{A}_1$$

5.2.2 TWO OUTRIGGERS

Consider the uniform core wall shown in Fig.[5.1b], which is braced by two outriggers positioned at levels x_1 and x_2 which are rigidly connected to the core. The state vectors of actions at point "1" on the structure may be expressed in terms of the state vectors at the significant positions "0" by the relationship,

$$\mathbb{Z}_1^{-} = \mathbb{B}_1.\mathbb{Z}_0 \qquad (5.17)$$

The state vector at point "2" along the core may be expressed in terms of the state vectors at point "1" as

$$\mathbb{Z}_2^- = \mathbb{B}_2 . \mathbb{Z}_1^+ \qquad (5.18)$$

and the state vector at point "3" at the top of the structure may be expressed as

$$\mathbb{Z}_3 = \mathbb{B}_3 . \mathbb{Z}_2^+ \qquad (5.19)$$

Matrices $\mathbb{B}_1$, $\mathbb{B}_2$ and $\mathbb{B}_3$ are transfer matrices of a form similar to $\mathbb{U}$ with corresponding elements, $a1_{ij}$, $a2_{ij}$ and $a3_{ij}$, to those given in Appendix I.

By establishing the compatibility for the rotations at the inboard end of the outriggers where they attach to the core, the restraining moments M_1 and M_2 due to the outriggers at levels x_1 and x_2 can be expressed in terms of the slopes as,

$$\mathbb{M}_2 = \mathbb{T}_2 . \Psi_2 \qquad (5.20a)$$

where

$$\mathbb{M}_2 = \begin{bmatrix} M_2 \\ M_1 \end{bmatrix} \qquad (5.20b)$$

$$\mathbb{T}_2 = \begin{bmatrix} S_1 + S_2 x_2 & S_2 x_1 \\ S x_1 & S_1 + S_2 x_1 \end{bmatrix}^{-1} \qquad (5.20c)$$

$$\Psi_2 = \begin{bmatrix} \psi_2 \\ \psi_1 \end{bmatrix} \tag{5.20d}$$

From equation (5.20a), M_1 and M_2 can be expressed as,

$$\begin{bmatrix} 0 \\ 0 \\ M_1 \\ 0 \end{bmatrix} = \mathbb{K}_2 . \Psi_2 \tag{5.21a}$$

$$\begin{bmatrix} 0 \\ 0 \\ M_2 \\ 0 \end{bmatrix} = \mathbb{K}_3 . \Psi_2 \tag{5.21b}$$

where $\mathbb{K}_2$ and K_3 are the matrices of the order 4x2

$$\mathbb{K}_2 = \begin{bmatrix} 0 & 0 \\ 0 & 0 \\ t2_{21} & t2_{22} \\ 0 & 0 \end{bmatrix}$$

$$\mathbb{K}_3 = \begin{bmatrix} 0 & 0 \\ 0 & 0 \\ t2_{11} & t2_{12} \\ 0 & 0 \end{bmatrix}$$

in which $t2_{11}$, $t2_{12}$, $t2_{21}$ and $t2_{22}$ are the elements of matrix $\mathbb{T}_2$.

The relationship between the state vectors $\mathbb{Z}_1^+$ and $\mathbb{Z}_1^-$ at point "1" on the structure is,

$$\mathbb{Z}_1^+ = \mathbb{Z}_1^- + \mathbb{K}_2 . \Psi_2 \tag{5.22}$$

Substituting equation (5.17) into (5.22), $\mathbb{Z}_1^+$ becomes,

$$\mathbb{Z}_1^+ = \mathbb{B}_1.\mathbb{Z}_0 + \mathbb{K}_2.\Psi_2 \qquad (5.23)$$

By substituting equation (5.23) into (5.18), $\mathbb{Z}_2^-$ at point "2" on the structure is,

$$\mathbb{Z}_2^- = \mathbb{B}_2.\mathbb{B}_1.\mathbb{Z}_0 + \mathbb{B}_2.\mathbb{K}_2.\Psi_2 \qquad (5.24)$$

and the relationship between the state vectors $\mathbb{Z}_2^+$ and $\mathbb{Z}_2^-$ at point "2" on the structure is,

$$\mathbb{Z}_2^+ = \mathbb{Z}_2^- + \mathbb{K}_3.\Psi_2 \qquad (5.25)$$

After substituting equation (5.24) into (5.25), it becomes,

$$\mathbb{Z}_2^+ = \mathbb{B}_2.\mathbb{B}_1.\mathbb{Z}_0 + [\ \mathbb{B}_2.\mathbb{K}_2 + \mathbb{K}_3\ ].\Psi_2 \qquad (5.26)$$

From equation (5.17), ψ_1 can be expressed as

$$\psi_1 = \mathbb{G}.\mathbb{B}_1.\mathbb{Z}_0 \qquad (5.27)$$

From equation (5.22), ψ_2 can be expressed as

$$\psi_2 = \mathbb{G}.\mathbb{B}_2.\mathbb{B}_1.\mathbb{Z}_0 + \mathbb{G}.\mathbb{B}_2.\mathbb{K}_2.\Psi_2 \qquad (5.28)$$

Equations (5.27) and (5.28) can be expressed in matrix form as,

$$\begin{bmatrix} \psi_1 \\ \psi_2 \end{bmatrix} = \begin{bmatrix} \mathbb{G}.\mathbb{B}_1.\mathbb{Z}_0 \\ \mathbb{G}.\mathbb{B}_2.\mathbb{B}_1.\mathbb{Z}_0 + \mathbb{G}.\mathbb{B}_2.\mathbb{K}_2.\Psi_2 \end{bmatrix} \qquad (5.29)$$

Equation (5.29) can be simplified further in terms of the state vector $\mathbb{Z}_0$ as,

$$\psi_2 = \mathbb{J}_1^{-1}.\mathbb{J}_2.\mathbb{Z}_0 \qquad (5.30)$$

where $\mathbb{J}_1$ and $\mathbb{J}_2$ are the matrices of the order 2x2 and 2x4 respectively and are given by,

$$\mathbb{J}_1 = \mathbb{I} - \begin{bmatrix} 0 & 0 \\ \mathbb{G}.\mathbb{B}_2.\mathbb{K}_2 \end{bmatrix}$$

$$\mathbb{J}_2 = \begin{bmatrix} \mathbb{G}.\mathbb{B}_1 \\ \mathbb{G}.\mathbb{B}_2.\mathbb{B}_1 \end{bmatrix}$$

and $\mathbb{I}$ is a 2x2 unit matrix.

Substituting equations (5.30), (5.24) and (5.25) into (5.19), the transfer matrix linking the point "0" at the base to the state vector of actions at point "3" at the top of structure is obtained as,

$$\mathbb{Z}_3 = \mathbb{R}_2.\mathbb{Z}_0 \qquad (5.31)$$

where $\mathbb{R}_2$ is a matrix of the order 4x4,

$$\mathbb{R}_2 = \mathbb{B}_3.\{\ \mathbb{B}_2.\mathbb{B}_1 + [\ \mathbb{B}_2.\mathbb{K}_2 + \mathbb{K}_3\ ].\mathbb{J}_1^{-1}.\mathbb{J}_2\ \}$$

5.2.3 THREE OUTRIGGERS

Similarly, for three outriggers positioned at levels x_1, x_2 and x_3 as shown in Fig.[5.2a], by establishing the compatibility for the rotations at the inboard ends of the outrigger where they are attached to the core, the restraining moment M_1, M_2 and M_3 due to the outriggers at level x_1 x_2 and x_3 can be expressed in terms of the slope as,

$$\mathbb{M}_3 = \mathbb{T}_3 . \Psi_3 \tag{5.32a}$$

where

$$\mathbb{M}_3 = \begin{bmatrix} M_3 \\ M_2 \\ M_1 \end{bmatrix} \tag{5.32b}$$

$$\mathbb{T}_3 = \begin{bmatrix} S_1 + S_2x_3 & S_2x_2 & S_2x_1 \\ Sx_2 & S_1 + S_2x_2 & S_2x_1 \\ Sx_1 & Sx_1 & S_1 + S_2x_1 \end{bmatrix}^{-1} \tag{5.32c}$$

$$\Psi_3 = \begin{bmatrix} \psi_3 \\ \psi_2 \\ \psi_1 \end{bmatrix} \tag{5.32d}$$

Therefore M_1 , M_2 and M_3 can be expressed in terms of Ψ_3 as,

$$\begin{bmatrix} 0 \\ 0 \\ M_1 \\ 0 \end{bmatrix} = \mathbb{K}_5 . \Psi_3 \qquad (5.33)$$

$$\begin{bmatrix} 0 \\ 0 \\ M_2 \\ 0 \end{bmatrix} = \mathbb{K}_6 . \Psi_3 \qquad (5.34)$$

$$\begin{bmatrix} 0 \\ 0 \\ M_3 \\ 0 \end{bmatrix} = \mathbb{K}_7 . \Psi_3 \qquad (5.35)$$

where $\mathbb{K}_5$, $\mathbb{K}_6$ and $\mathbb{K}_7$ are matrices of the order 4x3,

$$\mathbb{K}_5 = \begin{bmatrix} 0 & 0 & 0 \\ 0 & 0 & 0 \\ t3_{31} & t3_{32} & t3_{33} \\ 0 & 0 & 0 \end{bmatrix}$$

$$\mathbb{K}_6 = \begin{bmatrix} 0 & 0 & 0 \\ 0 & 0 & 0 \\ t3_{21} & t3_{22} & t3_{23} \\ 0 & 0 & 0 \end{bmatrix}$$

$$\mathbb{K}_7 = \begin{bmatrix} 0 & 0 & 0 \\ 0 & 0 & 0 \\ t3_{11} & t3_{12} & t3_{13} \\ 0 & 0 & 0 \end{bmatrix}$$

Following the same procedure as in the previous sections, the state vectors of actions at point "1", "2", "3" and "4" on the structure may be expressed in terms of the state vectors at

position "0" by the relationships,

$$\mathbb{Z}_1^- = \mathbb{C}_1.\mathbb{Z}_0 \tag{5.36}$$

$$\mathbb{Z}_1^+ = \mathbb{C}_1.\mathbb{Z}_0 + \mathbb{K}_4.\Psi_3 \tag{5.37}$$

$$\mathbb{Z}_2^- = \mathbb{C}_2.\mathbb{C}_1.\mathbb{Z}_0 + \mathbb{C}_2.\mathbb{K}_4.\Psi_3 \tag{5.38}$$

$$\mathbb{Z}_2^+ = \mathbb{C}_2.\mathbb{C}_1.\mathbb{Z}_0 + [\mathbb{C}_2.\mathbb{K}_4 + \mathbb{K}_5].\Psi_3 \tag{5.39}$$

$$\mathbb{Z}_3^- = \mathbb{C}_3.\mathbb{C}_2.\mathbb{C}_1.\mathbb{Z}_0 + \mathbb{C}_3.[\mathbb{C}_2.\mathbb{K}_4 + \mathbb{K}_5].\Psi_3 \tag{5.40}$$

$$\mathbb{Z}_3^+ = \mathbb{C}_3.\mathbb{C}_2.\mathbb{C}_1.\mathbb{Z}_0 + \{\mathbb{C}_3.[\mathbb{C}_2.\mathbb{K}_4 + \mathbb{K}_5] + \mathbb{K}_6\}.\Psi_3 \tag{5.41}$$

$$\mathbb{Z}_4 = \mathbb{C}_4.\mathbb{C}_3.\mathbb{C}_2.\mathbb{C}_1.\mathbb{Z}_0 + \{\mathbb{C}_4.\mathbb{C}_3.[\mathbb{C}_2.\mathbb{K}_4 + \mathbb{K}_5] + \mathbb{C}_4.\mathbb{K}_6\}.\Psi_3 \tag{5.42}$$

From equations (5.36), (5.38) and (5.40), ψ_1, ψ_2 and ψ_3 can be extracted and written in a single matrix as,

$$\begin{bmatrix} \psi_1 \\ \psi_2 \\ \psi_3 \end{bmatrix} = \begin{bmatrix} \mathbb{G}.\mathbb{C}_1.\mathbb{Z}_0 \\ \mathbb{G}.\mathbb{C}_2.\mathbb{C}_1.\mathbb{Z}_0 + \mathbb{G}.\mathbb{C}_2.\mathbb{K}_4.\Psi_3 \\ \mathbb{G}.\mathbb{C}_3.\mathbb{C}_2.\mathbb{C}_1.\mathbb{Z}_0 + \mathbb{G}.\mathbb{C}_3.[\mathbb{C}_2.\mathbb{K}_4+\mathbb{K}_5].\Psi_3 \end{bmatrix} \tag{5.43}$$

Equation (5.43) can be simplified further in terms of the state vector $\mathbb{Z}_0$ as,

$$\Psi_3 = \mathbb{J}_3^{-1} . \mathbb{J}_4 . \mathbb{Z}_0 \qquad (5.44)$$

where $\mathbb{J}_3$ and $\mathbb{J}_4$ are matrices of the order 3x3 and 3x4 respectively and are given by,

$$\mathbb{J}_3 = \mathbb{I} - \begin{bmatrix} 0 & 0 & 0 \\ \mathbb{G}.\mathbb{C}_2.\mathbb{K}_4 & & \\ \mathbb{G}.\mathbb{C}_3.[\mathbb{C}_2.\mathbb{K}_4.+\mathbb{K}_5] & & \end{bmatrix}$$

$$\mathbb{J}_4 = \begin{bmatrix} \mathbb{G}.\mathbb{C}_1 \\ \mathbb{G}.\mathbb{C}_2.\mathbb{C}_1 \\ \mathbb{G}.\mathbb{C}_3.\mathbb{C}_2.\mathbb{C}_1 \end{bmatrix}$$

and $\mathbb{I}$ is a 3x3 unit matrix.

Substituting equation (3.57) into (3.55), the transfer matrix linking the point "0" at the base to the top of structure is obtained as,

$$\mathbb{Z}_4 = \mathbb{R}_3 . \mathbb{Z}_0 \qquad (5.45)$$

where

$$\mathbb{R}_3 = \mathbb{C}_4.\mathbb{C}_3.\mathbb{C}_2.\mathbb{C}_1.\mathbb{Z}_0 + \{\mathbb{C}_4.\mathbb{C}_3.[\mathbb{C}_2.\mathbb{K}_4+\mathbb{K}_5]+\mathbb{C}_4.\mathbb{K}_6\}.\mathbb{J}_3^{-1}.\mathbb{J}_4$$

5.2.4 n OUTRIGGERS

For n outriggers positioned at levels x_1, x_2 .. x_i .. and x_n, as shown in Fig.[5.2b], by establishing the compatibility for the

rotations at the inboard ends of the outrigger where they are attached to the core, the restraining moment M_1, M_2, .. M_i .. and M_n due to the outriggers at levels x_1, x_2, .. x_i .. and x_n can be expressed in terms of the slope as,

$$\mathbb{M} = \mathbb{T}_n . \Psi_n \tag{5.46a}$$

where

$$\mathbb{M} = \begin{bmatrix} M_n \\ \vdots \\ M_i \\ \vdots \\ M_2 \\ M_1 \end{bmatrix} \tag{5.46b}$$

$$\mathbb{T}_n = \begin{bmatrix} S_1+S_2x_n & S_2x_{n-1} & \cdots & S_2x_2 & S_2x_1 \\ \vdots & \vdots & \vdots & \vdots & \vdots \\ S_2x_i & S_1+S_2x_i & \cdots & \cdots & S_2x_1 \\ \vdots & \vdots & \vdots & \vdots & \vdots \\ S_2x_2 & S_2x_2 & \cdots & S_1+S_2x_2 & S_2x_1 \\ S_2x_1 & S_2x_1 & \cdots & S_2x_1 & S_1+S_2x_1 \end{bmatrix}^{-1} \tag{5.46c}$$

$$\Psi_n = \begin{bmatrix} \psi_n \\ \vdots \\ \psi_i \\ \vdots \\ \psi_2 \\ \psi_1 \end{bmatrix} \qquad (5.46d)$$

Therefore the restraining moments M_1, M_2, .. M_i .. and M_n can be expressed as,

$$\begin{bmatrix} 0 \\ 0 \\ M_1 \\ 0 \end{bmatrix} = \mathbb{K}1.\Psi_n \qquad (5.47a)$$

$$\begin{bmatrix} 0 \\ 0 \\ M_2 \\ 0 \end{bmatrix} = \mathbb{K}2.\Psi_n \qquad (5.47b)$$

$$\begin{bmatrix} 0 \\ 0 \\ M_3 \\ 0 \end{bmatrix} = \mathbb{K}3.\Psi_n \qquad (5.47c)$$

$$\begin{bmatrix} 0 \\ 0 \\ M_i \\ 0 \end{bmatrix} = \mathbb{K}i.\Psi_n \qquad (5.47d)$$

$$\begin{bmatrix} 0 \\ 0 \\ M_n \\ 0 \end{bmatrix} = \mathbb{K}n.\Psi_n \qquad (5.47e)$$

where $\mathbb{K}1$, $\mathbb{K}2$, $\mathbb{K}3$, .. $\mathbb{K}i$ .. $\mathbb{K}n$ are the matrices of the order 4xn,

$$\mathbb{K}1 = \begin{bmatrix} 0 & .. & 0 & .. & 0 \\ 0 & .. & 0 & .. & 0 \\ tn_{n1} & .. & tn_{ni} & .. & tn_{nn} \\ 0 & .. & 0 & .. & 0 \end{bmatrix}$$

$$\mathbb{K}2 = \begin{bmatrix} 0 & .. & 0 & .. & 0 \\ 0 & .. & 0 & .. & 0 \\ tn_{n-1\ 1} & .. & tn_{n-1\ i} & .. & tn_{n-1\ n} \\ 0 & .. & 0 & .. & 0 \end{bmatrix}$$

$$\mathbb{K}i = \begin{bmatrix} 0 & .. & 0 & .. & 0 \\ 0 & .. & 0 & .. & 0 \\ tn_{n-i+1\ 1} & .. & tn_{n-i+1\ i} & .. & tn_{n-i+1\ n} \\ 0 & .. & 0 & .. & 0 \end{bmatrix}$$

$$\mathbb{K}n = \begin{bmatrix} 0 & .. & 0 & .. & 0 \\ 0 & .. & 0 & .. & 0 \\ tn_{11} & .. & tn_{1i} & .. & tn_{1n} \\ 0 & .. & 0 & .. & 0 \end{bmatrix}$$

By extension of the earlier analysis, the state vector at the point top of the structure may be expressed in a generalised form as,

$$\mathbb{Z}_{n+1} = \mathbb{U}_n.\mathbb{U}_{n-1}..\mathbb{U}_0.\mathbb{Z}_0 + [\ \mathbb{U}_n.\mathbb{U}_{n-1}..\mathbb{U}_1.\mathbb{K}1 + \mathbb{U}_n.\mathbb{U}_{n-1}..\mathbb{U}_2.\mathbb{K}2 + ..+ \mathbb{U}_n.\mathbb{U}_{n-1}..\mathbb{U}_i.\mathbb{K}i + .. + \mathbb{U}_n.\mathbb{K}n\ ].\Psi_n \qquad (5.48)$$

where

$\mathbb{Z}_n$ is the state vector at the top of the structure

$\mathbb{Z}_0$ is the state vector at the bottom of the structure

$\mathbb{U}_n$, $\mathbb{U}_{n-1}$, $\mathbb{U}_{n-2}$ .. $\mathbb{U}_i$ .. $\mathbb{U}_0$ are the transfer matrices

$\mathbb{K}1$, $\mathbb{K}2$, .. $\mathbb{K}i$ .. $\mathbb{K}n$ are the matrices formed from the elements of the matrix $\mathbb{T}_n$

Following the same procedure as in the previous sections, the general expression for ψ_1, ψ_2, ψ_3 .. ψ_i ..and ψ_n can be expressed as

$$\Psi_n = \mathbb{J}1^{-1}.\mathbb{J}2.\mathbb{Z}_0 \qquad (5.49)$$

where $\mathbb{J}1$ and $\mathbb{J}2$ are matrices of order nxn and nx4 respectively and are given by,

$$J1 = \mathbb{I} - \begin{bmatrix} 0 & \cdots & 0 \\ G.U_1.K1 & & \\ G.U_2.U_1.K1 + G.U_2.K2 & & \\ \vdots & & \\ G.U_n.U_{n-1}\ldots U_1.K1 + G.U_n.U_{n-1}\ldots U_2.K2 & & \\ + \ldots + G.U_n.Kn & & \end{bmatrix}$$

$$J2 = \begin{bmatrix} G.U_0 \\ G.U_1.U_0 \\ G.U_2.U_1.U_0 \\ \vdots \\ G.U_n.U_{n-1}\ldots U_i\ldots U_0 \end{bmatrix}$$

where $\mathbb{I}$ is a nxn unit matrix.

Substituting equation (3.62) into (3.61), the transfer matrix linking the point "0" at the base to the top of structure is obtained as,

$$Z_{n+1} = R_n.Z_0 \qquad (5.50)$$

where R_n is the transfer matrix of order 4x4,

$$R_n = U_n.U_{n-1}..U_0 + [\, U_n.U_{n-1}..U_1.K1 + U_n.U_{n-1}..U_2.K2 + .. + U_n.U_{n-1}..U_i.Ki + .. + U_n.Kn \,].J1^{-1}.J2$$

5.2.5 FREQUENCY EQUATION

If the structure is rigidly built in at the base and free at the top, the boundary conditions are,

$$y_B = \psi_B = 0 \tag{5.51}$$

$$M_T = V_T = 0 \tag{5.52}$$

where the subscript "B" and "T" denote bottom and top position of the structure respectively.

Substitution of the boundary conditions, equations (5.51) and (5.52), into equation (5.50) gives,

$$\begin{bmatrix} rn_{33} & rn_{34} \\ rn_{43} & rn_{44} \end{bmatrix} \cdot \begin{bmatrix} M_B \\ V_B \end{bmatrix} = \begin{bmatrix} 0 \\ 0 \end{bmatrix} \tag{5.53}$$

where rn_{ij} are the elements of the transfer matrix $\mathbb{R}_n$ in equation (5.50).

Since M_B and V_B are non-zero, a non-trivial solution of equation (5.53) is possible only if the determinant of the matrix of coefficients rn is zero, and the frequency equation becomes,

$$(rn_{33} \cdot rn_{44} - rn_{34} \cdot rn_{43}) = 0 \tag{5.54}$$

The solutions of equation (5.54) give the natural frequencies of vibration of the structure.

If a certain degree of base flexibilities is considered, the boundary conditions at the base become,

$$y_B = 0 \tag{5.55}$$

$$\psi_B = K_\vartheta M_B \tag{5.56}$$

The boundary conditions at the top would be the same as in equation (5.52).

Substitution of the boundary conditions, equations (5.55) and (5.56), into equation (5.50) gives,

$$\begin{bmatrix} rn_{32}.K_\vartheta+rn_{33} & rn_{34} \\ rn_{42}.K_\vartheta+rn_{43} & rn_{44} \end{bmatrix} . \begin{bmatrix} M_B \\ V_B \end{bmatrix} = \begin{bmatrix} 0 \\ 0 \end{bmatrix} \tag{5.57}$$

Therefore the frequency equation becomes,

$$(rn_{32}.K_\vartheta+rn_{33}).rn_{44} - (rn_{42}.K_\vartheta+rn_{43}).rn_{34} = 0 \tag{5.58}$$

The solutions of equation (5.58) gives the natural frequencies of vibration of the structure.

5.2.6 NORMAL MODES OF VIBRATION

Having determined the natural frequencies from the relevant frequency equation, the normal modes of free undamped vibrations may be obtained. The relationship between bending moment M_a and shear force V_a at the base of the core, for a rigid foundation case, may be obtained by substituting equations (5.51) and (5.52) into (5.53) as,

$$V_B = - \frac{rn_{33}}{rn_{34}} M_B \qquad (5.59)$$

On substituting equation (5.54) into the appropriate equation for each state vector point along the core, the displacements can be obtained.

For the single outrigger case, by substituting equation (5.59) into equations (5.6) and (5.7), the displacement of each vector point becomes,

$$\begin{bmatrix} -y_1 \\ \psi_1 \end{bmatrix} = \begin{bmatrix} a1_{13} & a1_{14} \\ a1_{23} & a1_{24} \end{bmatrix} . \begin{bmatrix} 1 \\ \frac{-r1_{33}}{r1_{34}} \end{bmatrix} . M_a \qquad (5.60a)$$

$$\begin{bmatrix} -y_2 \\ \psi_2 \end{bmatrix} = \begin{bmatrix} r1_{13} & r1_{14} \\ r1_{23} & r1_{24} \end{bmatrix} . \begin{bmatrix} 1 \\ \frac{-r1_{33}}{r1_{34}} \end{bmatrix} . M_a \qquad (5.60b)$$

where $r1_{ij}$ and $a1_{ij}$ are the elements of the transfer matrices $\mathbb{A}_1$ and $\mathbb{R}_1$.

For a two outrigger case, by substituting equation (5.59) into (5.17), (5.18) and (5.19), the displacement of each vector point becomes,

$$\begin{bmatrix} -y_1 \\ \psi_1 \end{bmatrix} = \begin{bmatrix} b1_{13} & b1_{14} \\ b1_{23} & b1_{24} \end{bmatrix} \cdot \begin{bmatrix} 1 \\ \dfrac{-r2_{33}}{r2_{34}} \end{bmatrix} . M_a \qquad (5.61a)$$

$$\begin{bmatrix} -y_2 \\ \psi_2 \end{bmatrix} = \begin{bmatrix} v1_{13} & v1_{14} \\ v1_{23} & v1_{24} \end{bmatrix} \cdot \begin{bmatrix} 1 \\ \dfrac{-r2_{33}}{r2_{34}} \end{bmatrix} . M_a \qquad (5.61b)$$

$$\begin{bmatrix} -y_3 \\ \psi_3 \end{bmatrix} = \begin{bmatrix} r2_{13} & r2_{14} \\ r2_{23} & r2_{24} \end{bmatrix} \cdot \begin{bmatrix} 1 \\ \dfrac{-r2_{33}}{r2_{34}} \end{bmatrix} . M_a \qquad (5.61c)$$

where $r2_{ij}$ and $b1_{ij}$ are the elements of the transfer matrices $\mathbb{R}_2$ and $\mathbb{B}_1$, and $v1_{ij}$ are the elements of the transfer matrix $\mathbb{V}_1$ given by,

$$\mathbb{V}_1 = \mathbb{B}_2 . \mathbb{B}_1 + [\ \mathbb{B}_2 . \mathbb{K}_2\ ] . \mathbb{J}_1^{-1} . \mathbb{J}_2$$

For a three outrigger case, by substituting equation (5.59) into (5.36), (5.38), (5.40) and (5.42), the displacement of each vector point becomes,

$$\begin{bmatrix} -y_1 \\ \psi_1 \end{bmatrix} = \begin{bmatrix} c1_{13} & c1_{14} \\ c1_{23} & c1_{24} \end{bmatrix} . \begin{bmatrix} 1 \\ \frac{-r3_{33}}{r3_{34}} \end{bmatrix} . M_a \qquad (5.62a)$$

$$\begin{bmatrix} -y_2 \\ \psi_2 \end{bmatrix} = \begin{bmatrix} v2_{13} & v2_{14} \\ v2_{23} & v2_{24} \end{bmatrix} . \begin{bmatrix} 1 \\ \frac{-r3_{33}}{r3_{34}} \end{bmatrix} . M_a \qquad (5.62b)$$

$$\begin{bmatrix} -y_3 \\ \psi_3 \end{bmatrix} = \begin{bmatrix} v3_{13} & v3_{14} \\ v3_{23} & v3_{24} \end{bmatrix} . \begin{bmatrix} 1 \\ \frac{-r3_{33}}{r3_{34}} \end{bmatrix} . M_a \qquad (5.62c)$$

$$\begin{bmatrix} -y_4 \\ \psi_4 \end{bmatrix} = \begin{bmatrix} r3_{13} & r3_{14} \\ r3_{23} & r3_{24} \end{bmatrix} . \begin{bmatrix} 1 \\ \frac{-r3_{33}}{r3_{34}} \end{bmatrix} . M_a \qquad (5.62d)$$

where $r3_{ij}$ and $c1_{ij}$ are the elements of the transfer matrices $\mathbb{R}_3$ and $\mathbb{C}_1$.

$v1_{ij}$ and $v2_{ij}$ are the elements of the transfer matrix $\mathbb{V}_2$ and $\mathbb{V}_3$, given by,

$$\mathbb{V}_2 = \mathbb{C}_2 . \mathbb{C}_1 + [\mathbb{C}_2 . \mathbb{K}_4 + \mathbb{K}_5] . \mathbb{J}_3^{-1} . \mathbb{J}_4$$

$$\mathbb{V}_3 = \mathbb{C}_3 . \mathbb{C}_2 . \mathbb{C}_1 + \{\mathbb{C}_3 . [\mathbb{C}_2 . \mathbb{K}_4 + \mathbb{K}_5]\} . \mathbb{J}_3^{-1} . \mathbb{J}_4$$

For the case of a flexible base, the relationship between bending moment M_a and shear force V_a at the base of the core may be obtained by substituting equations (5.55) and (5.56) into equation (5.57) as,

$$V_B = - \frac{rn_{32} \cdot K_\vartheta + rn_{33}}{rn_{34}} M_B \qquad (5.63)$$

In a similar way, the displacement of each vector point for one outrigger or two or three outriggers can be found substituting equation (5.63) into the appropriate equations at each state vector point.

For a one outrigger case, the displacements become,

$$\begin{bmatrix} -y_1 \\ \psi_1 \end{bmatrix} = \begin{bmatrix} a1_{12} \cdot K_\vartheta + a1_{13} - \frac{a1_{14} \cdot [r1_{32} \cdot K_\vartheta + r1_{33}]}{r1_{34}} \\ a1_{22} \cdot K_\vartheta + a1_{23} - \frac{a1_{24} \cdot [r1_{32} \cdot K_\vartheta + r1_{33}]}{r1_{34}} \end{bmatrix} . M_a \qquad (5.64a)$$

$$\begin{bmatrix} -y_2 \\ \psi_2 \end{bmatrix} = \begin{bmatrix} r1_{12} \cdot K_\vartheta + r1_{13} - \frac{r1_{14} \cdot [r1_{32} \cdot K_\vartheta + r1_{33}]}{r1_{34}} \\ r1_{22} \cdot K_\vartheta + r1_{23} - \frac{r1_{24} \cdot [r1_{32} \cdot K_\vartheta + r1_{33}]}{r1_{34}} \end{bmatrix} . M_a \qquad (5.64b)$$

For a two outriggers case, the displacements become,

$$\begin{bmatrix} -y_1 \\ \\ \psi_1 \end{bmatrix} = \begin{bmatrix} b1_{12}.K_\vartheta + b1_{13} - \dfrac{b1_{14}.[r2_{32}.K_\vartheta + r2_{33}]}{r2_{34}} \\ \\ b1_{22}.K_\vartheta + b1_{23} - \dfrac{b1_{24}.[r2_{32}.K_\vartheta + r2_{33}]}{r2_{34}} \end{bmatrix} .M_a \qquad (5.65a)$$

$$\begin{bmatrix} -y_2 \\ \\ \psi_2 \end{bmatrix} = \begin{bmatrix} v1_{12}.K_\vartheta + v1_{13} - \dfrac{v1_{14}.[r2_{32}.K_\vartheta + r2_{33}]}{r2_{34}} \\ \\ v1_{22}.K_\vartheta + v1_{23} - \dfrac{v1_{24}.[r2_{32}.K_\vartheta + r2_{33}]}{r2_{34}} \end{bmatrix} .M_a \qquad (5.65b)$$

$$\begin{bmatrix} -y_3 \\ \\ \psi_3 \end{bmatrix} = \begin{bmatrix} r2_{12}.K_\vartheta + r2_{13} - \dfrac{r2_{14}.[r2_{32}.K_\vartheta + r2_{33}]}{r2_{34}} \\ \\ r2_{22}.K_\vartheta + r2_{23} - \dfrac{r2_{24}.[r2_{32}.K_\vartheta + r2_{33}]}{r2_{34}} \end{bmatrix} .M_a \qquad (5.65c)$$

For a three outriggers case, the displacements become,

$$\begin{bmatrix} -y_1 \\ \\ \psi_1 \end{bmatrix} = \begin{bmatrix} c1_{12}.K_\vartheta + c1_{13} - \dfrac{c1_{14}.[r3_{32}.K_\vartheta + r3_{33}]}{r3_{34}} \\ \\ c1_{22}.K_\vartheta + c1_{23} - \dfrac{c1_{24}.[r3_{32}.K_\vartheta + r3_{33}]}{r3_{34}} \end{bmatrix} .M_a \qquad (5.66a)$$

$$\begin{bmatrix} -y_2 \\ \psi_1 \end{bmatrix} = \begin{bmatrix} v2_{12}.K_\vartheta + v2_{13} - \dfrac{v2_{14}.[r3_{32}.K_\vartheta + r3_{33}]}{r3_{34}} \\ v2_{22}.K_\vartheta + v2_{23} - \dfrac{v2_{24}.[r3_{32}.K_\vartheta + r3_{33}]}{r3_{34}} \end{bmatrix} .M_a \qquad (5.66b)$$

$$\begin{bmatrix} -y_3 \\ \psi_3 \end{bmatrix} = \begin{bmatrix} v3_{12}.K_\vartheta + v3_{13} - \dfrac{v3_{14}.[r3_{32}.K_\vartheta + r3_{33}]}{r3_{34}} \\ v3_{22}.K_\vartheta + v3_{23} - \dfrac{v3_{24}.[r3_{32}.K_\vartheta + r3_{33}]}{r3_{34}} \end{bmatrix} .M_a \qquad (5.66b)$$

$$\begin{bmatrix} -y_4 \\ \psi_4 \end{bmatrix} = \begin{bmatrix} r3_{12}.K_\vartheta + r3_{13} - \dfrac{r3_{14}.[r3_{32}.K_\vartheta + r3_{33}]}{r3_{34}} \\ r3_{22}.K_\vartheta + r3_{23} - \dfrac{r3_{24}.[r3_{32}.K_\vartheta + r3_{33}]}{r3_{34}} \end{bmatrix} .M_a \qquad (5.66c)$$

5.3 CORRESPONDING CASE OF LINKED SHEAR WALLS

As stated in Section 4.2 of Chapter 4, there is an analogy between the structural actions of laterally loaded stiffened linked walls and outrigger-braced structures. The theory developed in this Chapter can be used directly for the analysis of linked shear walls. In that case, the bending of the core wall under the action

of lateral forces corresponds to the bending of the two walls, and the axial deformations in the columns correspond directly to the axial deformations in the two walls. The resisting moment produced by the outrigger corresponds to the resisting moment produced by the stiffening beam in inducing the axial forces in the walls. Consequently, the theory for dynamic analysis may be developed in an identical manner, the only differences in the analysis are the structural parameters s_1 and s_2 for the linked shear wall instead of S_1 and S_2 for the outrigger-braced core.

For linked shear walls, the structural parameters s_1 and s_2 in the analysis are given in equations (4.6c) and (4.7c).

The general expression of the restraining moment M_1, M_2, .. M_i .. and M_n due to stiffening beams at levels x_1, x_2 .. x_i .. x_n, can be obtained from equation (4.59).

The equations derived for the case of outrigger-braced structures may thus be used directly for the dynamic analysis of linked shear walls structures, provided the structural parameter S_1 and S_2 are changed to s_1 and s_2.

5.4 APPLICATION TO COUPLED SHEAR WALL STRUCTURES

As stated in Section 4.3 of Chapter 4, there is an analogy between the structural actions of laterally loaded stiffened linked walls and outrigger-braced structures. As the number of stiffening beams in the linked shear walls increases, the structural action will change that of linked shear walls towards that of coupled shear

walls. The dynamic analysis developed in this Chapter can be applied to analyse the coupled shear walls in a similar manner. The number of outriggers in the earlier analysis will correspond to the number of connecting beams considered in the coupled shear wall structure.

Consider a pair of coupled shear walls with n connecting beams positioned at heights x_1, x_2 ..x_i.. and x_n, as shown in Fig. [4.8] in Chapter 4. The restraining moments M_1, M_2, .. M_i .. and M_n due to the outriggers at levels x_1, x_2,...x_i... and x_n can be expressed in terms of the slope and are defined in equation (4.59).

Therefore the restraining moments M_1, M_2, .. M_i .. and M_n due to the connecting beams of the shear walls can be obtained in the same form as in equations (5.47a) to (5.47e), in which tn_{ij} of the matrices $\mathbb{K}1$ to $\mathbb{K}n$ are the elements of matrix $\mathbb{T}_n$ defined in equation (4.59).

The state vector at the point top of the structure may be obtained from equation (5.48). Following the same procedure as in the previous sections, the same expression as in equation (5.49) for ψ_1, ψ_2, ψ_3 .. ψ_i .. and ψ_n can be obtained. Finally the expression for the matrix linking the base to the top of structure is obtained in equation (5.50). Then the expression for the frequency equations for the coupled shear walls can be obtained from equations (5.54) and (5.58).

5.5 NUMERICAL RESULTS

In order to examine the validity of the methods and to illustrate the influence of the significant parameters on the structural behaviour, two particular examples of the outrigger-braced structure are employed. The first one is taken from the earlier paper by Moudarres and Coull[37] and is used to demonstrate mainly the variation of circular frequency with different locations of outriggers and different base flexibilities. The second example is to demonstrate the structural behaviour of the structure due to the influence of a flexible foundation.

5.5.1 EXAMPLE (5.1)

In order to verify the theory and to compare the relative influences of outrigger/s on the behaviour of an outrigger-braced structure on a flexibile foundation, the example structure studied by Moudarres and Coull was considered. The structure is 42m high with concrete core , outrigger and steel exterior columns. The structural properties are given as follows,

$E=E_o=24.5E+09N/m^2$

$E_c=206E+09N/m^2$

$G=0.33E$

$I=36m^4$

$A=5m^2$

$d=17.5m$

The clear span of the outrigger arm is 5.25m and the mass per unit height of the core is assummed to be 18,500kg/m.

The curves which demonstrate the influence of outrigger location on the primary natural frequency for the case of a single outrigger and a rigid base, are shown in Fig.[5.4] to [5.6]. Over the range of structural parameters considered, the optimum location of outrigger for this example structure varies between 0.5 to 0.6H. However, the actual magnitude of the first natural frequency appears to be very sensitive to the relative flexural and axial stiffnessess of the outrigger and external columns. The results which demontrate the effect of different base flexibilities are presented in Table [5.1].

5.5.2 EXAMPLE (5.2)

The basic structural parameters of this example are based on the 42 storey First Wisconsin Centre, Milwaukee. The configuration of the structure is shown in Fig.[5.3]. The structure is assumed to be 185m high with a concrete core braced by three levels of outrigger arms attached to steel exterior columns. It is assumed that the structural core is composed of eight 400mmx400mm columns located at a lever arm of 12m. The structural properties are given below,

E_c=206E+09N/m^2

E=E_o=24.5E+09N/m^2

G=0.33E=8.1E+09N/m^2

I=200m^4, A=10m^2, d=36m

The clear span of the outrigger arm is 12m. The mass per unit height of the core is as assumed to be 100,000kg/m.

The curves which demonstrate the influence of the outrigger location on the first natural frequency for the case of a single outrigger structure with a rigid base, are shown in Fig.[5.7] to [5.9]. Over the range of structural parameters considered, the optimum location of outrigger for this example structure is found to be around 0.6H. Again the actual magnitude of the first natural frequency appears to be very sensitive to the relative flexural and axial stiffnessess of the outrigger and external columns. Figs.[5.10] to [5.12] demonstrate the influence of the outrigger location on the first natural frequency for a the case of a single outrigger and a flexible base of $5x10^{-11}$ (rad/Nm). The results which demonstrate the effect of different base flexibilities are presented in Table [5.2]. The corresponding mode shapes for the case of a rigid and flexible base are presented in Figs.[5.13] to [5.21]. The general effect of the base flexibility tends to reduce both the primary and secondary natural frequencies quite substantially though the decrease depends on the degree of flexibility at the base.

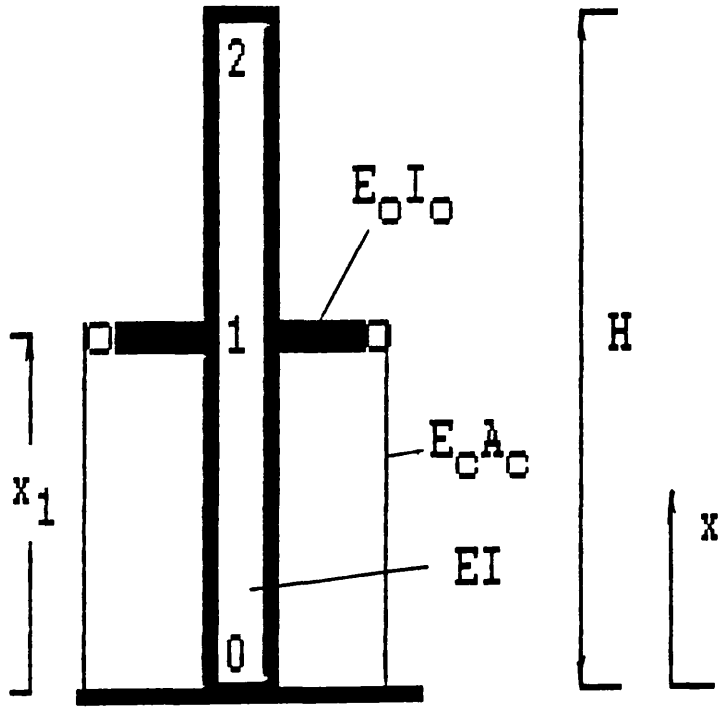

FIG. [5.1a] ONE OUTRIGGER CASE

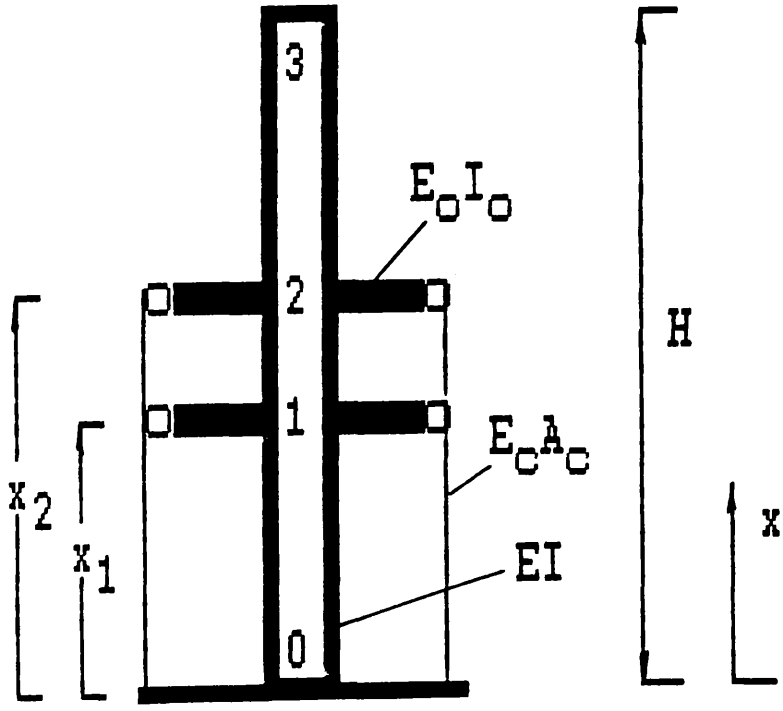

FIG. [5.1b] TWO OUTRIGGER CASE

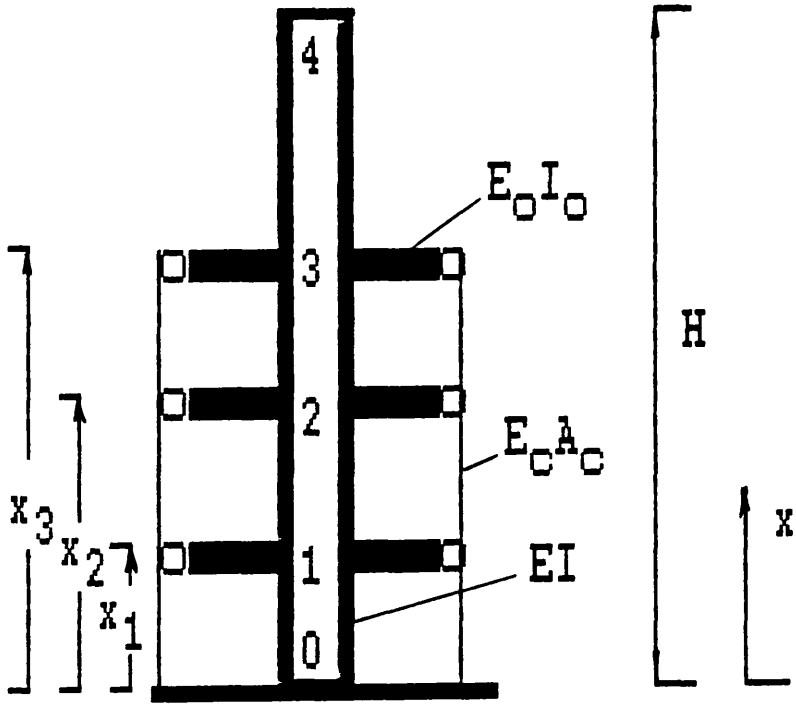

FIG.[5.2a] THREE OUTRIGGER CASE

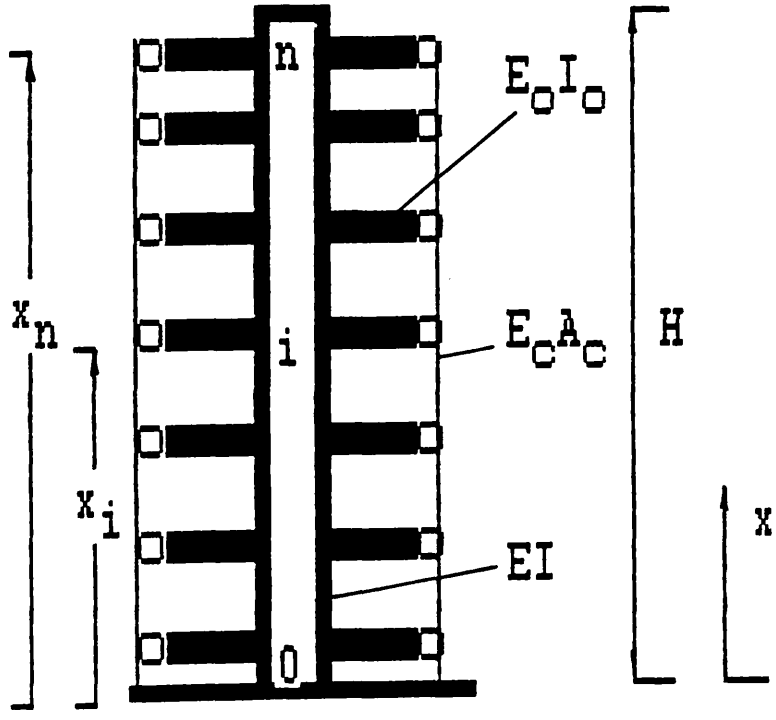

FIG.[5.2b] n OUTRIGGER CASE

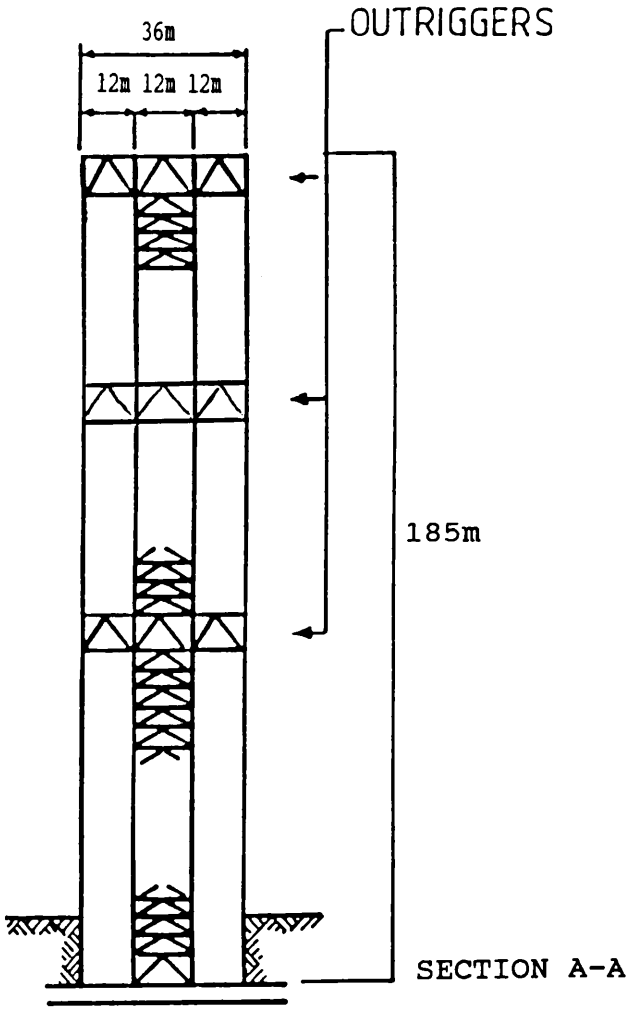

42 STORY FIRST WISCONSIN CENTRE, MILWAUKEE

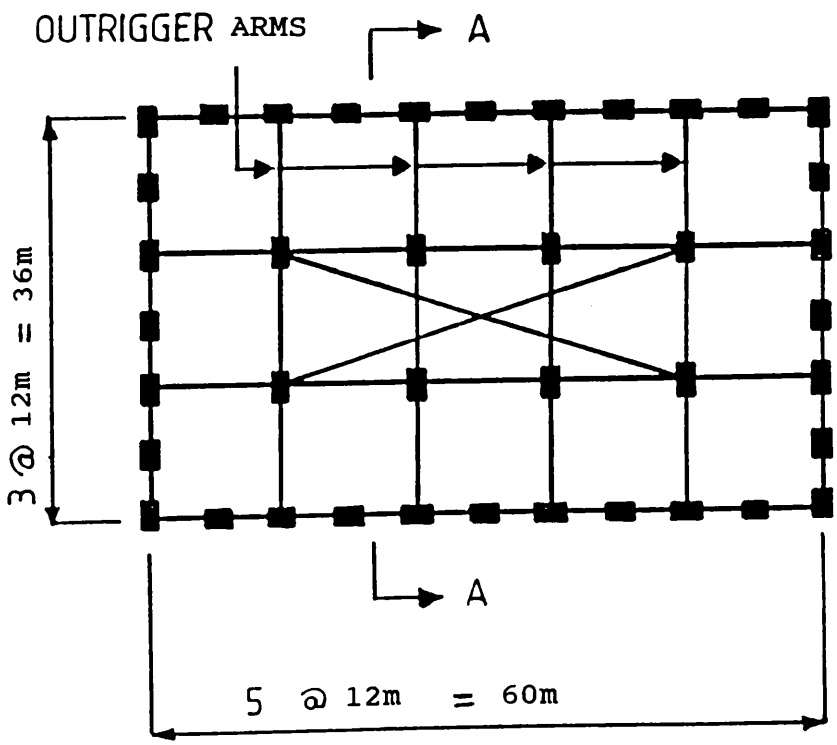

TYPICAL PLAN

FIG. [5.3] EXAMPLE STRUCTURE [5.2]

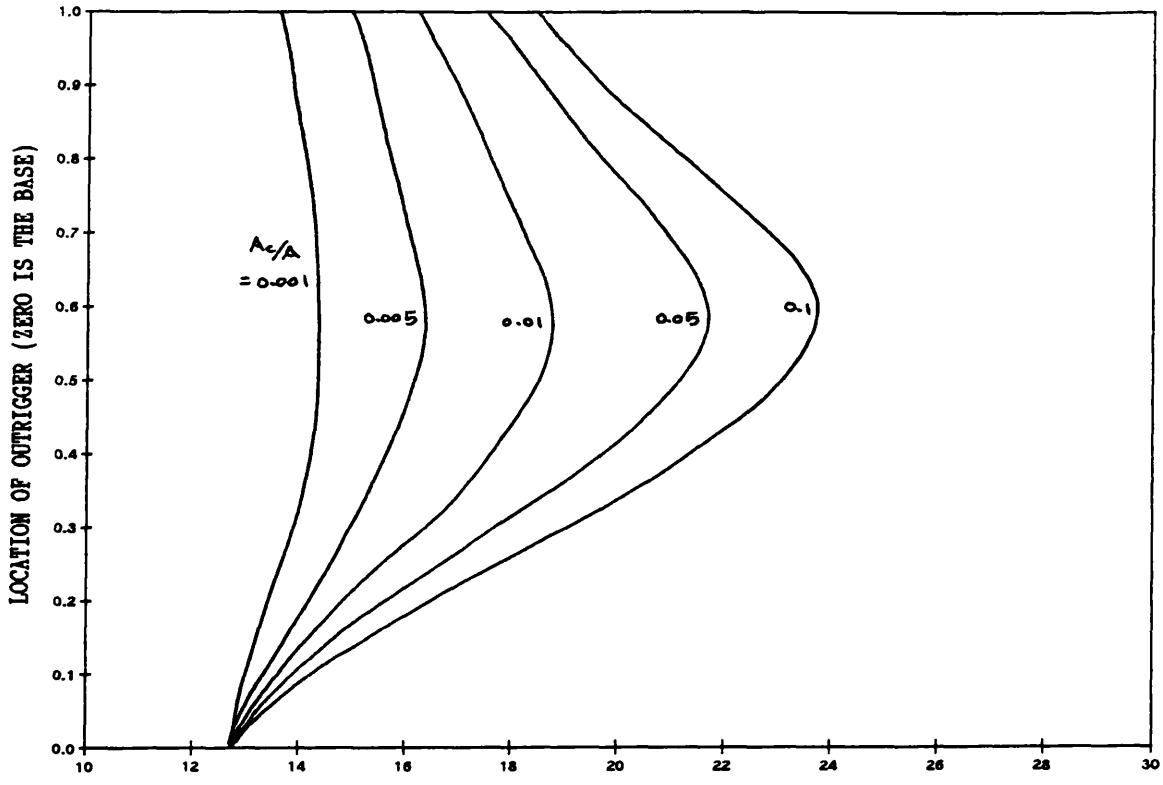

FIG. [5.4] VARIATION OF FIRST NATURAL FREQUENCY WITH OUTRIGGER LOCATIONS FOR DIFFERENT COLUMN/CORE AREA RATIO
(EXAMPLE 5.1, ONE OUTRIGGER CASE)
(BASE FLEXIBILITY=0, $E_o I_r/EI=0.1$)

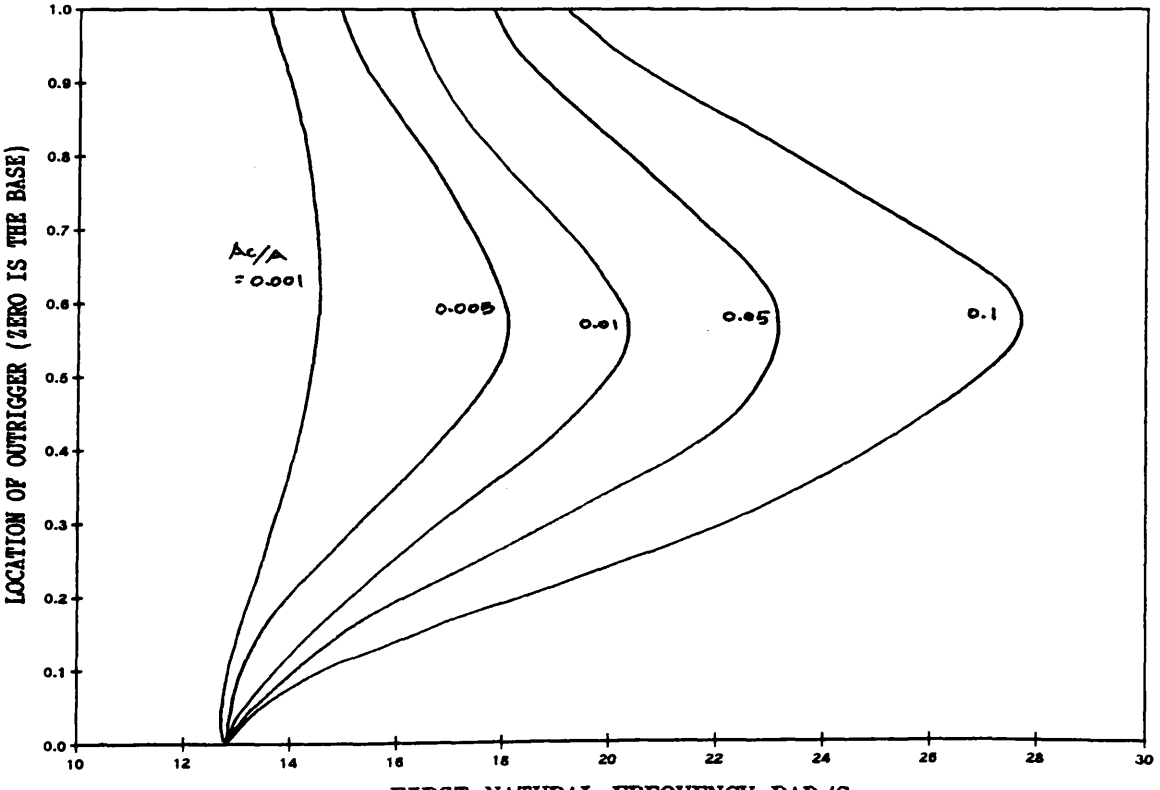

FIG. [5.5] VARIATION OF FIRST NATURAL FREQUENCY WITH LOCATIONS OF RIGID OUTRIGGER FOR DIFFERENT COLUMN/CORE AREA RATIO
(EXAMPLE 5.1, ONE OUTRIGGER CASE)
(BASE FLEXIBILITY=0, $E_o I_r/EI=$INFINITE)

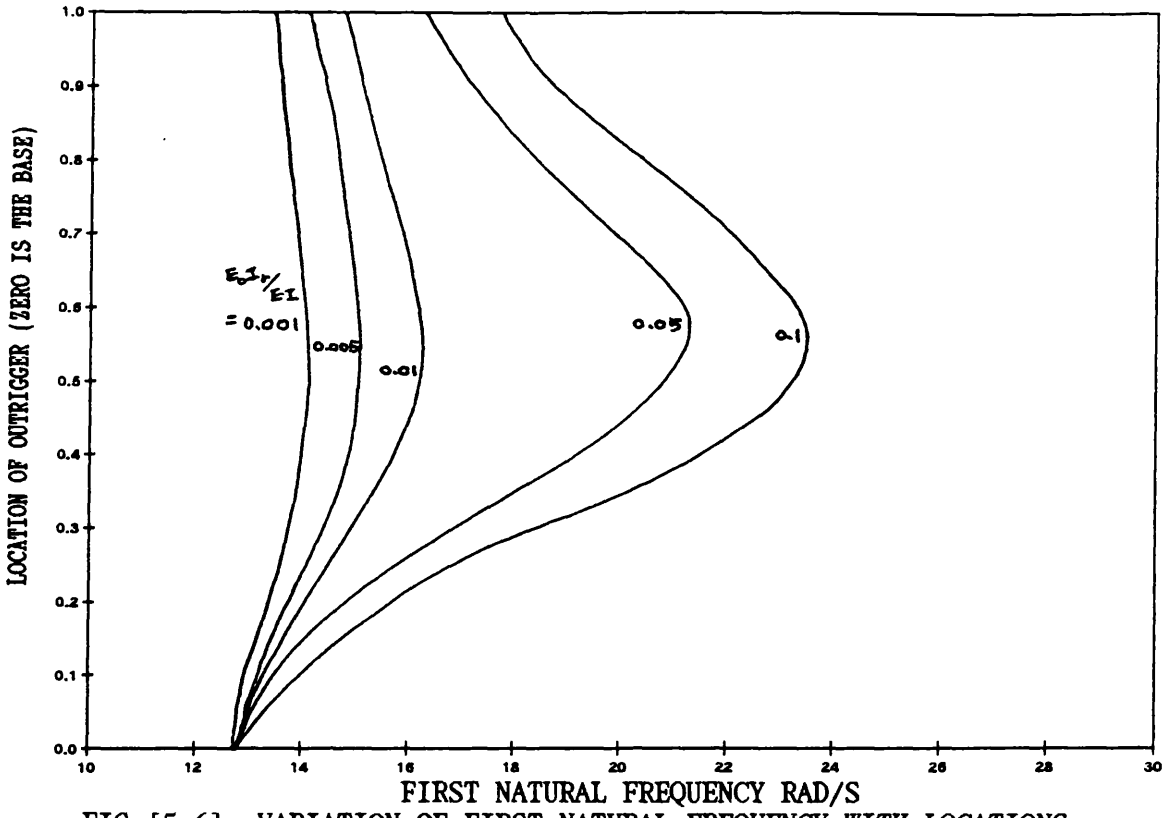

FIG. [5.6] VARIATION OF FIRST NATURAL FREQUENCY WITH LOCATIONS OF OUTRIGGER FOR DIFFERENT FLEXURAL RATIO E_oI_r/EI AND AXIALLY RIGID COLUMNS
(EXAMPLE 5.1, ONE OUTRIGGER CASE)
(BASE FLEXIBILITY=0, A_c/A=INFINITE)

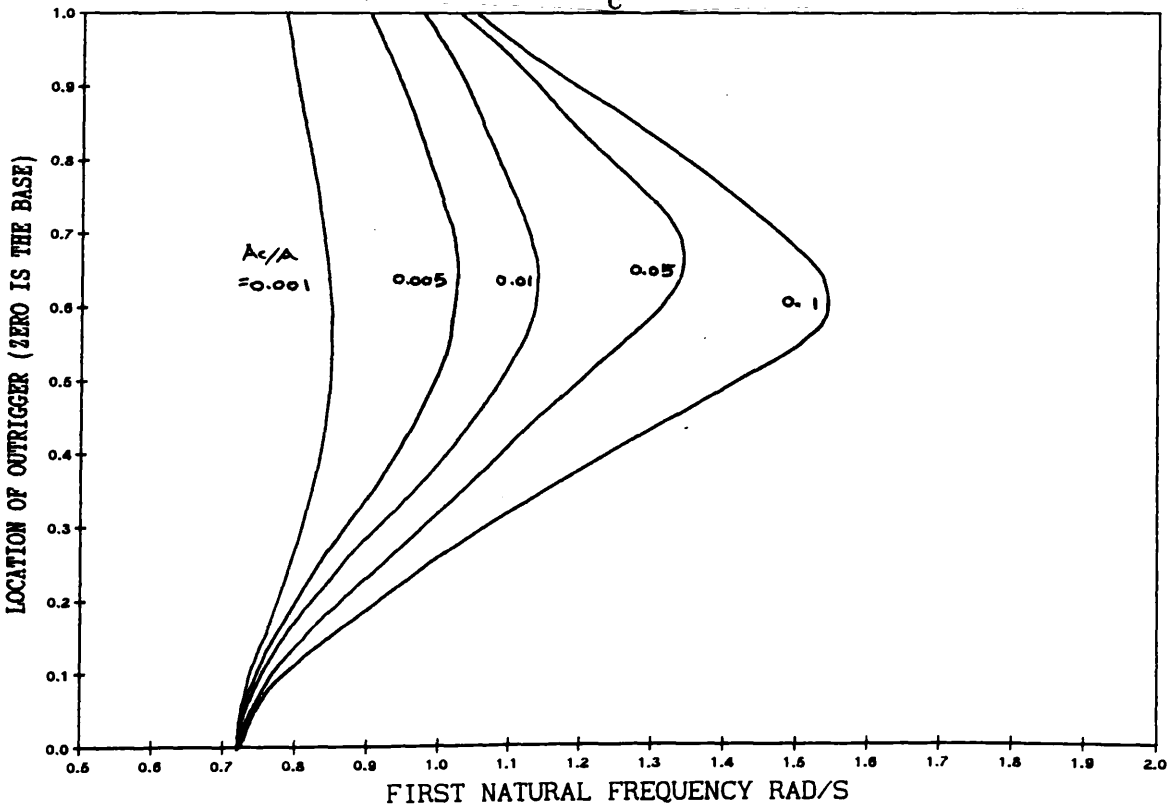

FIG. [5.7] VARIATION OF FIRST NATURAL FREQUENCY WITH OUTRIGGER LOCATIONS FOR DIFFERENT COLUMN/CORE AREA RATIO
(EXAMPLE 5.2, ONE OUTRIGGER CASE)
(BASE FLEXIBILITY=0, E_oI_r/EI=0.1)

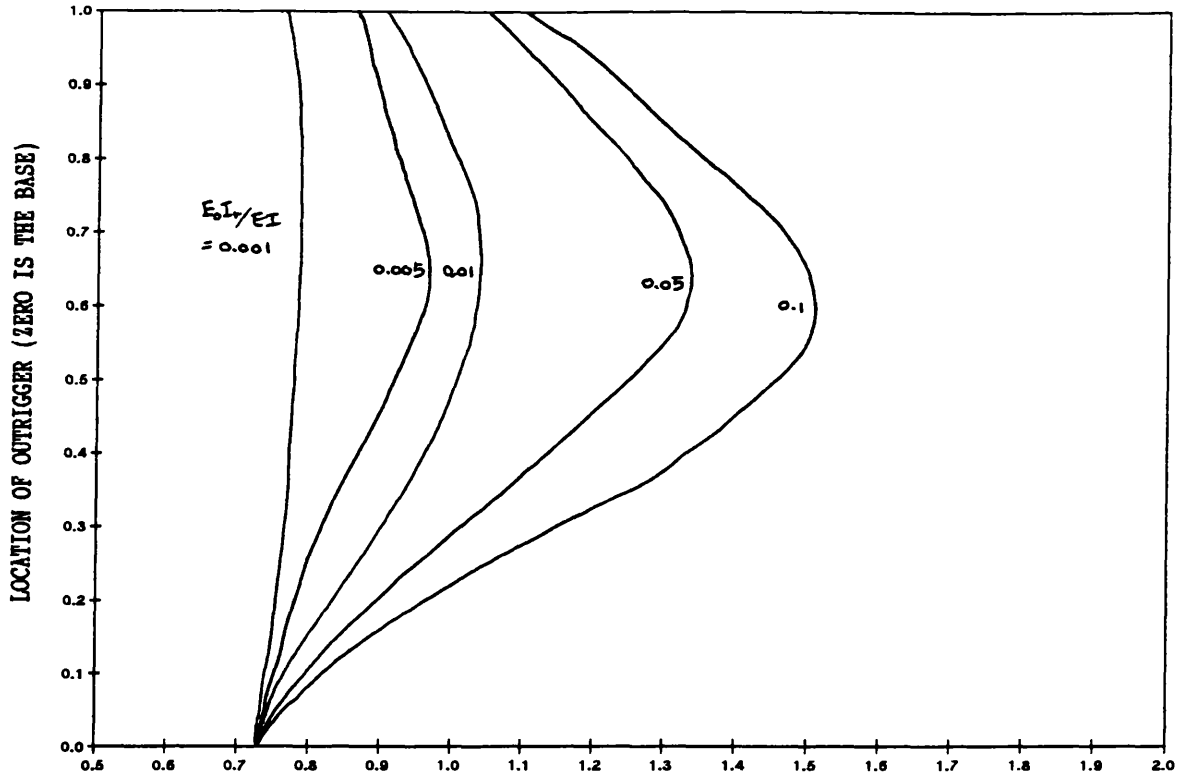

FIG. [5.8] VARIATION OF FIRST NATURAL FREQUENCY WITH LOCATIONS OF OUTRIGGER FOR DIFFERENT FLEXURAL RATIO E_oI_r/EI

(EXAMPLE 5.2, ONE OUTRIGGER CASE)
(BASE FLEXIBILITY=0, A_c/A=0.1)

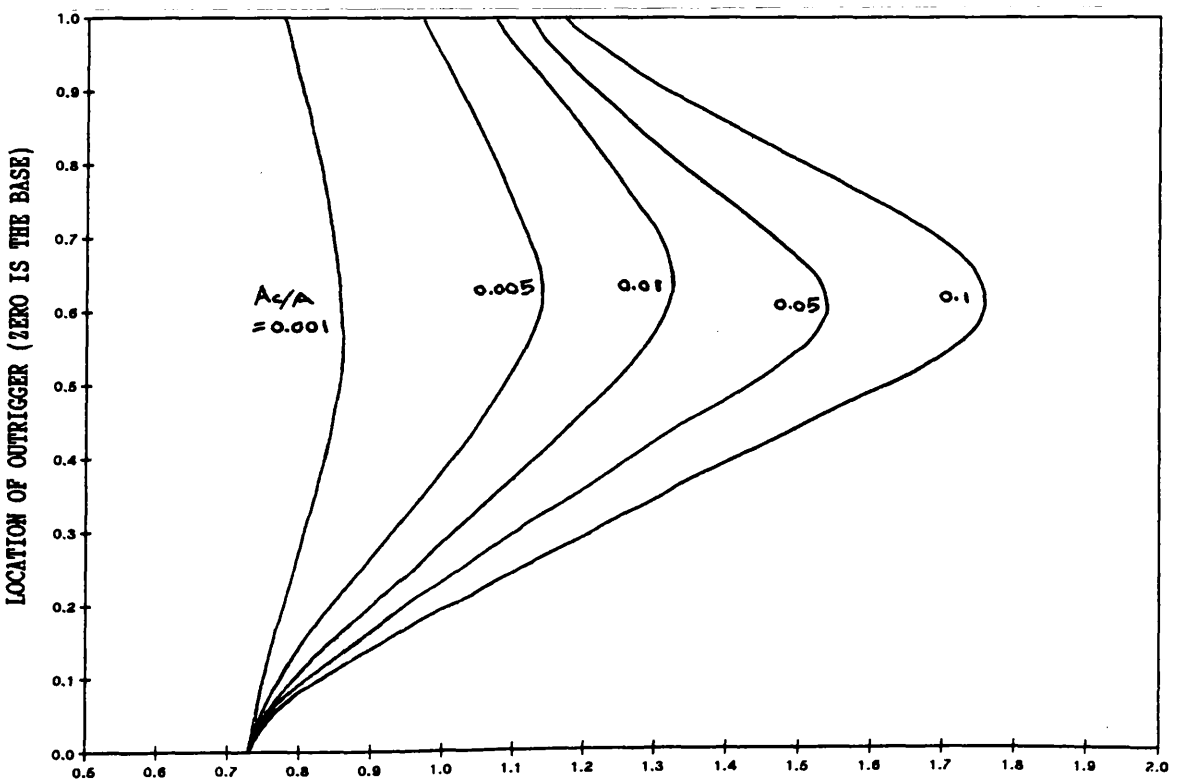

FIG. [5.9] VARIATION OF FIRST NATURAL FREQUENCY WITH LOCATIONS OF RIGID OUTRIGGER FOR DIFFERENT COLUMN/CORE AREA RATIO

(EXAMPLE 5.2, ONE OUTRIGGER CASE)

(BASE FLEXIBILITY=0, E_oI_r/EI=INFINITE)

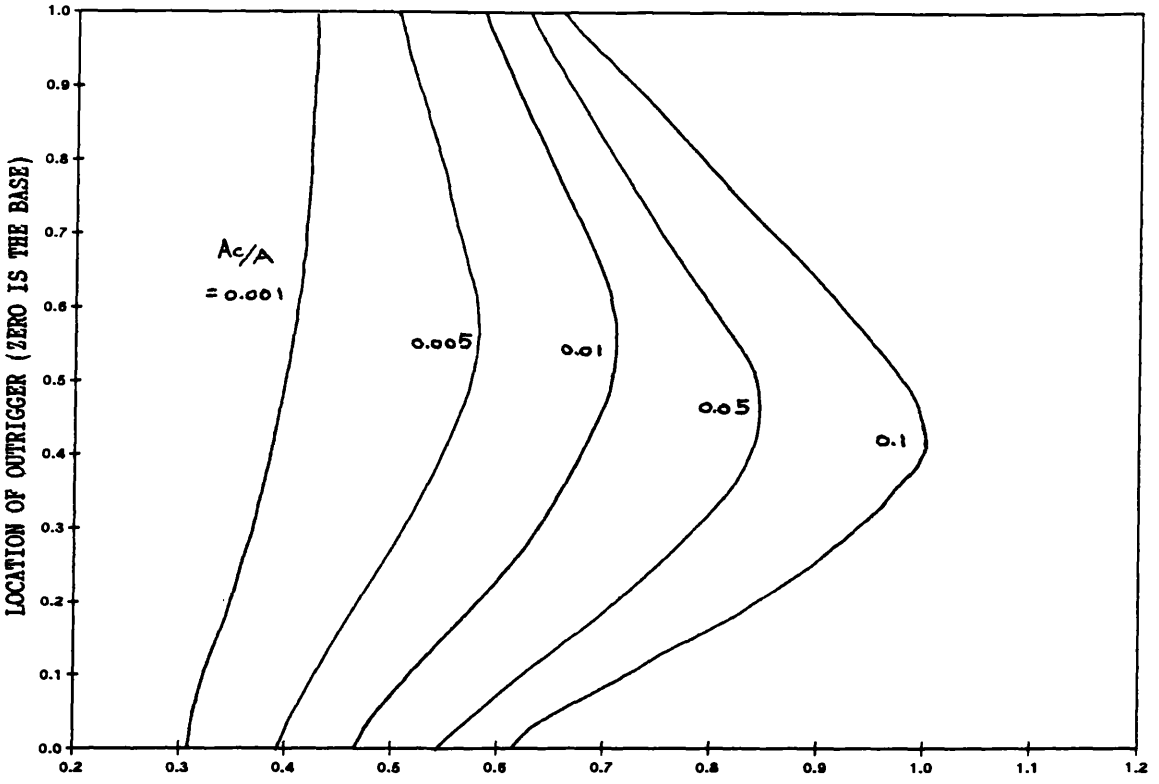

FIG. [5.10] VARIATION OF FIRST NATURAL FREQUENCY WITH OUTRIGGER LOCATIONS FOR DIFFERENT COLUMN/CORE AREA RATIO (EXAMPLE 5.2, ONE OUTRIGGER CASE) (BASE FLEXIBILITY=5*10^-11 RAD/NM, $E_o I_r$/EI=0.1)

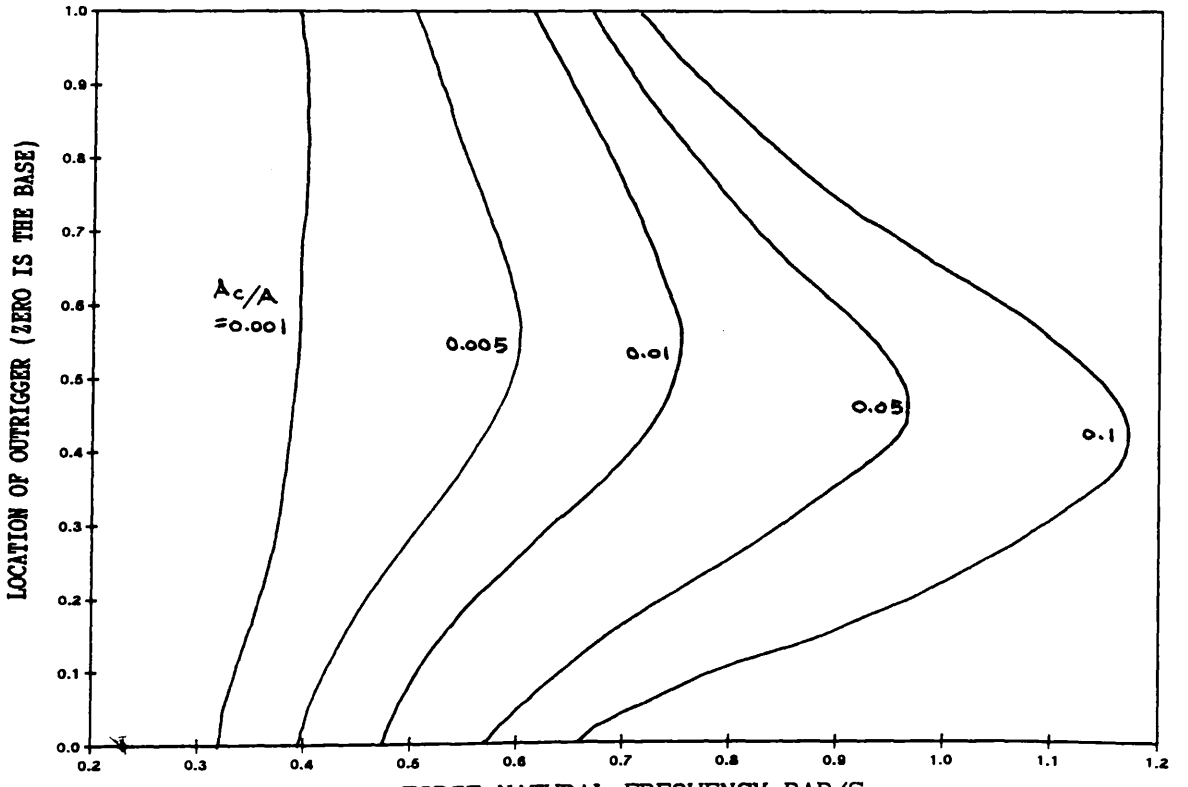

FIG. [5.11] VARIATION OF FIRST NATURAL FREQUENCY WITH LOCATIONS OF RIGID OUTRIGGER FOR DIFFERENT COLUMN/CORE AREA RATIO (EXAMPLE 5.2, ONE OUTRIGGER CASE) (BASE FLEXIBILITY=5*10^-11 RAD/NM, $E_o I_r$/EI=INFINITE)

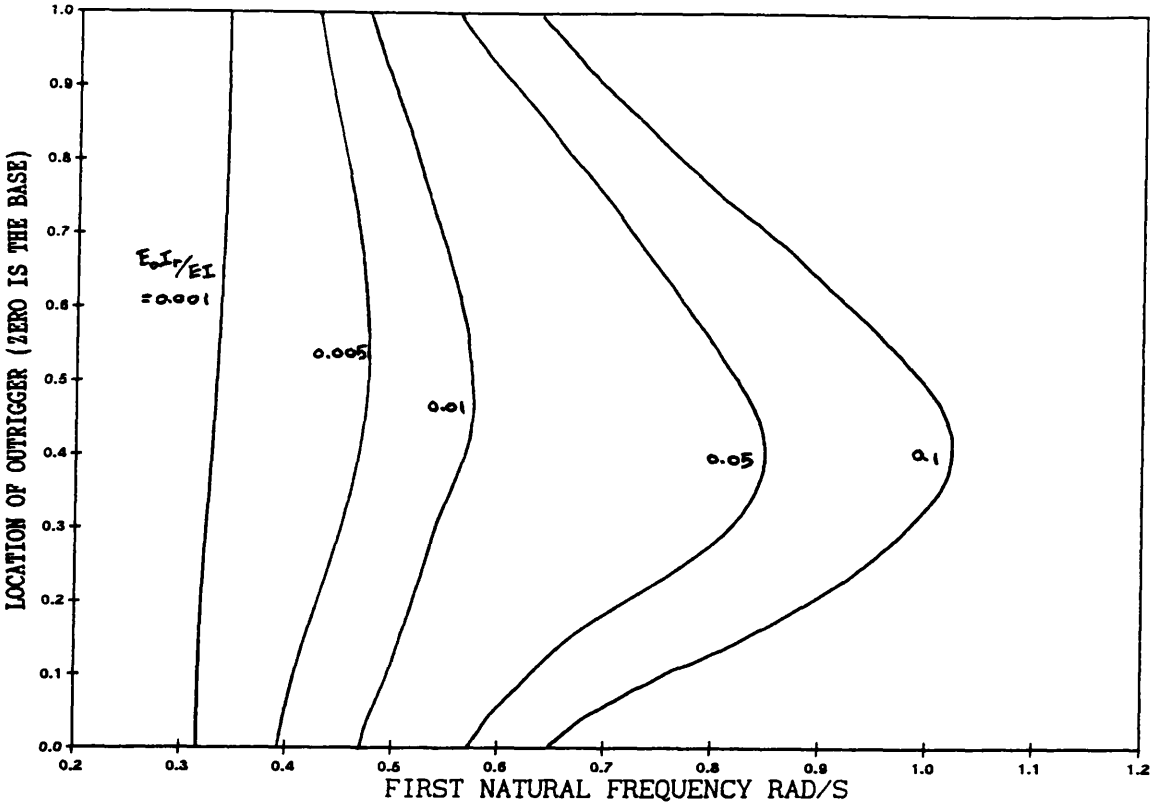

FIG. [5.12] VARIATION OF FIRST NATURAL FREQUENCY WITH LOCATIONS OF RIGID OUTRIGGER FOR DIFFERENT FLEXURAL RATIO E_oI_r/EI AND AXIALLY RIGID COLUMNS
(EXAMPLE 5.2, ONE OUTRIGGER CASE)
(BASE FLEXIBILITY=5*10^-11 RAD/NM, A_C/A=INFINITE)

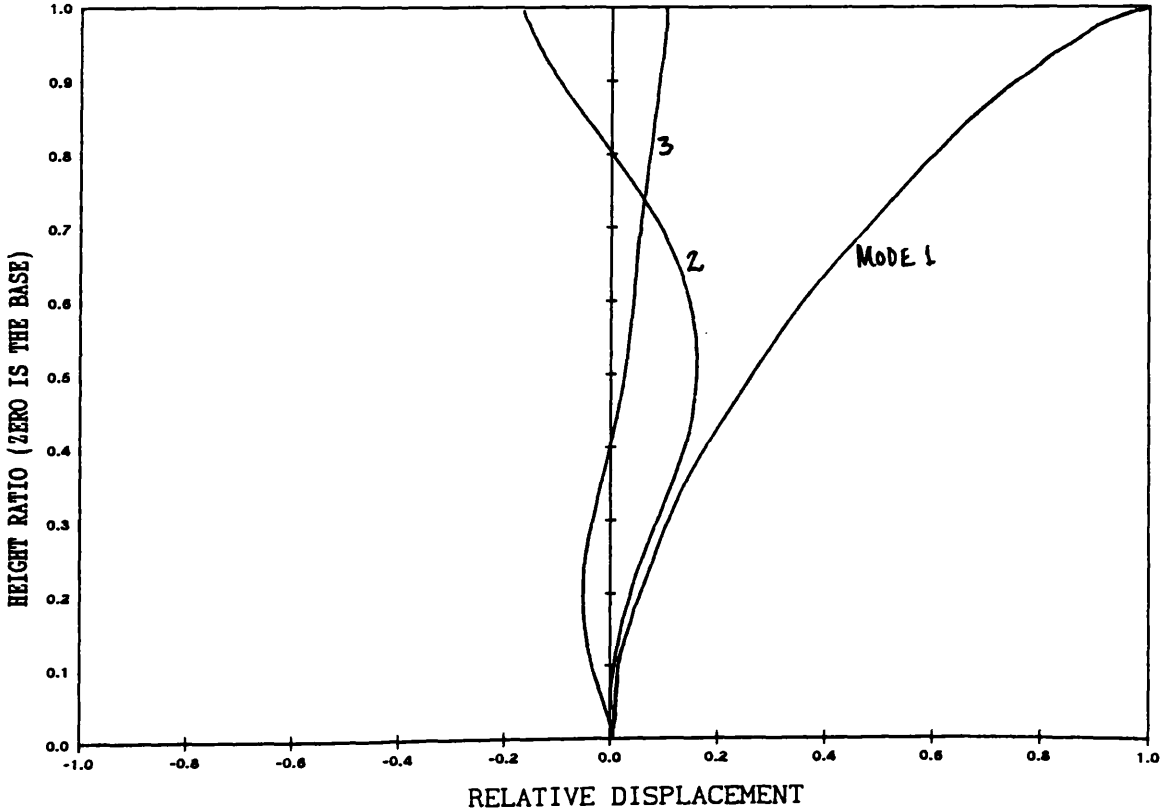

FIG. [5.13] MODE SHAPES CORRESPONDING TO THE FIRST THREE NATURAL FREQUENCIES
(EXAMPLE 5.2, ONE OUTRIGGER CASE)
(BASE FLEXIBILITY=0, X1=0.4)

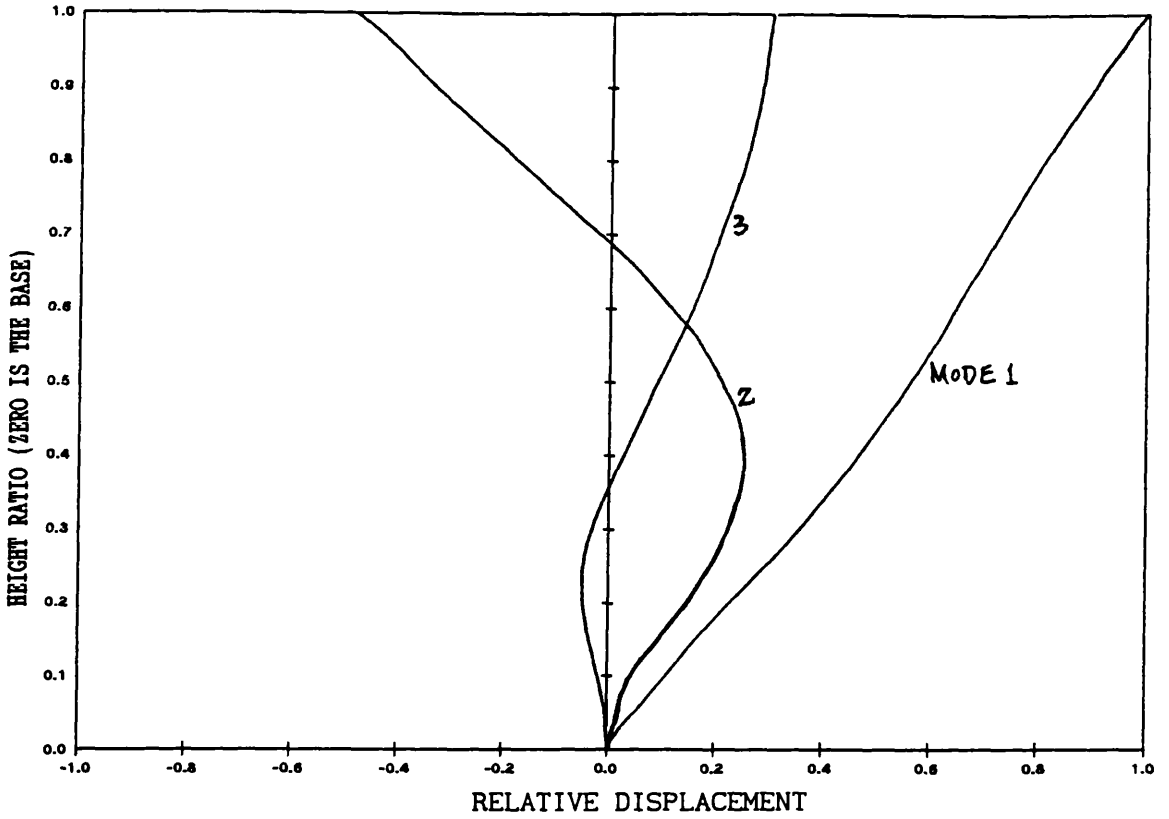

FIG. [5.14] MODE SHAPES CORRESPONDING TO THE FIRST THREE NATURAL FREQUENCIES
(EXAMPLE 5.2, ONE OUTRIGGER CASE)
(BASE FLEXIBILITY=5*10^-11 RAD/KN, X1=0.4)

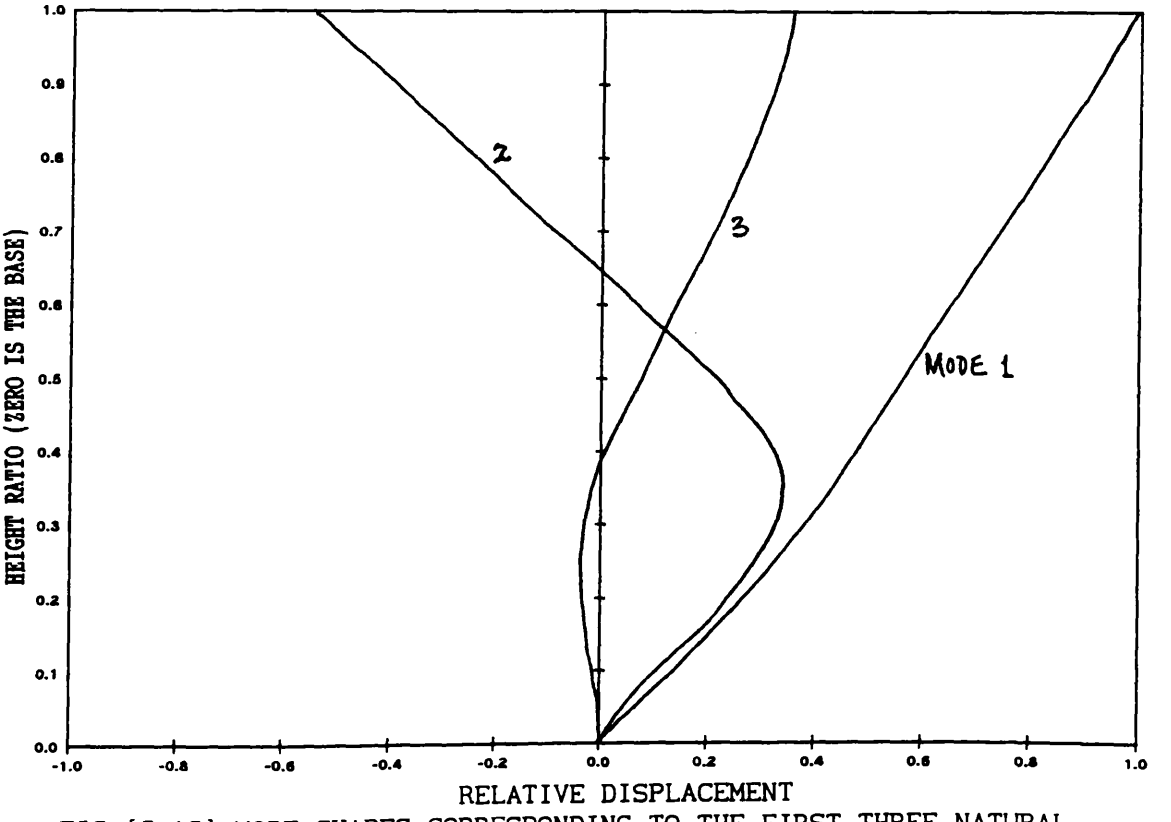

FIG. [5.15] MODE SHAPES CORRESPONDING TO THE FIRST THREE NATURAL FREQUENCIES
(EXAMPLE 5.2, ONE OUTRIGGER CASE)
(BASE FLEXIBILITY=1*10^-10 RAD/KN, X1=0.4)

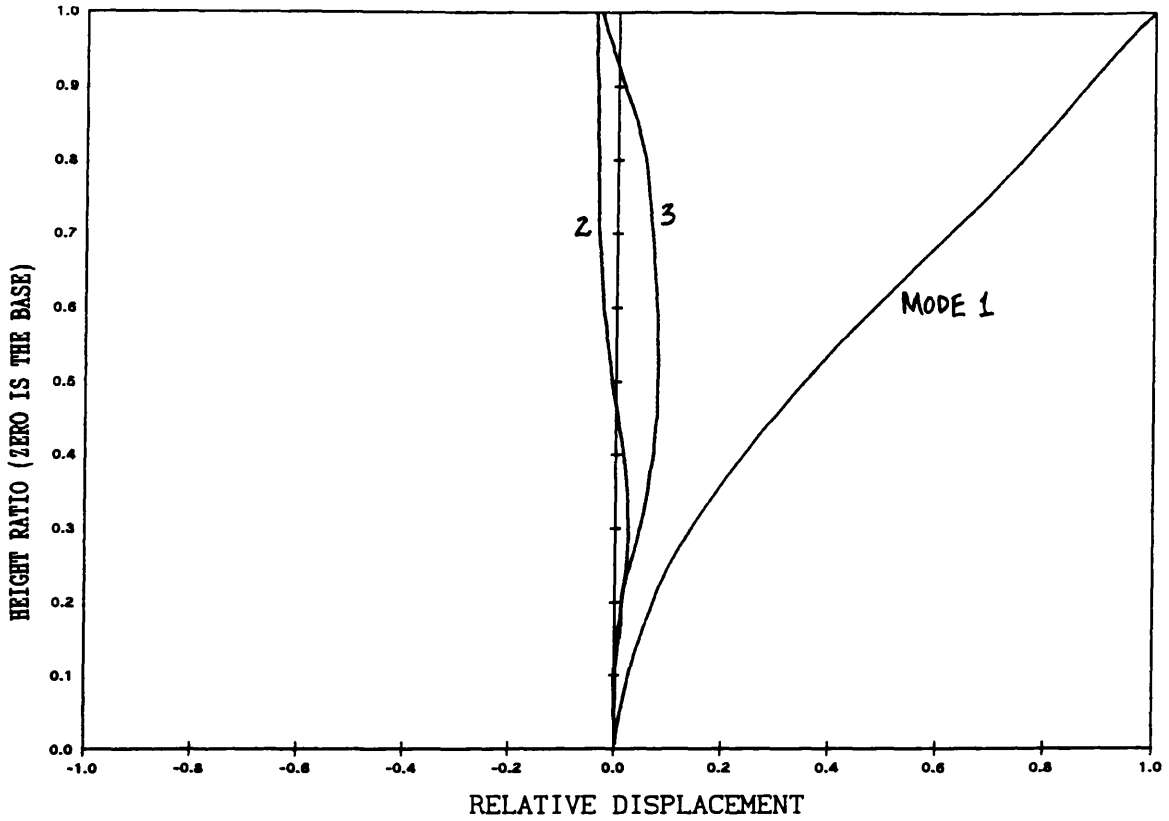

FIG. [5.16] MODE SHAPES CORRESPONDING TO THE FIRST THREE NATURAL FREQUENCIES
(EXAMPLE 5.2, TWO OUTRIGGER CASE)
(BASE FLEXIBILITY=0, X1=0.25, X2=0.75)

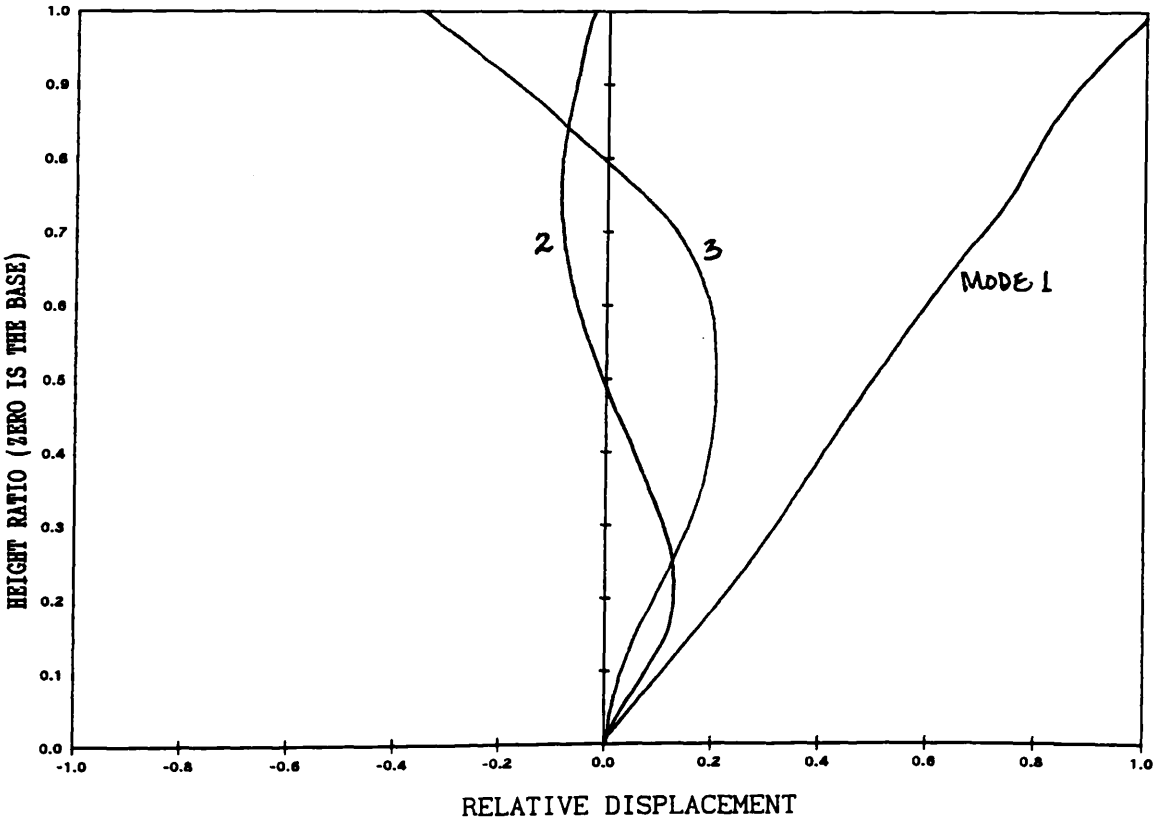

FIG. [5.17] MODE SHAPES CORRESPONDING TO THE FIRST THREE NATURAL FREQUENCIES
(EXAMPLE 5.2, TWO OUTRIGGER CASE)
(BASE FLEXIBILITY=5*10^-11 RAD/KN, X1=0.25, X2=0.75)

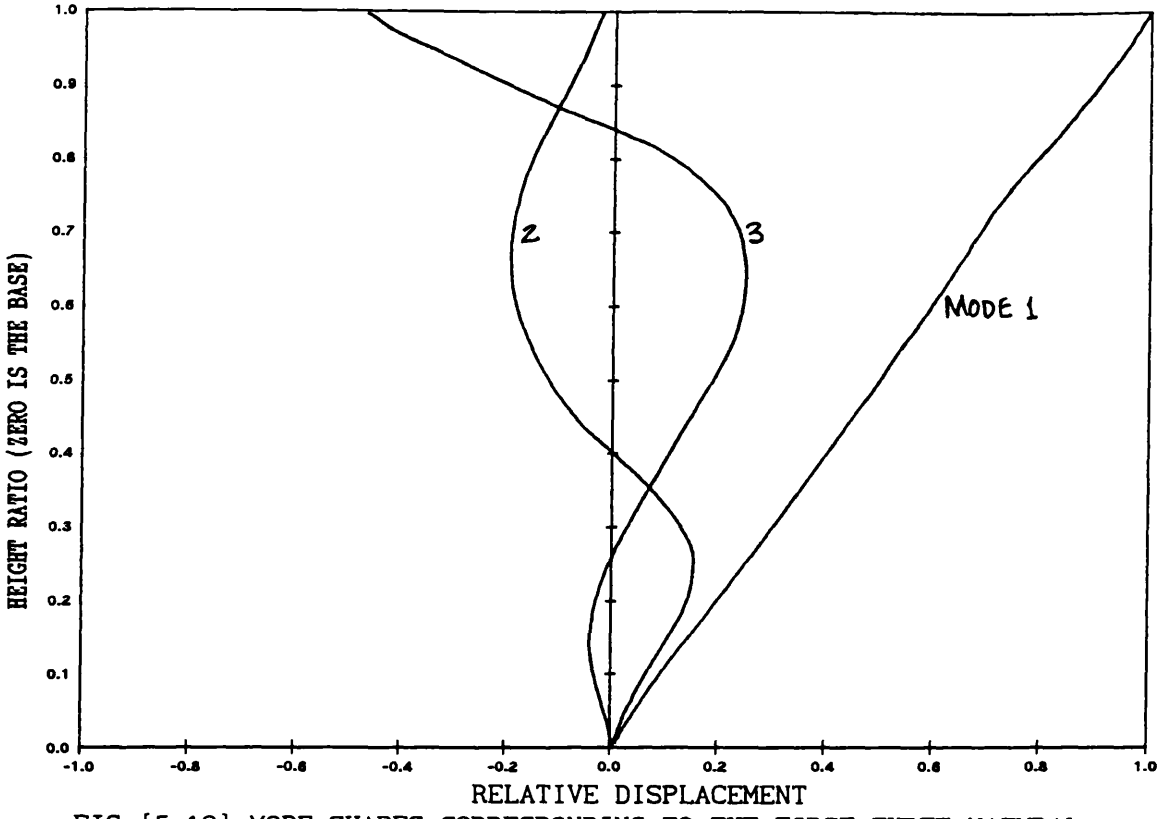

FIG.[5.18] MODE SHAPES CORRESPONDING TO THE FIRST THREE NATURAL FREQUENCIES
(EXAMPLE 5.2, TWO OUTRIGGER CASE)
(BASE FLEXIBILITY=1*10^-10 RAD/KN, X1=0.25, X2=0.75)

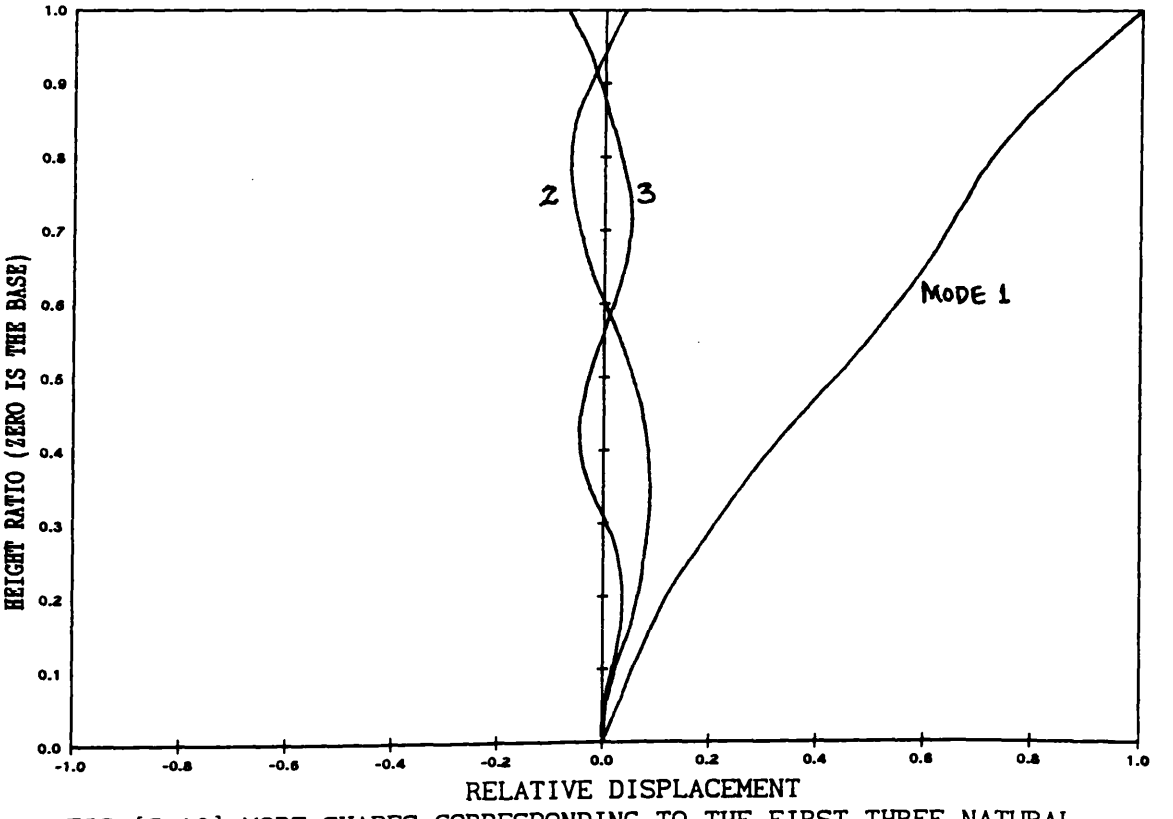

FIG.[5.19] MODE SHAPES CORRESPONDING TO THE FIRST THREE NATURAL FREQUENCIES
(EXAMPLE 5.2, THREE OUTRIGGER CASE)
(BASE FLEXIBILITY=0, X1=0.25, X2=0.50, X3=0.75)

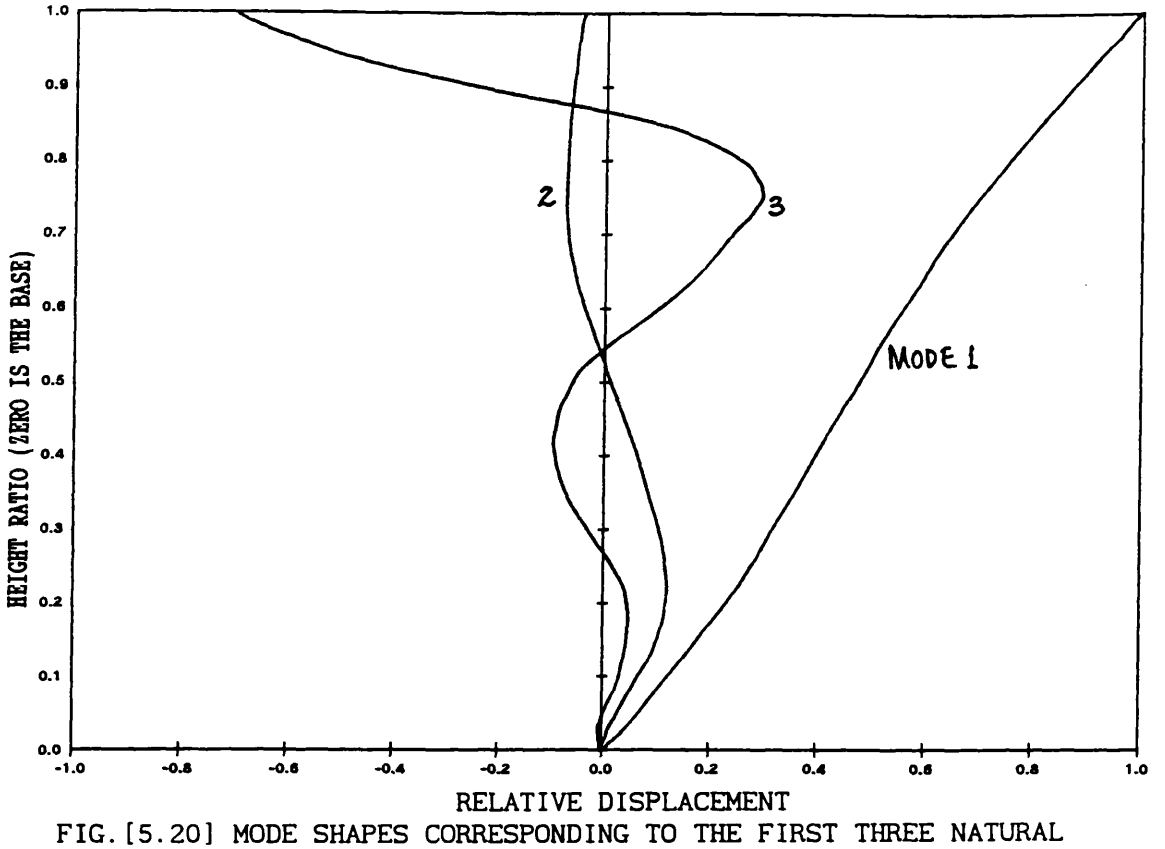

FIG. [5.20] MODE SHAPES CORRESPONDING TO THE FIRST THREE NATURAL FREQUENCIES
(EXAMPLE 5.2, THREE OUTRIGGER CASE)
(BASE FLEXIBILITY=5*10^-11 RAD/KN, X1=0.25, X2=0.50, X3=0.75)

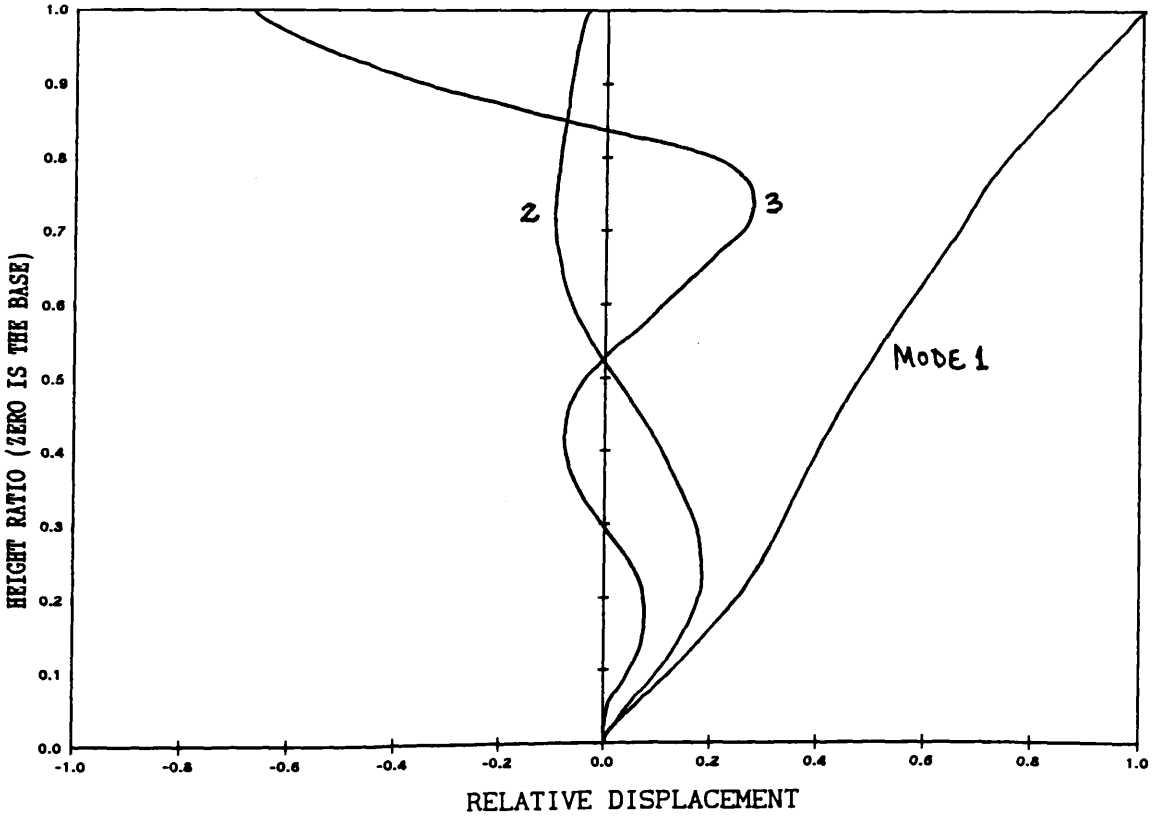

FIG. [5.21] MODE SHAPES CORRESPONDING TO THE FIRST THREE NATURAL FREQUENCIES
(EXAMPLE 5.2, THREE OUTRIGGER CASE)
(BASE FLEXIBILITY=1*10^-10 RAD/KN, X1=0.25, X2=0.50, X3=0.75

Table [5.1] Results for example structure [5.1] with different base flexibility (A_c=0.1A, $E_o I_r$=0.1EI, $K_{\vartheta 1}$=0rad/Nm, $K_{\vartheta 2}$=5x10^{-11}rad/Nm and $K_{\vartheta 3}$=1x10^{-10}rad/Nm)

n	Mode	x_1	x_2 (H)	$K_{\vartheta 1}$ ω	$K_{\vartheta 2}$ ω (rad/s)	$K_{\vartheta 3}$ ω
1	1	0.0		12.568	10.616	10.531
	2			67.963	61.762	61.531
	3			162.251	153.741	153.472
	1	0.2		15.821	14.056	13.835
	2			73.609	61.455	60.439
	3			163.294	146.299	145.266
	1	0.4		21.229	16.525	15.851
	2			68.467	54.094	52.944
	3			170.699	156.495	155.611
	1	0.6		23.446	15.188	14.126
	2			76.791	67.256	66.518
	3			166.914	148.201	147.072
	1	0.8		21.442	12.775	11.640
	2			95.439	79.953	78.777
	3			179.835	166.972	166.238
	1	1.0		18.601	11.035	9.937
	2			86.242	70.979	69.822
	3			182.889	167.016	166.110
2	1	0.33	0.67	27.665	21.765	21.143
	2			124.671	123.467	121.438
	3			213.418	191.603	191.540
	1	0.25	0.75	25.733	21.594	21.193
	2			134.298	127.366	125.582
	3			220.454	201.565	200.199
	1	0.50	1.00	28.694	19.992	18.937
	2			110.036	96.418	95.476
	3			202.988	198.765	195.376

Table [5.2] Results for example structure [5.2] with different base flexibility (E_cA_c=0.1A, E_oI_r=0.1EI, $K_{\vartheta 1}$=0rad/Nm, $K_{\vartheta 2}$=5x10^{-11}rad/Nm and $K_{\vartheta 3}$=1x10^{-10}rad/Nm)

n	Mode	x_1	x_2	x_3 (H)	$K_{\vartheta 1}$ ω	$K_{\vartheta 2}$ ω (rad/s)	$K_{\vartheta 3}$ ω
1	1	0.0			0.714	0.616	0.614
	2				4.342	3.915	3.907
	3				11.624	10.745	10.730
	1	0.2			0.938	0.848	0.840
	2				5.030	3.933	3.872
	3				12.015	9.857	9.788
	1	0.4			1.333	1.009	0.977
	2				4.460	3.219	3.162
	3				12.471	11.103	11.053
	1	0.6			1.480	0.879	0.824
	2				4.989	4.297	4.260
	3				12.327	10.108	10.031
	1	0.8			1.270	0.709	0.652
	2				6.612	5.190	5.127
	3				13.452	11.976	11.931
	1	1.0			1.095	0.592	0.542
	2				5.671	4.376	4.317
	3				13.398	11.510	11.449
2	1	0.33	0.67		1.535	1.358	1.324
	2				8.454	6.999	6.887
	3				14.063	11.998	11.995
	1	0.25	0.75		1.668	1.369	1.348
	2				9.568	7.872	7.738
	3				13.555	11.381	11.352
	1	0.50	1.00		1.621	1.139	1.086
	2				5.894	4.884	4.840
	3				16.878	15.200	15.001
3	1	0.25	0.50	0.75	2.014	1.588	1.560
	2				9.308	8.079	7.939
	3				18.255	17.087	17.071
	1	0.17	0.50	0.83	1.871	1.598	1.580
	2				9.517	8.163	8.032
	3				18.222	17.247	17.231
	1	0.33	0.67	1.00	2.087	1.533	1.422
	2				8.208	6.948	6.871
	3				17.942	17.867	17.865

CHAPTER SIX

STATIC ANALYSIS OF STIFFENED COUPLED SHEAR WALL STRUCTURES

NOTATION of Chapter 6

A_1, A_2	cross-section area of walls 1 and 2
c	clear span length of lintel beams
d	vertical foundational deformation
d_c	depth of connecting beams
E	elastic modulus of walls
E_c	elastic modulus of the connecting beams
E_{c1}, E_{c2}	elastic moduli of the connecting beams in the lower and upper media
E_{s1}, E_{s2}	elastic moduli of stiffening beams 1 and 2
G1, G2, G3	non-dimensional terms
H	height of structure
h	storey height
I_1, I_2	second moment of walls 1 and 2
I	$I_1 + I_2$
K1, K2	non-dimensional terms
l	distance between centroidal axes of walls
M_a	applied moment due to external loads
M_{aB}	applied moment at the base of the structure
M_c	maximum reduction of base moment
M_{Bir}	base moment of a pair of coupled shear walls with infinite stiff connecting beams
M_B	moment at the base of the structure
n	number of storeys
P	point load at the top of the structure
q, q_1, q_2, q_3	laminar shear in the connecting medium
T, T_1, T_2, T_3	axial forces in walls
w	horizontal load per unit height

w_t	load intensity of a upper triangular distributed load
x_1, x_2	positions of the stiffening beams
V	non-dimensional terms
y_1, y_2, y_3	deflection of the structure
y_c	maximum possible top drift reduction
y_{Tir}	top drift of the free bending of a pair of unstiffened walls
y_T	top drift of the structure
α, α_1, α_2	structural parameters
β, β_1, β_2	structural parameters
γ_1, γ_2, γ_3	relative flexural rigidity of the stiffening beams
ϑ	rotation of walls

Other subsidiary symbols are defined locally in the text.

6.1 INTRODUCTION

Most of the construction of buildings consist entirely of wall and floor slab elements which are extremely stiff in their own plane. The slabs serve not only to collect and distribute the lateral forces to walls, but by complex structural interaction with the walls, increase the lateral stiffness of the building. Load-bearing walls normally contain openings for doors, windows and corridors, and may even be discontinued completely at lower levels to allow large uninterrupted areas for a concourse. Shear walls are used in addition to the partition walls to enclose lift shafts and stair wells to form the open section box structures which act as main lateral resisting elements in the building.

In practice, shear walls of various shapes; planar, flanged or box-shaped; may be coupled together in cross-wall structures. The connection between the wall sections is provided by either connecting beams which form part of the wall or by floor slabs, or by a combination of both. Such assemblies are normally termed coupled shear walls, as shown in Fig.[6.1].

The importance of determining the stresses in, and deflections of, such coupled wall structures is reflected by a large number of technical papers devoted to this subject. The stiffness developed by coupled walls depends on the stiffness of the joints between the walls and connecting beams or floor slabs. The presence of moment-resistant connections greatly increases the stiffness and efficiency of the wall assembly, in a similar manner to that of a stiffening beam on a system of linked walls as discussed in

When the walls deflect, shears and moments are induced in the connecting beams or slabs. The coupling beams, in turn, induce axial forces in the walls, tensile in one and compressive in the other. Coupled shear walls with relatively weak coupling beams will behave more like two independent cantilever walls and for a given horizontal load the walls will experience high bending moments and low axial fores. On the other hand, coupled shear walls with stiffer coupling beams will tend to act more as a monolithic cantilever and for the same external load the walls will experience relatively lower bending moments and higher axial forces. As coupled shear walls are usually designed for resisting both gravitational and lateral loads, the tensile stress uplift in the "tensile" wall ~~is~~ should be suppressed by its share of gravitational load.

In most residential or office buildings, the depth of lintel connecting beam and the thickness of the floor slabs will usually be limited by the difference between the floor to floor height and the floor clear height. Because of the limitations, the stiffening effect due to the two elements is very restricted. As a result, the coupling effect of the lintel beams on shear walls may not be sufficiently predominant and, therefore, the top drift and the flexural bending moments at the bottom of the walls may become excessive. Hence, it is sometimes necessary to insert some form of stiffening element, such as a deep beam or a rigid truss, somewhere in the height of the walls to increase the coupling effect. A suitable position for the stiffening beam can be

conveniently found either at the top of the building, at podium level or at an intermediate level reserved for building services or for safety purposes, and sometimes even at the bottom level if the foundation is flexible.

A large number of publications have been devoted to the important subject of coupled shear walls in the past. Based on the continuum method, Coull[18] studied the influence of a stiff top beam on the structural response of coupled shear walls supported on flexible foundations. Choo and Coull[19,20] extended the study to cover the case of a stiff base beam. In this Chapter, based on the previous continuum technique, an analysis for the design of a coupled shear wall structure with up to two stiffening beams is presented, and the optimum location/s of the stiffening beams is investigated. A coupled shear wall structure with two different stiffnesses of connecting beams is also investigated in this Chapter. Results showing the effect of different types of stiffened shear wall structures are presented through a series of design curves. An attempt is made to define the structural efficiency of the stiffening systems in shear wall structures. The results of the finding are tabulated to illustrate the influence and performance of connecting beams and stiffening beams on the structural response of coupled shear wall structures on rigid foundations. In addition the results of a study are also given, comparing the effects of stiffening beams on the structural response of laterally loaded coupled shear walls situated on deformable foundations. In order to estimate the foundation movements, it is assumed that the walls are situated on elastic supports which yield vertically and rotationally under the action of axial forces and moments.

After the completion of this Chapter, a paper was later published by Chan and Kuang[40] who considered the effect of an intermediate stiffening beam. They showed that the particular location of the beam has a significant effect on the structural behaviour.

6.2 ANALYSIS

Consider laterally loaded coupled shear walls with dimensions as given in Fig.[6.1]. An approximate analysis of the structure is achieved by replacing the set of discrete connecting beams by an equivalent substitute medium. The following assumptions are made:-

(i)Plane sections of both walls and beams which are plane before bending remain plane after bending.

(ii)The discrete set of connecting beams, with their flexural rigidities be replaced by an equivalent continuous connecting medium or set of laminae of flexural rigidity EI_c/h per unit height, where h is the storey height.

(iii)Both walls deflect equally as a result of the high axial stiffness of the connecting beams. As such, the connecting beams will deflect with a point of contraflexure at the mid-span position. This is also true of the continuous medium.

(iv)The discrete shear and axial force at the line of contraflexure may be replaced by continuous distributions of shear flow q, and axial forces of intensity t per unit height.

6.2.1 COUPLED SHEAR WALLS WITH AN INTERMEDIATE STIFFENING BEAM

Consider a coupled shear wall system with a stiffening beam at level x_1 between two walls, as shown in Fig.[6.2], resting on a

flexible foundation. By employing the continuum approach, the connecting beams above and below the stiffening beam are replaced by a continuous laminae with equivalent stiffness. It is assumed that the centre-line of the laminae passes through the points of contraflexure of the connecting beams.

If a "cut" is made along the points of contraflexure, as shown in Fig.[6.3], the relative vertical deflection of the cut ends of the laminae must be zero. Therefore the general compatibility equation for the lamina is given by,

$$l\frac{dy}{dx} - \frac{hc^3q}{12E_cI_c} - \frac{1}{E}\left(\frac{1}{A_1} + \frac{1}{A_2}\right)\int_0^x T\,dx - \delta = 0 \qquad (6.1)$$

where

l is the distance between centroids of walls 1 and 2

$\frac{dy}{dx}$ is the slope of the walls at any level x

h is the storey height

c is the clear span of the coupling beams

E is the elastic modulus of the wall material

I_c is the second moment of area of the coupling beams

A_1, A_2 is the cross-sectional area of walls 1 and 2

T is the axial force in the walls at any level x

δ is the relative vertical foundation deformation

The successive terms of the above equation represent the vertical deflection of the midpoint of the lamina due to the slopes of the walls, bending of the laminae, axial deformation of the walls and the relative vertical foundation deformation.

On differentiating with respect to x, equation (6.1) becomes,

$$l\frac{d^2y}{dx^2} - \frac{hc^3}{12E_cI_c}\frac{dq}{dx} - \frac{AT}{EA_1A_2} = 0 \qquad (6.2)$$

The moment curvature relationships for the walls are,

$$EI\frac{d^2y_1}{dx^2} = M_a - T_1 l \qquad (x_1 \leq x \leq H) \qquad (6.3a)$$

$$EI\frac{d^2y_2}{dx^2} = M_a - T_2 l \qquad (0 \leq x \leq x_1) \qquad (6.3b)$$

where

$I = I_1 + I_2$

M_a is the applied bending moment at any level due to the external loads P, w and w_t, given by,

$$M_a = P(H-x) + \frac{w(H-x)^2}{2} + \left[\frac{w_t(H-x)^2}{2} - \frac{w_t(H-x)^3}{6H}\right] \qquad (6.4)$$

In equations (6.3a) and (6.3b), M_a represents three kinds of typical lateral load - namely uniformly distributed load, upper triangularly distributed load and a concentrated load acting at the top of the structure.

For the upper segment of the wall, the axial force at any level x is given by,

$$T_2 = \int_x^H q_2 dx \qquad (6.5)$$

Thus

$$q_2 = - \frac{dT_2}{dx} \qquad (6.6)$$

and

$$\frac{dT_2^2}{dx^2} = - \frac{dq_2}{dx} \qquad (6.7)$$

where T_2 and q_2 are the axial force and laminar shear in the walls above level x_1 respectively.

Similarly, for the lower segment of the wall, the axial force at any level x is given by,

$$T_1 = \int_x^{x_1} q_1 dx + Q_1 + T_{2(x=x_1)}$$

$$= \int_x^{x_1} q_1 dx + Q_1 + \int_{x_1}^H q_2 dx \qquad (6.8)$$

where q_1 and T_1 are the laminar shear and the axial force in the walls below level x_1 respectively. Q_1 is the shear force in the stiffening beam at the height x_1.

Substituting equations (6.3) and (6.7) into equation (6.2) to

eliminate the variables y and q yields,

$$\frac{d^2T_2}{dx^2} - \alpha^2 T_2 = -\beta^2 M_a \qquad (6.9)$$

where

$$\beta^2 = \frac{12 I_c l}{hc^3 I} \qquad (6.10)$$

$$\alpha^2 = \beta^2 \left(1 + \frac{AI}{A_1 A_2 l} \right) \qquad (6.11)$$

$$A = A_1 + A_2$$

The complete solution to the governing ordinary differential equation (6.9) is given by the sum of the complementary function and the particular integral. The complementary function, T_{2c}, of T_2 is,

$$T_{2c} = D_1 \cosh\alpha x + E_1 \sinh\alpha x \qquad (6.12)$$

where D_1 and E_1 are integration constants to be found from the boundary conditions. For the load system as shown in Fig.[6.1]. The particular integral, T_{2p}, of T_2 is given by,

$$T_{2p} = \frac{\beta^2}{\alpha^2} \left\{ M_a + \frac{w}{\alpha^2} + \frac{w_t Hx}{(\alpha H)^2} \right\} \qquad (6.13)$$

Therefore the complete solution to equation (6.9) is,

$$T_2 = D_1 \cosh\alpha x + E_1 \sinh\alpha x + \frac{\beta^2}{\alpha^2}\left\{ M_a + \frac{w}{\alpha^2} + \frac{w_t H x}{(\alpha H)^2} \right\} \tag{6.14}$$

Substituting equation (6.14) into (6.6), the laminar shear flow q_1 is given by,

$$q_2 = -\alpha\,(D_1 \sinh\alpha x + E_1 \cosh\alpha x) - \frac{\beta^2}{\alpha^2}\left\{ \frac{dM_a}{dx} + \frac{w_t H}{(\alpha H)^2} \right\} \tag{6.15}$$

where

$$\frac{dM_a}{dx} = -P - w(H-x) - \frac{w_t(H^2-x^2)}{2H}$$

Similarly, the governing equation for the wall axial force below level x_1, T_1, is given by,

$$\frac{dT_1^2}{dx^2} - \alpha^2 T_1 = -\beta^2 M_a \tag{6.16}$$

The complete solution to equation (6.16) is,

$$T_1 = B_1 \cosh\alpha x + C_1 \sinh\alpha x + \frac{\beta^2}{\alpha^2}\left\{ M_a + \frac{w}{\alpha^2} + \frac{w_t H x}{(\alpha H)^2} \right\} \tag{6.17}$$

where B_1 and C_1 are integration constants.

Differentiating equation (6.17), the expression for q_1 is given by,

$$q_1 = -\alpha\ (B_1\ \sinh\alpha x + C_1\ \cosh\alpha x) - \frac{\beta^2}{\alpha^2}\left\{\frac{dM_a}{dx} + \frac{w_t H}{(\alpha H)^2}\right\}$$

(6.18)

The shear force Q_1 in the stiffening beam located at the level x_1 is obtained by equating the corresponding terms from the equations of compatibility at the point of contraflexure of the lamina just above and below the stiffening beam and the stiffening beam. They are given as follows,

$$l\frac{dy_1}{dx} - \frac{hc^3 q_1}{12E_c I_c} - d_1 - \delta = 0 \qquad (6.19)$$

$$l\left(\frac{dy}{dx}\right)_b - \frac{c^3 Q_1}{12E_s I_s} - d_1 - \delta = 0 \qquad (6.20)$$

$$l\ \frac{dy_2}{dx} - \frac{hc^3 q_2}{12E_c I_c} - d_1 - \delta = 0 \qquad (6.21)$$

where

y_1 is the deflection below the level x_1

y_2 is the deflection above the level x_1

$E_s I_s$ is the flexural rigidity of the stiffening beam

$\left(\frac{dy}{dx}\right)_b$ is the slope of the stiffening beam

and d_1 is the deformation of the wall below the level x_1 given by,

$$d_1 = \frac{1}{E}\left(\frac{1}{A_1} + \frac{1}{A_2} \right) \int_0^{x_1} T_1 \, dx$$

At $x = x_1$,

$$\frac{dy_1}{dx} = \left(\frac{dy}{dx}\right)_b = \frac{dy_2}{dx} \qquad (6.22)$$

The slope at the laminae below and above the level x_1 must be equal to that of the stiffening beam. Therefore,

$$Q_1 = \gamma_1 q_1 = \gamma_1 q_2 \qquad (6.23a)$$

where

$$\gamma_1 = \frac{E_s I_s h}{E_c I_c} \qquad (6.23b)$$

The integration constants B_1, C_1, D_1 and E_1 are found by considering the upper and lower boundary conditions of the structure. For a coupled shear wall, the boundary conditions are as follows:-

The boundary condition at the top depends on whether or not there is a top stiffening beam to help stiffen the structure. Consider the case where there is not a stiff top beam. There can be no axial force at the top of the structure, thus at x=H,

$$T_2(H) = 0 \tag{6.24}$$

Substituting equation (6.24) into (6.14) and simplifying gives,

$$D_1 = -E_1 \tanh\alpha H - \Delta_1 \tag{6.25}$$

where

$$\Delta_1 = \frac{\beta^2}{\alpha^4} \frac{1}{\cosh\alpha H} (w + w_t)$$

From equation (6.8), the boundary condition at level x_1 for the axial forces of the walls is,

$$T_{1(x=x_1)} = Q_1 + T_{2(x=x_1)}$$

$$= \gamma_1 q_{2(x=x_1)} + \int_{x_1}^{H} q_2 dx \tag{6.26}$$

Substituting T_1 and q_2 from equations (6.17) and (6.15) into equation (6.26) and simplifying yields,

$$B_1 \cosh\alpha x_1 + C_1 \sinh\alpha x_1 = D_1 \Delta_2 + E_1 \Delta_3 + \Delta_4 \tag{6.27a}$$

where

$$\Delta_2 = \cosh\alpha x_1 - \alpha\gamma_1 \sinh\alpha x_1 \tag{6.27b}$$

$$\Delta_3 = \sinh\alpha x_1 - \alpha\gamma_1 \cosh\alpha x_1 \tag{6.27c}$$

$$\Delta_4 = \frac{\beta^2}{\alpha^2}\gamma_1\left[P + w(H-x_1) + \frac{w_t(H^2-x_1^2)}{2H} - \frac{w_t H}{(\alpha H)^2}\right] \qquad (6.27d)$$

Substituting D_1 from equation (6.25) into equation (6.27a) and simplifying yields,

$$E_1 = \frac{B_1\ \cosh\alpha x_1 + C_1\ \sinh\alpha x_1 + \Delta_1\Delta_2 - \Delta_4}{\Delta_3 - \Delta_2 \tanh\alpha H} \qquad (6.28)$$

From equation (6.23a), the laminar shear of both substitute mediums at height x_1 must be equal, that is,

$$q_{1(x=x_1)} = q_{2(x=x_1)} \qquad (6.29)$$

Substituting $x=x_1$ into equations (6.15) and (6.18), the following relationship is obtained,

$$E_1 = \frac{C_1 + \tanh\alpha x_1\ (B_1+\Delta_1)}{(\ 1 - \tanh\alpha H\ \tanh\alpha x_1)} \qquad (6.30)$$

The boundary condition at the base depends on whether the foundation is considered to be fully rigid or elastically flexible.

Case 1

Consider the case where the walls are built into fully rigid

foundations. The boundary condition can be obtained from the basic compatibility equation (6.1) and can be expressed as,

$$1\left(\frac{dy_1}{dx}\right)_{(x=0)} - \frac{hc^3 q_{(x=0)}}{12E_c I_c} - \delta = 0 \qquad (6.31)$$

As the foundation is rigid,

$$1\left(\frac{dy_1}{dx}\right)_{(x=0)} = \delta = 0 \qquad (6.32)$$

Therefore from equation (6.31),

$$q_{(x=0)} = 0 \qquad (6.33)$$

Case 2

Where the separate wall bases rest on elastic foundations, the boundary condition is also obtained by using the base compatibility equation as given by equation (6.31). Both vertical and rotational deformations of the separate bases will be considered. Since the foundation is elastic, the vertical displacement is proportional to the axial load $T_{1(x=0)}$ at the base. The following relationship is obtained,

$$\delta = K_d \, T_{1(x=0)} \qquad (6.34)$$

where K_d is a constant which depends on the characteristics of the foundation system. In the case of the wall bases resting on

elastic soil,

$$K_d = \frac{1}{k_1 a_1} + \frac{1}{k_2 a_2} \tag{6.35}$$

where

k_1 = modulus of subgrade reaction of the soil under wall 1

k_2 = modulus of subgrade reaction of the soil under wall 2

a_1 = area of base 1

a_2 = area of base 2

The rotational deformations of the wall bases ϑ_1 and ϑ_2 are,

$$\vartheta_1 = K_{\vartheta 1} M_{1(x=0)} = \frac{K_\vartheta I_1 M_{(x=0)}}{I} \tag{6.36a}$$

$$\vartheta_2 = K_{\vartheta 2} M_{2(x=0)} = \frac{K_\vartheta I_2 M_{(x=0)}}{I} \tag{6.36b}$$

where

M_1 and M_2 are the moments in wall 1 and wall 2

$$K_{\vartheta 1} = \frac{1}{k_1 I_{b1}}$$

$$K_{\vartheta 2} = \frac{1}{k_2 I_{b2}}$$

I_{b1} are the second moment of area of wall 1

I_{b2} are the second moment of area of wall 2

M_B is the moment at the base of the structure given by,

$$M_B = M_{aB} - T_{1(x=0)}l$$

and M_{aB} is the applied moment at the base given by,

$$M_{aB} = PH + \frac{wH^2}{2} + \frac{w_t H^2}{3}$$

Since the walls deflect equally, the rotations of the wall bases must be the same and the slope at the base of the walls $\left(\frac{dy}{dx}\right)_{(x=0)}$ is given by,

$$\left(\frac{dy_1}{dx}\right)_{(x=0)} = K_\vartheta M_{(x=0)} = \vartheta_{(x=0)} \qquad (6.37)$$

where

$$\frac{1}{K_\vartheta} = \frac{1}{K_{\vartheta 1}} + \frac{1}{K_{\vartheta 2}}$$

Substituting for d and $\left(\frac{dy}{dx}\right)_{(x=0)}$ from equations (6.34) and (6.37) into equation (6.31), and simplifying, results in the base condition for flexible foundations.

$$q_{1(x=0)} = K_r M_{a(x=0)} - K_{rv} T_{1(x=0)} \qquad (6.38)$$

where

$$K_r = \frac{12EI_c lK_\vartheta}{hc^3}$$

$$K_{rv} = l\,K_r + K_v$$

and

$$K_v = \frac{12EI_c lK_d}{hc^3}$$

Substituting $q_{1(x=0)}$ and $T_{1(x=0)}$ from equations (6.18) and (6.17) into equation (6.38) and simplifying, the following expression is obtained.

$$C_1 = \Delta_5 + K_{rv}\frac{B_1}{\alpha} \qquad (6.39a)$$

where

$$\Delta_5 = -\frac{\beta^2}{\alpha^3}\left[-P - wH - \frac{w_t H}{2} + \frac{w_t H}{(\alpha H)^2}\right] - \frac{K_r M_{a(x=0)}}{\alpha}$$

$$+ \frac{(lK_r + K_v)}{\alpha} + \frac{\beta^2}{\alpha^2}K_{rv}\left(M_{a(x=0)} + \frac{w}{\alpha^2}\right) \qquad (6.39b)$$

For the case of a rigid foundation, the terms K_r, K_v and K_{rv} becomes zero. Therefore, the integration constant C_1 reduces to,

$$C_1 = -\frac{\beta^2}{\alpha^3}\left[-P - wH - \frac{w_t H}{2} + \frac{w_t H}{(\alpha H)^2}\right] \qquad (6.40c)$$

The analysis assumes that the coupled shear wall structure is built on a flexible foundation. Substituting C_1 from equation (6.39a) into equations (6.28) and (6.30), the solution of the two simultaneous equations (6.28) and (6.30), give the expression for the integration constant B_1,

$$B_1 = \frac{\Delta_8 - \Delta_7}{\Delta_6 - \Delta_9} \qquad (6.40a)$$

where

$$\Delta_6 = \frac{\cosh\alpha x_1 + \frac{K_{rv}}{\alpha}\sinh\alpha x_1}{\Delta_3 - \Delta_2 \tanh\alpha H} \qquad (6.40b)$$

$$\Delta_7 = \frac{\Delta_5 \sinh\alpha x_1 + \Delta_1\Delta_2 - \Delta_4}{\Delta_3 - \Delta_2 \tanh\alpha H} \qquad (6.40c)$$

$$\Delta_8 = \frac{\Delta_5 + \Delta_1 \tanh\alpha x_1}{1 - \tanh\alpha H \tanh\alpha x_1} \qquad (6.40d)$$

$$\Delta_9 = \frac{\frac{K_{rv}}{\alpha} + \tanh\alpha x_1}{1 - \tanh\alpha H \tanh\alpha x_1} \qquad (6.40e)$$

Substituting B_1 from equation (6.40a) into (6.39a) and simplifying, the integration constant C_1 becomes,

$$C_1 = \Delta_5 + \left(\frac{\Delta_8 - \Delta_7}{\Delta_6 - \Delta_9}\right)\frac{K_{rv}}{\alpha} \qquad (6.41)$$

Then substituting B_1 and C_1 into (6.28), the expression for the integration constant E_1 can be obtained as,

$$E_1 = \left(\frac{\Delta_8 - \Delta_7}{\Delta_6 - \Delta_9}\right) \Delta_6 + \Delta_7$$

Substituting E_1 into equation (6.25), gives the expression of the integration constant D_1,

$$D_1 = -\left[\left(\frac{\Delta_8 - \Delta_7}{\Delta_6 - \Delta_9}\right) \Delta_6 + \Delta_7 \right] \tanh\alpha H - \Delta_1 \qquad (6.42)$$

Once the axial forces T_1 and T_2 are determined, then by integrating equations (6.3a) and (6.3b) twice, and using the boundary conditions,

$$y_{1(x=0)} = 0 \qquad (6.43a)$$

$$\left(\frac{dy_1}{dx}\right)_{(x=0)} = \vartheta_{(x=0)} \qquad (6.43b)$$

$$y_{2(x=x_1)} = y_{1(x=x_1)} \qquad (6.43c)$$

$$\left(\frac{dy_1}{dx}\right)_{(x=x_1)} = \left(\frac{dy_2}{dx}\right)_{(x=x_1)} \tag{6.43d}$$

the equations governing the lateral deflection of the structure can be found as,

$$y_1 = \frac{L(x)}{EI} - \frac{1}{EI}\,1\left\{\frac{B_1}{\alpha^2}\cosh\alpha x + \frac{C_1}{\alpha^2}\sinh\alpha x + \frac{\beta^2}{\alpha^2}\left[L(x) + \frac{wx^2}{2\alpha} + \frac{w_t H x^3}{6(\alpha H)^2}\right]\right\} + F_1 x + G_1 \tag{6.44}$$

$$y_2 = \frac{L(x)}{EI} - \frac{1}{EI}\,1\left\{\frac{D_1}{\alpha^2}\cosh\alpha x + \frac{E_1}{\alpha^2}\sinh\alpha x + \frac{\beta^2}{\alpha^2}\left[L(x) + \frac{wx^2}{2\alpha} + \frac{w_t H x^3}{6(\alpha H)^2}\right]\right\} + H_1 x + I_1 \tag{6.45a}$$

where

$$L(x) = \frac{P(H-x)^3}{6} + \frac{w(H-x)^4}{24} + \left[\frac{w_t(H-x)^4}{24} - \frac{w_t(H-x)^5}{120H}\right] \tag{6.45b}$$

Using the boundary condition in equation (6.43b),

$$F_1 = \frac{1}{EI}\left[\frac{PH^2}{2} + \frac{wH^3}{6} + \frac{w_tH^3}{8} + \frac{C_1 l}{\alpha} - \frac{\beta^2}{\alpha^2} l \left(\frac{wH^3}{6} + \frac{w_tH^3}{8} + \frac{PH^2}{2}\right)\right] + \vartheta_{(x=0)} \tag{6.46}$$

Using the boundary condition in equation (6.43a),

$$G_1 = \frac{1}{EI}\left[\frac{B_1 l}{\alpha^2} + \frac{\beta^2}{\alpha^2} l \left(\frac{wH^4}{24} + \frac{w_tH^4}{30} + \frac{PH^3}{6}\right) - \left(\frac{wH^4}{24} + \frac{w_tH^4}{30} + \frac{PH^3}{6}\right)\right] \tag{6.47}$$

Using the boundary condition in equation (6.43d),

$$H_1 = \frac{1}{EI}\left[\frac{l \sinh\alpha x_1}{\alpha}(D_1-B_1) + \frac{l \cosh\alpha x_1}{\alpha}(E_1-C_1)\right] + F_1 \tag{6.48}$$

Using the boundary condition in equation (6.43c),

$$I_1 = \frac{1}{EI}\left[\frac{l \cosh\alpha x_1}{\alpha^2}(D_1-B_1) + \frac{l \sinh\alpha x_1}{\alpha^2}(E_1-C_1)\right] + x_1(F_1-H_1) + G_1 \tag{6.49}$$

The maximum deflection $y_{(x=H)}$ is obtained by substituting x=H into equation (6.45) and is given by,

$$y_{2(x=H)} = -\frac{1}{EI}\,1\left\{\frac{D_1}{\alpha^2}\cosh\alpha H + \frac{E_1}{\alpha^2}\sinh\alpha H + \frac{\beta^2}{\alpha^2}\left[\frac{wH^2}{2\alpha} + \frac{w_t H^4}{6(\alpha H)^2}\right]\right\} + H_1 H + I_1 \qquad (6.50)$$

The analysis in the above section (6.2.1) is a general analysis for the coupled shear wall structure with an intermediate beam. This also includes the treatment for plain coupled shear walls or coupled shear walls with a top or bottom stiffening beam. The solution of these is reviewed and given in the following sections.

PLAIN COUPLED SHEAR WALLS

The solution for the plain coupled shear walls can be obtained from the above analysis by substituting γ_1=0 into the equations in section (6.2.1). Therefore all the terms which include γ_1 will vanish. The expression for the axial force in the walls T, laminar shear q and lateral deflection y are given as below,

$$T = N_1\cosh\alpha x + N_2\sinh\alpha x + \frac{\beta^2}{\alpha^2}\left\{M_a + \frac{w}{\alpha^2} + \frac{w_t H x}{(\alpha H)^2}\right\} \qquad (6.51)$$

$$q = -\alpha\,(N_1\sinh\alpha x + N_2\cosh\alpha x) - \frac{\beta^2}{\alpha^2}\left\{\frac{dM_a}{dx} + \frac{w_t H}{(\alpha H)^2}\right\} \qquad (6.52)$$

$$y = \frac{L(x)}{EI} - \frac{1}{EI} 1 \left\{ \frac{N_1}{\alpha^2} \cosh\alpha x + \frac{N_2}{\alpha^2} \sinh\alpha x \right.$$

$$\left. + \frac{\beta^2}{\alpha^2} \left[L(x) + \frac{wx^2}{2\alpha} + \frac{w_t H x^3}{6(\alpha H)^2} \right] \right\} + N_3 x + N_4$$

(6.53)

By using the boundary conditions,

$$T_{(x=H)} = 0 \tag{6.54a}$$

$$q_{(x=0)} = K_r M_{a(x=0)} - K_{rv} T_{(x=0)} \tag{6.54b}$$

$$y_{(x=0)} = 0 \tag{6.54c}$$

$$\left(\frac{dy}{dx}\right)_{(x=0)} = \vartheta_{(x=0)} \tag{6.54d}$$

The integration constants of equations of (6.51), (6.52) and (6.53) are obtained as follows,

$$N_1 = -N_2 \tanh\alpha H - \frac{\beta^2}{\alpha^4} \frac{1}{\cosh\alpha H} (w + w_t)$$

$$N_2 = -\frac{\beta^2}{\alpha^3} \left[P - wH + \frac{w_t H}{2} + \frac{w_t H}{(\alpha H)^2} \right] - \frac{K_r M_{a(x=0)}}{\alpha}$$

$$+ \frac{(1K_r + K_v)}{\alpha} + \frac{\beta^2}{\alpha^2} K_{rv} \left(M_{a(x=0)} + \frac{w}{\alpha^2} \right)$$

$$N_3 = \frac{1}{EI} \left[\frac{PH^2}{2} + \frac{wH^3}{6} + \frac{w_t H^3}{8} + \frac{N_2 1}{\alpha} \right.$$

$$\left. - \frac{\beta^2}{\alpha^2} 1 \left(\frac{wH^3}{6} + \frac{w_t H^3}{8} + \frac{PH^2}{2} \right) \right] + \vartheta_{(x=0)}$$

$$N_4 = \frac{1}{EI}\left[\frac{N_1 l}{\alpha^2} + \frac{\beta^2 l}{\alpha^2}\left(\frac{wH^4}{24} + \frac{w_t H^4}{30} + \frac{PH^3}{6}\right)\right]$$

$$- \left(\frac{wH^4}{24} + \frac{w_t H^4}{30} + \frac{PH^3}{6}\right)\Bigg]$$

COUPLED SHEAR WALLS WITH A TOP STIFFENING BEAM

The analysis also allows for the treatment of coupled shear walls with a top stiffening beam which was studied by Coull[18]. By substituting x_1=H into the equations in section (6.2.1), the expression for the axial force in the walls T, laminar shear q and lateral deflection y are given as below,

$$T = N_5 \cosh\alpha x + N_6 \sinh\alpha x + \frac{\beta^2}{\alpha^2}\left\{M_a + \frac{w}{\alpha^2} + \frac{w_t H x}{(\alpha H)^2}\right\} \tag{6.55}$$

$$q = -\alpha\,(N_5 \sinh\alpha x + N_6 \cosh\alpha x) - \frac{\beta^2}{\alpha^2}\left\{\frac{dM_a}{dx} + \frac{w_t H}{(\alpha H)^2}\right\} \tag{6.56}$$

$$y = \frac{L(x)}{EI} - \frac{1}{EI} 1\left\{\frac{N_5}{\alpha^2}\cosh\alpha x + \frac{N_6}{\alpha^2}\sinh\alpha x\right.$$

$$\left. + \frac{\beta^2}{\alpha^2}\left[L(x) + \frac{wx^2}{2\alpha} + \frac{w_t H x^3}{6(\alpha H)^2}\right]\right\} + N_7 x + N_8 \tag{6.57}$$

By using the boundary conditions,

$$T_{(x=H)} = \gamma_1 \, q_{(x=H)} \tag{6.58a}$$

$$q_{(x=0)} = K_r M_{a(x=0)} - K_{rv} T_{(x=0)} \tag{6.58b}$$

$$y_{(x=0)} = 0 \tag{6.58c}$$

$$\left(\frac{dy}{dx}\right)_{(x=0)} = \vartheta_{(x=0)} \tag{6.58d}$$

The integration constants of equations of (6.55), (6.56) and (6.57) are obtained as follows,

$$N_5 = - \frac{(\gamma\alpha\cosh\alpha H+\sinh\alpha H)}{(\gamma\alpha\sinh\alpha H+\cosh\alpha H)} N_6 - \frac{\beta^2}{\alpha^4} \frac{(w+w_t)}{(\cosh\alpha H+\gamma\alpha\sinh\alpha H)}$$

$$N_6 = - \frac{\beta^2}{\alpha^3} \left[P - wH + \frac{w_t H}{2} + \frac{w_t H}{(\alpha H)^2} \right] - \frac{K_r M_{a(x=0)}}{\alpha}$$

$$+ \frac{(1K_r+K_v)}{\alpha} + \frac{\beta^2}{\alpha^2} K_{rv} \left(M_{a(x=0)} + \frac{w}{\alpha^2} \right)$$

$$N_7 = \frac{1}{EI} \left[\frac{PH^2}{2} + \frac{wH^3}{6} + \frac{w_t H^3}{8} + \frac{N_6 l}{\alpha} \right.$$

$$\left. - \frac{\beta^2}{\alpha^2} l \left(\frac{wH^3}{6} + \frac{w_t H^3}{8} + \frac{PH^2}{2} \right) \right] + \vartheta_{(x=0)}$$

$$N_8 = \frac{1}{EI} \left[\frac{N_5 l}{\alpha^2} + \frac{\beta^2 l}{\alpha^2} \left(\frac{wH^4}{24} + \frac{w_t H^4}{30} + \frac{PH^3}{6} \right) \right.$$

$$\left. - \left(\frac{wH^4}{24} + \frac{w_t H^4}{30} + \frac{PH^3}{6} \right) \right]$$

COUPLED SHEAR WALLS WITH A BOTTOM STIFFENING BEAM

The analysis allows for the treatment of coupled shear walls with a bottom stiffening beam which was studied by Choo and Coull[20]. The use of a bottom stiffening beam was proved to be effective for stiffening the structure on a flexible foundation. By substituting x_1=0 into the equations in section (6.2.1), the expression for the axial force in the walls T, laminar shear q and lateral deflection y are given as below,

$$T = N_9 \cosh\alpha x + N_{10} \sinh\alpha x + \frac{\beta^2}{\alpha^2}\left\{ M_a + \frac{w}{\alpha^2} + \frac{w_t H x}{(\alpha H)^2} \right\} \tag{6.59}$$

$$q = -\alpha\,(N_9 \sinh\alpha x + N_{10} \cosh\alpha x) - \frac{\beta^2}{\alpha^2}\left\{ \frac{dM_a}{dx} + \frac{w_t H}{(\alpha H)^2} \right\} \tag{6.60}$$

$$y = \frac{L(x)}{EI} - \frac{1}{EI} 1 \left\{ \frac{N_9}{\alpha^2} \cosh\alpha x + \frac{N_{10}}{\alpha^2} \sinh\alpha x + \frac{\beta^2}{\alpha^2}\left[L(x) + \frac{w x^2}{2\alpha} + \frac{w_t H x^3}{6(\alpha H)^2} \right] \right\} + N_{11} x + N_{12} \tag{6.61}$$

By using the boundary conditions,

$$T_{(x=H)} = \gamma_1 \, q_{(x=H)} \tag{6.62a}$$

$$q_{(x=0)} = \frac{K_r M_{a(x=0)} - K_{rv} T_{(x=0)}}{1 + K_{rv}\gamma} \tag{6.62b}$$

$$y_{(x=0)} = 0 \tag{6.62c}$$

$$\left(\frac{dy}{dx}\right)_{(x=0)} = \vartheta_{(x=0)} \tag{6.62d}$$

The integration constants of equations of (6.59), (6.60) and (6.61) are obtained as follows,

$$N_9 = -N_2 \tanh\alpha H - \frac{\beta^2}{\alpha^4} \frac{1}{\cosh\alpha H} (w + w_t)$$

$$N_{10} = \frac{\frac{\beta^2}{\alpha^2}\left[(1+K_{rv}\gamma)N_{13}+K_{rv}N_{14}\right] - K_r M_{a(x=0)}}{K_{rv}\tanh\alpha H + \alpha(1+K_{rv}\gamma)}$$

$$N_{11} = \frac{1}{EI}\left[\frac{PH^2}{2} + \frac{wH^3}{6} + \frac{w_t H^3}{8} + \frac{N_{10}l}{\alpha} - \frac{\beta^2}{\alpha^2} l \left(\frac{wH^3}{6} + \frac{w_t H^3}{8} + \frac{PH^2}{2}\right)\right] + \vartheta_{(x=0)}$$

$$N_{12} = \frac{1}{EI}\left[\frac{N_9 l}{\alpha^2} + \frac{\beta^2 l}{\alpha^2}\left(\frac{wH^4}{24} + \frac{w_t H^4}{30} + \frac{PH^3}{6}\right) - \left(\frac{wH^4}{24} + \frac{w_t H^4}{30} + \frac{PH^3}{6}\right)\right]$$

$$N_{13} = P + wH + \frac{w_t H}{2} - \frac{w_t H}{(\alpha H)^2}$$

$$N_{14} = M_{a(x=0)} + \frac{w}{\alpha^2} - \Delta_1 \frac{\alpha^2}{\beta^2}$$

6.2.2 COUPLED SHEAR WALLS WITH TWO INTERMEDIATE STIFFENING BEAMS

Consider a coupled shear wall system on a flexible foundation with two stiffening beams, as shown in Fig.[6.4]. The relative flexural rigidities of the stiffening beams are γ_1 and γ_2 at levels x_1 and x_2 respectively. between two walls resting on a flexible foundation. By employing the continuum analysis as in the previous section, the connecting beams above, between and below the stiffening beams are replaced by a continuous laminae with equivalent stiffness.

For the upper segment of the wall, the axial force at any level x is given by,

$(H \geq x \geq x_2)$

$$T_3 = \int_x^H q_3 dx \qquad (6.63a)$$

Similarly, for the middle and lower segment of the wall, the axial force at any level x is given by,

$(x_2 \geq x \geq x_1)$

$$T_2 = \int_x^{x_2} q_1 dx + Q_2 + \int_{x_2}^H q_2 dx \qquad (6.63b)$$

$(x_1 \geq x \geq 0)$

$$T_1 = \int_x^{x_1} q_1 dx + Q_1 + \int_{x1}^{x_2} q_1 dx + Q_2 + \int_{x_2}^{H} q_2 dx \qquad (6.63c)$$

where q_1, q_2 and q_3 are the laminar shear in the walls below, between and above the stiffening beams. T_1, T_2 and T_3 are the axial force in the walls below, between and above the stiffening beams respectively. Q_1 and Q_2 are the shear force in the stiffening beams located at the height x_1 and x_2.

The moment-curvature relationships for the walls is,

$$EI \frac{d^2 y_1}{dx^2} = M_a - T_1 l \qquad (0 \leq x \leq x_1) \qquad (6.64a)$$

$$EI \frac{d^2 y_2}{dx^2} = M_a - T_2 l \qquad (x_1 \leq x \leq x_2) \qquad (6.64b)$$

$$EI \frac{d^2 y_3}{dx^2} = M_a - T_3 l \qquad (x_2 \leq x \leq H) \qquad (6.64c)$$

Differentiating equation (6.1) and combining equations (6.63a), (6.63b), (6.63c), (6.64a), (6.64b) and (6.64c) to eliminate the variables y and q yields the solution of governing differential equations for the axial forces T_1, T_2 and T_3.

$$T_3 = F_2 \cosh\alpha x + G_2 \sinh\alpha x + \frac{\beta^2}{\alpha^2} \left\{ M_a + \frac{w}{\alpha^2} + \frac{w_t H x}{(\alpha H)^2} \right\} \qquad (6.65a)$$

$$T_2 = D_2 \cosh\alpha x + E_2 \sinh\alpha x + \frac{\beta^2}{\alpha^2}\left\{ M_a + \frac{w}{\alpha^2} + \frac{w_t H x}{(\alpha H)^2} \right\} \tag{6.65b}$$

$$T_1 = B_2 \cosh\alpha x + C_2 \sinh\alpha x + \frac{\beta^2}{\alpha^2}\left\{ M_a + \frac{w}{\alpha^2} + \frac{w_t H x}{(\alpha H)^2} \right\} \tag{6.65c}$$

where B_2, C_2, D_2, E_2, F_2 and G_2 are the integration constants. Differentiating equations (6.65a), (6.65b) and (6.65c) yields the expressions for the laminae shears.

$$q_3 = -\alpha\,(F_2 \sinh\alpha x + G_2 \cosh\alpha x) - \frac{\beta^2}{\alpha^2}\left\{ \frac{dM_a}{dx} + \frac{w_t H}{(\alpha H)^2} \right\} \tag{6.66a}$$

$$q_2 = -\alpha\,(D_2 \sinh\alpha x + E_2 \cosh\alpha x) - \frac{\beta^2}{\alpha^2}\left\{ \frac{dM_a}{dx} + \frac{w_t H}{(\alpha H)^2} \right\} \tag{6.66b}$$

$$q_1 = -\alpha\,(B_2 \sinh\alpha x + C_2 \cosh\alpha x) - \frac{\beta^2}{\alpha^2}\left\{ \frac{dM_a}{dx} + \frac{w_t H}{(\alpha H)^2} \right\} \tag{6.66c}$$

The values of the integration constants B_2, C_2, D_2, E_2, F_2 and G_2 can be determined by considering the boundary conditions in the problem.

At the top of the structure, x=H, the axial force in the walls is equal to zero, that is

$$T_{3(x=H)} = 0 \tag{6.67}$$

From equation (6.63b), the boundary condition at level x_2 for the axial forces of the wall is

$$T_{2(x=x_2)} = Q_2 + T_{3(x=x_2)} \tag{6.68}$$

where Q_2 is the shear force in the stiffening beam given by,

$$Q_2 = \gamma_2 q_2 = \gamma_2 q_3$$

and

$$\gamma_2 = \frac{E_{s2} I_{s2} h}{E_c I_c}$$

$E_{s2}I_{s2}$ is the flexural rigidity of the stiffening beam at level x_2.

By establishing compatibility equations as in equations (6.19), (6,20) and (6.21) at the level $x=x_2$, it yields,

$$q_3 = q_2 \tag{6.69}$$

Similarly at level x_1, the corresponding equations as in equations (6.68) and (6.69) are obtained.

$$T_{1(x=x_1)} = Q_1 + T_{2(x=x_1)} \tag{6.70}$$

$$q_1 = q_2 \tag{6.71}$$

where

$$Q_1 = \gamma_1 q_1 = \gamma_1 q_2$$

and

$$\gamma_1 = \frac{E_{s1} I_{s1} h}{E_c I_c}$$

$E_{s1} I_{s1}$ is the flexural rigidity of the stiffening beam at level x_1.

Considering the compatibility equation at the base, x=0, the following equation is obtained.

$$q_{1(x=0)} = K_r M_{a(x=0)} - K_{rv} T_{1(x=0)} \tag{6.72}$$

Solving equations (6.67), (6.68), (6.69), (6.70), (6.71) and (6.72), the integration constants B_2, C_2, D_2, E_2, F_2 and G_2 are obtained.

$$B_2 = D_2 + E_2 \phi_{18} - \phi_{19} \tag{6.73a}$$

$$C_2 = \phi_8 + K_{rv} \frac{B_1}{\alpha} \tag{6.73b}$$

$$D_2 = E_2 \phi_{20} + \phi_{21} \tag{6.73c}$$

$$E_2 = \frac{\phi_{21} - \phi_{23}}{\phi_{22} - \phi_{20}} \tag{6.73d}$$

$$F_2 = -G_2 \tanh\alpha H - \phi_1 \tag{6.73e}$$

$$G_2 = D_2 \phi_{12} + E_{12} \phi_{13} + \phi_{14} \tag{6.73f}$$

where

$$\phi_1 = \frac{\beta^2}{\alpha^4} \frac{1}{\cosh\alpha H} (w + w_t)$$

$$\phi_2 = \cosh\alpha x_2 - \alpha\gamma_2 \sinh\alpha x_2$$

$$\phi_3 = \sinh\alpha x_2 - \alpha\gamma_2 \cosh\alpha x_2$$

$$\phi_4 = \frac{\beta^2}{\alpha^2} \gamma_2 \left[P + w(H-x_2) + \frac{w_t(H^2-x_2^2)}{2H} - \frac{w_t H}{(\alpha H)^2} \right]$$

$$\phi_5 = \cosh\alpha x_1 - \alpha\gamma_1 \sinh\alpha x_1$$

$$\phi_6 = \sinh\alpha x_1 - \alpha\gamma_1 \cosh\alpha x_1$$

$$\phi_7 = \frac{\beta^2}{\alpha^2} \gamma_1 \left[P + w(H-x_1) + \frac{w_t(H^2-x_2^2)}{2H} - \frac{w_t H}{(\alpha H)^2} \right]$$

$$\phi_8 = -\frac{\beta^2}{\alpha^3}\left[-P - wH - \frac{w_t H}{2} + \frac{w_t H}{(\alpha H)^2}\right] - \frac{K_r M_{a(x=0)}}{\alpha}$$

$$+ \frac{(1K_r + K_v)}{\alpha} + \frac{\beta^2}{\alpha^2} K_{rv}\left(M_{a(x=0)} + \frac{w}{\alpha^2}\right)$$

$$\phi_9 = \frac{\cosh\alpha x_2}{\phi_3 - \phi_2 \tanh\alpha H}$$

$$\phi_{10} = \frac{\sinh\alpha x_2}{\phi_3 - \phi_2 \tanh\alpha H}$$

$$\phi_{11} = \frac{\phi_1\phi_2 - \phi_4}{\phi_3 - \phi_2 \tanh\alpha H}$$

$$\phi_{12} = \frac{\tanh\alpha x_2}{1 - \tanh\alpha H \tanh\alpha x_2}$$

$$\phi_{13} = \frac{1}{1 - \tanh\alpha H \tanh\alpha x_2}$$

$$\phi_{14} = \frac{\phi_1 \tanh\alpha x_1}{1 - \tanh\alpha H \tanh\alpha x_2}$$

$$\phi_{15} = \frac{\phi_5}{\cosh\alpha x_1 + \frac{K_{rv}}{\alpha}}$$

$$\phi_{16} = \frac{\phi_6}{\cosh\alpha x_1 + \frac{K_{rv}}{\alpha}}$$

$$\phi_{17} = \frac{\phi_7 - \phi_8 \sinh\alpha x_2}{\cosh\alpha x_1 + \frac{K_{rv}}{\alpha}}$$

$$\phi_{18} = \frac{1}{\tanh\alpha x_1 + \frac{K_{rv}}{\alpha}}$$

$$\phi_{19} = \frac{\phi_8}{\tanh\alpha x_1 + \frac{K_{rv}}{\alpha}}$$

$$\phi_{20} = \frac{\phi_{13} - \phi_{10}}{\phi_9 - \phi_{12}}$$

$$\phi_{21} = \frac{\phi_{14} - \phi_{11}}{\phi_9 - \phi_{12}}$$

$$\phi_{22} = \frac{\phi_{18} - \phi_{16}}{\phi_{15} - 1}$$

$$\phi_{23} = \frac{\phi_{19} - \phi_{17}}{\phi_{15} - 1}$$

Then by integrating equations (6.64a), (6.64b) and (6.64c) twice and using the boundary conditions,

$$y_{1(x=0)} = 0 \qquad (6.74a)$$

$$\left(\frac{dy_1}{dx}\right)_{(x=0)} = \vartheta_{(x=0)} \tag{6.74b}$$

$$y_{2(x=x_1)} = y_{1(x=x_1)} \tag{6.74c}$$

$$\left(\frac{dy_1}{dx}\right)_{(x=x_1)} = \left(\frac{dy_2}{dx}\right)_{(x=x_1)} \tag{6.74d}$$

$$y_{2(x=x_2)} = y_{3(x=x_2)} \tag{6.74e}$$

$$\left(\frac{dy_2}{dx}\right)_{(x=x_2)} = \left(\frac{dy_3}{dx}\right)_{(x=x_2)} \tag{6.74f}$$

the lateral deflection of the structure can be found as,

$$y_1 = \frac{L(x)}{EI} - \frac{1}{EI} 1 \left\{ \frac{B_2}{\alpha^2} \cosh\alpha x + \frac{C_2}{\alpha^2} \sinh\alpha x + \frac{\beta^2}{\alpha^2} \left[L(x) + \frac{wx^2}{2\alpha} + \frac{w_t H x^3}{6(\alpha H)^2} \right] \right\} + H_2 x + I_2 \tag{6.75a}$$

$$y_2 = \frac{L(x)}{EI} - \frac{1}{EI} 1 \left\{ \frac{D_2}{\alpha^2} \cosh\alpha x + \frac{E_2}{\alpha^2} \sinh\alpha x + \frac{\beta^2}{\alpha^2} \left[L(x) + \frac{wx^2}{2\alpha} + \frac{w_t H x^3}{6(\alpha H)^2} \right] \right\} + J_2 x + K_2 \tag{6.75b}$$

$$y_3 = \frac{L(x)}{EI} - \frac{1}{EI} l \left\{ \frac{F_2}{\alpha^2} \cosh\alpha x + \frac{G_2}{\alpha^2} \sinh\alpha x \right.$$

$$\left. + \frac{\beta^2}{\alpha^2} \left[L(x) + \frac{wx^2}{2\alpha} + \frac{w_t H x^3}{6(\alpha H)^2} \right] \right\} + L_2 x + M_2$$

(6.75c)

where H_2, I_2, J_2, K_2, L_2 and M_2 are the integration constants and are found as,

$$H_2 = \frac{1}{EI} \left[\frac{PH^2}{2} + \frac{wH^3}{6} + \frac{w_t H^3}{8} + \frac{C_2 l}{\alpha} \right.$$

$$\left. - \frac{\beta^2}{\alpha^2} l \left(\frac{wH^3}{6} + \frac{w_t H^3}{8} + \frac{PH^2}{2} \right) \right] + \vartheta_{(x=0)}$$

$$I_2 = \frac{1}{EI} \left[\frac{B_2 l}{\alpha^2} + \frac{\beta^2}{\alpha^2} l \left(\frac{wH^4}{24} + \frac{w_t H^4}{30} + \frac{PH^3}{6} \right) \right.$$

$$\left. - \left(\frac{wH^4}{24} + \frac{w_t H^4}{30} + \frac{PH^3}{6} \right) \right]$$

$$J_2 = \frac{1}{EI} \left[\frac{l \sinh\alpha x_1}{\alpha} (D_2 - B_2) + \frac{l \cosh\alpha x_1}{\alpha} (E_2 - C_2) \right] + H_2$$

$$K_2 = \frac{1}{EI} \left[\frac{l \cosh\alpha x_1}{\alpha^2} (D_2 - B_2) + \frac{l \sinh\alpha x_1}{\alpha^2} (E_2 - C_2) \right]$$

$$+ x_1 (H_2 - J_2) + I_2$$

$$L_2 = \frac{1}{EI} \left[\frac{l \sinh\alpha x_2}{\alpha} (F_2 - B_2) + \frac{l \cosh\alpha x_2}{\alpha} (G_2 - C_2) \right] + J_2$$

$$M_2 = \frac{1}{EI}\left[\frac{1}{\alpha^2}\cosh\alpha x_2\,(F_2-B_2) + \frac{1}{\alpha^2}\sinh\alpha x_2\,(G_2-C_2)\right]$$

$$+ x_1(J_2-L_2) + K_2$$

The maximum deflection $y_{(x=H)}$ is obtained by substituting x=H into equation (6.45) and is given by,

$$y_{3(x=H)} = -\frac{1}{EI}\,1\left\{\frac{F_2}{\alpha^2}\cosh\alpha H + \frac{G_2}{\alpha^2}\sinh\alpha H + \frac{\beta^2}{\alpha^2}\left[\frac{wH^2}{2\alpha} + \frac{w_t H^4}{6(\alpha H)^2}\right]\right\} + L_2 H + M_2 \qquad (6.76)$$

The analysis in the above section (6.2.2) is a general analysis for the coupled shear wall structure with two intermediate beams. This also includes the treatment for coupled shear walls with a top and bottom stiffening beam, a top and an intermediate stiffening beam and a bottom and an intermediate stiffening beam. The solutions of these are briefly discussed in the following sections.

COUPLED SHEAR WALLS WITH A TOP AND BOTTOM STIFFENING BEAM CASE

Sometimes, it is necessary to insert more than one stiffening element somewhere in the height of the structure to enhance the coupling effect of the normal lintel or connecting beams. stiffening the structure by using a top or bottom stiffening beam

has been proved effective in the past. It will be of interest to assess the effectiveness of using a top and bottom stiffening beams to reduce both the top drift and base moment of the structure. The solution for the coupled shear walls with a top and bottom stiffening beam can be obtained from the above analysis by substituting x_1=0 and x_2=H into the equations in section (6.2.2). The terms γ_1 and γ_2 represent the relative flexural rigidities of the bottom and top stiffening beams.

COUPLED SHEAR WALLS WITH A TOP AND AN INTERMEDIATE STIFFENING BEAMS

It is sometimes convenient to insert some form of stiffening element, such as a deep beam or rigid truss, at the top of the structure. If it is required to reduce the deflection and stresses in the walls further, an intermediate stiffening beam will be needed. The performance of the intermediate stiffening beam will depend on its location in the height of the structure. The solution for the coupled shear wall with a top and an intermediate stiffening beam can be obtained from the above analysis by substituting x_2=H into the equations in section (6.2.2). The terms γ_1 and γ_2 represent the relative flexural rigidities of the intermediate and top stiffening beams.

COUPLED SHEAR WALLS WITH A BOTTOM AND INTERMEDIATE STIFFENING BEAMS

In the case where the foundations are flexible, the provision of a

local stiffening beam at the base of the structure may be more effective in reducing the effects of foundation flexibility. The solution for the coupled shear walls with a bottom and intermediate stiffening beam can be obtained from the above analysis by substituting $x_1=0$ into the equations in section (6.2.2). The terms γ_1 and γ_2 represent the relative flexural rigidity of the bottom and intermediate stiffening beams.

6.2.3 COUPLED SHEAR WALLS WITH TWO DIFFERENT TYPES OF CONNECTING BEAMS

Normally, the maximum laminar shear occurs at around one-third of the height from the base. It will be of interest to find out the effect on the distribution of the laminar shear for adopting two different types of connecting beams. In this section, an analysis is presented for coupled shear walls with two different types of connecting beams.

Consider a coupled shear wall system, with two different types of connecting beams or connecting beams with two different types of connection, meeting at level x_1 as shown in Fig.[6.5]. By employing the continuum approach, the connecting beams are replaced by a continuous laminae with equivalent stiffness. If a cut is made along the line of contraflexure, a continuous distribution of shear force and axial force along the cut will be released. Similar to the earlier sections, let q denote the shear flow per unit height. The compatibility consideration of the vertical displacement in the upper and lower connecting media requires that,

$$l\frac{dy_1}{dx} - \frac{hc^3 q_1}{12E_{c1}I_{c1}} - \frac{1}{E}\left(\frac{1}{A_1} + \frac{1}{A_2}\right)\int_0^x T_1 dx - \delta_1 = 0 \qquad (6.77a)$$

$$l\frac{dy_2}{dx} - \frac{hc^3 q_2}{12E_{c2}I_{c2}} - \frac{1}{E}\left(\frac{1}{A_1} + \frac{1}{A_2}\right)\left(\int_0^{x_1} T_1 dx + \int_{x_1}^x T_2 dx\right) - \delta_1 = 0 \qquad (6.77b)$$

where $E_{c1}I_{c1}$ and $E_{c2}I_{c2}$ are the flexural rigidities of the connecting beams in the lower and upper media.

The moment-curvature relationships for the walls are,

$$EI\frac{d^2y_1}{dx^2} = M_a - T_1 l \qquad (x_1 \le x \le H) \qquad (6.78a)$$

$$EI\frac{d^2y_2}{dx^2} = M_a - T_2 l \qquad (0 \le x \le x_1) \qquad (6.78b)$$

For the upper and lower segments of the walls, the axial force at any level x is given by,

$$T_2 = \int_x^H q_2 dx \qquad (6.79a)$$

$$T_1 = \int_x^{x_1} q_1 dx + \int_{x_1}^H q_2 dx \qquad (6.79b)$$

Differentiating equations (6.77a) and (6.77b) and combining equations (6.78a) and (6.78b), yields the governing differential

equations for the axial force T,

$$\frac{dT_1^2}{dx^2} - \alpha_1^2 T_1 = -\beta_1^2 M_a \tag{6.80a}$$

$$\frac{dT_2^2}{dx^2} - \alpha_2^2 T_2 = -\beta_2^2 M_a \tag{6.80b}$$

where

$$\beta_1^2 = \frac{12 I_{c1} l}{hc^3 I} \tag{6.81a}$$

$$\alpha_1^2 = \beta_1^2 \left(1 + \frac{AI}{A_1 A_2 l} \right) \tag{6.81b}$$

$$\beta_2^2 = \frac{12 I_{c2} l}{hc^3 I} \tag{6.82a}$$

$$\alpha_2^2 = \beta_2^2 \left(1 + \frac{AI}{A_1 A_2 l} \right) \tag{6.82b}$$

Therefore,

$$\alpha_2^2/\beta_2^2 = \alpha_1^2/\beta_1^2 = \left(1 + \frac{AI}{A_1 A_2 l} \right) \tag{6.83}$$

The complete solutions to equations (6.80a) and (6.80b) are as follows,

$$T_1 = B_3 \cosh\alpha_1 x + C_3 \sinh\alpha_1 x + \frac{\beta_1^2}{\alpha_1^2}\left\{ M_a + \frac{w}{\alpha^2} + \frac{w_t H x}{(\alpha H)^2} \right\} \tag{6.84a}$$

$$T_2 = D_3 \cosh\alpha_2 x + E_3 \sinh\alpha_2 x + \frac{\beta_2^2}{\alpha_2^2}\left\{ M_a + \frac{w}{\alpha^2} + \frac{w_t H x}{(\alpha H)^2} \right\} \tag{6.84b}$$

where B_3, C_3, D_3 and E_3 are integration constants.

Differentiating equations (6.83a) and (6.83b), the expressions for q_1 and q_2 are given by,

$$q_1 = -\alpha_1 (B_3 \sinh\alpha_1 x + C_3 \cosh\alpha_1 x) - \frac{\beta_1^2}{\alpha_1^2}\left\{ \frac{dM_a}{dx} + \frac{w_t H}{(\alpha_1 H)^2} \right\} \tag{6.85a}$$

$$q_2 = -\alpha_2 (D_3 \sinh\alpha_2 x + E_3 \cosh\alpha_2 x) - \frac{\beta_2^2}{\alpha_2^2}\left\{ \frac{dM_a}{dx} + \frac{w_t H}{(\alpha_2 H)^2} \right\} \tag{6.85b}$$

The values of the integration constants B_3, C_3, D_3 and E_3 can be determined by considering the boundary conditions.

At the top of the structure, x=H, the axial force in the walls is equal to zero, that is

$$T_{2(x=H)} = 0 \tag{6.86}$$

From equations (6.77a) and (6.77b) the boundary condition at level x_1 for the laminar shear flow intensity q_1 and q_2 is,

$$q_1 = \gamma_3 \, q_2 \tag{6.87}$$

where $\gamma_3 = \dfrac{E_{c1} I_{c1}}{E_{c2} I_{c2}}$

From equations (6.79a) and (6.79b) the boundary condition at level x_1 for the axial forces of the wall is,

$$T_{1(x=x_1)} = T_{2(x=x_1)} \tag{6.88}$$

Considering the compatibility equation at the base, x=0, the following equation is obtained.

$$q_{1(x=0)} = K_r M_{a(x=0)} - K_{rv} T_{1(x=0)} \tag{6.89}$$

Solving equations (6.86), (6.87), (6.88) and (6.89), the integration constants B_3, C_3, D_3 and E_3 can be obtained.

$$B_3 = \frac{\psi_{11} - \psi_{10}}{\psi_9 - \psi_{12}} \tag{6.90a}$$

$$C_3 = \psi_5 + \left(\frac{\psi_{11} - \psi_{10}}{\psi_9 - \psi_{12}}\right)\frac{K_{rv}}{\alpha_1} \tag{6.90b}$$

$$D_3 = -\left[\left(\frac{\psi_{11} - \psi_{10}}{\psi_9 - \psi_{12}}\right)\psi_9 + \psi_{10}\right]\tanh\alpha_2 H - \psi_1 \qquad (6.90c)$$

$$E_3 = \left(\frac{\psi_{11} - \psi_{10}}{\psi_9 - \psi_{12}}\right)\psi_9 + \psi_{10} \qquad (6.90d)$$

where

$$\psi_1 = \frac{\beta_2^2}{\alpha_2^2}\frac{1}{\cosh\alpha H}(w + w_t)$$

$$\psi_2 = \cosh\alpha_2 x_1$$

$$\psi_3 = \sinh\alpha_2 x_1$$

$$\psi_4 = \frac{\beta_2^2}{\alpha_2^2}\left(\frac{1}{\alpha_1^2} - \frac{1}{\alpha_2^2}\right)\left(w - \frac{w_t x_1}{H}\right)$$

$$\psi_5 = \gamma_3 \frac{\alpha_1 \sinh\alpha_1 x_1}{\alpha_2 \cosh\alpha_2 x_1}$$

$$\psi_6 = \gamma_3 \frac{\alpha_1 \cosh\alpha_1 x_1}{\alpha_2 \cosh\alpha_2 x_1}$$

$$\psi_7 = \frac{\beta_2^2}{\alpha_2^3}\frac{1}{\cosh\alpha_2 x_1}\left\{\left[\frac{dM_a}{dx} + \frac{w_t H}{(\alpha_1 H)^2}\right] - \gamma_3\left[\frac{dM_a}{dx} + \frac{w_t H}{(\alpha_2 H)^2}\right]\right\}$$

$$\psi_8 = -\frac{\beta_1^2}{\alpha_1^3}\left[-P - wH - \frac{w_t H}{2} + \frac{w_t H}{(\alpha_1 H)^2}\right] - \frac{K_r M_{a(x=0)}}{\alpha_1}$$

$$+ \frac{(1K_r + K_v)}{\alpha_1} + \frac{\beta_1^2}{\alpha_1^2} K_{rv}\left(M_{a(x=0)} + \frac{w}{\alpha_1}\right)$$

$$\psi_9 = \frac{\cosh\alpha x_1 + \frac{K_{rv}}{\alpha_1}}{\psi_3 - \psi_2 \tanh\alpha_2 H}$$

$$\psi_{10} = \frac{\psi_8 \sinh\alpha_1 x_1 + \psi_1\psi_2 - \psi_4}{\psi_3 - \psi_2 \tanh\alpha_2 H}$$

$$\psi_{11} = \frac{\psi_8\psi_6 + \psi_1 \tanh\alpha_2 x_1 + \psi_7}{1 - \tanh\alpha_2 H \tanh\alpha_2 x_1}$$

$$\psi_{12} = \frac{\psi_5 + \frac{K_{rv}}{\alpha_2}}{1 - \tanh\alpha_2 H \tanh\alpha_2 x_1}$$

Once the axial forces T_1 and T_2 are determined, then by integrating equations (6.3a) and (6.3b) twice, and using the boundary conditions,

$$y_{1(x=0)} = 0 \qquad (6.91a)$$

$$\left(\frac{dy_1}{dx}\right)_{(x=0)} = \vartheta_{(x=0)} \qquad (6.91b)$$

$$y_{2(x=x_1)} = y_{1(x=x_1)} \tag{6.91c}$$

$$\left(\frac{dy_1}{dx}\right)_{(x=x_1)} = \left(\frac{dy_2}{dx}\right)_{(x=x_1)} \tag{6.91d}$$

The equations governing the lateral deflection of the structure can be found as,

$$y_1 = \frac{L(x)}{EI} - \frac{1}{EI} 1 \left\{ \frac{B_3}{\alpha_1^2} \cosh\alpha_1 x + \frac{C_3}{\alpha_1^2} \sinh\alpha_1 x + \frac{\beta_1^2}{\alpha_1^2} \left[L(x) + \frac{wx^2}{2\alpha_1} + \frac{w_t H x^3}{6(\alpha_1 H)^2} \right] \right\} + F_3 x + G_3 \tag{6.92a}$$

$$y_2 = \frac{L(x)}{EI} - \frac{1}{EI} 1 \left\{ \frac{D_3}{\alpha_2^2} \cosh\alpha_2 x + \frac{E_3}{\alpha_2^2} \sinh\alpha_2 x + \frac{\beta_2^2}{\alpha_2^2} \left[L(x) + \frac{wx^2}{2\alpha_2} + \frac{w_t H x^3}{6(\alpha_2 H)^2} \right] \right\} + H_3 x + I_3 \tag{6.92b}$$

Using the boundary condition in equation (6.43b),

$$F_3 = \frac{1}{EI} \left[\frac{PH^2}{2} + \frac{wH^3}{6} + \frac{w_t H^3}{8} + \frac{C_3 1}{\alpha} - \frac{\beta_1^2}{\alpha_1^2} 1 \left(\frac{wH^3}{6} + \frac{w_t H^3}{8} + \frac{PH^2}{2} \right) \right] + \vartheta_{(x=0)}$$

$$G_3 = \frac{1}{EI}\left[\frac{B_1 l}{\alpha_1^2} + \frac{\beta_1^2}{\alpha_1^2} l \left(\frac{wH^4}{24} + \frac{w_t H^4}{30} + \frac{PH^3}{6}\right)\right.$$

$$\left. - \left(\frac{wH^4}{24} + \frac{w_t H^4}{30} + \frac{PH^3}{6}\right)\right]$$

$$H_3 = \frac{1}{EI}\left[\frac{l \sinh\alpha_2 x_1}{\alpha_2} D_3 + \frac{l \cosh\alpha_2 x_1}{\alpha_2} E_3\right]$$

$$+ \frac{1}{EI}\left[\frac{l \cosh\alpha_2 x_1}{\alpha_2} B_3 + \frac{l \sinh\alpha_2 x_1}{\alpha_2} C_3\right]$$

$$+ \frac{\beta_2^2}{\alpha_2^2}\left(\frac{1}{\alpha_2^2} - \frac{1}{\alpha_1^2}\right)\left(wx_1 - \frac{w_t x_1^2}{2H}\right) + F_3$$

The above equations have been derived to assist in the design of stiffened coupled walls, with different stiffening arrangements, supported on elastic foundations and subjected to the standard pattern of lateral loadings. As more stiffening beams are introduced, the equations for determining the forces in the system become more complex.

The equations for laminar shear q, the axial force in the walls T, the shear force in the stiffening beam Q and the lateral deflection of the structure y for the above cases are established. It is more convenient and useful to use their nondimensional form to enable design curves to be drawn.

$$q = \frac{\beta^2}{\alpha^2} (wH + w_t H + P)\, q^*$$

$$\frac{\beta^2}{\alpha^2} = \frac{1}{(1+\eta)1}$$

where

$$\eta = \frac{AI}{A_1 A_2 l^2}$$

$$Q = \frac{\beta^2}{\alpha^2} (wH^2 + w_t H^2 + PH)\, Q^*$$

$$T = \frac{\beta^2}{\alpha^2} (wH^2 + w_t H^2 + PH)\, T^*$$

$$y = \left(\frac{wH^4}{8EI} + \frac{11 w_t H^4}{120EI} + \frac{PH^3}{3EI} \right) y^*$$

where q*, Q*, T* amd y* are the nondimensional form of q, Q, T and y respectively.

From the equations derived in the above sections for any given loads, the terms q, T and Q are related to the structural parameters x, x_1, x_2, $\beta^2 l/\alpha^2$, αH, $\alpha_1 H$, $\alpha_2 H$, γ_1, γ_2 and γ_3, which can be expressed more conveniently in nondimensional form as,

$x/H = \xi$ (height ratio)

$x_1/H = \xi_1$ (height ratio for stiffening beam 1)

$x_2/H = \xi_2$ (height ratio for stiffening beam 2)

$\beta^2 l/\alpha^2 = V$ (drift reduction factor)

$\alpha H = K$ (effectiveness of the coupling beams)

$\alpha_1 H = K1$ (effectiveness of the coupling beams 1)

$\alpha_2 H = K2$ (effectiveness of the coupling beams 2)

$\gamma_1/H = G1$ (relative stiffness of the stiffening beam 1)

$\gamma_2/H = G2$ (relative stiffness of the stiffening beam 2)

$\gamma_3/H = G3$ (relative stiffness of coupling beams

For convenience the above nondimensional structural parameters K, K1, K2 and G1, G2 and G3 are used in the design curves.

6.3 SIGNIFICANCE OF STRUCTURAL PARAMETERS

The preceding mathematical developments of the analysis give rise to several parameters such as V, K, K1, K2, G1, G2 and G3. As shown in equations (6.50), (6.57), (6,76) and (6.93), drift depends upon the parameter $\beta^2 l/\alpha^2$ or V. The dimensionless parameter V is defined as

$$V = \frac{\beta^2}{\alpha^2} l = \frac{1}{(1+\eta)}$$

It can be seen from the above expressions that V is a function of the properties of the walls as well as the spacing of the centroids of the walls. It shows that V can assume a maximum value of unity (i.e. for AI very small in comparison to $A_1 A_2 l^2$) and V decreases as the ratio $AI/(A_1 A_2 l^2)$ increases. The influence of the drift reduction factor on the deflection of the top of the

structure can be seen later in the design graphs.

In order to illustrate the physical meaning of V, the structural data in the example structure shown in Fig.[6.6] are used. With other properties remaining constant and varying only the parameters l, I, A_1 and A_2, a summary of the study is given below.

I m^4	l m	A_1 m^2	A_2 m^2	η	V	Comment
42.6	10	4	4	0.213	0.824	Example structure as basis
64.0	10	6	6	0.213	0.824	Wall thickness increase by 50%
42.6	15	4	4	0.0947	0.914	Longer coupling lever arm

It can be seen from the above study that the spacing of the centroids of the walls is the governing factor for V. Increase or decrease in wall thickness will not change the reduction factor V.

The other governing dimensionless parameter for the deflection of the structure is αH or K which is defined as

$$K = \left[(1+\eta)\frac{12 I_c l^2 Hn}{c^3 I} \right]^{0.5}$$

where n (=H/h) is the number of storeys.

Based on the example structure (H=60m, n=20), a summary of a study to illustrate the physical meaning of K is given below.

I_c m^4	l m	c m	I m^4	K	Comment
0.001543	10	2	42.6	2.812	Example structure,beam depth=0.33m
0.005208	10	2	42.6	5.167	Beam depth increase to 0.50m
0.001543	15	2	42.6	4.007	Coupling lever arm increase by 50%
0.001543	10	4	42.6	0.994	The connecting beam more slender
0.001543	10	2	64	2.294	Wall thickness increase by 50%

It can be seen that the parameter K represents the strength of the connecting beams. It is dependent on the clear span and depth of connecting beam. The stiffer the connecting beams, other factors being constant, the less the deflection of the structure will become. Usually, the values of K range from 1 to 10.

For the coupled shear wall structure further stiffened by one stiffening beam, deflection will depend on the dimensionless parameter G1. If the structure involves two stiffening beams, the deflection will depend on G1 and G2. If, as is commonly the case, the elastic modulus for both stiffening beams and coupling beams is the same. Also, if the beams are rectangular and of the same thickness, the depth of a stiffening beam to that of the main connecting beams is equal to $(G_1 n)^{1/3}$ or $(G_2 n)^{1/3}$. For coupled shear walls of ten to thirty storeys (i.e.n=10 to 30) with connecting beam depth d_c, the depth of the stiffening beams corresponding to the relative stiffness factors G1 or G2 are tabulated below.

G1 or G2	Depth of stiffening beam		
	n=10	n=20 (d_c)	n=30
0.2	1.26	1.59	1.82
1.0	2.15	2.71	3.10
5	3.68	4.64	5.31
10	4.64	5.85	6.69

The relative stiffness factor G_1 or G_2 of above 5 would imply virtually no opening between floors and utilising the whole storey height for the implementation of the stiffening beam. The way to ease the problem might be to either increase the beam width or adopt a steel stiffening beam. There could still be a problem of headroom. The depth of stiffening beam adopted to control the deflection and stress very often will be restrained by the minimum required headroom of the floor. Usually the stiffening beams are implemented on the storeys which are used for purposes such as storage or mechanical plant.

6.4 PERFORMANCE OF COUPLED SHEAR WALL STRUCTURES

On the basis of the above derivations, similar studies as in Chapter 2 can be made on the performance of stiffening systems which involve the use of stronger coupling beams and one or more stiffening beams in the height of the structure. The structural performance of the whole structure will depend on the arrangement

of the stiffening system employed. In order to achieve an economical and efficient design of the coupled shear wall structure, it is important to gain knowledge in the efficiency of the stiffening system on structural performance of the structure.

In the following sections, an attempt is made to define the efficiency of the stiffening system of a coupled shear wall structure for a rigid foundation case with respect to the reduction of top drift and base moment.

6.4.1 REDUCTION OF THE TOP DRIFT

A useful measure of the influence of the stiffening on top drift is to express the reduction in the top drift as a percentage of the maximum possible top drift reduction y_c which is given by

$$y_c = y_{FT} - y_{Tir} \tag{6.93}$$

where y_{FT} is the top drift of the free bending of a pair of unstiffened walls with a rigid base. For a uniformly distributed load case, for example, y_{FT} is given by

$$y_{FT} = \frac{wH^4}{8EI}$$

y_{Tir} is the top drift of a pair of coupled shear walls with infinitely stiff connecting beams throughout the height. It can be

obtained by substituting a very high value of αH into equation (6.53).

The drift reduction efficiency r_y is given by

$$r_y = (y_{FT} - y_T).100/y_c \qquad (6.94)$$

where y_T is the top drift of the stiffened structure.

6.4.2 REDUCTION OF THE BASE MOMENT

The moment performance of the stiffening system can also be usefully expressed as a moment reduction efficiency r_m. In this case, the moment reduction due to the stiffening system is expressed as a percentage of the base moment reduction M_c which is given by

$$M_c = M_{aB} - M_{Bir} \qquad (6.95)$$

where M_{Bir} is the base moment of a pair of coupled shear walls with infinitely stiff connecting beams throughout the height. It can be obtained by substituting a very high value of αH into equation (6.51). Once the base axial force is obtained, the base moment can then be determined.

The moment reduction efficiency r_m is given by

$$r_m = (M_{aB} - M_B).100/M_c \qquad (6.96)$$

where M_B is the base moment of the stiffened structure.

6.5 NUMERICAL RESULTS

The numerical investigations conducted on the elastic behaviour are presented in three parts. Firstly, design curves for laminar shear flow, axial force in the walls, shear force in the stiff top beam and the maximum deflection are plotted against values of the stiffness parameter K for the case of a uniformly distributed load. These graphs compare and illustrate the influence of up to two stiffening beams on the elastic response of a coupled shear wall resting on a rigid foundation. Optimum locations of the stiffening beams are discussed. Curves showing the variation of the optimum location for one and two stiffening beams case are presented to enable the designer to determine the optimum location of the stiffening beam within the assumptions made in this Chapter. Secondly, in order to assess the effectiveness of the stiffening system on coupled shear wall structures, comparisons with efficiencies for different stiffening systems for a wide range of connecting beam stiffnesses are conducted and presented in tabular form. Thirdly, in order to investigate the influence of stiffening beams on the behaviour of a coupled shear wall structure supported on an elastic foundation, an example structure as shown in Fig.[6.6] studied by Coull [18] was considered. The results of the study are also presented in tabular form.

Graphs showing the influence of the reduction factor V on the top deflection of the structure are given in Fig.[6.7]. It can be seen that as V increases, the deflection decreases. The other factor

controlling the drift is K. The effect of K on reducing the deflection of the structure diminishes quickly when K is above 4. Figs.[6.8] and [6.9] show deflection profiles with different K values for V=0.5 and V=1.0. The variations of top drift with different locations of stiffening beams are given in Figs.[6.10] to [6.12] for different values of V. These demonstrate that the influence of the stiffening beam is most significant when the connecting beams are weak. The deflection profiles of the structure for the stiffening beam at different locations are given Fig.[6.13] and [6.14] for weak (K=1) and strong connecting beam (K=8) cases. The influence of two stiffening beams is shown in Fig.[6.15] and [6.16]. It can be seen that the influence of using two stiffening beams become less effective as K increases. For a pair of coupled shear walls with strong connecting beams (K greater than 2), the use of two stiffening beams will hardly be justified. The optimum location of a single stiffening beam is given in Fig.[6.17] for different values of G. Since the use of two stiffening beams will normally involve one being placed at the top of the structure, the optimum location of the lower stiffening beam is examined and is given in Figs.[6.17] to [6.21]. For two intermediate stiffening beams, the efficiency of use is low. However, a set of recommended optimum locations for two intermediate stiffening beam case is given in Fig.[6.22]. It is noted that for the structure with stiff connecting beams, the use of one stiffening beam or two close to each other is recommended.

The variation of laminar shear q* (in dimensionless form) with height for various values of K for coupled shear walls subjected to a uniformly distributed lateral loading is given in Figs.[6.23]

to [6.31]. It is shown that the optimum location of the stiffening beam to reduce the laminar shear in the connecting beams is around 0.3H from the base.

The axial force in the walls at the bottom of the structure plotted against values of K is given in Figs.[6.32] to [6.34]. It is noted that one of the penalties of using the stiffening beam is the higher axial force induced at the base of the structure. However, since the prime purpose of coupled shear walls is load bearing, the force at the base will normally be dominated by the compressive force. It is also noted that the stiffening beam placed near to the base of the structure will normally attract more base axial force. Variation of shear force Q* in the stiffening beam for different values of K and different stiffening beam stiffnesses is given in Figs.[6.35] to [6.37].

The wall bending moments for different stiffening beam stiffnesses and locations are presented in Figs.[6.38) to [6.45]. It is shown that the stiffening beam is quite effective in reducing the bending moment in the walls. The optimum location of the stiffening beam for minimising the bending moment in the walls is found to be around 0.3H from the base.

Normally, the maximum laminar shear occurs at around one-third of the height from the base. Therefore a study was made to investigate the use of two different connecting beams with an attempt to reduce the laminar shears in connecting beams below the one-third of the height of the structure. The general deflection profiles against different stiffness factors of the connecting

beams are given in Figs.[6.46] to [6.47]. Figs.[6.48] to [6.50] give the variation of laminar shear with locations where different connecting beams meet. The attempt to reduce the laminar shear was not successful. Fig.[6.51] to [6.53] show the variation of bending moment with height for different combinations of different connecting beam stiffnesses. The results indicate that the use of two different connecting beams can reduce the bending moment at the base of the walls by as much as 35%. The most economical position for the meeting point of different connecting beams will be near to the base. In Fig.[6.51], the maximum moment induced in the walls for K1=8 and K2=1 is 0.41 of M_{aB} whereas for walls with K=8 the maximum at the base is 0.85 M_{aB}. Similar findings to the above study are obtained for point load or triangularly distributed load and the corresponding plots for the point load case are given in Fig.[6.54] to [6.71].

The above study has demonstrated that improvement in structural performance depends on the relative flexural stiffness factors of the connecting beams αH or K and of the stiffening beam γH or G. Table [6.1] shows the results of the investigation and the comparison of efficiency of different stiffening systems on coupled shear walls. It was shown that the performance of the structure depends critically on the structural parameters αH and γH. For a plain coupled shear wall, that is without stiffening beams, the stronger the connecting beams, other factors being constant, the greater the drift reduction. However, the "law of diminishing returns" applies in that the increments of increase in efficiency reduce for each increment of αH. This diminishing effect suggests that a pair of coupled shear walls with αH of 3 to

4 would be most efficient. For plain coupled shear walls, the efficiency of the structure remains the same for other values of V as shown in Table [6.1]. For a single stiffening beam case, the improvement in efficiency due to the stiffening beam becomes less as αH increase. Generally, the justifiable maximum value of αH in the structure for the use of a single stiffening beam is around 3. For a two stiffening beams case, the results have shown that the justifiable maximum value of αH in the structure is around 2. Since the position of the critical moment in the coupled shear walls is greatly dependent on the location of stiffening beams, the base moment efficiency may not reflect the actual efficiency corresponding to the reduction in critical moment. Therefore, for the case of one or more stiffening beams, the base moment reduction efficiency is not tabulated.

The stiffness properties of the foundations chosen in the example structure are the limiting cases of dense gravel and dense sand with elastic moduli of 207 and 69 MN/m^2 respectively. For each type of supporting soil, vertical foundation flexibility alone, rotational foundational flexibility alone and a combination of both vertical and rotational flexibility were considered. The response of the structure, resting on a rigid foundation or on dense gravel and sand while subjected to a uniformly distributed lateral load of 600KN are given in Tables [6.2] to [6.4]. The cases considered are no stiffening beam, a stiffening beam at the base, at 0.3H, at 0.6H, at 1.0H and both top and bottom stiffening beams. The comparisons are made against the case where there is no stiffening beam at all in the structure.

It can be seen from column y_T of Tables [6.2] to [6.4] that the maximum deflection of laterally loaded coupled shear walls resting on a flexible foundation is larger than when the structure is resting on a rigid foundation. The introduction of a stiffening beam with G=1.35 or γ=81m at the top will normally reduce the deflection values by about 10 percent. For the flexible foundation case, the reduction of drift for γ=81 at the base and $K_\vartheta=3.22\text{x}10^{-8}$(rad/KN) due to the introduction of a stiffening beam can increase to 33%.

It is evident from the above that reductions in deflections value, caused by introducing a bottom beam into the configuration of the coupled shear wall, are lower when the structure is resting on stiff soil than on weak soil. The optimum location of the stiffening beam is around 0.3H from the base for minimising the top drift.

The vertical base deformations d are given in column 9 of Tables [6.2] to [6.3]. The introduction of top, and/or intermediate and/or bottom stiffening beams (of G=1.35 or γ=81m) causes increase in the vertical base deformation (of around 6% and 18% for weak and stiff soils respectively) when both rotation and vertical foundation flexibility are considered. Where only vertical flexibility is considered, the introduction of a top stiffening beam alone results in relatively small increases in the vertical base deformations. When a bottom stiffening beam is present, there is a big decrease (65% and 45% percent for vertical base deformation. It is evident that a stiffening beam placed at the base is very effective in reducing the vertical base

deformation when only vertical foundation flexibility is considered.

The effects of the base rotational deformation are given in column 10 of the Tables [6.3] to [6.4]. It is noted that the presence of a top stiffening beam does not cause a significant reduction in base rotations; however an intermediate stiffening beam (γ=81m) placed at 0.3H or a bottom stiff beam are much more efficient in reducing base rotations. Relatively it is more so on a weaker soil than on the stiff one. In reducing rotational deformation, the performance of a bottom stiffening beam is 20% better than an intermediate stiff beam placed at 0.3H.

The magnitude of the maximum laminar shear flow q_{max} and its position x_{max} is given in the last two columns of Tables [6.2] to [6.4]. Where only rotational foundation flexibility, or where vertical and rotational foundation flexibility are considered simultaneously, it is observed that the introduction of a top stiffening beam results in a small reduction in q_{max}. However, where an intermediate stiffening beam (0.3H) is introduced, a much larger reduction in q_{max} is achieved. The reduction is greater when only rotation flexibility is considered than when rotational and vertical flexibility are considered simultaneously. Where the soil is stiff (Table [6.3]) and only vertical flexibility is considered, the introduction of a top stiffening beam lowered q_{max}, while the introduction of only a bottom stiffening beam raised q_{max}. In the case where the soil is weak (Table [6.4]) and where only rotational flexibility is considered, the position of maximum laminar shear is near to the base of the structure.

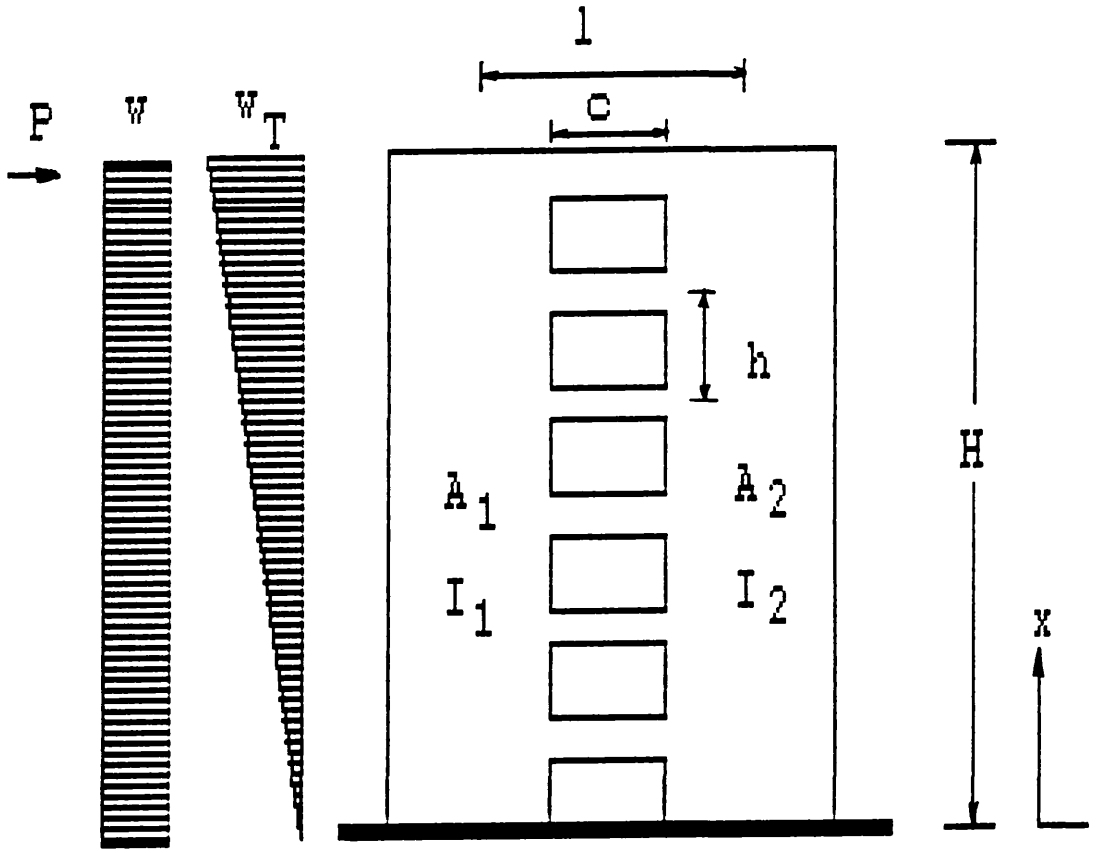

Coupled shear wall and external loads

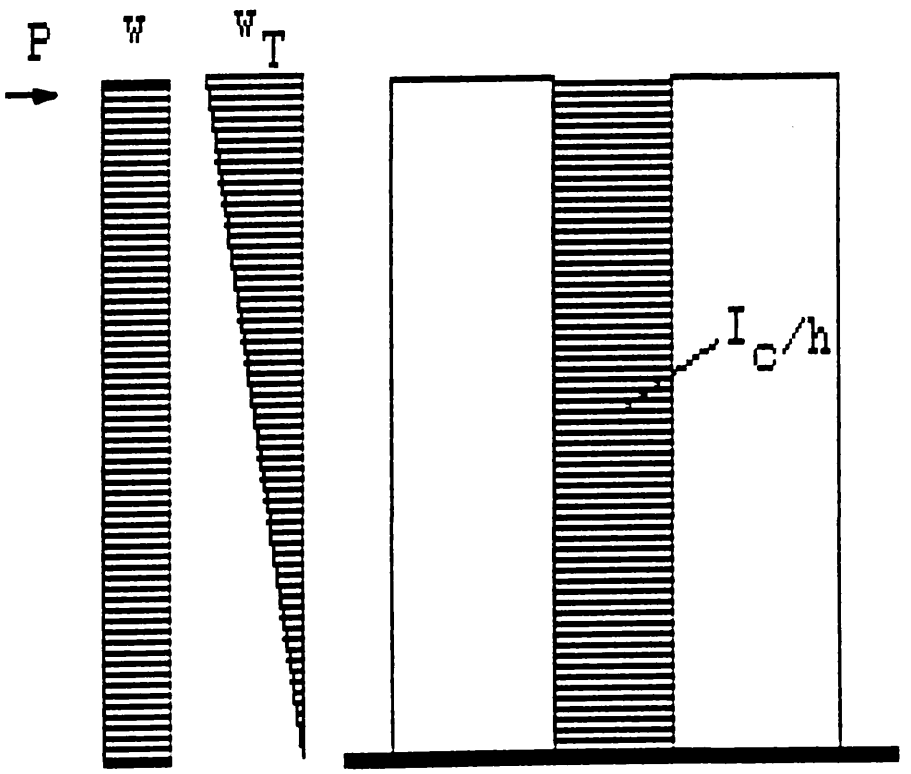

Equivalent substitute system

FIG. [6.1]

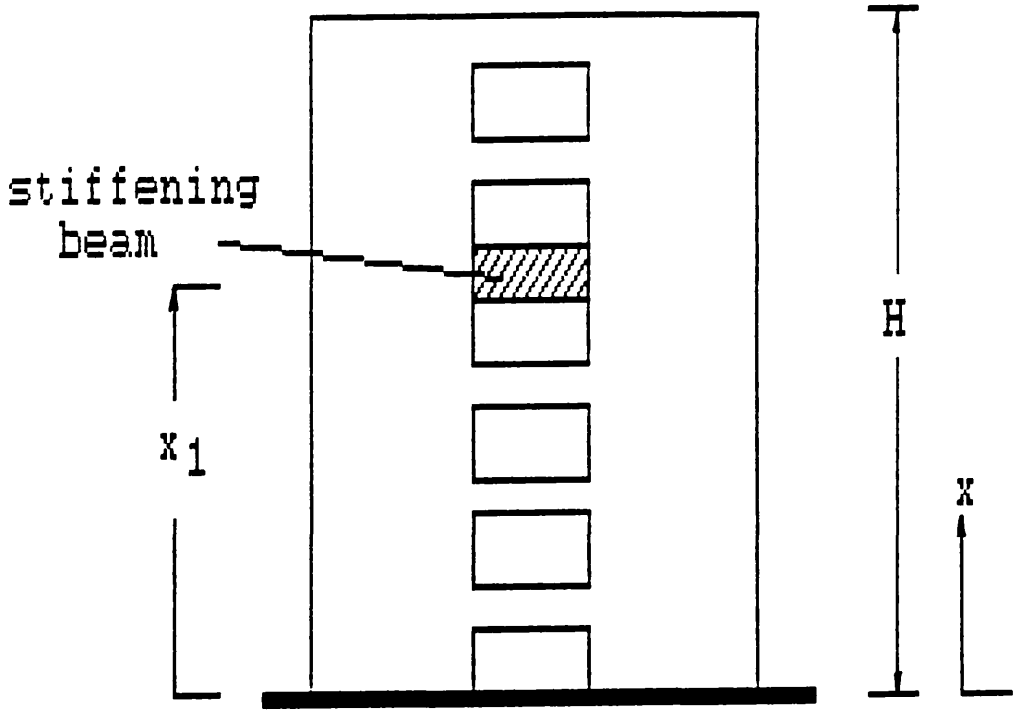

Coupled shear walls with an intermediate stiff beam

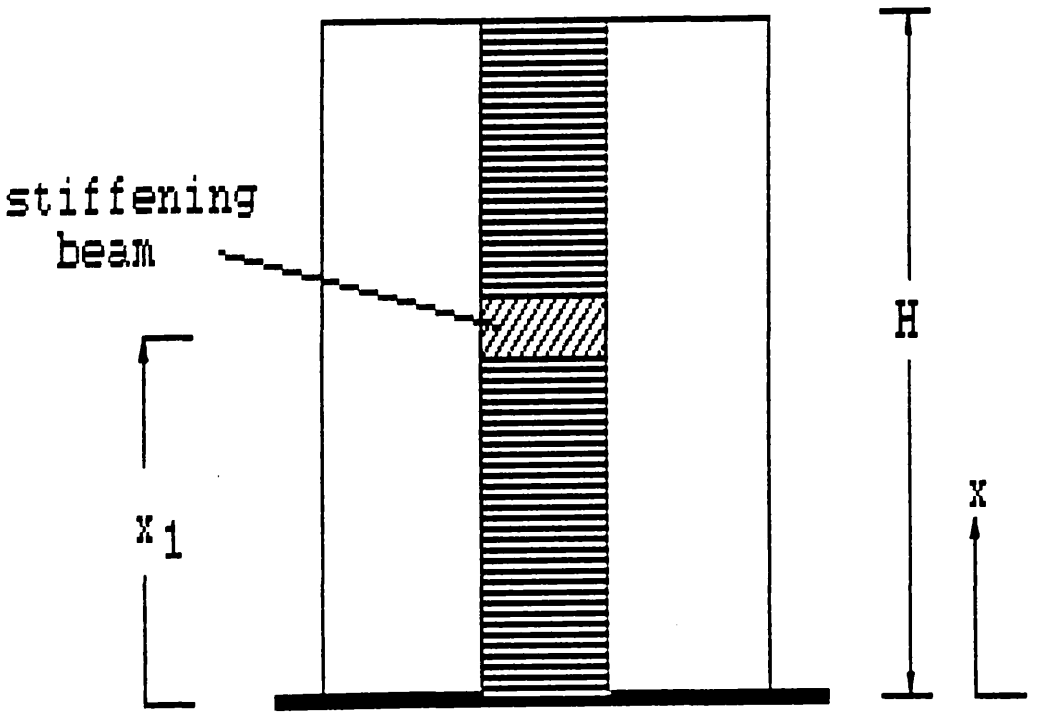

Equivalent substitute system

FIG. [6.2]

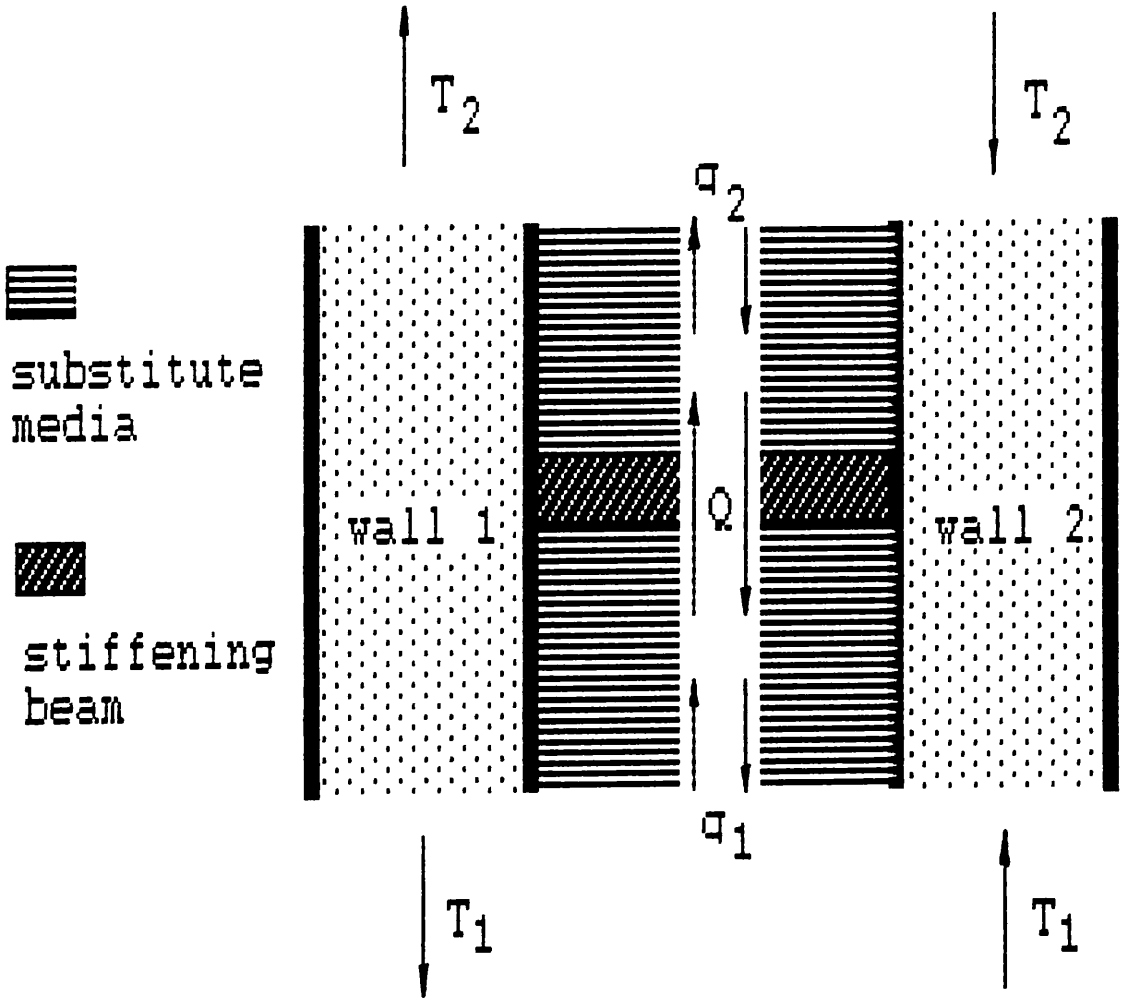

FIG. [6.3] EQUILIBRIUM OF VERTICAL FORCES AT THE STIFFENING BEAM

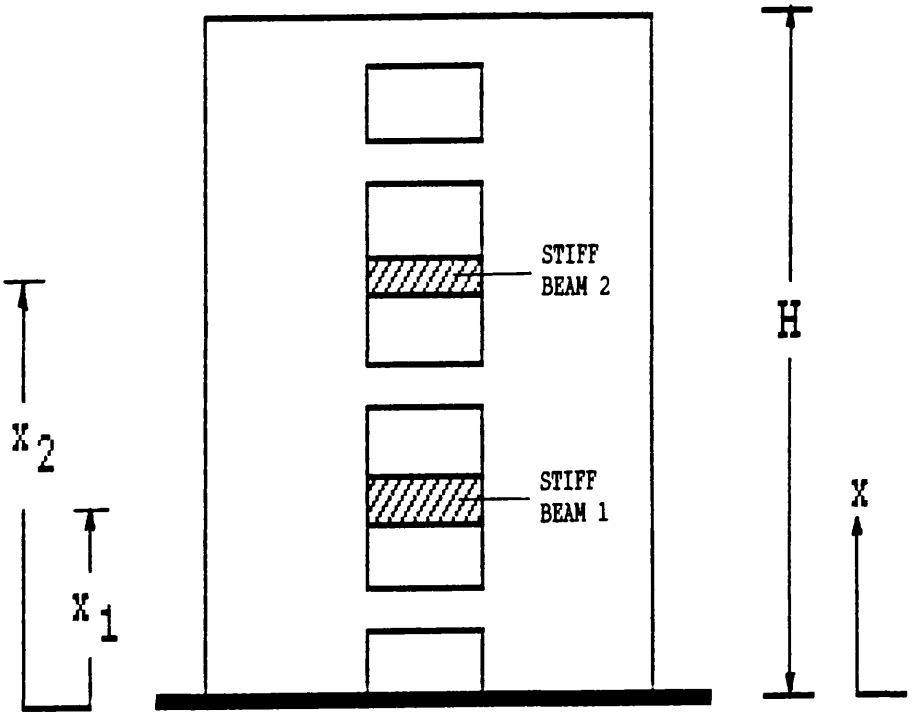

Coupled shear walls with two intermediate stiff beams

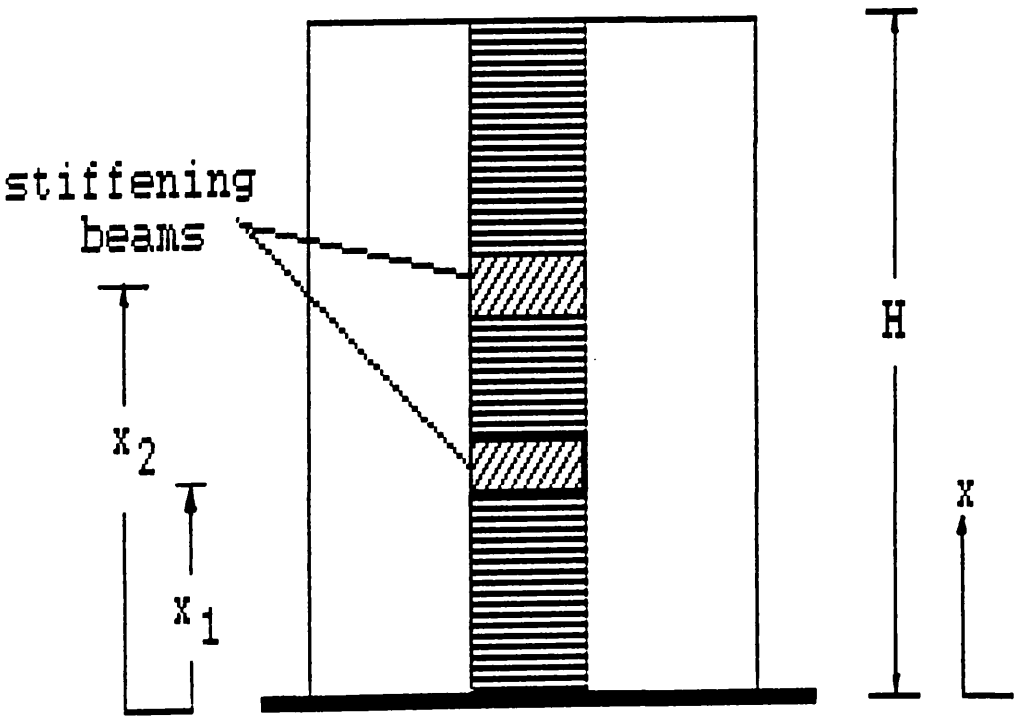

Equivalent substitue system

FIG. [6.4]

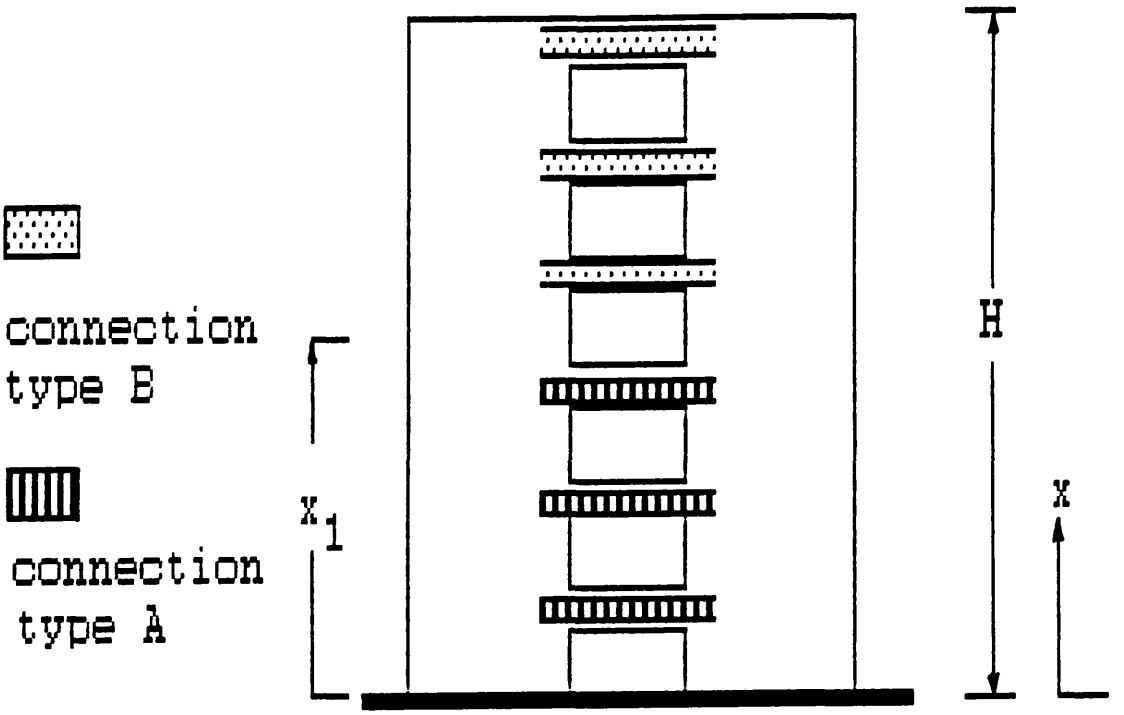

Coupled shear walls with two
different media of connecting beams

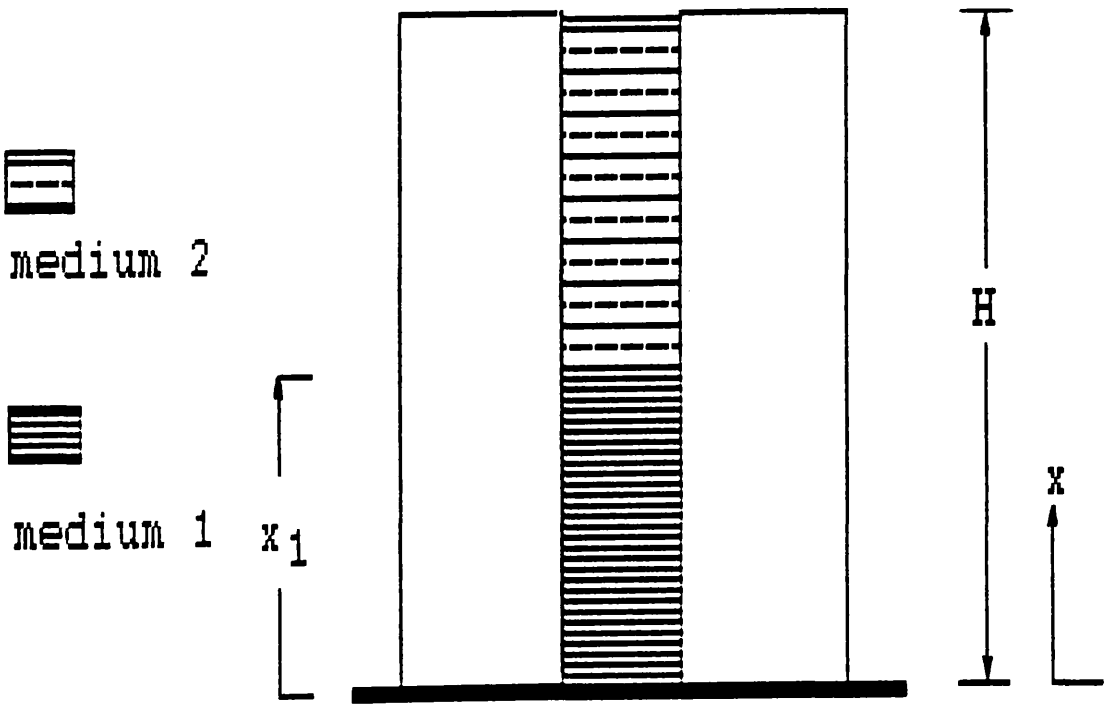

Equivalent substitute system

FIG. [6.5]

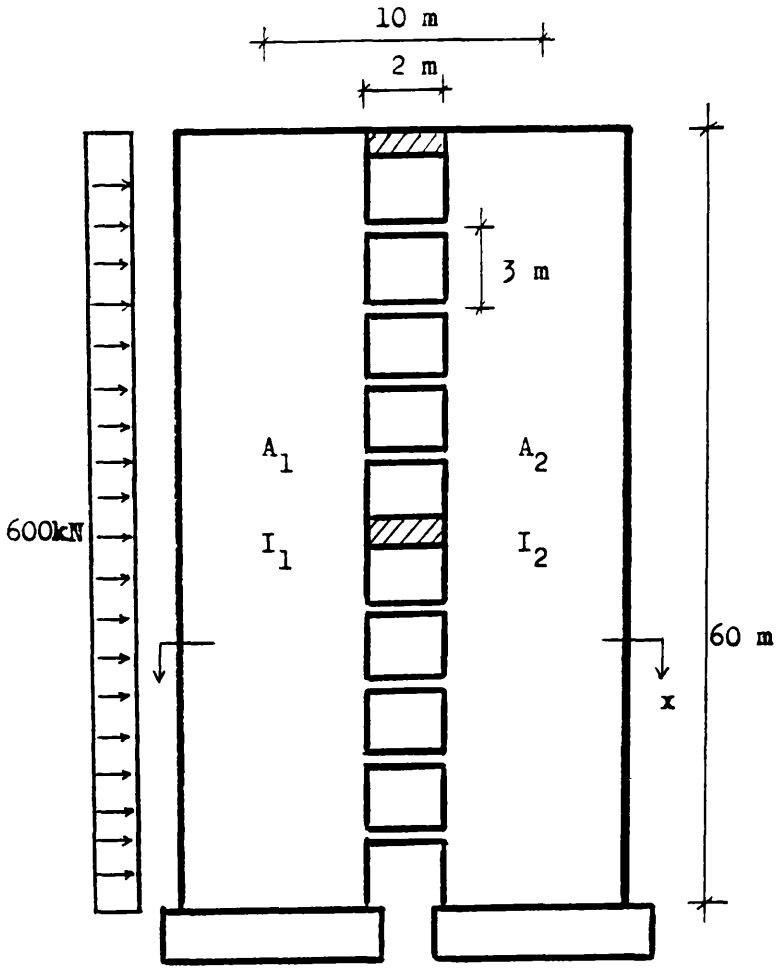

Elevation

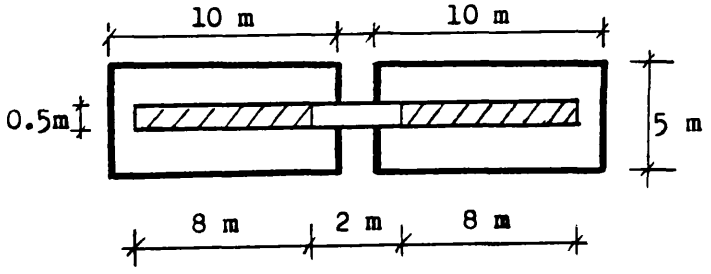

Section x-x

H = 60 m

h = 3 m

l = 10 m

c = 2 m

A_1 = 4 m^2

A_2 = 4 m^2

I_1 = 21.3 m^4

I_2 = 21.3 m^4

I_c = 0.001543 m^4

I_s = 0.04167 m^4

$\gamma_1 = \gamma_2$ = 81 m

αH = 2.812

$\frac{\beta^2}{\alpha^2} l$ = 0.8244

$E = E_s = 15 \times 10^6 kN/m^2$

E_{soil} = 207 or 69 MN/m^2

ν_{soil} = 0.3

k = stiffness moduli of the soil

$$k = \frac{E_{soil}}{i B (1 - \nu^2_{soil})}$$

B = breath of foundation

i = influence factor = 1.22

FIG. [6.6] EXAMPLE STRUCTURE [6.1]

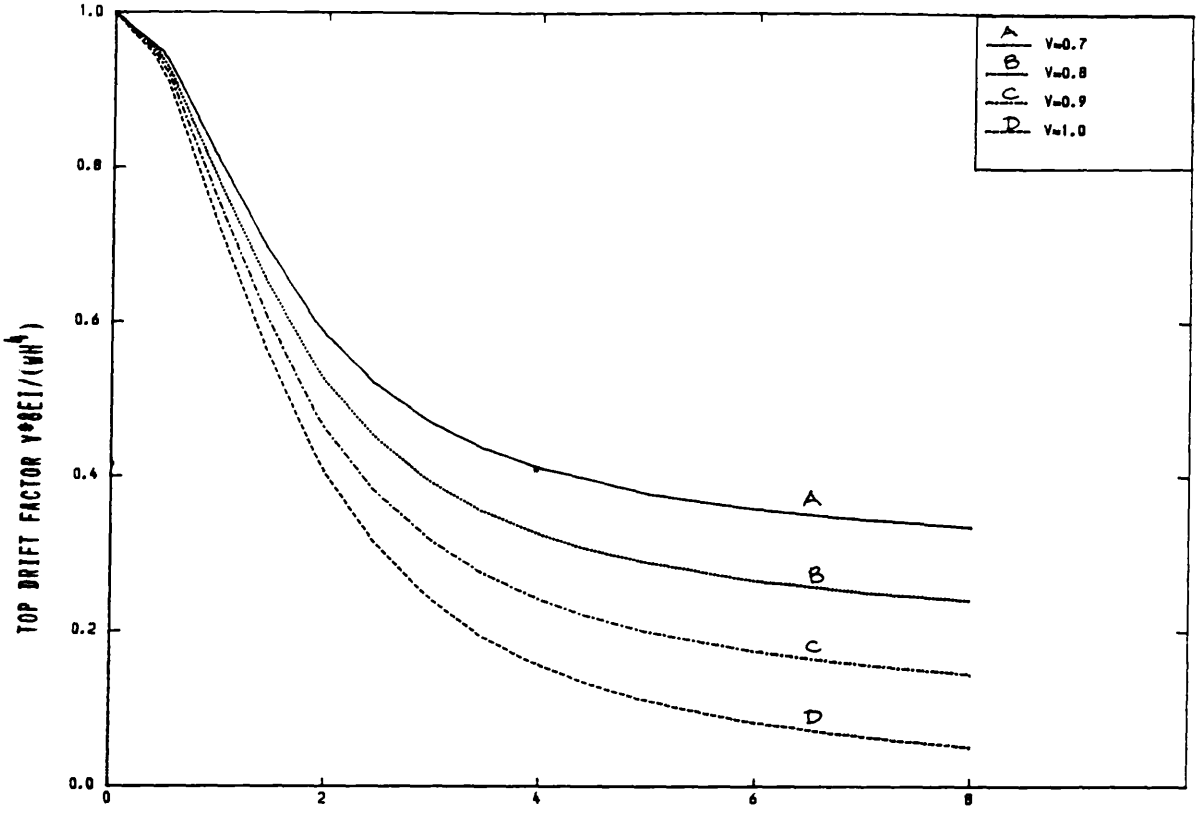

FIG. [6.7] VARIATION OF TOP DRIFT WITH STIFFNESS FACTOR K FOR DIFFERENT V
(G=0, U.D.L.)

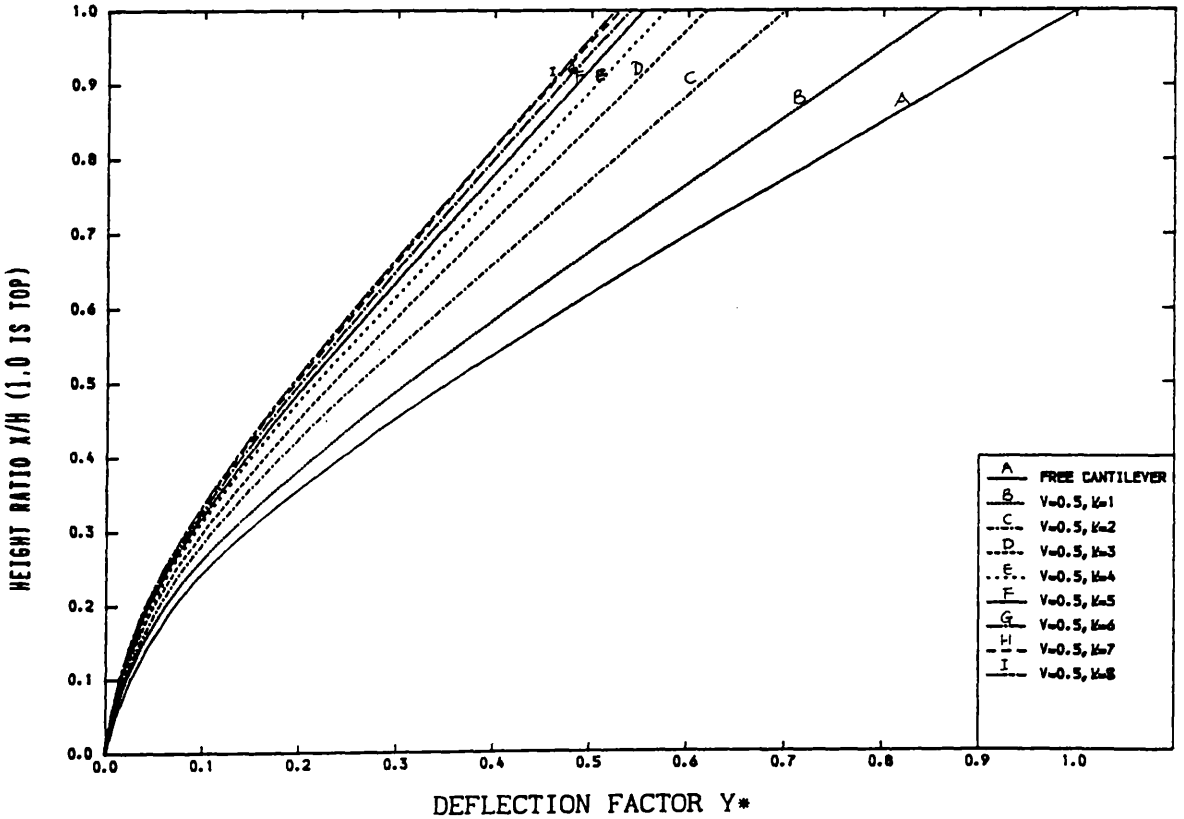

FIG. [6.8] VARIATION OF DEFLECTION WITH HEIGHT FOR DIFFERENT V AND K
(G=0, U.D.L.)

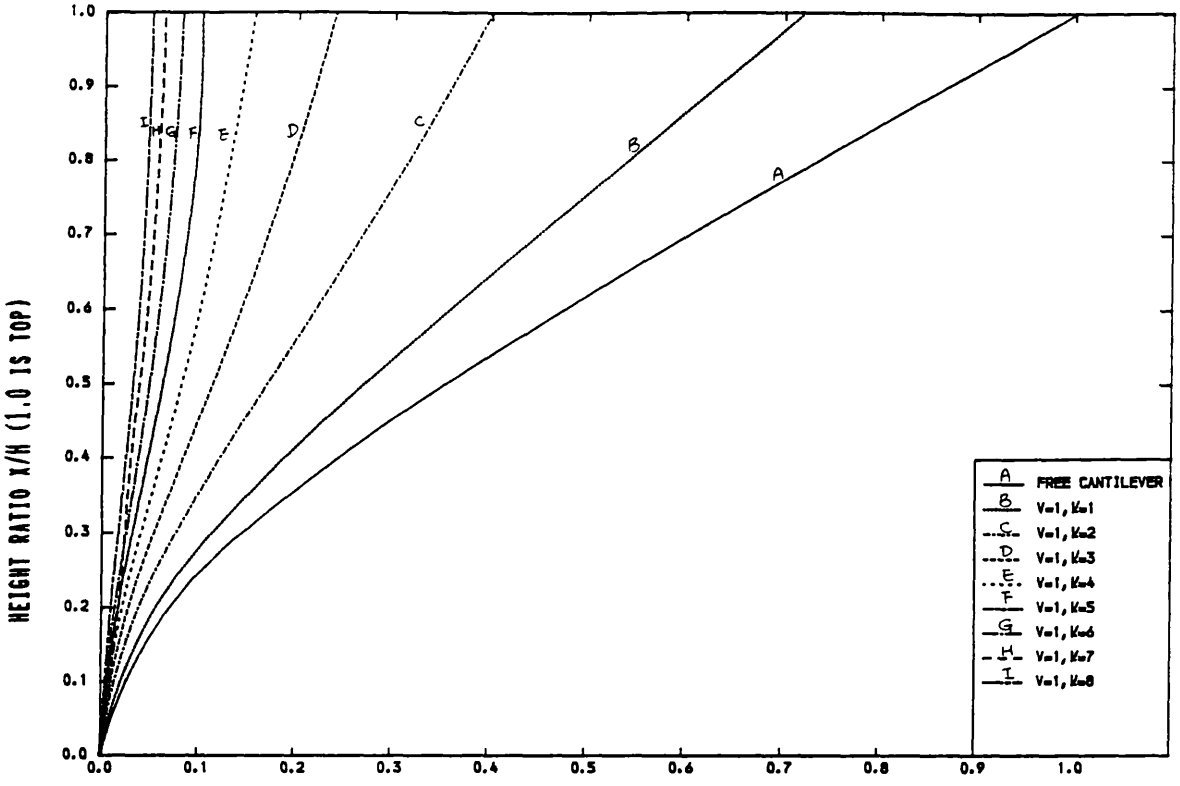

FIG. [6.9] VARIATION OF DEFLECTION WITH HEIGHT FOR DIFFERENT V AND K
(G=0, U.D.L.)

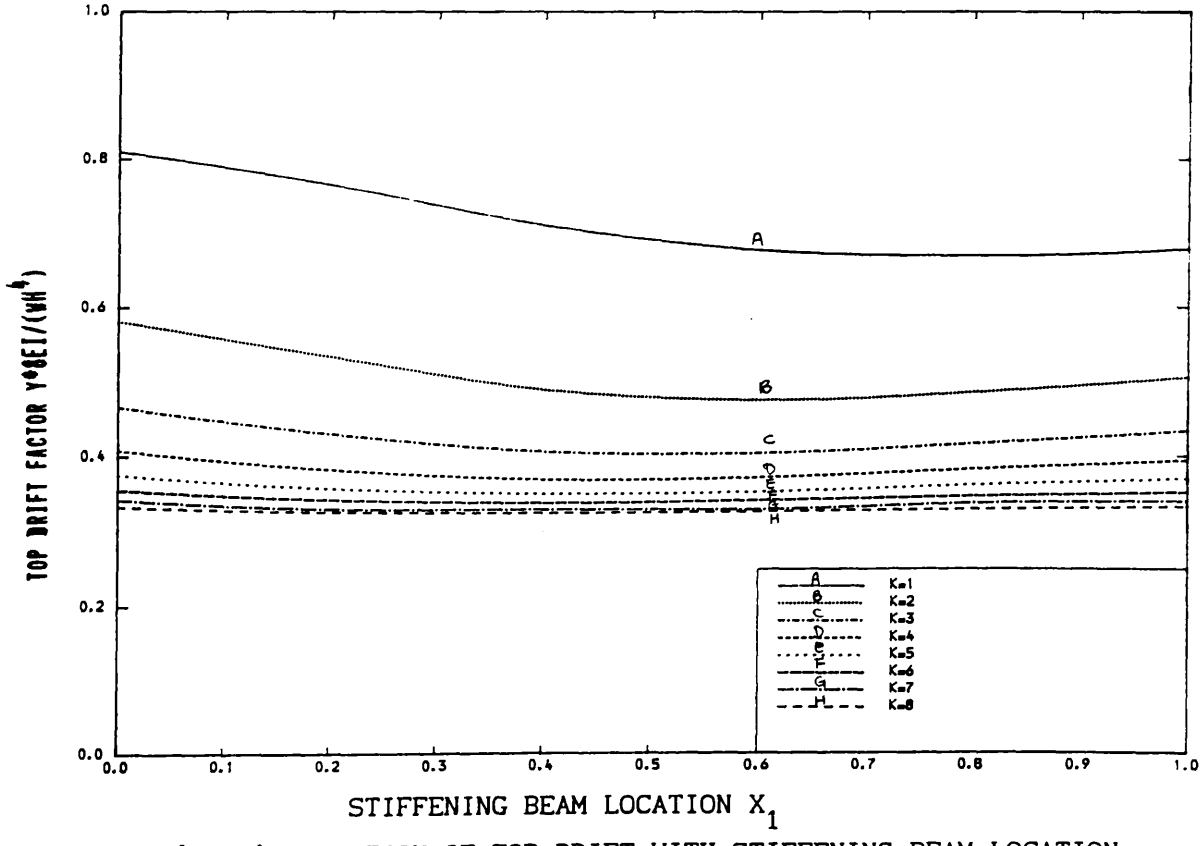

FIG. [6.10] VARIATION OF TOP DRIFT WITH STIFFENING BEAM LOCATION
(V=0.7, G=1, U.D.L.)

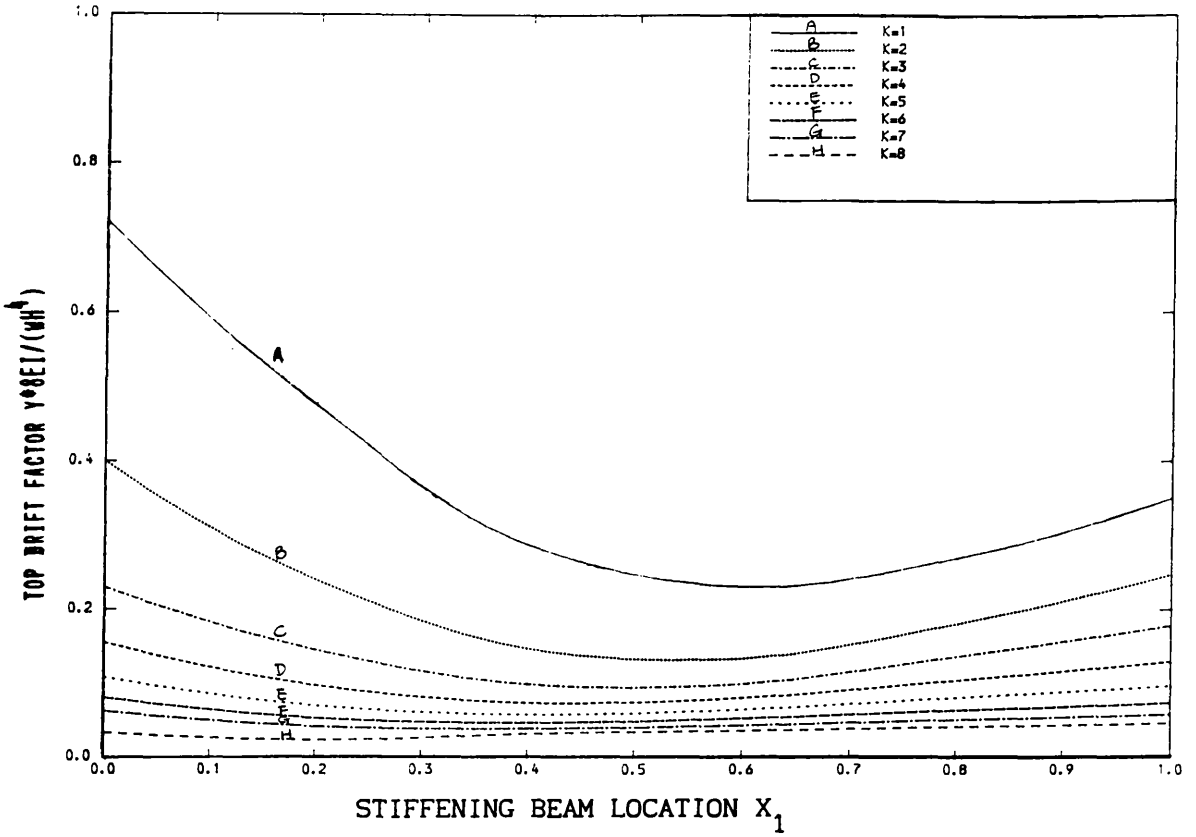

FIG. [6.11] VARIATION OF TOP DRIFT WITH STIFFENING BEAM LOCATION
(V=1.0, G=1, U.D.L.)

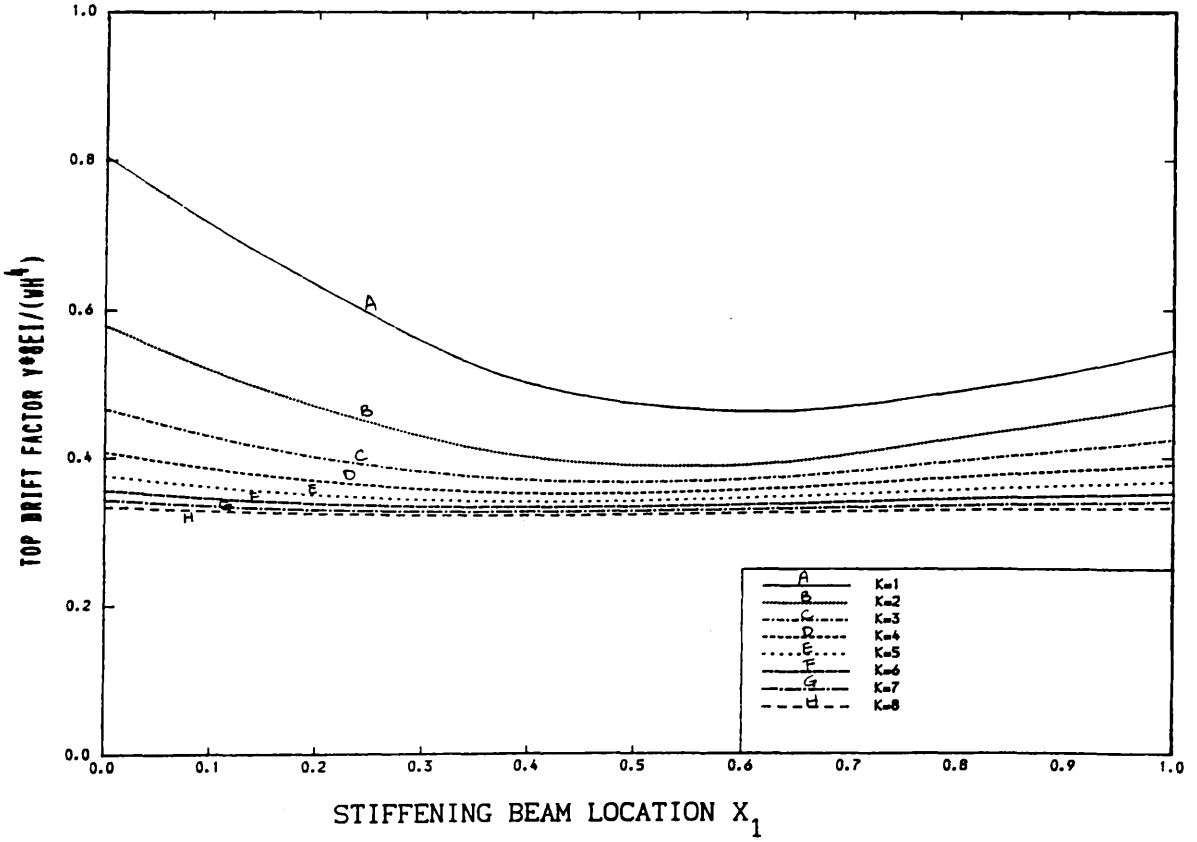

FIG. [6.12] VARIATION OF TOP DRIFT WITH STIFFENING BEAM LOCATION
(V=0.7, G=10, U.D.L.)

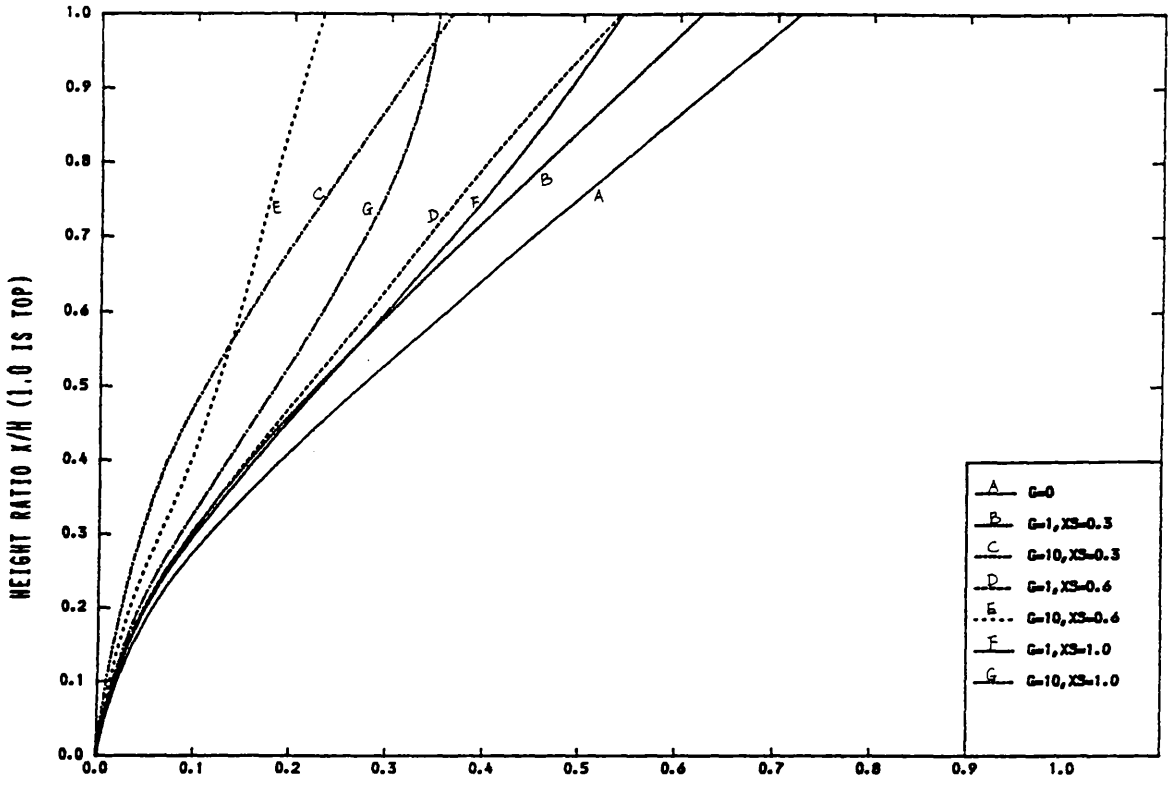

FIG. [6.13] VARIATION OF DEFLECTION WITH HEIGHT FOR DIFFERENT STIFFENING CONDITIONS
(V=1.0, K=1, U.D.L.)

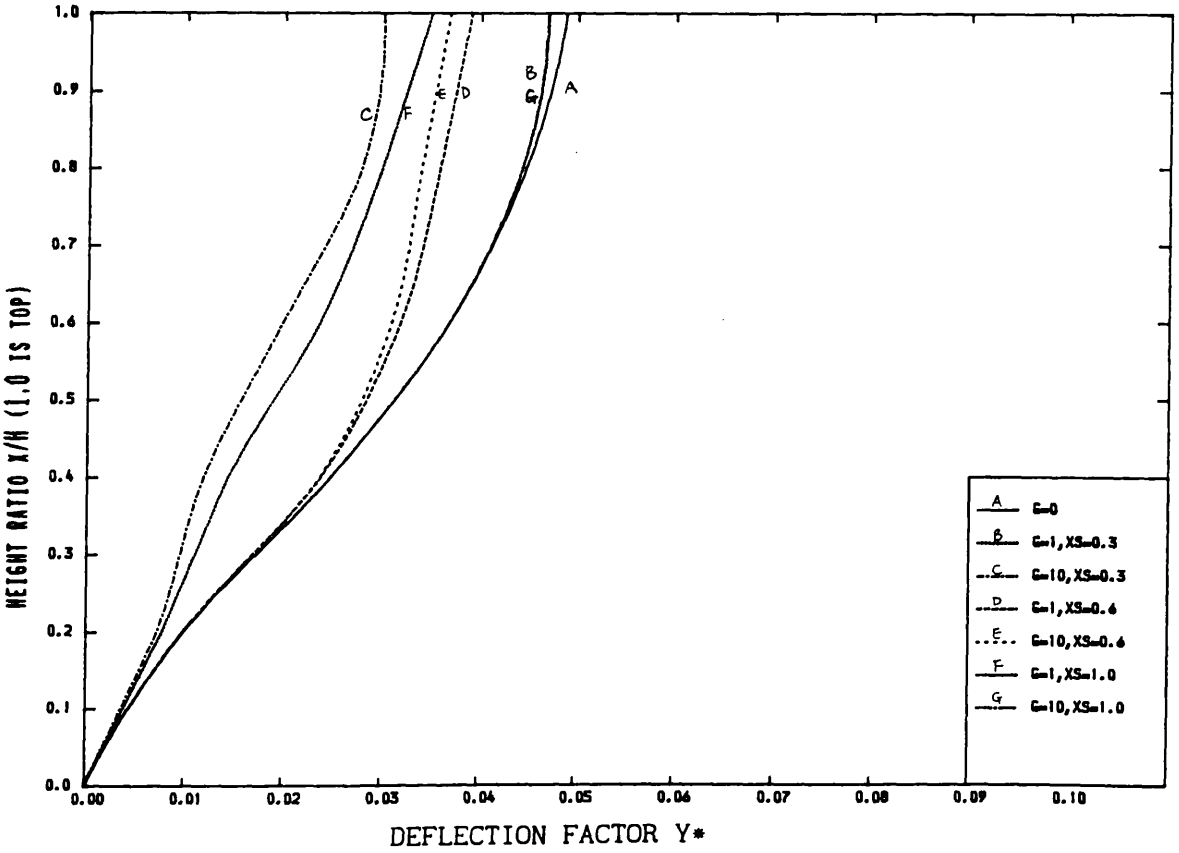

FIG. [6.14] VARIATION OF DEFLECTION WITH HEIGHT FOR DIFFERENT STIFFENING CONDITIONS
(V=1.0, K=8, U.D.L.)

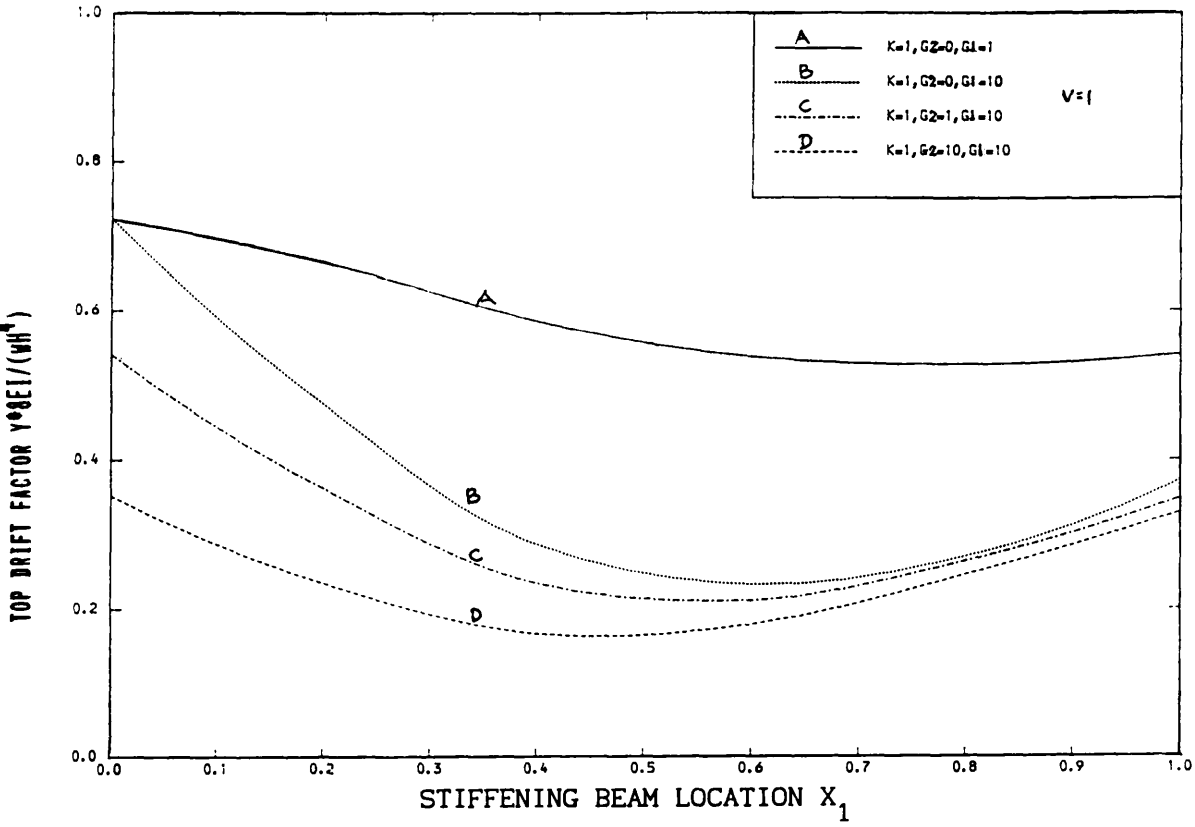

FIG. [6.15] VARIATION OF TOP DRIFT WITH STIFFENING BEAM LOCATIONS
(TOP AND INTERMEDIATE STIFFENING BEAM)
(V=1.0, U.D.L.)

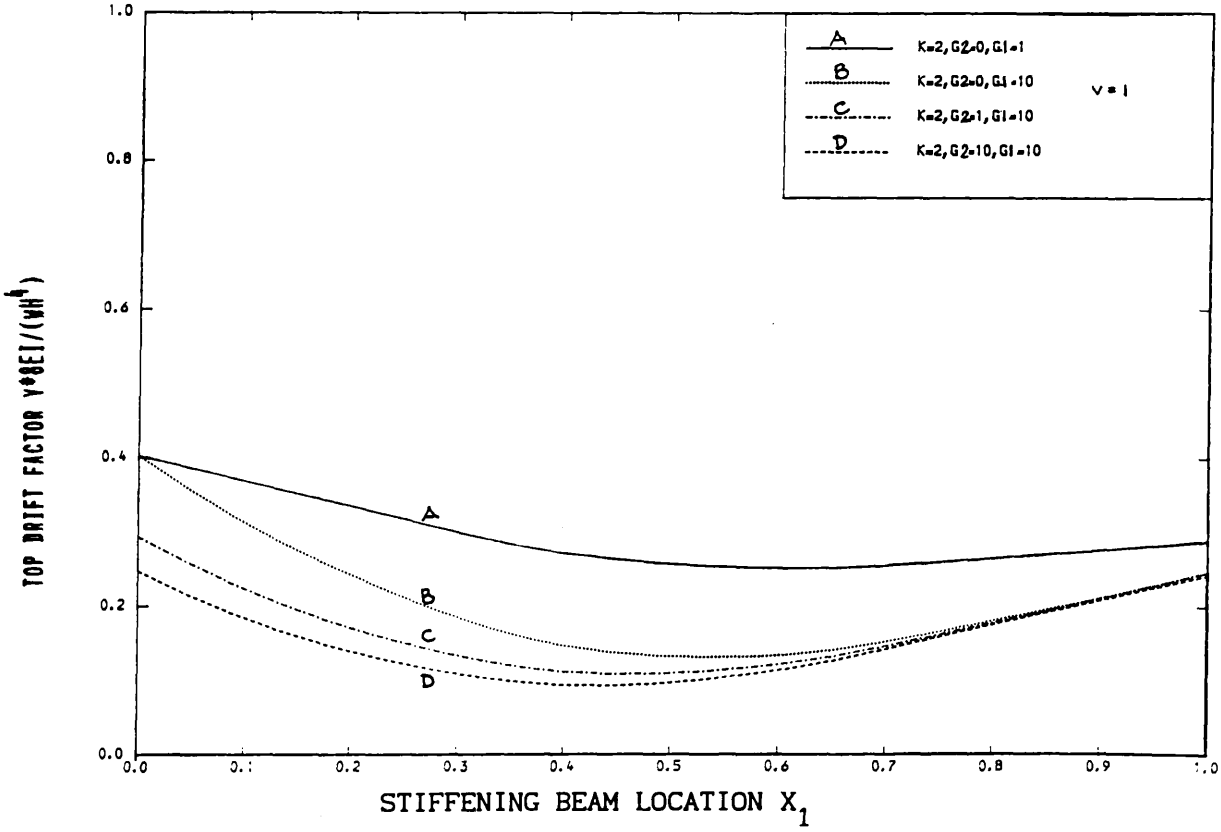

FIG. [6.16] VARIATION OF TOP DRIFT WITH STIFFENING BEAM LOCATIONS
(TOP AND INTERMEDIATE STIFFENING BEAM)
(V=1.0, U.D.L.)

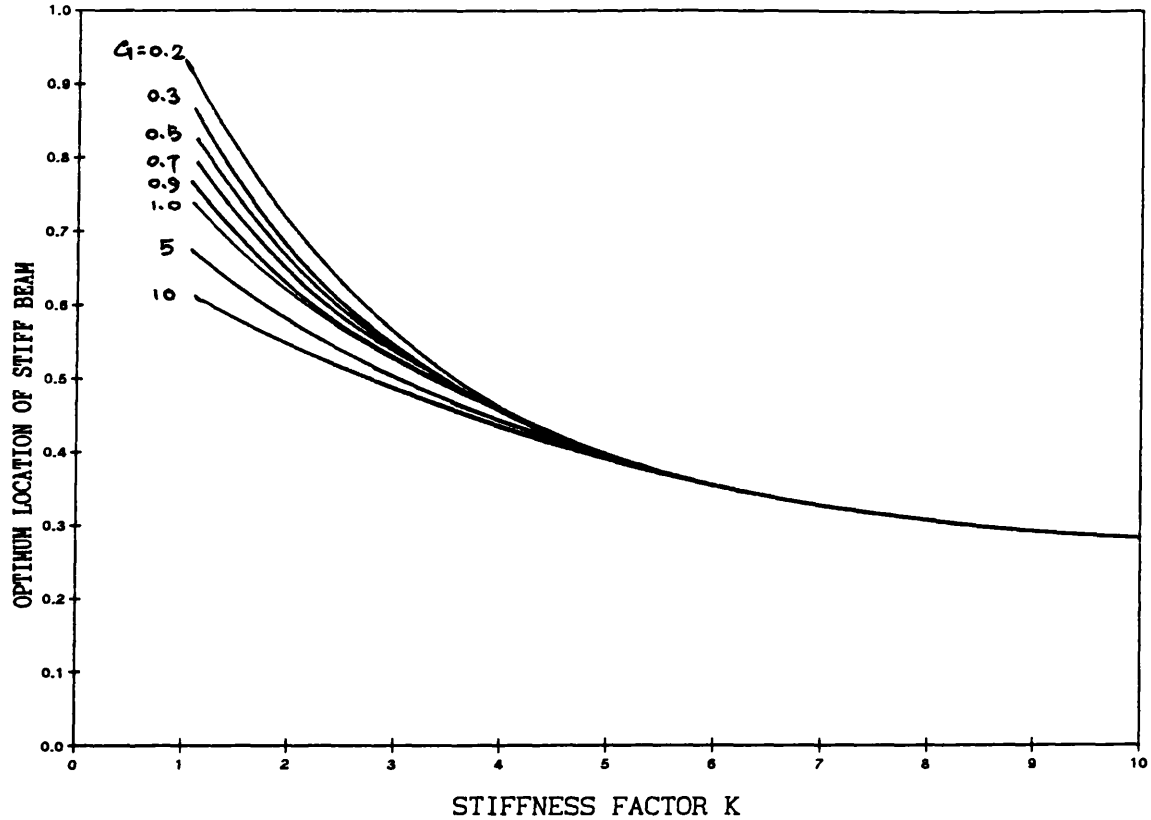

FIG. [6.17] VARIATION OF OPTIMUM LOCATION OF STIFF BEAM WITH STIFFNESS FACTOR K (U.D.L.)
(ONE INTERMEDIATE STIFFENING BEAM)

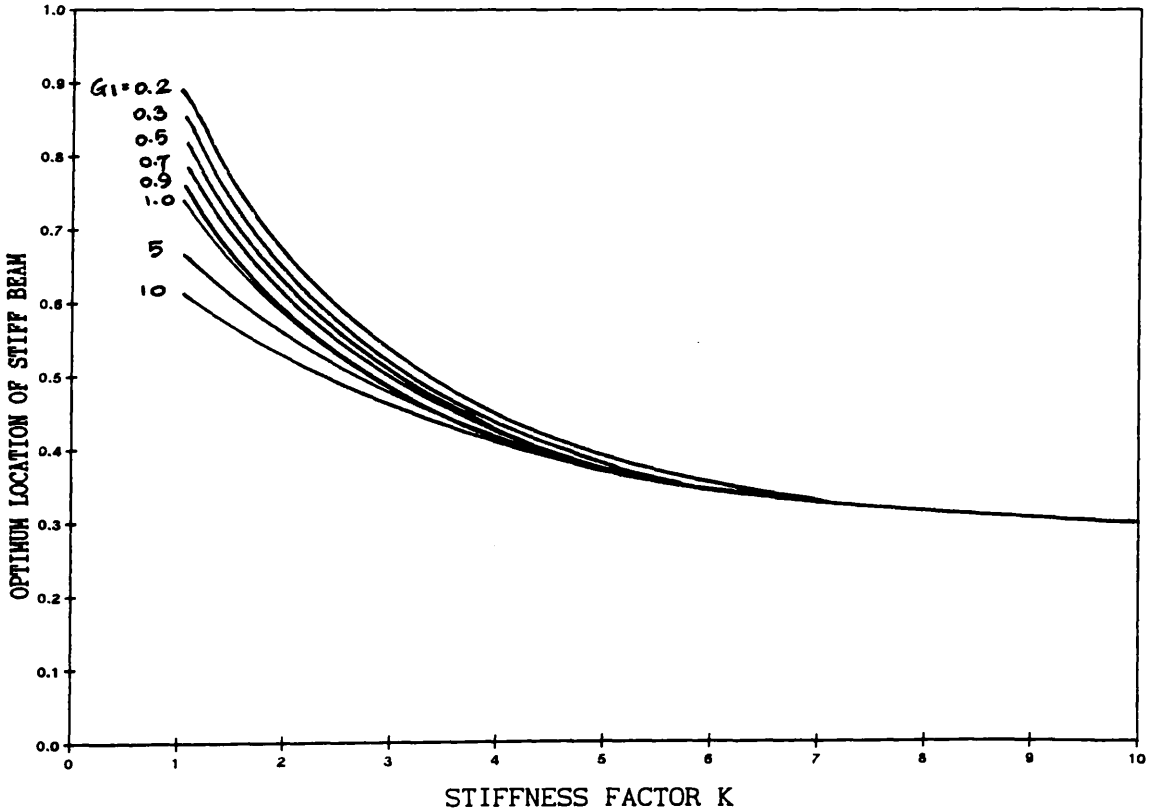

FIG. [6.18] VARIATION OF OPTIMUM LOCATION OF STIFF BEAM WITH STIFFNESS FACTOR K (U.D.L.)
(TOP AND INTERMEDIATE STIFFENING BEAMS, G2=0.1)

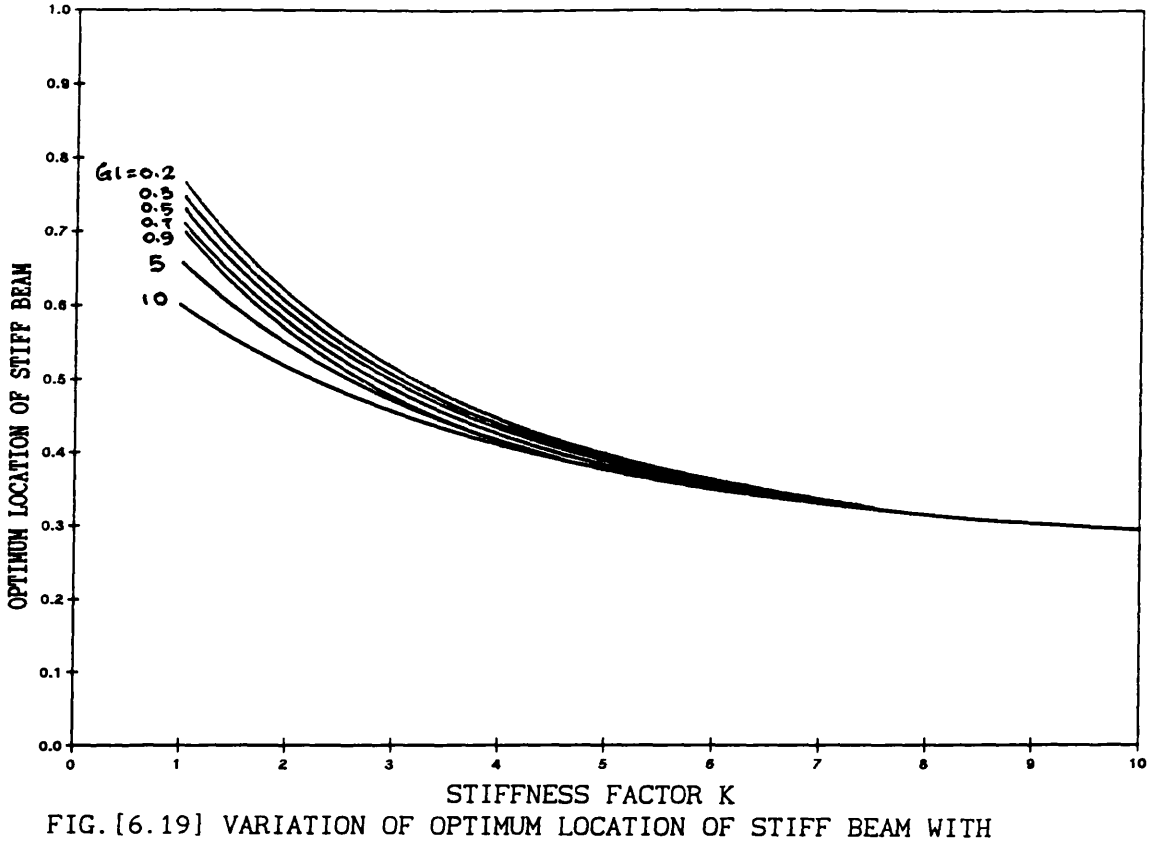

FIG.[6.19] VARIATION OF OPTIMUM LOCATION OF STIFF BEAM WITH STIFFNESS FACTOR K (U.D.L.)
(TOP AND INTERMEDIATE STIFFENING BEAMS, G2=0.3)

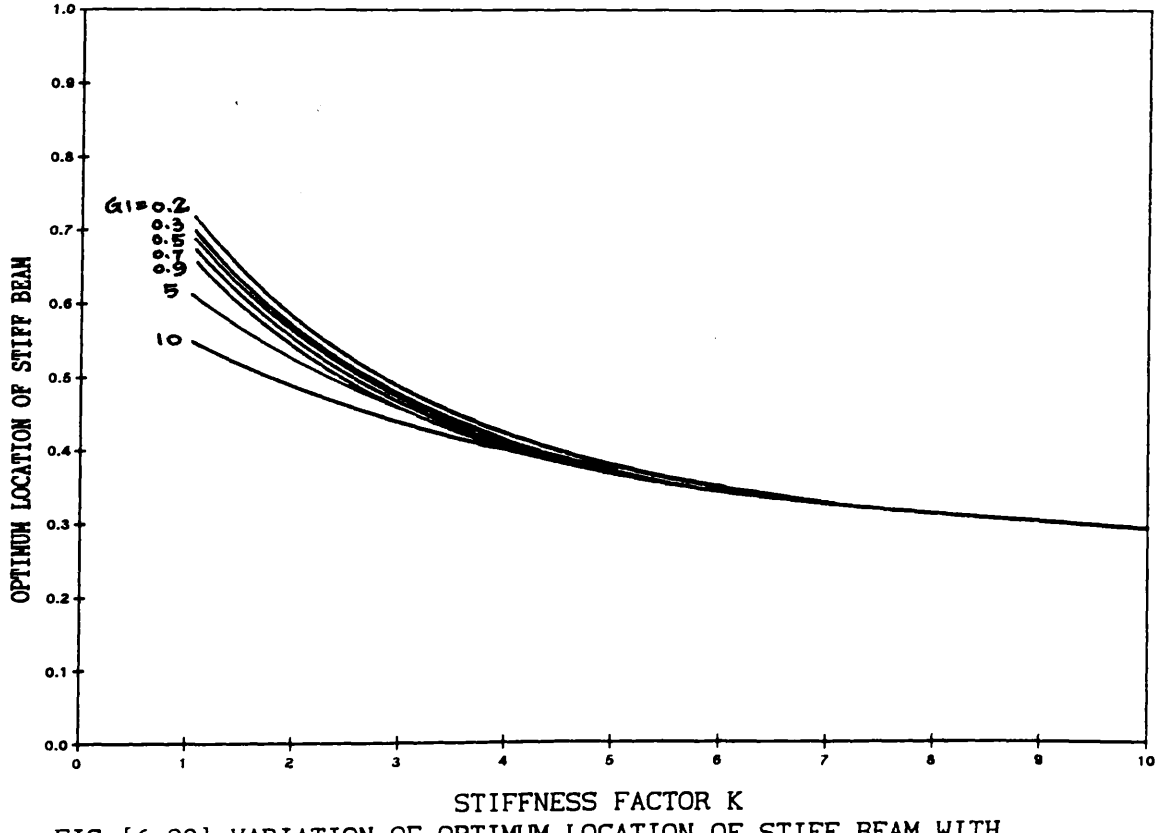

FIG.[6.20] VARIATION OF OPTIMUM LOCATION OF STIFF BEAM WITH STIFFNESS FACTOR K (U.D.L.)
(TOP AND INTERMEDIATE STIFFENING BEAMS, G2=0.5)

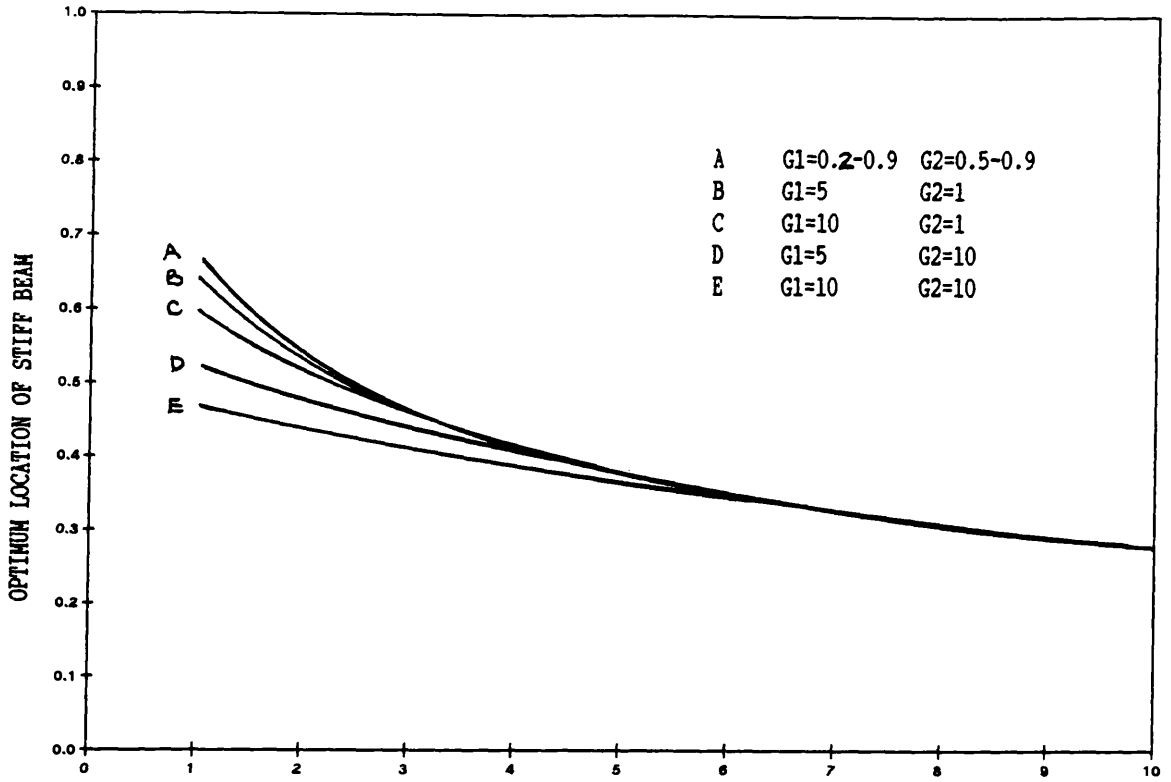

FIG. [6.21] VARIATION OF OPTIMUM LOCATION OF STIFF BEAM WITH STIFFNESS FACTOR K (U.D.L.)
(TOP AND INTERMEDIATE STIFFENING BEAMS)

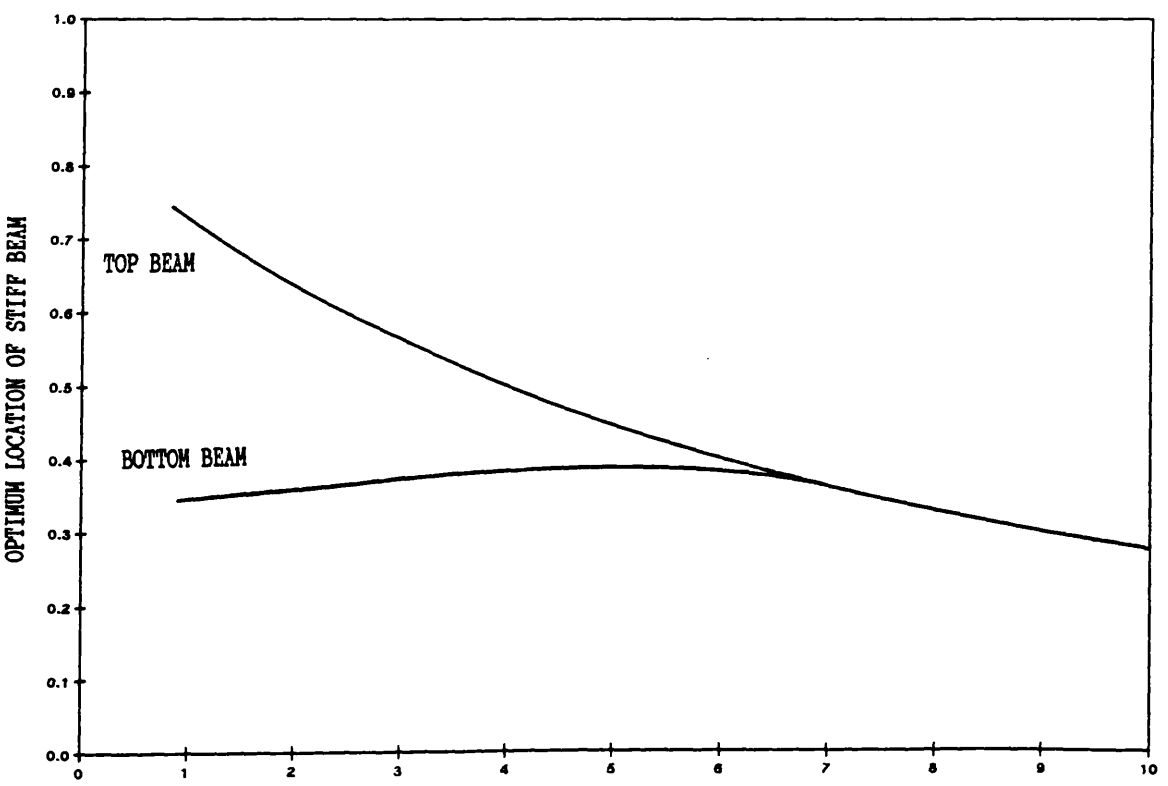

FIG. [6.22] VARIATION OF RECOMMENDED OPTIMUM LOCATIONS OF STIFF BEAMS WITH STIFFNESS FACTOR K (U.D.L.)
(TWO INTERMEDIATE STIFFENING BEAMS)

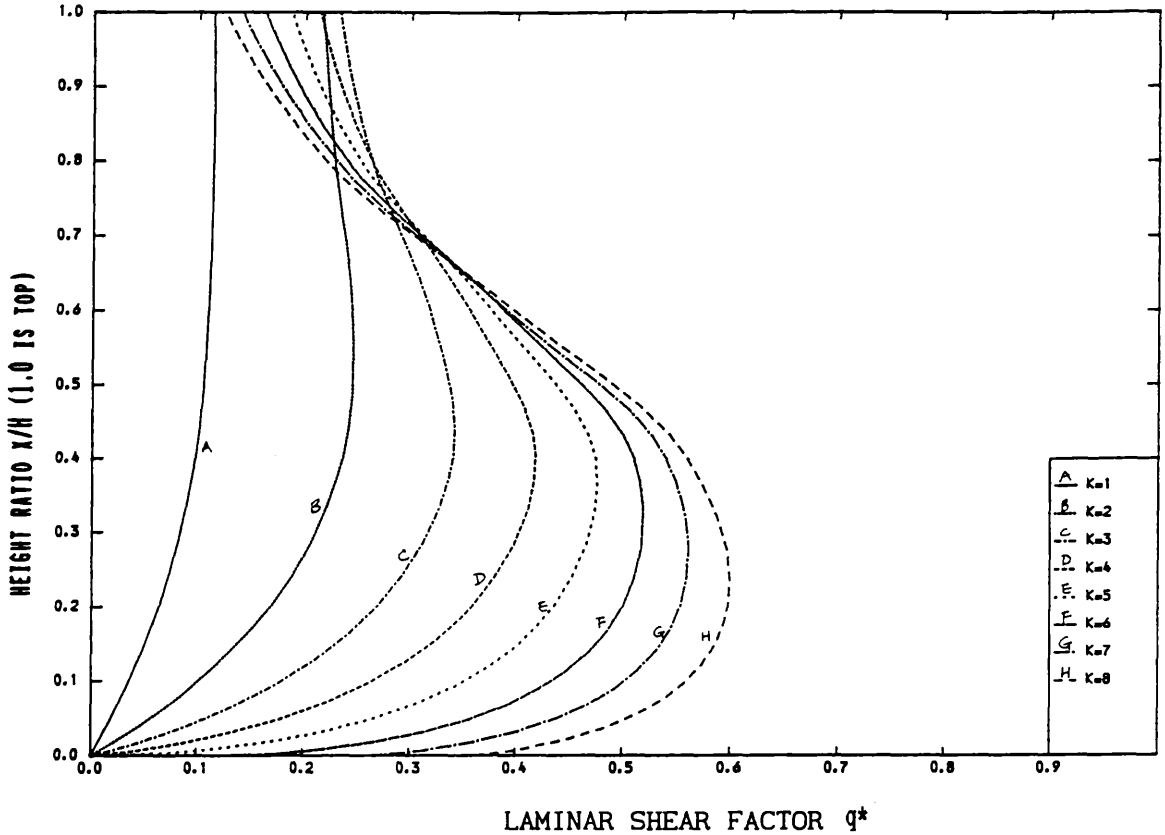

FIG. [6.23] VARIATION OF LAMINAR SHEAR WITH HEIGHT
(G=0, U.D.L.)

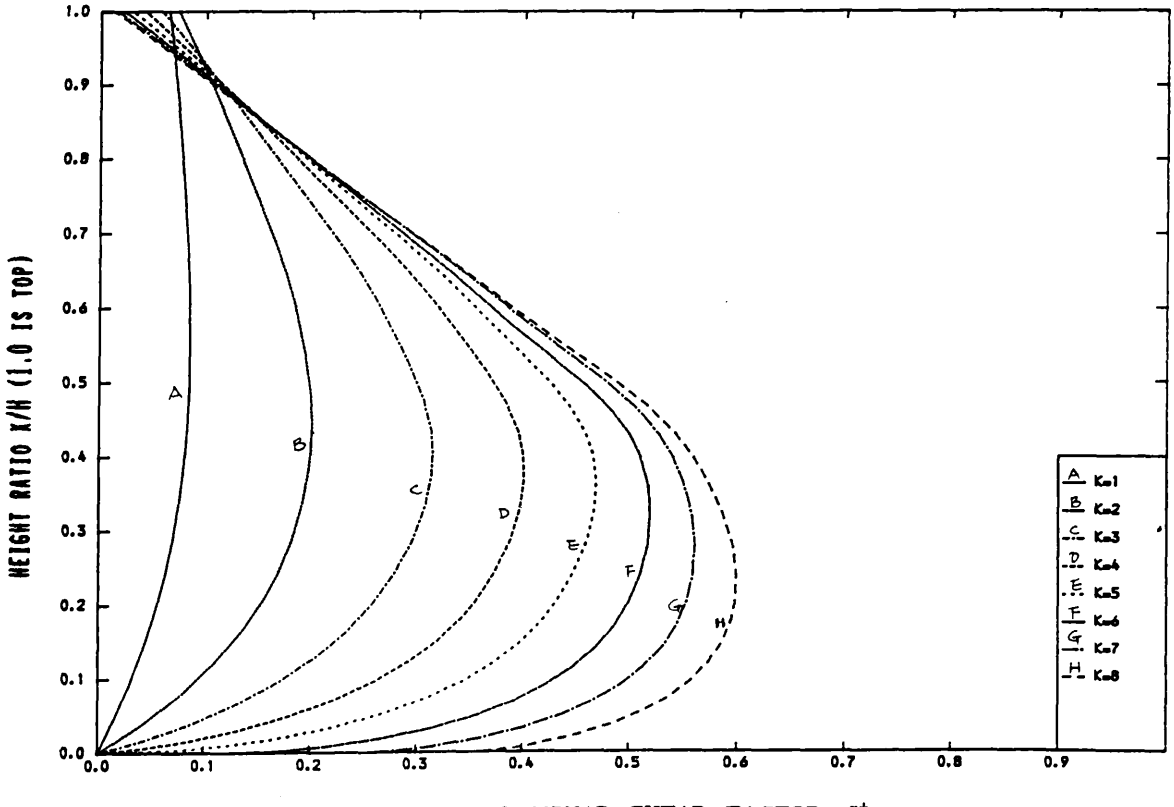

FIG. [6.24] VARIATION OF LAMINAR SHEAR WITH HEIGHT
(ONE INTERMEDIATE STIFFENING BEAM)
(G=1, X_1/H=1.0, U.D.L.)

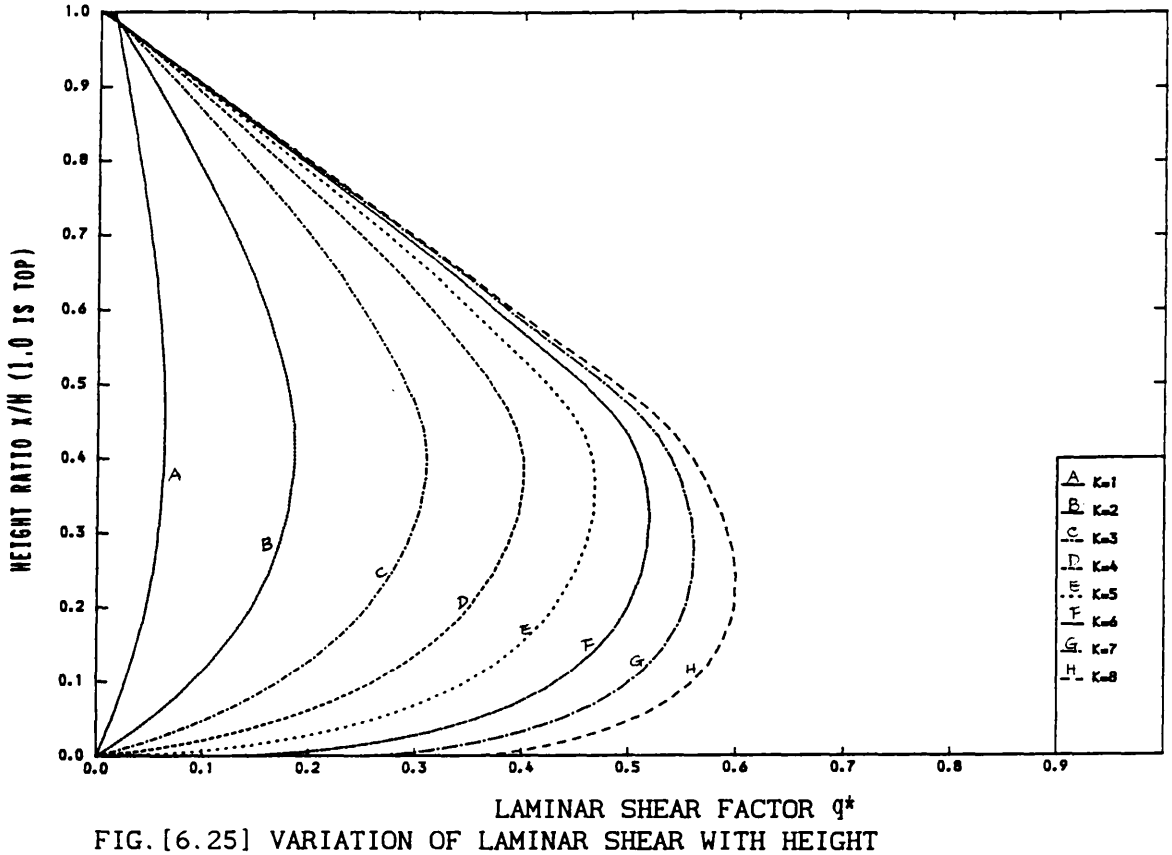

FIG.[6.25] VARIATION OF LAMINAR SHEAR WITH HEIGHT
(ONE INTERMEDIATE STIFFENING BEAM)
(G=10, X_1/H=1.0, U.D.L.)

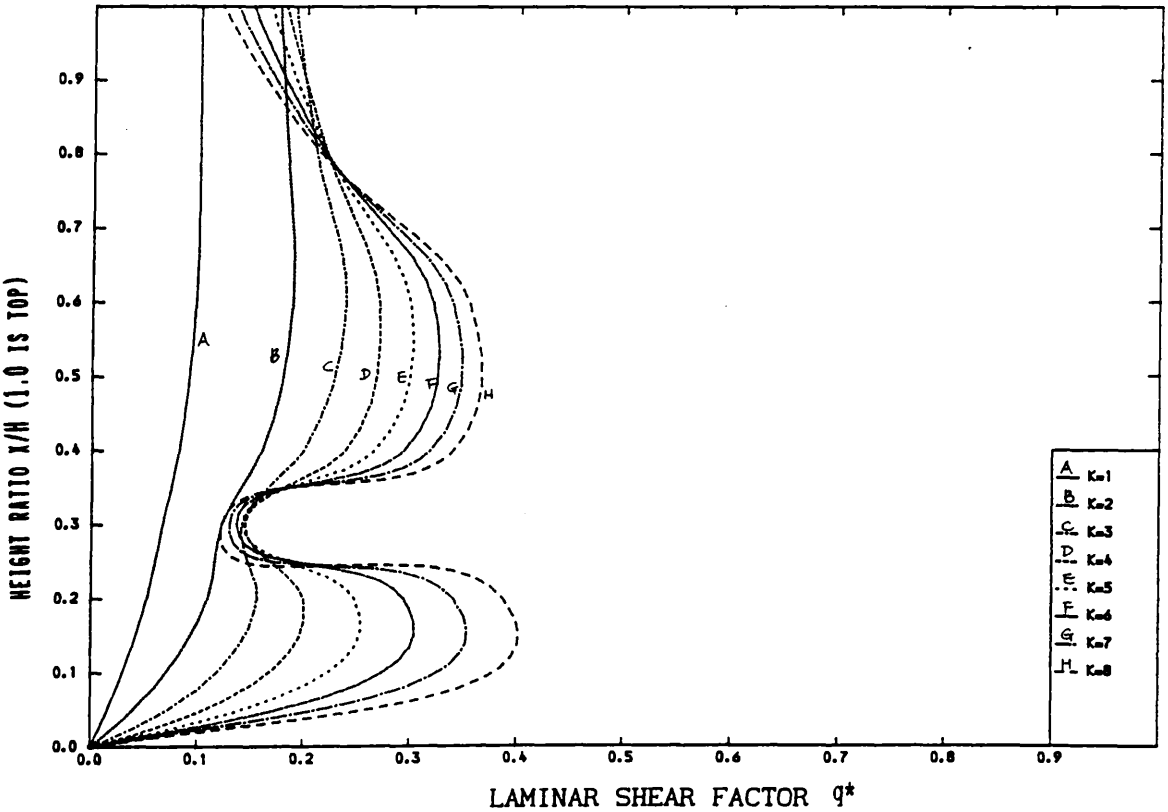

FIG.[6.26] VARIATION OF LAMINAR SHEAR WITH HEIGHT
(ONE INTERMEDIATE STIFFENING BEAM)
(G=1, X_1/H=0.3, U.D.L.)

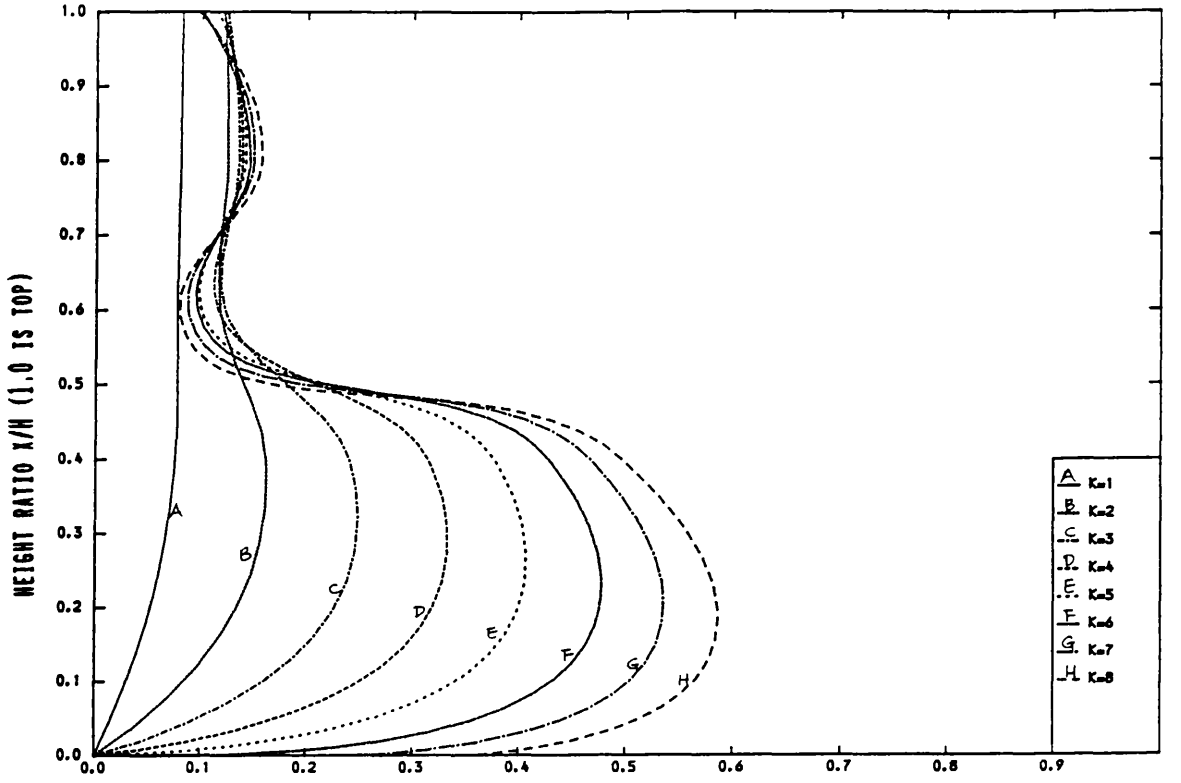

FIG. [6.27] VARIATION OF LAMINAR SHEAR WITH HEIGHT
(ONE INTERMEDIATE STIFFENING BEAM)
(G=1, X_1/H=0.6, U.D.L.)

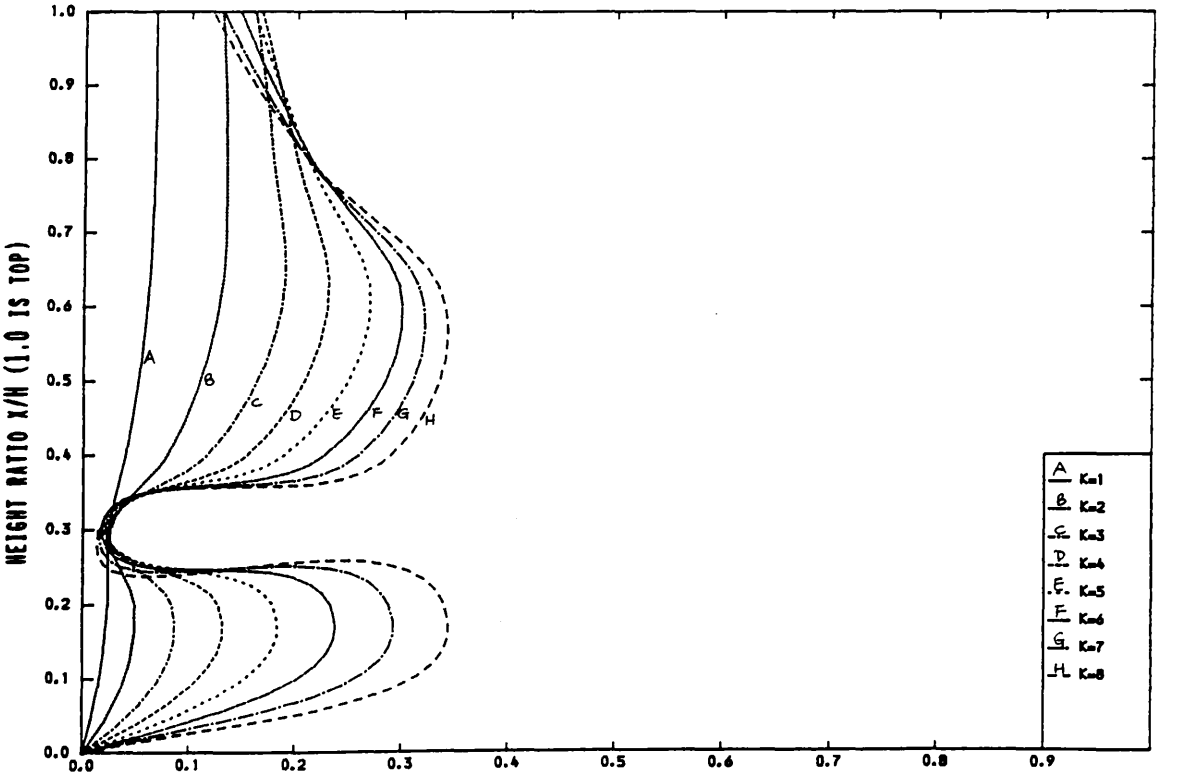

FIG. [6.28] VARIATION OF LAMINAR SHEAR WITH HEIGHT
(ONE INTERMEDIATE STIFFENING BEAM)
(G=10, X_1/H=0.3, U.D.L.)

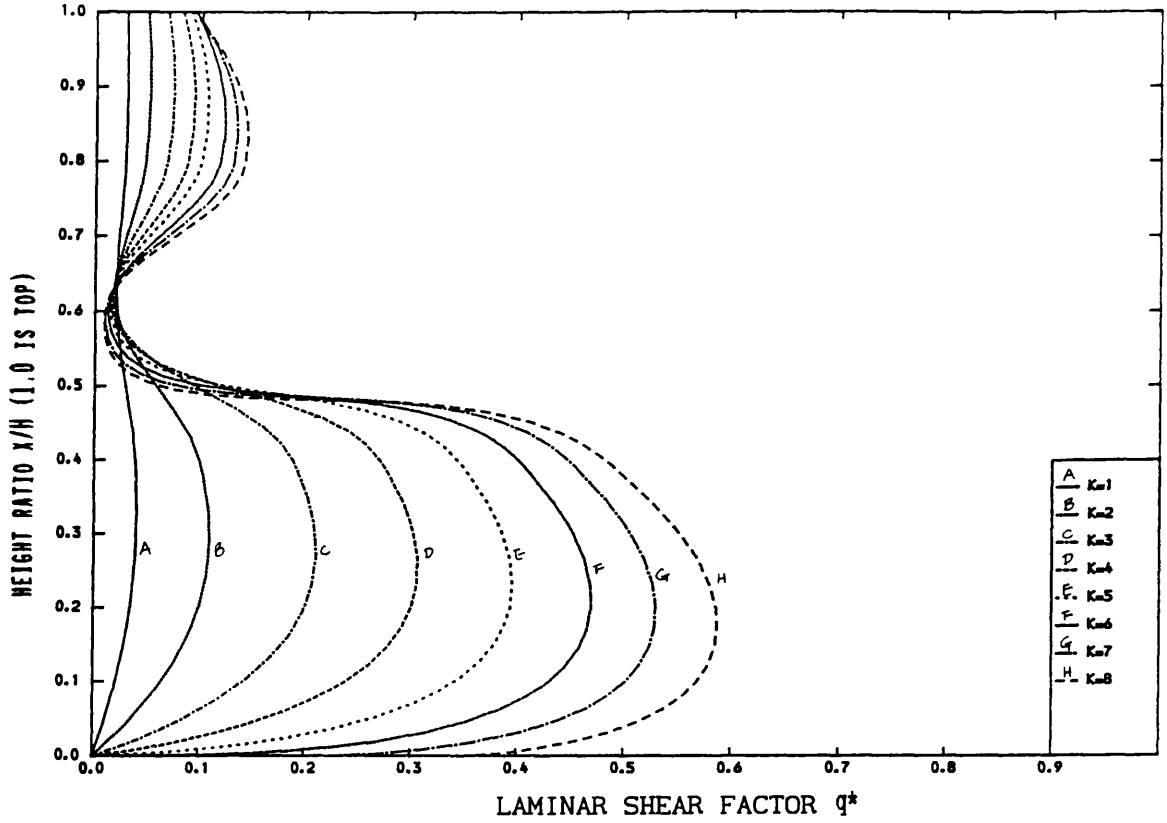

FIG. [6.29] VARIATION OF LAMINAR SHEAR WITH HEIGHT
(ONE INTERMEDIATE STIFFENING BEAM)
(G=10, $X_1/H=0.6$, U.D.L.)

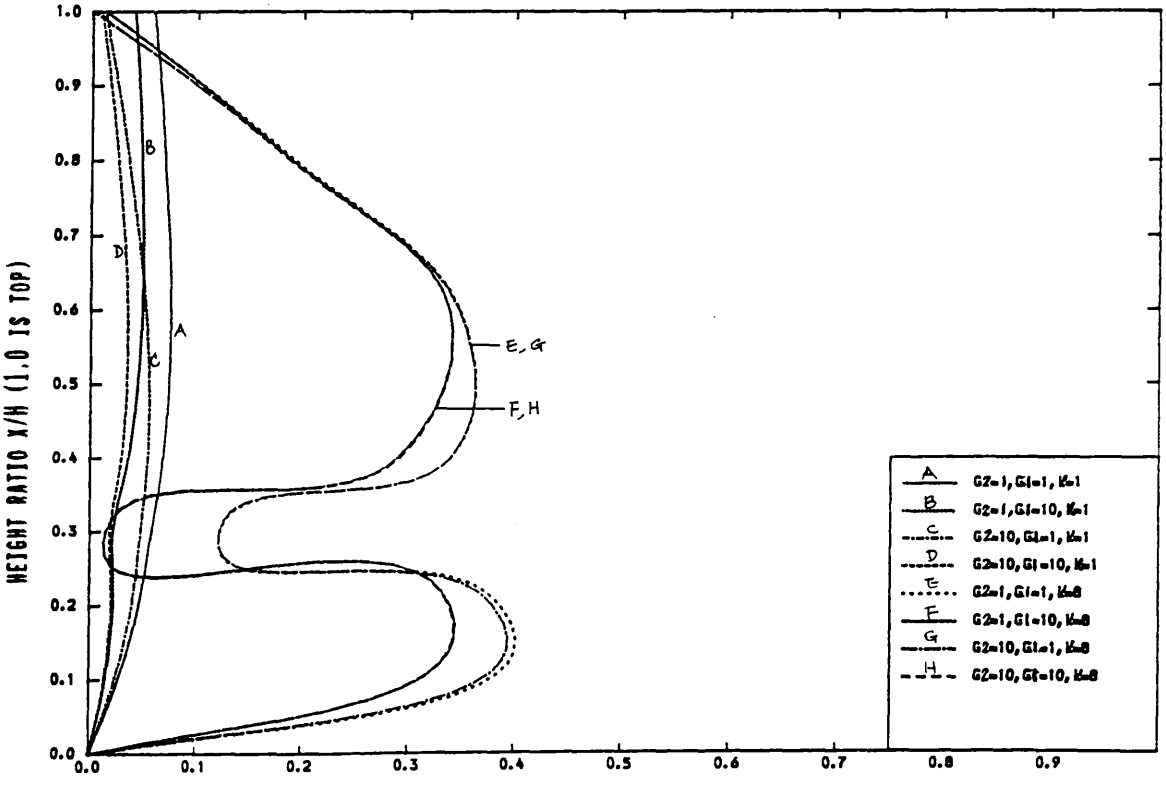

FIG. [6.30] VARIATION OF LAMINAR SHEAR WITH HEIGHT
(TWO INTERMEDIATE STIFFENING BEAMS)
(G=10, $X_1/H=0.3$, $X_2/H=1.0$, U.D.L.)

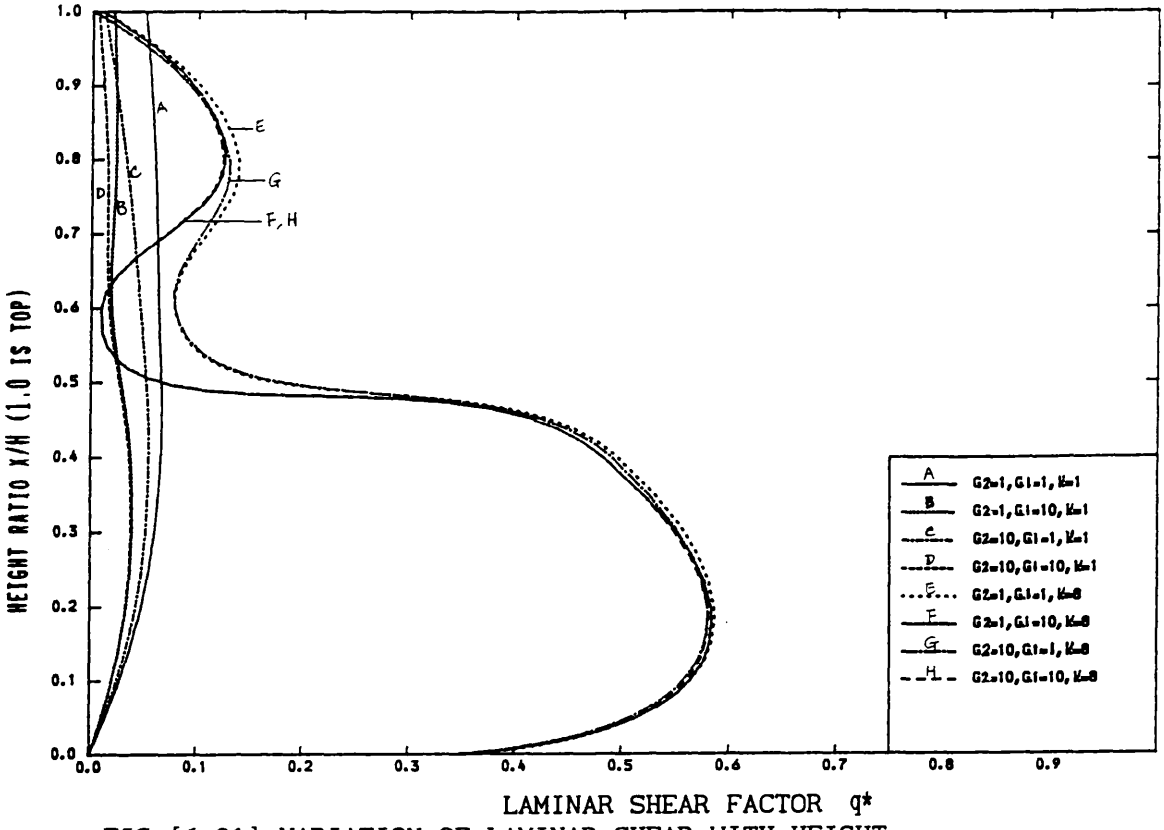

FIG. [6.31] VARIATION OF LAMINAR SHEAR WITH HEIGHT
(TWO INTERMEDIATE STIFFENING BEAMS)
(G=10, $X_1/H=0.6$, $X_2/H=1.0$, U.D.L.)

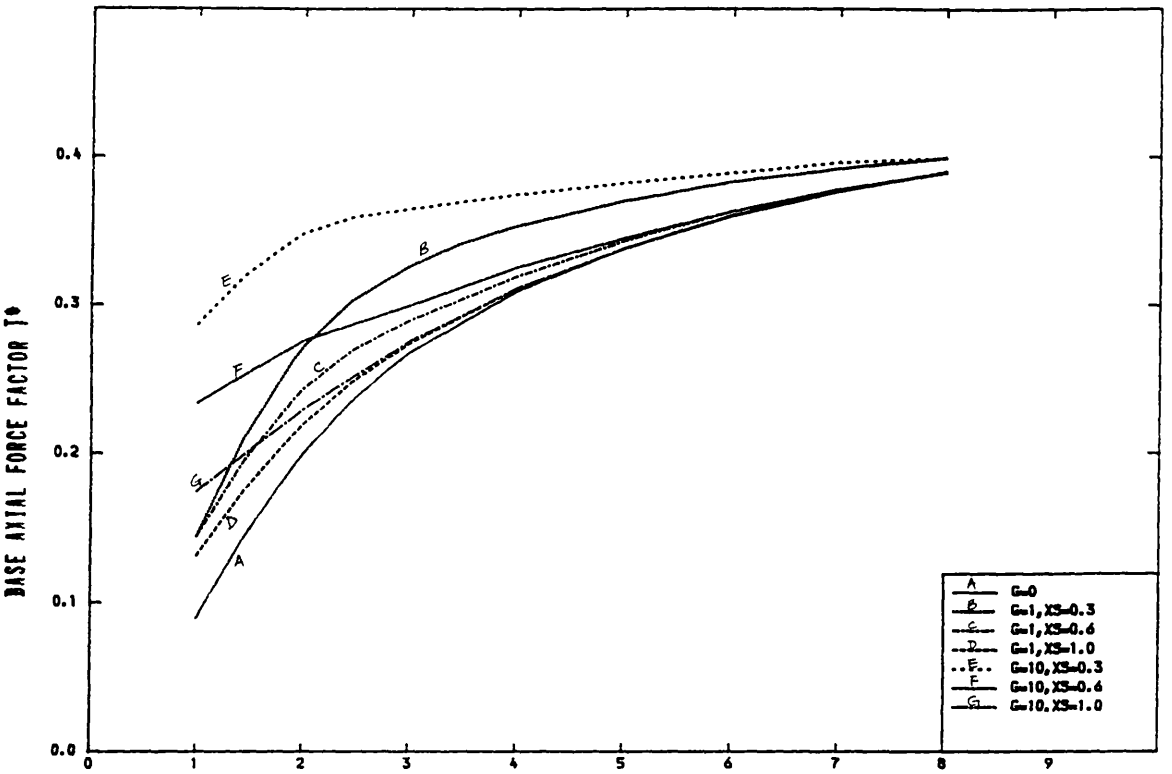

FIG. [6.32] VARIATION OF BASE AXIAL FORCE WITH STIFFNESS FACTOR K
(ONE INTERMEDIATE STIFFENING BEAM)
(U.D.L.)

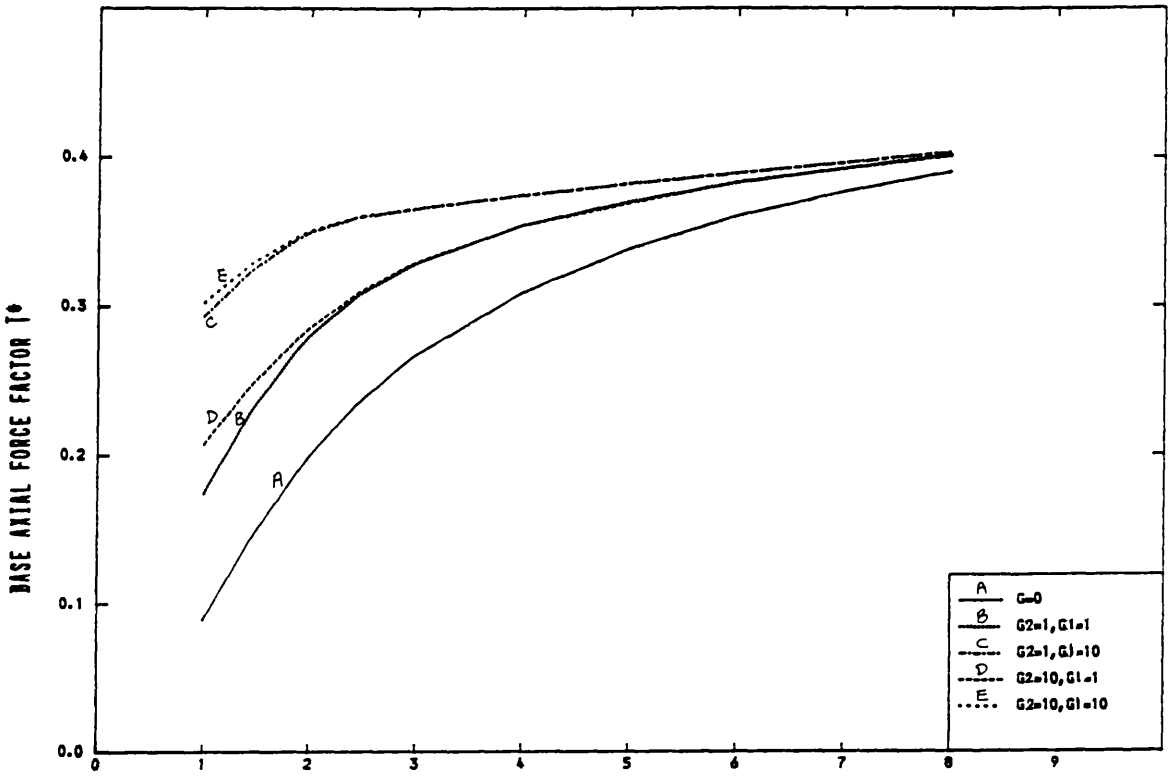

FIG. [6.33] VARIATION OF BASE AXIAL FORCE WITH STIFFNESS FACTOR K
(TWO INTERMEDIATE STIFFENING BEAMS)
($X_1/H=0.3$, $X_2/H=1.0$, U.D.L.)

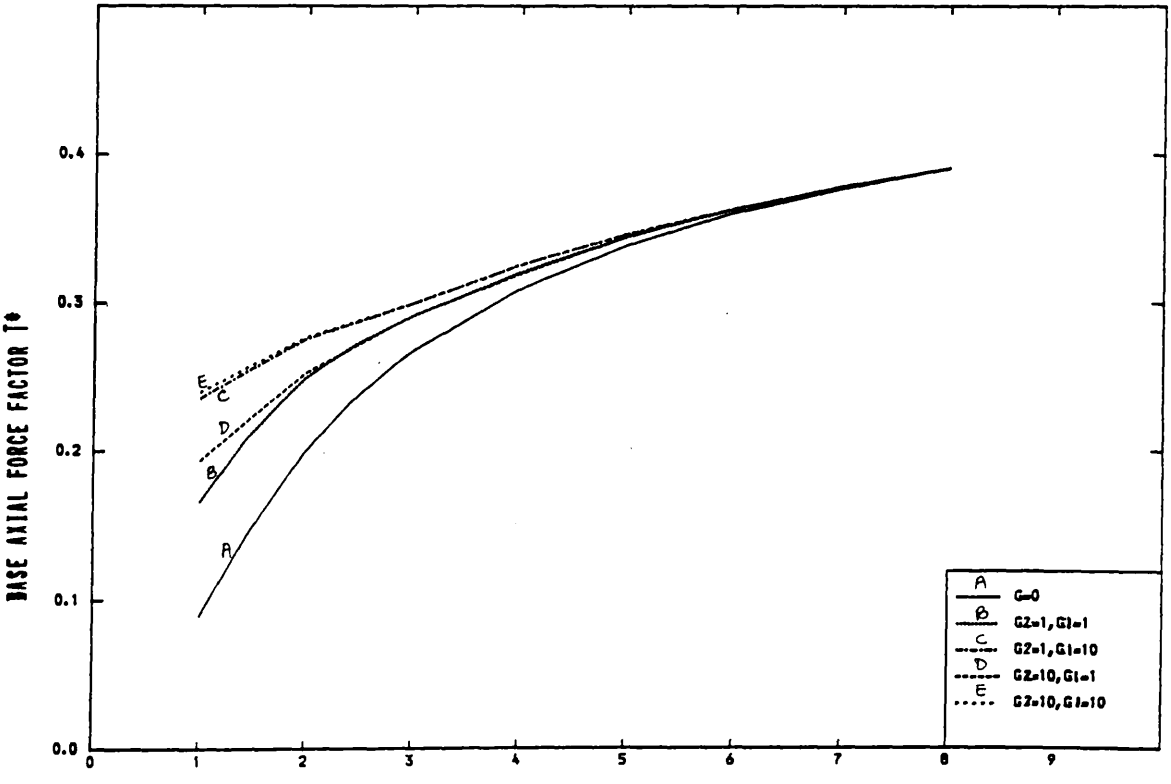

FIG. [6.34] VARIATION OF BASE AXIAL FORCE WITH STIFFNESS FACTOR K
(TWO INTERMEDIATE STIFFENING BEAMS)
($X_1/H=0.6$, $X_2/H=1.0$, U.D.L.)

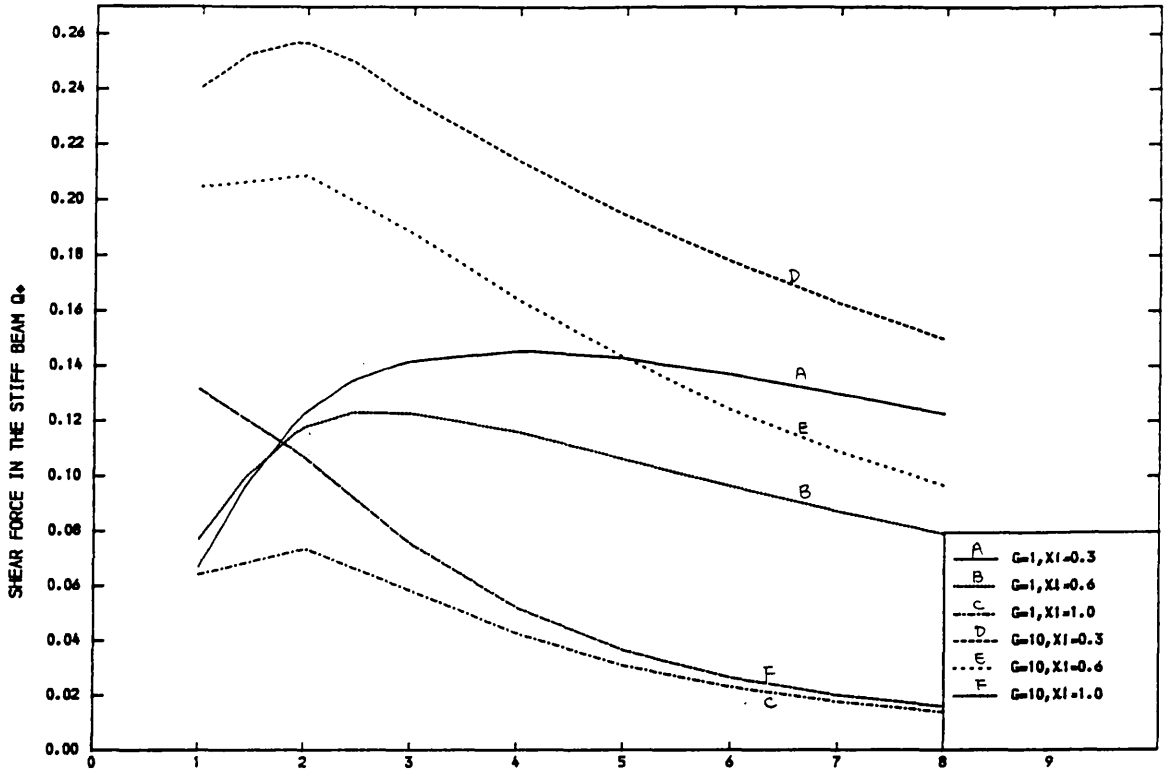

FIG. [6.35] VARIATION OF STIFFENING BEAM SHEAR FORCE FACTOR Q* WITH STIFFNESS FACTOR K
(ONE INTERMEDIATE STIFFENING BEAM)
(U.D.L.)

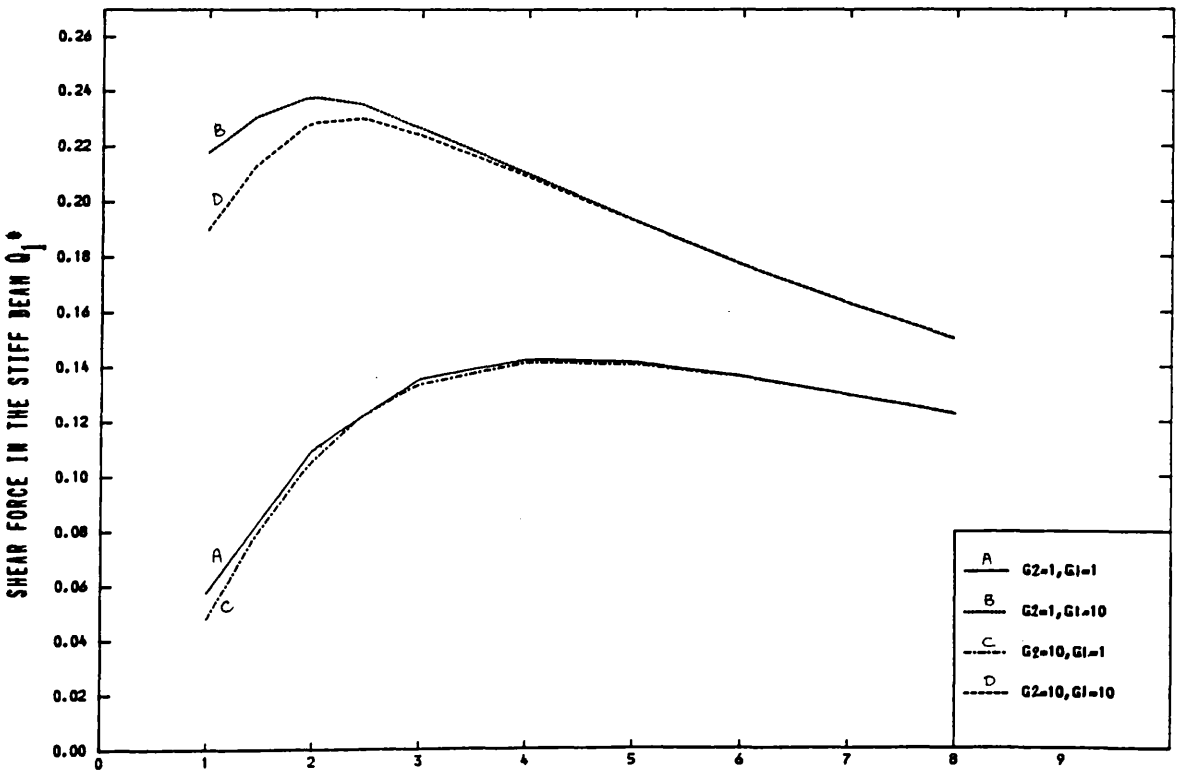

FIG. [6.36] VARIATION OF STIFFENING BEAM SHEAR FORCE FACTOR Q* WITH STIFFNESS FACTOR K
(TWO INTERMEDIATE STIFFENING BEAMS)
($X_1/H=0.3$, $X_2/H=1.0$, U.D.L.)

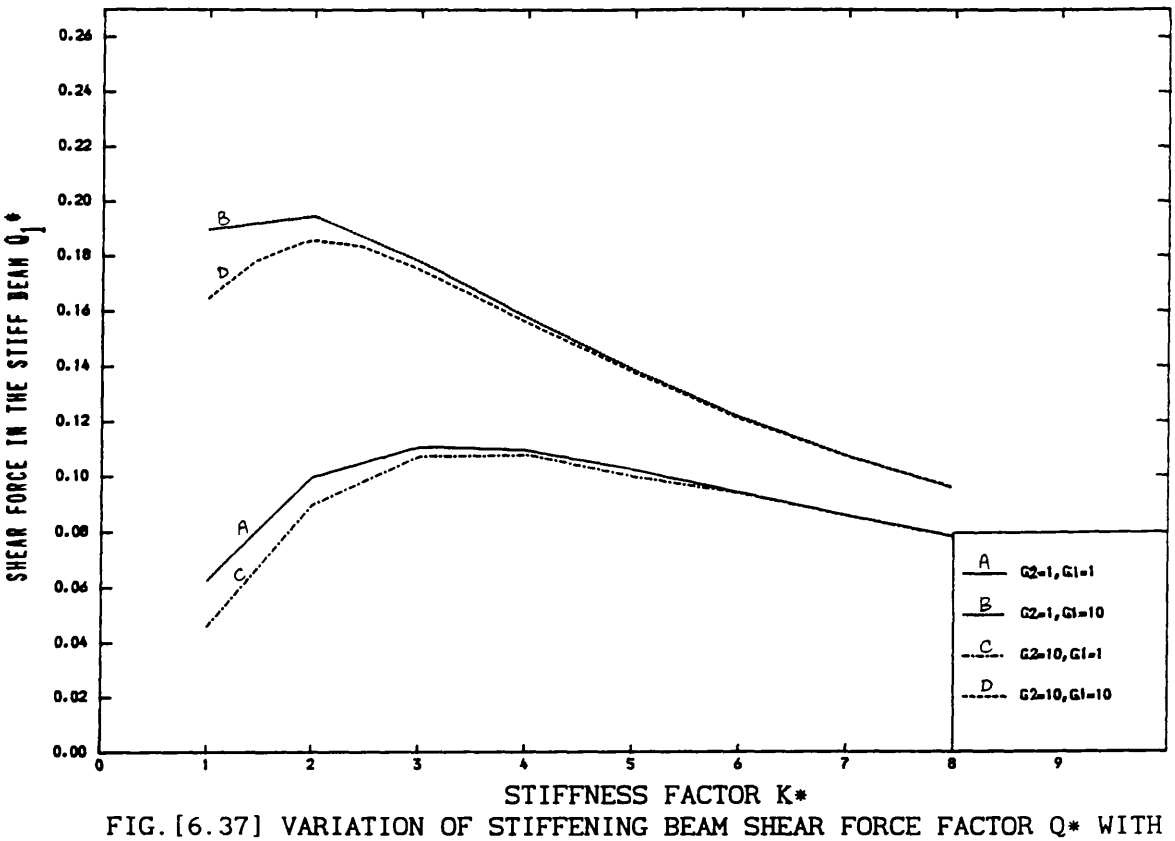

FIG. [6.37] VARIATION OF STIFFENING BEAM SHEAR FORCE FACTOR Q* WITH STIFFNESS FACTOR K
(TWO INTERMEDIATE STIFFENING BEAMS)
($X_1/H=0.6$, $X_2/H=1.0$, U.D.L.)

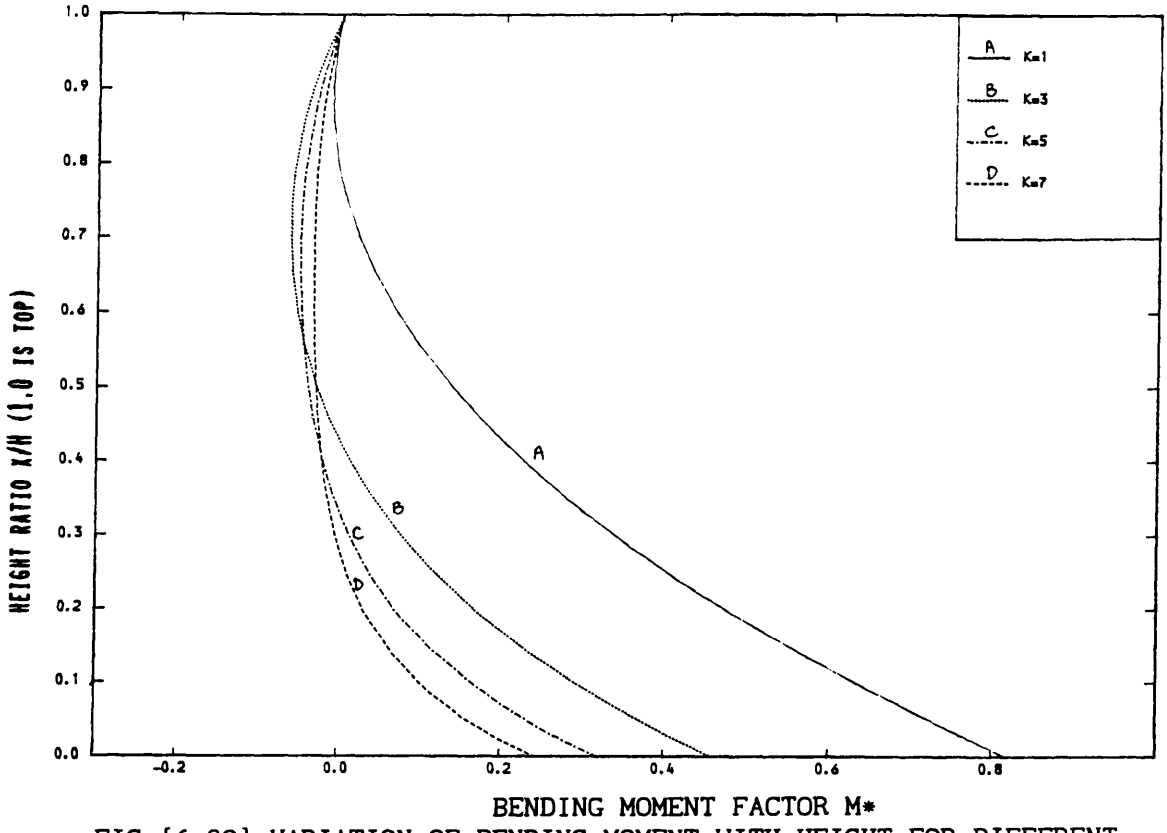

FIG. [6.38] VARIATION OF BENDING MOMENT WITH HEIGHT FOR DIFFERENT STIFFNESS FACTOR K
(V=1.0, G=0, U.D.L.)

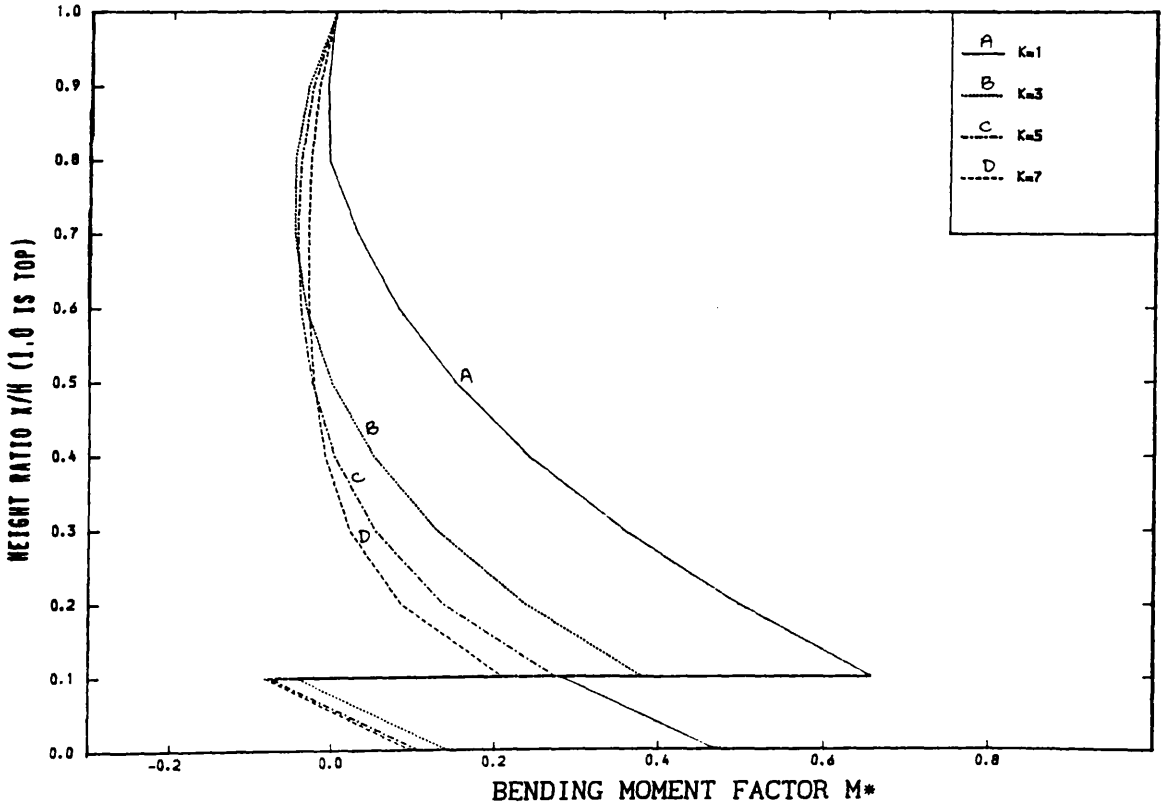

FIG. [6.39] VARIATION OF BENDING MOMENT WITH HEIGHT FOR DIFFERENT STIFFNESS FACTOR K
(ONE INTERMEDIATE STIFFENING BEAM)
(V=1.0, X_1/H=0.1, G=10, U.D.L.)

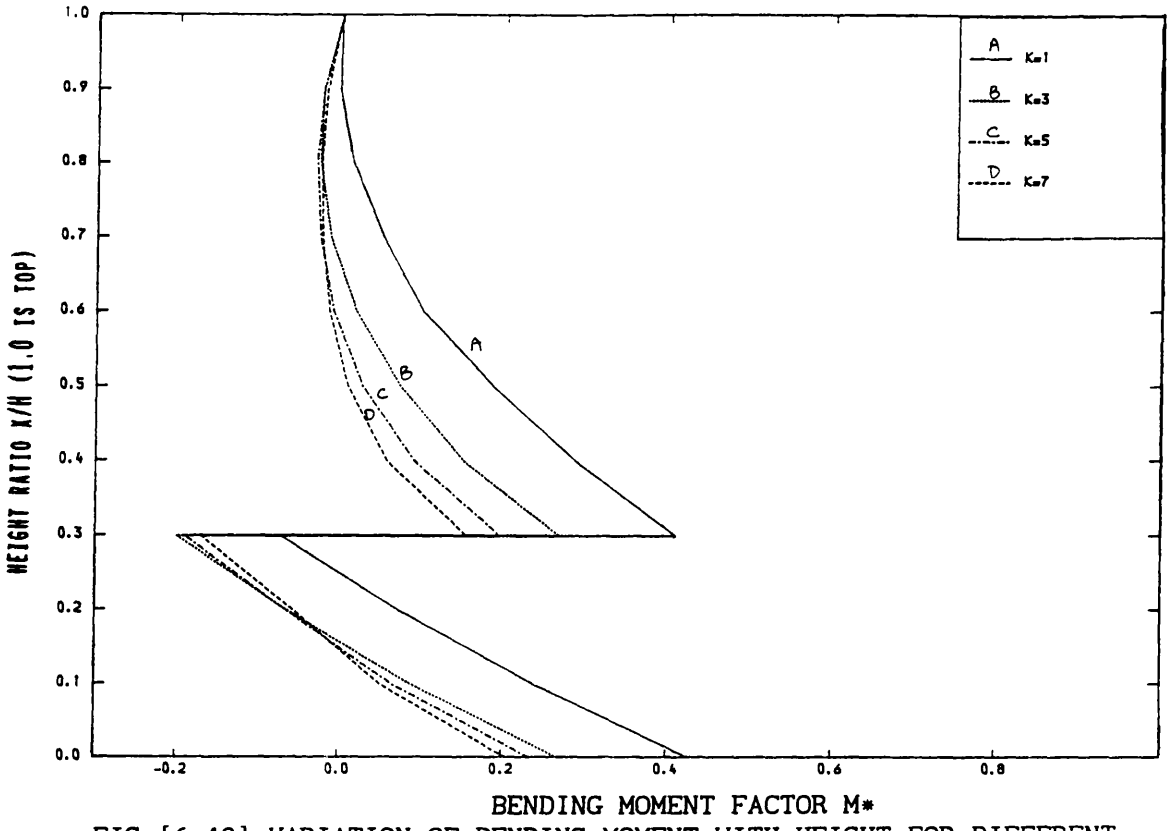

FIG.[6.40] VARIATION OF BENDING MOMENT WITH HEIGHT FOR DIFFERENT STIFFNESS FACTOR K
(ONE INTERMEDIATE STIFFENING BEAM)
(V=1.0, X_1/H=0.3, G=10, U.D.L.)

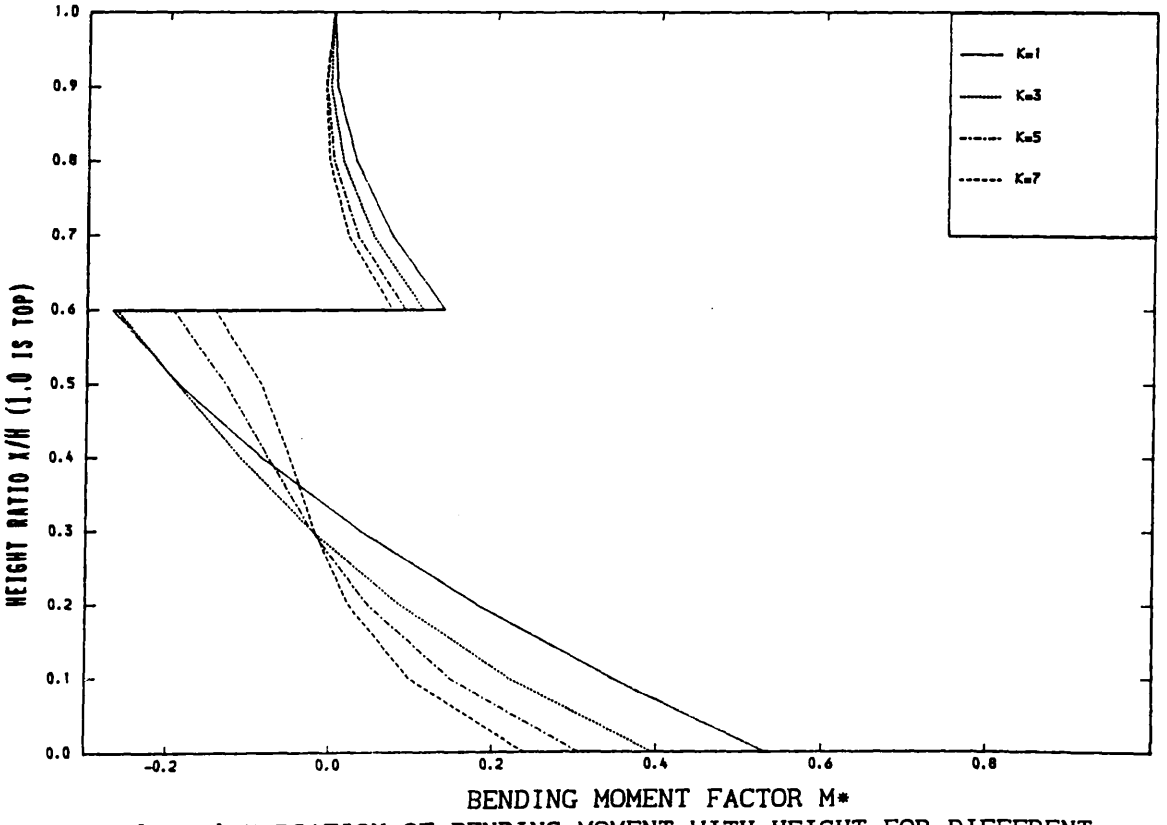

FIG.[6.41] VARIATION OF BENDING MOMENT WITH HEIGHT FOR DIFFERENT STIFFNESS FACTOR K
(ONE INTERMEDIATE STIFFENING BEAM)
(V=1.0, X_1/H=0.6, G=10, U.D.L.)

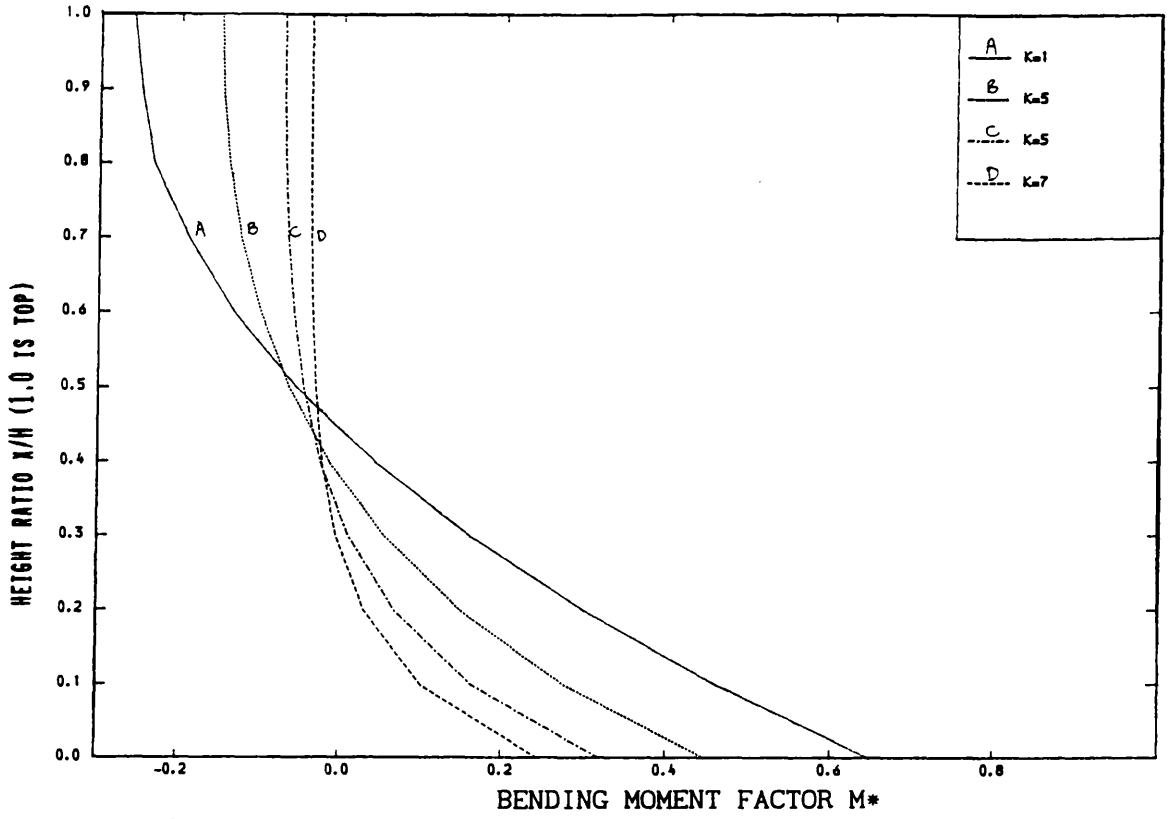

FIG. [6.42] VARIATION OF BENDING MOMENT WITH HEIGHT FOR DIFFERENT STIFFNESS FACTOR K
(ONE INTERMEDIATE STIFFENING BEAM)
(V=1.0, X_1/H=1.0, G=10, U.D.L.)

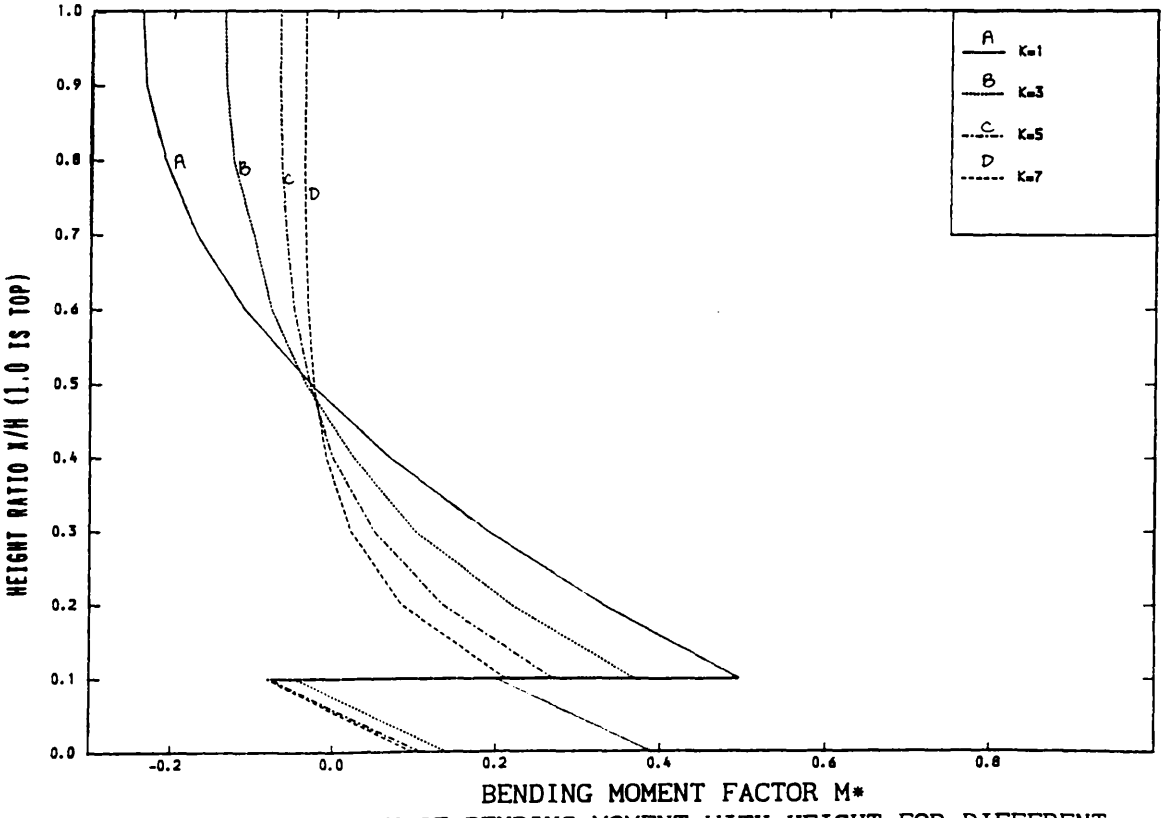

FIG. [6.43] VARIATION OF BENDING MOMENT WITH HEIGHT FOR DIFFERENT STIFFNESS FACTOR K
(TWO INTERMEDIATE STIFFENING BEAMS)
(V=1.0, X_1/H=0.1, X_2/H=1.0, G=10, U.D.L.)

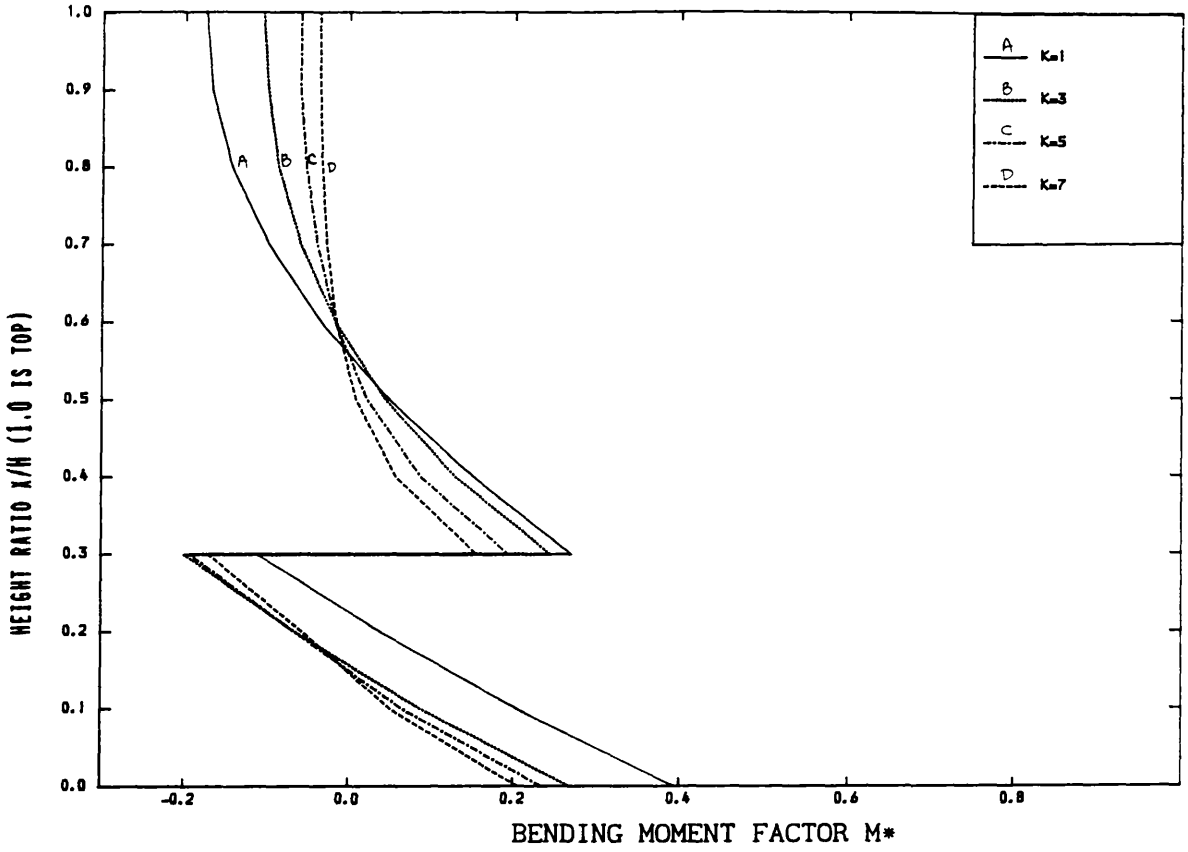

FIG.[6.44] VARIATION OF BENDING MOMENT WITH HEIGHT FOR DIFFERENT STIFFNESS FACTOR K
(TWO INTERMEDIATE STIFFENING BEAMS)
(V=1.0, X_1/H=0.3, X_2/H=1.0, G=10, U.D.L.)

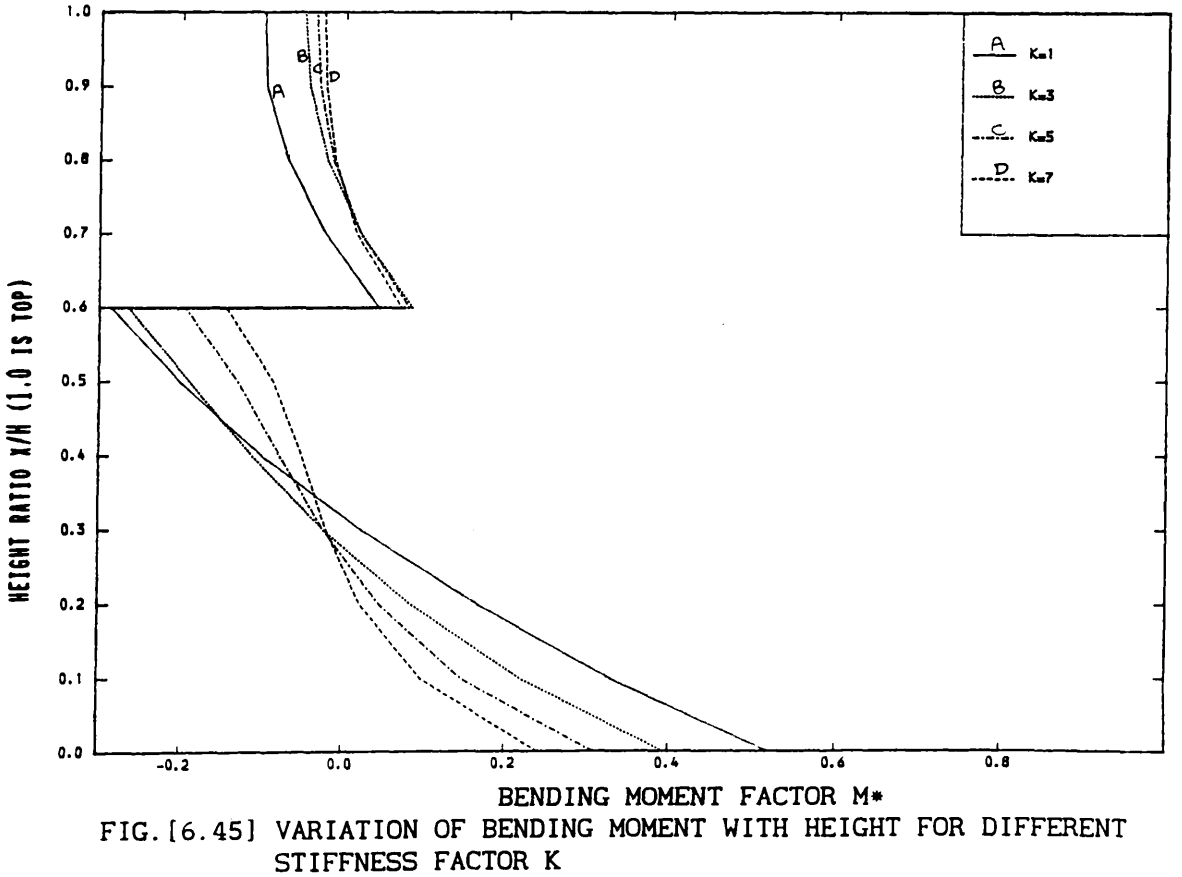

FIG.[6.45] VARIATION OF BENDING MOMENT WITH HEIGHT FOR DIFFERENT STIFFNESS FACTOR K
(TWO INTERMEDIATE STIFFENING BEAMS)
(V=1.0, X_1/H=0.6, X_2/H=1.0, G=10, U.D.L.)

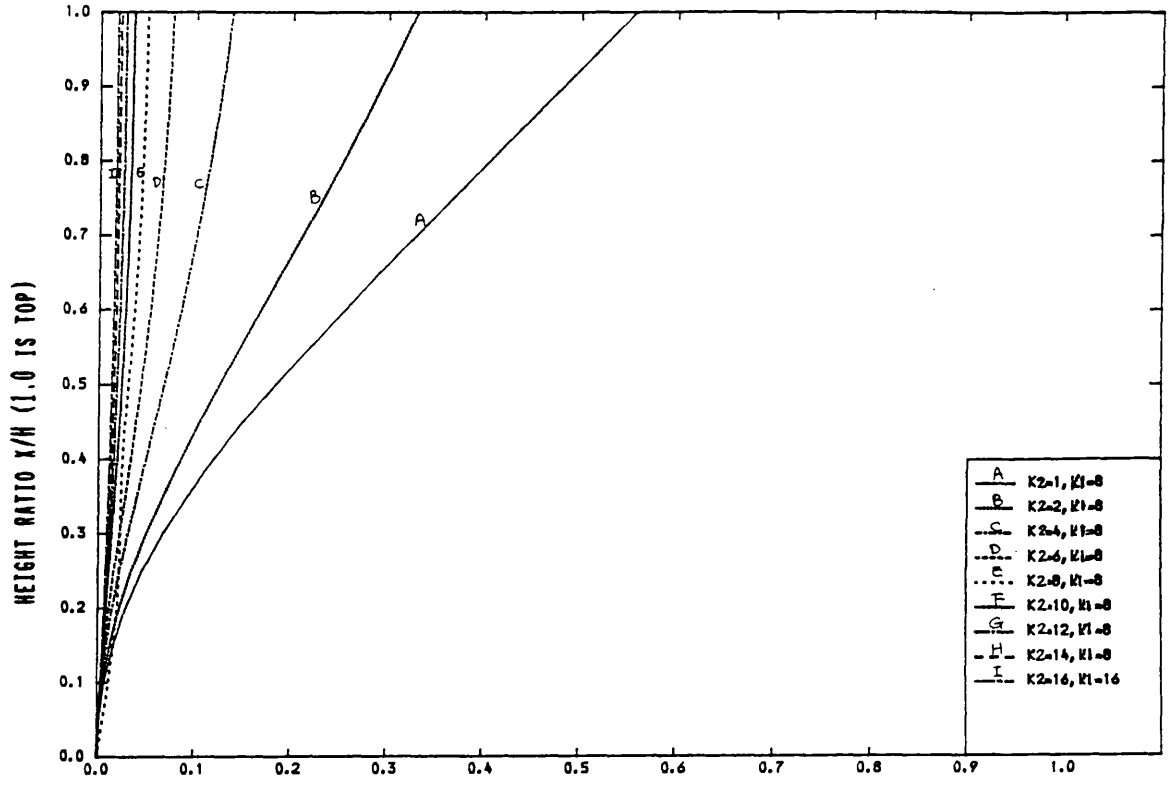

FIG. [6.46] VARIATION OF DEFLECTION WITH HEIGHT FOR DIFFERENT STIFFNESS FACTOR K
(TWO DIFFERENT TYPES OF CONNECTING BEAMS)
(V=1.0, X_1/H=0.2, U.D.L.)

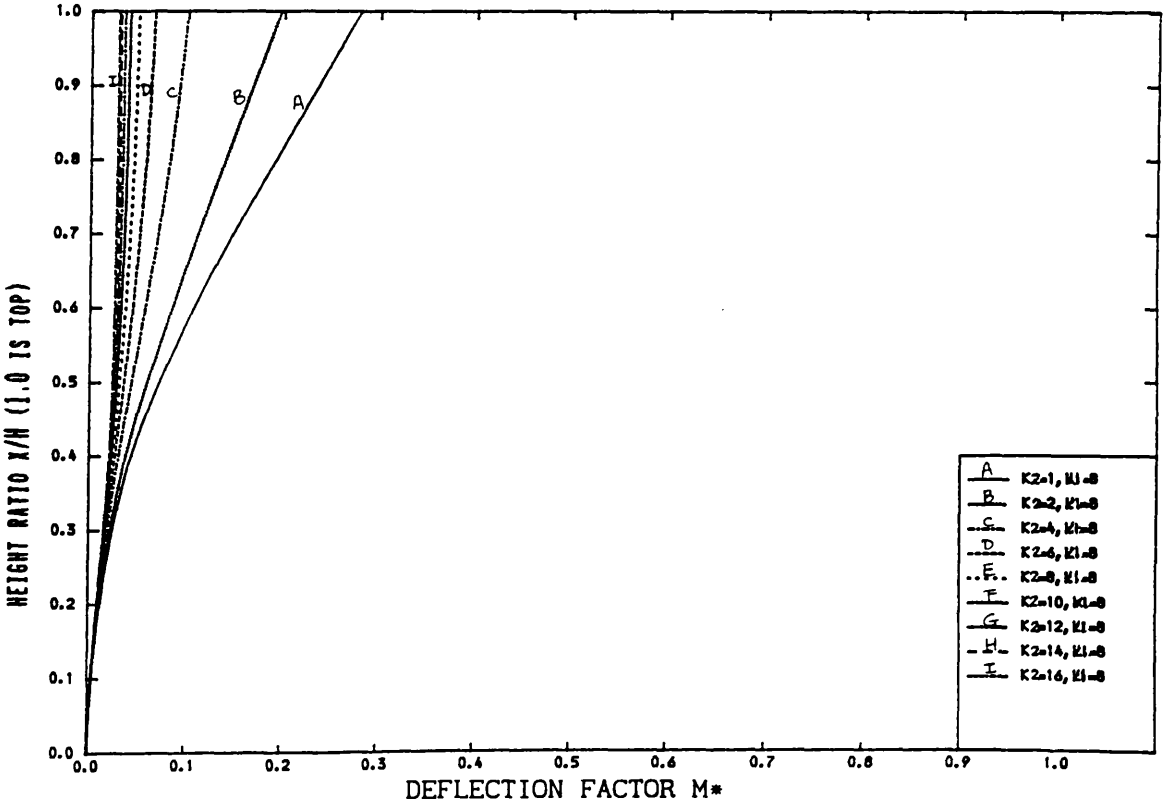

FIG. [6.47] VARIATION OF DEFLECTION WITH HEIGHT FOR DIFFERENT STIFFNESS FACTOR K
(TWO DIFFERENT TYPES OF CONNECTING BEAMS)
(V=1.0, X_1/H=0.4, U.D.L.)

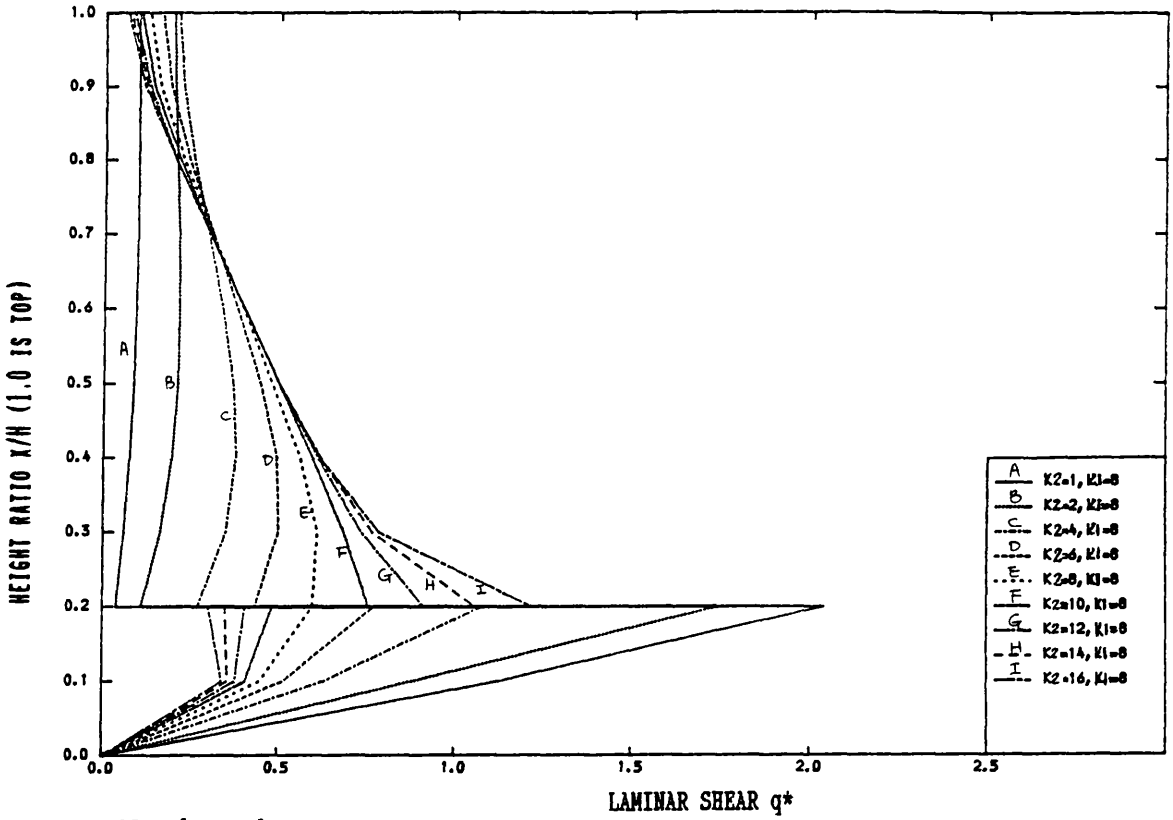

FIG. [6.48] VARIATION OF LAMINAR SHEAR WITH HEIGHT
(TWO DIFFERENT TYPES OF CONNECTING BEAMS)
(X_1/H=0.2,, U.D.L.)

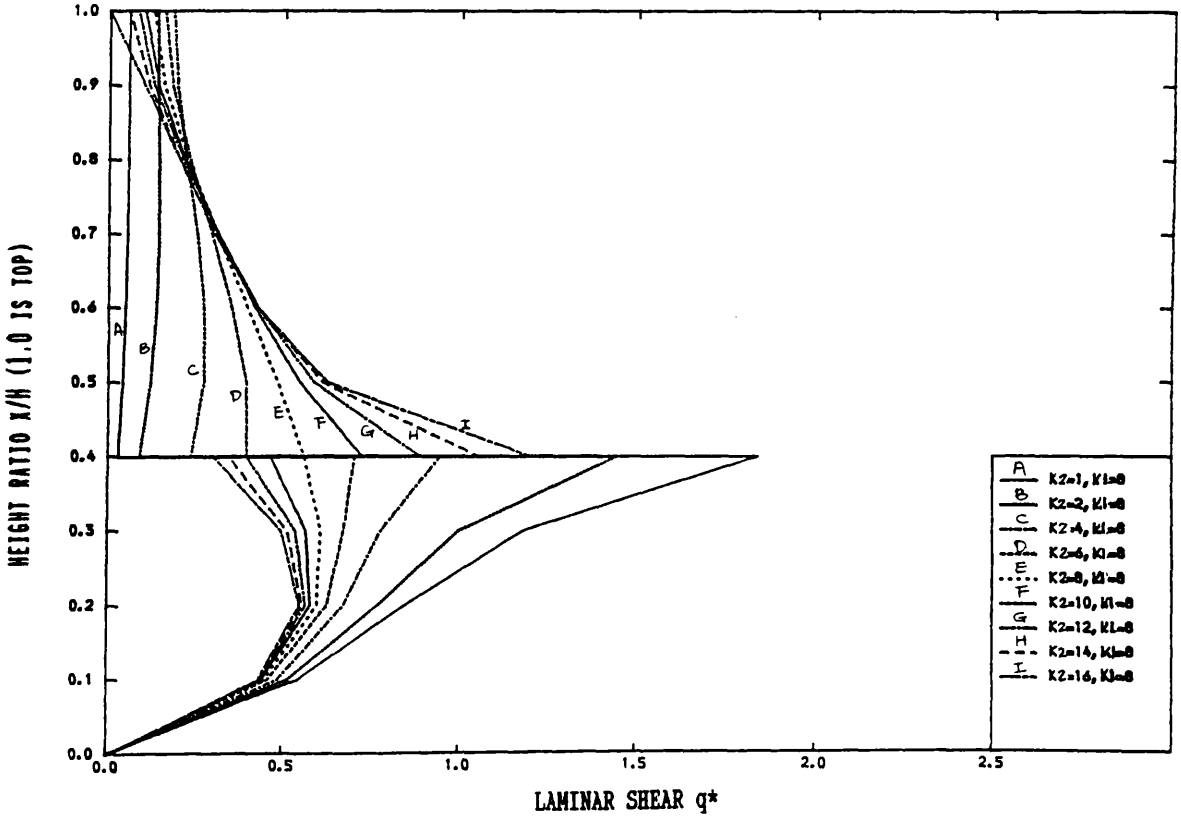

FIG. [6.49] VARIATION OF LAMINAR SHEAR WITH HEIGHT
(TWO DIFFERENT TYPES OF CONNECTING BEAMS)
(X_1/H=0.4,, U.D.L.)

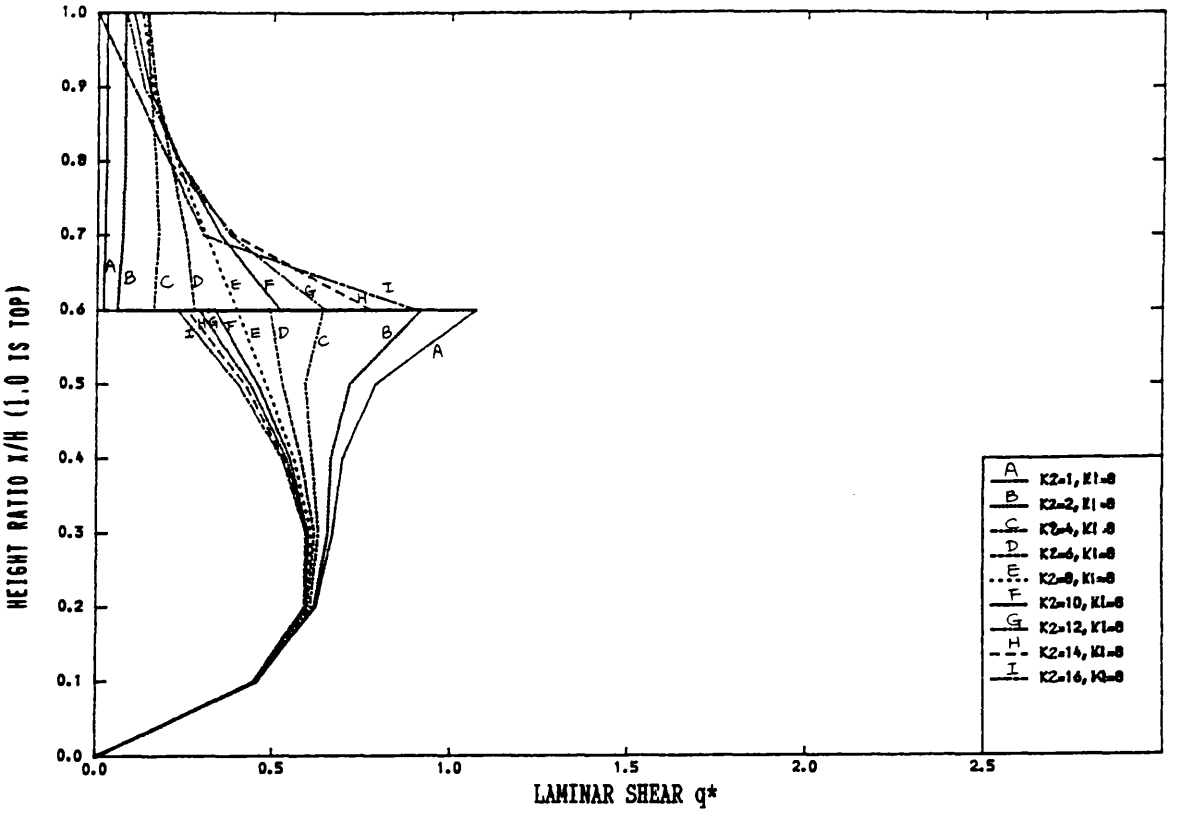

FIG. [6.50] VARIATION OF LAMINAR SHEAR WITH HEIGHT
(TWO DIFFERENT TYPES OF CONNECTING BEAMS)
(X_1/H=0.6,, U.D.L.)

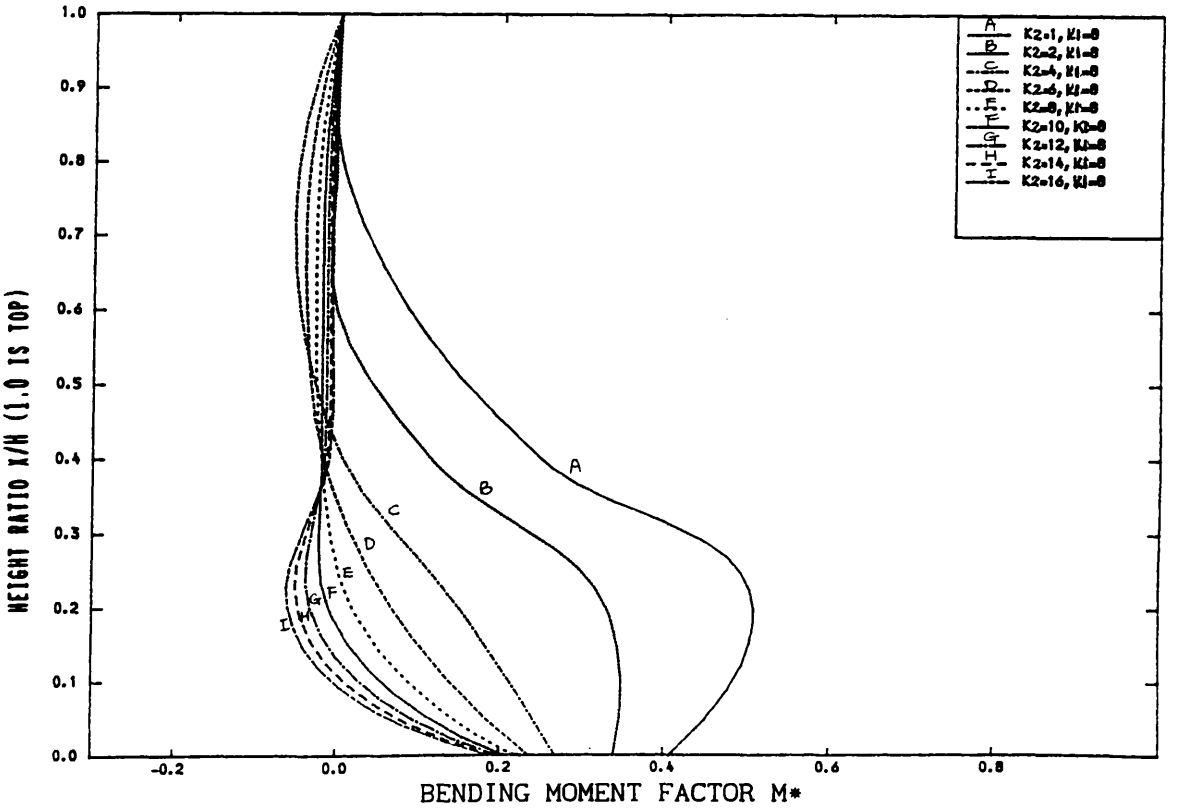

FIG. [6.51] VARIATION OF BENDING MOMENT WITH HEIGHT FOR DIFFERENT STIFFNESS FACTORS K1 AND K2
(TWO DIFFERENT TYPES OF CONNECTING BEAMS)
(X_1/H=0.2, U.D.L.)

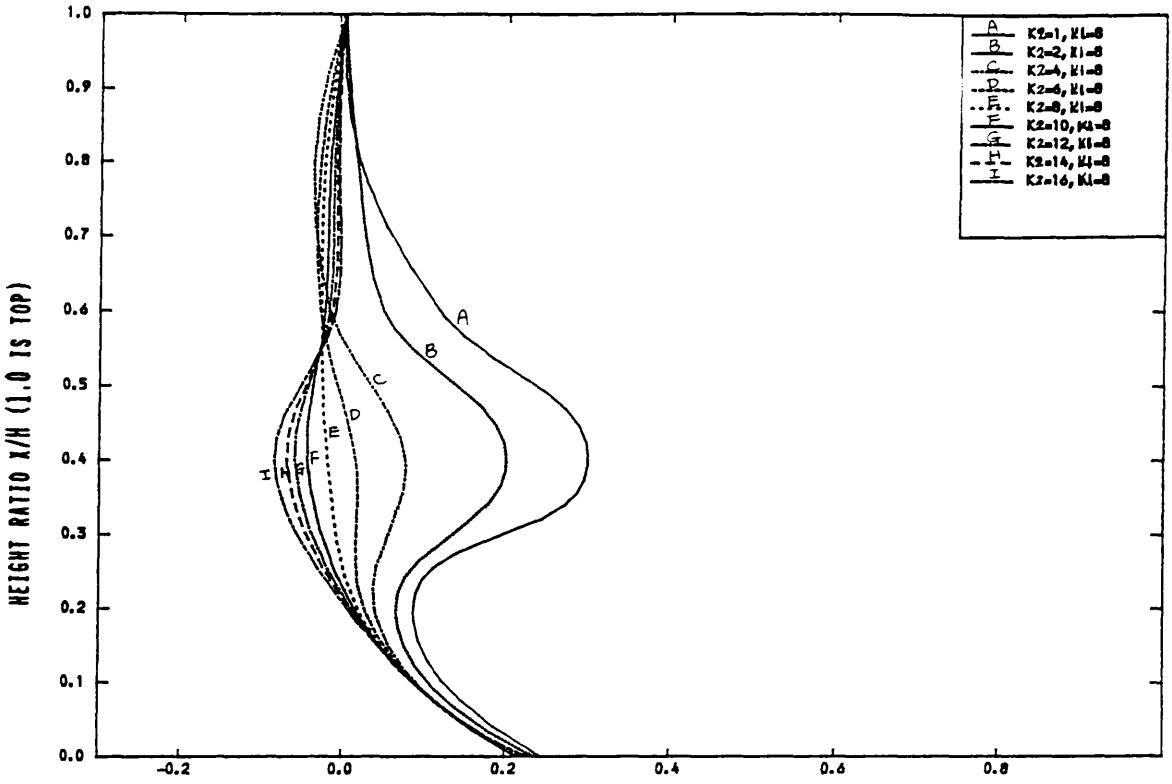

FIG. [6.52] VARIATION OF BENDING MOMENT WITH HEIGHT FOR DIFFERENT STIFFNESS FACTORS K1 AND K2
(TWO DIFFERENT TYPES OF CONNECTING BEAMS)
(X_1/H=0.4, U.D.L.)

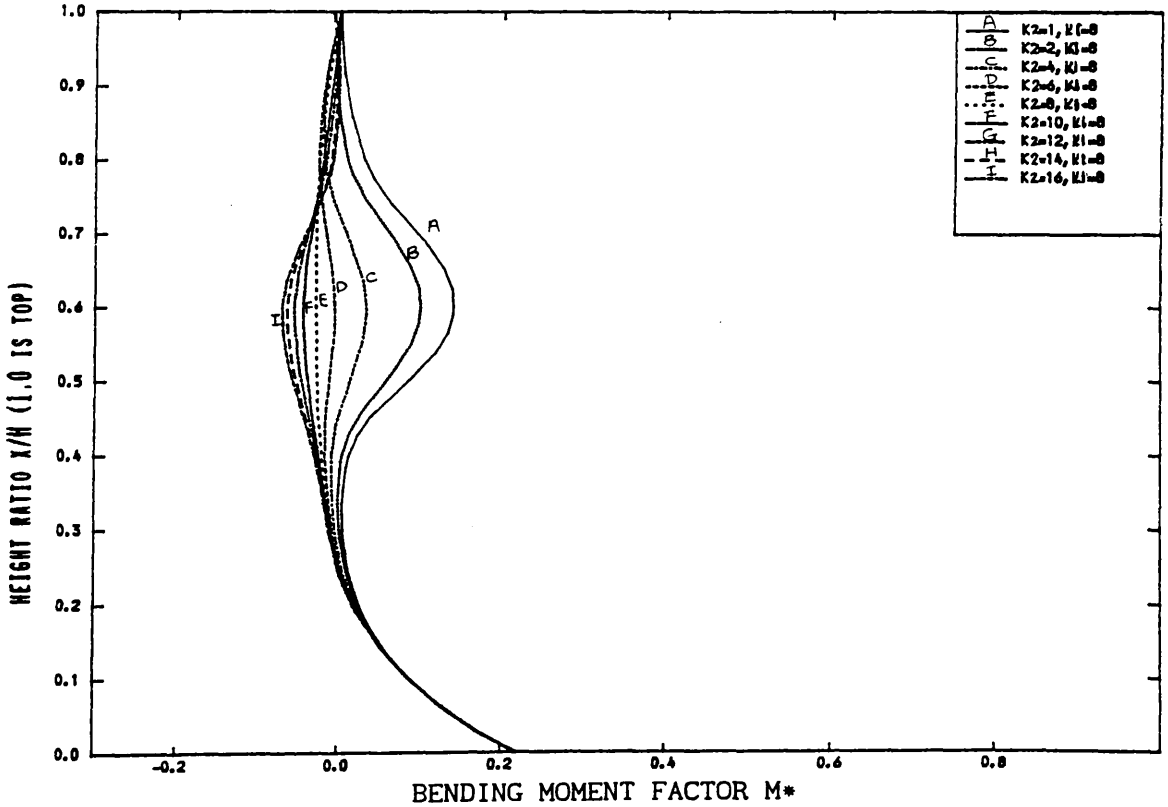

FIG. [6.53] VARIATION OF BENDING MOMENT WITH HEIGHT FOR DIFFERENT STIFFNESS FACTORS K1 AND K2
(TWO DIFFERENT TYPES OF CONNECTING BEAMS)
(X_1/H=0.6, U.D.L.)

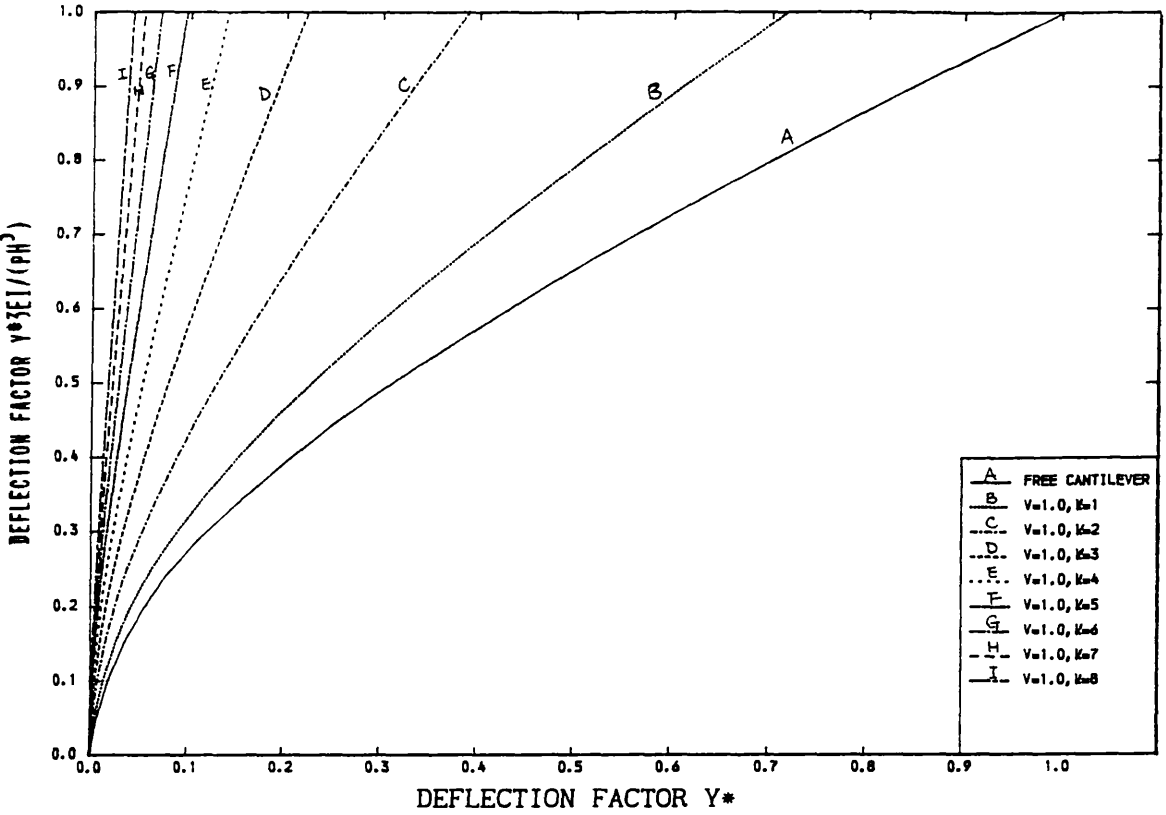

FIG.[6.54] VARIATION OF DEFLECTION WITH HEIGHT FOR DIFFERENT STIFFNESS FACTORS
(G=0, POINT LOAD AT THE TOP)

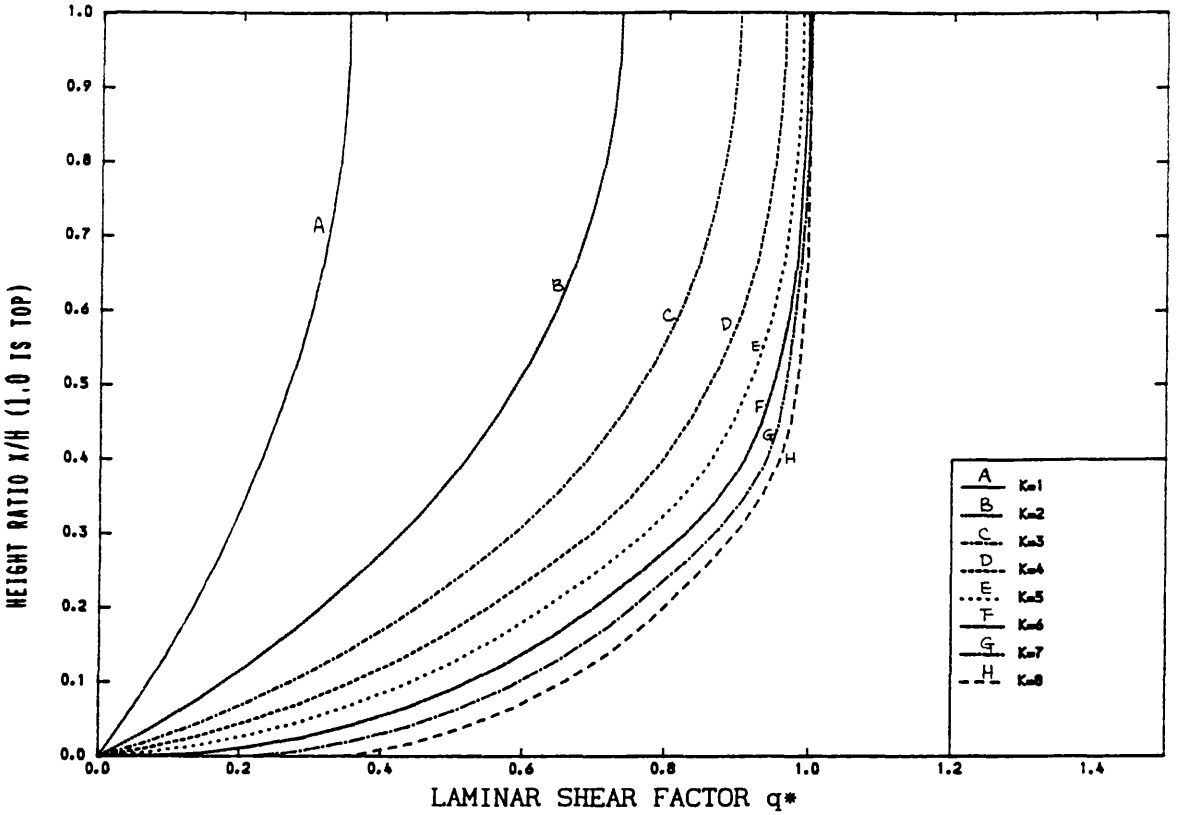

FIG. [6.55] VARIATION OF LAMINAR SHEAR WITH HEIGHT
(G=10, POINT LOAD AT THE TOP)

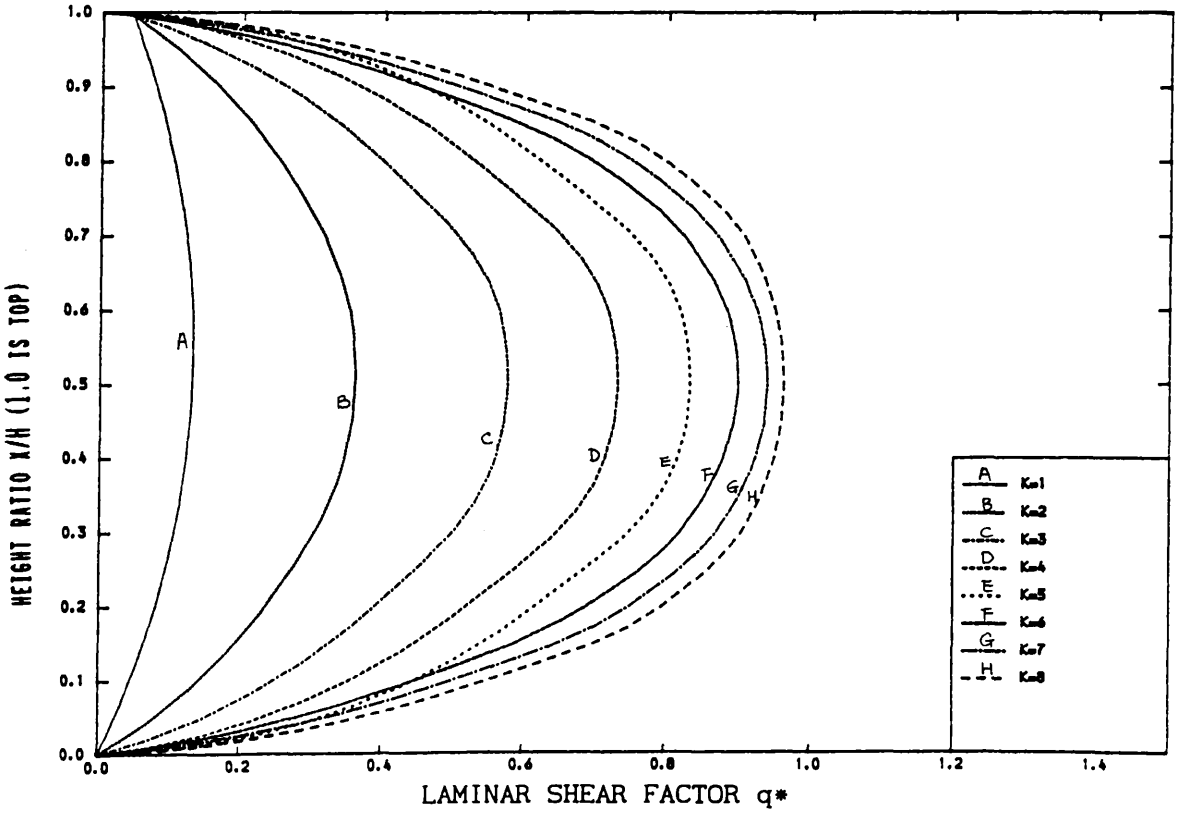

FIG. [6.56] VARIATION OF LAMINAR SHEAR WITH HEIGHT
(ONE INTERMEDIATE STIFFENING BEAM)
(G=10, X_1/H=1.0, POINT LOAD AT THE TOP)

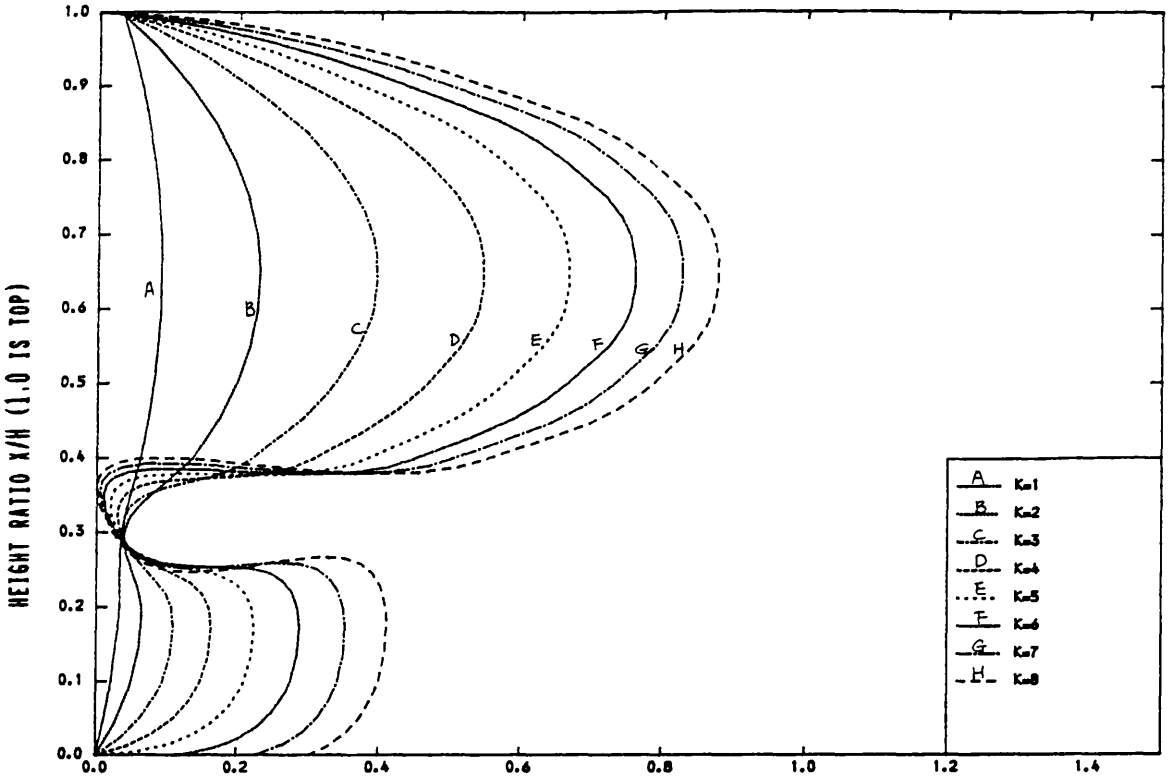

FIG. [6.57] VARIATION OF LAMINAR SHEAR WITH HEIGHT
(TWO INTERMEDIATE STIFFENING BEAM)
(G1=10, G2=10, X_1/H=.0.3, X_2/H=1.0)
(POINT LOAD AT THE TOP)

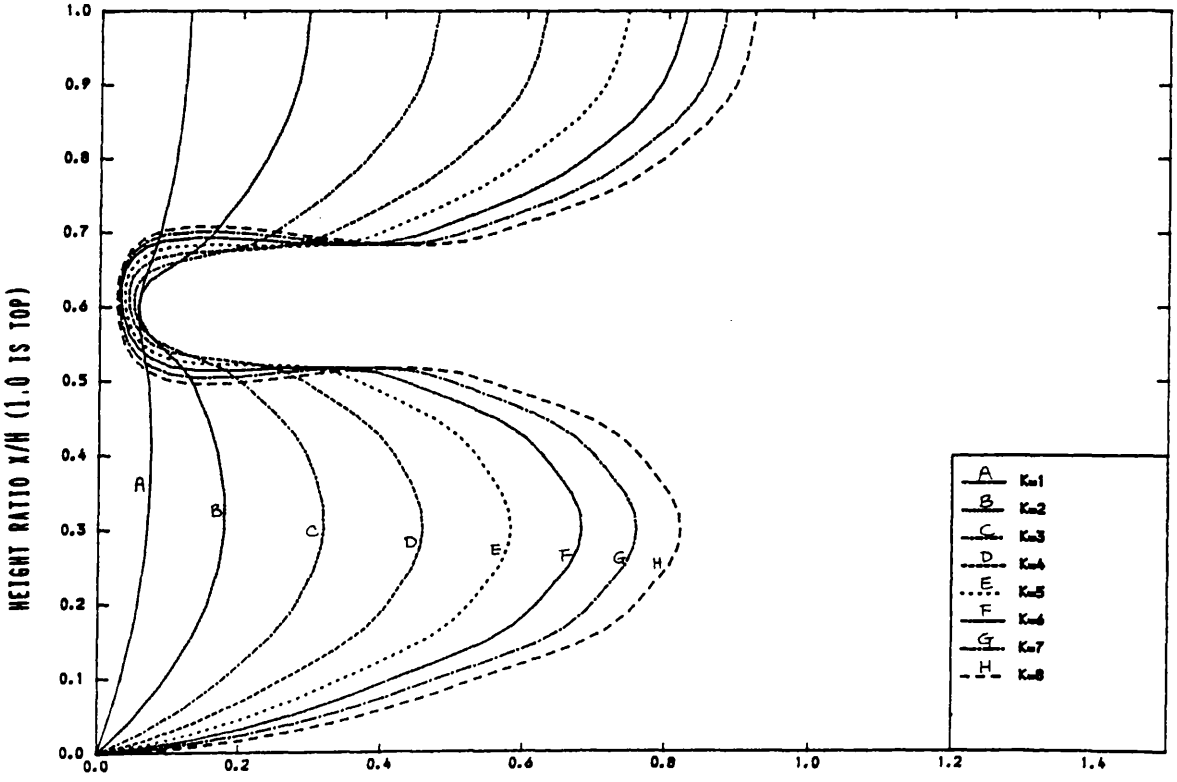

FIG. [6.58] VARIATION OF LAMINAR SHEAR WITH HEIGHT
(ONE INTERMEDIATE STIFFENING BEAM)
(G=10, X_1/H=0.6, POINT LOAD AT THE TOP)

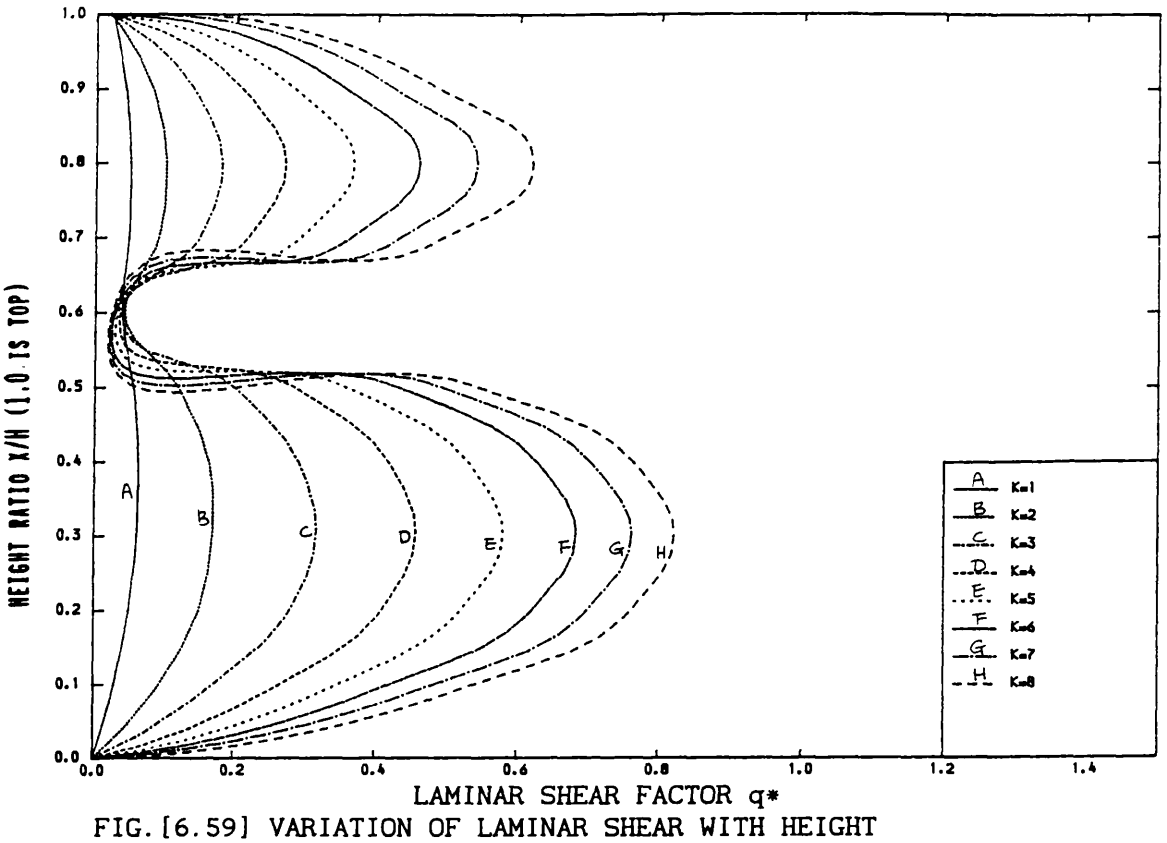

FIG. [6.59] VARIATION OF LAMINAR SHEAR WITH HEIGHT
(TWO INTERMEDIATE STIFFENING BEAMS)
(G1=10, G2=10, $X_1/H=0.6$, $X_2/H=1.0$)
(POINT LOAD AT THE TOP)

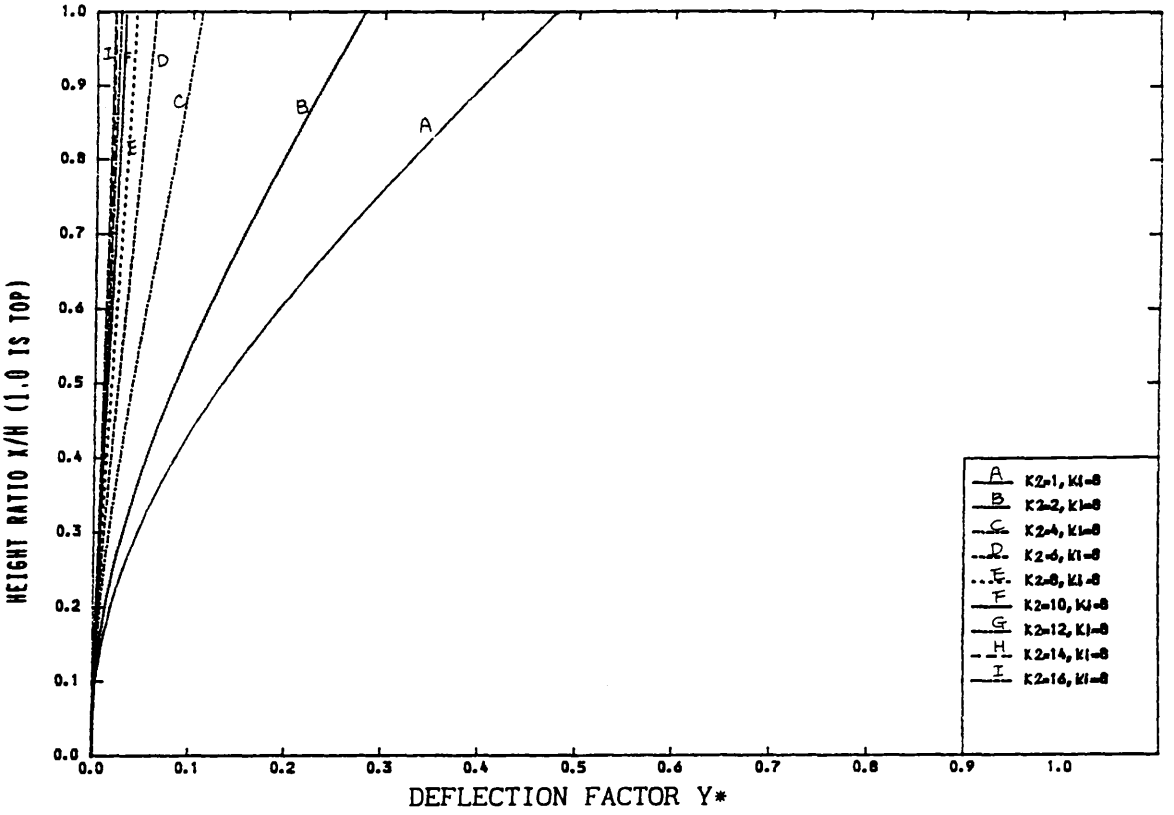

FIG. [6.60] VARIATION OF DEFLECTION WITH HEIGHT FOR DIFFERENT STIFFNESS FACTORS
(TWO DIFFERENT TYPES OF CONNECTING BEAMS)
(V=1.0, $X_1/H=0.2$, POINT LOAD AT THE TOP)

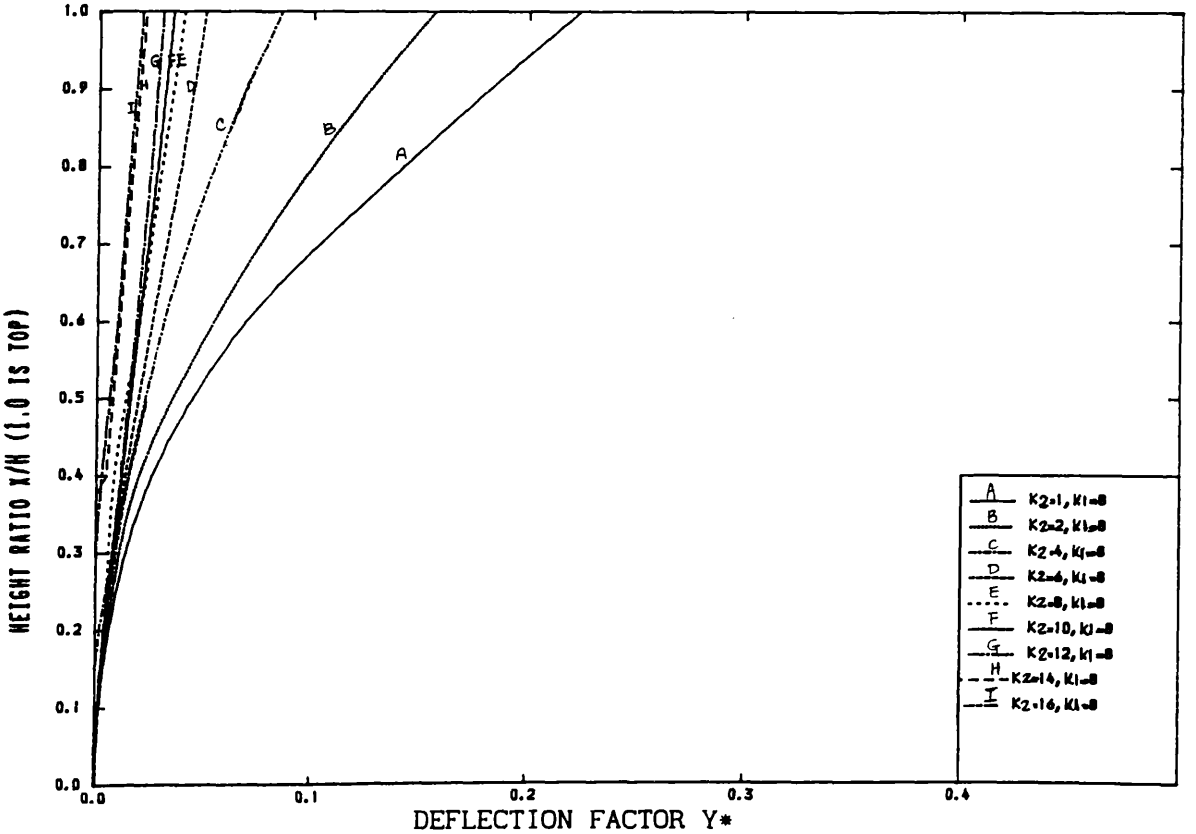

FIG. [6.61] VARIATION OF DEFLECTION WITH HEIGHT FOR DIFFERENT STIFFNESS FACTORS
(TWO DIFFERENT TYPES OF CONNECTING BEAMS)
(V=1.0, $X_1/H=0.4$, POINT LOAD AT THE TOP)

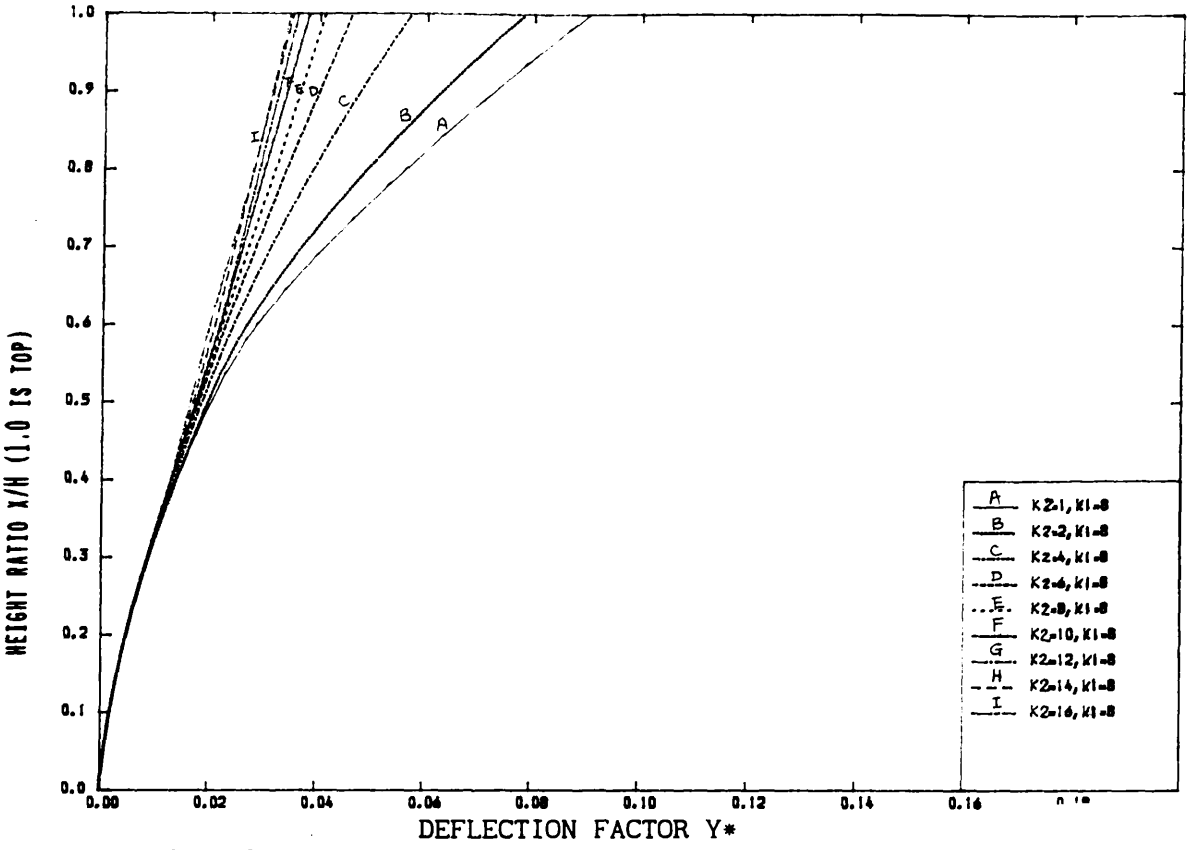

FIG. [6.62] VARIATION OF DEFLECTION WITH HEIGHT FOR DIFFERENT STIFFNESS FACTORS
(TWO DIFFERENT TYPES OF CONNECTING BEAMS)
(V=1.0, X_1/H=0.6, POINT LOAD AT THE TOP)

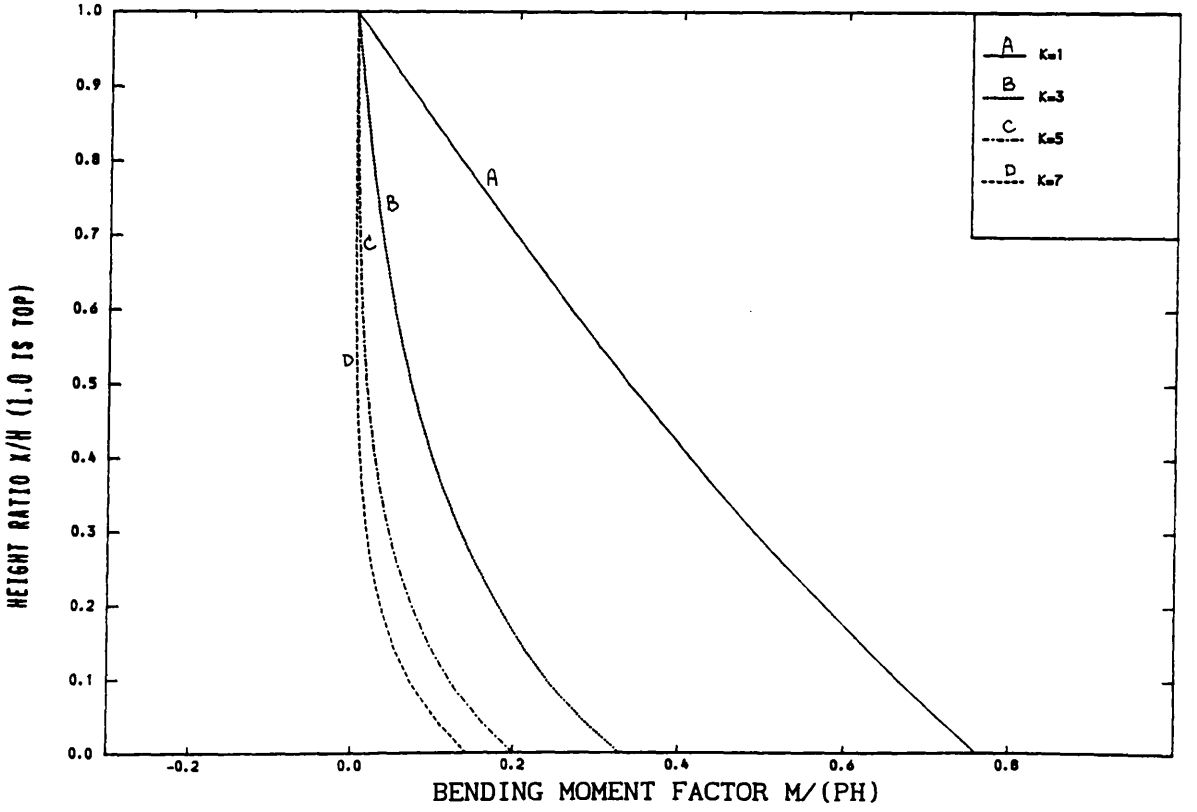

FIG. [6.63] VARIATION OF BENDING MOMENT WITH HEIGHT FOR DIFFERENT STIFFNESS FACTORS
(V=1.0, G=0, POINT LOAD AT THE TOP)

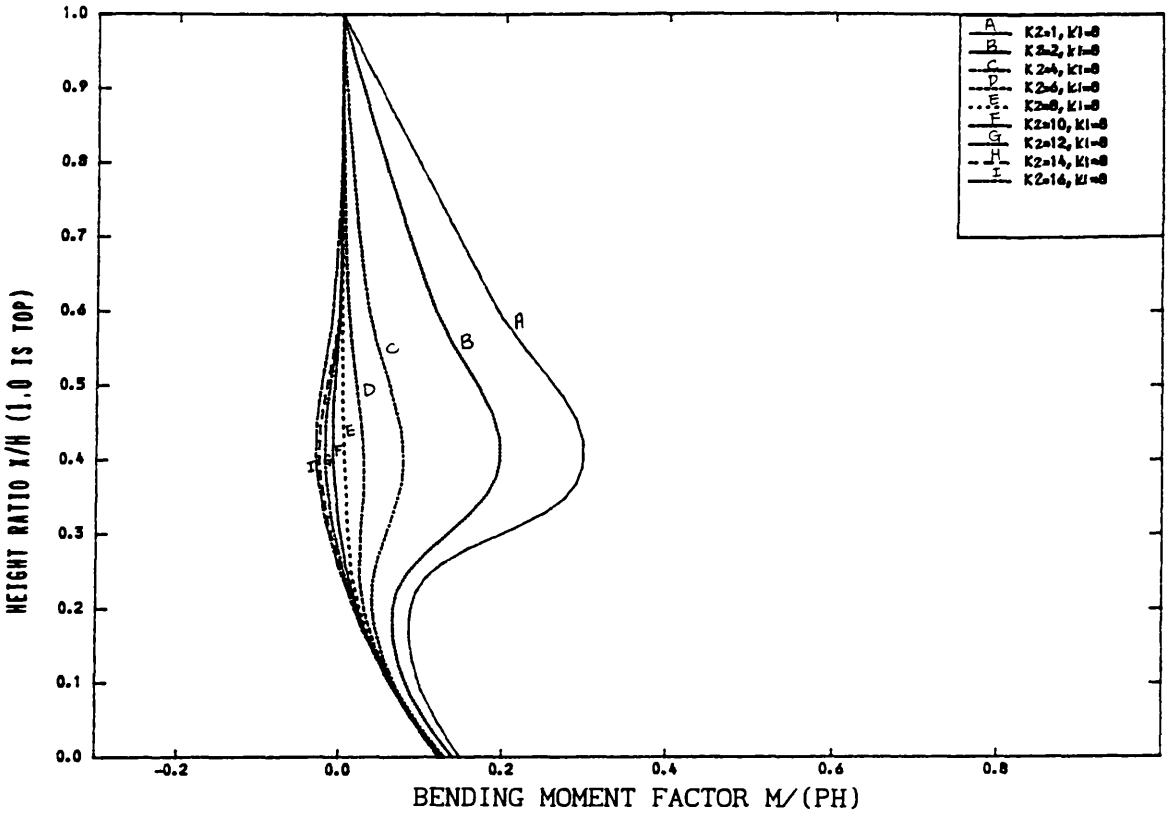

FIG. [6.68] VARIATION OF BENDING MOMENT WITH HEIGHT FOR DIFFERENT STIFFNESS FACTORS
(V=1.0, X_1/H=.0.4, POINT LOAD AT THE TOP)

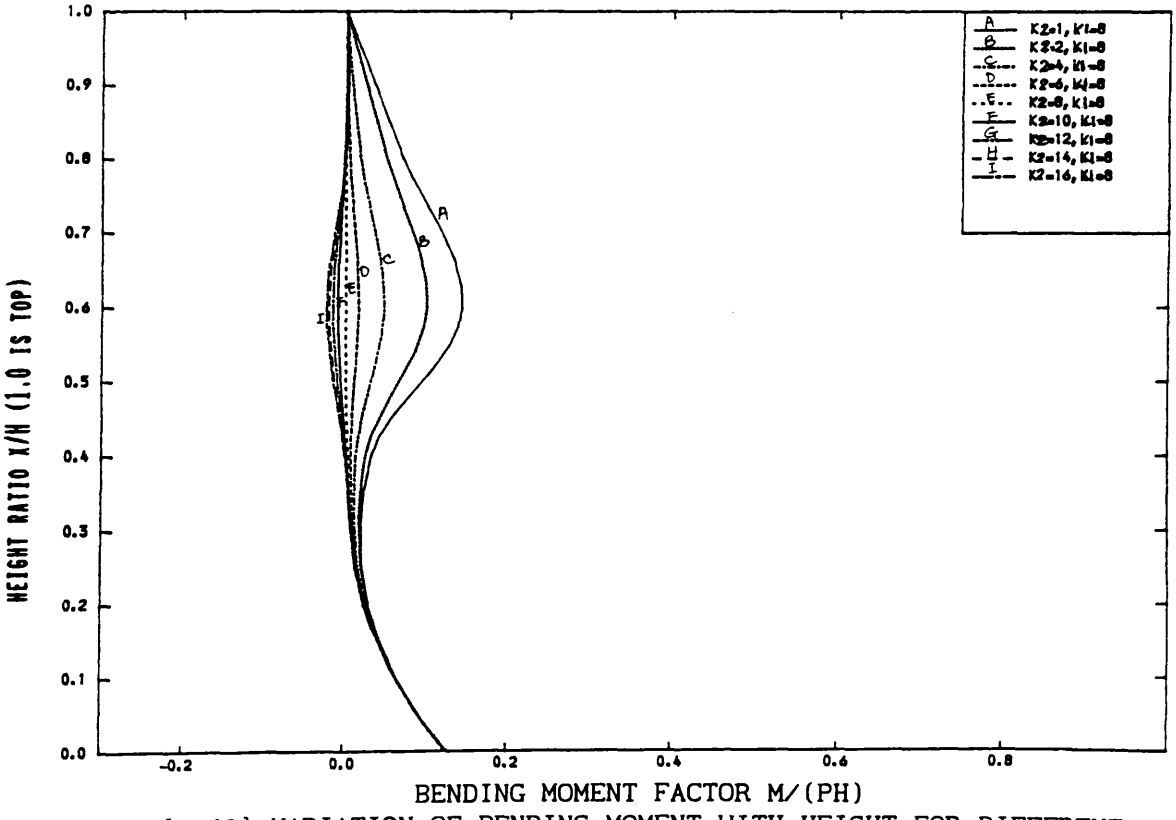

FIG. [6.69] VARIATION OF BENDING MOMENT WITH HEIGHT FOR DIFFERENT STIFFNESS FACTORS
(V=1.0, X_1/H=.0.6, POINT LOAD AT THE TOP)

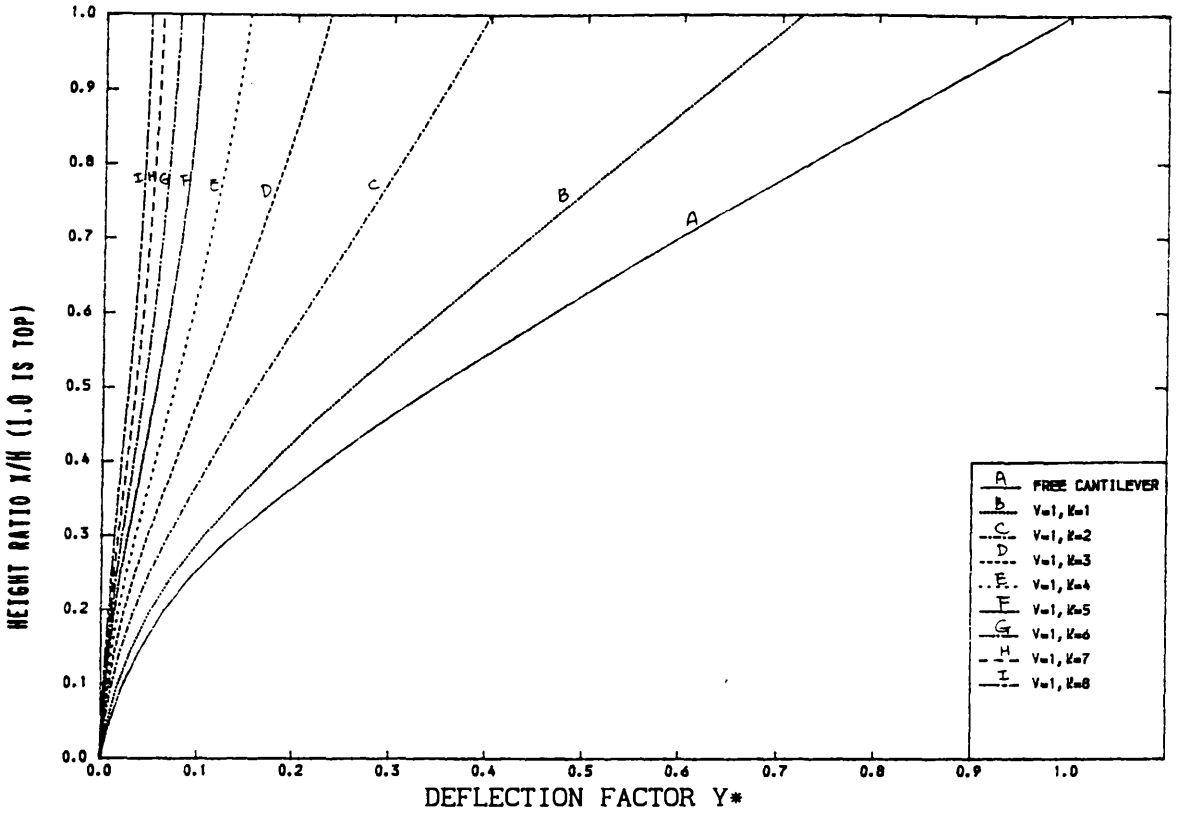

FIG. [6.70] VARIATION OF DEFLECTION WITH HEIGHT FOR DIFFERENT STIFFNESS FACTORS
(TWO DIFFERENT TYPES OF CONNECTING BEAMS)
(V=1.0, G=0, TRIANGULARLY DISTRIBUTED LOAD)

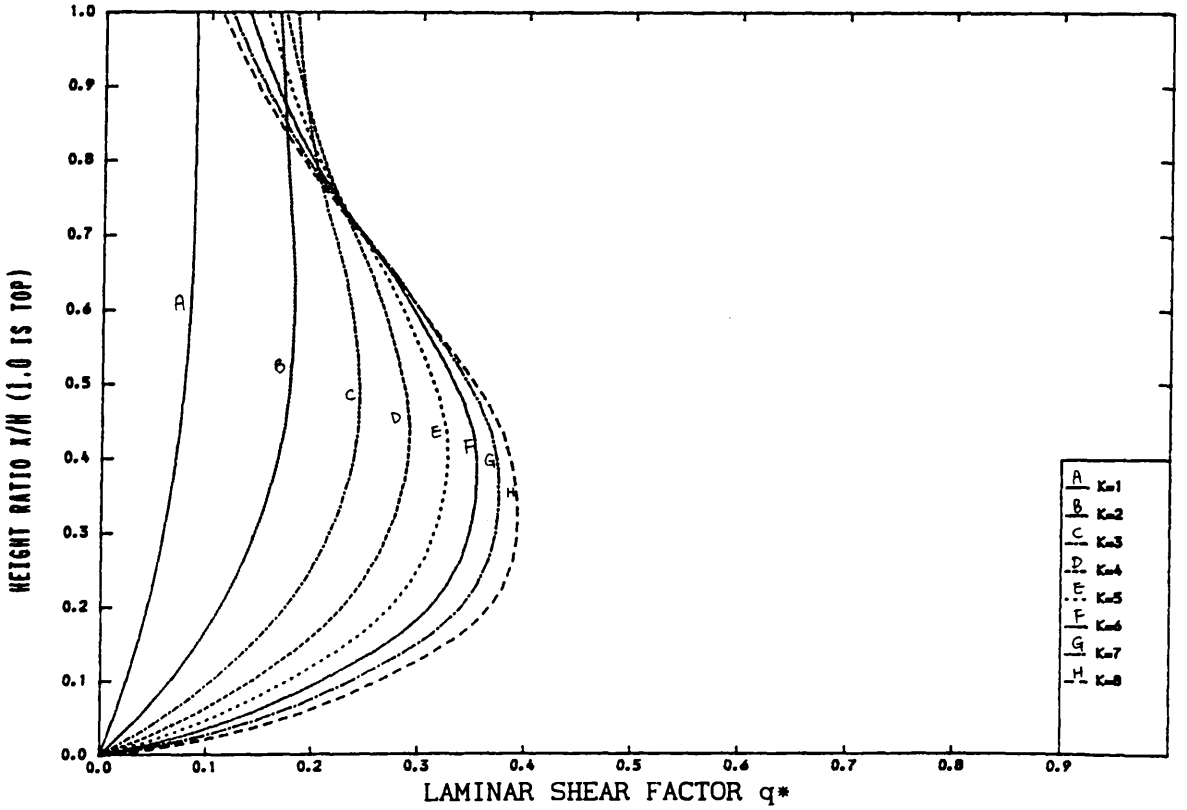

FIG. [6.71] VARIATION OF LAMINAR SHEAR WITH HEIGHT
(TWO DIFFERENT TYPES OF CONNECTING BEAMS)
(G=0, TRIANGULARLY DISTRIBUTED LOAD)

Table [6.1] Comparisons of structural efficiencies of different stiffening system (U.D.L., rigid foundation)

Type of structure	1/EIS	αH	y_T	M_B	y_{Tir}	M_{Bir}	r_y	r_m
			$*y_T$	$*M_{aB}$	$*y_T$	$*M_{aB}$	%	%
Plain coupled shear walls	0.1	1.0	0.972	0.982	0.900	0.900	27.75	18.48
		2.0	0.940	0.960	0.900	0.900	59.75	41.22
		3.0	0.924	0.946	0.900	0.900	76.22	54.90
		4.0	0.916	0.938	0.900	0.900	84.57	63.49
		5.0	0.911	0.932	0.900	0.900	89.23	69.44
		6.0	0.908	0.928	0.900	0.900	92.07	73.84
		7.0	0.906	0.924	0.900	0.900	93.93	77.22
		8.0	0.905	0.922	0.900	0.900	95.21	79.90
		9.0	0.904	0.920	0.900	0.900	96.13	82.07
		10.0	0.903	0.918	0.900	0.902	96.82	83.86
		11.0	0.903	0.917	0.900	0.900	97.34	85.37
		12.0	0.902	0.915	0.900	0.900	97.74	86.65
		13.0	0.902	0.914	0.900	0.900	98.07	87.75
		14.0	0.902	0.913	0.900	0.900	98.33	88.71
		15.0	0.902	0.912	0.900	0.900	98.53	89.55
		16.0	0.901	0.912	0.900	0.900	97.73	90.29
	0.2	1.0	0.945	0.964	0.800	0.800	27.75	18.48
		8.0	0.810	0.844	0.800	0.800	95.21	79.90
	0.4	1.0	0.889	0.928	0.600	0.600	27.75	18.48
		8.0	0.620	0.688	0.600	0.600	95.21	79.90
	0.6	1.0	0.834	0.892	0.400	0.400	27.75	18.48
		8.0	0.642	0.758	0.400	0.400	95.21	79.90
	0.8	1.0	0.778	0.855	0.200	0.200	27.75	18.48
		8.0	0.239	0.375	0.201	0.218	95.21	79.90
G1=0.3, xs/H=0.86	0.1	1.0	0.964				35.68	
G1=0.3, xs/H=0.65		2.0	0.933				66.92	
G1=0.3, xs/H=0.46		4.0	0.911				87.70	
G1=0.3, xs/H=0.41		5.0	0.909				91.41	
G1=0.3, xs/H=0.34		7.0	0.905				95.08	
G1=0.3, xs/H=0.32		8.0	0.904				96.07	
G1=0.5, xs/H=0.82		1.0	0.960				39.73	
G1=0.5, xs/H=0.46		4.0	0.911				88.78	
G1=0.5, xs/H=0.32		8.0	0.904				96.28	
G1=0.9, xs/H=0.77		1.0	0.954				46.02	
G1=0.9, xs/H=0.45		4.0	0.910				90.02	
G1=0.9, xs/H=0.32		8.0	0.904				96.49	
G1=0.5, xs/H=0.82	0.3	1.0	0.881				39.73	
G1=0.5, xs/H=0.46		4.0	0.734				88.78	
G1=0.5, xs/H=0.32		8.0	0.711				96.28	
G1=0.9, xs/H=0.77		1.0	0.862				46.02	
G1=0.9, xs/H=0.45		4.0	0.730				90.02	
G1=0.9, xs/H=0.32		8.0	0.711				96.49	
G1=.0.9, G2=0.9 xs1/H=0.63,xs2/H=1.00	0.1	1.0	0.944				55.35	
G1=.0.9, G2=0.9 xs1/H=0.44,xs2/H=1.00		3.0	0.913				86.74	
G1=.0.9, G2=0.9 xs1/H=0.38,xs2/H=1.00		5.0	0.907				93.28	
G1=.0.9, G2=0.9		7.0	0.904				95.82	

Table [6.2] Forces and deformations for example structure [6.1] (rigid foundation, U.D.L. of 600kN)

Foundation flexibility		Stiff beam				$T_{(x=0)}$	$M_{(x=0)}$	d	$\vartheta_{(x=0)}$	y_T	q_{max}	x_{qmax}
k_d	k_ϑ	γ_1	γ_2	xs_1	xs_2				$x10^{-6}$			
$x10^{-6}$ m/kN	$x10^{-8}$ rad/kNm	m	m	m	m	kN	kNm	mm	rad	mm	kN/m	m
rigid	rigid	/	/	/	/	766	10335	0	0	9.9	16.1	26
rigid	rigid	10	/	60	/	775	10239	0	0	9.4	15.4	24
rigid	rigid	/	10	/	18	821	9777	0	0	9.4	14.5	30
rigid	rigid	/	10	/	33	794	10041	0	0	9.2	14.1	24
rigid	rigid	/	10	/	36	790	10083	0	0	9.2	14.4	24
rigid	rigid	10	10	60	18	828	9702	0	0	8.9	13.7	30
rigid	rigid	10	10	60	36	797	10018	0	0	8.8	13.9	18
rigid	rigid	81	/	60	/	789	10105	0	0	8.7	14.5	24
rigid	rigid	/	81	/	18	971	8270	0	0	8.0	10.9	36
rigid	rigid	/	81	/	30	881	9175	0	0	7.5	9.8	18
rigid	rigid	/	81	/	36	849	9504	0	0	7.6	11.3	18
rigid	rigid	81	81	60	18	979	8197	0	0	7.1	9.1	30
rigid	rigid	81	81	60	27	906	8920	0	0	6.6	8.7	18
rigid	rigid	81	81	60	36	853	9462	0	0	7.2	11.1	18
rigid	rigid	273	/	60	/	793	10059	0	0	8.5	14.2	24
rigid	rigid	/	273	/	18	1049	7491	0	0	7.3	9.3	42
rigid	rigid	/	273	/	30	918	8799	0	0	6.8	8.2	18
rigid	rigid	/	273	/	36	874	9251	0	0	6.9	10.2	18
rigid	rigid	273	273	60	18	1052	7459	0	0	6.4	7.2	36
rigid	rigid	273	273	60	24	980	8188	0	0	6.2	6.5	18
rigid	rigid	273	273	60	36	875	9237	0	0	6.6	10.1	18

Table [6.3] Forces and deformations for example structure [6.1] (stiff soil, U.D.L. of 600kN)

Foundation flexibility		Stiff beam				$T_{(x=0)}$	$M_{(x=0)}$	d	$\vartheta_{(x=0)}$	y_T	q_{max}	x_{qmax}
k_d	k_ϑ	γ_1	γ_2	xs_1	xs_2				$x10^{-6}$			
$x10^{-6}$ m/kN	$x10^{-8}$ rad/kNm	m	m	m	m	kN	kNm	mm	rad	mm	kN/m	m
1.07	rigid	/	/	/	/	606	11933	0.65	0	12.0	14.0	30
1.07	rigid	10	/	60	/	613	11858	0.66	0	11.6	13.2	30
1.07	rigid	/	10	/	0	551	12480	0.59	0	11.8	14.2	30
1.07	rigid	10	10	60	0	558	12416	0.57	0	11.4	13.4	30
1.07	rigid	81	/	60	0	623	11762	0.67	0	10.9	12.0	27
1.07	rigid	/	81	/	0	337	14616	0.36	0	11.1	14.9	29
1.07	rigid	81	81	60	0	347	14525	0.37	0	9.9	13.2	24
1.07	rigid	273	/	60	/	627	11727	0.67	0	10.7	11.8	25
1.07	rigid	/	273	/	0	164	16351	0.18	0	10.5	15.4	28
1.07	rigid	/	273	/	3	694	11045	0.74	0	10.0	6.3	48
1.07	rigid	273	273	60	0	170	16294	0.18	0	9.0	13.6	24
rigid	3.22	/	/	/	/	1222	5770	0	186	15.1	24.8	12
rigid	3.22	10	/	60	/	1228	5702	0	184	14.4	24.3	18
rigid	3.22	/	10	/	0	1323	4753	0	153	14.2	22.8	18
rigid	3.22	10	10	60	0	1328	4701	0	151	13.5	22.2	15
rigid	3.22	81	/	60	/	1238	5610	0	181	13.5	23.7	11
rigid	3.22	/	81	/	0	1585	2140	0	69	11.8	18.8	22
rigid	3.22	/	81	/	9	1463	3345	0	107	11.3	15.8	27
rigid	3.22	81	81	60	0	1590	2081	0	67	10.4	17.3	20
rigid	3.22	80	81	60	9	1469	3269	0	106	10.0	14.1	27
rigid	3.22	273	/	60	/	1241	5580	0	179	13.2	23.4	12
rigid	3.22	/	273	/	0	1714	844	0	27	10.6	17.1	24
rigid	3.22	/	273	/	9	1564	2334	0	75	8.5	11.4	27
1.07	3.22	/	/	/	/	1065	7350	1.14	236	20.2	21.2	18
1.07	3.22	10	/	60	/	1071	7277	1.15	234	19.6	20.6	18
1.07	3.22	/	10	/	0	1122	6765	1.20	217	19.8	19.9	18
1.07	3.22	10	10	60	0	1126	6723	1.21	217	19.3	19.4	18
1.07	3.22	81	/	60	/	1078	7206	1.16	232	18.7	19.7	16
1.07	3.22	/	81	/	12	1184	6143	1.27	198	18.2	15.0	30
1.07	3.22	81	81	60	0	1258	5410	1.35	174	17.3	16.0	21
1.07	3.22	81	81	60	12	1188	6103	1.27	197	17.1	13.5	24
1.07	3.22	273	/	60	/	1081	7178	1.17	231	18.4	19.5	18
1.07	3.22	/	273	/	0	1314	4849	1.41	156	18.8	16.6	24
1.07	3.22	/	273	/	21	1187	6116	1.27	197	16.6	9.7	38
1.07	3.22	273	273	60	0	1315	4831	1.40	156	17.3	14.8	24
1.07	3.22	273	273	60	18	1212	5866	1.30	189	15.7	8.5	30

Table [6.4] Forces and deformations for example structure [6.1] (weak soil, U.D.L. of 600kN)

Foundation flexibility		Stiff beam				$T_{(x=0)}$	$M_{(x=0)}$	d	$\vartheta_{(x=0)}$	y_T	q_{max}	x_{qmax}
k_d	k_ϑ	γ_1	γ_2	xs_1	xs_2				$x10^{-6}$			
$x10^{-6}$ m/kN	$x10^{-8}$ rad/kNm	m	m	m	m	kN	kNm	mm	rad	mm	kN/m	m
3.22	rigid	/	/	/	/	428	13718	1.38	0	14.3	-15.9	0
3.22	rigid	10	/	60	/	432	13672	1.39	0	14.0	11.1	30
3.22	rigid	/	10	/	0	353	14466	1.14	0	13.4	12.5	30
3.22	rigid	/	10	/	3	320	14795	1.03	0	13.4	13.2	33
3.22	rigid	10	10	60	0	357	14428	1.15	0	13.2	11.8	30
3.22	rigid	10	10	60	3	324	14755	1.04	0	13.0	12.3	30
3.22	rigid	81	/	60	/	439	13608	1.41	0	13.4	-16.4	0
3.22	rigid	/	81	/	0	159	16406	0.51	0	11.6	14.4	24
3.22	rigid	81	81	60	0	164	16360	0.53	0	10.5	12.5	26
3.22	rigid	273	/	60	/	440	13588	1.41	0	13.3	9.6	30
3.22	rigid	/	273	/	0	64	17360	0.21	0	10.6	15.3	30
3.22	rigid	273	273	60	0	66	17338	0.20	0	9.2	13.5	24
rigid	9.66	/	/	/	/	1493	3060	0	295	18.1	34.3	0
rigid	9.66	10	/	60	/	1496	3016	0	291	17.3	33.9	0
rigid	9.66	/	10	/	0	1570	2276	0	219	16.0	27.1	12
rigid	9.66	10	10	60	0	1573	2250	0	217	15.3	26.6	12
rigid	9.66	81	/	60	/	1502	2961	0	286	16.2	33.3	0
rigid	9.66	/	81	/	0	1717	820	0	79	12.1	19.1	21
rigid	9.66	/	81	/	3	1693	1053	0	102	12.0	18.3	21
rigid	9.66	81	81	60	0	1719	793	0	77	10.7	17.8	18
rigid	9.66	81	81	60	3	1694	1031	0	99.7	10.6	16.9	21
rigid	9.66	273	/	60	/	1503	2944	0	284	16.1	33.3	0
rigid	9.66	/	273	/	0	1770	285	0	27.5	10.6	17.1	24
rigid	9.66	/	273	/	6	1721	767	0	74.2	10.2	14.7	30
rigid	9.66	/	273	/	0	1770	285	0	27.5	10.6	17.1	24
rigid	9.66	/	273	/	6	1721	767	0	74.2	10.2	14.7	30
3.22	9.66	/	/	/	/	1209	5894	3.90	569	38.3	24.5	13
3.22	9.66	10	/	60	/	1212	5864	3.90	566	37.6	23.9	12
3.22	9.66	/	10	/	0	1247	5515	4.02	531	37.6	21.7	18
3.22	9.66	10	10	60	0	1249	5496	4.02	531	37.0	21.1	18
3.22	9.66	81	/	60	/	1216	5826	3.92	563	36.7	23.1	12
3.22	9.66	/	81	/	0	1314	4850	4.23	468	36.5	17.8	24
3.22	9.66	/	81	/	0	1283	5159	4.13	498	36.3	17.5	24
3.22	9.66	81	81	60	0	1315	4840	4.24	467	35.2	16.3	21
3.22	9.66	81	81	60	6	1301	4973	4.19	480	35.1	16.1	21
3.22	9.66	273	/	60	/	1217	5812	3.92	561	36.4	22.8	12
3.22	9.66	/	273	/	0	1336	4615	4.30	446	36.1	16.7	24
3.22	9.66	/	273	/	15	1286	5122	4.14	495	34.7	12.6	32
3.22	9.66	273	273	60	0	1338	4608	4.31	445	34.6	14.8	24
3.22	9.66	273	273	60	12	1301	4974	4.19	480	33.5	11.1	30

CHAPTER SEVEN

DYNAMIC ANALYSIS OF OUTRIGGER-BRACED STRUCTURES USING CONTINUUM TECHNIQUE

NOTATION of Chapter 7

A_c	sectional area of column
d	distance between columns
E	elastic modulus of core
E_c	elastic modulus of column
E_o	elastic modulus of outrigger
H	height of structure
I	moment inertia of core
I_o	effective moment of inertia of outrigger
I_r	actual moment of inertia of outrigger
m	mass of walls per unit height
M_a	applied moment due to external loads
q	shear force per unit height in the medium
T	axial force in column
α', β', λ	structural parameters
ϕ	function describing variation of deflection with height
ψ	ϕ/H
ρ	mass per unit height of the system of core wall
η	function describing variation of deflection with time

Other subsidiary symbols are defined locally in the text.

7.1 INTRODUCTION

Chapter 3 highlighted the use of the continuous connection technique for the static analysis of outrigger-braced structures. The method is simple and yet accurate. It assumes that the discrete system of outrigger arms connecting the core walls and the columns may be replaced by an equivalent continuous medium. By assuming that the set of outriggers is smeared over the height to give an equivalent uniform bracing system, the equations of equilibrium and compatibility yield a second-order governing differential equation. This enables a general closed solution to the problem to be obtained, and allows simple design curves to be generated. As far as statical behaviour is concerned, the method has been proved to give reasonably accurate results for even a very small number of outriggers.

It has been shown that there is an analogy between the structural action of laterally loaded coupled shear walls and multi-outrigger-braced structures for very tall structures. The dynamic analysis of both forms of structure, which are essentially uniform throughout their height, but contain several structural discontinuities where stiffening girders are introduced has been shown to be handled by the transfer matrix technique in Chapter 5. The field transfer matrix technique has been demonstrated to be applicable to the dynamic analysis of multi-outrigger-braced and coupled shear wall structures to give natural frequencies and modes of vibration. However, as the number of structural discontinuities due to the outriggers or connecting beams increases, the operation of the matrices for final solutions will

become more complex.

The free bending and torsional vibrations of regular symmetric cross-wall structures has already been studied by Coull[41]. In this Chapter, his analysis which is based on the continuous connection technique is extended to cover the multi-outrigger-braced structures. The Galerkin technique as described in detail in Ref.[41] was applied to determine the natural modes and frequencies of vibration.

7.2 ANALYSIS

Consider the multi-outrigger-braced structure replaced by continuous medium,as shown in Fig.[7.1]. The n outriggers are rigidly connected to the central core and pin-connected to external columns to ensure that the latter carry only axial forces. The discrete set of outriggers, each of flexural rigidity E_oI_o, is assumed smeared over the height to produce an equivalent uniform bracing medium of flexural rigidity E_oI_on/H per unit height. The basic assumptions are given in detail in Chapter 3.

If the axial force at any level in a column is T, consideration of the equilibrium of a small element of column and outrigger medium shows that

$$T = \int_x^H q\, dx \qquad (7.1)$$

In equation (7.1), x is the distance measured from the base of the structure and q is the shear force per unit height in the bracing medium, as shown in Fig.[7.1]. Equation (7.1) can be written as

$$q = - \frac{dT}{dx} \tag{7.2}$$

The equation of vertical deflection compatibility at the junction between external columns and outriggers, is

$$\frac{d}{2}\frac{dy}{dx} - \frac{q(d/2)^3 H}{3E_o I_o n} - \frac{1}{E_c A_c}\int_0^x T\,dx = 0 \tag{7.3}$$

where

d is the distance between columns

$E_c A_c$ is the axial rigidity of the columns

$E_o I_o$ is the flexural rigidity of the outrigger

In equation (4.3), the three terms represent the relative vertical displacement due, respectively, to bending of the core, bending of the outriggers, and axial deformations of the columns.

The moment-curvature relationship for the core is

$$EI \frac{d^2 y}{dx^2} = M = M_a - Td \tag{7.4}$$

where

M is the moment in the core

M_a is the applied moment

EI is the flexural rigidity of the core

Differentiation of equation (7.3) once and (7.4) twice, and using (7.1) yields, respectively,

$$\frac{d}{2}\frac{d^2y}{dx^2} + \frac{d^3H}{24E_oI_on}\frac{d^2T}{dx^2} - \frac{1}{E_cA_c}T = 0 \qquad (7.5)$$

$$EI\frac{d^4y}{dx^4} = \frac{d^2M_a}{dx^2} - d\frac{d^2T}{dx^2} \qquad (7.6)$$

Eliminating T and d^2T/dx^2 from equations (7.4), (7.5) and (7.6) and rearranging, yields the equation

$$EI\frac{d^4y}{dx^4} - EI\alpha'\frac{d^2y}{dx^2} = \frac{d^2M_a}{dx^2} - \beta'M_a \qquad (7.7a)$$

where

$$\alpha' = \frac{24E_oI_on}{EId^2H}\left(\frac{d}{2} + \frac{EI}{E_cA_cd}\right) \qquad (7.7b)$$

$$\beta' = \frac{24E_oI_on}{E_cA_cd^3H} \qquad (7.7c)$$

Equation (7.6) is the differential equation for the deflection of a statically loaded multi-outrigger-braced structure. By d'Alembert's principle, the dynamic equation of a vibrating structure may be derived from equation (7.6) provided that the

external forces are augmented by the inertia forces. In the case of free vibrations, the only forces acting are the inertia forces and the lateral force intensity is given by,

$$\frac{\partial^2 M}{\partial x^2} = -\rho \frac{\partial^2 y}{\partial t^2} \tag{7.8}$$

where ρ is the mass per unit height of the system of core wall. The use of a continuous system allows the masses of the floor slabs to be incorporated in the total mass of the core wall.

On changing to partial derivatives to take account of the two variables x and t, differentiating equation (7.6) twice with respect to x, and substituting for $\partial^2 M/\partial x^2$ from (7.8), the governing equation becomes,

$$\frac{\partial^6 y}{\partial x^6} - \alpha' \frac{\partial^4 y}{\partial x^4} = -\frac{\rho}{EI} \left(\frac{\partial^4 y}{\partial x^2 dt^2} - \beta' \frac{\partial^2 y}{\partial t^2} \right) \tag{7.9}$$

Assuming that the deflection y may be expressed in terms of a height function $\phi(x)$ and a time function $\eta(t)$ such that,

$$y = \phi(x)\eta(t) \tag{7.10}$$

and using the method of separation of variables, two equations involving ordinary derivatives may be obtained as

$$\frac{d^2\eta}{dt^2} + \omega^2\eta = 0 \qquad (7.11)$$

and

$$\frac{d^6\phi}{dx^6} - \alpha'\frac{d^4\phi}{dx^4} = \frac{\omega^2\rho}{EI}\left(\frac{d^2\phi}{dx^2} - \beta'\phi\right) \qquad (7.12)$$

where ω is the circular frequency.

The solution of equation (7.7a) may be expressed in terms of the frequency ω as

$$\eta = P\cos\omega t + Q\sin\omega t \qquad (7.13)$$

where P and Q are the integration constants and must be determined from the initial conditions at time t=0.

By introducing for convenience a system of non-dimensional parameters defined as,

$$z = \frac{x}{H}$$

$$\psi = \frac{\phi}{H}$$

$$\alpha = \alpha' H^2$$

$$\beta = \beta' H^2$$

and

$$\lambda = \frac{\rho\omega^2 H^4}{EI} \qquad (7.14)$$

equation (7.12) may be rewritten in the form,

$$(D^6 - \alpha D^4)\psi = \lambda(D^2 - \beta)\psi \qquad (7.15)$$

where the operator D represents differentiation with respect to the non-dimensional height coordinate z.

For the structure rigidly built-in at the base and free at the top, the relevant boundary conditions are:

At x = 0, t (z = 0,t)

$$y = 0 \quad \text{i.e. } \psi = 0 \qquad (7.16a)$$

$$\frac{\partial y}{\partial x} = 0 \quad \text{i.e. } D\psi = 0 \qquad (7.16b)$$

$$q = 0 \qquad (7.16c)$$

At x = H, t (z = 1,t)

$$\frac{\partial^2 y}{\partial x^2} = 0 \quad \text{i.e. } D^2\psi = 0 \qquad (7.16d)$$

$$\frac{\partial q}{\partial x} = 0 \qquad (7.16e)$$

$$\frac{\partial M}{\partial x} = 0 \qquad (7.16f)$$

On using equations (7.4), (7.1), (7.10) and (7.13), the boundary conditions (7.16c), (7.16e) and (7.16f) may be expressed in terms of the displacement function ψ as,

At $z = 0$, t

$$D^5\psi - (\alpha-\beta)D^3\psi = 0 \qquad (7.16g)$$

At $z = 1$, t

$$D^4\psi = \lambda\psi \qquad (7.16h)$$

$$(D^5 - \alpha D^3)\psi = \lambda D\psi \qquad (7.16i)$$

Equation (7.15) is a sixth-order equation, and its solution in closed form is not practical, although theoretically possible. It is therefore necessary to seek a numerical solution to obtain the characteristic equation for the determination of the natural frequencies and modes of vibration. Practically important numerical methods lead to a matrix characteristic equation of the form $\mathbb{A}.\mathbb{X} = \lambda.\mathbb{B}.\mathbb{X}$ which can be solved readily provided the matrices $\mathbb{A}$ and $\mathbb{B}$ are symmetric and of positive definite form.

In the present case, the Galerkin technique is employed to achieve a closed form solution.

The chosen solution of ψ which satisfy the homogeneous boundary conditions of equation (7.16) is used.

$$\psi = \sum_{j=1,2,3}^{r} c_j(1 - \cos m\pi z/2) \qquad (m = 2j-1)$$

(7.17)

Following the same procedure as described in Ref.[41], the following matrix characteristic equation is obtained.

$$\mathbb{A}.\mathbb{C} = \lambda.\mathbb{B}.\mathbb{C} \tag{7.18}$$

In equation (7.18) $\mathbb{C}$ is a column vector of the unknown coefficients c_j for the determination of mode shape function, and $\mathbb{A}$ and $\mathbb{B}$ are square matrices containing element a_{jk} and b_{jk} given by,

$$a_{jk} = \left\{\left(\frac{m\pi}{2}\right)^6 + \alpha\left(\frac{m\pi}{2}\right)^4\right\} \qquad \text{if } j \neq k$$

$$a_{jk} = 0 \qquad \text{if } j = k$$

(7.19a)

A similar calculation yields $b_{jk}(=b_{kj})$, as

$$b_{jk} = 1 + \beta\left\{1 + \frac{2}{\pi}\left[\frac{1}{m}(-1)^{(m+1)/2} + \frac{1}{n}(-1)^{(n+1)/2}\right]\right\} \qquad \text{if } j \neq k$$

$$b_{jk} = 1 + \beta\left[\frac{3}{2} + \frac{4}{m\pi}(-1)^{(m+1)/2}\right] + \frac{1}{2}\left(\frac{m\pi}{2}\right)^2$$

$$\text{if } j = k \qquad (7.19b)$$

where m = jk-1 and n = 2k-1. The matrix $\mathbb{A}$ is thus a diagonal matrix.

The matrix characteristic equation may then be set up and solved for λ and $\mathbb{C}$ using standard techniques.

7.4 NUMERICAL RESULTS

The numerical investigations using the developed theory based on the continuum method on the dynamic behaviour of an multi-outrigger braced structure are presented and compared to that based on the transfer matrix technique.

In order to illustrate the theoretical technique, a representative structure with basic dimensions and structural data taken from example [5.2] is considered.

The matrices $\mathbb{A}$ and $\mathbb{B}$ are first calculated by substituting the structural data into equations (7.19a) and (7.19b). The eigenvalues and eigenvectors are then evaluated from the solution of the characteristic equation $\mathbb{AC} = \lambda\mathbb{BC}$. Solutions are obtained using three terms in the general series in equation (7.17). Once the eigenvalues λ are obtained, the corresponding circular

frequencies ω can be determined from equation (7.14). Table [7.1] shows the comparison of results obtained by the continuum technique to that of the transfer matrices technique for the example structure [5.2]. By substituting the corresponding eigenvectors into equation (7.17), the relative deflection of the structure can be obtained. Figs.[7.1] to [7.5] respectively describe the mode shapes of the structure for n=1, 2, 3, and 4 where n is the number of outriggers considered. Tables [7.2] to [7.4] show the variation of the first, second and third eigenvalues and the corresponding eigenvectors with parameters α and β based on a three terms solution.

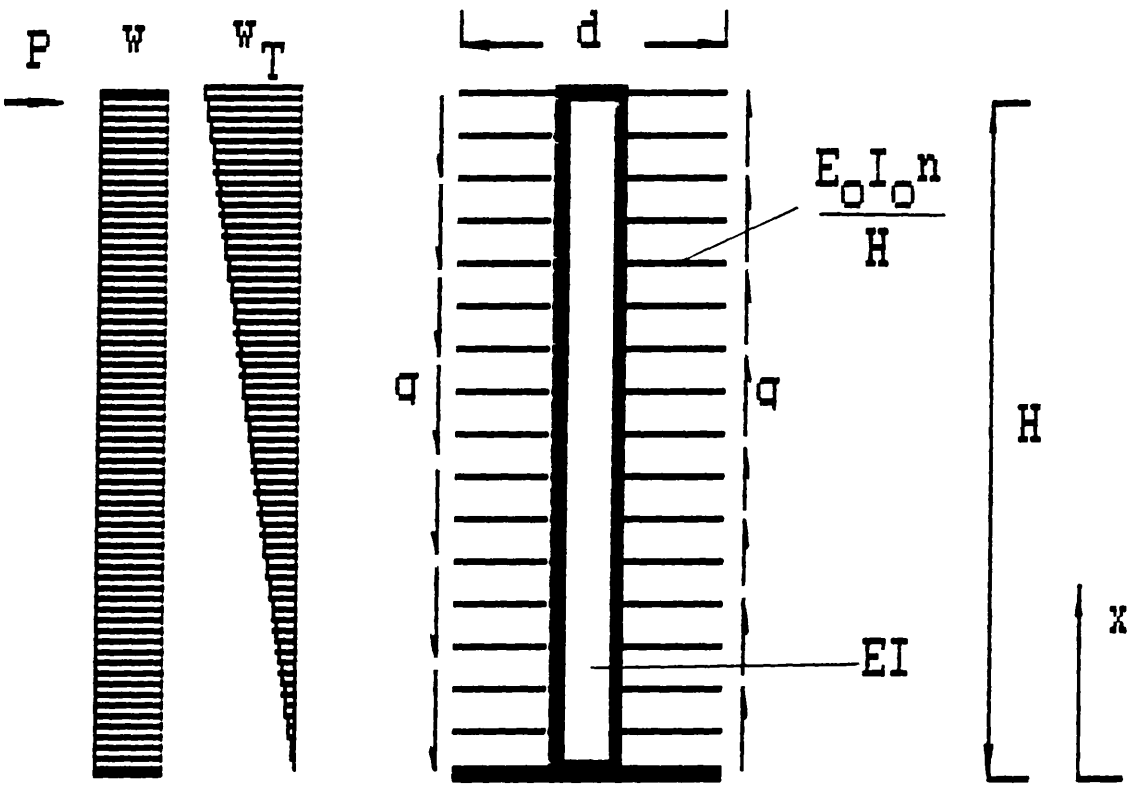

FIG. [7.1] A MULTI-OUTRIGGER-BRACED STRUCTURE REPLACED BY CONTINUOUS MEDIUM

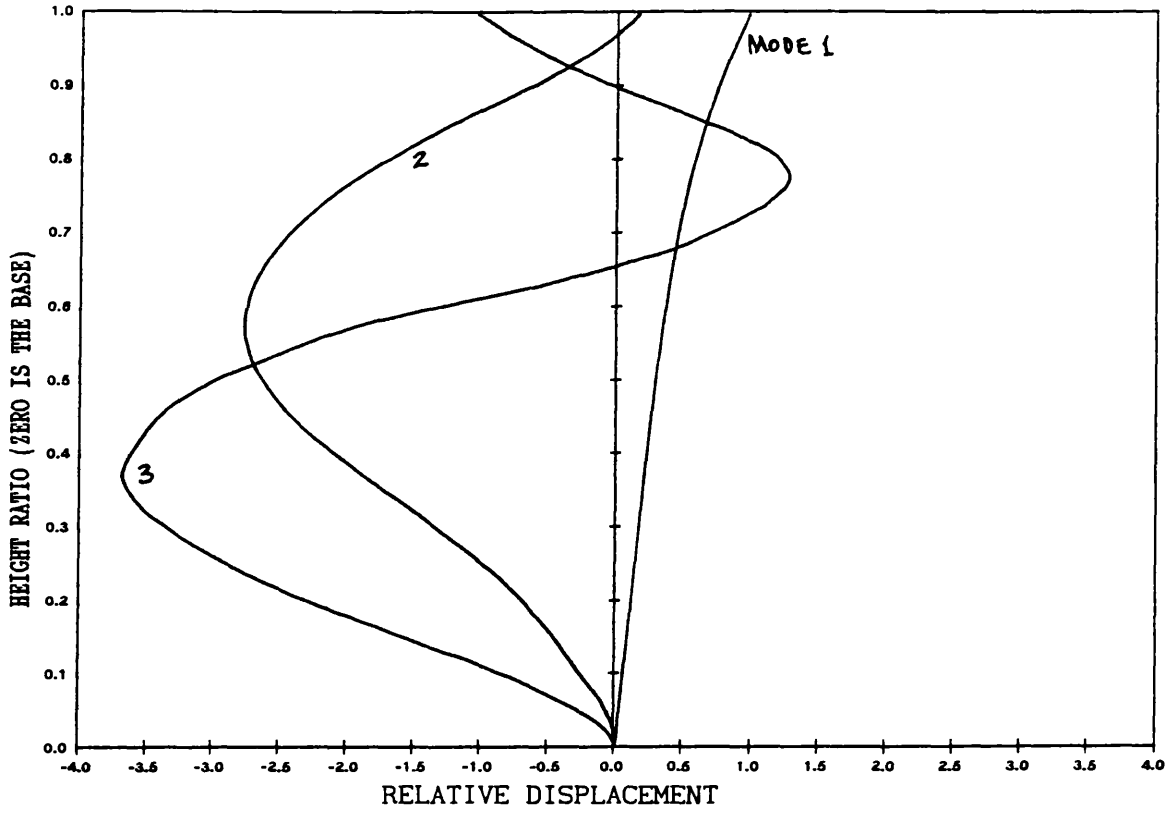

FIG. [7.2] MODE SHAPES CORRESPONDING TO THE FIRST THREE NATURAL FREQUENCIES
(EXAMPLE 5.2, n=1)

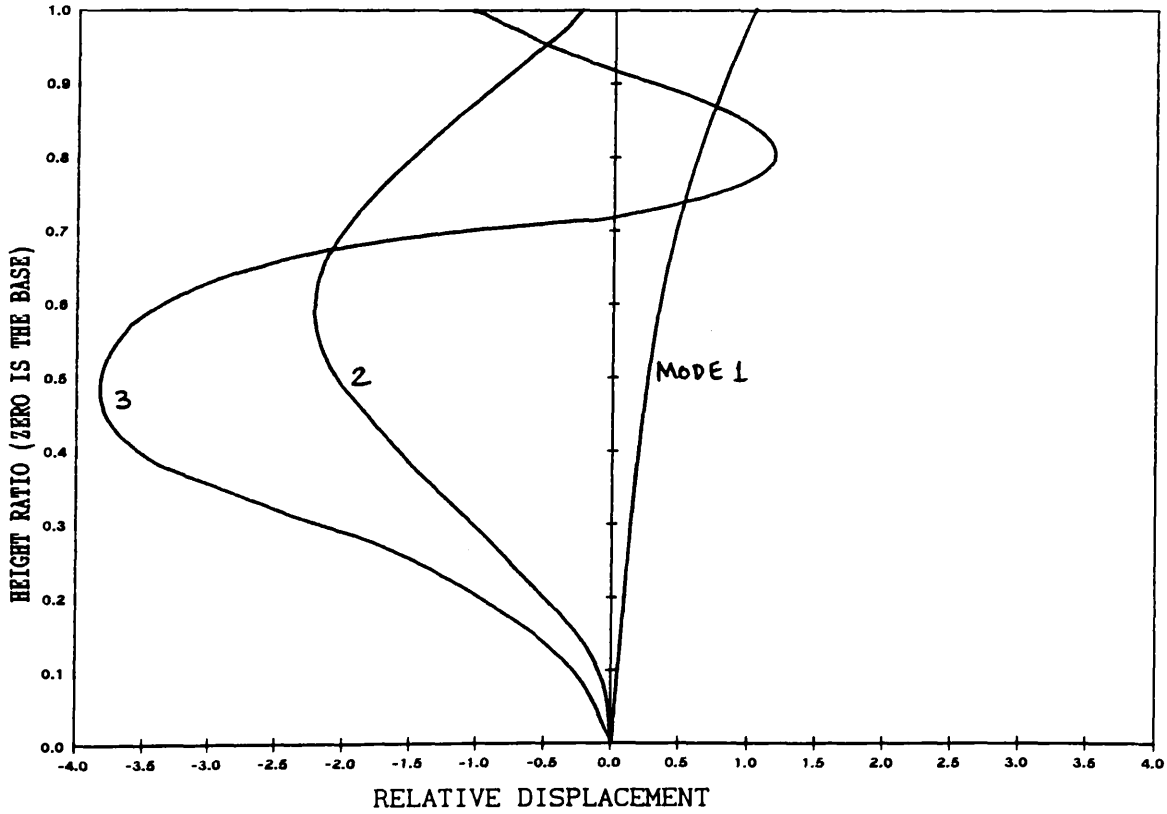

FIG. [7.3] MODE SHAPES CORRESPONDING TO THE FIRST THREE NATURAL FREQUENCIES
(EXAMPLE 5.2, n=2)

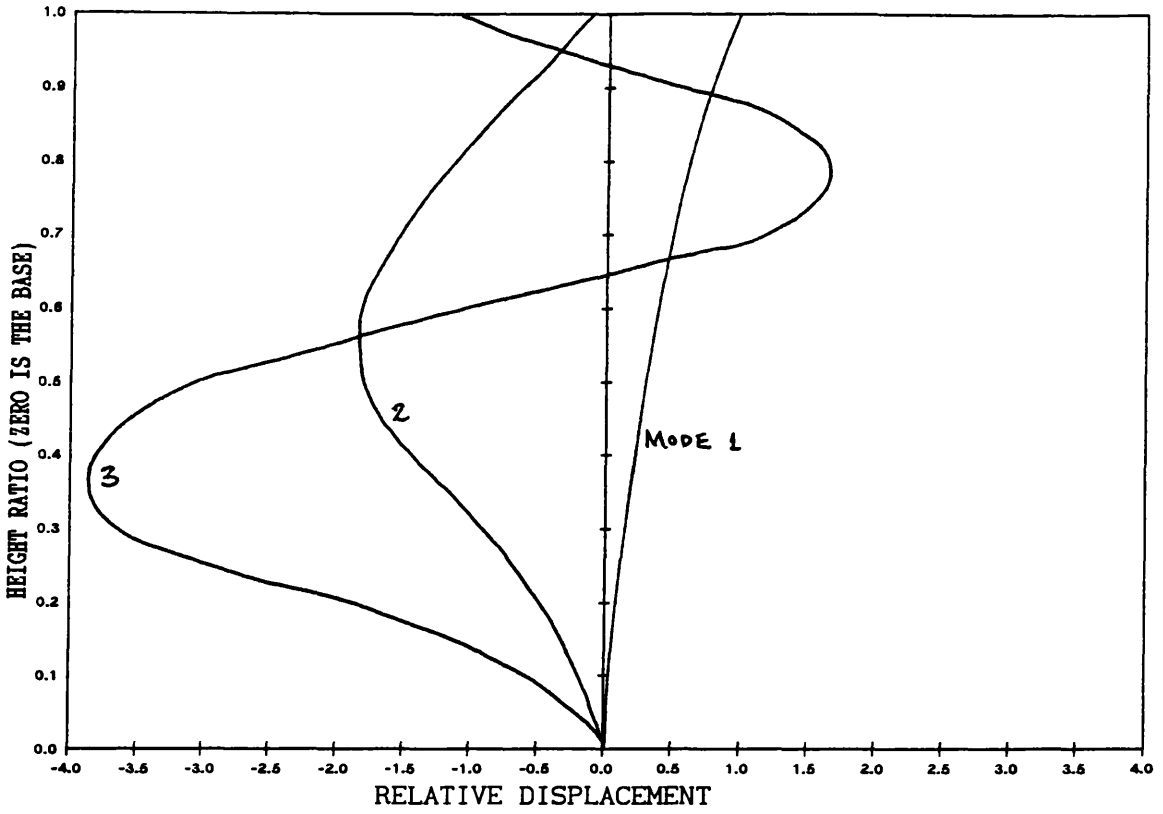

FIG. [7.4] MODE SHAPES CORRESPONDING TO THE FIRST THREE NATURAL FREQUENCIES
(EXAMPLE 5.2, n=3)

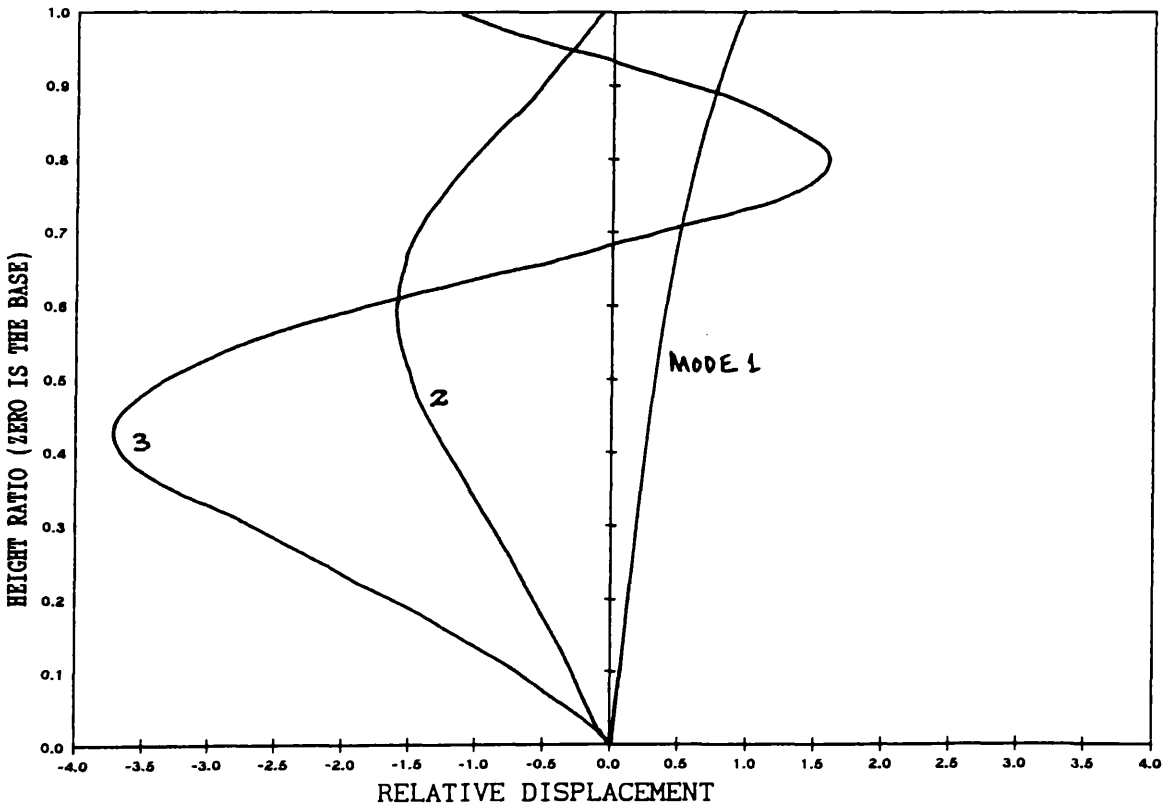

FIG. [7.5] MODE SHAPES CORRESPONDING TO THE FIRST THREE NATURAL FREQUENCIES
(EXAMPLE 5.2, n=4)

Table [7.1] Comparison of results obtained by continum technique to that of transfer matrices technique for example structure [5.2]

				Transfer Matrices			Continuum		
n	x1	x2	x3	ω_1	ω_2	ω_3	ω_1	ω_2	ω_3
	(height ratio)			(rad/sec)					
1	0.2			0.938	5.030	12.015	1.126	5.966	14.369
	0.4			1.333	4.460	12.471			
	0.6			1.480	4.989	12.327			
	0.8			1.270	6.612	13.452			
2	0.33	0.67		1.535	8.454	14.063	1.497	7.033	15.956
	0.25	0.75		1.668	9.568	13.555			
	0.50	1.00		1.621	5.894	16.878			
3	0.25	0.50	0.75	2.014	9.308	18.255	1.757	7.866	17.351
	0.17	0.50	0.83	1.871	9.517	18.222			
	0.33	0.67	1.00	2.087	8.208	17.942			
4							1.956	8.556	18.602
10							2.618	11.298	24.293
50							3.459	17.572	40.572

Table [7.2] Variation of the first eigenvalues and corresponding eigenvectors with parameters α and β (Three-term solution)

		Eigenvalue	Eigenvectors		
α	β	λ_1	C_1	C_2	C_3
0	0	3.352	1.000	0.000619	0.000029
	0.5	3.190	1.000	0.000758	0.000031
	1.0	3.043	1.000	0.000885	0.000032
5	0	10.159	1.000	0.001544	0.000080
	0.5	9.666	1.000	0.001893	0.000086
	1.0	9.218	1.000	0.002210	0.000090
10	0	16.963	1.000	0.002194	0.000125
	0.5	16.137	1.000	0.002690	0.000133
	1.0	15.386	1.000	0.003141	0.000141
15	0	23.763	1.000	0.002676	0.000164
	0.5	22.961	1.000	0.002407	0.000171
	1.0	21.551	1.000	0.003830	0.000185
20	0	30.563	1.000	0.003047	0.000199
	0.5	29.069	1.000	0.003736	0.000212
	1.0	27.712	1.000	0.004361	0.000223

Table [7.3] Variation of the second eigenvalues and corresponding eigenvectors with parameters α and β (Three-term solution)

		Eigenvalue	Eigenvectors		
α	β	λ_1	C_1	C_2	C_3
0	0	469.866	1.000	-1.908026	-0.004793
	0.5	443.114	1.000	-1.623387	-0.006440
	1.0	420.632	1.000	-1.423672	-0.007431
5	0	575.885	1.000	-2.071495	-0.005963
	0.5	543.197	1.000	-1.715868	-0.007806
	1.0	515.738	1.000	-1.482075	-0.008872
10	0	681.907	1.000	-2.095946	-0.006718
	0.5	643.280	1.000	-1.725799	-0.008746
	1.0	610.841	1.000	-1.485732	-0.009906
15	0	787.928	1.000	-2.101547	-0.007352
	0.5	763.847	1.000	-1.760162	-0.009794
	1.0	705.941	1.000	-1.483529	-0.010795
20	0	893.949	1.000	-2.102067	-0.007910
	0.5	843.441	1.000	-1.723555	-0.010257
	1.0	801.038	1.000	-1.480337	-0.011584

Table [7.4] Variation of the third eigenvalues and corresponding eigenvectors with parameters α and β (Three-term solution)

		Eigenvalue	Eigenvectors		
α	β	λ_1	C_1	C_2	C_3
0	0	3741.747	1.000	0.127770	-2.359474
	0.5	3684.398	1.000	0.198618	-2.325974
	1.0	3631.025	1.000	0.260585	-2.320539
5	0	4045.200	1.000	0.130025	-2.358115
	0.5	3983.311	1.000	0.202185	-2.326803
	1.0	3925.740	1.000	0.265352	-2.323603
10	0	4348.654	1.000	0.132041	-2.357022
	0.5	4282.231	1.000	0.205374	-2.327655
	1.0	4220.464	1.000	0.269615	-2.326449
15	0	4652.111	1.000	0.133855	-2.356131
	0.5	4560.312	1.000	-1.698209	-1.937321
	1.0	4515.196	1.000	0.273449	-2.329084
20	0	4955.569	1.000	0.135495	-2.355400
	0.5	4880.081	1.000	0.210835	-2.329334
	1.0	4809.935	1.000	0.276917	-2.331528

CHAPTER EIGHT

CONCLUSIONS AND RECOMMENDATIONS FOR FUTURE WORK

8.1 CONCLUSIONS

Both static and dynamic analyses of outrigger-braced and shear wall structures are presented in this thesis. The discrete matrix approach is used to cover the effects due to different degrees of base flexibilities on the optimum location/s of the outrigger/s based on minimisation of top drift and core moment. The static behaviour of outrigger structures subjected to different lateral load cases including uniformly distributed load, point load, triangularly distributed load, polynomial distributed load and a combination of point and triangularly distributed load are investigated. A study of the equal spacing/s of the outrigger/s is made. A multiple regression technique is applied to the established results to develop formulae for the optimum locations of the outriggers.

Curves have been presented to show the variation of the optimum locations to minimise either the top drift or the core moment. The results show that the outrigger-braced system is an efficient way of controlling both the top drift and the core moment of the structure by mobilising the axial stiffness of peripheral columns. In any outrigger-braced structure, it is shown that there is a set of optimum levels of the outriggers to give minimum top drift or minimum core moment. The behaviour of an idealised outrigger-braced structure within the assumptions stated can be expressed in terms of non-dimensional physical and structural parameters such as R, ω and k.

The particular levels of the outrigger/s and the behaviour of the structure depend upon a single non-dimensional characteristic parameter, ω, which is a function of the core-to-column and core-to-outrigger flexural rigidity ratios. The optimum levels of the outriggers to give minimum top drift can be expressed as a function of ω.

Decreasing the stiffness of the outrigger/s will tend to reduce the drift and moment efficiencies of the structure, but with a smaller reduction for more flexible column systems. It is shown that the more flexible the outriggers, other properties being constant, the lesser the drift and core moment reduction. The effect of increased outrigger flexibility is to diminish the restraining effects of the outrigger system on drift and core moment.

The primary function of the bracing system is the reduction in drift and the associated merit of the outrigger bracing system is reduction in core moment. The lower the outrigger the greater the resisting moment it usually provides. Outriggers could be placed very low in the structure to give a high resisting moment but this benefit would be offset by the fact that they would not be as effective in reducing drift. Only if drift of the structure is not a primary consideration, should additional reductions in the core moments be achieved by placing the outriggers at lower level of the structure.

As the outriggers become more flexible and the other properties

remain constant, their optimum levels for the reduction of drift usually become higher in the structure. As the core to outrigger inertia ratio increases, the structure becomes more sensitive to the outrigger flexibility.

As the number of outriggers in a structure increases and other properties remain constant, the reduction in drift or core moment will eventually reach a limit. The increment of increase in efficiency reduces for each additional outrigger. This effect of diminishing returns suggests that around three outriggers is probably the maximum number for a practical and economical solution to be used for the reductions in drift and core moment.

For the rigid foundation case, the maximum moment always occurs at the base of the structure. When a certain degree of rotational flexibility exists at the base of the structure or basement substructure, this is no longer the case. If the flexibility at the base of the structure due to a weak basement substructure or soil foundation is taken into consideration, the optimum locations of the outrigger/s tend to shift to lower levels. It follows that if drift control is not critical, additional reductions in the core moments may be achieved by placing the outriggers at lower than the optimum drift levels. The location where the maximum moment occurs is never far from the base of the structure and outriggers placed at a low levels are always an effective means of reducing base core moment. For outrigger structures with a flexible base, it is found that the flexural rigidity of the outrigger is the governing factor accounting for the structural

efficiency of the system. However, as the outrigger system becomes flexible its structural efficiency drops sharply. The optimum locations for the outrigger structures are found to be close to the base of the structure and if possible outriggers of very high stiffness should be used in order to achieve the best structural performance.

For the case of outrigger structures with a rigid base, the maximum reduction in drift and core moment is related to the parameter k which is associated with the core-to-column ratio. This is also found to be the case for flexible base. The maximum reduction in drift or core moment can be obtained by using a hypothetical infinitely rigid multi-outrigger structure with a rigid or flexible base. A closed form solution based on the continuum approach is presented in Chapter 4.

A multiple regression analysis has been applied to the analytical results for outrigger structures to develop formulae for the optimum locations of the outriggers. It is shown that the introduction of higher order terms in ω results in good approximations to the optimum locations of outrigger. The formulae are developed to allow rapid hand solutions of the optimum outrigger locations which may then be used to determine moments and drift in the structure. This serves as a useful guide to the behaviour and for estimating the forces and deflections in outrigger structures.

An approximate analysis based on the continuum approach is

presented for multi-outrigger structures. Design curves have been presented for assessing the lateral drift and the core base moment for any structural configuration defined in terms of three controlling parameters, ω, κ and R. A set of limiting values of maximum reduction of top drift and base moment of an infinitely rigid multi-outrigger structure are obtained and are used as a basis for assessing the efficiency of outrigger systems. Comparisons with results from an accurate flexibility analysis based on the discrete matrix approach, for a wide range of structural configurations, have shown that continuum analysis can give reasonably accurate results for even a very small number of outriggers. By establishing the maximum possible reductions in lateral deflection and core base moment for a very large number of outriggers, the relative efficiency of a limited number may be assessed. Once the continuous distributions of forces have been determined, the localised values in the real discrete system may be derived by integration over the length involved. For example, the shear force in any outrigger arm will be obtained by integrating the shear intensity q over half a height distance above and below the level of outrigger concerned.

The field transfer matrix technique has been used to investigate the static and dynamic behaviour of linked shear walls with multi-stiffening beams. The proposed method essentially combines the simplicity of the continuum method and the flexibility method. Complexity in the structural configuration can be handled by dividing the structure into a series of segments where each segment has a uniform structural property within itself.

Therefore, variations in the thickness and width of the walls, clear span width and size of the connecting beams and change in storey height of the building can be accommodated easily.

In the determination of the natural frequencies of vibration, the effects of bending, shear, rotatory inertias and base flexibility are included in the analysis. The field transfer matrix technique has been applied to handle the discontinuities at the outrigger or the stiffening beams positions. In addition, the possibility of any elastic rotational flexibility at the core base is included. Its influence on the natural frequencies is investigated by numerical studies. A series of numerical studies are made, and the first few natural frequencies are determined for one, two and three outriggers. The relative influences of the flexural rigidities of the core and outriggers, and the axial rigidities of the columns are examined. The determination of the first natural frequency is more important for wind actions, but the higher modes become of importance when considering seismic behaviour. The behaviour of outrigger braced core and stiffened linked shear walls is analogous, and so the analysis, equations and results apply equally well to both forms of stiffened structure. Only the important governing parameters need to be redefined in a manner appropriate to the particular structure being considered. Outrigger bracing is proved to be extremely efficient in greatly increasing the dominant natural frequencies of the structures particularly those with a flexible base.

An analysis based on the continuum approach is derived for

investigating the effect of up to two stiffening beams and connecting beams with two different types of stiffnesses on the structural behaviour of fully elastic coupled shear walls supported on flexible foundations. It is demonstrated that the adoption of a stiffening beam into coupled shear walls will reduce considerably the maximum shear force in the lintel beams, the base moment in the walls and the top drift of the structure. An attempt was made to define the efficiency of both top drift and base moment of the stiffened coupled shear wall structures. For a single stiffening beam case, the improvement in efficiency due to the stiffening beam becomes less as αH increase. Generally, the justifiable maximum value of αH in the structure for the use of a single stiffening beam is around 3. For a two stiffening beams case, the results have shown that the justifiable maximum value of αH in the structure is around 2. The efficiency of the structural performance of the stiffening beam is high when the stiffness of the connecting beams is low. For the case of one intermediate stiffening beam, the optimum location for the minimisation of top drift becomes closer to the base as the connecting beams become weaker. Reductions to both the top drift, base moment and shear force in the lintel beams diminish rapidly with two stiffening beams placed in a coupled shear walls system. For the flexible foundation case, it is found that it is usually efficient to put a stiffening beam near to the base in order to achieve optimum structural performance. It is also shown that a change of stiffness in the two different connecting types has little beneficial effect on reducing the drift and moment of the structure.

The continuous connection technique has been extended to describe the free vibrations of a system of outrigger-braced structure, and an approximate solution to the governing equation has been obtained by the Galerkin method. The results are used to evaluate the dynamic response following an imposed lateral displacement of the structure. The method is designed to be suitable for hand computations, and so is particularly useful for preliminary design calculations for outrigger-braced structures which are regular in form. The assumptions made in the theory are more questionable for the higher modes of vibration than the fundamental mode, and the higher natural frequencies are liable to become less accurate. A comparison between the proposed methods by the continuous approach and by the field transfer matrix technique was carried out. Reasonable agreement was achieved when comparing the results obtained from both methods for the frequencies of the first three modes of vibration. The same agreement could not be achieved when comparing the mode shapes because of the fundamental differences in the assumptions made in each method. The continuous medium approach has obvious limitations in that it applies to structures which are essentially regular in form. If more than one or two structural discontinuities are present, the derivation of the approximation solution become very complex and virtually impossible to be solved by hand methods.

8.2 RECOMMENDATIONS FOR FUTURE WORK

In this thesis, static and dynamic analysis on outrigger/s and

shear wall structures based on a number of simplifying assumptions have been presented. Clearly, there is scope for further refinement and extension of the present study. Some of the recommendations for future work are put forward as below:-

1).All the analyses presented so far are only applicable to symmetric outrigger structures. It would be useful to cover the case of asymmetric outrigger systems to find the effect on the structural behaviour of the structure resulting from the eccentricity of the core.

2).One of the assumptions made in the analysis of outrigger structures is that the sectional properties of the core and columns are uniform throughout the height. It would be useful to determine the optimum locations of outrigger and the structural behaviour of a structure comprising core and columns with non-prismatic sections. This would more closely approach practical design requirements.

3).In the analysis it was assumed that the sectional properties of the outriggers are the same throughout the height. From the results, it was found that the outrigger located nearest to the base usually takes up a higher proportion of restraining moments. Clearly, there is scope to investigate the distribution of the amount of resources required in each outrigger arm such that an optimum solution in the light of cost effectiveness and structural performance is achieved.

4).It has been shown that outrigger bracing is an efficient way to control drift and core moment in the structure. It would be interesting to find out the improvement in and efficiency of the structural performance after implementing the outrigger system to those shear wall structures in which the floors are projected beyond the walls or the facades to form balconies. The optimum number of outriggers and their corresponding optimum locations in such outrigger-braced shear wall structures should be determined.

5).All the dynamic analyses reported in this thesis are on the free vibration of outrigger-braced structure. Clearly there is room for developing the analysis to determine the structural response due to forced vibration.

6).It has been shown that the overall stiffness and structural behaviour of shear wall structures supported on flexible foundations may be improved by introducing stiff beams near to the base. For a rigid foundation case, these beams should be nearer the mid-height of the structure. There are no reasons for limiting the use of stiff beams for shear wall structures. These principles could well be applied to both open and partially closed core structures. It would be useful to determine the influence of the location of stiff beams in the height of the core on achieving the most effective improvement in structural response due to torsional and bending actions.

7).The work reported in this thesis on the static analysis of outrigger-braced and shear wall structures is concerned with

static equivalent loads which are time-independent. It would be valuable to investigate the effect on the structural behaviour and performance of the outrigger system under the application of a time-dependent loading such as transient load, seismic and blast loads. An outrigger-braced system could be used to tune the dynamic characteristic of a building which is, for example, required to be seismically qualified in its design. The outrigger braced system has been proved as an efficient way to improve overall stiffness and is relatively stiffer and involves less mass than conventional type of structural bracings. Both of these will reduce the inertia forces resulting from dynamic loading.

8).The use of outrigger-braced system has been proved to be an effective way of improving the structural efficiency of the structure. The idea can be expanded and applied to the area of laterally loaded structures which consist of different load bearing and lateral load resisting elements, such as shear walls, coupled shear walls, cores and rigidly-jointed frame works.

9).The investigation of the outrigger-braced structures reported in this thesis is based on the linear elastic concept. In order to further improve savings in the materials and reduce cost, the incorporation of the bilinear elasto-plastic concept into the present type of analysis should be attempted.

REFERENCES

1. Iyengar S.H. "Bundled-tube structure for Sears Tower" Civil Engineering, A.S.C.E., Nov.1972, pp.71-75.

2. Iyengar S.H. Khan F.R. and Zils Z.Z. "The Sears Tower (Chicago): World's Tallest Building" Acier-Stahl-Steel, 7-8/1973, pp.308-313.

3. Iyengar S.H. Amin N. and Carpenter L. "Computerised design of world's tallest building" Computers and Structures, Vol.2 pp.771-783.

4. Coull A. and Stafford Smith B. "Tall buildings", Proceedings of a Symposium on tall buildings, University of Southampton, April 1966, Pergamon Press.

5. ASCE and IABSE Proceedings of the International Conference on planning and design of tall buildings, Lehigh University, Bethlehem, Pennsylvania, U.S.A., 5 Vols., 1972.

6. ASCE Monographs on the planning and design of tall buildings, 5 Vols.: planning and environmental criteria for tall buildings; SC, tall building criteria and loadings; SB, structural design of tall steel buildings; CB, structural design of tall concrete and masonry buildings, published separately.

7. Chitty L. and Wen-Yuh Wan — "Tall building structures under wind load", 7th International Conference for Applied Mechanics, Vol.1, Paper 22, 1948, pp.254-268.

8. Beck H. — "Contribution to the analysis of coupled shear walls", ACI Journal, Proceedings Vol. 59, No.8, August 1962, pp.1055-1070.

9. Rosman R. — "An approximate method of analysis of walls of multistorey buildings", Civil Engineering and Public Works Review (London), Vol. 59, No.690, Jan.1964, pp.67-70.

10. Rosman R. — "Approximate analysis of shear walls subjected to lateral loads", ACI Journal, Proceedings Vol.61, No.6, June 1964, pp. 717-734.

11. Magnus D. — "Pierced shear walls", Concrete and Constructional Engineering (London), Vol. 60: No.3, Mar.1965, pp.89-98; No.4, April 1965, pp.127-136; No.5, May 1965. pp.77-185.

12. Coull A. and Choudhoury J.R. — "Stresses and deflections in coupled shear walls", ACI Journal, Proceedings Vol.64, No.2, Feb.1967, pp.65-72.

13. Coull A and Choudhoury J.R. "Analysis of coupled shear walls", ACI Journal, Proceedings Vol.64, Sept.1967, pp.587-593.

14. Coull A and Puri R.D. "Analysis of coupled shear walls of variable variable thickness", Building Science, Vol.2, 1967, pp.181-188.

15. Coull A. and Choudhoury J.R. "Analysis of coupled shear walls of variable cross-section", Building Science, Vol.2, 1968, pp.313-320.

16. Coull A. "Interaction of coupled shear walls with elastic foundations", ACI Journal Proceedings Vol.68, June 1971, pp.457-461.

17. Tso W.K. and Chan P.C.K. "Flexible foundation effect on Coupled Shear Walls", Journal of Am.Concr.Inst. Vol.69, Nov. 1972, pp.678-683.

18. Coull A. "Stiffening of coupled shear walls against foundation movements", Structural Engineer, No.1, Vol.52, Jan. 1974, pp.23-26.

19. Choo B.S. "Elastic and elasto-plastic behaviour of shear wall structures" PhD thesis, University of Glasgow, 1981.

20. Choo B.S. and Coull A. "Stiffening of laterally loaded coupled shear walls on elastic foundations", Build. Environ. Vol.19, n.4,1984, pp.251-256.

21. Jenkins, W.M. and Harrison T. "Analysis of tall buildings with shear walls under bending and torsion", 'Tall buildings' by Coull A. and Stafford Smith B., Pergamon Press, 1967, pp.413-449.

22. Stafford Smith B. and Taranath B.S. "The analysis of tall core-supported to Torsion", Proc. Inst. of Civil Eng., Vol.53, Part 2, Sept. 1972, pp.173-187.

23. Heidbrecht A.C. and Stafford Smith B. "Approximate analysis of open-section shear walls subjected to torsional loading" Journal of Structural Division, A.S.C.E., Vol.99, No.ST12, 2355-2373.

24. Khan M.A.H. and Stafford Smith B. "Restraining action of bracing in thin walled open section beams" Proc. ICE 59, Part 2, pp.67-78, 1975.

25. Michael D. "Torsional coupling of core walls in tall buildings" Structural Engineer, Vol.47, 67-71, 1969.

26. Tso W.K.and Biswas J.K. "Analysis of core wall structure subjected to applied torque", Building Science, Vol.8, 1973, pp.251-257.

27. Coull A. "Torsion of structural cores on deformable foundations", Building Science, Vol.10, 1975, pp.57-64.

28. Tawfik S.Y. "Torsional analysis of core structure buildings", PhD thesis, University of Glasgow, 1982.

29. Coull A. and Tawfik S.Y. "Analysis of core structures subjected to Torsion", Building and Environment, Vol.16 No.3, pp.221-228, 1981.

30. Taranath B.S. "Optimum belt truss location for high-rise structures", Structural Engineer, Vol.53, No.8, August 1975, pp.345-347.

31. McNabb J.W and Muvdi B.B. "Drift reduction factors for belt high-rise structures", Engineering Journal, American Institute of Steel Construction, 3rd Quarter, 1975, pp.88-91.

32. Stafford Smith B. and Nwake I.O. "The behaviour of multi-outrigger braced tall buildings", American Concrete Institute sponsored by Committee 442, 1980.

33. Stafford Smith B. and Salim I. "A parameter study of outrigger-braced tall building structures", Proc. ASCE, Structural Division, No.ST10, pp2001-2004, 1981.

34. Stafford Smith, Smith B. and Salim I. "Formulae for optimum drift resistance of outrigger braced tall building structures" Computer and Structure, Vol.17, No.1, pp.45-50, 1983.

35. Boggs P.C. and Gasparini D.A. "Lateral stiffness of core/outrigger system", Engineering Journal, American Institute of Steel Construction, Fourth Quarter, pp.172-180, 1983.

36. Rutenberg A. "Earthquake analysis of belted high-rise building structures", Eng. Struct., Vol.1, July, 1979, pp. 191 - 196.

37. Moudarres F.R. and Coull A. "Free vibration of outrigger-braced structures", Proc. Inst. Civil Engrs, Part 2, March 1985, pp. 105 - 117.

38. Moudarres F.R. and Coull A. "Stiffening of linked shear walls", Journal of Eng. Mech. Vol.112, No.3, March 1966, pp.223-237.

39. Pestel E.C. and Leckie F.A "Matrix methods in elastomechanics", McGraw-Hill, New York, 1963.

40. Chan H.C. and Kuang J.S. "Effect of a single deep beam on twin shear walls with relational coupling", Proc. Instn. Civil Engrs., Pt.2, Sept. 1988, pp.503-515.

41. A. Coull "Free vibrations of regular symmetrical shear wall buildings", Build. Sci., Vol.10, 1975, pp.127-133.

42. National Building Code of Canada, 1990, National Research Council, Ottawa, Canada.

PUBLICATIONS

43. Coull A. and Lau O.W.H. "Analysis of multioutrigger-braced structures", Journal of Structural Engineering, A.S.C.E. Vol.115, No.7, July 1989, pp.1811-1815.

44. Coull A. and Lau O.W.H. "Outrigger-braced structures subjected to equivalent static seismic loading", Proc. 4th International Conference on Tall Buildings Hong Kong at Shanghai, Y.K. Cheung and P.K.K. Lee(Eds) Vol.1, Hong Kong, 1988, pp.395-401.

APPENDIX I

ELEMENTS OF FIELD TRANSFER MATRIX $\mathbb{U}$

The elements of the transfer matrix $\mathbb{U}$ of equation (5.1) are,

$$u_{11} = u_{44} = c_o - \sigma c_2$$

$$u_{22} = u_{33} = c_o - \tau c_2$$

$$u_{21} = u_{43} = \beta^4 EI c_3 / l^2$$

$$u_{31} = u_{42} = \beta^4 EI c_2 / l^2$$

$$u_{41} = \beta^4 EI (c_1 - \sigma c_3) / l^3$$

$$u_{12} = u_{34} = l[c_1 - (\sigma+\tau)c_3]$$

$$u_{32} = EI[-\tau c_1 + (\beta^4+\tau^2)c_3]/l$$

$$u_{13} = u_{24} = l^2 c_2 / EI$$

$$u_{23} = l(c_1 - \tau c_3)/EI$$

$$u_{14} = l^3[-\sigma c_1 + (\beta^4+\sigma^2)c_3]/(\beta^4 EI)$$

where

$$\sigma = \frac{m l^2 \omega^2}{GA}$$

$$\tau = \frac{m i^2 l^2 \omega^2}{EI}$$

$$\beta^4 = \frac{m l^4 \omega^2}{EI}$$

$$c_o = \Lambda\ (\lambda_2^{\,2}\cosh\lambda_1 + \lambda_1^{\,2}\cosh\lambda_2)$$

$$c_1 = \Lambda\ (\lambda_2^{\,3}\sinh\lambda_1 + \lambda_1^{\,3}\sinh\lambda_2)/(\lambda_1\lambda_2)$$

$$c_2 = \Lambda\ (\cosh\lambda_1 - \cosh\lambda_2)$$

$$c_3 = \Lambda\ (\lambda_2\sin\lambda_1 - \lambda_1\sinh\lambda_2)/(\lambda_1\lambda_2)$$

$$\Lambda = 1/(\lambda_1^{\,2} + \lambda_2^{\,2})$$

m is the mass per unit length

EI is the flexural rigidity

GA is the shearing rigidity

i is the radius of gyration about the centroidal axis

ω is the circular natural frequency

l is the length of beam considered

and λ_1 and λ_2 are the repeated roots of the characteristic equation (5.1), given by

$$\lambda_1,\ \lambda_2 = \{\ \beta^4 + \tfrac{1}{4}(\sigma-\tau)^2 \mp \tfrac{1}{2}(\sigma+\tau)\ \}^{1/2}$$

APPENDIX II

EVALUATION OF PARAMETER K_ϑ

A rigid base transmitting vertical loads into the underlying soil will cause initial compressive stresses under the foundation. The underlying soil might be said to be prestressed. When applied moment M are superimposed on this system, induced stresses will relieve the initial compression on the tensile side. As long as the resultant does not become tensile and the base can be considered to be rigid, the modulus of subgrade reaction may be used to develop a moment/theta relationship. Consider the base of dimension B by D. If the base rotates ϑ about the centre of the base D then the extreme edge deflects $D\vartheta/2$ into the soil. If the modulus of subgrade reaction is K N/m^3, the stress in the soil is $KD\vartheta/2$. It follows from the simple bending theory

$$\sigma = \frac{My}{I_B} \qquad \text{(A2.1)}$$

where $\sigma = KD\vartheta/2$

$y = D/2$

$I_B = BD^3/12$

From equation (A2.1), $M = KI_B\vartheta$ and therefore K_ϑ is given as

$$K_\vartheta = \vartheta/M = 1/(KI_B) \qquad \text{(A2.2)}$$

For a relatively stiff foundation (stiff clay, $K=2.9E+7N/m^3$) with the following properties,

I_B (a square base of 12m x 12m) = $1728m^4$

$I = 50m^4$

$H = 100m$

$K_\vartheta = 2E-11(Rad/Nm)$

$R = EI/(K_\vartheta I_B H) = 0.24$

For a relatively weak foundation (weak clay, $K=5.8E+6N/m^3$),

$K_\vartheta = 10E-11(Rad/Nm)$

$R = 1.22$

Generally, R ranges from 0 to 1.0

Range of values of modulus of subgrade reaction K can be referred from "Foundation analysis and design" by J.E. Bowles, McGraw-hill International Book Company, 1982, pp.324.